Pavement-ME Rehabilitation Design Protocols for MDOT Implementation

Final Report

Michigan Department of Transportation
Research Administration
8885 Ricks Road
Lansing, MI 48909

by

Syed Waqar Haider, Faizan Ahmad Lali, M. Emin Kutay, and Karim Chatti
(Michigan State University)

Linda M. Pierce, Nichols Consulting Engineering (NCE)

Report Number: SPR-1763

Michigan State University
Department of Civil and Environmental Engineering
3546 Engineering Building
East Lansing, MI 48824

March 2026

Technical Report Documentation Page

1. Report No. SPR-1763	**2. Government Accession No.**	**3. MDOT Project Manager** Justin Schenkel	
4. Title and Subtitle Pavement-ME Rehabilitation Design Protocols for MDOT Implementation		**5. Report Date**	
		6. Performing Organization Code	
7. Author(s) Syed Waqar Haider, Faizan Ahmad Lali, M. Emin Kutay, Karim Chatti, and Linda M. Pierce		**8. Performing Org. Report No.**	
9. Performing Organization Name and Address Michigan State University Department of Civil and Environmental Engineering 428 S. Shaw Lane, 3546 Engineering Building East Lansing, MI 48824 Tel: (517) 355-5107, Fax: (517) 432-1827		**10. Work Unit No. (TRAIS)**	
		11. Contract No. Contract #2023-0342	
		11(a). Authorization No. Z5	
12. Sponsoring Agency Name and Address Michigan Department of Transportation Research Administration 8885 Ricks Road Lansing MI 48909		**13. Type of Report & Period Covered** 7/13/2023 – 03/31/2026	
		14. Sponsoring Agency Code	
15. Supplementary Notes			

16. Abstract

This study delivers a Michigan-specific mechanistic-empirical framework for rehabilitation pavement design by locally calibrating PMED V2.6 across all major MDOT rehabilitation fixes, including asphalt over asphalt/concrete/rubblized concrete/crushed asphalt, and concrete over asphalt/concrete. Using 14 field projects, FWD, GPR, LWD, and field cores data were evaluated. The PMED materials inputs were established for existing aggregate base, sand subbase, pavements, crushed asphalt, rubblized concrete, and ASCRL asphalt mix. Calibration employed 336 pavement sections (308 asphalt, 28 concrete) and included fatigue cracking (top/bottom), rutting, transverse cracking (thermal + reflective), faulting, and IRI. Bootstrapping and reliability analyses produced revised local coefficients and standard-error equations that reduce bias relative to national defaults. Validation against AASHTO 93 showed calibrated PMED overlay thicknesses typically within ±1 to ±1.5 inches, aligning mechanistic predictions with current practice while improving sensitivity to materials, climate, and distress interactions. The PMED limitations were identified for some rehabilitation fix types, leading to recommended alternate layer inputs or modeling approaches. Sensitivity analyses also defined PMED input constraints, including minimum HMA overlay thicknesses of 3.5 inches over existing HMA and 4.5 inches over existing concrete pavements. Key outcomes include statewide layer modulus guidance, rehab-specific performance threshold recommendations, adoption of rehabilitation Level 2 inputs for HMA over HMA, and recommended design reliability levels to effectively integrate mechanistic-empirical rehabilitation design into MDOT standard practice.

17. Key Words Pavement-ME, local calibration, resampling techniques, pavement rehabilitation analysis, and design		**18. Distribution Statement** No restrictions. This document is available to the public through the Michigan Department of Transportation.	
19. Security Classification - report Unclassified	**20. Security Classification - page** Unclassified	**21. No. of Pages** 348	**22. Price**

ACKNOWLEDGMENTS

The authors would like to thank the Michigan Department of Transportation (MDOT) for funding this project, specifically the Research Advisory Panel (RAP) members. During this study, the authors appreciate the continuous interaction with the MDOT pavement group, Justin P. Schenkel, Michael Eacker, and Fawaz Kaseer. Thanks to Ethan Akerly for the material samples and in-situ test data collection on the field projects. Their inputs were invaluable to the researchers and helped improve the quality and results of the Report.

TABLE OF CONTENTS

CHAPTER 1 - INTRODUCTION 1
1.1 PROBLEM STATEMENT 1
1.2 BACKGROUND AND SIGNIFICANCE OF WORK 2
1.3 RESEARCH OBJECTIVES 3
1.4 RESEARCH TASKS 3
1.4.1 Task 1: Review of Literature and Rehabilitation Design Practices 4
1.4.2 Task 2: Characterization of Existing Layers 4
1.4.3 Task 3: Rehabilitation Modeling Selection for Analysis and Design 4
1.4.4 Task 4: Comparison of Rehabilitation/Material Input Levels 5
1.4.5 Task 5: Input Database 5
1.4.6 Task 6: Review of Project Data for Calibration 6
1.4.7 Task 7: Compare Rehabilitation Design PMED vs. AASHTO 93 6
1.4.8 Task 8: Identify Limitations 6
1.4.9 Task 9: Evaluate the Impact of Recalibration on Design 7
1.4.10 Task 10: Final Report and Technology Transfer 7
1.5 OUTLINE OF REPORT 7

CHAPTER 2 - LITERATURE REVIEW 9
2.1 INTRODUCTION 9
2.2 MDOT EXISTING DESIGN PRACTICES – AASHTO 93 GUIDE 10
2.2.1 HMA Overlays 10
2.2.2 Concrete Overlays 13
2.3 ME DESIGN PHILOSOPHY 15
2.4 REHABILITATION DESIGN STRATEGY 16
2.5 CHARACTERIZATION OF EXISTING PAVEMENT LAYERS 19
2.5.1 Existing HMA Layer Characterization 20
2.5.2 Existing PCC Layer Characterization 22
2.5.3 Existing Unbound Layer Characterization 24
2.5.4 Characterization of Existing Pavement Layers Across Different States 26
2.6 LOCAL CALIBRATION EFFORTS AND CHALLENGES 36
2.6.1 Local Calibration Efforts for HMA Overlays 38
2.6.2 Local Calibration Efforts for Concrete (bonded & unbonded) Overlays 50
2.7 PMED SENSITIVITY INPUTS 56
2.7.1 Summary of Sensitivity Investigations 56
2.7.2 Michigan Implementation Efforts 59
2.8 STATE OF PRACTICES FOR MATERIAL TESTING 63
2.8.1 Field Testing 64
2.8.2 Laboratory Testing 65

CHAPTER 3 - MATERIAL TESTING RESULTS 69
3.1 INTRODUCTION 69
3.2 FIELD CHARACTERIZATION OF MATERIALS 72
3.2.1 Falling Weight Deflectometer Testing 72
3.2.2 Light Weight Deflectometer Testing 98

3.2.3 Ground Penetrating Radar Testing 100
3.2.4 Traffic Speed Deflectometer Testing 101
3.3 LABORATORY CHARACTERIZATION OF MATERIALS 109
3.3.1 HMA Material Testing 110
3.3.2 PCC Material 117
3.3.3 C&S Material 118
3.4 SUMMARY 133

CHAPTER 4 - DATA SYNTHESIS FOR LOCAL CALIBRATION 135
4.1 INTRODUCTION 135
4.2 MDOT CONDITION DATA 135
4.2.1 Pavement Condition Measures and PMED Data Conversions 136
4.2.2 Condition Database for Local Calibration 140
4.3 PROJECT SELECTION CRITERIA FOR LOCAL CALIBRATION 140
4.3.1 Minimum Number of Recommended Sections for Calibration 140
4.3.2 Available In-Service Pavement Projects 141
4.3.3 Project Selection Criteria 142
4.3.4 Summary of the Selected Projects for Local Calibration 144
4.4 CALIBRATION SECTION PERFORMANCE DATA SUMMARY 146
4.4.1 Asphalt Overlay Performance Data 147
4.4.2 JPCP Unbonded Overlay Performance Data: 150
4.5 CALIBRATION INPUTS FOR MATERIALS, TRAFFIC, AND CLIMATE 153
4.5.1 Pavement Cross-Section and Layer Configuration 153
4.5.2 Material Inputs 155
4.5.3 Traffic Inputs 164
4.5.4 Climatic Inputs 165
4.6 SUMMARY 167

CHAPTER 5 - REHABILITATION MODEL SELECTION 168
5.1 INTRODUCTION 168
5.2 FIX TYPES MODELED DIRECTLY IN THE PMED 169
5.2.1 HMA over HMA 170
5.2.2 HMA over JPCP or JRCP 174
5.2.3 HMA over CRCP 177
5.2.4 JPCP (Unbonded) overlay of Existing JPCP, JRCP, or CRCP 180
5.2.5 Concrete over Full-Depth HMA Pavements 181
5.2.6 SJPCP over HMA 181
5.2.7 HMA over C&S Pavement 182
5.2.8 HMA over Rubblized Concrete 183
5.3 FIX TYPES REPRESENTED THROUGH EQUIVALENT MODELING APPROACHES 184
5.3.1 HMA over HMA/JPCP, JRCP, or CRCP (composite pavement) 184
5.3.2 HMA or JPCP over Aggregate-Lift (Agg-Lift) Sections 186
5.3.3 Concrete over Composite Pavements 190
5.3.4 HMA with ASCRL over JPCP or JRCP 192
5.3.5 HMA with ASCRL over CRCP 194
5.4 FIX TYPES NOT ADDRESSED BY PMED 195
5.4.1 SJPCP over Existing PCC or AC/JPCP, JRCP, or CRCP (composite) 195

5.5 DISTRESS THRESHOLDS 195
5.5.1 Asphalt Overlays (of intact pavements) 196
5.5.2 Concrete Overlays 198
5.6 PMED LIMITATIONS 201
5.7 SUMMARY 202

CHAPTER 6 - LOCAL CALIBRATION PROCEDURES 203
6.1 INTRODUCTION 203
6.2 CALIBRATION APPROACHES 203
6.3 CALIBRATION TECHNIQUES 208
6.3.1 No-Sampling Technique 208
6.3.2 Bootstrapping 208
6.3.3 Summary of Resampling Techniques 209
6.4 PROCEDURE FOR CALIBRATION OF PERFORMANCE MODELS 210
6.4.1 Testing the Accuracy of the Global Calibration Coefficients 210
6.5 TRANSFER FUNCTION COEFFICIENTS OF ASPHALT OVERLAY 211
6.5.1 Fatigue Cracking Model (bottom-up) 211
6.5.2 Fatigue Cracking Model (top-down) 212
6.5.3 Rutting Model 212
6.5.4 Thermal Cracking Model 213
6.5.5 Reflective Cracking Model 215
6.5.6 IRI Model for Asphalt Overlay Pavements 215
6.6 TRANSFER FUNCTION COEFFICIENTS OF CONCRETE OVERLAY 216
6.6.1 Transverse Cracking Model 216
6.6.2 Transverse Joint Faulting Model 216
6.6.3 IRI Model for JPCP (Unbonded) Overlay Pavements 216
6.7 DESIGN RELIABILITY 217
6.7.1 Reliability Estimation 218
6.8 SUMMARY 220

CHAPTER 7 - LOCAL CALIBRATION 221
7.1 INTRODUCTION 221
7.2 LOCAL CALIBRATION OF ASPHALT OVERLAYS 222
7.2.1 HMA Overlay of C&S Pavement 222
7.2.2 HMA Overlays of Rubblized PCC Pavements 239
7.2.3 HMA Overlays of Existing HMA Pavements 255
7.2.4 HMA Overlays of PCC/Composite Pavements 271
7.3 LOCAL CALIBRATION OF CONCRETE OVERLAYS 282
7.3.1 Transverse Cracking Model 282
7.3.2 Faulting Model 285
7.3.3 Rigid Pavement Roughness (IRI) Model 286
7.3.4 Summary of JPCP (Unbonded) Overlays 288
7.4 COMPARISON AND VALIDATION OF REHABILITATION DESIGNS USING CALIBRATED MODELS 289
7.4.1 HMA Overlay of C&S Pavement 290
7.4.2 HMA Overlay of Rubblized PCC Pavement 291
7.4.3 HMA Overlay of Existing HMA Pavement 292
7.4.4 HMA Overlay of PCC/Composite Pavement 294

7.4.5 JPCP (Unbonded) Overlay of existing JPCP (or JRCP) 295
7.4.6 JPCP Overlay of existing HMA Pavement 297
7.4.7 HMA/PCC over Aggregate Lift over Existing Pavement 298
7.5 CATALOG DESIGN 302
7.5.1 Traffic Levels 302
7.5.2 Condition of Existing HMA Pavement 303
7.5.3 Subgrade Modulus 303
7.5.4 Cross-section of Existing Pavement Layers 304
7.5.5 Climate Region Grouping 304
7.5.6 Selection of Material Properties 305
7.5.7 Design Selection Criteria and Performance Evaluation 305
7.5.8 Summary of Catalog Results and Limitations 308
7.6 SUMMARY OF FINDINGS 309

CHAPTER 8 - CONCLUSIONS AND RECOMMENDATIONS 311
8.1 SUMMARY 311
8.2 MATERIAL CHARACTERIZATION 312
8.2.1 Field Testing 312
8.2.2 Laboratory Testing 313
8.3 MDOT REHABILITATION FIX TYPES AND PMED MODELING 314
8.4 LOCAL CALIBRATION FINDINGS 316
8.4.1 HMA Overlay of C&S Pavements 317
8.4.2 HMA Overlay of Rubblized PCC Pavements 318
8.4.3 HMA Overlay of Existing HMA Pavements 319
8.4.4 HMA overlay of PCC/Composite Pavements 320
8.4.5 JPCP (Unbonded) Overlays of existing JPCP (or JRCP) 323
8.5 COMPARISON AND VALIDATION OF REHABILITATION DESIGNS 324
8.6 CATALOG DESIGN 326
8.7 RECOMMENDATIONS 326

REFERENCES 334

APPENDICES

Note: Appendices A through E are maintained as standalone electronic supplements, available upon request.

Appendix A: FWD backcalculation results (Excel file)
Appendix B: Input data summaries for rehab model calibration (Excel file)
Appendix C: Performance data (Excel file)
Appendix D: Input data summaries for validation (Excel file)
Appendix E: Examples of TSD data analysis in Michigan (Technical Memorandum)

LIST OF TABLES

Table 2-1 Typical design lives for HMA pavements (*19*) 10
Table 2-2 Typical layer thicknesses of MDOT pavement designs (*19*)..... 11
Table 2-3 MDOT recommended values of structural coefficients per layer (*19*)..... 12
Table 2-4 Elastic modulus ranges for pavement layers (*19*) 12
Table 2-5 Thickness matrix for thin concrete overlays on existing concrete (≤ 6 in.) 13
Table 2-6 Thickness matrix for thin concrete overlays on existing asphalt (≤ 6 in.)..... 14
Table 2-7 Design thickness matrix for concrete overlays on existing HMA (≥ 6 in.) 14
Table 2-8 C-factor values for overlay on existing concrete pavements (*19*)..... 15
Table 2-9 C-factor values for HMA over HMA (*19*)..... 15
Table 2-10 PMED Structural Overlays 17
Table 2-11 Impact of input variables on PMED asphalt rehabilitation options..... 18
Table 2-12 List of significant inputs — HMA over HMA..... 19
Table 2-13 List of significant inputs — HMA over composite pavement..... 19
Table 2-14 List of significant inputs — HMA over rubblized concrete 19
Table 2-15 List of significant inputs — Unbonded concrete overlay..... 19
Table 2-16 HMA damage based on pavement condition rating..... 22
Table 2-17 C values for in-situ subgrade modulus to optimum moisture (*48*) 27
Table 2-18 PMED input data levels for Missouri DOT (*53*)..... 31
Table 2-19 HMA and base thicknesses comparison from GPR and coring (*59*) 35
Table 2-20 Rehabilitation input levels used by other SHAs..... 36
Table 2-21 SHA calibration efforts for HMA overlays of existing asphalt pavements 42
Table 2-22 SHA local calibration coefficients for the bottom-up cracking model 44
Table 2-23 SHA local calibration coefficients for the top-down cracking model 45
Table 2-24 SHA local calibration coefficients for the rutting model 47
Table 2-25 SHA local calibration coefficients for the stress intensity factor, *K* 48
Table 2-26 SHA local calibration coefficients for reflective cracking model..... 49
Table 2-27 SHA IRI model local calibration coefficients..... 50
Table 2-28 Confusion matrix for comparing field-measured and PMED predictions 52
Table 2-29 SHA calibration efforts for concrete overlays 52
Table 2-30 SHA local calibration coefficients for the concrete transverse cracking 54
Table 2-31 SHA local calibration coefficients for the faulting model..... 55
Table 2-32 SHA local calibration coefficients for the concrete overlay IRI model..... 56
Table 2-33 Summary of sensitive input parameters for asphalt pavements *(66, 67)*..... 57
Table 2-34 Summary of sensitive input parameters for concrete pavements (*68, 69*) .. 60
Table 2-35 Impact of input variables on concrete pavement performance 61
Table 2-36 Impact of input variables on asphalt pavement performance 61
Table 2-37 Conclusions and recommendations for traffic input levels 62
Table 2-38 Average subgrade modulus values 63

Table 3-1 Selected projects for the year 2023 construction season..... 71
Table 3-2 Selected projects for the year 2024 construction season..... 71
Table 3-3 Selected projects for the year 2025 construction season..... 71
Table 3-4 Coefficients for the corrected deflection coefficient (6)..... 74
Table 3-5 Adjustment factors for backcalculated modulus (10)..... 77
Table 3-6 Cross-sectional details of flexible pavements before overlay placement 78
Table 3-7 Cross-sectional details of flexible pavements after overlay placement 78

Table 3-8 Cross-sectional details of composite pavements before overlay placement . 79
Table 3-9 Cross-sectional details of composite pavements after overlay placement 79
Table 3-10 Summary FWD data available for existing asphalt pavement sections 81
Table 3-11 Summary FWD data available for asphalt pavement sections 81
Table 3-12 Pre-overlay average layer moduli for 3-layered analysis..... 82
Table 3-13 Post-overlay average layer moduli for 3-layered analysis 82
Table 3-14 Pre-overlay average moduli for 4-layered analysis 85
Table 3-15 Post-overlay average moduli for 4-layered analysis..... 85
Table 3-16 Summary FWD data available for existing composite pavements..... 90
Table 3-17 Summary FWD data available for existing composite pavements..... 90
Table 3-18 Pre-overlay average moduli for 3-layered analysis 91
Table 3-19 Post-overlay average moduli for 3-layered analysis..... 91
Table 3-20 Summary of the available LWD data..... 98
Table 3-21 LWD-based layer moduli..... 99
Table 3-22 GPR vs. field cores thickness comparison for AC/PCC layers..... 100
Table 3-23 Project selection summary for TSD analysis..... 102
Table 3-24 Tested field core samples for damaged |E*| that have FWD data..... 111
Table 3-25 Summary of damaged dynamic modulus..... 113
Table 3-26 Percent passing of extracted aggregate from cores after ignition 117
Table 3-27 Percent passing of extracted aggregate from C&S material after ignition . 117
Table 3-28 PCC core compressive strength results from composite pavements 118
Table 3-29 Testing sequences for base and subbase materials 120
Table 3-30 Summary of resilient modulus testing 121
Table 3-31 Regression parameters (slope and intercept) of |E*| per frequency..... 127
Table 3-32 Dynamic modulus slope and intercept per confinement..... 130
Table 3-33 Summary MR (ksi) for C&S at 20 °C using DTS30 133

Table 4-1 Asphalt pavement distress measurement by MDOT..... 136
Table 4-2 HMA minimum thicknesses for top-down cracking..... 137
Table 4-3 Concrete pavement distress measurement by MDOT 139
Table 4-4 Minimum number of sections required for rehabilitation calibration..... 141
Table 4-5 Selection matrix displaying selected rehabilitation sections 146
Table 4-6 Average rehabilitation treatment thicknesses..... 154
Table 4-7 As-constructed percent air voids for HMA layers 156
Table 4-8 HMA layer average aggregate gradation 156
Table 4-9 MDOT recommended values, volumetrics, and gradation 157
Table 4-10 Structural rating criteria per corresponding bottom-up fatigue cracking 158
Table 4-11 Environmental rating criteria per corresponding thermal cracking..... 158
Table 4-12 Summary of existing base and subbase resilient modulus values 161
Table 4-13 Structural layer coefficients for existing unbound layers 162
Table 4-14 Summary of C&S layer resilient modulus values..... 162
Table 4-15 Average roadbed soil resilient modulus values (2)..... 164
Table 4-16 MDOT Level 2 Attributes and Subcategories for Traffic inputs..... 164
Table 4-17 Ranges of AADTT for all rehabilitation projects..... 165
Table 4-18 Michigan climate station information 166

Table 5-1 FHWA pavement condition rating..... 171
Table 5-2 Sensitivity of predicted IRI..... 175

Table 5-3 Sensitivity of predicted JPCP transverse cracking 175
Table 5-4 Sensitivity of predicted total transverse cracking..... 176
Table 5-5 MDOT pavement condition criteria based on DI (*19*) 185
Table 5-6 Predicted performance comparison 191
Table 5-7 PMED default thresholds for asphalt overlays..... 196
Table 5-8 Recommended thresholds for HMA overlays 198
Table 5-9 PMED default thresholds for concrete overlays (*1*) 200

Table 6-1 Model transfer functions and calibration approaches for asphalt 206
Table 6-2 Model transfer functions and calibration approaches for concrete 207
Table 6-3 Summary of calibration techniques 210
Table 6-4 Global values for the bottom-up cracking model coefficients 212
Table 6-5 Example statistics for reliability analysis of HMA overlay 218
Table 6-6 Global SE equations for each distress and smoothness model 220

Table 7-1 Calibration of bottom-up cracking model for C&S (No sampling) 223
Table 7-2 Hypothesis testing results for bottom-up cracking (No sampling)..... 223
Table 7-3 Bootstrapping global model summary 224
Table 7-4 Bootstrapping local calibration results summary 224
Table 7-5 SE equation of the bottom-up cracking model for C&S pavements..... 225
Table 7-6 Calibration results for top-down cracking for C&S 226
Table 7-7 SE equation of the top-down cracking model for C&S pavements 227
Table 7-8 Hypothesis testing results of rutting models for C&S pavements 229
Table 7-9 Calibration summary results for C&S pavements – Method 1 229
Table 7-10 Global rutting model for C&S pavements (bootstrapping) 230
Table 7-11 Local rutting model for C&S pavements (bootstrapping)..... 230
Table 7-12 Hypothesis testing results for total rutting 231
Table 7-13 Total rutting model calibration results..... 231
Table 7-14 Global model summary for total rutting of C&S pavements..... 232
Table 7-15 Local calibration summary for total rutting of C&S pavements 232
Table 7-16 SE equations of rutting models for C&S pavements 233
Table 7-17 Transverse (thermal) cracking results – C&S pavements 234
Table 7-18 SE equations for the thermal cracking model of C&S pavements 235
Table 7-19 IRI model hypothesis testing results..... 236
Table 7-20 IRI model calibration results (No sampling)..... 236
Table 7-21 Global model summary for IRI of C&S pavements (bootstrapping)..... 237
Table 7-22 Local calibration summary for IRI of C&S pavements (bootstrapping) 238
Table 7-23 Summary coefficients for HMA overlay over C&S pavements..... 239
Table 7-24 SE equations for HMA overlay over C&S pavements 239
Table 7-25 Calibration of the bottom-up cracking model for rubblized PCC..... 240
Table 7-26 Hypothesis testing results for bottom-up cracking (No sampling)..... 241
Table 7-27 Bootstrapping global model summary 241
Table 7-28 Bootstrapping local calibration results summary 241
Table 7-29 SE equations of the bottom-up cracking model for rubblized PCC..... 242
Table 7-30 Calibration results of the top-down cracking model for rubblized PCC..... 243
Table 7-31 SE equations of the top-down cracking model for rubblized PCC 244
Table 7-32 Hypothesis testing results of rutting models for rubblized PCC..... 246
Table 7-33 Calibration summary results for rubblized PCC – Method 1..... 246

Table 7-34 Global rutting model for rubblized PCC (bootstrapping) 247
Table 7-35 Local rutting model for rubblized PCC (bootstrapping) 247
Table 7-36 Hypothesis testing results for total rutting 248
Table 7-37 Total rutting model calibration results 249
Table 7-38 Global model summary for total rutting of rubblized PCC 249
Table 7-39 Local calibration summary for total rutting of rubblized PCC 249
Table 7-40 SE equations of rutting models for rubblized PCC 250
Table 7-41 Transverse (thermal) cracking results for rubblized PCC 251
Table 7-42 SE equations for the thermal cracking model of rubblized PCC 252
Table 7-43 IRI model hypothesis testing results 252
Table 7-44 IRI model calibration results (No sampling) 252
Table 7-45 Global model summary for IRI of rubblized PCC (bootstrapping) 253
Table 7-46 Local calibration summary for IRI of rubblized PCC (bootstrapping) 254
Table 7-47 Summary coefficients for HMA overlay over rubblized PCC 255
Table 7-48 SE equations for HMA overlay over rubblized PCC 255
Table 7-49 Calibration of the total fatigue cracking model for HMA over HMA 256
Table 7-50 SE equations of the total fatigue cracking model for HMA over HMA 257
Table 7-51 Calibration results of the top-down cracking model for HMA over HMA 258
Table 7-52 SE equations of the top-down cracking model for HMA over HMA 259
Table 7-53 Hypothesis testing results of rutting models for HMA over HMA 262
Table 7-54 Calibration summary results for HAM over HMA (No sampling) 262
Table 7-55 Global rutting model for HMA over HMA (bootstrapping) 262
Table 7-56 Local rutting model for HAM over HMA (bootstrapping) 262
Table 7-57 Hypothesis testing results for the total rutting of HMA over HMA 263
Table 7-58 Total rutting model calibration results for HMA over HMA 263
Table 7-59 Global model summary for total rutting of HMA over HMA 264
Table 7-60 Local calibration for total rutting of HAM over HMA (bootstrapping) 264
Table 7-61 SE equations of rutting models for HMA over HMA 265
Table 7-62 Total transverse cracking results for HMA over HMA 267
Table 7-63 SE equations of the total transverse cracking for HMA over HMA 267
Table 7-64 IRI model hypothesis testing results 268
Table 7-65 IRI model calibration results (No sampling) 268
Table 7-66 Global model summary for IRI of HMA over HMA (bootstrapping) 269
Table 7-67 Local calibration summary for IRI of HMA over HMA (bootstrapping) 269
Table 7-68 Summary coefficients for HMA over HMA 270
Table 7-69 SE equations for HMA over HMA 271
Table 7-70 Calibration results of the top-down cracking model for HMA over PCC 273
Table 7-71 SE equation of the top-down cracking model for HMA over PCC 273
Table 7-72 Hypothesis testing results of HMA rutting for HMA over PCC 274
Table 7-73 HMA rutting model calibration results for HMA over PCC 274
Table 7-74 Global model summary for total rutting of rubblized PCC (bootstrapping) 275
Table 7-75 Calibration summary for total rutting of rubblized PCC (bootstrapping) 275
Table 7-76 SE equations of rutting models for rubblized PCC 275
Table 7-77 Total transverse cracking results for HMA over PCC 276
Table 7-78 SE equations of the total transverse cracking for HMA over PCC 277
Table 7-79 IRI model hypothesis testing results for HMA over PCC 278
Table 7-80 IRI model calibration results for HMA over PCC (No sampling) 278
Table 7-81 Global model summary for IRI of HMA over PCC (bootstrapping) 279

Table 7-82 Local calibration summary for IRI of HMA over PCC (bootstrapping) 280
Table 7-83 Summary coefficients for HMA overlay over PCC 281
Table 7-84 SE equations for HMA overlay over PCC 281
Table 7-85 Global model hypothesis testing results 283
Table 7-86 Local calibration results using the entire dataset (No sampling) 283
Table 7-87 Transverse cracking global model using bootstrapping 284
Table 7-88 Transverse cracking local model using bootstrapping 284
Table 7-89 SE equations for transverse cracking 285
Table 7-90 Summary of faulting model calibration 286
Table 7-91 SE equations for the faulting model 286
Table 7-92 Calibration results for IRI (No sampling) 287
Table 7-93 IRI global model using bootstrapping for unbonded overlays 288
Table 7-94 IRI local model using bootstrapping for unbonded overlays 288
Table 7-95 Summary of unbonded overlay pavement performance models 289
Table 7-96 SE equations of unbonded overlays 289
Table 7-97 Summary of validation sections for HMA overlays of C&S pavements 290
Table 7-98 Summary of validation sections for HMA overlays 291
Table 7-99 Summary of validation sections for HMA over HMA 293
Table 7-100 Summary of validation sections for HMA over PCC 294
Table 7-101 Summary of validation sections for JPCP (unbonded) overlays 296
Table 7-102 Summary of validation sections for JPCP overlay of existing HMA 297
Table 7-103 Mix and binder selection by climate region, traffic level, and layer 305
Table 7-104 Performance-based design thicknesses for HMA over HMA 307
Table 7-105 Final catalog thicknesses for HMA over HMA 307
Table 7-106 Performance-based design thicknesses for HMA over C&S 307
Table 7-107 Final catalog thicknesses for HMA over C&S 308
Table 7-108 Performance-based design thicknesses for HMA over rubblized PCC 308
Table 7-109 Final catalog thicknesses for HMA over rubblized PCC 308
Table 7-110 Summary of calibrated rehabilitation fix types 310

Table 8-1 Final local calibrated coefficients for HMA overlay of C&S pavements 318
Table 8-2 SE equations for HMA overlay of C&S pavements 318
Table 8-3 Final local calibrated coefficients for HMA overlay of rubblized pavements 319
Table 8-4 SE equations for HMA overlay of rubblized pavements 319
Table 8-5 Final local calibrated coefficients for HMA overlay of HMA pavements 321
Table 8-6 SE equations for HMA overlay of HMA pavements 322
Table 8-7 Final local calibrated coefficients for HMA overlay 322
Table 8-8 SE equations for HMA overlay of PCC/composite pavements 323
Table 8-9 Locally calibrated coefficients of unbonded overlay pavements 324
Table 8-10 SE equations of unbonded overlay pavements 324
Table 8-11 Summary of asphalt overlay rehabilitation fix types 332
Table 8-12 Summary of concrete overlay rehabilitation fix types 333

LIST OF FIGURES

Figure 1-1 Overlay modeling options available in the PMED 5

Figure 2-1 Effect of traffic on serviceability and structural capacity (*18*)..... 10
Figure 2-2 Flowchart of the PMED methodology (*22*) 16
Figure 2-3 Procedure for selecting the preferred rehabilitation strategy (*23*) 18
Figure 2-4 HMA layer damage computation at Level 1 21
Figure 2-5 Ratio of measured to predicted asphalt concrete |*E**| in one core (*58*) 35

Figure 3-1 Location of the selected 2023, 2024, and 2025 construction 70
Figure 3-2 FWD time histories and time delay vs. location of the sensors 76
Figure 3-3 Comparison of deflection basin for flexible pavement..... 80
Figure 3-4 Pre- and post-overlay comparison for asphalt pavements 84
Figure 3-5 Pre- and post-overlay results for asphalt pavements 86
Figure 3-6 Comparison of Backcalculated subgrade moduli for asphalt pavements 87
Figure 3-7 Statistical comparison of backcalculation methods for asphalt pavements .. 88
Figure 3-8 Pre- and post-overlay comparison for composite pavements 92
Figure 3-9 Pre- and post-overlay results for composite pavements 94
Figure 3-10 Comparison of Backcalculated subgrade moduli for asphalt pavements ... 95
Figure 3-11 Statistical comparison of backcalculation methods 96
Figure 3-12 Comparison of LWD-based resilient moduli..... 99
Figure 3-13 GPR testing of I-96 (Grand) EB (composite pavement)..... 101
Figure 3-14 TSD analysis summary for I69EB HMA over HMA 104
Figure 3-15 TSD analysis summary for US131 NB HMA over C&S..... 105
Figure 3-16 JPCP layer thickness US131 NB 106
Figure 3-17 TSD analysis summary for US131 NB HMA over rubblized concrete 107
Figure 3-18 TSD analysis summary for US127 NB full-depth HMA 108
Figure 3-19 Field cores collected from full depth and a composite pavement..... 109
Figure 3-20 Collected C&S and rubblized material 110
Figure 3-21 Samples extracted from field cores for |E*| testing..... 111
Figure 3-22 Comparison of mean percent air voids for WP and NWP samples 112
Figure 3-23 Laboratory-measured damaged |E*| comparison..... 114
Figure 3-24 Laboratory-measured damaged |E*| ratios for WP and NWP cores..... 115
Figure 3-25 ASCRL laboratory testing results for |E*| 115
Figure 3-26 Summary percent binder extraction 116
Figure 3-27 Concrete compressive strength testing..... 119
Figure 3-28 Laboratory testing of C&S materials 120
Figure 3-29 Resilient modulus summary..... 122
Figure 3-30 Testing Setup using DTS-30..... 123
Figure 3-31 Variation of the average dynamic modulus of M-117 124
Figure 3-32 Variation of the average dynamic modulus of I-75BL..... 125
Figure 3-33 Variation of the average dynamic modulus of US-41 126
Figure 3-34 Variation of the average dynamic modulus of M-117 with frequency 128
Figure 3-35 Variation of average dynamic modulus of I-75BL with frequency..... 129
Figure 3-36 Variation of average dynamic modulus of US-41 with frequency 130
Figure 3-37 Resilient modulus (MR) at 5 psi confining pressure 132

Figure 4-1 Example of distress progression of HMA over C&S 142
Figure 4-2 Example of distress progression of HMA over rubblized concrete 143
Figure 4-3 Example of distress progression of multicourse HMA over HMA 143
Figure 4-4 Geographical location of selected HMA over C&S and rubblized 144
Figure 4-5 Geographical location of selected HMA over HMA sections (2) 145
Figure 4-6 Geographical location of selected JPCP (unbonded) 145
Figure 4-7 Selected asphalt rehabilitation sections — Bottom-up cracking 147
Figure 4-8 Selected asphalt rehabilitation sections — Top-down cracking 148
Figure 4-9 Selected asphalt rehabilitation sections — Transverse cracking 148
Figure 4-10 Selected asphalt rehabilitation sections — Total rutting 148
Figure 4-11 Selected asphalt rehabilitation sections — IRI 149
Figure 4-12 Condition distribution of asphalt overlay sections 150
Figure 4-13 Selected JPCP unbonded overlay sections — Transverse cracking 151
Figure 4-14 Selected JPCP unbonded overlay sections — Joint faulting 151
Figure 4-15 Selected JPCP unbonded overlay sections — IRI 152
Figure 4-16 Condition distribution of concrete overlay sections 153
Figure 4-17 Layer thickness distribution amongst different rehabilitation types 154
Figure 4-18 The PMED characterization of existing HMA at rehabilitation 157
Figure 4-19 Distribution of fatigue and transverse cracking for HMA overlays 158
Figure 4-20 Distribution of resilient modulus values of existing base and subbase 163
Figure 4-21 Distribution of 2-way AADTT 165

Figure 5-1 Overlay modeling options available in the PMED V2.6 (*1*) 170
Figure 5-2 The PMED rehabilitation Levels 2 and 3 171
Figure 5-3 Load cycles vs. plastic axial strain (*1*) 172
Figure 5-4 Horizontal strain profiles in overlay and existing layers from MATLEA 173
Figure 5-5 Comparison of thermal and total transverse cracking 178
Figure 5-6 HMA overlay of JPCP vs. CRCP cross-sections 179
Figure 5-7 Predicted performance comparison of HMA over JPCP vs. CRCP 179
Figure 5-8 Predicted transverse cracking versus overlay thickness 180
Figure 5-9 PMED modeling of SJPCP over AC 182
Figure 5-10 Distribution of composite pavement sections' condition based on DI 185
Figure 5-11 PMED design approach for HMA over agg-lift over existing HMA 187
Figure 5-12 PMED design approach for HMA over agg-lift over existing PCC 188
Figure 5-13 PMED design approach for HMA over agg-lift over existing HMA/PCC 188
Figure 5-14 PMED design approach for PCC over agg-lift over existing HMA 189
Figure 5-15 PMED design approach for PCC over agg-lift over existing PCC 189
Figure 5-16 PMED design approach for PCC over agg-lift over existing HMA/PCC 190
Figure 5-17 Theoretical cross-sections modeled for concrete-over-composite 191
Figure 5-18 PMED structural configurations for ASCRL and 3EMH sections 193
Figure 5-19 Total fatigue cracking comparison 194
Figure 5-20 Total transverse cracking comparison 194
Figure 5-21 Field-measured performance for asphalt overlay sections 199
Figure 5-22 Measured performance of concrete overlay sections 201

Figure 6-1 Schematic representation of bias and standard error (5) 204
Figure 6-2 Rutting profile analysis results 214
Figure 6-3 Design reliability concept for IRI (*8*) 218

Figure 6-4 Fitting curve for the reliability of bottom-up cracking 219

Figure 7-1 Calibration results of bottom-up cracking for C&S (No sampling) 223
Figure 7-2 Distribution of local calibration parameters (bootstrapping) 224
Figure 7-3 SE of global and local models for C&S pavements 225
Figure 7-4 Measured and predicted top-down-cracking for C&S (time series) 226
Figure 7-5 SE of global and local top-down cracking models 227
Figure 7-6 Predicted vs. measured rutting (No sampling) 228
Figure 7-7 Time series of individual layers' rutting for C&S pavements 229
Figure 7-8 Distribution of calibration parameters - AC rutting (Bootstrapping) 231
Figure 7-9 Predicted vs measured total rutting (No sampling) 232
Figure 7-10 Distribution of calibration parameters - total rutting 233
Figure 7-11 SE comparison for C&S rutting models 234
Figure 7-12 Predicted vs. measured thermal cracking for C&S pavements 235
Figure 7-13 SE comparison of thermal cracking model for C&S pavements 236
Figure 7-14 Measured vs predicted IRI for C&S pavements 237
Figure 7-15 Distribution of calibration parameters of the IRI model 238
Figure 7-16 Calibration results of bottom-up cracking for rubblized (No sampling) 240
Figure 7-17 Distribution of local calibration parameters (bootstrapping) 242
Figure 7-18 SE of global and local models for rubblized PCC 242
Figure 7-19 Measured and predicted top-down-cracking for rubblized PCC 243
Figure 7-20 SEof the global and local top-down cracking model for rubblized 244
Figure 7-21 Predicted vs. measured rutting for rubblized PCC (No sampling) 245
Figure 7-22 Individual layers rutting time series for the rubblized PCC 246
Figure 7-23 Distribution of calibration parameters - AC rutting (Bootstrapping) 247
Figure 7-24 Predicted vs measured Total rutting (No sampling) 248
Figure 7-25 Distribution of calibration parameters - total rutting 249
Figure 7-26 SE comparison for rubblized PCC 250
Figure 7-27 Predicted vs. measured thermal cracking for rubblized PCC 251
Figure 7-28 SE comparison of thermal cracking model for rubblized PCC 252
Figure 7-29 Measured vs predicted IRI for rubblized PCC 253
Figure 7-30 Distribution of calibration parameters of the IRI model 254
Figure 7-31 Calibration of the total fatigue cracking model for HMA over HMA 257
Figure 7-32 SE of global and local models of total fatigue cracking 258
Figure 7-33 Measured and predicted top-down-cracking for HMA over HMA 259
Figure 7-34 SE of the top-down cracking model for HMA over HMA 260
Figure 7-35 Predicted vs. measured rutting for HMA over HMA (No sampling) 261
Figure 7-36 Individual layers rutting time series for HMA over HMA 261
Figure 7-37 Distribution of calibration parameters of the rutting model 263
Figure 7-38 Predicted vs measured total rutting of HMA over HMA (No sampling) 264
Figure 7-39 Distribution of calibration parameters - total rutting (bootstrapping) 265
Figure 7-40 SE comparison for HMA over HMA 265
Figure 7-41 Predicted vs. measured total transverse cracking for HMA over HMA 266
Figure 7-42 SE of the total transverse cracking for HMA over HMA 267
Figure 7-43 Measured vs predicted IRI for HMA over HMA 268
Figure 7-44 Distribution of parameters of the IRI model for HMA over HMA 269
Figure 7-45 Measured and predicted top-down-cracking for HMA over PCC 272
Figure 7-46 SE of the top-down cracking model for HMA over PCC 273

Figure 7-47 Predicted vs measured HMA rutting for HMA over PCC (No sampling)... 274
Figure 7-48 Distribution of calibration parameters of HMA rutting 275
Figure 7-49 SE comparison of HMA rutting for HMA over PCC 276
Figure 7-50 Predicted vs. measured total transverse cracking for HMA over HMA..... 277
Figure 7-51 SE of the total transverse cracking for HMA over PCC 278
Figure 7-52 Measured vs predicted IRI for HMA over PCC..... 279
Figure 7-53 Parameters distribution of the IRI model for HMA over PCC 280
Figure 7-54 Local calibration results of transverse cracking..... 283
Figure 7-55: Bootstrap sampling calibration results for the transverse cracking 284
Figure 7-56 Calibration results of joint faulting for unbonded overlays 285
Figure 7-57 IRI calibration results for unbonded overlays using no sampling 287
Figure 7-58 Bootstrap sampling calibration results for the IRI model 288
Figure 7-59 Design thickness comparison for C&S pavements 291
Figure 7-60 Design thickness comparison for rubblized PCC pavements..... 292
Figure 7-61 Design thickness comparison for HMA over HMA 294
Figure 7-62 Design thickness comparison for HMA over PCC/composite pavements 295
Figure 7-63 Design thickness comparison for JPCP (unbonded) overlays..... 296
Figure 7-64 Design thickness (20-years) comparison for JPCP over HMA pavement 298
Figure 7-65 HMA over aggregate-lift over existing pavement 299
Figure 7-66 PCC over aggregate-lift over existing pavement..... 300
Figure 7-67 Design thickness (20-years) comparison for HMA/PCC over agg-lift..... 301

EXECUTIVE SUMMARY

This study establishes a comprehensive mechanistic-empirical (ME) framework for rehabilitation pavement design in Michigan by locally calibrating and validating the Pavement-ME Design (PMED V2.6) performance models for asphalt and concrete overlays. The research builds on MDOT's prior calibration efforts for new and reconstructed pavements (SPR-1723) and extends ME principles to rehabilitation applications. This study addresses limitations of national default models and inconsistencies between empirical AASHTO 1993 (AASHTO 93) designs and ME predictions. The project scope encompasses all major MDOT rehabilitation fix types: Hot Mix Asphalt (HMA) overlay of existing HMA, Portland Cement Concrete (PCC), rubblized PCC, or crush-and-shaped (C&S) HMA pavements; HMA overlays with asphalt stabilized crack relief layer (ASCRL); PCC overlay of existing HMA or PCC pavement; and HMA or PCC over aggregate-lift sections (thick aggregate base separating existing pavement).

Fourteen representative projects were evaluated through field investigations using Falling Weight Deflectometer (FWD), Ground Penetrating Radar (GPR), Light-Weight Deflectometer (LWD), supplemented by laboratory characterization of asphalt, concrete, C&S, and ASCRL materials. Backcalculated resilient moduli from FWD and laboratory tests were used to establish practical input ranges for existing layers: 28 ksi for aggregate base, 18 ksi for sand subbase, 60 ksi for C&S HMA, and 70 ksi for rubblized concrete. Asphalt cores indicated that existing HMA mixtures were, on average, most similar to MDOT's 4E mix volumetrics. Concrete cores from composite pavements have an average compressive strength of 9,215 psi, corresponding to a design elastic modulus of approximately 3,000 ksi. Laboratory-compacted ASCRL specimens with 20% air voids yielded dynamic modulus values appropriate for design application. In addition, a separate set of five in-service pavement sections was evaluated to demonstrate the applicability of Traffic Speed Deflectometer (TSD) data for rehabilitation design and existing pavement characterization.

A total of 336 MDOT sections were used for calibration, including 308 asphalt overlays and 28 concrete overlays, representing a wide range of traffic levels, climate, and construction practices across Michigan. Model calibration covered bottom-up and top-down fatigue cracking, rutting, transverse cracking (thermal and reflective), faulting, and IRI models for each rehabilitation fix type. Bootstrapping and reliability analyses yielded revised calibration coefficients and standard-error equations that reduced bias and standard error relative to national defaults. Validation of AASHTO 93 designs indicated that locally calibrated PMED thicknesses are typically within ±1 to ±1.5 inches for most rehabilitation types, demonstrating consistency while offering improved sensitivity to material, climate, and distress-interaction effects.

The calibrated models provide direct and equivalent modeling pathways within PMED. However, analysis revealed limitations in modeling certain PMED rehabilitation types (e.g., composite pavements with ASCRL layers or short-jointed fiber-reinforced PCC), yielding recommendations for alternate layer configurations and/or modeling types that more accurately simulate these within PMED. Additionally, sensitivity analyses identified PMED input limitations, including minimum HMA overlay thicknesses of 3.5 and 4.5

inches for existing asphalt and concrete, respectively. The key findings include: (1) updated layer modulus values for unbound materials for statewide use; (2) recommended performance thresholds for different rehabilitation fix types; (3) validated rehabilitation Level 2 as the preferred input for design of HMA over HMA; and (4) examined PMED rehabilitation performance predictions and practical outcomes to identify recommended design reliability. These recommendations will improve accuracy, consistency, and efficiency in Michigan's rehabilitation design practice, supporting MDOT's continued integration of PMED for pavement design applications.

CHAPTER 1 - INTRODUCTION

1.1 PROBLEM STATEMENT

For several decades, state highway agencies (SHAs) in the United States have primarily relied on the American Association of State Highway and Transportation Officials 1993 (AASHTO 93) Guide for the Design of Pavement Structures and its companion DARWin software to design new and rehabilitated pavements (*1*). This methodology is primarily based on empirical observations and was initially developed using performance data from the American Association of State Highway Officials (AASHO) Road Test conducted from the late 1950s to early 1960s. Although the AASHTO 93 Guide incorporated refinements in material characterization and design procedures, its empirical foundation has increasingly limited its applicability as pavement engineering has advanced (*2, 3*). To overcome these limitations, the AASHTO Mechanistic-Empirical Pavement Design (PMED) Guide was developed under the National Cooperative Highway Research Program (NCHRP) Project 1-37A (*4*). PMED's framework integrates site-specific inputs for traffic, climate, material properties, and structural characteristics with mechanistic models to predict pavement stresses and strains. The mechanistic responses are used to estimate incremental damage over time, which is subsequently translated into pavement distress using empirically derived and calibrated transfer functions (*5, 6*). This approach represents a significant improvement over purely empirical design, as it allows for more rational, science-based predictions of pavement performance.

The Michigan Department of Transportation (MDOT) has been proactive in adopting mechanistic-empirical (ME) methods. MDOT has implemented PMED and its accompanying software (PMED V2.6) for new and reconstruction projects and has sponsored a series of studies to improve its applicability in Michigan (*7-13*). These studies, conducted in collaboration with Michigan State University (MSU), have characterized regional climate and traffic, refined material properties, and calibrated performance models to reflect Michigan conditions better. As a result, reliance on national default values has been reduced, and design predictions have become more accurate. Nevertheless, the primary emphasis of these studies was on new and reconstructed pavements. Rehabilitation design received limited attention, and many analyses continued to rely on PMED default inputs because of a lack of consistent field data (*13*). Reliance on default input values limits the accuracy of pavement prediction and underscores the need for further research, particularly focused on rehabilitation applications.

The application of the PMED to rehabilitation design presents unique challenges. Rehabilitation requires accurate characterization of the condition and properties of existing pavement layers, which is inherently more complex than new or reconstruction designs. Historical records for older pavements are often incomplete, and many hot-mix asphalt (HMA) mixtures and asphalt binder specifications historically used in Michigan

have since been modified or replaced, complicating the development of representative input parameters. In addition, for rehabilitation projects, the lack of standardized procedures for material sampling may have limited the quality of past calibration efforts. These limitations must be addressed to improve the accuracy and reliability of PMED rehabilitation designs in Michigan.

This study addresses these challenges by developing a Michigan-specific framework for applying PMED to rehabilitation design. The study focuses on refining approaches for characterizing existing pavement materials, selecting appropriate pavement types in PMED for common rehabilitation treatments, and establishing clear, practical protocols for MDOT engineers. Through these efforts, the project will provide a foundation for improving the accuracy, consistency, and efficiency of rehabilitation designs, thereby complementing MDOT's ongoing efforts to implement PMED for new/reconstructed and rehabilitation pavements.

1.2 BACKGROUND AND SIGNIFICANCE OF WORK

The development and nationwide adoption of ME design principles have marked a major shift in pavement engineering practice. While the nationally calibrated models provide a foundation, the accuracy of PMED predictions depends heavily on local calibration and validation to reflect state-specific materials, traffic spectra, and climatic conditions (*14*). MDOT, in collaboration with MSU, has been proactive in this regard. A series of projects addressed climate inputs, traffic characterization, HMA and binder properties, and local calibration of asphalt and concrete pavement models (*13*). These studies reduced reliance on the PMED national default input values and improved prediction accuracy for new and reconstructed pavements in Michigan.

SHAs have emphasized that rehabilitation requires more detailed characterization of existing pavement layers than new design, including forensic evaluation of accumulated damage and aging. These challenges include:

(a) Accurate structural characterization of existing layers requires backcalculating moduli using deflection data from falling weight deflectometer (FWD) testing, coring, and ground penetrating radar (GPR). Still, these methods are resource-intensive and can yield variable results across projects (*15, 16*).
(b) PMED rehabilitation designs often rely on Level 3 assumptions when field data (e.g., the thickness and condition of existing layers) are unavailable, thereby reducing the accuracy of local calibration and performance predictions (*13, 16, 17*).
(c) Many SHAs have calibrated the PMED bottom-up fatigue cracking prediction model, neglecting the distinct mechanisms of top-down and reflective cracking. Transverse cracking has often been treated generically without explicit calibration of reflective cracking models, which limits predictive reliability (*18, 19*).
(d) Pavement surface condition survey data and pavement management system outputs are not always directly compatible with PMED input requirements,

creating challenges for integrating network-level data into project-level rehabilitation design (*6*).

This study identifies critical inputs and appropriate levels for applying PMED to rehabilitation design. It provides procedures for estimating missing or incomplete data and establishes standardized methods of section selection for local calibration, material characterization, and data archiving. Moreover, performance model calibration using PMED V2.6 with expanded datasets will provide MDOT with greater confidence in applying ME procedures to rehabilitation designs.

1.3 RESEARCH OBJECTIVES

The following are the specific study objectives:

1. Review and evaluate current MDOT pavement design practices, protocols, data, and past research for reconstruction and rehabilitation. The scope of the work includes the following rehabilitation fix types:

    - HMA over rubblized concrete
    - Unbonded concrete overlay (6 inches or more)*
    - Thin concrete overlay (less than 6 inches)*
    - HMA over crush & shaped HMA (C&S)
    - Multicourse HMA overlay*
    - Multicourse HMA with Asphalt Stabilized Crack Relief Layer (ASCRL) overlay of existing concrete pavement

* Over existing concrete, asphalt, or composite (asphalt over concrete) pavements

2. Recommend the appropriate PMED pavement type selection (i.e., PMED design type and pavement type categories) for each rehabilitation fix type.
3. Compare different hierarchical input levels for rehabilitation pavement designs, including (a) evaluation of reliability and performance criteria thresholds, (b) recommendations on how to characterize existing pavement cross-section materials (including thicknesses) based on the readily available data in MDOT's databases, and (c) MDOT practicality.
4. If warranted, evaluate and update the PMED performance model calibration coefficients for each rehabilitation treatment type.
5. Provide a comparison of performance predictions and/or design thicknesses for selected pavements designed using the AASHTO 1993 Guide and PMED to quantify and qualify the differences for each rehabilitation treatment type.
6. Provide updated guidance for MDOT pavement rehabilitation designs.

1.4 RESEARCH TASKS

The research includes the following nine (9) tasks.

1.4.1 Task 1: Review of Literature and Rehabilitation Design Practices

This task included a review of MDOT's current rehabilitation design practices under the AASHTO 1993 Guide and an evaluation of the PMED framework for overlays. In addition, strategies for characterizing existing pavement layers, highlighting national practices, and identifying sensitive inputs in PMED were summarized. Local calibration efforts and challenges reported by other SHAs were also reviewed. The developed synthesis provides the foundation for developing Michigan-specific procedures for PMED rehabilitation design.

1.4.2 Task 2: Characterization of Existing Layers

In this task, existing pavement layers were characterized to establish inputs for PMED rehabilitation design. FWD backcalculation, GPR, and core testing results were used to evaluate in-situ asphalt concrete (or HMA), Portland cement concrete (PCC), and unbound aggregate layers, including rubblized concrete and C&S material. Laboratory testing of extracted cores was performed to determine bitumen content, aggregate gradation, dynamic modulus master curves for HMA, compressive strength for concrete, and resilient modulus for unbound materials. The combined results provided input levels for the PMED to support rehabilitation performance modeling and calibration.

1.4.3 Task 3: Rehabilitation Modeling Selection for Analysis and Design

This task identified the most appropriate PMED pavement type for each MDOT rehabilitation design type. The research team prioritized rehabilitation strategies by identifying those that can be represented directly using available PMED pavement types, those that require adjustments to approximate equivalent conditions, and those that cannot currently be evaluated within the software.

The PMED provides several pavement type options for new, reconstruction, and overlay design. Figure 1-1 illustrates all overlay options available in PMED V2.6. The selection of the overlay design type was crucial and was based on the existing pavement layer, the availability of design inputs, and PMED performance prediction models. The recommended PMED pavement type approach was based on the literature review and MDOT practices for each rehabilitation fix type.

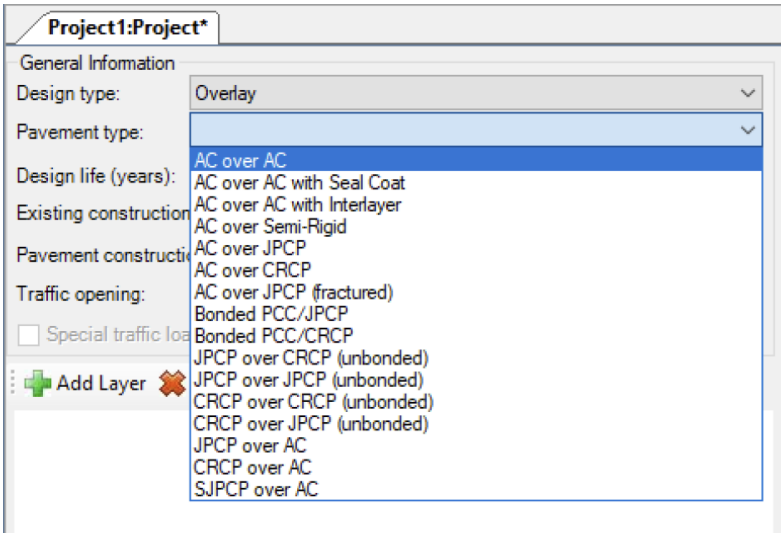


Figure 1-1 Overlay modeling options available in the PMED

Available PMED pavement types were evaluated for different MDOT rehabilitation types by assessing both predicted and field performance. While transfer functions for different performance prediction models can be locally calibrated, the recommended model was the one with the least difference between predicted and measured performance. In addition, ease of use and data availability were also considered as criteria for model selection.

1.4.4 Task 4: Comparison of Rehabilitation/Material Input Levels

This study identified applicable PMED hierarchical input levels for characterizing existing pavement layers in rehabilitation design. For HMA overlays, Level 1 characterization relied on FWD-based backcalculated moduli and damaged modulus master curves; Level 2 incorporated field condition surveys and laboratory-measured |E*|; and Level 3 used pavement condition ratings and volumetric properties (*20-22*). In the case of HMA overlays of existing jointed plain concrete pavement (JPCP), the PMED allows three hierarchical input levels for the structural capacity (or "strength") of the existing concrete: Level 1 uses FWD or core-based elastic modulus adjusted by condition factors, Level 2 uses compressive strength correlations, and Level 3 uses historical compressive strength data from DOT records (*20*). It is essential to note that the hierarchical levels refer to material input levels and should not be confused with rehabilitation input levels. Unbound aggregate bases, rubblized concrete, and C&S layers were modeled as aggregate bases with resilient modulus values derived from testing or adjusted correlations. This comparison established the relative accuracy and practicality of input levels to guide Michigan-specific rehabilitation design and calibration.

1.4.5 Task 5: Input Database

Relevant material, traffic, and climate inputs for rehabilitation design were compiled and organized into a ready-to-use database. Data from MDOT construction records, quality

control/acceptance forms, mix design sheets, and historical mix databases were processed and stored in Microsoft Excel files. These files provide standardized values and estimation procedures for key inputs, including HMA volumetrics, binder properties, layer thicknesses, and resilient moduli. The resulting database serves as a practical catalog of inputs for PMED analyses, facilitating future calibration and rehabilitation design efforts by MDOT.

1.4.6 Task 6: Review of Project Data for Calibration

Existing MDOT local and global calibration coefficients were evaluated for applicability to the recommended PMED procedures and inputs identified in Tasks 3, 4, and 5 for each rehabilitation option. Where new coefficients were required, the research team recalibrated the relevant transfer functions. Representative rehabilitated sections were selected from the pavement management system database based on age, geographical location, and measured performance trends.

PMED performance prediction models were nationally calibrated using in-service pavement material properties, pavement structures, climate, and truck loadings, along with performance data from the Long-Term Pavement Performance (LTPP) program (*4*). However, the globally calibrated models did not comprehensively represent Michigan's materials, construction practices, or climatic conditions.

The standard error of estimates (SEE) and bias values confirmed the need for local calibration across all rehabilitation performance models. The research team therefore recalibrated the rehabilitation performance prediction models using PMED V2.6, the Calibration Assistant Tool (CAT), and resampling techniques to develop Michigan-specific coefficients.

1.4.7 Task 7: Compare Rehabilitation Design PMED vs. AASHTO 93

Overlay design thicknesses from representative projects were evaluated and compared using AASHTO 93 and PMED (with Michigan-calibrated performance prediction models). Most of the selected pavement sections originated from projects previously analyzed via MDOT's Life Cycle Cost Analysis (LCCA) process. Analyses were conducted using 15- and 20-year design lives to reflect typical MDOT rehabilitation applications.

1.4.8 Task 8: Identify Limitations

In this task, the applicability of PMED for MDOT rehabilitation treatment types was evaluated, and areas were identified where PMED's use is most suitable from both practical and data availability perspectives. While PMED provides a rational design framework, its application to rehabilitation is constrained by the availability of detailed inputs and the need for state-specific calibration. Similar challenges have been reported by other highway agencies, where nationally calibrated models were found to be insufficient for routine use without local calibration (*17, 23*). Implementation studies further highlight that extensive input data, including material characterization, traffic loading, and climate parameters, are critical to achieving reliable performance

predictions, and that limitations in cracking models and transfer functions remain a concern (*24, 25*). Accordingly, this task documented where PMED can be reliably applied to MDOT rehabilitation designs and where additional data collection, calibration, or model refinement is required to support broader implementation.

1.4.9 Task 9: Evaluate the Impact of Recalibration on Design

The impact of the model recalibration on pavement designs was quantified using results from Task 8. A set of pavement sections was analyzed using both the previous and new calibration coefficients, and comparisons were documented based on PCC and HMA layer thicknesses (i.e., AASHTO 93 and PMED V2.6). Based on these comparisons, recommendations were made to modify Michigan calibration coefficients.

1.4.10 Task 10: Final Report and Technology Transfer

The final report documents all work performed during the study, including a comprehensive review of literature on PMED rehabilitation design, evaluation of national and MDOT practices, methodologies for characterizing existing pavement layers, comparison of modeling approaches for various rehabilitation options, assessment of backcalculation and data analysis tools, evaluation of input levels for existing materials, recalibration of performance models, design comparisons between AASHTO 93 and PMED, and identification of limitations with recommendations for future implementation. The report also summarizes the input database developed for this study and provides practical guidance for future MDOT projects. Also, a technology transfer workshop will be developed and presented to MDOT engineers and practitioners. The workshop will include (a) what inputs are critical for rehabilitation in Michigan, (b) the delineation of the project into uniform sections, (c) how to best characterize the existing layers, (d) which input levels are most appropriate for characterizing existing materials, (e) how to use the PMED for rehabilitation design options with demonstrative examples (f) compare the designs between AASHTO 93 and the PMED, and (g) recommendations for rehabilitation and source of data availability.

1.5 OUTLINE OF REPORT

This report contains eight chapters, and the summary of each chapter is given below:

1. Chapter 1 introduces the problem statement, background and significance, research objectives, MDOT benefits, and details of the research plan.
2. Chapter 2 presents a comprehensive literature review covering rehabilitation design practices used by MDOT and other agencies, including AASHTO 93 and PMED procedures, rehabilitation design strategies, characterization of existing pavement layers, calibration efforts, and identification of sensitive inputs.
3. Chapter 3 summarizes the results from the field and laboratory testing conducted in this study, including FWD, light-weight deflectometer (LWD), traffic speed deflectometer (TSD), dynamic modulus, compressive strength, and resilient modulus testing.

4. Chapter 4 synthesizes available MDOT Pavement Management System (PMS) condition data, project selection criteria, condition data for local calibration, and the input database assembled for rehabilitation fixes.
5. Chapter 5 establishes the framework for selecting appropriate pavement types for MDOT rehabilitation fix types within PMED. It classifies rehabilitation strategies by their modeling feasibility, presents equivalent and direct modeling approaches, defines performance thresholds, and summarizes software limitations relevant to local calibration and design implementation.
6. Chapter 6 details the local calibration process, including calibration approaches, techniques, and refinements to transfer functions.
7. Chapter 7 presents the results of local calibration for rehabilitation treatment types and validates the calibrated models using past MDOT project designs.
8. Chapter 8 provides conclusions, recommendations, and implementation guidance for MDOT.
9. Appendix A summarizes the FWD backcalculated results.
10. Appendix B contains input data summaries used for calibration.
11. Appendix C presents measured performance data for the calibration section
12. Appendix D documents the input data for validation sections.
13. Appendix E shows examples of TSD data analysis in Michigan.

CHAPTER 2 - LITERATURE REVIEW

2.1 INTRODUCTION

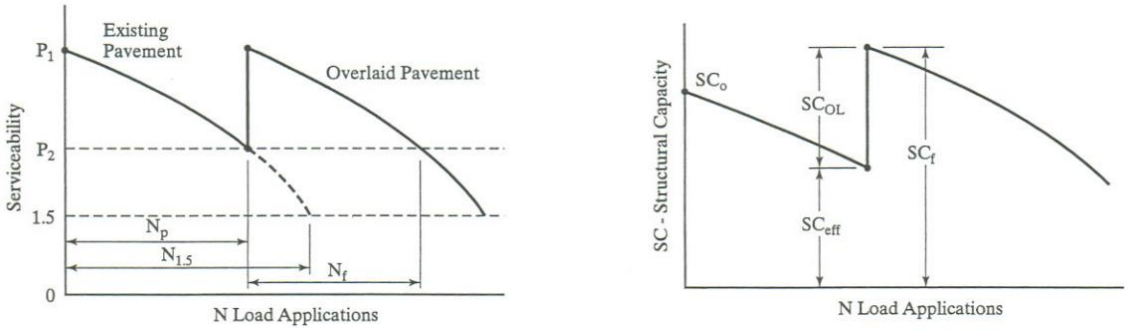
The AASHTO PMED was developed under the NCHRP Project 1-37A, Development of the 2002 Guide for the Design of New and Rehabilitated Pavement Structures: Phase II, to provide a state-of-the-art pavement design tool to the highway community (*1*). Many SHAs have adopted or are implementing the PMED to design new or rehabilitated pavements, replacing, in whole or in part, the old empirical design approach from the AASHTO 93 Guide (*2*). The PMED uses pavement mechanistic responses (stresses and strains) to compute damage accumulation, accounting for various distress mechanisms and considering axle load levels and climate variation. Subsequently, the accumulated damage is used to estimate field-observed pavement distress through transfer functions for performance prediction. The PMED performance prediction models were developed and calibrated using the data from the LTPP program, necessitating validation and potential local calibration to account for local materials, traffic, and climatic conditions (*3*).

While the use of PMED performance prediction models has increased over the past few years, accurate model calibration is critical for reliable performance predictions. Several researchers have attempted to calibrate the PMED models since the implementation of the mechanistic-empirical pavement design guide (MEPDG) (*4-6*). To date, 17 SHAs have implemented the PMED as a primary design method, and 20 SHAs use PMED with other methods for the design of new asphalt and concrete pavements and overlays. With advances in calibration tools and techniques, these efforts have become more rigorous and robust, driven by computational methods. Haider et al. used resampling methods (i.e., bootstrapping and repeated sampling) to calibrate transverse cracking and IRI in Michigan *(7)*. These techniques are beneficial for accommodating model prediction variability. Tabesh and Sakhaeifar calibrated Oklahoma's bottom-up, top-down, rutting, transverse cracking, and IRI models using a narrow-down iterative approach to minimize the standard error *(8).*

MDOT has been using PMED since 2014 in conjunction with the AASHTO 93 Guide. Currently, MDOT allows a deviation of ±1 inch between the AASHTO 93 Guide and the PMED results for all new/reconstruction projects (*9*). MDOT has sponsored several research efforts to assist with PMED implementation (*7, 9-17*). The focus of this research effort is to review and evaluate current MDOT pavement design practices, protocols, data, and past research for reconstruction and rehabilitation. In addition, this study extends the review to national practices and lessons learned from other SHA’s regarding the implementation of PMED for rehabilitation design. Emphasis is placed on the characterization of existing pavement layers, sensitivity of input levels, and calibration challenges that influence rehabilitation design accuracy. The findings from this review provide a foundation for identifying gaps in current MDOT practices and for developing Michigan-specific procedures for PMED rehabilitation design.

2.2 MDOT EXISTING DESIGN PRACTICES – AASHTO 93 GUIDE

The AASHTO 93 Guide approach determines the overlay thickness to address the structural deficiency of the existing pavement and sustain the estimated design traffic (*18*). Figure 2-1 represents the decrease in structural capacity (SC) and serviceability of any pavement type with increased load repetitions (N). The SC is expressed as the structural number (SN) for asphalt pavements and the slab thickness (D) for JPCP. At initial serviceability (P_1), the pavement has an initial structural capacity (SC_o) and reaches an effective structural capacity (SC_{eff}) at acceptable serviceability (P2) due to load repetitions (N_p). Additional structural capacity (SC_{OL}) is required to upgrade the pavement's structural capacity to the serviceability conditions at the time of rehabilitation.



a. Remaining life approach b. Structural capacity approach

Figure 2-1 Effect of traffic on serviceability and structural capacity (*18*)

Equation 2-1 represents the general overlay design equation.

$$(\mathrm{SC}_{OL})^n = \left(\mathrm{SC}_f\right)^n - \left(\mathrm{SC}_{eff}\right)^n \quad (2\text{-}1)$$

where;
SC_{OL} = additional structural capacity of the overlay.
SC_{eff} = existing structural capacity of the pavement.
SC_f = structural capacity of newly designed pavement for projected future overlay traffic (N_f).
n = constant; n=2 for unbonded concrete overlays over existing JPCP; n=1 for all other pavement types.

2.2.1 HMA Overlays

MDOT follows the AASHTO 93 Guide for the design of HMA overlays using the DARWin 3.1 software platform. Typical design lives range from 15 to 20 years, depending on the pavement fix type (Table 2-1). For example, HMA over rubblized concrete and multicourse HMA over an ASCRL are typically designed for 20 years, while overlays such as HMA over C&S may be designed for either 15 or 20 years (*19*).

Table 2-1 Typical design lives for HMA pavements (*19*)

Pavement Fix	Design Life (Years)
New/Reconstructed HMA Pavements	20
HMA over Rubblized Concrete	20
HMA over C&S	15 or 20
Multicourse HMA with ASCRL	20
Multicourse HMA Overlay	15 or 20

In addition to design life, MDOT specifies minimum thicknesses for standard overlay and base layers (Table 2-2). These include 1.5 to 2.5 inches for HMA surface courses, 2 to 3.75 inches for leveling courses, and 3 to 5 inches for HMA base courses. Stabilized bases (cement or asphalt/emulsion treated) are typically 4 to 6 inches, while unbound aggregate layers vary from 6 to 18 inches, depending on the region and the fix type (*19*).

Table 2-2 Typical layer thicknesses of MDOT pavement designs (*19*)

Layer	Typical Thickness (inches)
HMA Surface (Top) Course	1.5 to 2.5
HMA Leveling Course	2 to 3.75
HMA Base Course	3 to 5
ASCRL	3 to 5
Cement Stabilized Base	4 to 6
Asphalt/Emulsion Stabilized Base	4 to 6
Dense-Graded Aggregate Base	6
Open-Graded Drainage Course	6 (16 in Metro Region)
Sand Subbase	8 to18 depending on region & design

Another critical factor in overlay design is the assignment of structural layer coefficients (a_i), which are used to translate material thicknesses into structural numbers that reflect the layers' contributions to pavement performance (Table 2-3). For HMA layers, a coefficient of 0.42 is used, while coefficients for recycled or treated materials range between 0.12 and 0.30, depending on condition and type. Existing HMA layers are assigned coefficients based on their structural condition, ranging from 0.36 (excellent) to 0.12 (very poor) (*19*).

MDOT also recommends elastic modulus values for each pavement layer. These values are used in the AASHTO 93 Guide layered design analysis to estimate structural capacity and determine overlay thicknesses (Table 2-4). Modulus values for HMA surface courses typically range from 390,000 to 410,000 psi, while base courses range from 275,000 to 320,000 psi. Recycled materials and stabilized bases range from 45,000 psi for rubblized concrete to 1,000,000 psi for cement-stabilized bases (*19*).

Table 2-3 MDOT recommended values of structural coefficients per layer (*19*)

Layer		Structural coefficient
HMA top, leveling, and base course		0.42
ASCRL		0.30
Cement-stabilized base		0.26
Asphalt/emulsion stabilized base		0.22
C&S		0.20
Rubblized concrete		0.18
Dense-graded aggregate base		0.14
Open-graded drainage course		0.13
Sand subbase		0.10
Existing HMA**	Excellent condition – little or no alligator cracking and/or low-severity transverse cracking	0.36
Existing HMA**	Good condition • < 10% low-severity alligator cracking and/or • < 5% medium and high-severity transverse cracking	0.30
Existing HMA**	Fair condition • > 10% low-severity alligator cracking and/or • < 10% medium-severity alligator cracking and/or • 5-10% medium and high severity transverse cracking	0.24
Existing HMA**	Poor condition • > 10% medium-severity alligator cracking and/or • < 10% high-severity alligator cracking and/or • > 10% medium and high severity transverse cracking	0.17
Existing HMA**	Very poor condition • > 10% high-severity alligator cracking and/or • > 10% high-severity transverse cracking	0.12
Existing aggregate base	No evidence of pumping, degradation, or contamination by fines	0.13
	Evidence of pumping, degradation, or contamination by fines	0.06
Existing sand subbase	No evidence of pumping, degradation, or contamination by fines	0.09
	Evidence of pumping, degradation, or contamination by fines	0.04

** Multiple layers can represent the existing HMA, but one layer is sufficient. The existing HMA structural coefficient should represent the material present after milling or repair(s), to be overlaid.

Table 2-4 Elastic modulus ranges for pavement layers (*19*)

Layer	Elastic modulus (psi)
HMA top and leveling course	390,000 to 410,000
HMA base course	275,000 to 320,000
ASCRL	210,000
Cement-stabilized base	1,000,000
Asphalt/emulsion stabilized base	160,000
C&S	100,000 to 150,000
Rubblized concrete	45,000 to 55,000
Dense-graded aggregate base	30,000
Open-graded drainage course	24,000
Sand subbase	13,500
Existing aggregate base	15,000* to 28,000**
Existing sand subbase	7,500* to 12,500**

* Evidence of pumping, degradation, or contamination by fines.

** No evidence of pumping, degradation, or contamination by fines.

These standardized design lives, thickness requirements, and structural layer coefficients allow MDOT to maintain consistency across HMA rehabilitation projects while ensuring adequate performance for projected traffic levels.

2.2.2 Concrete Overlays

MDOT also employs the AASHTO 93 Guide methodology for designing concrete overlays of existing concrete and asphalt pavements (*19*). The design procedure relies on the modified U.S. Army Corps of Engineers (USACE) empirical equation that relates required overlay thickness to the thickness of a new concrete pavement, the thickness of the existing pavement, and a condition-dependent adjustment factor (C-factor). The C-factor reflects the structural integrity of the existing pavement and is derived from field inspections, coring, FWD data, and historical performance records.

2.2.2.1. Thin Concrete Overlays (< 6 inches)

For thin overlays, typically applied over existing concrete or HMA pavements, a minimum thickness of 4 inches is required. The design life for these overlays is generally set at 15 years. Tables 2-5 and 2-6 summarize the recommended design thicknesses for thin concrete overlays on existing concrete and existing asphalt surfaces, respectively.

Table 2-5 Thickness matrix for thin concrete overlays on existing concrete (≤ 6 in.)

Design lane CADT	CADT (2-way)	CESAL	C Factor	C Factor	C Factor	C Factor
			0.80	**0.75**	**0.70**	**0.65**
100	≤ 220	650,000	4.0	4.0	4.0	4.0
150	330	970,000	4.0	4.0	4.0	4.0
200	440	1,300,000	4.0	4.0	4.0	4.0
250	550	1,630,000	4.0	4.0	4.0	4.0
300	650	1,950,000	4.0	4.0	4.0	4.0
350	760	2,270,000	4.0	4.0	4.0	4.0
400	870	2,590,000	4.0	4.0	4.0	4.5
450	980	2,900,000	4.0	4.0	4.5	5.0
500	1090	3,230,000	4.0	4.5	4.5	5.0
600	1310	3,900,000	4.5	5.0	5.0	5.5
700	1525	4,500,000	5.0	5.0	5.5	-
800	1750	5,200,000	5.0	5.5	-	-
900	1950	5,800,000	5.5	-	-	-
1000	2000	6,450,000	5.5	-	-	-

2.2.2.2. Standard Concrete Overlays (> 6 inches)

For thicker overlays (6 inches or more), MDOT assumes a 20-year design life. Table 2-7 presents the overlay thicknesses as a function of commercial average daily traffic (CADT) or commercial equivalent single axle load (CESAL) and pavement condition.

Table 2-6 Thickness matrix for thin concrete overlays on existing asphalt (≤ 6 in.)

Design lane CADT	CADT (2-way)	CESAL	C Factor	C Factor	C Factor	C Factor
			0.42	**0.38**	**0.34**	**0.30**
100	≤ 220	650,000	4.0	4.0	4.0	4.5
150	330	970,000	4.0	4.5	4.5	5.0
200	440	1,300,000	4.5	5.0	5.0	5.5
250	550	1,630,000	5.0	5.5	5.5	
300	650	1,950,000	5.5	5.5	-	-
350	760	2,270,000	5.5	-	-	-
400	870	2,590,000	-	-	-	-
450	980	2,900,000	-	-	-	-
500	1090	3,230,000	-	-	-	-
600	1310	3,900,000	-	-	-	-
700	1525	4,500,000	-	-	-	-
800	1750	5,200,000	-	-	-	-
900	1950	5,800,000	-	-	-	-
1000	2000	6,450,000	-	-	-	-

Table 2-7 Design thickness matrix for concrete overlays on existing HMA (≥ 6 in.)

Design lane CADT	CADT (2-way)	CESAL	C Factor	C Factor	C Factor	C Factor
			0.42	**0.38**	**0.34**	**0.30**
250	550	2,210,000	-	-	-	6.0
300	650	2,650,000	-	-	6.0	6.0
350	760	3,090,000	-	6.0	6.0	6.5
400	870	3,540,000	6.0	6.0	6.5	6.5
450	980	3,980,000	6.0	6.5	6.5	7.0
500	1090	4,420,000	6.5	6.5	7.0	7.0
600	1310	5,300,000	6.5	7.0	7.0	7.5
700	1525	6,190,000	7.0	7.5	7.5	7.5
800	1750	7,070,000	7.5	7.5	7.5	8.0
900	1950	7,960,000	7.5	7.5	8.0	8.0
1000	2000	8,840,000	7.5	8.0	8.0	8.5
1100	2400	9,720,000	8.0	8.0	8.5	8.5
1200	2600	10,610,000	8.0	8.5	8.5	8.5
1400	3050	12,380,000	8.5	8.5	8.5	9.0
1600	3500	14,150,000	8.5	9.0	9.0	9.0
1800	3925	15,910,000	9.0	9.0	9.0	9.5
2000	4350	17,680,000	9.0	9.0	9.5	9.5
2500	5450	22,100,000	9.5	9.5	10.0	10.0
3000	6550	26,520,000	10.0	10.0	10.0	10.5
3500	7625	30,940,000	10.0	10.5	10.5	10.5
4000	8700	35,360,000	10.5	10.5	10.5	11.0
4500	9800	39,780,000	10.5	11.0	11.0	11.0
5000	10,900	44,200,000	11.0	11.0	11.0	11.5
5500	12,000	48,620,000	11.0	11.0	11.5	11.5
6000	13,075	53,040,000	11.5	11.5	11.5	11.5

2.2.2.3. C-Factor Values for Existing Pavements

The C-factor is critical in determining overlay thickness, as it accounts for the effective structural contribution of the existing pavement. MDOT specifies different ranges for overlays on existing concrete and asphalt pavements based on condition surveys, FWD testing, and coring (*19*).

For overlays of existing concrete pavements, fair structural condition with minimal cracking corresponds to a C-factor from 0.75 to 0.80, while pavements exhibiting mid-slab and "D" cracking but with adequate load transfer are assigned a lower C-factor of 0.65 to 0.70 (Table 2-8).

Table 2-8 C-factor values for overlay on existing concrete pavements (*19*)

Existing pavement condition	C – factor
Fair overall condition with minimum cracking	0.75 – 0.80
Mid–slab and D cracking, with adequate load transfer	0.65 – 0.70

For HMA over HMA, fair condition with uniform support and minimal cracking or rutting corresponds to a C-factor of 0.38-0.42. In contrast, HMA over HMA with adequate support but rutting greater than 0.1 inch and some cracking is assigned a range of 0.30 to 0.34 (Table 2-9).

Table 2-9 C-factor values for HMA over HMA (*19*)

Existing pavement condition	C – factor
Fair overall condition with uniform support • Alligator cracking, transverse cracking, and rutting are minimal	0.38 – 0.42
Has an adequate structural condition • Alligator cracking and high-severity transverse cracking are minimal • Rutting (after milling) is greater than 0.1 inch	0.30 – 0.34

2.3 ME DESIGN PHILOSOPHY

ME design is an engineering mechanics approach for computing pavement responses and predicting pavement performance, associating pavement responses with field performance data (*20*). For pavement rehabilitation designs, PMED allows the users to select any rehabilitation design strategy and other critical inputs, including traffic, climate, and layer properties (Figure 2-2). Advantages of an ME-based pavement design approach compared to the empirical approach include (*21*):

- Agency- or site-specific design criteria.
- Material characterization based on in-service pavement performance.
- Ability to assess the extent of damage resulting from specific loading configurations or higher axle loads.
- Incorporate the impacts of seasonal variations.
- Explore alternative design strategies and additional design features.

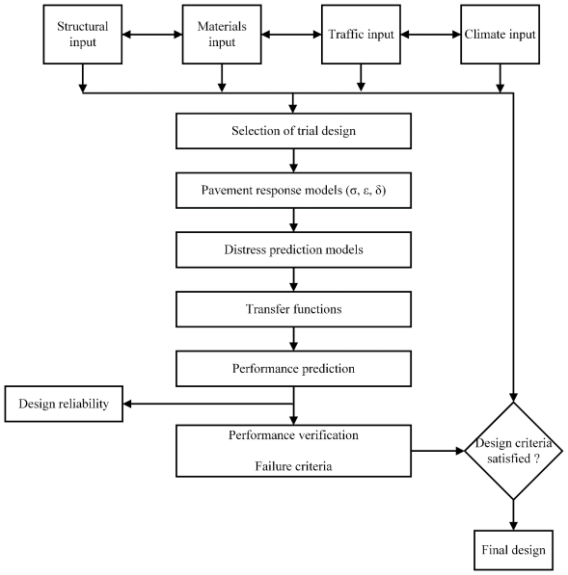


Figure 2-2 Flowchart of the PMED methodology (*22*)

Unlike the empirical AASHTO 93 Guide, PMED requires a wide range of input parameters to characterize the pavement system (*20*). These include traffic load spectra, climate records, cross-section details, and detailed material properties. To account for variability in the available data, inputs are categorized into hierarchical levels:

- Level 1 inputs are project-specific, obtained through laboratory testing or field measurements (e.g., dynamic modulus, modulus of rupture [MOR], coefficient of thermal expansion [CTE]).
- Level 2 inputs are based on regional correlations or cluster analyses (e.g., axle-load spectra and resilient modulus estimates).
- Level 3 inputs represent statewide or default values when no project-specific information is available.

For rehabilitation designs, existing pavement condition is explicitly incorporated through distress surveys, FWD backcalculation, and PMS data conversion to ensure compatibility with PMED distress models. This framework highlights the difference between the AASHTO 93 Guide, where design inputs were mainly limited to equivalent single axle load (ESALs) and empirical structural numbers. The ME design philosophy, therefore, demands a more rigorous data-driven approach, ensuring that predictions of distresses such as rutting, fatigue cracking, thermal cracking, and IRI reflect local conditions and material performance.

2.4 REHABILITATION DESIGN STRATEGY

The combined effects of traffic loading, climatic conditions, and other material-related deficiencies cause pavements to deteriorate. Pavement rehabilitation is the restoration of the structural capacity of existing pavements to prevent further deterioration under

future traffic loadings and climatic conditions. PMED rehabilitation strategies include (*20*):

- Reconstruction without lane addition.
- Reconstruction with lane addition.
- Structural overlays.
- Nonstructural overlays.
- Reconstruction without overlays.

Reconstruction can be applied to all pavement types; however, certain criteria should be considered when selecting the most appropriate rehabilitation strategy. For example, high-severity load-related distresses in asphalt pavements, and a high percentage of cracked slabs, deteriorated joints, inadequate foundation support, and D cracking in JPCP are candidates for reconstruction. Structural overlays are recommended when routine pavement maintenance does not address the cause of distress and when they reduce the time to distress recurrence. Table 2-10 shows the structural overlays evaluated in PMED (*20*):

Table 2-10 PMED Structural Overlays

Asphalt Pavement	Concrete Pavement
• HMA over HMA • HMA over HMA with seal coat • HMA over HMA with an interlayer • HMA over semi-rigid • HMA over JPCP • HMA over CRCP • HMA over fractured JPCP	• Bonded concrete over JPCP • Bonded concrete over CRCP • Unbonded JPCP over CRCP • Unbonded JPCP over JPCP • Unbonded CRCP over CRCP • Unbonded CRCP over JPCP • JPCP over HMA pavement • CRCP over HMA pavement • Short-jointed plain concrete pavement (SJPCP) over HMA pavement

The selection of the preferred rehabilitation strategy includes a detailed analysis and thorough engineering judgment to assess current and future conditions. Figure 2-3 illustrates steps for evaluating and selecting the preferred rehabilitation strategy.

MDOT's typical pavement rehabilitation activities include HMA over HMA, JPCP, and composite pavements. MDOT is currently using the AASHTO 93 Guide for all rehabilitation designs. Although the AASHTO 93 Guide has proven to be a simple and powerful pavement design tool, its empirical nature limits its applicability as a modern design method compared to PMED. The PMED approach is more rational, as it uses site-specific traffic and climate inputs, along with existing pavement conditions, for pavement rehabilitation analysis and design.

MDOT sponsored a sensitivity study to evaluate the PMED pavement design procedure for local construction, materials, and design practices. The PMED approach can be used to analyze and design new, reconstructed, and rehabilitated pavements; however, differences exist in how damage is calculated across pavement layers (*9*). These differences include:

- Location within the pavement layer where damage is calculated for asphalt rehabilitation designs.
- Age hardening of the existing asphalt layers.
- Characterization of the existing pavement damage. Rehabilitation options also consider reflective cracking.

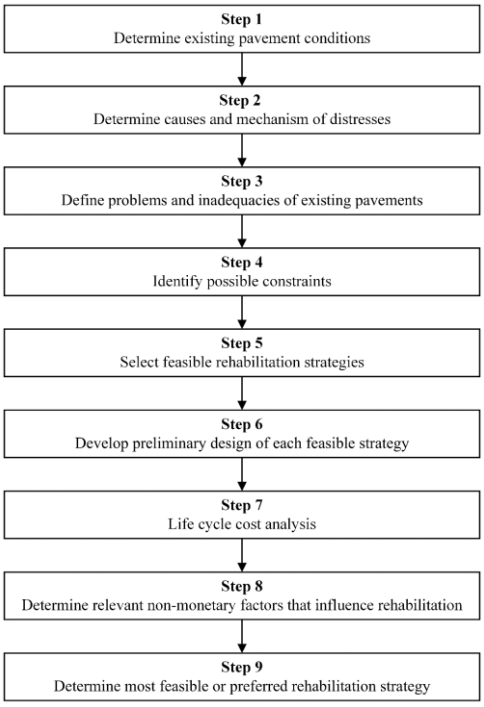


Figure 2-3 Procedure for selecting the preferred rehabilitation strategy (*23*)

The AASHTO 93 Guide requires less input data than the PMED; therefore, it is crucial to understand the impact of the different design inputs on the predicted pavement performance of the various rehabilitation options. Table 2-11 summarizes the PMED predicted distress/condition and the associated influential inputs (*9, 24, 25*).

Table 2-11 Impact of input variables on PMED asphalt rehabilitation options (*9, 24, 25*)

Fatigue cracking	Longitudinal cracking	Transverse cracking	Rutting	IRI
• HMA thickness • HMA effective binder content • HMA air voids • Base type • Subbase type	• HMA thickness • HMA air voids • HMA effective binder content • Base type • Subbase type • Subgrade type	• HMA binder grade • HMA thickness • HMA effective binder content • HMA air voids • HMA aggregate gradation	• HMA thickness • Subgrade material • Subgrade modulus • HMA effective binder content • HMA air voids • Base type • Subbase type • Base thickness • Subbase thickness	• HMA thickness • HMA aggregate gradation • HMA effective binder content • HMA air voids • Base type • Subbase thickness • Subbase type • Subgrade type

The interaction between the HMA overlay air voids and the existing asphalt thickness significantly impacts all asphalt pavement rehabilitation performance measures. The HMA overlay thickness and the interaction between the existing PCC layer modulus and the unbonded concrete overlay significantly affect the predictions of the unbonded concrete overlay. MDOT RC-1594 identified sensitive inputs for pavement rehabilitation options using the Normalized Sensitivity Index (NSI), which quantifies the relative effect of input variables on predicted pavement distress (*9*). NSI is defined as the percentage change in predicted distress relative to its global prediction, caused by a given percentage change in the input coefficient (*26*). The ranking of significant input values for each rehabilitation options are summarized in Tables 2-12 to 2-15.

Table 2-12 List of significant inputs — HMA over HMA

Inputs	Ranking (NSI)
HMA air voids	1 (6)
Existing thickness	2 (5)
HMA thickness	3 (4)
Existing pavement condition rating	4 (4)
HMA effective binder	5 (2)
Subgrade modulus	6 (2)
Subbase modulus	7 (1)

Table 2-13 List of significant inputs — HMA over composite pavement

Inputs	Ranking (NSI)
HMA air voids	1 (9)
HMA thickness	2 (2)
Existing PCC thickness	3 (1)

Table 2-14 List of significant inputs — HMA over rubblized concrete

Inputs	Ranking (NSI)
HMA air voids	1 (6)
HMA effective binder	2 (2)
HMA thickness	3 (1)

Table 2-15 List of significant inputs — Unbonded concrete overlay

Inputs	Ranking (NSI)
Concrete overlay thickness	1 (23)
Concrete overlay CTE	2 (12)
Concrete overlay MOR	3 (8)
Concrete overlay joint spacing	4 (5)
Existing PCC elastic modulus	6 (1)
Climate	7 (1)

In this framework, higher NSI values indicate that slight variations in the input have a significant influence on predicted performance, while lower values suggest minimal impact.

2.5 CHARACTERIZATION OF EXISTING PAVEMENT LAYERS

Characterizing the existing pavement layers is a critical step in rehabilitation design. Damage accumulated in the existing layer is a crucial factor for the future deterioration rate of the overlay. PMED considers the propagation of damage through the existing pavement layers and the development of distress in the overlay (*20*). The first step in

the rehabilitation design is to assess the overall condition of the existing pavement. The following categories for assessing the existing pavement condition include.

- Structural (e.g., existing distress, layer modulus, layer thickness, joint load transfer).
- Functional (e.g., smoothness, noise, friction resistance).
- Subsurface drainage (e.g., moisture, temperature, existing facilities).
- Material durability (e.g., stripping, base erosion).
- Shoulder profile (e.g., surface condition).
- Variability in condition or performance of existing pavement (e.g., lane to lane, cut and fill).
- Miscellaneous (e.g., load transfer adequacy, centerline joint spalling, joint seal damage).
- Constraints (e.g., available detours, bridge clearance, lateral clearance).

The characterization process is further described in the following sections for individual pavement layers, including the existing HMA, PCC, and unbound layers, along with a review of how other SHAs have approached similar evaluations.

2.5.1 Existing HMA Layer Characterization

Accurate damage assessment of existing pavements and in situ material properties is the most challenging in the characterization process. Damaged modulus is one of the critical factors in characterizing the existing pavement condition (*20*). Volumetric properties, including percent air voids, effective binder content, Poisson's ratio, and unit weight, are also vital in characterizing the existing asphalt layers. Three hierarchical input levels are used to represent the existing asphalt layer.

2.5.1.1. Rehabilitation Level 1

For rehabilitation Level 1, PMED estimates the damaged dynamic modulus master curve for the existing HMA layer from FWD measurements (*20, 27, 28*). The steps include:

- *Step 1:* Calculate the undamaged modulus master curve of the existing HMA layer using the Witczak |*E**| predictive equation. To calculate |*E**|, the delta, alpha, beta, and gamma fit parameters are estimated based on the mix volumetric and binder properties of existing pavement cores.
- *Step 2:* Calculate the viscosity $\left(\eta_{T_{FWD}}\right)$ at the FWD test temperature (T_{FWD}) using the existing asphalt binder activation energy–viscosity–temperature shift (A-VTS) parameters, as shown in Equation (2-2).

$$log\ log\left(\eta_{T_{FWD}}\right) = A + VTS \times log(459.67 + T_{FWD}) \quad (2\text{-}2)$$

- *Step 3:* Calculate the viscosity at the reference temperature (T_{Ref}) using the A-VTS parameters, as shown in Equation (2-3).

$$log\ log\left(\eta_{T_{Ref}}\right) = A + VTS \times \log\left(459.67 + T_{Ref}\right) \quad (3)$$

- *Step 4:* Calculate the reduced time log(t_r) using the FWD test frequency (f), viscosity at the FWD test temperature, and reference temperature, as shown in Equation (2-4).

$$log(t_r) = log\left(\frac{1}{f}\right) - c \times \left(log\left(\eta_{T_{FWD}}\right) - log\left(\eta_{T_{ref}}\right)\right) \quad (2\text{-}4)$$

- *Step 5:* Calculate the equivalent undamaged modulus at the adjusted reduced time, as shown in Equation (2-5).

$$log_{10}\left|E^*_{undamaged}\right| = \delta + \frac{\alpha}{1 + e^{\beta+\gamma \log(t_r)}} \quad (2\text{-}5)$$

- *Step 6:* Calculate the fatigue damage factor (d_{HMA}) as shown in Equation (2-6), corresponding to the backcalculated modulus, $|E^*|_{FWD}$ entered by the user, and the undamaged modulus ($E^*_{undamaged}$), calculated in Step 5.

$$log(\,d_{HMA}) = 0.2 \times \left[\ln\left(\frac{E^*_{undamaged} - E^*_{damaged}}{E^*_{FWD} - 10^{\delta}}\right) + 0.3\right] \quad (2\text{-}6)$$

- *Step 7:* Redefine the dynamic modulus master curve using the undamaged modulus ($E^*_{undamaged}$), log(d_{HMA}), and the delta parameter at a range of reduced time values. Equation (2-7) below is a rearranged version of Equation (2-6).

$$E^*_{Damaged} = E^*_{FWD} = 10^{\delta} + \frac{E^*_{undamaged} - 10^{\delta}}{1 + e^{-0.3+5\times log(d_{HMA})}} \quad (2\text{-}7)$$

Figure 2-4 shows the PMED characterization of the damaged dynamic modulus master curve for Rehabilitation Level 1 (*20*).

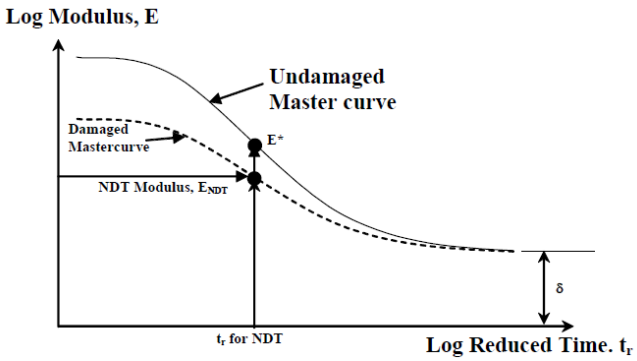


Figure 2-4 HMA layer damage computation at Level 1

2.5.1.2. Rehabilitation Level 2

At rehabilitation Level 2, the damaged dynamic modulus is determined using the field-observed or measured bottom-up fatigue (i.e., alligator cracking) before overlay repairs (*20, 27, 28*). The d_{HMA} is measured as a percentage of the total lane area. The bottom-up fatigue cracking transfer function, represented by Equation (2-8), is rearranged to calculate the damage in the existing asphalt layer, as shown in Equation (2-11).

$$FC_{HMA} = \left(\frac{1}{60}\right) + \frac{C_4}{1 + e^{C_1 C_1^* - C_2 C_2^* log(DI_{HMA})}} \quad (2\text{-}8)$$

where:
FC_{HMA} = Fatigue cracking (in the percentage of area).
DI_{HMA} = cumulative damage at the bottom of the HMA layer. Same as d_{HMA} in Equation 8.
C_1, C_2, C_4 = Transfer function coefficients where C2 is a function of HMA thickness between 5 and 12 in.

C1* and C2* can be determined using Equations (2-9) and (2-10).

$$C_1^* = -2C_2^* \quad (2\text{-}9)$$

$$C_2^* = -2.40874 \; - \; 39.748(1 + H_{HMA})^{-2.856} \quad (2\text{-}10)$$

where:
H_{HMA}= thickness of HMA layer

Now, d_{HMA} can be calculated using equation 2-11.

$$d_{HMA} = 10^{\left(\frac{\ln\left(\frac{C_4}{60 * FC_{HMA}} - 1\right) - C_1^* C_1}{C_2^* C_2}\right)} \Big/ 100 \quad (2\text{-}11)$$

After estimating the fatigue damage in existing pavement, Equation (2-7) is used to develop the damaged dynamic modulus master curve.

2.5.1.3. Rehabilitation Level 3

At rehabilitation Level 3, the pavement's structural rating is used to assess the existing pavement damage. Table 2-16 represents the d_{HMA} corresponding to the pavement's general condition ratings (*20, 27, 28*). As with rehabilitation Level 1, the undamaged modulus master curve is obtained from HMA volumetric and binder properties. With an undamaged modulus and estimated d_{HMA}, Equation (2-7) is used to predict the damaged modulus.

Table 2-16 HMA damage based on pavement condition rating

Category	d_{HMA}
Excellent	0.00 – 0.20
Good	0.20 – 0.40
Fair	0.40 – 0.80
Poor	0.80 – 1.20
Very poor	> 1.20

It is important to note that the characterization of existing asphalt layers at all hierarchical levels is typically performed before milling the surface, ensuring the determined properties reflect the pavement's in situ condition.

2.5.2 Existing PCC Layer Characterization

PMED's characterization of the existing PCC layer depends on the rehabilitation treatment type: (1) HMA or bonded PCC overlay or (2) an unbonded PCC overlay.

2.5.2.1. HMA or Bonded PCC Overlays

When an HMA overlay is placed on existing JPCP or CRCP, a thorough characterization of the underlying PCC layer is required to accurately capture the residual structural capacity and model its interaction with the HMA overlay. The presence of the overlay alters thermal gradients, reducing fatigue damage accumulation at both the top and the bottom of the slab. Even thin asphalt overlays can significantly mitigate future fatigue damage, although the extent of reflection cracking remains highly dependent on overlay thickness and often governs overall performance criteria (*20*).

A critical step in this process is estimating the accumulated fatigue damage in the existing PCC layer. For JPCP, this is assessed by combining the proportion of slabs with transverse cracks (all severities) with the percentage of repaired or replaced slabs. Pre-overlay repairs further modify this estimate, and the difference between pre-repair and post-repair conditions establishes the percentage of remaining cracked slabs at the time of rehabilitation (*20*). For example, if 6% of slabs currently exhibit transverse cracking and 4% of slabs were previously replaced, the total past fatigue damage is 10%. After pre-overlay repair, if 9% of slabs were replaced, then only 1% of cracked slabs remain before overlay. For CRCP, a similar approach is applied using the number of medium- and high-severity punchouts per mile, adjusted for repairs. These values are used in PMED, which applies nationally calibrated fatigue-damage curves to project future cracking and punchout development over the design period.

Another key parameter is the modulus of elasticity of the existing intact PCC slab, which reflects the slab stiffness at the time of rehabilitation and is typically greater than the 28-day modulus. This value is not directly reduced for slab cracking. Still, it is indirectly accounted for through computed fatigue damage and the percentage of cracked slabs, which also influence reflection-cracking projections via overlay performance models (*20*).

Finally, PMED requires characterization of the MOR and E of the underlying PCC layer. These properties capture the flexural strength and stiffness behavior of the slab, which significantly influence overlay performance predictions. Accurate input of these parameters ensures the distress transfer functions properly account for existing slab conditions. To reflect the quality and availability of project-specific data, PMED provides a hierarchical framework for PCC strength and stiffness inputs (*20*):

- *Level 1*: Project-specific laboratory or field data, including MOR and elastic modulus at multiple curing ages (7-, 14-, 28-, and 90-day values). Ratio of 20-year to 28-day properties is also required. This level provides the highest accuracy and is the preferred approach.
- *Level 2*: Compressive strength measurements at similar curing intervals, with long-term to 28-day compressive strength ratios used to estimate modulus relationships. This approach is less direct but still provides a reasonable representation of slab properties.
- *Level 3*: Limited or default strength indicators, such as 28-day MOR, 28-day compressive strength, or combinations with elastic modulus. These inputs offer

flexibility when project-specific testing is unavailable, though with reduced reliability.

2.5.2.2. Unbonded PCC Overlays

Unbonded overlays are typically used when an existing concrete pavement has reached the end of its service life but can still provide a sound foundation for an additional PCC layer. These overlays, usually six inches or thicker, are placed on existing JPCP, CRCP, or composite pavements with an appropriate separator layer. The separator layer is commonly a thin asphalt interlayer, about one to two inches thick, or a geotextile fabric. Its primary function is to prevent direct bonding between the new and old slabs, thereby limiting the reflection of existing distress into the overlay. In design, complete frictional contact between the overlay and separator layer is assumed, consistent with the global calibration used to replicate field cracking performance.

Unlike bonded or asphalt overlays, unbonded overlays do not require characterization of both PCC stiffness and strength. Instead, the existing PCC slab is represented by its elastic or resilient modulus, which is adjusted to account for the overall pavement condition. This simplification applies across different overlay configurations:

- Unbonded JPCP over JPCP.
- Unbonded JPCP over CRCP.
- Unbonded CRCP over JPCP.
- Unbonded CRCP over CRCP.

In all unbonded overlay cases, the elastic modulus serves as the primary input for existing PCC characterization, with adjustments guided by the AASHTO Manual of Practice to reflect the in situ pavement condition (*20*).

2.5.3 Existing Unbound Layer Characterization

The performance of rehabilitation treatment depends heavily on the characterization of the unbound base, subbase, and subgrade layers. The primary parameter used to represent these layers in the PMED is the resilient modulus (M_R), which quantifies the foundation's elastic recovery under repeated traffic loading and governs its overall load-carrying capacity (*1, 20*). A variety of approaches are available to determine the resilient modulus values, ranging from direct field measurements to empirical correlations.

- *Field testing*: FWD testing and backcalculation are widely recognized as the most reliable techniques for in situ characterization, as it captures the variability of materials under actual field conditions, including seasonal moisture changes.
- *Laboratory testing*: Repeated-load triaxial testing (AASHTO T307) is used to determine the resilient modulus under controlled stress states but results often differ from field conditions due to differences in boundary conditions and sample disturbance.
- *Empirical correlations*: Resilient modulus may also be estimated from simpler tests such as the Dynamic Cone Penetrator (DCP), California Bearing Ratio (CBR), aggregate gradation, or Atterberg limits. While practical, these

correlations provide only approximate values and cannot fully capture horizontal and vertical variability.

2.5.3.1. Input Hierarchy in PMED

Pavement ME incorporates a hierarchical input framework:

- *Level 1*: No formal Level 1 input exists for unbound layers, though advanced FWD testing and backcalculation, and laboratory resilient modulus testing provide the highest accuracy.
- *Level 2*: Direct input of resilient modulus values, or estimates derived from correlations with soil indices and strength properties.
- *Level 3*: Default resilient modulus values based on soil classification, aggregate gradation, and Atterberg limits, often adjusted for in situ moisture and density conditions.

2.5.3.2. Environmental Sensitivity

Numerous studies have confirmed that the subgrade modulus is highly sensitive to environmental conditions such as moisture and temperature. Salour and Erlingsson reported a 48% reduction in base stiffness during spring thaw in Sweden (*29*). Dawson et al. and Watson and Rajapakse documented that freeze–thaw cycles in Canada and other cold climates significantly decrease subgrade modulus during thaw, with a fourfold increase in deflection at peak thaw (*30, 31*). Cary and Zapata enhanced the PMED moisture model by linking the subgrade modulus to soil properties and seasonal saturation (*32*). Muslim et al. observed strong seasonal and even diurnal variations in backcalculated moduli from Michigan FWD tests, further highlighting the dynamic nature of unbound layers (*33*). Similar trends were reported by Ji et al. in Indiana and Popik et al. in Canada, where the subgrade modulus fluctuated from 1.98 ksi during thaw to 7.35 ksi in frozen winter conditions (*34, 35*). Hodek and Mayrberger further demonstrated that the subgrade modulus of natural gravel, dolomite, slag, and recycled concrete bases in Michigan decreased substantially under saturated conditions, emphasizing the role of drainage in preserving base stiffness (*36*). Overall, studies consistently show the subgrade modulus can vary by more than 200–300% seasonally, underscoring the importance of using seasonally adjusted values in PMED (*37-40*).

2.5.3.3. Field versus Laboratory Characterization

Discrepancies between FWD backcalculated and laboratory triaxial subgrade modulus are widely reported. Lab tests, such as AASHTO T307, often yield lower subgrade modulus values because in situ stress states, moisture content, anisotropy, or sample preloading history cannot be fully replicated (*41-43*). Field studies indicate that base and subgrade modulus values can be generally 1.8 times higher (depending on material type) in FWD testing than in laboratory tests under the same conditions (*44, 45*). Nazarian and Yuan noted that coarse aggregates can lose nearly 85% of their stiffness with moisture infiltration, explaining why FWD-measured subgrade modulus values are often higher in drier field conditions than in lab-prepared samples (*45*). Baladi et al., analyzing Michigan base and subbase layers, also found consistent differences

between field and lab subgrade modulus values, with laboratory results often 20–40% lower than FWD-based values (*46*). These findings confirm that direct adoption of laboratory resilient modulus without adjustment can misrepresent actual pavement performance.

2.5.4 Characterization of Existing Pavement Layers Across Different States

Several SHAs have undertaken studies to adapt PMED to local traffic, climate, and material conditions, with a particular focus on characterizing existing pavement layers for rehabilitation design. These efforts typically rely on a combination of FWD testing, laboratory measurements, PMS data, and hierarchical input levels to capture the structural condition of in-service HMA, PCC, and unbound materials. A review of these initiatives highlights recurring challenges, including reconciling laboratory and field modulus values and converting PMS distress data into formats compatible with PMED. At the same time, the literature documents practical strategies that agencies have applied to improve the reliability of data input. Examining these experiences provides context for MDOT's current efforts and illustrates how lessons from other SHAs can support more effective calibration and implementation of PMED.

2.5.4.1. Arizona

Arizona DOT conducted a comprehensive study to evaluate PMED for both new construction and rehabilitation designs, assembling a database of 152 pavement sections. Of these, 57 sections represented rehabilitation projects, including 42 HMA over HMA and 15 HMA over JPCP, either intact or fractured. Additional rehabilitation strategies included HMA over rubblized concrete and unbonded PCC over concrete pavements (*47*).

Characterization of existing asphalt layers was primarily conducted using Level 3 inputs, in which mixture volumetric properties, such as air voids, effective binder content, and unit weight, were assigned default values. Asphalt binder modulus data were available at Levels 1 and 2 for selected mixtures, but Level 3 defaults were used for indirect tensile strength and creep compliance due to limited testing. Existing PCC layers were also predominantly represented with Level 3 defaults. Typical elastic modulus and modulus of rupture values were adopted from standard practice, while CTE values were assigned based on the aggregate type commonly used in Arizona pavements. Rubblized concrete was modeled as a bound granular material with resilient modulus values ranging from 50,000 to 75,000 psi. Unbonded PCC overlays were modeled assuming a thin asphalt separator layer, as used in the national calibration effort (*47*). Unbound base and subgrade layers were characterized using FWD testing conducted at nearly all sections. In situ subgrade elastic moduli were backcalculated from deflection data and adjusted to laboratory-equivalent resilient modulus at optimum moisture content using soil-specific correction factors: 0.55 for fine-grained soils and 0.67 for coarse-grained soils. Gradation and Atterberg limits for unbound materials were based on DARWin-ME default values, with average resilient modulus values summarized by soil classification, including approximately 34,000 psi for A-1 materials and 14,400–15,000 psi for fine-grained soils (*47*).

In summary, Arizona's rehabilitation sections were characterized by Level 3 defaults for bound layers and FWD-adjusted values for unbound layers and subgrades. The inclusion of 42 HMA over HMA and 15 HMA over JPCP sections in the calibration database provided a broad representation of rehabilitation strategies. However, the heavy reliance on Level 3 defaults for existing HMA and PCC layers underscored the need for additional project-specific testing to strengthen rehabilitation design predictions in PMED (*47*).

2.5.4.2. Colorado

Colorado DOT assembled a large dataset of 126 projects (new and rehabilitated) and conducted detailed field investigations of 56 rehabilitation projects, including new HMA over HMA and HMA over JPCP. The characterization of existing layers relied on a multi-tiered program that combined construction quality control/quality assurance (QA/QC) records, FWD testing, coring, and laboratory measurements (*48*). Field testing included FWD deflection testing at 25-ft intervals on HMA and composite pavements, and at slab centers, transverse joints, and slab corners for JPCP. These data were backcalculated using Evercalc© to estimate in situ HMA, base, and subgrade moduli, as well as k-values for concrete pavements. Coring was performed to recover HMA samples for volumetric testing (air voids, binder content) and to obtain unbound material and soil samples for moisture and classification testing (*48*). Laboratory testing complemented field efforts by measuring the strength and classification properties of extracted materials. However, many missing data were supplemented with Colorado DOT QA/QC databases (e.g., gradation, binder type, CTE). For subgrade soils, PMED requires a subgrade modulus value at an optimum moisture content. Since FWD testing provides the subgrade modulus (E_{SG}) at in-situ moisture conditions, Equation (2-12) was used to adjust the FWD-derived modulus to its equivalent laboratory resilient modulus at optimum moisture content. (*48*):

$$M_{r,eq} = E_{SG} \times C \times {M_r}/{M_{r(opt)}} \quad (2\text{-}12)$$

where:
$M_{r,eq}$ = equivalent "lab" resilient modulus at optimum moisture.
E_{SG} = backcalculated subgrade elastic modulus.
C = correction factors accounting for layer type and location (Table 2-17).
M_r = resilient modulus at in situ moisture.
$M_{r(opt)}$ = resilient modulus at optimum moisture.

Table 2-17 C values for in-situ subgrade modulus to optimum moisture (*48*)

Layer Type / Location	C Value
Aggregate base/subbase – between stabilized & HMA layer	1.43
Aggregate base/subbase – below PCC layer	1.32
Aggregate base/subbase – below HMA layer	0.62
Subgrade/embankment – below stabilized subgrade/embankment	0.75
Subgrade/embankment – below HMA or PCC layer	0.52
Subgrade/embankment – below unbound aggregate base	0.35

This framework ensured that inputs for HMA, PCC, and unbound layers met PMED requirements. Importantly, Colorado DOT's calibration effort showed that using

unadjusted national defaults introduced bias in distress and IRI predictions, necessitating local calibration of performance models to improve prediction accuracy (*48*).

2.5.4.3. Georgia

The Georgia DOT study assembled a comprehensive database of both LTPP and non-LTPP sites to evaluate PMED inputs for new and rehabilitated pavements. For rehabilitation, the focus was mainly on HMA over HMA and JPCP, with 32 rehabilitated asphalt and semi-rigid sections documented in the calibration database (*49*). Characterization of existing asphalt layers was based on combining field condition surveys with layer thickness data obtained from construction records, coring, and, in some cases, GPR. Initial air voids of HMA overlays were back-casted from PMS and project data, while volumetric properties and performance grades were obtained from Georgia DOT mix designs. For unbound bases and subgrades, both laboratory resilient modulus testing and FWD backcalculation were used. Where direct measurements were not available, average values by soil type were applied to non-LTPP sites. A comparison of laboratory and backcalculated values showed high variability, leading Georgia DOT to determine project-specific C-factors that adjusted field-derived elastic modulus values to laboratory-equivalent resilient modulus values. For example, average C-values for aggregate bases below HMA layers were about 0.37, compared to the national PMED default of 0.62 (*49*). PCC layers were characterized by using laboratory-derived compressive strength and modulus data when available; otherwise, backcasting procedures and national defaults were applied. Reported 28-day modulus values typically ranged between 3,000,000 and 5,000,000 psi, with flexural strengths of 600–800 psi. Thermal expansion coefficients were taken from prior Georgia DOT-sponsored work and ranged from 4 to 6 microstrain/°F (*49*).

Overall, Georgia DOT's approach to characterizing existing layers emphasized integrating multiple data sources, including laboratory testing, FWD backcalculation, PMS records, and construction archives, to develop Levels 1 and 2 rehabilitation inputs. The results illustrated the high variability between field and laboratory modulus values and demonstrated the need for local default values and correction factors calibrated to Georgia's soils and materials (*49*).

2.5.4.4. Kansas

Islam et al. 2023 conducted a study to implement PMED for the design of HMA over HMA (25 sections) and HMA over JPCP (18 sections) (*22*). Data was collected at the time of HMA overlay construction, when possible. In situ material properties were assumed based on a review of the Kansas DOT construction management system (CMS) database. The study used 7% as constructed air voids for all HMA mixes, an effective binder content (by volume) was obtained by the difference of voids in mineral aggregate (VMA), and the target air voids, unit weight of 128 to150 pcf, and a Poisson's ratio of 0.35 was assumed for all HMA mix types. For level 1 rehabilitation input, FWD backcalculated layer moduli were used. The study used pre-overlay FWD data from 16 HMA over HMA sections. Kansas DOT does not conduct pre-overlay FWD testing for HMA over JPCP. Evercalc© was used to backcalculate the layer moduli for each drop at

a 9,000 lb load level. Any calculated values with a root mean square error greater than 5% were removed from the analysis. FWD testing data were unavailable for 9 projects; therefore, level 2 inputs for these sections were used for the analysis. Distress data was collected using a Laser Crack Measurement System (LCMS) and manual condition surveys. For pre-overly condition data, all load-related cracking was considered top-down. For PCC mix inputs, the data for 7-, 14-, 28-, and 90-day elastic modulus and MOR were not available for Level 1 inputs; instead, Levels 2 and 3 mix properties were characterized using default PMED equations. Specifically, default PMED regression equations were applied to estimate compressive strength at different ages and long-term strength. For Level 3 inputs, the 28-day modulus of rupture and elastic modulus were also determined using default PMED relationships (*22*).

2.5.4.5. Louisiana

The Louisiana Department of Transportation and Development (DOTD) has conducted multiple studies to support the implementation and local calibration of PMED. The initial investigation examined 33 rehabilitation projects consisting of HMA over HMA. In comparison, the subsequent statewide study expanded the database to encompass more than 160 projects, capturing regional variability in climate, traffic, and materials (*50, 51*). Both efforts emphasized the importance of establishing representative material properties for existing pavement layers. However, they relied mainly on defaults and PMS data because Level 1 laboratory or field testing was limited in availability. HMA layers were generally entered with Level 3 inputs. Effective binder contents of about 9.2–9.5 percent, in-place air voids near 7 percent, and unit weights of approximately 144 pcf were used as default volumetric properties (*50*). Rehabilitation inputs were taken from PMS rutting and condition ratings, and where ratings were missing, sections were conservatively assumed to be in poor condition with a rut depth of 0.25 in (*51*). PCC layers lacked project-specific testing and were therefore represented by statewide defaults.

An elastic modulus of 4.2 million psi and a 28-day modulus of rupture of 600 psi were adopted in both studies, consistent with Louisiana DOTD design practice. Rubblized concrete was modeled with a resilient modulus of about 200,000 psi, supported by field testing along I-10 and national calibration values (*50, 51*). Stabilized and unbound bases were characterized according to material type and condition. Cement- and lime-treated bases were assigned resilient modulus values between 80,000 and 100,000 psi. Still, older soil-cement layers showing deterioration were reduced to approximately 25,000 psi and entered as crushed stone due to software limitations. For granular bases, resilient modulus values of 30,500 psi were applied to Kentucky limestone, 23,500 psi to Mexican limestone, and 27,000 psi to recycled concrete or generic crushed stone. Where an aggregate layer was placed between stabilized layers, the modulus was increased to 50,000 psi to reflect confinement effects (*50, 51*). Subgrade layers were not tested at the project level in either study. Instead, the Louisiana DOTD used county-level default values derived from parish soil maps to assign resilient modulus uniformly across the calibration database. Lime-treated working platform layers, which are common in Louisiana DOTD construction, were not credited with additional stiffness and were modeled as untreated subgrade (*50, 51*).

In both the initial and expanded studies, the reliance on Level 3 defaults and PMS condition data provided consistency across many projects. Still, it also introduced limitations in capturing true material variability. Sensitivity analyses confirmed that overlay performance was most influenced by overlay thickness, subgrade modulus, and asphalt mixture properties such as binder content and air voids. The combined findings underscore the importance of accurately representing base and subgrade stiffness for reliable rutting and reflective cracking predictions (*50, 51*).

2.5.4.6. Maryland

Maryland DOT developed a PMED input database as part of its implementation efforts (*52*). Existing asphalt pavements were characterized primarily through Level 3 inputs, which relied on pavement condition ratings rather than direct material testing. For these rehabilitated sections, thermal conductivity, heat capacity, unit weight, and Poisson's ratio were assumed to be the same as values typically used for new asphalt pavement design. This simplified approach allowed Maryland DOT to populate the extensive input database necessary for PMED. Still, it also highlighted a limitation: the characterization of in-service layers was not based on project-specific testing. The study concluded that while this Level 3, assumption-driven framework provided consistency across projects, it reduced the sensitivity of performance predictions to actual field conditions, underscoring the importance of upgrading to higher input levels where feasible.

2.5.4.7. Michigan

MDOT developed an extensive rehabilitation database in support of PMED implementation. The SPR-1723 study assembled 203 rehabilitation sections, comprising 175 HMA-over-HMA sections and 28 unbonded PCC overlay sections. The objective was to represent MDOT's full range of rehabilitation practices across traffic levels, overlay thicknesses, and pavement types (*17*). All rehabilitation designs were modeled using Level 3 inputs for existing materials, reflecting MDOT's practice of relying on statewide defaults and construction records rather than project-specific testing. Aggregate bases were assigned a resilient modulus of 30,000 psi, while a modulus of 13,500 psi represented sand subbases. Subgrade resilient modulus values were selected from soil classification–based defaults established in earlier Michigan DOT studies. For HMA over HMA, the condition of the existing asphalt pavement was standardized by assuming "fair" ratings for both structural and environmental conditions across all sections. This approach provided consistent input for overlay performance predictions. For HMA over JPCP, MDOT's dataset covered a broad range of concrete pavements, including JPCP, JRCP, and CRCP. In PMED, these were modeled under the standard category of "HMA overlay of JPCP." Standardized inputs included an existing concrete layer elastic modulus of 3,000,000 psi, a slab width of 15 ft, a dowel diameter of 1.25 in, a dowel spacing of 12 in, and untied shoulders for all sections. For rubblized concrete, the fractured concrete layer was treated as an unbound aggregate base with a resilient modulus of 70,000 psi, and the overlay was designed as a new asphalt pavement. Similarly, C&S layers were modeled as new asphalt pavements by treating the processed HMA as an unbound aggregate base with a modulus of 125,000 psi.

In summary, MDOT's characterization of existing layers for rehabilitation in PMED relied on default Level 3 inputs and fixed modulus assumptions tailored to each rehabilitation strategy. This standardized framework allowed consistent modeling of 203 sections, ensuring asphalt overlays, intact PCC, rubblized concrete, and C&S layer could all be represented in a uniform manner suitable for statewide calibration (*17*).

2.5.4.8. Missouri

Missouri DOT conducted a recent study to recalibrate the pavement distress and IRI prediction models for new and rehabilitated asphalt and concrete pavements using PMED v2.5.5. (*53*). The Missouri DOT performed FWD testing for asphalt pavement sections and backcalculated in situ layer resilient modulus. FWD testing was conducted in accordance with LTPP FWD testing protocols. Four load levels (i.e., 6000, 9000, 12,000, and 16,000 lb) and four replicates were used at each load level. Evercalc© was used to backcalculate the subgrade resilient modulus. The researchers also collected loose HMA material and field cores to test HMA material inputs. The Asphalt Mixture Performance Tester (AMPT) was used to measure the dynamic modulus, which was then converted to PMED Level 1 inputs. Creep compliance and tensile strength (AASHTO T322) tests were conducted and included in a material input library. The study found that tensile strength increased and creep compliance decreased with increasing air voids. Time series data for distress and IRI performance models were obtained from the pavement management information system (PMIS) and LTTP projects. Table 2-18 summarizes the hierarchical input levels used for this study.

Table 2-18 PMED input data levels for Missouri DOT (*53*)

Input Data Elements	Hierarchical Level
Truck volume distribution and vehicle class distribution	Level 1 project-specific data
Axle load distributions	Level 1 or 2 using weigh-in-motion (WIM) data when available, or PMED defaults
Monthly adjustment factors	Level 1 when available or PMED default
All others	Level 3 PMED defaults
Temperature, wind speed, percent sunshine, precipitation, and relative humidity	MERRA data for 31asphalt pavements and NARR data for concrete pavements
HMA dynamic modulus	Level 1 for PMIS sections and Level 2 for LTPP sections
HMA air voids	Level 1 field air void data and LTPP database
HMA binder	Level 1 for PMIS sections and Level 3 for LTPP sections
HMA creep compliance & indirect tensile strength	Level 1 laboratory test data for PMIS sections; Level 2 computed data for LTPP sections
Other HMA inputs	Level 3 PMED defaults
PCC strength over time and mix design inputs	Level 1 strength data from previous laboratory test results for different specification gradations, and Levels 2 and 3 for CTE and other inputs
Unbound base and subgrade: Resilient modulus Atterberg limits, & gradation	Level 1 backcalculated data and field test data for PMIS sections, and Level 3 data for LTPP sections.
Performance (distress & IRI)	Level 1: Field measured

2.5.4.9. Oregon

The Oregon DOT study evaluated the use of PMED for both new construction and rehabilitation, with particular emphasis on characterizing existing materials (*54*). Oregon DOT compiled a database of 44 pavement sections that included HMA overlays of existing asphalt pavements and HMA overlays of JPCP. Because FWD data were not available, the characterization of existing asphalt pavements relied primarily on Level 3 rehabilitation inputs. Oregon DOT assumed a pavement rating of "fair" and a total rut depth of zero inches. to represent the pre-overlay condition. For HMA material properties, Oregon DOT selected hierarchical inputs depending on data availability. Dynamic modulus values were obtained from laboratory testing (Level 1), and asphalt binder properties were based on Levels 1 and 2. Creep compliance and indirect tensile strength were characterized through Level 3 defaults due to the absence of project-specific measurements. Other mixture properties, including unit weight, Poisson's ratio, and thermal properties, were assumed to be the same as those used for new asphalt pavement designs. Oregon DOT conducted field distress surveys to support the assumed Level 3 rehabilitation inputs. The surveys recorded rutting and thermal cracking across the study sections. Average rut depths ranged from 0.044 in. to 0.3 in., and thermal cracking was absent in the coastal and valley regions but observed in the eastern region (*54*). To summarize the distribution of thermal cracking severities, a weighted function was used, as shown in Equation (2-13):

$$TC = \frac{LowseverityTC + 3 * MediumseverityTC + 5 * HighseverityTC}{9} \quad (2\text{-}13)$$

where:
TC = thermal cracking.
Lowseverity = unsealed crack, mean width ≤ 0.25 in., or sealed crack with sealant in good condition and indeterminable width.
Mediumseverity = any crack with a mean width > 0.25 in. and ≤ 0.75 in., or any crack with a mean width < 0.75 in. and adjacent low severity random cracking.
Highseverity = any crack with a mean width > 0.75 in., or any crack with a mean width ≤ 0.75 in. and adjacent moderate to high severity random cracking.

For unbound and subgrade layers, default values from DARwinME were used. Soil classification data were supplemented with information from web soil surveys and historic modulus estimates. In summary, Oregon DOT's characterization of existing pavements for rehabilitation design relied heavily on Level 3 assumptions, supported by condition surveys and limited laboratory testing for asphalt mixtures (*54*).

2.5.4.10. Tennessee

Tennessee DOT evaluated the use of PMED for both new construction and rehabilitation designs through a statewide calibration study (Huang et al., 2017). A total of 20 rehabilitation sections were included from the PMS database, consisting of 14 asphalt overlays of existing asphalt pavements and six asphalt overlays of existing concrete pavements (*55*). For asphalt overlays of existing asphalt pavements, all existing asphalt layers were combined and modeled as a single asphalt base. PMED treats overlays thicker than 3.94 in. using the same rutting transfer functions as for new

asphalt pavements; therefore, these sections were characterized with inputs equivalent to those for new asphalt pavement designs. Volumetric properties, such as air voids, binder content, and gradation, were obtained from PMS records or design files, and dynamic modulus values were assigned using predictive equations or available laboratory data (*55*). For asphalt overlays of existing concrete pavements, the asphalt layer was characterized using the same methods as overlays on existing asphalt pavements. At the same time, the existing concrete layer was represented with Level 3 national default values for elastic modulus, modulus of rupture, and CTE. No project-specific testing of PCC was performed. Unbound bases and subgrades were characterized using PMS data, soil classification, and default resilient modulus values. Reported values for granular base layers ranged between 25,000 and 35,000 psi, while fine-grained subgrades were assigned values between 8,000 and 20,000 psi across the selected sections (*55*).

In summary, Tennessee DOT's rehabilitation design in PMED involved combining all existing asphalt layers into a single asphalt base, applying predictive or default properties to overlays, and adopting national defaults for PCC slabs. The inclusion of base and subgrade modulus values from PMS records provided some site-specificity. Still, reliance on defaults for PCC inputs highlighted the need for more detailed testing to represent better existing concrete pavements in rehabilitation design (*55*).

2.5.4.11. Utah

Utah DOT has developed a framework for characterizing existing pavement layers in PMED rehabilitation design that relies primarily on Level 3 inputs, supported by condition surveys and local adjustment factors (*56*). For HMA layers, dynamic modulus values are estimated using predictive equations based on gradation, binder properties, air voids, and effective binder content, while pavement condition surveys provide percent alligator cracking (all severities) and an overall rating, which are used to refine the dynamic modulus estimates. PCC layers are characterized depending on the rehabilitation strategy. For JPCP restoration or unbonded JPCP overlays, the elastic modulus is obtained from cores or the 28-day modulus and multiplied by 1.2 to approximate long-term values. For fractured slab techniques, modulus assignments vary by method, with typical values ranging from 150,000 to 250,000 psi for crack-and-seat and 50,000 to 75,000 psi for rubblization. For HMA over rubblized concrete, an effective PCC modulus of 60,000 psi is assumed (*56*).

Unbound bases and subgrades are generally entered using Level 3 resilient modulus values based on AASHTO soil classification. Typical ranges include 40,000 psi for coarse granular bases (A-1-a) and 8,000 to 18,000 psi for fine-grained subgrades (A-5 to A-7). UDOT practice recommends limiting unbound base modulus to no more than two to three times the assigned subgrade modulus to avoid unrealistic stiffness contrasts. Where feasible, FWD testing and backcalculation are encouraged to establish Level 2 subgrade modulus values, which can be adjusted to optimum moisture conditions to represent laboratory-equivalent properties (*56*). This characterization approach demonstrates that, while Level 3 defaults are widely used, Utah DOT

supplements them with condition surveys, empirical relationships, and modulus constraints to better reflect local material behavior in rehabilitation design.

2.5.4.12. Virginia

Virginia DOT adopted PMED for the design of new and reconstructed pavements on interstate and primary routes in 2018, but continues to rely on the AASHTO 93 Guide for rehabilitation while preparing to extend PMED to the most common overlay strategies. To investigate appropriate input levels for rehabilitation, several studies evaluated existing asphalt layers across nine sites, where a total of 33 cores were extracted and tested for dynamic modulus over a wide range of temperatures and loading frequencies (*57*-*59*).

Level 1 characterization used FWD data to backcalculate in-place moduli, providing realistic values for the full asphalt thickness. Level 2 relied on laboratory resilient modulus tests on cores, which frequently overestimated stiffness and sometimes produced unrealistic or even negative damage factors because they reflected only portions of the asphalt layer. Level 3 inputs applied pavement condition ratings, but these surface-based assessments did not adequately capture deeper structural deterioration, particularly in previously overlaid sections. Typical backcalculated FWD moduli ranged from about 1,600 to 4,100 MPa, while laboratory resilient modulus values averaged 3,200 to 6,500 MPa depending on site and mix type (*57*-*59*). A key outcome of this evaluation was the comparison between predicted and measured dynamic modulus master curves. Witczak-predicted undamaged curves and laboratory measurements were generally of the same order of magnitude, but the ratio of predicted-to-measured values ranged from 0.3 to 3.3 across sites. While some mixtures showed close agreement (ratios between 0.77 and 1.44), others diverged substantially, with predicted curves overstating stiffness. Level 1 FWD-based inputs provided dynamic modulus ($|E^*|$) master curves for damaged asphalt concrete that are most closely aligned with laboratory measurements, demonstrating their suitability for representing field-damaged asphalt concrete. This relationship is illustrated in Figure 2-5, which compares measured and predicted $|E^*|$ master curves for representative Virginia DOT mixes (*58*). In addition to modulus characterization, layer thicknesses were evaluated using GPR surveys with coring verification. GPR provided reliable estimates of asphalt and base thicknesses, though it was unable to consistently identify the bottom of very thick base layers (>20 in.). Table 2-19 summarizes the comparison between GPR and coring results for selected sites.

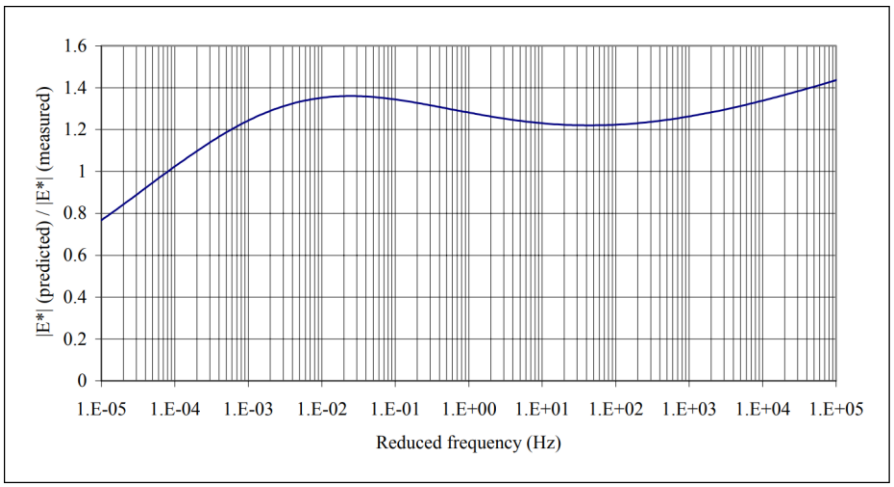


Figure 2-5 Ratio of measured to predicted asphalt concrete |*E**| in one core (*58*)

Table 2-19 HMA and base thicknesses comparison from GPR and coring (*59*)

Site	Coring average asphalt layer thickness (inch)	GPR average asphalt layer thickness (inch)	Core average base thickness (inch)	GPR average base thickness (inch)
1	12.0	11.3	8.0	7.0
2	7.5	7.0	4.0 to 8.0	8.0
3	11.6	10.8	4.0 to 8.0	7.1

For bases and subgrades, modulus values were drawn from the materials database and soil surveys, with typical ranges of 25,000 to 35,000 psi for aggregate bases and 8,000 to 20,000 psi for subgrades. When available, deflection basin data were adjusted to laboratory-equivalent values following PMED guidelines (*59*). The studies concluded that Level 1 FWD-based inputs are the most reliable method for characterizing existing asphalt layers in Virginia. Laboratory Level 2 inputs were unsuitable due to poor agreement with damaged master curves, and Level 3 survey-based values provided only broad approximations. This study reinforced the importance of capturing the degraded stiffness profile of the full asphalt thickness through field-based testing (*57-59*).

2.5.4.13. Summary

Table 2-20 summarizes the rehabilitation levels used by other SHAs to characterize damage in existing pavement layers.

Table 2-20 Rehabilitation input levels used by other SHAs for damage characterization

State	Level 1	Level 2	Level 3	Notes
Arizona (*47*)	No	No	Yes	Relied on Level 3 defaults for bound layers; FWD only for subgrades.
Colorado (*48*)	No	Yes	Yes	Utilized FWD, lab testing, and PMS, with reliance on Level 2 and 3 for overlays.
Georgia (*49*)	Yes	Yes	Yes	Used FWD and lab testing where available; defaults otherwise.
Kansas (*22*)	Yes	Yes	No	Pre-overlay FWD for AC over AC; defaults for AC over PCC; mainly Levels 1–2.
Louisiana (*50*)	No	No	Yes	Relied on Level 3 defaults for HMA and PCC; county-level soils.
Maryland (*52*)	No	No	Yes	Used Level 3 condition ratings; assumed new-pavement defaults.
Michigan (*17*)	No	No	Yes	Used Level 3 condition ratings.
Missouri (*53*)	No	No	Yes	Reported reliance on Level 3 default PMS ratings.
Oregon (*54*)	No	No	Yes	No FWD; all overlays characterized with Level 3 assumptions.
Tennessee (*55*)	No	Yes	Yes	PMS + predictive models for AC overlays; defaults for PCC.
Utah (*56*)	No	No	Yes	Default modulus and survey ratings; Level 3 for overlays.
Virginia (*57-59*)	Yes	Yes	Yes	Compared all levels, but recommended Level 1 as most reliable.

2.6 LOCAL CALIBRATION EFFORTS AND CHALLENGES

To date, very few SHAs are working towards or have implemented PMED for conducting asphalt and concrete pavement rehabilitation designs. Rehabilitation design poses almost similar challenges as new designs, and includes:

- Project selection: Identify the available sections with performance data.
- Existing layer characterization: Many agencies lack comprehensive FWD, GPR, or coring data for in-service pavements, leading to reliance on Level 3 defaults. Even when some testing is available, linking results to PMED inputs, such as damaged modulus master curves or resilient modulus correlations, can be problematic. Laboratory testing of extracted cores often fails to capture the degraded condition of full-depth layers, producing unrealistic inputs.
- PMED inputs: The level of detail needed for rehabilitation design often exceeds what agencies routinely collect. Challenges include reconciling laboratory and field resilient modulus values, establishing correction factors for unbound materials, assigning default moduli for processed layers such as rubblized concrete or C&S layer, and avoiding unrealistic stiffness contrasts between base and subgrade layers.
- Performance data: PMS distress measurements are rarely in formats that align with PMED requirements. Agencies frequently struggle to convert rutting, cracking, and IRI data into PMED-compatible definitions. This often requires assumptions, adjustment factors, or the creation of weighted indices to summarize the severity of distress.

- Local calibration techniques: Globally calibrated PMED models often produce systematic bias when applied to local conditions, such as overpredicting rutting or underpredicting cracking. Reducing bias and standard error requires careful statistical adjustments, but calibration datasets are sometimes too limited to capture the full variability in materials, traffic, and climates.
- Lack of consensus on how to represent processed or fractured layers, leading to reliance on defaults.
- Resource and cost constraints that limit the collection of high-level (Level 1) data, leading to widespread reliance on Level 3 assumptions.
- Challenges arise in incorporating seasonal or climatic variations in subgrade modulus, and there is uncertainty about whether to apply representative annual values or climate–station–based adjustments.

As noted above, PMED performance models are nationally calibrated using data from the LTPP program. Local calibration is crucial for accounting for SHA-specific materials and practices, thereby ensuring the accuracy of distress predictions. The general steps of local calibration include selecting inputs, developing a sampling strategy, conducting field investigations, validating global model coefficients, reducing bias, and quantifying the standard error of the estimate. Local includes the following steps:

- Step 1: Select input levels.
- Step 2: Develop an experimental plan and sampling strategy.
- Step 3: Assess the adequate sample size for each distress.
- Step 4: Select of pavement sections.
- Step 5: Obtain PMED inputs and measured distress data.
- Step 6: Conduct field and forensic investigation.
- Step 7: Validate global model coefficients for local conditions.
- Step 8: Eliminate the local bias for PMED performance prediction models.
- Step 9: Estimate the standard error of the estimate.
- Step 10: Eliminate the standard error of the estimate.
- Step 11: Assess the calibration process.

The PMED was updated over time as many national and SHA-level studies were completed to implement the new ME design approach. These studies focused on sensitivity analysis to determine the impact of inputs on distress prediction; the development of a database for SHAs; the calibration and validation of PMED performance prediction models; and the implementation of calibrated models for the design of new and rehabilitated pavements. As part of the initial implementation, most SHAs focused on new or reconstructed pavement designs; however, few SHAs worked on selective overlay designs using available (limited) input data.

The challenges discussed above have motivated agencies to pursue targeted calibration efforts for rehabilitation treatments. The following sections summarize these efforts.

2.6.1 Local Calibration Efforts for HMA Overlays

This subsection reviews local calibration studies that have focused on HMA overlays of existing asphalt pavements, highlighting how agencies have adapted PMED inputs and models to improve prediction accuracy for asphalt rehabilitation treatments.

2.6.1.1. Arizona

Arizona DOT conducted local calibration of PMED (V1.0) using a dataset of 180 pavement sections, including both new and rehabilitated pavements, with HMA overlays comprising a significant portion of the rehabilitation group. The calibration effort focused on the key performance models for rutting, fatigue cracking, thermal cracking, and reflection cracking, as well as IRI. Nationally calibrated models consistently overpredicted rutting and underpredicted transverse and thermal cracking in Arizona conditions. To address these issues, calibration coefficients were adjusted to reduce bias and standard error of the estimate. The recalibrated rutting model substantially improved prediction accuracy, aligning simulated permanent deformation more closely with measured field data. Similarly, adjustments to the fatigue cracking models provided a better representation of alligator and longitudinal cracking progression in overlays. However, the transverse cracking model remained problematic, with continued underprediction even after calibration. IRI predictions improved after recalibration, but site-to-site variability indicated the need for further refinement (*47*).

Overall, the Arizona DOT calibration showed that unadjusted national models were inadequate for asphalt overlays. Local recalibration of rutting, fatigue, and IRI models reduced error and improved bias, while thermal and reflection cracking remained the most difficult to predict accurately. These findings underscore the importance of continued calibration efforts to align PMED predictions with regional trends in rehabilitation performance (*47*).

2.6.1.2. Colorado

The Colorado DOT undertook a local calibration study using MEPDG version 1.0 to support implementation of ME design for both new and rehabilitated pavements. A total of 127 pavement sections, drawn from Colorado DOT's PMS and the LTPP database, were analyzed, including a substantial number of HMA overlays over existing asphalt and concrete pavements (*48*). Calibration targeted the distress models most critical to HMA overlays: alligator (bottom-up) cracking, fatigue damage, reflection cracking, rutting, and IRI. For fatigue and alligator cracking, locally calibrated models replaced the global coefficients with Colorado-specific values. Statistical evaluation demonstrated a good fit, with R^2 values of about 63% and an SEE near 9.4% of the lane area for fatigue damage, indicating improved prediction accuracy. The reflection cracking model, developed from both new HMA and HMA overlays of existing HMA projects, showed similarly strong performance, with R^2 values above 54% and SEE near 8.6% of the lane area, without introducing significant bias. The study concluded that national coefficients systematically underpredicted reflection cracking and overpredicted fatigue damage in Colorado overlays, but recalibration substantially improved accuracy. The locally

derived models provided unbiased predictions across the state's diverse climate zones, giving Colorado DOT confidence in applying PMED for overlay design (*48*).

2.6.1.3. Georgia

The Georgia DOT conducted a local calibration study to support the implementation of PMED for asphalt and rehabilitated pavements (*49*). A total of 20 HMA overlay sections were included, along with other asphalt projects. Calibration efforts focused on the key distress models for overlays, namely rutting, fatigue cracking, reflection cracking, and IRI. For rutting, bias reduction was achieved by using backcalculated FWD moduli rather than laboratory-derived resilient modulus values, thereby improving alignment between predicted and measured field performance. Reflection cracking was considered jointly with fatigue cracking, as PMED simulates total cracking in overlays rather than isolating reflection as a separate distress. The study also evaluated IRI predictions, which showed acceptable accuracy after bias adjustments but required continued refinement to capture the influence of varying traffic and climate zones. The study concluded that while global calibration coefficients provided a starting point, they introduced systematic bias in predicting rutting and cracking for overlays under Georgia conditions. Local recalibration using the 20 overlay sections improved prediction accuracy but highlighted the need for expanded datasets to better represent the diversity of Georgia's materials and environmental conditions (*49*).

2.6.1.4. Kansas

The Kansas DOT conducted a research study to implement the PMED design of rehabilitated pavements for state-managed roads in Kansas (*22*). Local calibration for HMA overlays of existing asphalt pavements (25 sections) and HMA overlays of existing JPCP (18 sections) was conducted using PMED v2.5 and verified using PMED v2.6.2.2. SEE and bias were used as criteria for model verification. Since the input hierarchical level directly affects performance prediction, Kansas DOT conducted a comprehensive study to select the optimal input level for traffic, climate, material properties, and existing pavement conditions. As-constructed material properties of the new layer were collected at the time of overlay construction from the Kansas DOT CMS database and by reviewing the QC/QA spreadsheets. Permanent deformation, transverse (thermal + reflection) cracking, load-related cracking (bottom-up + top-down), and IRI models for HMA overlays of existing asphalt pavements were calibrated in this study. The PMED did not predict thermal cracking under Kansas DOT conditions, so only reflection-cracking model coefficients were calibrated, and all load-related cracking was modeled as top-down cracking. An automated calibration technique employing three resampling methods (traditional split sampling, jackknife, and bootstrap) was used to calibrate the PMED performance prediction models in Python. The automated technique limitations include: (a) it cannot be implemented for parameters that need multiple runs of PMED software (i.e., β2r and β3r coefficients of permanent deformation model), and (b) identification of bounds of model coefficients. Local calibration improved the accuracy of rutting, load-related cracking, and IRI models for HMA overlays of existing asphalt pavement sections. However, local calibration of the transverse cracking model resulted in higher SEE because the HMA thermal cracking model was calibrated using global values, as the Kansas DOT does not distinguish between reflection and thermal

cracking. The top-down cracking model showed high accuracy, with lower bias and SEE than the globally calibrated values. However, SEE was high due to variability in data collection. Distress data on all sections overlaid before 2013 were collected manually, which contributed to high data variability.

Additionally, the Kansas DOT considers all load-related cracking to be top-down, a factor that also contributed to the high SEE. The research team also compared calibration results from PMED v2.5 and v2.6.2.2, which showed slightly higher distress predictions for HMA total fatigue cracking, especially for HMA bottom-up fatigue cracking; the remaining predicted distress values remained unchanged. The study emphasized the importance of collecting full-depth pavement cores to differentiate cracking types, conducting creep compliance and indirect tensile strength tests to assess low-temperature behavior, and incorporating layer-specific rutting contributions to improve calibration accuracy (*22*).

2.6.1.5. Louisiana

In Louisiana, the most recent calibration study focused specifically on asphalt overlays of existing asphalt pavements and evaluated 33 rehabilitation overlays distributed throughout the state using PMED v2.6. (*50*). The PMED v2.6 was used, with rehabilitation overlays manually calibrated and preservation overlays calibrated using a calibrator assistance tool. For rehabilitation overlays, fatigue cracking was consistently underpredicted, while the national models overpredicted rutting. Local calibration significantly reduced this bias, improving the match between measured and predicted performance. The findings demonstrated that local calibration is essential for Louisiana conditions, particularly because performance was strongly influenced by base type, pre-overlay condition, and total HMA thickness. These efforts recommended a set of locally calibrated coefficients for overlay designs that Louisiana DOTD uses for new flexible pavements (*50*).

2.6.1.6. Maryland

Maryland DOT has not conducted local calibration of PMED models for HMA overlays. Instead, the agency relied on Level 3 inputs derived from pavement ratings and assumed material properties rather than project-specific testing. The report emphasized that the lack of a sufficient database of rehabilitated sections (ten sections) limited calibration efforts, and, as a result, nationally calibrated models continued to be used to predict rutting, fatigue cracking, and IRI. The study concluded that developing a Maryland-specific database of overlay performance would be a prerequisite for any future calibration work (*52*).

2.6.1.7. Michigan

Calibration for rehabilitated pavements was carried out under the SPR-1723 study, which focused extensively on HMA overlays (*17*). A total of 175 rehabilitation pavement sections were analyzed, including HMA over existing HMA, HMA over rubblized concrete, HMA over intact PCC, and crush-and-shape treatments. Calibration targeted the performance models for rutting, top-down fatigue cracking, thermal cracking, and IRI. PMED inputs were obtained from MDOT’s PMS, supplemented by construction

records and previous studies. Model calibration was performed outside the PMED software environment using statistical approaches, including no-sampling and resampling techniques, while validation relied on split-sample strategies. The study revealed that national models consistently overestimated rutting and underestimated fatigue performance for asphalt overlays. Local calibration reduced model bias and improved the standard errors of estimate for rutting, fatigue, and IRI predictions, although thermal cracking remained variable due to limitations in the distress data (*17*).

2.6.1.8. Missouri

Missouri DOT conducted local calibration of PMED using v2.5.5, including asphalt pavements with both new AC and rehabilitated overlays of existing asphalt pavements (*53*). The calibration effort for asphalt overlays focused on the key performance models for alligator cracking, reflection cracking, thermal cracking, rutting, and IRI. Level 1 laboratory and field data were incorporated where available, and agency records were used to supplement older sections. The analysis revealed that the nationally calibrated models systematically misrepresented Missouri conditions, particularly by overpredicting rutting and underpredicting cracking progression in HMA overlays. Local recalibration of rutting, fatigue, and IRI models reduced SEE and improved bias, aligning predictions more closely with measured field performance. However, the reflection and thermal cracking models continued to exhibit variability, reflecting limitations in the coverage of distress data. Overall, the Missouri study demonstrated that recalibration of PMED v2.5.5 was necessary for overlays, and the adjustments significantly improved prediction accuracy for asphalt rehabilitation designs under local conditions (*53*).

2.6.1.9. Oregon

Calibration for HMA overlays was conducted using DARwin ME v1.1. A total of 44 pavement sections were included, covering a range of traffic levels, climatic regions, and performance conditions (*54*). The study evaluated distress models for rutting, alligator cracking, longitudinal cracking, and thermal cracking. The nationally calibrated models did not adequately represent field conditions, as rutting was overestimated, alligator and thermal cracking were underestimated, and longitudinal cracking exhibited high variability (*54*). Local calibration factors were developed, substantially improving the accuracy of rutting and alligator cracking predictions, although longitudinal and transverse cracking remained more variable than desired. Calibration relied on PMS data, field surveys, and dynamic modulus values from previous Oregon DOT studies, with verification and sensitivity analyses confirming the effectiveness of the adjusted models. The study recommended adopting calibrated rutting and alligator cracking models for use in rehabilitation overlay design, while noting that additional sections and data would be required to improve the reliability of cracking predictions (*54*).

2.6.1.10. Tennessee

Tennessee DOT conducted a local calibration study using PMED, focusing on HMA overlays of existing asphalt and concrete pavements (*55*). A total of 76 sections were analyzed, including HMA overlay of existing asphalt and HMA over existing concrete pavements, with data obtained from the PMS and supplemental construction records. Calibration targeted the distress models most relevant to overlays, namely rutting,

fatigue cracking, and IRI, while transverse cracking was excluded due to limited field data. The study design incorporates overlays thicker than 3.94 in., such as new asphalt pavements, and primarily uses Level 2 inputs for materials characterization. The findings indicated that the nationally calibrated models did not adequately reflect Tennessee field conditions. Rutting was generally overpredicted, while fatigue cracking was underpredicted, resulting in a systematic bias in performance predictions. Local calibration significantly reduced this bias and improved the standard error of estimates for rutting, fatigue, and IRI models. Although transverse cracking was not calibrated, its impact on IRI was considered minor for Tennessee conditions. The study demonstrated that locally calibrated models provided more reliable predictions for HMA overlays, highlighting the importance of expanding distress data to refine cracking models (*55*).

2.6.1.11. Virginia

Virginia DOT conducted local calibration of PMED v2.5.5 and v2.6 using a database of 61 pavement sections, including both new and rehabilitated pavements, with HMA overlays of existing asphalt pavements comprising most of the rehabilitation group (*59*). Calibration focused on the key distress models for asphalt overlays, namely rutting, fatigue cracking, and IRI, while transverse cracking was not calibrated because of limited field data. Inputs were drawn from PMS records, supported by GPR and coring, to establish existing layer thicknesses. The study found that the nationally calibrated models tended to overpredict rutting and underpredict fatigue cracking in Virginia overlays. Local calibration improved prediction accuracy by reducing bias and the standard error of estimates for rutting, fatigue, and IRI models. However, cracking models remained problematic due to variability in field data and the absence of reliable reflection-cracking inputs. The study concluded that additional overlay sections would be needed to strengthen calibration, particularly for cracking-related performance predictions (*59*).

2.6.1.12. HMA Distress Prediction

Table 2-21 summarizes the transfer functions for asphalt pavement performance prediction models and the SHA local calibration coefficients.

Table 2-21 SHA calibration efforts for HMA overlays of existing asphalt pavements

State	Number of Sections (Rehabilitation)	PMED Models Calibrated	Version	Year
Arizona	42	Rut, BU, TD, REF, IRI	v1.0	2014
Colorado	49	Rut, BU, REF, IRI, TC	v1.0	2013
Georgia	20	Rut, BU, TC, IRI	v1.0	2015
Kansas	43	Rut, BU, TD, REF, IRI, TC	v2.6.2.2	2016
Louisiana	33	Rut, BU, TD, TC, IRI	v2.6	2021
Maryland	10	Rut, BU, TD, IRI	v1.0	2011
Michigan	175	Rut, TD, TC, IRI	v2.6	2019
Missouri	11	Rut, BU, REF, TC, IRI	v2.5.5	2009
Oregon	44	Rut, BU, TD, TC	v1.1	2013
Tennessee	76	Rut, BU, TD, IRI	v2.2	2017
Virginia	59	Rut, BU, IRI	v2.2.6	2022

Note: BU = Bottom-up cracking; TD = Top-down cracking; TC = Thermal cracking; RUT = Total rutting; REF = Reflective cracking; IRI = International roughness index

2.6.1.12.1. Fatigue Bottom-up Cracking

Bottom-up cracking is a load-related distress resulting from repeated axle loads. It originates at the bottom of the HMA layer and progresses upward to the surface. The total cumulative damage can be estimated by summing the cumulative damage computed using Miner's law (*60*), as shown in Equation 2-14.

$$DI = \sum(\Delta DI)_{j,m,l,p,T} = \sum\left(\frac{n}{N_{f-HMA}}\right)_{j,m,l,p,T} \quad (2\text{-}14)$$

where,
n = number of actual axle load applications within a specific time.
j = axle load interval.
m = axle type (single, tandem, tridem, quad).
l = truck type classification.
p = month.
T = median temperature for five temperature quintiles (°F).
$N_{f\text{-}HMA}$ = allowable number of axle load applications computed using Equation 2-15.

$$N_{f-HMA} = C \times k_1 \times C_H \times \beta_{f1}(\varepsilon_t)^{-k_2\beta_{f2}}(E_{HMA})^{-k_3\beta_{f3}} \quad (2\text{-}15)$$

where,
ε_t = tensile strain at critical AC locations.
E_{HMA} = HMA dynamic modulus (psi).
k1, k2, k3 = laboratory regression coefficients.
β_{f1}, β_{f2}, β_{f3} = local or field calibration constants.
C = adjustment factor (laboratory to the field) as shown in Equations 2-16 and 2-17.
C_H = thickness correction factor for bottom-up cracking as shown in Equation 2-18.

$$C = 10^M \quad (2\text{-}16)$$

$$M = 4.84\left(\frac{v_{be}}{V_a + V_{be}} - 0.69\right) \quad (2\text{-}17)$$

where,
V_{be} = effective binder content by volume (%).
V_a = in situ air voids in the HMA mixture (%).

$$C_H = \frac{1}{0.000398 + \frac{0.003602}{1 + e^{(11.02 - 3.49H_{HMA})}}} \quad (2\text{-}18)$$

where,
H_{HMA} = HMA layer thickness (inch).

The bottom-up fatigue cracking is estimated using Equation 2-19.

$$FC_{\text{Bottom}} = \left(\frac{1}{60}\right)\left(\frac{C_4}{1 + e^{C_1C_1^* + C_2C_2^*\log(DI_{\text{Bottom}} \cdot 100)}}\right) \quad (2\text{-}19)$$

where,
FC_{Bottom} = bottom-up fatigue cracking (percent area).
DI_{Bottom} = cumulative damage at the bottom of the HMA layer.
C_1, C_2, C_4 = transfer function coefficients where C_2 is a function of thickness for HMA thickness between 5 and 12 in.
C_1^*, C_2^* can be determined using Equation 2-20 and Equation 2-21.

$$C_1^* = -2C_2^* \quad (2\text{-}20)$$

$$C_2^* = -2.40874 - 39.748(1 + H_{HMA})^{-2.856} \quad (2\text{-}21)$$

where,
H_{HMA} = HMA layer thickness (inch).

Table 2-22 summarizes the local calibration coefficients among several SHAs.

Table 2-22 SHA local calibration coefficients for the bottom-up cracking model

SHA	C_1	C_2	C_4
Arizona	1	4.5	6000
Colorado	0.07	2.35	6000
Georgia	2.2	2.2	6000
Louisiana	0.892	0.892	6000
Michigan	1.31	hac<5: 2.1585 5<hac<12: 0.867+0.1*hac Hac>12: 3.9666	6000
Missouri	-0.31	hac<5: 1.367 5<hac<12: 0.867+0.1*hac Hac>12: 2.067	6000
Oregon	0.56	0.225	6000
Tennessee	1.023	0.045	6000
Virginia	0.319	0.319	-

2.6.1.12.2. Top-down Cracking

Top-down or longitudinal cracking is a load-related distress where the crack initiates at the pavement surface and propagates downwards due to repeated axle loads. It appears as cracks parallel to the wheel path.

Old model: The damage calculation for top-down cracking is the same as bottom-up cracking for the old model, except for the thickness correction factor and the transfer function, as shown in Equations 2-22 and 2-23.

$$C_H = \frac{1}{0.01 + \frac{12.00}{1 + e^{(15.676 - 2.8186 H_{\text{HMA}})}}} \quad (2\text{-}22)$$

$$FC_{\text{Top}} = 10.56\left(\frac{C_3}{1 + e^{C_1 - C_2 Log(DI_{\text{Top}})}}\right) \quad (2\text{-}23)$$

where,
FC_{Top} = top-down fatigue cracking (in ft/mile)
DI_{Top} = cumulative damage at the top of the AC layer
C_1, C_2, C_3 = Transfer function coefficients
H_{HMA} = HMA layer thickness (inch).

New model: The top-down cracking model is based on fracture mechanics concepts (*61*). It is expressed in percentage area rather than length (ft/mi). The top-down cracking model encompasses crack initiation and propagation, as outlined in Paris' law (*62*). A crack length of 0.3 inches defines crack initiation. Equation 2-24 shows the time

to crack initiation formulated using regression over longitudinal and alligator cracking data from LTPP.

$$t_0 = \frac{\mathrm{K}_{L1}}{1 + e^{\mathrm{K}_{L2}\times 100\times(\mathrm{a}_0/2\mathrm{A}_0)+\mathrm{K}_{L3}\times\mathrm{H}_T+\mathrm{K}_{L4}\times\mathrm{L}_T+K_{L5}\times\log_{10}\ \mathrm{AADTT}}} \quad (2\text{-}24)$$

where,
t_0 = time to crack initiation (days).
H_T = annual number of days above 90˚F.
L_T = annual number of days below 32˚F.
AADTT = annual average daily truck traffic (initial year)
K_{L1}, K_{L2}, K_{L3}, K_{L4}, K_{L5} = calibration coefficients for time to crack initiation.
$a_0/2A_0$ = energy parameter (Equation 2-25).

$$\frac{a_0}{2A_0} = 0.1796 + 1.5\mathrm{x}10^{-5}E_1 - 0.69m - 7.1691.5\mathrm{x}10^{-4}H_a \quad (2\text{-}25)$$

where,
E_1 and m = relaxation modulus parameters,
H_a = HMA thickness (inch).

Top-down cracking is expressed as a percentage area using Equation 2-26.

$$L(t) = L_{MAX}e^{-\left(\frac{C_1\rho}{t-C_3t_0}\right)^{C_2\beta}} \quad (2\text{-}26)$$

where,
$L(t)$ = top-down cracking expressed (percent area).
L_{MAX} = maximum area of top-down cracking (%) – a value of 58% is assumed.
t = analysis month in days.
ρ = scale parameter for the top-down cracking curve (Equation 2-27).
β = Shape parameter for the top-down cracking curve (Equation 2-28).
C_1, C_2, C_3 = Transfer function coefficients

$$\rho = \alpha_1 + \alpha_2 \times \text{ Month} \quad (2\text{-}27)$$

where,
α_1 and α_2 are functions of the climatic zone (wet freeze, wet non-freeze, dry freeze, dry non-freeze).

$$\beta = 0.7319 \times (\log_{10}\ \text{Month}\ )^{-1.2801} \quad (2\text{-}28)$$

Table 2-23 summarizes the SHA local calibration coefficients for the top-down cracking model.

Table 2-23 SHA local calibration coefficients for the top-down cracking model

SHA	C_1	C_2	C_3	C4	K_{L1}	K_{L2}	K_{L3}	K_{L4}	K_{L5}
Kansas	4.5	-	36000	-	-	-	-	-	-
Michigan	0.084	2.007	-	-	-	0.714	0.093	0.102	0.191
Oregon	1.453	0.097	0	1000	-	-	-	-	-
Tennessee	6.44	0.27	204.54	-	-	-	-	-	-

Note: "-" = mean either no local calibration, or used as global coefficients

2.6.1.12.3. Rutting

Rutting is the total accumulated plastic strain in the different pavement layers (HMA, base/sub-base, and subgrade). It is calculated by summing the plastic strains at the mid-depth of each layer, accumulated over each time increment. The permanent plastic strain for the HMA layer is determined using Equation 2-29.

$$\Delta_{p(HMA)} = \varepsilon_{p(HMA)} h_{HMA} = \beta_{1r} k_z \varepsilon_{r(HMA)} 10^{k_{1r}} T^{k_{2r}\beta_{2r}} N^{k_{3r}\beta_{3r}} \quad (2\text{-}29)$$

where,
$\Delta_{p(HMA)}$ = permanent plastic deformation in the HMA layer.
$\varepsilon_{p(HMA)}$ = accumulated permanent or plastic axial strain in the HMA layer/sublayer
$\varepsilon_{r(HMA)}$ = resilient or elastic strain calculated by the structural response model at the mid-depth of each HMA sublayer
$h_{(HMA)}$ = HMA layer/sublayer thickness (inch).
N = number of axle load repetitions.
T =pavement temperature (ºF).
k_z = depth confinement factor.
k_{1r}, k_{2r}, k_{3r} = global field calibration parameters.
β_{1r}, β_{2r}, β_{3r} = local or mixture field calibration constants.

The permanent plastic strain in the unbound layers is given by Equation 2-30.

$$\Delta_{p(soil)} = \beta_{s1} k_{s1} \varepsilon_v h_{soil} \left(\frac{\varepsilon_o}{\varepsilon_r}\right) e^{-\left(\frac{\rho}{n}\right)^{\beta}} \quad (2\text{-}30)$$

where,
$\Delta_{p(Soil)}$ = permanent plastic deformation for the unbound layer/sublayer.
ε_o = intercept determined from laboratory repeated load permanent deformation tests.
n = number of axle load applications.
ε_r = resilient strain imposed in laboratory tests to obtain material properties ε_o, β, and ρ.
ε_v = average vertical resilient or elastic strain in the layer/sublayer and calculated by the structural response model.
h_{soil} = unbound layer thickness (inch).
k_{s1} = global calibration coefficients (different for granular and fine-grained material).
β_{s1} = local calibration constant for rutting in the unbound layers (base or subgrade).

The total rutting is calculated using Equation 2-31.

$$Rut\ Depth_{Total} = \Delta_{HMA} + \Delta_{Base/subbase} + \Delta_{Subgrade} \quad (2\text{-}31)$$

where,
$Rut\ Depth_{Total}$ = total permanent deformation due to deformation in all pavement layers (in.).
Δ_{HMA} = permanent deformation in HMA layer, (in.).
$\Delta_{Base/subbase}$ = permanent deformation in base/subbase layers, (in.).
$\Delta_{Subgrade}$= permanent deformation in subgrade layer, (in.).

A summary of SHAs' local calibration coefficients for the total rutting model is provided in Table 2-24.

Table 2-24 SHA local calibration coefficients for the rutting model

SHA	β_{1r}	β_{2r}	β_{3r}	β_{gb}	β_{sg}
Arizona	0.69	1	1	0.14	0.37
Colorado	1.34	1	1	0.4	0.84
Georgia	-	-	-	0.5	0.3
Louisiana	0.8		0.83	-	0.4
Kansas	0.9	-	-	-	0.3251
Michigan	1.0422	-	-	0.3823	0.1212
Missouri	0.899			1.0798	0.9779
Oregon	1.48	1	0.9	0	0
Tennessee	0.111	1	1	0.196	0.722
Virginia	0.687	-	-	0.153	0.153

2.6.1.12.4. Transverse (thermal) Cracking

Thermal cracking is caused by surface temperature fluctuations, leading to HMA contraction. This contraction causes volume changes and stresses, leading to thermal cracks under constrained conditions. A thermal crack forms when the tensile stresses within the HMA layer(s) reach or exceed the material's tensile strength. These initial cracks propagate through the HMA layer(s) with each subsequent thermal cycle. The amount of crack propagation induced by a given thermal cooling cycle is predicted using the Paris law of crack propagation. Experimental results indicate that reasonable estimates of *A* and *n* can be obtained from the indirect tensile creep-compliance and tensile strength (Equations 2-32 and 2-33).

$$\Delta C = A(\Delta K)^n \quad (2\text{-}32)$$

where,
ΔC = change in the crack depth due to a cooling cycle
ΔK = change in the stress intensity factor due to a cooling cycle
A, n = fracture parameters for the HMA mixture

$$A = k_t \beta_t 10^{[4.389 - 2.52 Log(E_{HMA} \sigma_m \eta)]} \quad (2\text{-}33)$$

where,
$\eta = 0.8\left[1 + \frac{1}{m}\right]$
k_t = Regression coefficient determined through field calibration.
E_{HMA} = HMA indirect tensile modulus (psi).
σ_m = Mixture tensile strength (psi).
m = derived from the measured indirect tensile creep compliance curve.
β_t = Local or mixture calibration factor.

The stress intensity factor, *K*, was incorporated into PMED using a simplified equation derived from theoretical finite element studies, as given by Equation 2-34.

$$K = \sigma_{tip}(0.45 + 1.99(C_0)^{0.56}) \quad (2\text{-}34)$$

where,
σ_{tip} = far-field stress from pavement response model at a depth of crack tip (psi).
C_o = current crack length (feet).

Equation 2-35 shows the PMED transfer function for determining transverse cracking.

$$TC = \beta_{t1} N(z) \left[\frac{1}{\sigma_d} \log \left(\frac{C_d}{H_{HMA}} \right) \right] \quad (2\text{-}35)$$

where,
TC = observed amount of thermal cracking (ft/500ft).
β_{t1} = regression coefficient determined through global calibration (=400).
N(z) = standard normal distribution evaluated at z.
σ_d = standard deviation of the log of the depth of cracks in the pavement (=0.769) (inch).
C_d = crack depth (inch).
H_{HMA} = HMA layer thickness (inch).

Table 2-25 summarizes the modified local calibration coefficients for various SHAs.

Table 2-25 SHA local calibration coefficients for the stress intensity factor, *K*

SHA	Level 1	Level 2	Level 3
Arizona	1.5	0.5	1.5
Colorado	7.5	-	-
Georgia	35	-	-
Michigan	MAAT x 0.55	-	-
Missouri	0.61	-	-
Oregon	-	-	10

Note: "-" = mean either no local calibration, or used as global coefficients

2.6.1.12.5. Reflective Cracking

Old model: The transverse reflection cracking model was originally empirical and predicted the percentage of the crack area as a function of time using Equation 2-36.

$$RC = \frac{1}{1 + e^{a(c) + bt(d)}} \quad (2\text{-}36)$$

where,
RC = reflected cracks (percent).
t = time (years).
a,b = regression fitting parameters defined through the calibration process and depend upon adequate HMA thickness as shown in Equations 2-37 and 2-38.
c,d = User-defined cracking progression parameter.

$$a = 3.5 + 0.75\left(H_{eff}\right) \quad (2\text{-}37)$$

$$b = -0.688684 - 3.37302\left(H_{eff}\right)^{-0.915469} \quad (2\text{-}38)$$

H_{eff} = Effective HMA overlay thickness.

New model: The new mechanistic-based transverse reflection cracking model, developed under the NCHRP Project 1-41, Models for Predicting Reflection Cracking of Hot-Mix Asphalt Overlays, replaced the empirical reflection cracking model and has been integrated into PMED *(63)*. The new mechanistic model combines finite element and fracture mechanics approaches based on the Paris Law *(64)*. The new reflection-cracking model also accounts for incremental crack growth due to flexure, shear, and thermal stress in the overlaid AC layer. Equations 2-39 to 2-45 show the transverse reflective crack model.

$$\Delta C = k_1 * \Delta_{Bending} + k_2 * \Delta_{Shearing} + k_3 * \Delta_{Thermal} \quad (2\text{-}39)$$

$$\Delta_{Bending} = A(SIF)_B^n \quad (2\text{-}40)$$

$$\Delta_{Shearing} = A(SIF)_S^n \quad (2\text{-}41)$$

$$\Delta_{Thermal} = A(SIF)_T^n \quad (2\text{-}42)$$

$$\Delta D = \frac{c_1 k_1 * \Delta_{Bending} + c_2 k_2 * \Delta_{Shearing} + c_3 k_3 * \Delta_{Thermal}}{h_{OL}} \quad (2\text{-}43)$$

$$D = \sum_{i=1}^{N} \Delta D \quad (2\text{-}44)$$

$$RCR = \left(\frac{100}{C_4 + e^{C_5 \log D}}\right) * EX_{CRK} \quad (2\text{-}45)$$

where,
ΔC = Crack length increment, in.
ΔD = Increment damage ratio.
$\Delta_{Bending}$, $\Delta_{Shearing}$, $\Delta_{Thermal}$, = Crack length increments due to bending, shearing, and thermal loading.
k_1, k_2, k_3, C_1, C_2, C_3 = Calibration factors.
A, n = HMA material fracture properties.
n = Total number of days.
$(SIF)_B$, $(SIF)_S$, $(SIF)_T$ = Stress intensity factor due to bending, shearing, and thermal loading.
D = Damage ratio.
h_{OL} = Overlay thickness, in.
RCR = Cracks in underlying layers, reflected, %.
C_4, C_5 = Calibration factors
EX_{CRK} = Transverse cracks in underlying layers ft/mile (transverse cracking).
Alligator cracking in underlying layers, % lane area (alligator cracking).

Table 2-26 presents the adjusted calibration coefficients in different SHAs.

Table 2-26 SHA local calibration coefficients for reflective cracking model

SHA	c*	d*	C_1#	C_2#	C_3#	C_4#	C_5#
Arizona	2.55	1.23	-	-	-	-	-
Colorado	2.5489	1.2341	-	-	-	-	-
Georgia	G	G	-	-	-	-	-
Louisiana	0.72	0.3	-	-	-	-	-
Maryland	-	-	-	-	-	-	-
Missouri	-	-	0.0456	0.0083	2.72	105.4	-7.02

* = Old model coefficients; # = New model coefficients

2.6.1.12.6. IRI

IRI is a measure of ride quality that affects the vehicle's operating costs, safety, and driver comfort. The asphalt IRI prediction model is based on the concept that IRI at any age is a function of the IRI immediately after construction and declines over time as various distresses develop. IRI is estimated from Equation 2-46.

$$IRI = IRI_o + C1(RD) + C2(FC_{\text{Total}}) + C3(TC) + C4(SF) \quad (2\text{-}46)$$

where,
IRI = international roughness index (in./mile).
IRI_o = initial IRI immediately after construction (in/mi).
FC_{Total} = alligator, longitudinal, and reflection cracking in the wheel path (percent area).
TC = transverse cracking (including the reflection of transverse cracks in existing HMA pavements) (feet).
RD = average rut depth (inch).
C1, C2, C3, C4 = calibration coefficients
SF = site factor, which can be expressed using Equations 2-47 to 2-49.

$$SF = (\text{ Frost } + \text{ Swell }) \times Age^{1.5} \quad (2\text{-}47)$$

$$\text{Frost } = \text{Ln}\,[(\text{ Rain } + 1) \times (FI + 1) \times P_4] \quad (2\text{-}48)$$

$$\text{Swell } = \text{Ln}\,[(\text{ Rain } + 1) \times (FI + 1) \times P_{200}] \quad (2\text{-}49)$$

where,
SF = site factor.
Age = pavement age (years).
FI = freezing index.
Rain = mean annual rainfall (in.).
P_4 = subgrade material passing No. 4 sieve (percent).
P_{200} = subgrade material passing No. 200 sieve (percent).

Table 2-27 summarizes SHA IRI calibration coefficients.

Table 2-27 SHA IRI model local calibration coefficients

SHA	C1	C2	C3	C4
Arizona	1.2281	0.1175	0.008	0.028
Colorado	35	0.3	0.02	0.019
Georgia	40	0.4	0.008	0.015
Kansas	95	0.04	0.001	-
Louisiana	40	0.4	0.008	0.015
Michigan	15.072	0.14	0.004	0.0192
Missouri	0.3	58.9	0.0072	0.0129
Tennessee	40	0.4	0.008	0.015
Virginia	-	-	-	0.0392

2.6.2 Local Calibration Efforts for Concrete (bonded & unbonded) Overlays

Several SHAs have undertaken local calibration of PMED models for bonded and unbonded concrete overlays, targeting distresses such as joint faulting, slab cracking, and IRI. These efforts provide SHA-specific adjustments to enhance predictive accuracy beyond the nationally calibrated defaults.

2.6.2.1. Colorado

The Colorado DOT conducted local calibration of the PMED (v1.0) for concrete pavements, including 25 new JPCP sections and 7 unbonded JPCP overlay sections, drawn from CDOT's PMS and the LTPP database (*48*). These sections provided a foundation for evaluating and, where necessary, recalibrating the performance models most critical to concrete overlays: transverse slab cracking, joint faulting, and IRI. Model evaluation indicated that the global IRI model for JPCP performed well under Colorado conditions, producing an R^2 of approximately 81% with a standard error of estimate near 9.9 in/mi, and no significant prediction bias. Accordingly, the IRI model was retained

without modification. In contrast, the faulting and slab cracking models showed systematic bias, particularly for unbonded overlays, necessitating local recalibration to reduce errors and align predicted values with field observations. These adjustments enhanced the predictive reliability of the models across Colorado's range of climatic and traffic conditions. In summary, the Colorado study demonstrated that while the nationally calibrated concrete pavement models provided acceptable predictions for IRI, local adjustments to faulting and cracking models were essential for unbonded JPCP overlays.

2.6.2.2. Michigan

Under the SPR-1723 study, MDOT calibrated PMED using a dataset of 28 unbonded JPCP overlay sections (*17*). Calibration targeted transverse cracking, joint faulting, and IRI, with distress data obtained from PMS records and validated through construction documentation. National models were found to underpredict slab cracking and faulting and to generate high variability in IRI. Local recalibration reduced bias and standard error of estimate, bringing faulting predictions within AASHTO limits and improving IRI accuracy. Resampling methods (jackknife and bootstrap) confirmed the robustness of the coefficients, supporting the need for continued overlay data collection to refine concrete pavement rehabilitation models under Michigan conditions.

2.6.2.3. Missouri

Missouri DOT's calibration study incorporated both new JPCP and nine unbonded JPCP overlay sections from the PMS and LTPP databases. PMED (v2.5.5) was applied to evaluate transverse slab cracking, joint faulting, and IRI models (*53*). Because of limited distress accumulation in the overlay dataset, complete regression-based recalibration was not feasible; instead, classification and sensitivity analyses were performed to assess model reasonableness. The study recommended that comprehensive calibration and validation are only possible once measured damage values are in the range of 0.01 to 1.0. A confusion matrix was created (see Table 2-28) to validate the accuracy of the transverse cracking model using Equation 2-50.

$$Accuracy = \frac{TP + TN}{TP + TN + FP + FN} \quad (2\text{-}50)$$

where:
TP = true positive, observation is greater than or equal to 1 percent, and the predicted is greater than or equal to 1 percent.
FN = false negative; observation is greater than or equal to 1 percent but is predicted as less than 1 percent.
TN = true negative, observation is less than 1 percent, and the predicted is less than 1 percent.
FP = false positive, observation is less than 1 percent but predicted is greater than or equal to 1 percent.

Table 2-28 Confusion matrix for comparing field-measured and PMED predictions

Distress Type	Predicted Category	Measured Category	Count
Transverse Cracking	< 1%	< 1%	22
Transverse Cracking	< 1%	≥ 1%	5
Transverse Cracking	≥ 1%	< 1%	0
Transverse Cracking	≥ 1%	≥ 1%	0
Transverse Faulting	High (>0.005)	High (>0.005)	9
Transverse Faulting	High (>0.005)	Low (<0.005)	5
Transverse Faulting	Low (<0.005)	High (>0.005)	13
Transverse Faulting	Low (<0.005)	Low (<0.005)	27
Transverse Faulting	Total	Total	54

The evaluation showed the global IRI model performed reasonably and was retained. In contrast, the cracking and faulting models revealed bias but could not be statistically recalibrated due to insufficient faulting and cracking progression in the field sections. The study recommended continued data collection from overlay projects to support future recalibration and highlighted the value of combining new JPCP and overlay sections for strengthening the calibration database.

2.6.2.4. Georgia

Georgia DOT evaluated concrete pavements using PMED (V1.0), incorporating a dataset of 8 LTPP and 12 non-LTPP JPCP sections distributed across the state (*49*). Although only one unbonded JPCP overlay of existing JPCP was available in Georgia through the LTPP program, it was included in the verification analysis alongside new JPCP sections. Calibration targeted joint faulting, slab cracking, and IRI, with global models. The analysis revealed that the global faulting model necessitated local adjustments, yielding unbiased predictions upon recalibration. The IRI regression equation also showed poor initial fit but improved substantially after recalibration. While transverse slab cracking models exhibited variability, their verification supported continued reliance on the global coefficients. Overall, the Georgia study confirmed that the global models for JPCP overlays were inadequate, and local recalibration of faulting and IRI models was necessary to reduce bias and improve prediction accuracy. The limited number of unbonded overlay sections restricted overlay-specific calibration, underscoring the need for expanded datasets to strengthen reliability under Georgia conditions.

Table 2-29 summarizes the concrete overlay calibration efforts for all the above-mentioned states.

Table 2-29 SHA calibration efforts for concrete overlays

State	Number of Sections (Rehabilitation)	PMED Models Calibrated	Version	Year
Colorado	7	TC, JF, IRI	v1.0	2013
Georgia	2	TC, JF	v1.0	2014
Michigan	28	TC, JF, IRI	v2.6	2023
Missouri	9	TC, JF, IRI	v2.5.5	2020

2.6.2.5. Distress Prediction

The following summarizes the PMED concrete pavement performance prediction models and the SHA local calibration coefficients.

2.6.1.12.7. Transverse Cracking

PMED transverse slab cracking is calculated as the percentage of cracked slabs at all severity levels. The mechanism involves independently predicting bottom-up and top-down cracking and combining them using a probabilistic relationship, thereby eliminating the possibility of their co-occurrence. The fatigue damage for both bottom-up and top-down is defined using Miner's law as given in Equation 2-51:

$$DI_F = \sum \frac{n_{i,j,k,l,m,n,o}}{N_{i,j,k,l,m,n,o}} \quad (2\text{-}51)$$

where,
DI_F = total fatigue damage (bottom-up or top-down)
$n_{i,j,k,l,m,n,o}$ = actual load applications applied at age *i*, month *j*, axle type *k*, load level *l*, the equivalent temperature difference between top and bottom PCC surfaces *m*, traffic offset path *n*, and hourly truck traffic fraction *o*
$N_{i,j,k,l,m,n,o}$ = allowable number of load applications applied at age *i*, month *j*, axle type *k*, load level *l*, the equivalent temperature difference between top and bottom PCC surfaces *m*, traffic offset path *n*, and hourly truck traffic fraction *o*

The allowable number of load applications is a function of PCC strength and applied stress and is calculated based on Equation 2-52:

$$\log\left(N_{i,j,k,l,m,n,o}\right) = C_1 \cdot \left(\frac{MOR_i}{\sigma_{i,j,k,l,m,n,o}}\right)^{C_2} \quad (2\text{-}52)$$

where,
MOR_i = Modulus of rupture of the PCC slab at the age *i*
$\sigma_{i,j,k,l,m,n}$ = applied stress at the age *i*, month *j*, axle type *k*, load level *l*, the equivalent temperature difference between top and bottom PCC surface *m*, traffic offset path *n*, and hourly truck traffic fraction *o*
C_1, C_2 = fatigue life calibration coefficients

The fraction of slabs cracked is predicted using Equation 2-53 for both bottom-up and top-down cracking:

$$CRK = \frac{1}{1 + C_4(DI_F)^{C_5}} \quad (2\text{-}53)$$

where,
CRK = predicted fraction of bottom-up or top-down cracking
C_4, C_5 = transfer function coefficients.

Once the bottom-up and top-down cracking is estimated, the percentage of slabs cracked is calculated using Equation 2-54.

$$TCRACK = \left(CRK_{\text{Bottom-up}} + CRK_{\text{Top-down}} - CRK_{\text{Bottom-up}} \cdot CRK_{\text{Top-down}}\right) \cdot 100 \quad (2\text{-}54)$$

where,
TCRACK = total transverse cracking (percentage of slabs cracked with all severities)
$CRK_{Bottom\text{-}up}$ = predicted fraction of bottom-up transverse cracking
$CRK_{Top\text{-}down}$ = predicted fraction of top-down transverse cracking

Table 2-30 summarizes the local calibration coefficients for the SHA transverse cracking model.

Table 2-30 SHA local calibration coefficients for the concrete transverse cracking model

SHA	C1	C2	C4	C5
Colorado	-	-	1.0	-1.98
Georgia	2.0	1.22	0.52	-2.17
Michigan	-	-	0.415	-0.965
Missouri	2.0	1.22	0.52	-2.17

2.6.1.12.8. Joint faulting model

Transverse joint faulting is calculated monthly using the material properties, climatic conditions, present faulting level, pavement design properties, and applied axle loads. Total faulting is the sum of the faulting increments from previous months and is predicted using Equations 2-55 to 2-58.

$$\text{Fault}_m = \sum_{i=1}^{m} \Delta\text{Fault}_i \tag{2-55}$$

$$\Delta\ \text{Fault}_i = C_{34} \times (\ \text{FAULTMAX}_{i-1} - \ \text{Fault}_{i-1})^2 \times\ \text{DE}_i \tag{2-56}$$

$$FAULTMAX_i = FAULTMAX_0 + C_7 \times \sum_{j=1}^{m} DE_j \times \log\left(1 + C_5 \times 5.0^{EROD}\right)^{C_6} \tag{2-57}$$

$$\text{FAULTMAX}\ \mathrm{X}_0 = \mathrm{C}_{12} \times \delta_{\text{curling}} \times \left[\log\left(1 + \mathrm{C}_5 \times 5.0^{\mathrm{EROD}}\right) \times \log\left(\frac{\mathrm{P}_{200} \times\ \text{WetDays}}{\mathrm{P}_\mathrm{s}}\right)\right]^{\mathrm{C}_6} \tag{2-58}$$

where,
Fault$_m$ = mean joint faulting at the end of month *m*
ΔFault$_i$ = incremental change (monthly) in mean transverse joint faulting during month *i*
FAULTMAXi = maximum mean transverse joint faulting for month *i*
FAULTMAX$_0$ = initial maximum mean transverse joint faulting
EROD = erodibility factor for base/subbase
DE$_i$ = differential deformation energy of subgrade deformation accumulated during month *i*.
δ$_{curling}$ = maximum mean monthly slab corner upward deflection PCC due to temperature curling and moisture warping
P$_S$ = overburden pressure on subgrade
P$_{200}$ = percent subgrade soil material passing the No. 200 sieve
WetDays = average annual number of wet days (greater than 0.1 in rainfall)
C$_{1,2,3,4,5,6,7,12,34}$ = calibration coefficients

C$_{12}$ and *C*$_{34}$ are defined by Equation 2-59 and Equation 2-60:

$$\mathrm{C}_{12} = \mathrm{C}_1 + \mathrm{C}_2 \times FR^{0.25} \tag{2-59}$$

$$\mathrm{C}_{34} = \mathrm{C}_3 + \mathrm{C}_4 \times FR^{0.25} \tag{2-60}$$

FR = base freezing index defined as the percentage of time (in hours) the top base temperature is below freezing (32 °F), temperature to the total number of hours in design life

Damage in a doweled transverse joint for the current month is estimated using Equation 2-61.

$$\Delta DOWDAM_{tot} = \sum_{j=1}^{N} C_8 \times F_j \frac{n_j}{10^6 d f_c^*} \quad (2\text{-}61)$$

where,
$\Delta DOWDAM_{tot}$ = cumulative dowel damage for the current month
n_j = number of axle load applications for the current increment and load group j for the current month
N = number of load categories
fc^* = estimated PCC compressive strength
d = dowel diameter; C_8 = calibration constant; F_j = effective dowel shear force induced by axle loading of load category j

The faulting model local calibration results for several SHAs are summarized in Table 2-31.

Table 2-31 SHA local calibration coefficients for the faulting model

States	C1	C2	C3	C4	C5	C6	C7	C8
Colorado	0.595	1.636	0.00217	0.00444	250	0.47	7.3	400
Georgia	0.595	1.636	0.00217	0.00444	250	0.47	7.3	400
Michigan	0.60	1.611	0.00217	0.00444	250	0.20	7.3	400
Missouri	0.595	1.636	0.00217	0.00444	250	0.47	7.3	400

2.6.1.12.9. IRI model (concrete pavements)

IRI prediction is based on a linear relationship between the IRI immediately after construction and the change in other distresses (transverse cracking, joint faulting, and joint spalling) over time. IRI is estimated from Equation 2-62.

$$IRI = IRI_I + C1 \times CRK + C2 \times SPALL + C3 \times TFAULT + C4 \times SF \quad (2\text{-}62)$$

where,
IRI = Predicted IRI
IRI_I = Initial IRI at the time of construction
CRK = Percent slabs with transverse cracking (all severities).
$SPALL$ = Percentage of joints with spalling (medium and high severities).
$TFAULT$ = Total joint faulting cumulated per mi
C_1, C_2, C_3, C_4 = Calibration coefficients
SF = Site factor, which can be calculated as shown in Equation 2-63.

$$SF = AGE(1 + 0.5556 \times FI)(1 + P_{200}) \times 10^{-6} \quad (2\text{-}63)$$

where,
AGE = Pavement age
FI = Freezing index, °F-days.
$P200$ = Percent subgrade material passing No. 200 sieve.

The joint faulting and transverse cracking for IRI calculation is obtained using the models described previously. The joint spalling is calculated from Equation 2-64

$$SPALL = \left[\frac{AGE}{AGE + 0.01}\right]\left[\frac{100}{1 + 1.005(-12 \times AGE + SCF)}\right] \quad (2\text{-}64)$$

where,
$SPALL$ = percentage joints spalled (medium- and high-severities)
AGE = pavement age since construction
SCF = scaling factor based on site-, design-, and climate-related variables, which is estimated as given in Equation 2-65.

$$SCF = -1400 + 350 \times ACPCC \times (0.5 + PREFORM) + 3.4 f_c'^{0.4} - 0.2(\text{FTcycles} \times AGE) + 43 h_{PCC} - 536 WC_{PCC} \quad (2\text{-}65)$$

where,
$ACPCC$ = PCC air content
AGE = time since construction
$PREFORM$ = 1 if preformed sealant is present; 0 if not
f'_c = PCC compressive strength
$FTcycles$ = average annual number of freeze-thaw cycles
h_{PCC} = PCC slab thickness
WC_{PCC} = PCC water/cement ratio

The IRI local calibration coefficients for various SHAs are summarized in Table 2-32.

Table 2-32 SHA local calibration coefficients for the concrete overlay IRI model

SHA	C1	C2	C3	C4
Colorado	0.8203	0.4417	1.4929	24.24
Georgia	1.05	0.5417	1.85	33.8
Michigan	0.0942	1.5471	1.797	23.7529
Missouri	0.8203	0.4417	1.4929	25.24

2.7 PMED SENSITIVITY INPUTS

The prioritization of influential inputs is crucial to local calibration, particularly in rehabilitation, where legacy conditions and interface behavior significantly impact the response. Because laboratory and field characterization are resource-intensive, agencies focus on inputs whose credible variation produces meaningful shifts in predicted distress and IRI. Inputs with high leverage merit Level 1 characterization; low-influence inputs can often be addressed with Level 2 or 3 values. This study adopts this philosophy, drawing directly on MDOT's published program—culminating in SPR-1723—to direct data collection toward inputs that matter most for Michigan conditions.

2.7.1 Summary of Sensitivity Investigations

Over two decades, the PMED implementation studies focused on:

- Traffic load spectra from weighing in motion (WIM) stations and truck composition for both asphalt and concrete pavements
- HMA dynamic modulus (|*E**|) and mixture volumetrics* for overlays.
- PCC CTE and load transfer/edge support for JPCP and concrete overlays.

Consistent with national guidance, and confirmed from MDOT's work (including SPR-1723), improved characterization of these categories, together with updated climatic files, reduces bias and dispersion in PMED predictions for rehabilitation designs(*17, 65*).

2.7.1.1. Asphalt Pavements

For asphalt pavements, sensitivity analyses have demonstrated that overlay air voids, effective binder content, and layer thickness are among the most influential variables for rehabilitation design. Existing pavement conditions, dynamic mixture modulus, and truck traffic spectra also strongly affect fatigue cracking, rutting, and IRI predictions. In contrast, inputs such as binder grade or gradation often play a moderate role, while groundwater table and base thickness are generally less influential. The national NCHRP Study 1-47, Sensitivity Evaluation of MEPDG Performance Prediction, further established a normalized sensitivity index, which classified parameters as hypersensitive, very sensitive, sensitive, or non-sensitive. Based on this framework, asphalt dynamic modulus parameters and thickness consistently emerged as highly sensitive or very sensitive to cracking and rutting models. Similar findings were observed in Michigan, where laboratory and field evaluations highlighted the importance of mixture volumetrics, overlay geometry, and initial IRI in rehabilitation projects. Michigan climate sensitivity analyses also showed that temperature, followed by wind speed and percent sunshine, were the most important environmental drivers of distress prediction. The following tables summarize the sensitivity results from national studies and multi-SHA investigations.

Table 2-33 Summary of sensitive input parameters for asphalt pavements *(66, 67)*

Distress type	Hypersensitive (NSI > 5)	Very sensitive (1 < NSI < 5)	Sensitive (0.1 < NSI <1)
Longitudinal Cracking	• HMA E^* alpha, delta • HMA thickness	• Base resilient modulus • Surface shortwave absorptivity • HMA air voids • HMA Poisson's ratio • Truck volume • HMA effective binder content • Subgrade resilient modulus • Base thickness • Subgrade % passing #200 • Truck speed	• HMA unit weight • Base Poisson ratio • HMA heat capacity • Subgrade liquid limit • Binder low-temperature PG • HMA thermal conductivity • Binder high-temperature PG • Subgrade Poisson's ratio • Groundwater depth • Subgrade plasticity index
AC Rut Depth	• HMA E^* alpha and delta	• HMA thickness, • Surface shortwave absorptivity, • HMA Poisson's ratio, • HMA air voids, • truck volume	• HMA effective binder content • Subgrade resilient modulus • Base thickness and resilient modulus • HMA air voids • Subgrade percent passing #200 • Truck speed • HMA unit weight • Base Poisson's ratio • HMA heat capacity • Subgrade LL and PI • Binder low-temperature PG • HMA thermal conductivity • Binder high-temperature PG • Subgrade Poisson's ratio

Table 2-33 Summary of sensitive input parameters for asphalt pavements (continued…)

Alligator Cracking	• HMA E^* alpha, delta HMA thickness	• Base resilient modulus • Surface shortwave absorptivity • HMA air voids • HMA Poisson's ratio • Truck volume • HMA effective binder content • Subgrade resilient modulus • Base thickness	• Subgrade % passing #200 • Truck speed • HMA unit weight • Base Poisson's ratio • HMA heat capacity • Subgrade liquid limit • Binder low-temperature PG • HMA thermal conductivity • Binder high-temperature PG • Subgrade Poisson's ratio • Groundwater depth • Subgrade plasticity index
Thermal Cracking		• HMA E^* delta, • HMA air voids, • HMA creep compliance	• HMA E^* • HMA thickness • Base resilient modulus • HMA Poisson's ratio • HMA air voids • Truck volume • HMA effective binder content • Subgrade resilient modulus • Base thickness • Surface shortwave absorptivity • Subgrade % passing #200 • Truck speed • HMA unit weight • Base Poisson's ratio • HMA heat capacity • Subgrade liquid limit • Binder low-temperature PG • HMA thermal conductivity • Binder high-temperature PG • Subgrade Poisson's ratio • Groundwater depth • Subgrade plasticity index
Total Rut Depth	HMA E^* alpha and delta	• HMA thickness, • surface shortwave absorptivity, • HMA Poisson's ratio, • HMA air voids	• HMA unit weight • Base Poisson's ratio • HMA heat capacity • Subgrade LL, PI, and resilient modulus • Binder low-temperature PG • HMA thermal conductivity • Binder high-temperature PG • Subgrade Poisson's ratio • Groundwater depth • HMA air voids • Truck volume • HMA effective binder content • Base thickness and resilient modulus • Subgrade percent passing #200 • Operational speed

Table 2-33 Summary of sensitive input parameters for asphalt pavements (continued…)

IRI		• HMA *E** alpha, delta • HMA thickness	• Base resilient modulus • Surface shortwave absorptivity • HMA air voids • HMA Poisson's ratio • Truck volume • HMA effective binder content • Base thickness • Subgrade percent passing #200 • Truck speed • HMA unit weight • base Poisson's ratio • HMA heat capacity • subgrade LL, PL, and resilient modulus • binder low-temperature PG • HMA thermal conductivity • binder high-temperature PG • Subgrade Poisson's ratio, • Groundwater depth

2.7.1.2. Concrete Pavements

For concrete pavements and concrete overlays, sensitivity studies have consistently highlighted the influence of slab thickness, joint spacing, coefficient of thermal expansion, modulus of rupture, and load transfer efficiency. Base type and edge support conditions also play a significant role, particularly in unbonded overlay designs. MDOT's recent study (SPR-1723) confirmed that the coefficient of thermal expansion is highly sensitive to faulting and transverse cracking, while joint spacing and slab geometry dominate IRI predictions (*17*). The national studies also identified curl and warp gradients, dowel bar diameter, and practical support as critical factors for faulting and cracking. Although variables such as unit weight and subgrade modulus show moderate or low effects, the results underscore that concrete thermal properties and structural configuration remain the most critical for calibration. Table 2-34 summarizes the sensitive inputs for different performance measures (*68, 69*).

2.7.2 Michigan Implementation Efforts

MDOT, in collaboration with MSU and other institutions, has produced a series of detailed studies that directly address sensitive inputs for PMED implementation. These efforts span evaluation of mixture properties, traffic characterization, unbound layer modulus, development of climatic files, and local calibration of performance models. Collectively, they provide the foundation for Michigan's adoption of PMED for both new and rehabilitated pavements. The most comprehensive calibration effort was documented in SPR-1723 (*17*), which developed and validated Michigan-specific calibration coefficients for all distress models. The results from these studies are considered throughout the local calibration process in this report. Brief findings from these works are summarized below.

Table 2-34 Summary of sensitive input parameters for concrete pavements (*68, 69*)

Distress type	Hypersensitive (NSI > 5)	Very sensitive (1< NSI < 5)	Sensitive (0.1 < NSI < 1)
Faulting	• Slab width	• design lane width • PCC unit weight • PCC CTE	• Subgrade resilient modulus, dowel diameter • PCC Poisson's ratio, Traffic volume, PCC cement content • Base resilient modulus & thickness • Groundwater table depth, edge support • LTE, MOR, PCC thickness • Erodibility index • MOR, E_c • Surface shortwave absorptivity • Joint spacing, PCC water-to-cement ratio, PCC thermal conductivity, and construction month
Transverse Cracking	• Slab width	• MOR • PCC thickness • Design lane width • PCC unit weight • CTE, MOR, E_c • Surface shortwave absorptivity • Joint spacing • PCC water to cement ratio • PCC thermal conductivity	• Subgrade resilient modulus • Dowel diameter • PCC Poisson's ratio • Traffic volume • PCC cement content • Base resilient modulus • Groundwater depth • Base thickness • Edge support, LTE • Erodibility index • Construction month
IRI	• Slab width	• PCC unit weight, PCC CTE	• Subgrade resilient modulus, • Dowel diameter • PCC Poisson's ratio • Traffic volume • PCC cement content • Base resilient modulus • Groundwater depth • Base thickness • MOR, E_c • Surface shortwave absorptivity • Joint spacing • PCC water-to-cement ratio • PCC thermal conductivity • Construction month

2.7.2.1. MDOT Sensitivity Study

The initial MDOT evaluation used both one-variable-at-a-time and factorial designs to assess the effects of PMED inputs. Results showed that PCC thickness, CTE, LTE, curl and warp, and truck volume had the most decisive influence on faulting, cracking, and IRI for HMA pavements, while thickness, air voids, effective binder content, and base

type dominated fatigue, rutting, and IRI. These results are presented in Table 2-35 for concrete pavements and Table 2-36 for asphalt pavements *(30)*.

Table 2-35 Impact of input variables on concrete pavement performance

Design/material variable	Transverse joint faulting	Transverse cracking	IRI
PCC thickness	High	High	High
PCC modulus of rupture	None	High	Low
PCC coefficient of thermal expansion	High	High	High
Joint spacing	Moderate	High	Moderate
Joint load transfer efficiency	High	None	High
PCC slab width	Low	Moderate	Low
Shoulder type	Low	Moderate	Low
Permanent curl/warp	High	High	High
Base type	Moderate	Moderate	Low
Climate	Moderate	Moderate	Moderate
Subgrade type/modulus	Low	Low	Low
Truck composition	Moderate	Moderate	Moderate
Truck volume	High	High	High
Initial IRI	NA	NA	High

Table 2-36 Impact of input variables on asphalt pavement performance

Fatigue cracking	Longitudinal cracking	Transverse cracking	Rutting	IRI
• HMA thickness • HMA effective binder content • HMA air voids • Base material type • Subbase material type	• HMA thickness • HMA air voids • HMA effective binder content • Base material • Subbase material • Subgrade material	• HMA binder grade • HMA thickness • HMA effective binder content • HMA air voids • HMA aggregate gradation	• HMA thickness • Subgrade material • Subgrade modulus • HMA effective binder content • HMA air voids • Base material • Subbase material • Base thickness • Subbase thickness	• HMA thickness • HMA aggregate gradation • HMA effective binder content • HMA air voids • Base material type • Subbase thickness • Subbase material type • Subgrade material type

Note: The input variables are listed in order of importance.

2.7.2.2. Sensitivity of Rehabilitation Treatments

A focused MDOT study investigated rehabilitation treatments and ranked inputs using NSI values. For asphalt overlays of existing asphalt and composite pavements, overlay air voids, overlay thickness, and existing condition were the most critical factors. For rubblized concrete pavements, asphalt overlay air voids and binder properties were the dominant factors; for unbonded PCC overlays, slab thickness, CTE, MOR, and joint spacing had the strongest influence. These findings were directly incorporated into the calibration framework of SPR-1723 (*17*). The detailed rankings are provided in Tables 2-11 to 2-14 in section 2.4 above (*9*).

2.7.2.3. HMA Mixture Characterization

Extensive laboratory testing was performed to provide Level 1 HMA inputs for Michigan mixtures. Critical properties included the dynamic modulus, the complex shear modulus of the asphalt binder, creep compliance, and indirect tensile strength. Artificial neural network (ANN) methods were also developed to estimate E* from volumetrics, and the DYNAMOD database was created to store mixture properties in formats compatible with PMED (*17, 70*).

2.7.2.4. Local Calibration and Validation of PMED Performance Models

The calibration effort in SPR-1723 included more than one hundred reconstructed and rehabilitated sections (*17*). Robust statistical approaches, such as split sampling and bootstrapping, were used to derive Michigan-specific calibration coefficients. Results demonstrated that national models were inadequate, with rutting frequently overpredicted and cracking underestimated. The Michigan calibration coefficients significantly reduced bias and error, thereby improving predictions of rehabilitation performance.

2.7.2.5. Traffic Inputs

Traffic input characterization relied on WIM data from 44 sites. Level 1 inputs were developed at site-specific locations, Level 2 inputs were created by clustering similar sites, and Level 3 statewide averages were determined. Results confirmed the sensitivity of truck classification, axle load distributions, and traffic composition for both asphalt and concrete pavements. Conclusions and recommendations for traffic input levels are summarized in Table 2-37 (*10, 13*).

Table 2-37 Conclusions and recommendations for traffic input levels

Traffic Characteristic	*Impact on pavement performance	*Suggested input levels (when level I data is not available)	#Impact on pavement performance	#Suggested input levels (when level I data is not available)
TTC	Significant	Level II	Moderate	Level II
HDF	Significant	Level II	Negligible	Level III[1]
MDF	Negligible	Level III (State average)	Negligible	Level III (State average)
AGPV	Negligible	Level III (State average)	Negligible	Level III (State average)
Single ALS	Negligible	Level III (State average)	Negligible	Level III (State average)
Tandem ALS	Significant	Level II (State average)	Moderate	Level II (State average)
Tridem ALS	Negligible	Level III (State average)	Negligible	Level III (State average)
Quad ALS	Negligible	Level III (State average)	Moderate	Level III (State average)

[1] Level III inputs were available for asphalt pavements in the MEPDG version 1.1 and are no longer available as input in PMED; * = Concrete pavements; # = asphalt pavements

2.7.2.6. Unbound Material Inputs in Michigan

MDOT studies characterized the subgrade and unbound base layers. These studies compared laboratory and FWD-based values and established recommended Level 2 and Level 3 inputs (33,000 psi for aggregate base and 20,000 psi for sand subbase). For Level 1 inputs, FWD testing at prescribed intervals is recommended, with design values based on the thirty-third percentile. The recommended subgrade modulus by soil type is presented in Table 2-38 (*71, 72*).

Table 2-38 Average subgrade modulus values

USCS classification	AASHTO classification	Laboratory determined (psi)	Back-calculated (psi)	Design value (psi)	Recommended design value (psi)
SM	A-2-4, A-4	17,028	24,764	5,290	5,200
SP1	A-1-a, A-3	28,942	27,739	7,100	7,000
SP2	A-1-b, A-3	25,685	25,113	6,500	6,500
SP-SM	A-1-b,A-2-4, A-3	21,147	20,400	7,000	7,000
SC-SM	A-2-4, A-4	23,258	20,314	5,100	5,000
SC	A-2-6, A-6,A-7-6	18,756	21,647	4,430	4,400
CL	A-4, A-6, A-7-6	37,225	15,176	4,430	4,400
ML	A-4	24,578	15,976	4,430	4,400
SC/CL/ML	A-2-6, A-4, A-6, A-7-6	26,853	17,600	4,430	4,400

2.7.2.7. Coefficient of Thermal Expansion

CTE values were determined for Michigan aggregates. Pavements in the University and Metro regions should use a CTE of 5.8×10^{-6} in/in/°F, while pavements in other regions should use 4.5×10^{-6} in/in/°F. These values are applied during calibration because CTE strongly influences faulting and cracking (*73*).

2.7.2.8. Michigan Specific Climatic Files for PMED

Climatic files were revised to correct missing data, update records, and add new weather stations. Automated Surface Observation Systems (ASOS) and Michigan Road Weather Information System (RWIS) data were integrated, yielding 15 climate zones defined by pavement surface temperatures and distress trends. Temperature, wind speed, and sunshine were confirmed as the most sensitive climatic variables. These updated files have been embedded in PMED and are used for rehabilitation design in Michigan *(74)*.

2.8 STATE OF PRACTICES FOR MATERIAL TESTING

Characterization of existing pavement layers is a critical PMED component for rehabilitation design; accurate representation of in situ properties governs the reliability of performance predictions. A variety of testing protocols are routinely employed to capture structural, material, and mechanistic behavior of pavement systems. Nondestructive testing with FWD and subsequent backcalculation (e.g., Backcalculation Tool [BCT], Modulus 7.0), reduced-area methods for composite sections, and FWD time-series analysis and pulse histories for subgrade modulus estimation provide the foundation for structural characterization. Laboratory testing complements field evaluation through dynamic modulus testing of HMA cores, concrete compressive

strength testing from cores, binder extraction from asphalt mixtures, and resilient modulus testing of unbound materials. More recently, advanced approaches such as TSD testing have been implemented to provide continuous deflection data at highway operating speeds, improving network- and project-level assessments. Together, these testing practices form the basis for developing accurate input parameters, which are essential for local calibration and effective rehabilitation design in PMED. The following subsections provide a detailed discussion of these methods, highlighting their applications, limitations, and relevance to pavement rehabilitation design.

2.8.1 Field Testing

Field testing plays a vital role in characterizing existing pavement layers, providing direct insight into in situ structural response and material behavior under loading. Accurate field-based measurements are essential for developing reliable inputs and for reducing bias in rehabilitation performance predictions.

2.8.1.1. Falling Weight Deflectometer

FWD testing is the most widely used nondestructive tool for characterizing the structural condition of existing pavements. The test applies a transient impulse load to the surface through a circular plate and records the resulting deflection basin using geophones or seismometers at specified radial offsets. The measured basin is subsequently used in backcalculation procedures to estimate in situ layer moduli and to assess subgrade and base support conditions (*75-78*). Extensive FWD data collection and backcalculation in Michigan were reported in RC-1531, which focused on statewide subgrade modulus characterization and seasonal effects, and in RC-1548, which provided detailed backcalculated moduli for granular base and subbase layers using large datasets of FWD deflections. These studies established design values that have since served as primary inputs for PMED (*46, 79*). An FHWA-sponsored investigation advanced the analysis of FWD deflection data by proposing enhanced backcalculation procedures and standardized evaluation of device performance. The study emphasized improved interpretation of deflection basins for asphalt pavements, offering recommendations that strengthen the integration of FWD testing into mechanistic–empirical pavement design and rehabilitation practices (*80*). For rehabilitation Level 1 inputs, Kansas DOT used EVERCALC v5.0 to backcalculate moduli at a 9-kip load, with QA/QC that discarded results with a root mean square error (RMSE) greater than 5% and removed statistical outliers via box-plot screening. (*22*). In Georgia, FWD testing was incorporated into the calibration process. Deflection basins were measured at 50-ft intervals within the wheel path of calibration sections and supplemented with DCP testing and coring. The backcalculated layer moduli derived from these FWD data were used, along with construction records, to refine PMED material property inputs (*49*). In Virginia, FWD testing was systematically applied to characterize existing pavement layers for both new and rehabilitated designs. Backcalculated moduli obtained from these tests were incorporated as PMED Level 1 inputs, with particular emphasis on JPCP and overlay projects. The use of site-specific FWD-based characterization enhanced the accuracy of performance predictions and provided a reliable foundation for local calibration of rehabilitation models (*59*). In Louisiana, FWD testing has been widely integrated into the state's PMS for network-level monitoring and evaluation of pavement structural

capacity. However, these deflection data were not directly employed as PMED Level 1 inputs. Instead, the calibration relied on PMS distress data and other project-level records. At the same time, FWD remained primarily a tool for condition assessment and statewide management rather than site-specific model calibration (*50*).

2.8.1.2. Light Weight Deflectometer

The LWD has also emerged as a complementary nondestructive device for field characterization of unbound and subgrade layers. It has been widely applied in QC/QA programs, with studies validating its correlations to DCP, moisture content, and compaction quality (*81, 82*). LWD provides rapid, repeatable stiffness measurements, though sensitivity to moisture and layer thickness must be considered. Recent field and simulation work has demonstrated that equipping LWD with radial sensors improves the accuracy of layered backcalculation, particularly in stiff-over-soft systems (*83*). Analytical modeling efforts further extended their application, showing that depth-varying anisotropic soils require advanced interpretation of LWD deflections for reliable modulus estimation (*84*). More recently, comparisons of different devices (e.g., Zorn and Dynatest) confirmed equipment sensitivity and led to the development of standardized protocols for agency adoption (*85*). Collectively, these efforts highlight LWD as a valuable supplement to traditional density-based QC/QA methods and a potential tool for refining input parameters in PMED, provided results are locally calibrated and interpreted with attention to moisture sensitivity.

2.8.1.3. Traffic Speed Deflectometer

The TSD can measure the pavement's response to loading at traffic speeds (up to 50 mph and a 10,000 lb axle weight), minimizing traffic disruptions and maximizing data-collection frequency. The TSD is equipped with Doppler lasers to measure instantaneous deflection velocity (typically averaged over 0.01 miles). The deflection velocity is divided by the survey vehicle speed to obtain the deflection slope. Deflections are mathematically calculated from the deflection velocity and slope measurements. A common mathematical calculation is the Area Under the Curve method, which produces deflection bowl results like those from FWD measurements. TSD measurements are made along the outer wheel path at approximately 6 locations (4, 8, 12, 24, 36, and 60 inches from the wheel load center).

2.8.2 Laboratory Testing

Laboratory testing provides the fundamental material properties required for PMED and rehabilitation analysis. While field tests, such as FWD, LWD, and TSD capture in situ responses, laboratory testing enables the controlled evaluation of mixture stiffness, strength, and durability parameters, ensuring an accurate representation of material behavior under a wide range of loading and climatic conditions. These tests are essential for PMED Level 1 inputs and play a critical role in local calibration efforts, as reliance on default correlations or Level 3 values often leads to significant errors in distress prediction. The following subsections discuss the major laboratory tests used in pavement rehabilitation design, including dynamic modulus, PCC compressive strength from cores, and resilient modulus for unbound materials.

2.8.2.1. Dynamic Modulus

Dynamic modulus testing is the primary laboratory method for characterizing the viscoelastic response of asphalt mixtures and represents the most critical PMED Level 1 input for asphalt pavement analysis. The test is performed on cylindrical asphalt specimens subjected to cyclic uniaxial compressive loading at multiple temperatures and loading frequencies, producing stiffness and phase angle data that are shifted to construct a master curve. This master curve captures the time–temperature dependent response of asphalt mixtures and serves as the basis for predicting fatigue cracking, rutting, and IRI (*86-88*). The procedures for conducting dynamic modulus testing and analyzing the results are well defined in national standards. AASHTO T 342-11 outlines the standard method for measuring the dynamic modulus of HMA mixtures using repeated load axial testing at various temperatures and loading frequencies. AASHTO T 378-17 specifies the determination of dynamic modulus and flow number of asphalt mixtures using the AMPT, providing a more automated and standardized framework for mixture characterization. AASHTO R 84-17 establishes the practice for developing dynamic modulus master curves, detailing the procedures for shifting frequency–temperature data to a reference temperature and ensuring consistency in constructing dynamic modulus master curves using Equation 2-66.

$$log_{10}|E^*| = \delta + \frac{\alpha}{1 + e^{\beta + \gamma \log(t_r)}} \quad (2\text{-}66)$$

where:
E^* = HMA layer modulus (psi).
δ = regression parameter (10^{δ} = minimum modulus).
α = range (determines steepness of the curve).
t_r = reduced time (seconds).
β & γ = regression parameters.

Research has shown that dynamic modulus is highly sensitive to mixture volumetrics, binder grade, aggregate mineralogy, and aging, highlighting the need for local testing to replace national default values (*87, 89*). The NCHRP 1-37A and 1-40D projects confirmed that reliance on default dynamic modulus correlations results in systematic bias in distress prediction, while laboratory-measured values substantially improve model accuracy (*1, 90*). State-level implementation efforts, such as those in Michigan, performed comprehensive dynamic modulus testing on locally produced mixtures and developed databases compatible with PMED. These efforts also incorporated artificial neural network models to enhance the prediction of the dynamic modulus from mixture volumetrics (*70*). Similar programs emphasized that adopting dynamic modulus testing is essential for reducing calibration bias and capturing material variability across climate zones (*91*). Collectively, these standards and research findings demonstrate that dynamic modulus testing forms the cornerstone of asphalt mixture characterization in PMED. Its widespread adoption by SHAs underscores its significance in developing accurate Level 1 inputs, improving the reliability of distress prediction, and supporting the calibration of performance models to local conditions.

2.8.2.2. Resilient Modulus

The resilient modulus is a fundamental parameter in mechanistic–empirical pavement design as it characterizes the nonlinear elastic response of subgrade soils and unbound granular layers under repeated traffic loading. Laboratory determination of resilient modulus is standardized in AASHTO T307-99, which prescribes repeated-load triaxial testing with controlled confining and deviatoric stresses to simulate in situ stress conditions. Test specimens are compacted at optimum moisture content and subjected to a series of loading sequences at varying confining pressures, with axial recoverable strains measured to compute the resilient modulus for each stress state. The resulting data provide PMED Level 1 inputs, offering a more reliable representation of soil behavior than correlations or default values. The predictive model most associated with resilient modulus is the Witczak–Uzan constitutive equation (*41*), which relates resilient modulus to bulk stress and octahedral shear stress:

$$M_R = k_1 P_a \left(\frac{\theta}{P_a}\right)^{k_2} \left(\frac{\tau_{oct}}{P_a} + 1\right)^{k_3} \quad (2\text{-}67)$$

where:
M_R = resilient modulus
P_a = atmospheric pressure.
k_1, k_2, and k_3 are regression constants.
θ = bulk stress $= \sigma_1 + \sigma_2 + \sigma_3 = \sigma_1 + 2\sigma_3$
τ_{oct} = octahedral shear stress $= \sqrt[1/3]{(\sigma_1 - \sigma_2)^2 + (\sigma_1 - \sigma_3)^2 + (\sigma_2 - \sigma_3)^2}$

Several SHA and national research programs have adopted triaxial resilient modulus testing to support design and calibration. The LTPP program employed resilient modulus testing to populate a national database of unbound material properties (*92, 93*). NCHRP Project 1-37A incorporated these data to develop national PMED default values (*1*). Many SHAs have conducted extensive triaxial resilient modulus testing of base and subgrade materials for local calibration (*49, 71, 72, 94-100*). These studies confirmed the importance of resilient modulus as a sensitive input affecting distress predictions, particularly rutting and IRI, thereby underscoring the need for high-quality laboratory data in rehabilitation design.

2.8.2.3. PCC Compressive Strength

PCC compressive-strength testing of cores is a widely adopted practice for assessing the mechanical integrity of existing concrete pavements. Core samples are extracted from in-service slabs and tested in accordance with AASHTO T 22 and ASTM C39. Measuring compressive strength provides a direct measure of in situ concrete quality, deterioration, and structural capacity, thereby informing the feasibility of bonded or unbonded concrete overlay strategies. Within PMED, compressive strength is incorporated as a Level 1 input that directly influences predicted transverse cracking, faulting, and IRI in JPCP and concrete overlay designs. Empirical relationships further enhance the role of compressive strength by linking it to other critical PMED inputs. The modulus of elasticity and modulus of rupture are often estimated from compressive strength using widely accepted correlations, such as (*2, 20, 101, 102*):

$$E = 57{,}000\sqrt{f_c'} \quad \text{(2-68)}$$

where:
E = PCC layer modulus (psi).
f_c' = compressive strength, tested in accordance with AASHTO T22 (psi).

$$MOR = 7.5 - 9.5\sqrt{f_c'} \quad \text{(2-69)}$$

where:
MOR = Modulus of rupture (psi).
f_c' = compressive strength, tested in accordance with AASHTO T22 (psi).

Several SHA calibration efforts have incorporated compressive strength from cores to improve the characterization of concrete materials (*49, 51, 103, 104*). These correlations allow agencies to reduce the need for extensive laboratory testing by deriving secondary parameters directly from core compressive strength, while still maintaining input consistency for PMED modeling.

CHAPTER 3 - MATERIAL TESTING RESULTS

3.1 INTRODUCTION

Task 2 of this project involved characterizing existing material properties to support the development and updating of the material property database. These material properties serve as inputs for pavement design and future PMED model calibration efforts. This chapter documents the sample collection and field-testing activities conducted under this task, along with the results of material characterization and analysis of field test data.

Fourteen projects were selected from the 2023, 2024, and 2025 construction seasons. Laboratory testing was performed on HMA, PCC, and unbound materials collected from the construction sites. In addition, where feasible, field testing, including FWD, LWD, and GPR, was conducted for these projects. FWD and GPR testing were performed before and after construction to capture changes in pavement structure and layer properties.

In addition to construction-related projects, a separate set of five in-service pavements, originally constructed between 1992 and 2014, was evaluated using TSD testing. These projects were reviewed to assess the applicability of TSD data for rehabilitation design and existing pavement characterization. Since the TSD projects were not under construction, material sampling and lab testing were not performed for these locations.

Projects were selected to represent a range of rehabilitation types, project lengths, climate regions, road classes, and traffic volumes, as summarized below:

- Pavement rehabilitation fix type (e.g., HMA over HMA, HMA over JPCP)
- Project length (adequate for developing in situ and laboratory testing protocols)
- Climatic region (per MDOT regions)
- Road classification (freeway and non-freeway)
- Traffic volume (low, medium, and high)

Locations and details of the 2023 to 2025 construction-related projects are provided in Figure 3-1 and Tables 3-1 to 3-3. Details of the TSD selected projects are shown in Table 3-23.



Figure 3-1 Location of the selected 2023, 2024, and 2025 construction-related projects

Table 3-1 Selected projects for the year 2023 construction season

Project No.	Surface type	Region	Job number	Route	Pavement type description	Road class	Project length (miles)	Two-way ADT	Two-way AADTT
1	Asphalt	Grand	200816	I-96	Milling and two-course HMA over composite	Freeway	3.022	69,457	4,167
2	Asphalt	North	208319	US-23	Multicourse HMA over C&S	Freeway	2.394	5,657	283
3	Asphalt	Bay	211095	M-84	Milling and single-course HMA over composite	Non-freeway	2.008	19,575	332
4	Asphalt	Metro	210076	M-3	Milling and two-course HMA over HMA and composite	Non-freeway	3.427	18,150	363
5	Asphalt	Superior	203783	M-117	Milling and two-course HMA over C&S	Non-freeway	9.969	1,850	259
6	Asphalt	Southwest	200115	US-131	Multicourse HMA with ASCRL over PCC	Freeway	2.9565	18,900	1,512
7	Asphalt	North	207956	US-10 EB	Milling and single-course HMA over HMA	Non-freeway	0.859	27,118	813

Table 3-2 Selected projects for the year 2024 construction season

Project No.	Surface type	Region	Job number	Route	Pavement type description	Road class	Project length (miles)	Two-way ADT	Two-way AADTT
1	Asphalt	North	204211	I-75 BL	Multicourse HMA over C&S	Non-freeway	2.213	13,000	390
2	Asphalt	Bay	201308	M-53	Milling and two-course HMA over composite	Non-freeway	8.178	8,068	807
3	Asphalt	Metro	217866	M-53	Milling and two-course HMA over composite	Non-freeway	2.474	65,800	1,974
4	Asphalt	Grand	204218	M-91	Multicourse HMA over C&S	Non-freeway	4.520	3,875	542

Table 3-3 Selected projects for the year 2025 construction season

Project No.	Surface type	Region	Job number	Route	Pavement type description	Road class	Project length (miles)	Two-way ADT	Two-way AADTT
1	Asphalt	Metro	210074	I-75	HMA milling and multicourse HMA with ASCRL over PCC	Freeway	14.748	66,150	2,646
2	Asphalt	Superior	204073	US-41	Multicourse HMA over C&S	Non-freeway	6.124	4,313	130
3	Asphalt	University	130001	I-96	Multicourse HMA over rubblized	Freeway	3.604	74,950	6,746

3.2 FIELD CHARACTERIZATION OF MATERIALS

Field material testing involved conducting in-situ tests on various pavement layers, which included FWD, LWD, TSD, and GPR tests. This section summarizes the methodology used to analyze field-testing data and presents results for all projects included in this study. Detailed descriptions of each test type are included in Appendix A.

3.2.1 Falling Weight Deflectometer Testing

MDOT provided FWD deflection data of the selected projects before and after overlay placement. This section presents the backcalculation methodology adopted and compares the results obtained from different backcalculation methods for each project.

3.2.1.1. Backcalculation Methodology

The team backcalculated the layer moduli from FWD data using five different approaches to capture the variability in structural response across flexible, composite, and rigid systems. Methods 1 to 3 primarily estimated the modulus of AC and PCC layers, while Method 4 focused on subgrade MR. Method 5 used time-history analysis to provide independent verification of subgrade properties. This multi-method framework enabled comparison of results and improved confidence in the modulus estimates.

Method 1 and 2 – Using the Backcalculation Tool and Modulus 7.0

The team used the BcT and MODULUS 7.0 to backcalculate the moduli for flexible and composite pavements. The pavement structure was analyzed using three-layer pavement systems by combining unbound layers for both pavement types. For HMA-over-aggregate base and subbase pavement systems, the base and subbase were combined. For composite pavements, the base, subbase, and subgrade were combined into a three-layer system. The backcalculation programs generally produced reasonable results for flexible and composite pavements; however, for the backcalculation of composite pavements, the team also adopted a closed-form solution approach similar to that recommended for concrete pavements by the FHWA (*1, 2*).

Method 3 – Outer Area Method

The FWD is a key tool for assessing HMA and PCC pavement performance. As with other pavement systems, FWD testing helps evaluate the structural soundness of underlying PCC slabs, foundation support conditions, and load transfer efficiency across joints and cracks. A key distinction in analyzing FWD data for composite pavements compared to conventional PCC pavements is the effect of HMA layer compression. Failure to account for this compression in backcalculation analyses can result in significant errors (*3*). The Outer AREA method compensates for this compression effect in the HMA layer.

The AREA parameter represents the standardized area of the deflection basin (*4*). Because the sensor deflections normalize deflections under the load plate (d_0) when calculating AREA, the results of backcalculation using this method are highly dependent

on d_0. Therefore, it is crucial to account for the compression occurring within the HMA layer.

Another approach involves correcting the deflection under the load plate to account for HMA layer compression, thereby replicating the deflection profile of PCC pavements (*5*). However, satisfactory results can only be obtained by excluding the central deflection (d_0) and using the deflections measured from sensors located 305 mm (12 in) and farther from the load plate (*3*). This method, commonly called the Outer AREA Method, was originally proposed by Hall et al. (*6*). The calculation methodology for the Outer AREA Method follows the same principles as the conventional AREA method, except that the d_0 deflection is excluded from the calculation. Instead, deflections are normalized by the d_{12} deflection. The outer AREA for seven sensors, spaced non-uniformly at 0, 8, 12, 24, 36, 48, and 60-inch intervals, is then determined using Equation 3-1.

$$Outer\ Area = 3 + 6\frac{d_{18}}{d_{12}} + 9\frac{d_{24}}{d_{12}} + 18\frac{d_{36}}{d_{12}} + 12\frac{d_{60}}{d_{12}} \quad (3\text{-}1)$$

where;
Outer Area = normalized deflection basin area used for backcalculation of composite pavement.
d_{12}, d_{18}, d_{24}, d_{36}, d_{60} = measured FWD surface deflections (mils) at radial offsets of 12 in., 18 in., 24 in., 36 in., and 60 in., respectively, from the load plate center.

Hall et al. and McPeak and Khazanovich derived the following relationship to calculate the radius of relative stiffness (*l*), as shown in Equation 3-2 (*3, 6*).

$$l = \left[\frac{\ln\left(\frac{60 - Outer\ Area}{301.8}\right)}{-0.6223}\right]^{2.501} \quad (3\text{-}2)$$

where;
l= radius of relative stiffness.
Outer Area = normalized deflection basin area used for backcalculation of composite pavement.

After establishing the radius of relative stiffness, the k-value can be derived from any recorded deflections using the following correlation (*6*).

$$k = \frac{P.d_r^*}{d_r.l} \quad (3\text{-}3)$$

where;
k = Modulus of subgrade reaction, MPa/mm, (lbf/in2/in).
P = Applied load, N (lbf).
d_r^* = Corrected deflection coefficient for deflection at radial distance r from the center of the load plate and can be calculated using Equation (3-4).
d_r = Measured deflection at radial distance r from the load, mm (in).
ℓ = Radius of relative stiffness, mm (in).

$$d_r^* = a.e^{\left(-b.e^{(-c.l)}\right)} \quad (3\text{-}4)$$

where;

a, b, c = Regression coefficients (see Table 3-4).
ℓ = Radius of relative stiffness, mm (in).

Table 3-4 Coefficients for the corrected deflection coefficient (*6*)

Radial distance, in.	a	b	c
12	0.12188	0.79432	0.07074
24	0.11634	2.06115	0.06775
36	0.10960	3.62187	0.06568
48	0.10241	5.41549	0.06402
60	0.09521	7.41241	0.06255
72	0.08822	9.59399	0.06118

After determining the radius of relative stiffness (ℓ) and the k-value, the effective elastic modulus of the surface layers (combined PCC and HMA overlay) can be calculated using Equation 3-5.

$$E_e = \frac{12.l^4.(1-\mu^2).k}{h_e^3} \quad (3\text{-}5)$$

where;
E_e = Effective elastic modulus of the combined HMA and PCC layers, MPa (lbf/in²MPa).
ℓ = Radius of relative stiffness, mm (in).
h_e = Effective HMA and PCC layers thickness, mm (in).
μ = PCC Poisson's ratio.
k = Modulus of subgrade reaction, MPa/mm (lbf/in²/in).

The backcalculation process for a two-layer plate on subgrade follows the method introduced by Ioannides and Khazanovich. This method models the two layers as a unified plate with equivalent stiffness to the original system. In the case of HMA/PCC pavements, the two surface layers are assumed to be bonded, and the equivalent modulus, E_e, can be calculated using Equation 3-6 (*7*).

$$\frac{E_e.h_e^3}{12} = \frac{E_1.h_1^3}{12} + E_1h_1.\left(x-\frac{h_1}{2}\right)^2 + \frac{E_2.h_2^3}{12} + E_2h_2.\left(h_1-x+\frac{h_2}{2}\right)^2 \quad (3\text{-}6)$$

where;
E_e = Effective elastic modulus of the combined HMA and PCC layers, MPa (lbf/in²).
h_e = Effective thickness of the HMA and PCC layers, mm (in.) = h_{HMA} + h_{PCC}
E_1 = Elastic modulus of the upper plate (HMA), MPa (lbf/in²).
E_2 = Elastic modulus of the lower plate (PCC), MPa (lbf/in²).
h_1 = Thickness of the upper plate (HMA), mm (in).
h_2 = Thickness of the lower plate (PCC), mm (in).
x = Depth to the neutral axis, mm (in) using Equation 3-7.

$$x = \frac{\frac{h_1^2}{2} + \beta.h_2\left(h_1+\frac{h_1}{2}\right)}{h_1+\beta.h_2} \quad (3\text{-}7)$$

where;
β = Modular ratio = E_2/E_1. The ratio β values are recommended by Khazanovich et al. (*2*).

The moduli of the HMA and PCC layers can be determined from the backcalculated *effective modulus* by rearranging Equation (3-6) and substituting βE_1 for E_2 and (h_1+ h_2) for h_e. Equations (3-8) and (3-9) can be used to calculate the HMA and PCC moduli, respectively.

$$E_{AC} = E_1 = \frac{E_e.(h_1 + h_2)^3}{h_1^3 + \beta h_2^3 + 12.h_1.\left(x - \frac{h_1}{2}\right)^2 + 12.h_2.\left(h_1 - x + \frac{h_2}{2}\right)^2} \quad (3\text{-}8)$$

$$E_{PCC} = E_2 = \beta.E_{AC} \quad (3\text{-}9)$$

where;
E_{AC} = Elastic modulus of the HMA layer
E_{PCC} = Elastic modulus of the PCC layer

Method 4 – Boussinesq Solution (Surface Modulus)

The backcalculation of surface modulus using the Boussinesq methodology involves determining the modulus of elasticity of pavement materials from measured surface deflections under known loading conditions. This methodology is essential for evaluating pavement structural capacity and for supporting the design of appropriate rehabilitation strategies. The surface modulus is computed using Boussinesq's Equation (*8*). In this study, the team used the deflection at a radial distance of 60 inches to estimate the subgrade resilient modulus (M_R).

$$E_o(0) = \frac{2 \times (1\text{-}\mu^2) \times \sigma_0 \times a}{d\,(0)} \quad (3\text{-}10)$$

$$E_o(r) = \frac{2 \times (1 - \mu^2) \times \sigma_0 \times a}{\left(r \times d\,(r)\right)} \quad (3\text{-}11)$$

where;
$E_o(r)$ = surface modulus at a distance r from the center of the FWD loading plate
μ = Poisson's ratio (a value of 0.5 is assumed)
σ_0= contact stress under the loading plate (σ_0 = 82 psi)
d(r) = deflection at a distance r
a = radius of loading plate (a = 5.91 inches)

Method 5 – Time Histories (Spectral Element Method)

Lei (2011) developed a method for estimating the subgrade modulus using FWD time histories and the modulus of subgrade reaction, k (*9*). The method is explained below.

a. Determine the Poisson's ratio (v) and mass density (ρ) of the subgrade layer. Poisson's ratio depends on the soil type. In contrast, factors such as soil classification, degree of compaction during construction, and groundwater table influence the mass density, which typically ranges from 1500 to 2000 kg/m³. However, the estimated elastic modulus is not significantly influenced by mass density. Engineering judgment is therefore required to make appropriate estimations.

b. Calculate the slope of the time delay versus sensor location. Six sensors are positioned at various locations during the FWD test, each recording a distinct peak deflection time. These time delays and their corresponding sensor locations are plotted on a single graph, and the slope (m) for the more distant sensors is obtained through linear regression. Figures 3-2a and 3-2b show the peak load with deflection peaks for each sensor, as well as the time-delay plot with respect to sensor distance.
c. Determine the Rayleigh wave velocity (V_R) as the inverse of the slope (m) from the time-delay versus location graph.
d. Calculate the Shear wave velocity (Vs) by dividing the Rayleigh wave velocity (V_R) by k = 0.8109.
e. Calculate the shear modulus (G) of the subgrade layer using Equation 3-12. The value of ρ depends on the soil type and can be estimated as described in Step 1. For this study, the team selected ρ =94 lb/ft^3.

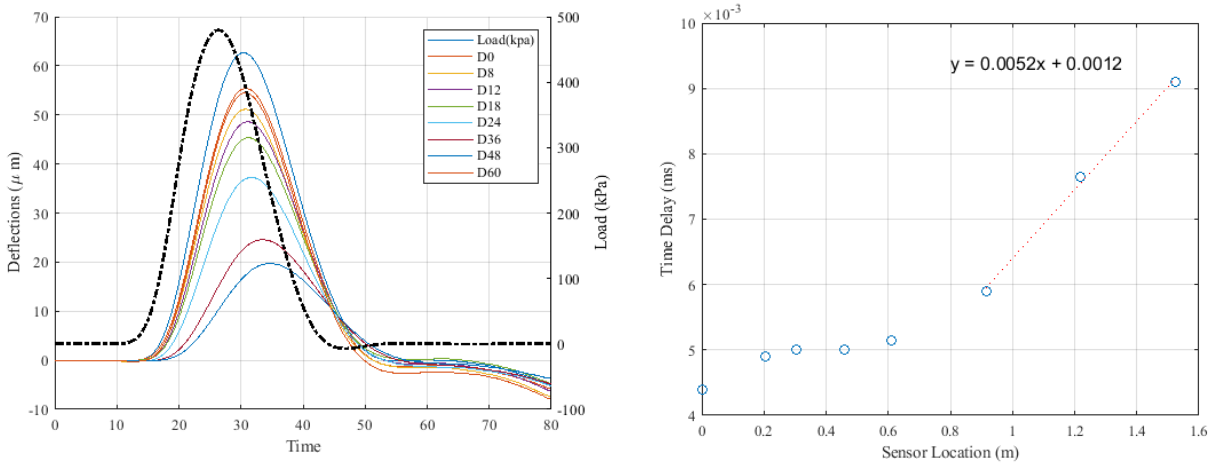
$$G = V_s^2 \times \rho \quad (3\text{-}12)$$

where;
G = subgrade shear modulus.
Vs = shear wave velocity.
ρ = mass density of subgrade.

f. Calculate the subgrade layer's elastic modulus (E) by Equation 3-13. The value of v was assumed as 0.45.

$$E = 2(1 + v)G \quad (3\text{-}13)$$

E = elastic modulus of subgrade.
v = Poisson ratio.
G = shear modulus of subgrade.



a. FWD load and deflection time histories

b. Time delay vs. location

Figure 3-2 FWD time histories and time delay vs. location of the sensors

Determining the appropriate number of sensors for Step 2 can be challenging. Typically, FWD tests employ 6 to 7 sensors, with the outer (more distant) sensors corresponding

to positions 4 to 6 or 5 to 7. Because of interactions between the interfaces of different pavement layers, the combined layer effects influence the time delays recorded by the nearby sensors. In contrast, the farther sensors experience less interlayer interaction, making them more suitable for deriving the slope (m-value). Therefore, the slope calculated from the farthest sensors is the most reliable indicator for determining the m-value (*9*).

Adjustment Factor for Backcalculated Values

The PMED performance models were calibrated using laboratory-measured values for existing layers. Therefore, backcalculated values from field FWD deflection data must be required to be adjusted to correspond with the laboratory-measured values for unbound layers (*10*). The PMED Guide generally recommends adjustment factors of 0.4 for subgrade and 0.67 for granular bases. Table 3-5 provides detailed adjustment factors based on pavement type.

Table 3-5 Adjustment factors for backcalculated modulus (*10*)

Layer types	Location	Adjustment factor
Unbound layers	Unbound base/subbase between two stabilized layers	1.43
Unbound layers	Unbound base/subbase under PCC	1.32
Unbound layers	Unbound base/subbase under HMA	0.62
Subgrade soils	Subgrade under stabilized subbase	0.75
Subgrade soils	Subgrade directly under flexible or rigid pavement without a granular base/subbase	0.52
Subgrade soils	Subgrade below a flexible or rigid pavement with a granular base/subbase	0.35

Adjustment factors of 0.52 and 0.35 were applied to flexible and composite pavements, respectively, to modify the back-calculated subgrade layer moduli. The following section contains the results of backcalculated moduli for flexible and composite pavements after these adjustments.

Pavement Structure Considered for Backcalculation

The study employed the following methodologies to analyze 3- and 4-layered flexible pavement structures, including both pre- and post-overlay analyses.

- Three-Layered Analysis – Pre-overlay
  - The existing AC layer is treated as the first layer.
  - The base and subbase layers are combined into a composite second layer.
  - The subgrade is the third layer.
- Three-Layered Analysis – Post-overlay for crushed and shaped projects only
  - The new AC overlay layer is treated as the first layer.
  - The existing C&S was treated as the second layer.
  - The base, subbase, and subgrade layers are combined into a composite third layer.

- Four-Layered Analysis – Pre-overlay
    - The existing AC layer is considered the first layer.
    - The aggregate base is treated as the second layer.
    - The subbase is treated as a distinct third layer.
    - The subgrade is the fourth layer.
- Four-Layered Analysis – Post-overlay for crushed and shaped projects only
    - The AC layer is considered the first layer.
    - The existing C&S AC was treated as the second layer.
    - The base and subbase layers are combined into a composite third layer.
    - The subgrade is the fourth layer.

Tables 3-6 and 3-7 present the flexible pavement structures considered before and after placement of an overlay, respectively.

Table 3-6 Cross-sectional details of flexible pavements before overlay placement

Road ID	Direction	AC (in.)	Base (in.)	Subbase (in.)
I-75 BL	NB	11.0	8.0	12.0
M-3	NB	11.0	6.0	12.0
M-53 (Bay)	NB	6.0	8.0	22.0
M-91	NB	8.0	12.0	12.0
M-117	NB and SB	8.0	6.0	9.0
M-84	NB	7.0	6.0	18.0
US-10	EB	10.0	6.0	12.0
US-23	NB	8.5	6.0	9.0
US-41	NB and SB	4.5	7.0	-
I-96 (Univ.)	EB	10.0†	4.0	10.0

† = Existing PCC to be rubblized base to be a flexible pavement

Table 3-7 Cross-sectional details of flexible pavements after overlay placement

Road ID	Direction	AC (in.)	Base (in.)	Subbase (in.)
I-75 BL	NB	6.5	11.0*	20.0#
M-3	NB	10.0	6.0	12.0
M-53 (Bay)	NB	6.0	8.0	22.0
M-91	NB	6.5	8.0*	24.0#
M-117	NB and SB	3.5	8.0*	15.0#
M-84	NB	7.0	6.0	18.0
US-10	EB	10.0	6.0	12.0
US-23	NB	4.0	8.0*	9.0
US-41	NB and SB	3.5	5.5	6.0
I-96 (Univ.)	EB	8.5	10.0†	14.0

* = Existing AC as C&S base
† = Existing PCC as rubblized base
# = Total is aggregate base and subbase combined

Tables 3-8 and 3-9 present the composite pavement structures considered before and after overlay placement, respectively.

Table 3-8 Cross-sectional details of composite pavements before overlay placement

Road ID	Direction	AC (in.)	PCC (in.)	Base (in.)	Subbase (in.)
I-96 (Grand)	EB	4.5	9.0	6.0	12.0
I-96 (Grand)	WB	4.5	9.0	6.0	12.0
M-3	SB	4.0	9.0	4.0	14.0
M-53 (Metro)	SB	3.5	10.0	3.0	12.0
US-131	NB	4.5	9.0	6.0	18.0
US-131	SB	4.5	9.0	6.0	18.0
I-75	NB and SB	6.0	9.0	4.0	10.0

Table 3-9 Cross-sectional details of composite pavements after overlay placement

Road ID	Direction	AC (in.)	PCC (in.)	Base (in.)	Subbase (in.)
I-96 (Grand)	EB	4.5	9.0	6.0	12.0
I-96 (Grand)	WB	4.5	9.0	6.0	12.0
M-3	SB	4.0	9.0	4.0	14.0
M-53 (Metro)	SB	3.5	10.0	3.0	12.0
US-131	NB	7.5	9.0	6.0	18.0
US-131	SB	7.5	9.0	6.0	18.0
I-75	NB and SB	6.5	9.0	4.0	10.0

3.2.1.2. Backcalculation Results

This section presents the backcalculation results for flexible and composite pavement sections based on FWD testing conducted before and after overlay placement. The results are organized to highlight differences in layer moduli across pavement types and to assess changes associated with the overlay.

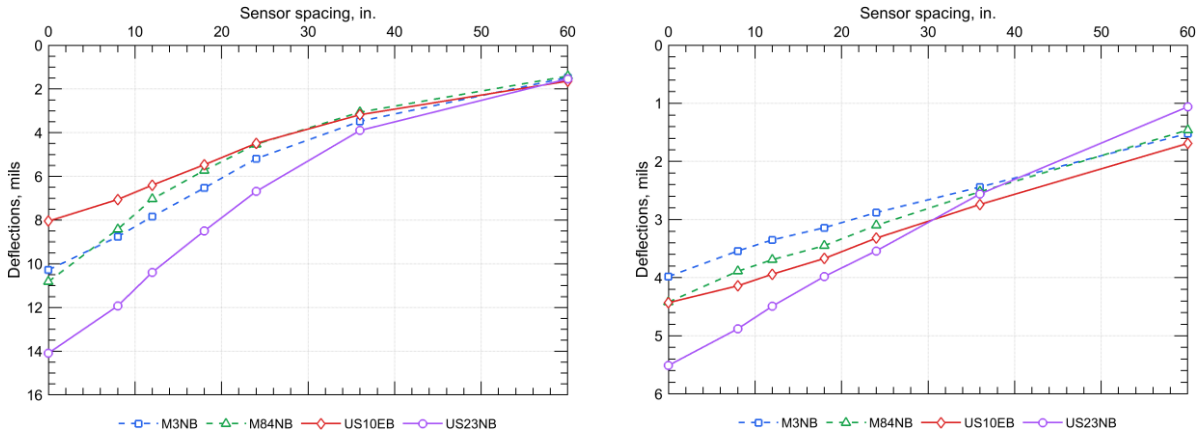
Flexible Pavement Sections

A detailed analysis was conducted on FWD data from nine flexible pavement sections, comparing results from 3- and 4-layered pavement structure analyses for pre- and post-overlay testing. The study aims to evaluate the structural capacity of flexible pavements using two widely employed back-calculation methods: MODULUS 7.0 and BcT. The summary reported includes the total number of FWD tests, convergence rates during back-calculation, average RMSE values, and the moduli of pavement layers. Tables 3-10 and 3-11 include information such as the region, road name, project job number, control section, FWD file name, number of tests conducted, tests that successfully converged during 3- and 4-layered analysis, and FWD temperature for pre-construction and post-construction analyses.

Three-Layered Analysis Results

FWD data were analyzed using a three-layered model for both pre- and post-overlay conditions. Across all projects, 672 FWD tests were performed before the overlay; 504 of these converged during backcalculation, yielding a 75% convergence rate. After the overlay, 771 FWD tests were performed, and 564 converged, yielding a 74% convergence rate. Convergence was defined based on two criteria: (1) RMSE < 5%, and (2) modulus values falling within acceptable ranges for each material type. The likelihood of convergence strongly depended on the shape of the measured deflection

basin. Figure 3-3 shows an example of a typical converged deflection basin compared with a non-converged case for a flexible pavement. Non-convergent tests were excluded from further analysis.



a. Normal deflection basin

b. Non-converged deflection basin

Figure 3-3 Comparison of deflection basin for flexible pavement

Tables 3-12 and 3-13 summarize the average layer moduli for the 3-layered analysis, including both pre- and post-overlay analysis for flexible pavements. The average RMSE values, which indicate the accuracy of the back-calculation, range from 0.52 to 1.3 mils. The modulus of the AC layer across different projects ranges from 233 ksi to 1570 ksi, indicating significant variation by pavement structure and region. Similarly, the combined Base-Subbase modulus ranges from 17 ksi to 50 ksi, while the Subgrade modulus varies between 7.0 ksi and 26.0 ksi.

Table 3-10 Summary FWD data available for existing asphalt pavement sections pre-overlay

Region	Road	Project Job Number	Control Section	FWD File Name	No. of Tests	3-Layered Analysis (No. of tests converged)	4-Layered Analysis (No. of tests converged)	FWD Temperature (°F)
Metro	M-3 NB	210076	50051	M3.FWD	78	52	54	68
Bay	M-84 NB	211095	73033	MDOT M-84.FWD	96	74	48	81
North	US-10 EB	207956	53021, 53032	US-10 EB Ludington Rt lane research pjct AM test.FWD	30	19	21	67
North	I-75 NB	204211	69011	75BL Gaylord morning.FWD	36	21	20	29
Bay	M-53 NB	201308	44032	M-53 NB am research.FWD	87	57	50	72
Grand	M-91 NB	204218	59032	M91 morning.FWD	144	112	116	72
Superior	M-117 NB	203783	49031	M-117.FWD	75	69	54	93
Superior	M-117 SB	203783	49031	M-117.FWD	60	51	39	98
North	US-23 NB	208319	1052	MDOT US-23.FWD	66	49	45	78
Total	**-**	**-**	**-**	**-**	**672**	**504**	**447**	-

Table 3-11 Summary FWD data available for asphalt pavement sections post-overlay

Region	Road	Project Job Number	Control Section	FWD File Name	No. of Tests	3-Layered Analysis (No. of tests converged)	4-Layered Analysis (No. of tests converged)	FWD Temperature (°F)
Metro	M-3 NB	210076	50051	M-3 NB outside lane AM run.FWD	93	50	51	72
Bay	M-84 NB	211095	73033	M-84 NB research.FWD	60	42	36	76
Bay	M-84 SB	211095	73033	M-84 SB research Bay City.FWD	66	46	42	77
North	US-10 EB	207956	53021, 53032	US-10 EB Ludington Rt lane research pjct 10-23-23.FWD	30	24	22	35
Bay	M-53 NB	201308	44032	NB AM.FWD	174	99	95	95
Grand	M-91 NB	204218	59032	M-91 NB RT lane OWP am run.FWD	147	120	110	76
North	US-23 NB	208319	1052	US-23 NB Spruce.FWD	36	33	33	78
North	US-23 SB	208319	1052	US-23 SB Spruce.FWD	36	33	33	76
Superior	M-117 NB	203783	49031	M117 Testing.FWD	66	60	58	43
Superior	M-117 SB	203783	49031	M117 Testing.FWD	63	57	53	52
Total	**-**	**-**	**-**	**-**	**771**	**564**	**533**	**-**

Table 3-12 Pre-overlay average layer moduli for 3-layered analysis of asphalt pavement sections

Project	AC (in.)	Total Base# (in.)	Mod. 7.0 – AC (ksi)	Mod. 7.0 – Total Base# (ksi)	Mod. 7.0 – Subgrade (ksi)	BcT – AC (ksi)	BcT – Total Base# (ksi)	BcT – Subgrade (ksi)	Average RMSE (%) – Mod. 7.0	Average RMSE (%) – BcT
M-3 NB	11	18	1,287	50	26	1,036	39	17	1.20	1.98
M-84 NB	7	24	639	35	21	618	42	9	1.30	1.80
US-10 EB	11	18	1,570	37	22	1,330	38	17	0.90	1.72
I-75 NB	11	20	500	17	7	450	21	11	0.75	1.60
M-53B NB	6	30	622	28	19	600	29	32	0.97	1.67
M-91 NB	8	24	233	26	11	213	31	9	1.06	0.70
M-117 NB	8	15	329	43	19	430	28	27	0.91	1.90
M-117 SB	8	15	293	39	17	371	22	24	0.99	1.99
US-23 NB	8.5	15	588	24	7	576	32	10	0.52	0.80

= Total base includes both unbound base and subbase layers.

Table 3-13 Post-overlay average layer moduli for 3-layered analysis for asphalt pavement sections

Project	AC (in.)	Total Base# (in.)	Mod. 7.0 – AC (ksi)	Mod. 7.0 – Total Base# (ksi)	Mod. 7.0 – Subgrade (ksi)	BcT – AC (ksi)	BcT – Total Base# (ksi)	BcT – Subgrade (ksi)	Average RMSE (%) – Mod. 7.0	Average RMSE (%) – BcT
M-3 NB	10	18	970	40	24	980	42	28	1.30	2.10
M-84 NB	7	24	1,000	57	22	1,270	50	18	1.05	2.20
M-84 SB	7	24	975	42	23	936	54	17	1.08	1.73
US-10 EB	10	18	1,790	27	13	1,450	32	16	0.71	1.57
M-53B NB	6	30	433	36	21	490	32	18	1.07	1.98
M-91 NB	6.5 5	8*	990	42	26	1,090	42	26	0.47	1.51
M-117 NB	3.5	8*	632	148	28	590	145	24	0.86	1.40
M-117 SB	3.5	8*	666	154	28	615	138	25	0.94	1.51
US-23 NB	4	8.5*	540	69	24	480	75	23	1.14	1.81
US-23 SB	4	8.5*	498	77	27	434	86	26	1.12	2.10

* = Existing HMA as C&S.

= Total base includes both unbound base and subbase layers.

Figure 3-4 compares the moduli of the pre- and post-overlay layers for a 3-layered analysis of flexible pavements. As expected, the AC modulus in the post-construction analysis generally increased due to the overlay, which provided additional stiffness to the pavement structure (Figures 3-4a and 3-4b), reflecting the intended enhancement in structural integrity. However, the behavior of the unbound layers is a key point of comparison, as they should ideally retain their characteristics after overlay placement. The MR values of the unbound layers remained within the same range as pre-overlay values, indicating consistent behavior (Figures 3-4c and 3-4d). This suggests that the overlay primarily strengthened the AC layer, with minimal impact on the underlying layers' stiffness, ensuring the pavement foundation remains robust and capable of supporting the new surface.
For C&S projects, the 3-layered post-overlay analysis combined all unbound layers beneath the existing C&S AC layer with the subgrade. The resulting increase in subgrade MR for US-23, M117, and M91 (Figures 3-4e and 3-4f) reflects the combined stiffness of the base, subbase, and subgrade.

Four-Layered Analysis Results

FWD data were also analyzed using a four-layered model for both pre- and post-overlay conditions. A total of 672 FWD tests were conducted before overlay placement, of which 447 converged successfully, yielding a 67% convergence rate. Post-overlay, 771 tests were performed, with 533 converging, corresponding to a 69% convergence rate. Tables 3-14 and 3-15 summarize the average layer moduli obtained from the four-layered analysis for flexible pavements under pre- and post-overlay conditions. Average RMSE values ranged from 0.27 to 1.38 mils for both MODULUS 7.0 and BcT, indicating acceptable backcalculation consistency. The AC layer moduli ranged from 490 ksi to 1695 ksi across projects, reflecting differences in pavement structure and regional conditions. The combined modulus of the aggregate base varied between 30 ksi and 60 ksi, while the C&S material exhibited higher stiffness, ranging from 45 ksi to 134 ksi. The subbase modulus values ranged from 18 ksi to 50 ksi, and the subgrade modulus ranged from 12.0 ksi to 30.0 ksi.

Figure 3-5 compares pre- and post-overlay layer moduli for the 4-layered analysis. As expected, the AC layer modulus generally increased post-construction (Figures 3-5a and 3-5b), reflecting the overlay’s structural contribution. The unbound layers (including base, subbase, and subgrade) retained similar moduli post-overlay, indicating consistent performance. Increases in subbase modulus for specific projects (M-91, M-117, and US-23) are attributed to the combined stiffness of the unbound layers beneath the existing C&S layer (Figures 3-5e and 3-5f). Overall, the four-layered analysis confirms that the overlay primarily strengthens the AC layer, while the underlying unbound layers maintain their intended structural behavior.

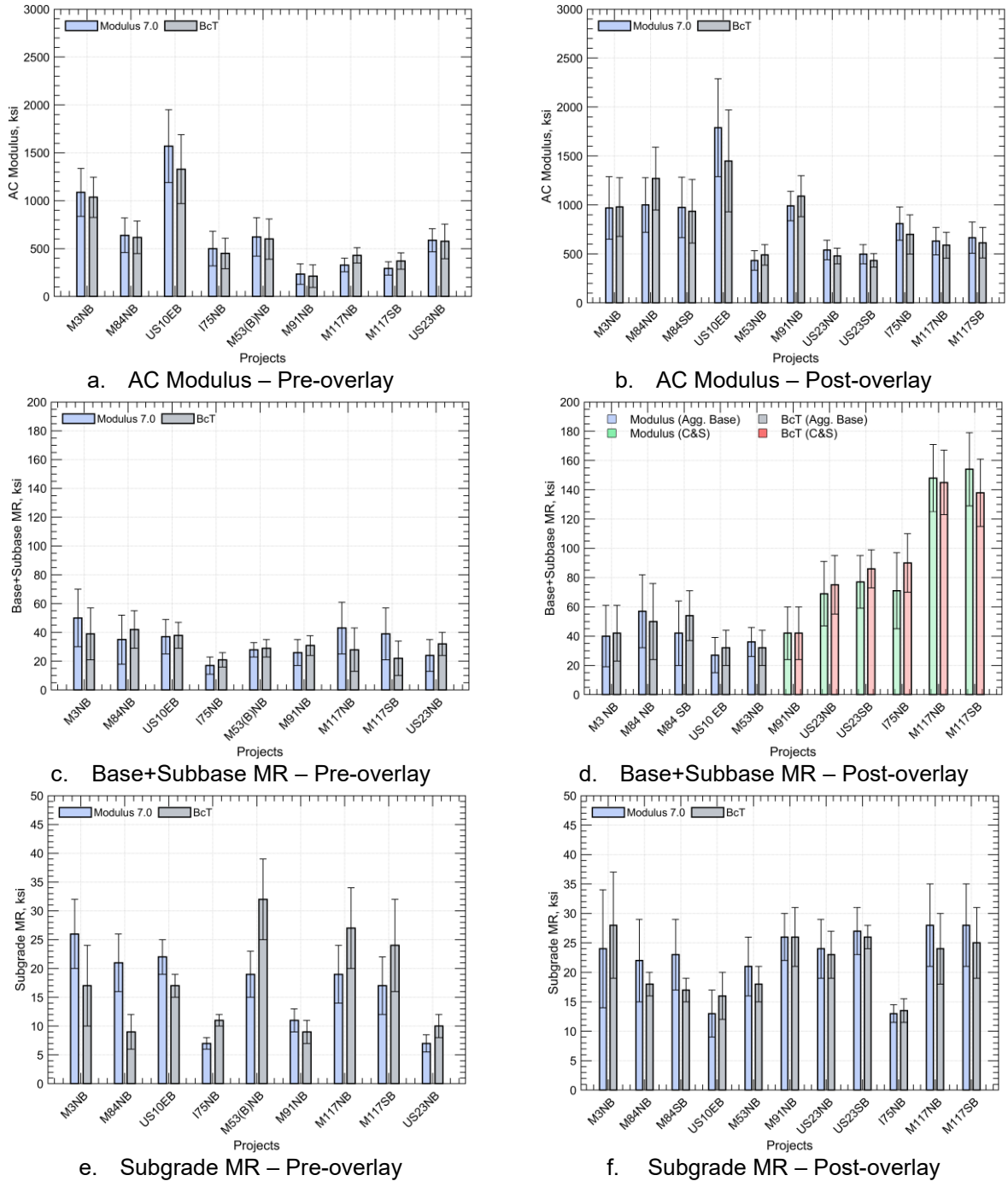


Figure 3-4 Pre- and post-overlay comparison for asphalt pavements – 3-layered analysis

Table 3-14 Pre-overlay average moduli for 4-layered analysis of asphalt pavement sections

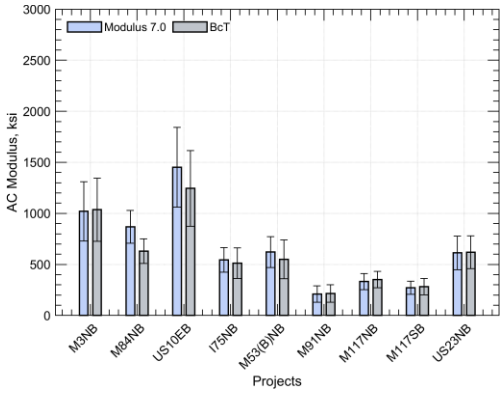
Project	AC (in.)	Base (in.)	Subbase (in.)	Mod. 7.0 – AC (ksi)	Mod. 7.0 – Base (ksi)	Mod. 7.0 – Subbase (ksi)	Mod. 7.0 – Subgrade (ksi)	BcT – AC (ksi)	BcT – Base (ksi)	BcT – Subbase (ksi)	BcT – Subgrade (ksi)	Average RMSE, (%) – Mod. 7.0	Average RMSE, (%) – BcT
M-3 NB	11	6	12	1,020	51	30	24	1,036	63	39	18	1.28	1.6
M-84 NB	7	6	18	869	36	33	16	630	44	40	9	0.92	1.4
US-10 EB	10	6	12	1,452	38	33	16	1,245	33	28	22	0.8	1.4
I-75 NB	11	8	12	545	34	18	8	512	48	22	11	0.9	1.43
M-53B NB	6	8	22	621	30	29	19	550	35	28	26	0.91	1.71
M-91 NB	8	12	12	210	30	25	13	216	37	27	9	0.89	0.96
M-117 NB	8	6	9	332	42	19	20	351	38	22	26	0.76	1.2
M-117 SB	8	6	9	272	39	19	19	282	37	18	24	0.72	1.3
US-23 NB	8.5	6	9	613	32	12	12	620	23	10	21	0.52	1.2

Table 3-15 Post-overlay average moduli for 4-layered analysis for asphalt pavement sections

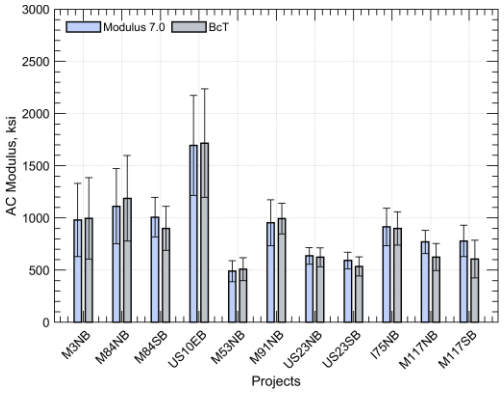
Project	AC (in.)	Base (in.)	Subbase (in.)	Mod. 7.0 – AC (ksi)	Mod. 7.0 – Base (ksi)	Mod. 7.0 – Subbase (ksi)	Mod. 7.0 – Subgrade (ksi)	BcT – AC (ksi)	BcT – Base (ksi)	BcT – Subbase (ksi)	BcT – Subgrade (ksi)	Average RMSE, (%) – Mod. 7.0	Average RMSE, (%) – BcT
M-3 NB	10	6	12	980	55	38	17	996	45	29	30	1.38	1.80
M-84 NB	7	6	18	1,112	43	33	24	1,188	55	42	18	1.17	1.90
M-84 SB	7	6	18	1,007	52	32	25	900	62	42	15	0.89	1.33
US-10 EB	10	6	12	1,695	43	18	13	1,717	49	34	16	0.76	1.24
M-53B NB	6	8	22	490	57	27	23	510	46	22	19	0.43	1.01
M-91 NB	6.55	8*	24	954	51	29	20	993	52	27	12	0.63	1.01
US-23 NB	4	8.5*	15#	637	58	29	25	624	57	35	22	0.68	1.37
US-23 SB	4	8.5*	15#	592	58	35	25	536	64	32	25	0.61	1.21
I-75 NB	6.5	11*	20#	914	53	27	16	900	52	19	20	0.40	0.99
M-117 NB	3.5	8*	15#	770	114	50	16	625	130	33	24	0.27	1.09
M-117 SB	3.5	8*	15#	780	134	47	16	606	137	32	25	0.46	1.08

* = Existing HMA as C&S.

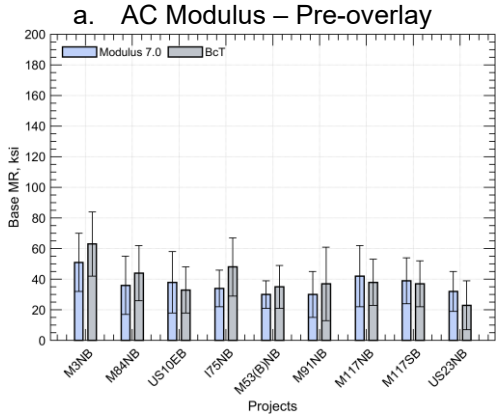
= Total base includes both unbound base and subbase layers.



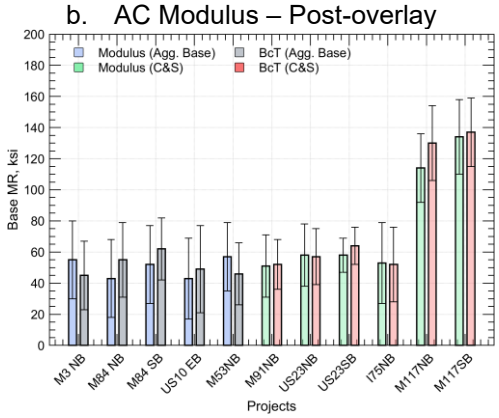
a. AC Modulus – Pre-overlay



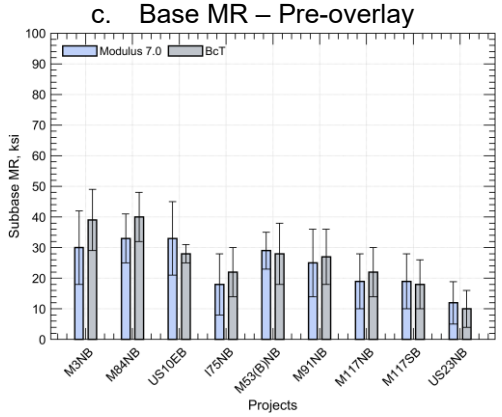
b. AC Modulus – Post-overlay



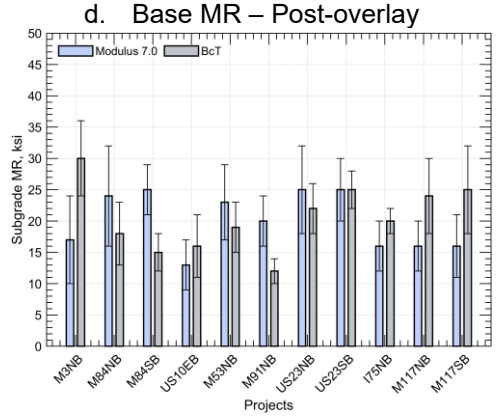
c. Base MR – Pre-overlay



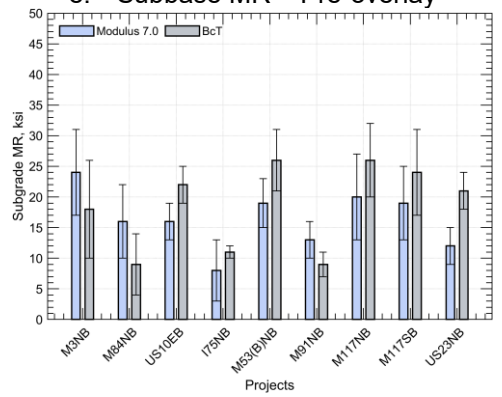
d. Base MR – Post-overlay



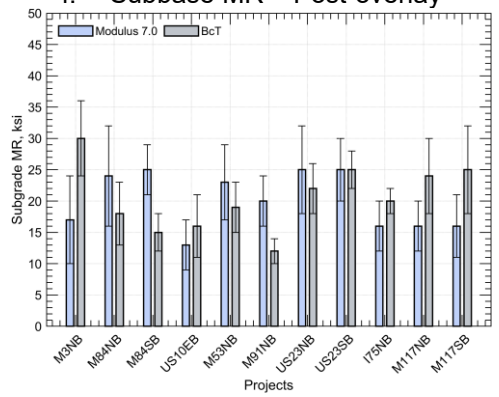
e. Subbase MR – Pre-overlay



f. Subbase MR – Post-overlay



g. Subgrade MR – Pre-overlay

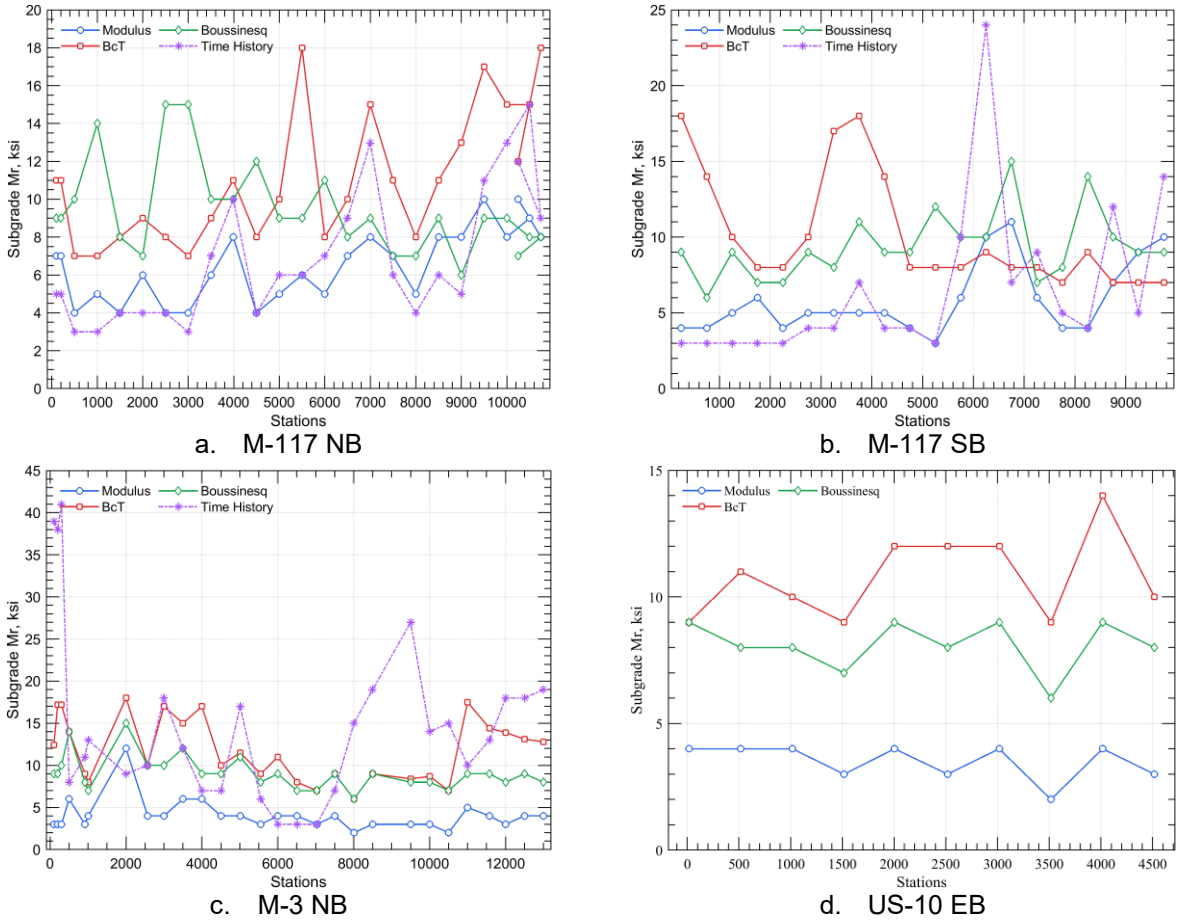


h. Subgrade MR – Post-overlay

Figure 3-5 Pre- and post-overlay results for asphalt pavements – 4-layered analysis

Subgrade Moduli

The team compared subgrade moduli separately across the four methods to verify the robustness of the backcalculation process. While earlier comparisons of AC, PCC, and other layers focused on MODULUS 7.0 and BcT, the subgrade warranted a more comprehensive evaluation given its critical role in pavement design and performance. Assessing subgrade response with MODULUS 7.0, BcT, Boussinesq, and time histories provided an additional check on the validity of the overall backcalculation methodology. Figures 3-6 and 3-7 illustrate the spatial distribution of backcalculated subgrade moduli and the cross-method comparison across all pavement sections. For US-10 EB, time-history data were unavailable; therefore, the comparison relied on the remaining three methods. After applying adjustment factors, BcT and the Boussinesq solution produced reasonable subgrade moduli of 7–15 ksi, whereas Modulus 7.0 yielded more conservative estimates.



a. M-117 NB

b. M-117 SB

c. M-3 NB

d. US-10 EB

Figure 3-6 Comparison of Backcalculated subgrade moduli for asphalt pavements

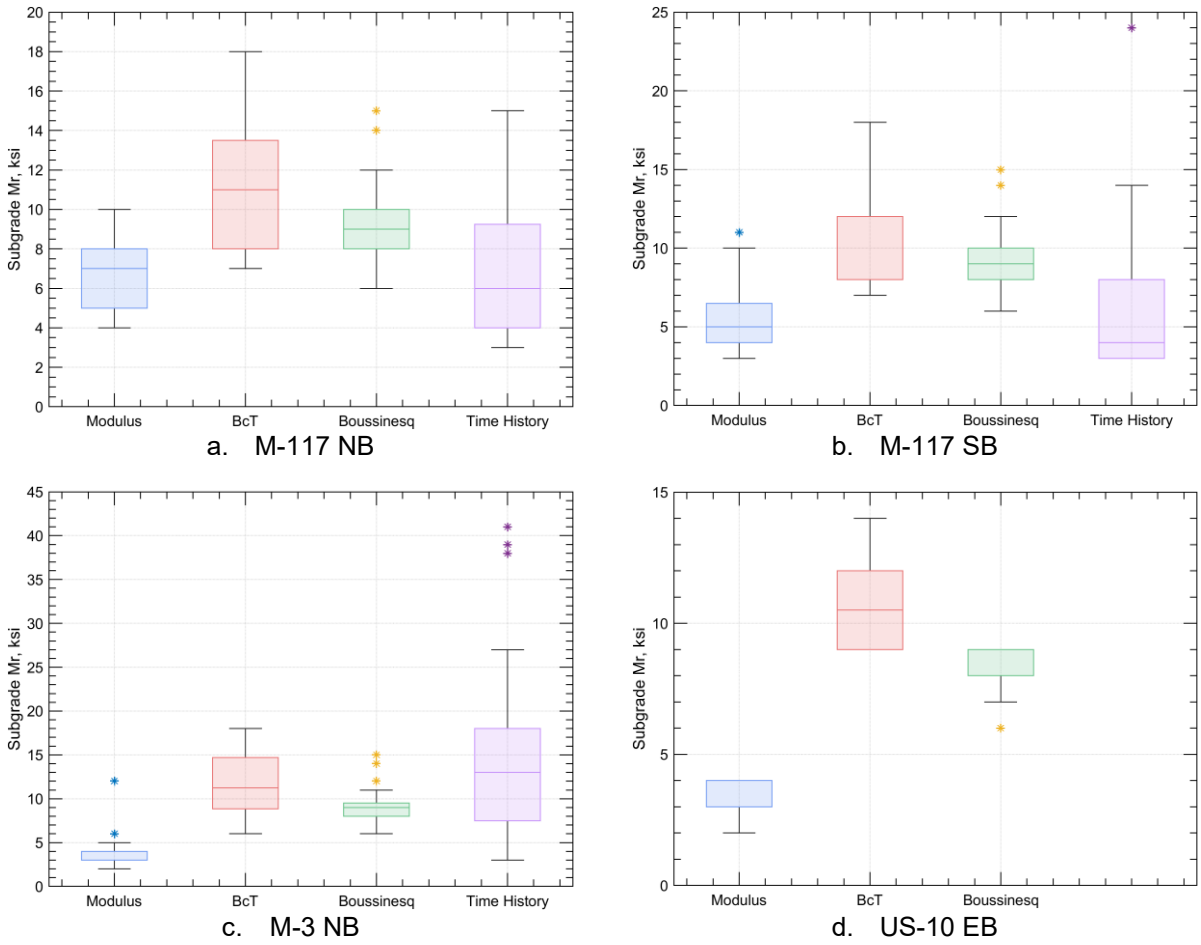


Figure 3-7 Statistical comparison of backcalculation methods for asphalt pavements

Composite Pavements

This section presents a detailed analysis of FWD data from six composite pavement sections, comparing results from 3- and 4-layered analyses for both pre- and post-overlay testing. Similarly to flexible pavements, the analysis evaluated the structural capacity of composite pavements using MODULUS 7.0 and BcT, using the equivalent modulus approach recommended by the FHWA report on the backcalculation of FWD deflection data (*1*). In addition to the four methods used for flexible pavements, the composite pavements were also analyzed using the "outer area" method. The key results reported include the total number of FWD tests, convergence rates during back-calculation, average RMSE values, and the modulus of pavement layers. The analysis was conducted on projects from various regions. Tables 3-16 and 3-17 include information such as the region, road name, project job number, control section, FWD file name, number of tests conducted, and the number of tests that successfully converged during the 3- and 4-layered analyses, and the FWD temperature for pre-construction and post-construction analyses.

Three-Layered Analysis Results

Using a three-layered model, 447 FWD tests were conducted on composite pavement sections: 306 pre-overlay and 309 post-overlay, yielding an overall convergence rate of 69%. The reduced AREA method was applied to estimate AC, PCC, and subgrade moduli. Tables 3-18 and 3-19 summarize results, and Figure 3-8 compares pre- and post-overlay layer moduli.

Post-overlay results show a substantial increase in AC modulus across all projects, confirming the overlay's stiffening effect. For example, in project I96EB, Modulus 7.0 reported an increase from 880 ksi pre-overlay to 2027 ksi post-overlay, while BcT indicated a similar rise from 878 ksi to 2013 ksi. The AREA method showed the same trend but consistently yielded higher values, suggesting an overestimation of AC stiffness relative to the other two methods.

For the PCC layer, pre-overlay moduli from MODULUS 7.0 and BcT were generally consistent, while the AREA method overestimated post-overlay moduli. In project I96EB, the PCC modulus increased from 15,350 ksi to 22,388 ksi using the AREA method, whereas MODULUS 7.0 and BcT produced values much closer to pre-overlay levels. This trend indicates that the outer AREA method may overestimate PCC stiffness in post-overlay conditions. Subgrade moduli from MODULUS 7.0 and BcT showed only minor variations between pre- and post-overlay analyses, suggesting that overlays had a minimal effect on subgrade behavior. For example, in project US131NB, the subgrade modulus increased modestly from 20 ksi to 26 ksi using MODULUS 7.0. By contrast, the outer AREA method consistently underestimated subgrade modulus across all projects. Average RMSE values for MODULUS 7.0 and BcT were similar in both pre- and post-overlay analyses, indicating stable predictions.

In summary, MODULUS 7.0 and BcT provided consistent and reliable estimates of AC and PCC moduli, while the outer AREA method tended to overestimate PCC stiffness and underestimate subgrade response. The overlay’s effect was most evident in the AC layer, confirming the structural enhancement it provided.

Four-Layered Analysis Results

Using a four-layered model, 447 pre-overlay FWD tests were conducted, with 309 converging (69% convergence rate). For post-overlay testing, 573 FWD tests were conducted, with 383 converging, corresponding to a 66% convergence rate. The outer AREA method was not applied, as FHWA does not recommend its use for estimating the MR of unbound base or subbase layers.

Compared to the three-layered model, the four-layered approach allowed separate characterization of base and subbase responses. In pavement rehabilitation, the modulus of existing layers is critical for accurate performance predictions; therefore, the base and subbase moduli were estimated separately for direct use in PMED.

Table 3-16 Summary FWD data available for existing composite pavement sections pre-overlay

Region	Road	Project Job Number	Control Section	FWD File Name	No. of Tests	3-Layered Analysis (No. of tests converged)	4-Layered Analysis (No. of tests converged)	FWD Temperature (°F)
Grand	I-96 EB	200816	41025	96 mdot.FWD	75	54	50	74
Grand	I-96 WB	200816	41025	97 mdot.FWD	78	67	67	86
Metro	M-3 SB	210076	50051	M3.FWD	81	51	48	73
Southwest	US-131 NB	200115	78013	US131.FWD	63	46	48	88
Southwest	US-131 SB	200115	78013	US131.FWD	63	43	48	83
Metro	M-53 SB	218766	50011	M53SB morning.FWD	87	45	48	72
Total	**-**	**-**	**-**	**-**	**447**	**306**	**309**	**-**

Table 3-17 Summary FWD data available for existing composite pavement sections post-overlay

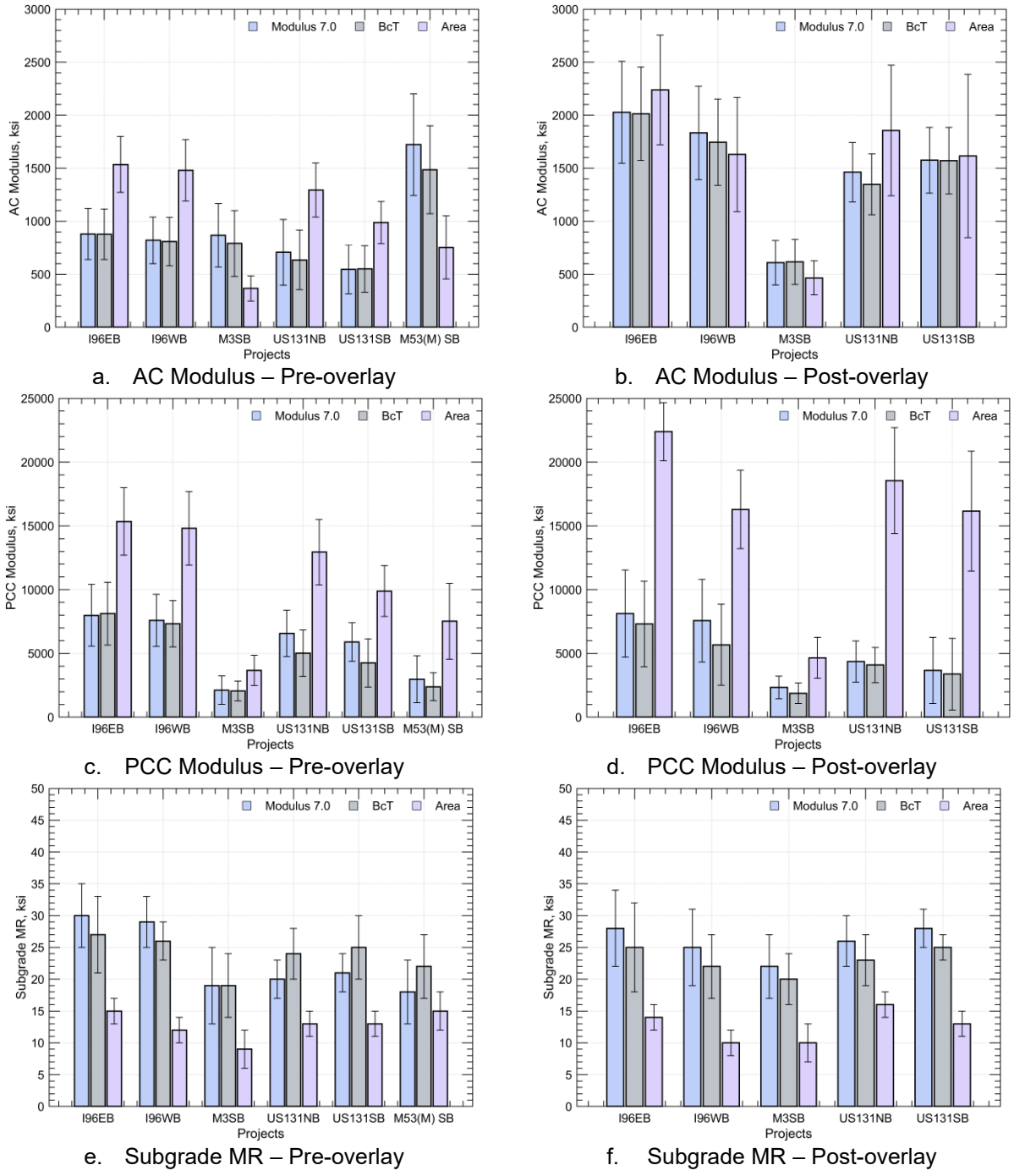
Region	Road	Project Job Number	Control Section	FWD File Name	No. of Tests	3-Layered Analysis (No. of tests converged)	4-Layered Analysis (No. of tests converged)	FWD Temperature (°F)
Grand	I-96 EB	200816	41025	96 mdot.FWD	93	79	63	52
Grand	I-96 WB	200816	41025	97 mdot.FWD	93	48	57	52
Metro	M-3 SB	210076	50051	M3.FWD	93	52	60	76
Southwest	US-131NB	200115	78013	US131.FWD	156	120	116	39
Southwest	US-131SB	200115	78013	US131.FWD	138	87	87	45
Total	**-**	**-**	**-**	**-**	**573**	**386**	**383**	**-**

Table 3-18 Pre-overlay average moduli for 3-layered analysis of composite pavement sections

Project	AC (in.)	PCC (in.)	Mod. 7.0 – AC (ksi)	Mod. 7.0 – PCC (ksi)	Mod. 7.0 – Subgrade (ksi)	BcT – AC (ksi)	BcT – PCC (ksi)	BcT – Subgrade (ksi)	AREA – AC (ksi)	AREA – PCC (ksi)	AREA – Subgrade (ksi)	RMSE (%) – Mod. 7.0	RMSE (%) – BcT
I-96 (Grand) EB	4.5	9	880	7,990	30	878	8,119	27	1,535	15,350	15	0.64	1.21
I-96 (Grand) WB	4.5	9	820	7,595	29	808	7,326	26	1,481	14,809	12	0.67	1.30
M-3 SB	4	9	867	2,120	19	790	2,053	19	366	3,664	9	1.3	1.73
US-131 NB	4.5	9	707	6,568	20	635	5,020	24	1,294	12,943	13	0.66	1.88
US-131 SB	4.5	9	545	5,905	21	550	4,258	25	988	9,885	13	0.89	1.97
M-53 (Metro) SB	3.5	10	1,722	2,982	10	1,486	2,384	23	753	7,525	15	0.82	2.20

Table 3-19 Post-overlay average moduli for 3-layered analysis of composite pavement sections

Project	AC (in.)	PCC (in.)	Mod. 7.0 – AC (ksi)	Mod. 7.0 – PCC (ksi)	Mod. 7.0 – Subgrade (ksi)	BcT – AC (ksi)	BcT – PCC (ksi)	BcT – Subgrade (ksi)	AREA – AC (ksi)	AREA – PCC (ksi)	AREA – Subgrade (ksi)	RMSE (%) – Modulus 7.0	RMSE (%) – BcT
I-96 (Grand) EB	4.5	9	2,027	8,128	28	2,013	7,315	25	2,239	22,388	14	0.57	1.12
I-96 (Grand) WB	4.5	9	1,833	7,566	25	1,745	5,680	22	1,629	16,290	10	0.66	1.97
M-3 SB	4	9	609	2,331	22	616	1,880	20	466	4,657	10	0.84	2.45
US-131 NB	7.5	9	1,462	4,365	26	1,348	4,090	23	1,855	18,551	16	0.59	1.22
US-131 SB	7.5	9	1,575	3,667	28	1,571	3,379	25	1,616	16,157	13	0.55	1.26



a. AC Modulus – Pre-overlay

b. AC Modulus – Post-overlay

c. PCC Modulus – Pre-overlay

d. PCC Modulus – Post-overlay

e. Subgrade MR – Pre-overlay

f. Subgrade MR – Post-overlay

Figure 3-8 Pre- and post-overlay comparison for composite pavements – 3-layered analysis

For the AC layer, post-overlay results show a marked increase in stiffness across all projects using both MODULUS 7.0 and BcT, reflecting the expected effect of the overlay. In the I96EB project, for example, the AC modulus rose from 853 ksi to 2074 ksi with MODULUS 7.0 and from 914 ksi to 1941 ksi with BcT. These results confirm the structural improvement achieved through the overlay. The PCC base layer, by contrast,

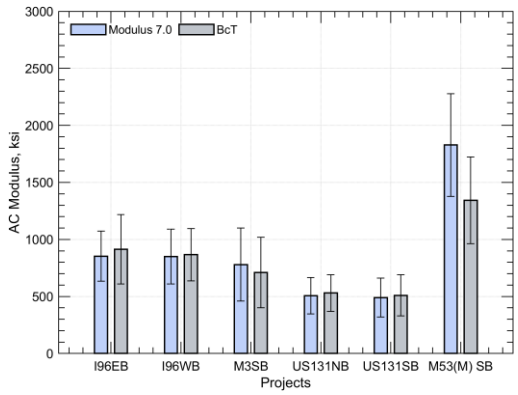
showed little change, though minor variability was observed across projects. The aggregate base + subbase (B+SB) layer displayed negligible variation in modulus between pre- and post-overlay conditions. In project US131NB, the modulus shifted only from 42 ksi to 43 ksi with MODULUS 7.0 and from 30 ksi to 32 ksi with BcT, indicating minimal effect. Subgrade moduli also remained stable in both methods with only slight fluctuations, further demonstrating that overlay treatments did not alter subgrade behavior. Average RMSE values ranged from 0.55 to 1.77 mils, reflecting acceptable backcalculation accuracy across analyses.

Figure 3-9 illustrates the comparison of pre- and post-overlay moduli for the four-layered analysis. Overall, the results reinforce that overlay treatments substantially increase AC layer stiffness, while the PCC base, B+SB, and subgrade layers remain essentially unchanged.

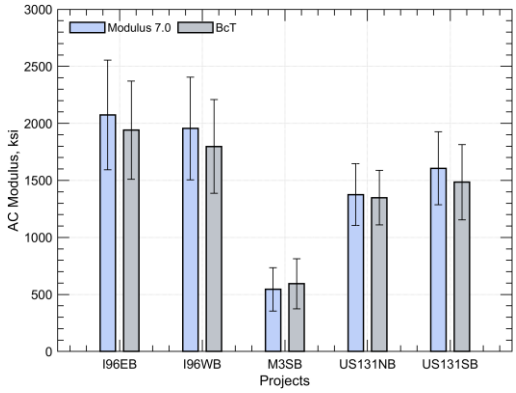
Subgrade Modulus (MR)

The team analyzed six composite pavement sections using the methods explained in the methodology section above. The underlying concrete slabs influenced the response, contributing to relatively high subgrade moduli. In addition to the four methods used for flexible pavements, the team employed the reduced AREA method for composite sections to backcalculate the subgrade MR. BcT and the Boussinesq solution produced subgrade moduli in the 10-15 ksi range, while the Outer AREA Method yielded consistent values with lower variability across the testing limits. Both the Outer AREA Method and MODULUS 7.0 estimated subgrade moduli in the 5-10 ksi range. Because no laboratory testing characterized the unbound layers in this project, the comparisons relied entirely on backcalculated values. Figures 3-10 and 3-11 illustrate the spatial variability and the statistical comparison of subgrade moduli across all methods.

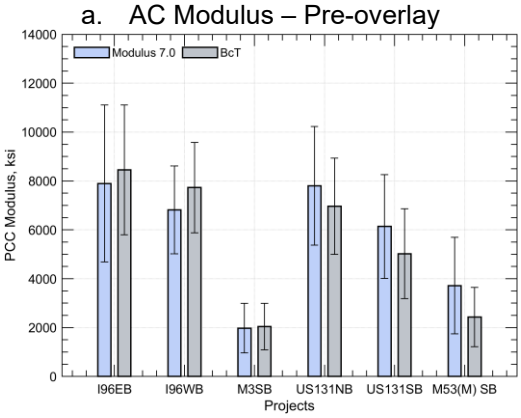
Overall, BcT and the Boussinesq solution provided the most reliable estimates for composite pavement subgrade layers, while the Outer AREA Method offered stable results with reduced variability.



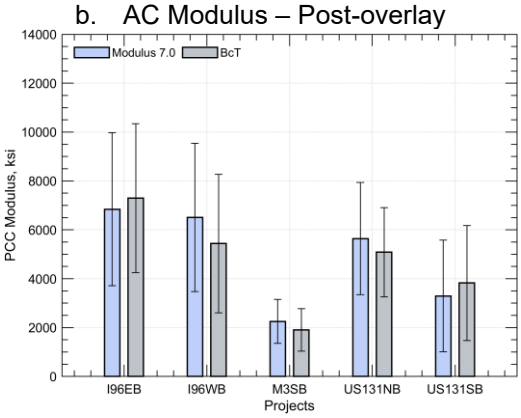
a. AC Modulus – Pre-overlay



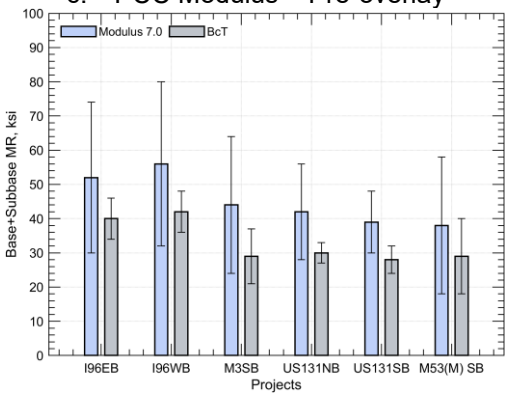
b. AC Modulus – Post-overlay



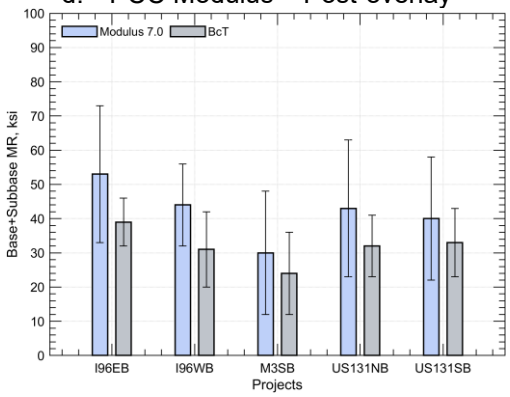
c. PCC Modulus – Pre-overlay



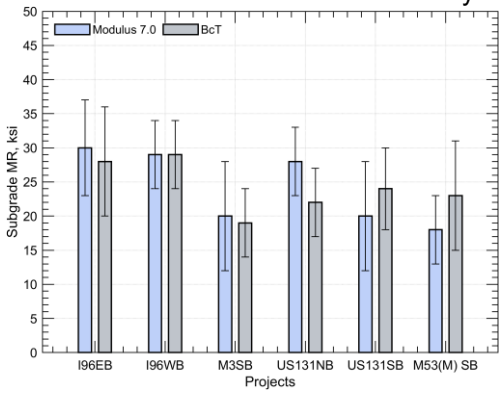
d. PCC Modulus – Post-overlay



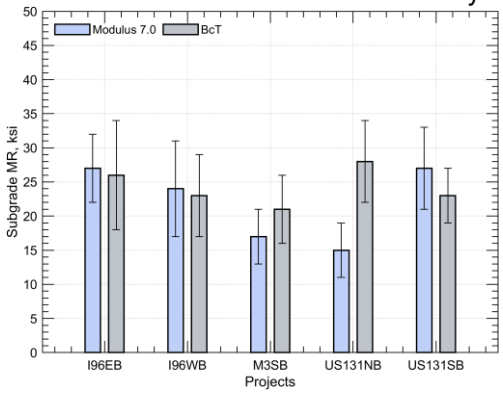
e. Base+Subbase MR – Pre-overlay



f. Base+Subbase MR – Post-overlay

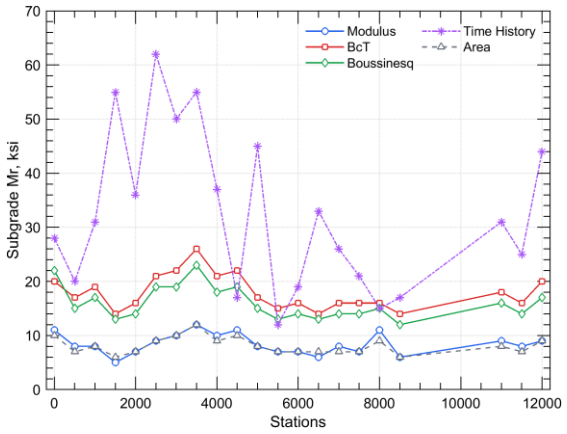


g. Subgrade MR – Pre-overlay

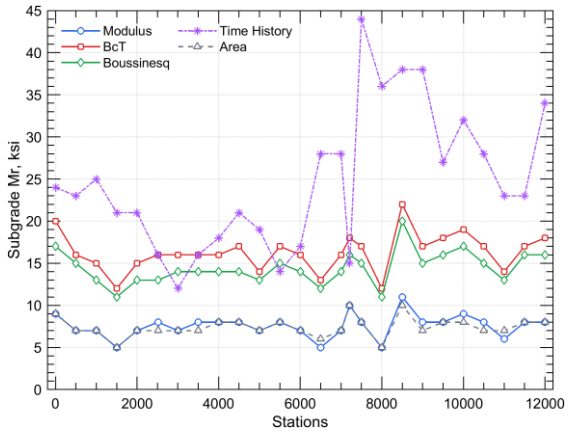


h. Subgrade MR – Post-overlay

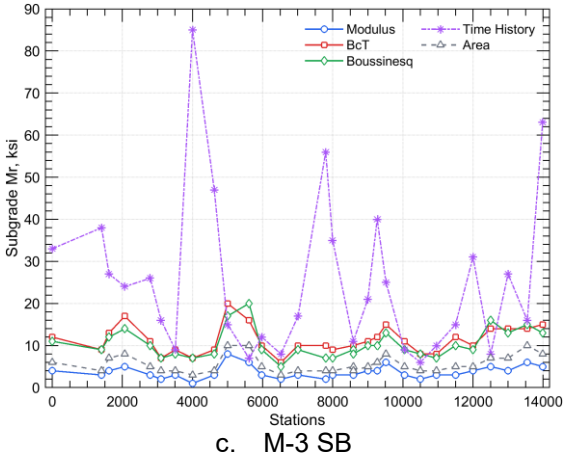
Figure 3-9 Pre- and post-overlay results for composite pavements – 4-layered



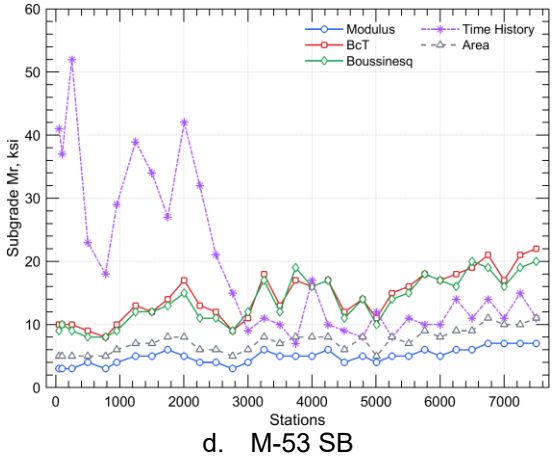
a. I-96 (Grand) EB



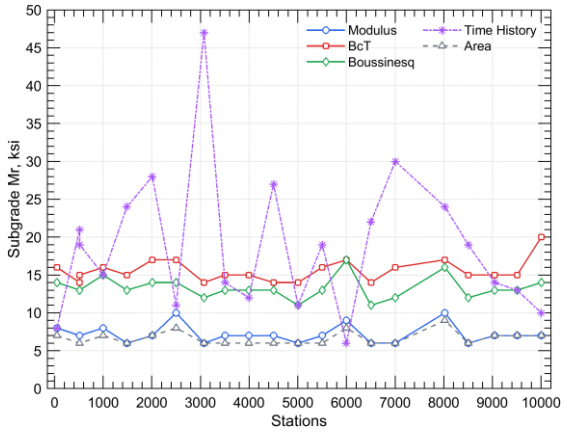
b. I-96 (Grand) WB



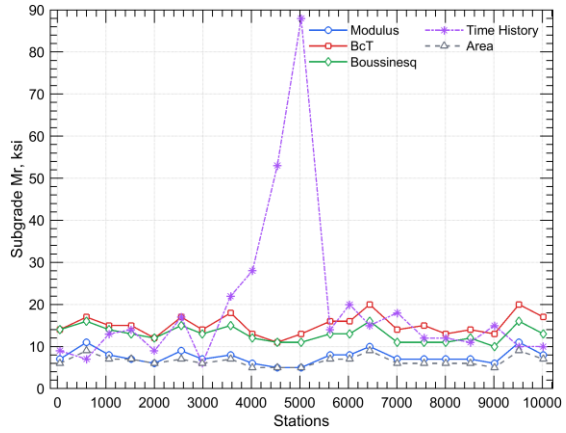
c. M-3 SB



d. M-53 SB



e. US-131 NB



f. US-131 SB

Figure 3-10 Comparison of Backcalculated subgrade moduli for asphalt pavements

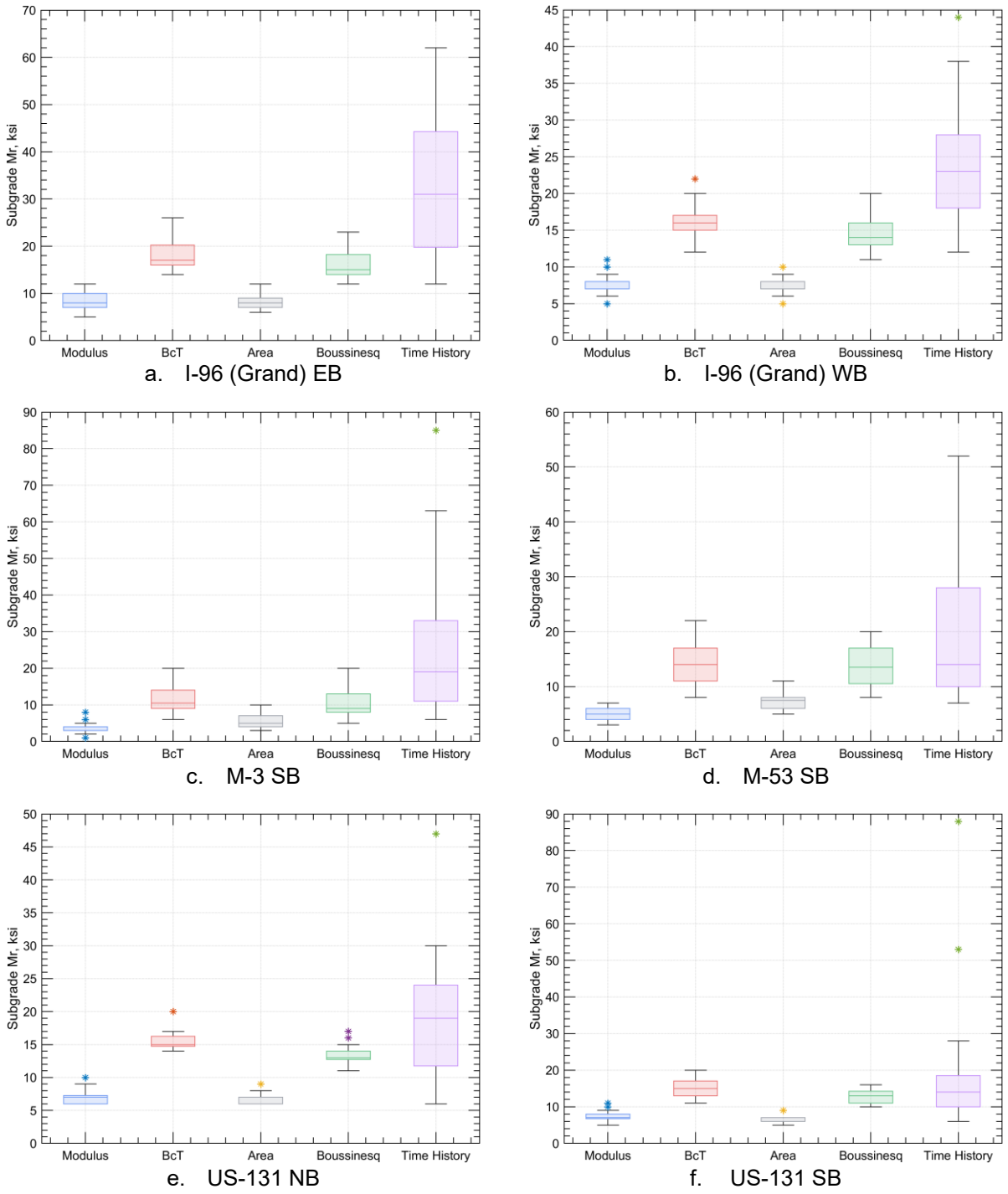


Figure 3-11 Statistical comparison of backcalculation methods for composite pavements

3.2.1.3. Summary

This section presents the key findings and recommendations based on the backcalculation results discussed above.

Findings

The analysis provided clear insights into pavement layers' response under overlays and the performance of different backcalculation methods:

- FWD backcalculation achieved strong convergence, with 75% of tests converging under pre-overlay conditions and 74% under post-overlay conditions for flexible pavements. For composite pavements, convergence rates reached 69% pre-overlay and 66% post-overlay.
- Overlays increased the AC modulus across all sections, confirming the surface stiffening effect of rehabilitation treatments.
- PCC layers in composite sections showed minimal change in modulus, indicating stable performance before and after overlay.
- The base, subbase, and subgrade layers displayed only minor variations in stiffness, suggesting a limited influence of overlays on the deeper layers.
- MODULUS 7.0 and BcT produced consistent results for the moduli of existing layers.
- BcT and the Boussinesq solution provided the most reliable subgrade moduli, while the reduced AREA method tended to overestimate PCC stiffness and underestimate subgrade response.
- A three-layered analysis adequately represented overlays on intact pavements but combined unbound layers, thereby limiting characterization of individual layers.
- A four-layered analysis separated base and subbase responses, captured the effect of C&S layers, and provided direct moduli for the unbound layers (base, subbase, and subgrade) required by PMED.

Recommendations

Based on these findings, the following practices are recommended for MDOT's backcalculation and design input selection:

- Adopt the four-layered backcalculation approach as the standard practice to characterize all existing layers individually.
- Use BcT or MODULUS 7.0 for backcalculating layer moduli; the Boussinesq solution can also serve as a quick check for subgrade MR.
- Avoid relying on the reduced AREA method for rehabilitation design, as it tends to overestimate PCC stiffness and underestimate subgrade response.
- Apply the 15th percentile values of backcalculated AC moduli, rather than mean values, to address spatial variability and provide conservative, field-representative PMED inputs.

3.2.2 Light Weight Deflectometer Testing

LWD data were collected on C&S and rubblized PCC projects, as summarized in Table 3-20. The force applied by the LWD at each drop was obtained using Equation 3-14. Boussinesq's elastic half-space equation was used to determine the elastic modulus values using Equation 3-15 (*11*).

Table 3-20 Summary of the available LWD data

Project	DGAB	Subbase	OGDC	Subgrade	C&S HMA base	Rubblized PCC base
I-75 BL NB	×	×	×	×	✓	×
I-75 BL SB	×	×	×	×	✓	×
M-91 NB	×	×	×	×	✓	×
US-41 NB	×	×	×	×	✓	×
I-96 (Univ.) EB	×	×	×	×	×	✓

Note: ✓ data available, × data not available, or layer not part of the structure, DGAB = Dense-graded aggregate base, OGDC = Open-graded drainage course.

$$F_{LWD} = \sqrt{2mghC} \tag{3-14}$$

where;
F_{LWD} = force applied by the LWD equipment (lbf)
m = dropped mass (lb)
g = acceleration due to gravity (32.2 ft/s^2)
h = drop height (ft)
C = spring constant (2.07x10^6 lbs/ft)

$$E_{LWD} = \frac{(1 - v^2)\sigma_0 r}{d_0} f \tag{3-15}$$

where;
E_{LWD} = LWD elastic modulus (ksi)
v = Poisson's ratio [0.35 and 0.40 for tests performed on base and subgrade layers, respectively];
σ_0 = applied stress (psi)
r = radius of the plate (in.)
d_0 = average deflection (in.)
f = shape factor [8/3 (rigid plate on granular material) and π/2 (rigid plate on material with intermediate characteristics) for tests performed on base and subgrade layers, respectively].

Table 3-21 summarizes the LWD-based resilient modulus results for four C&S projects and one rubblized concrete project, including the average, variability, and range of measured values. Figure 3-12 presents the corresponding boxplots, illustrating the spatial variability of LWD-measured moduli within each project along its length.

Table 3-21 LWD-based layer moduli

Project	Layer	No. of tests	Average (psi)	Standard Deviation (psi)	Minimum (psi)	Maximum (psi)
I-75 BL NB	C&S	16	6,538	975	4,702	8,018
I-75 BL SB	C&S	16	7,920	1,825	4,982	10,261
M-91 NB	C&S	12	9,205	1,076	7,220	11,100
US-41 NB	C&S	5	13,126	3,754	7,079	17,358
I-96 (Univ.) EB	Rubblized	38	8,803	1,848	4,930	12,599

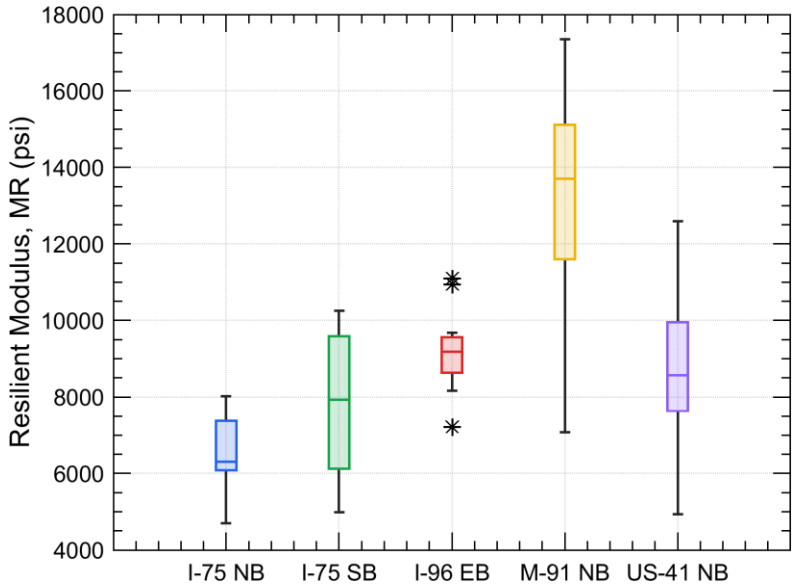


Figure 3-12 Comparison of LWD-based resilient moduli

The C&S sections (I-75 NB, I-75 SB, M-91 NB, and US-41 NB) exhibited MR values ranging from about 4,700 psi to 17,000 psi, with medians generally between 7,500 psi and 9,500 psi. The distributions for I-75 NB and I-75 SB were relatively narrow, while M-91 NB and US-41 NB showed broader spreads, reflecting greater field variability. The rubblized section on I-96 EB (University) showed values in a similar range, with several results extending beyond 11,000 psi. Some of the observed variability, especially in projects with fewer tests, likely stems from the limited number of field measurements and localized material differences.

The LWD-derived MR values for the C&S and rubblized layers ranged from about 4,700 psi to 17,000 psi, with medians generally between 7,500 psi and 9,500 psi. These values were consistently lower than those backcalculated from FWD, reflecting LWD's tendency to underpredict modulus relative to laboratory or analytical methods. Nevertheless, the results captured the relative stiffness trends across sections and highlighted spatial variability, particularly in projects with fewer test points. Previous studies have reported similar findings, noting that LWD provides reliable relative measures of stiffness and uniformity, but should be applied primarily as a field QA tool for unbound and processed layers rather than as a direct source of design-level modulus inputs (*12-14*).

3.2.3 Ground Penetrating Radar Testing

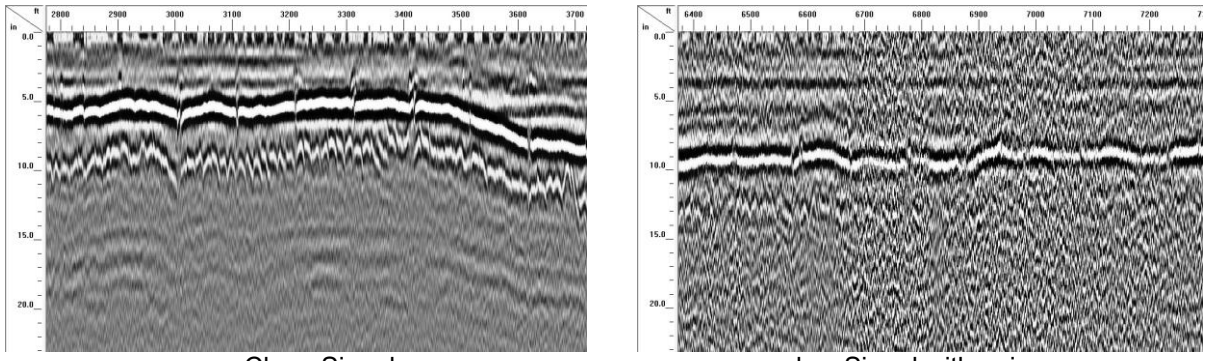
MDOT provided GPR data from six projects to compare GPR-recorded layer thicknesses with field-core measurements. MDOT analyzed the GPR data and provided results for all projects. Table 3-22 summarizes the GPR-recorded thicknesses and field-core thicknesses for AC/PCC layers.

Table 3-22 GPR vs. field cores thickness comparison for AC/PCC layers

Project	Station	HMA Cores (in.)	HMA GPR (in.)	HMA Difference (in.)	PCC Cores (in.)	PCC GPR (in.)	PCC Difference (in.)
I-96 (Grand) EB	648+54	7.25	8.98	1.73	9.00	N/A	N/A
I-96 (Grand) EB	648+64	7.50	9.01	1.51	9.00	N/A	N/A
I-96 (Grand) WB	645+00	7.00	7.75	0.75	9.00	3.30	-5.7
I-96 (Grand) WB	644+90	6.50	7.59	1.09	9.00	3.54	-5.46
I-96 (Grand) WB	603+00	4.25	5.30	1.05	9.00	N/A	N/A
M-84 SB	168+86	6.50	7.37	0.87	N/A	N/A	N/A
M-84 SB	128+96	12.00	14.66	2.66	N/A	N/A	N/A
M-84 SB	128+96	13.25	14.66	1.41	N/A	N/A	N/A
M-84 SB	90+76	9.65	14.34	4.69	N/A	N/A	N/A
M-117 NB	372+50	6.50	8.96	2.46	N/A	N/A	N/A
M-117 NB	329+00	8.45	10.07	1.62	N/A	N/A	N/A
M-117 NB	317+00	8.00	11.73	3.73	N/A	N/A	N/A
M-117 NB	278+00	8.75	9.92	1.17	N/A	N/A	N/A
M-117 SB	372+50	7.00	9.75	2.75	N/A	N/A	N/A
M-117 SB	329+00	8.00	10.84	2.84	N/A	N/A	N/A
M-117 SB	317+00	6.50	11.81	5.31	N/A	N/A	N/A
M-117 SB	278+00	6.50	11.54	5.04	N/A	N/A	N/A
US-10 EB	25+75	12.25	12.26	0.01	N/A	N/A	N/A
US-10 EB	45+75	11.75	2.35	-9.4	N/A	N/A	N/A
US-10 EB	45+80	12.00	2.09	-9.91	N/A	N/A	N/A
US-10 EB	66+00	11.25	11.02	-0.23	N/A	N/A	N/A
US-23 NB	4078+00	7.35	8.01	0.66	N/A	N/A	N/A
US-23 NB	138+00	7.25	6.20	-1.05	N/A	N/A	N/A
US-23 NB	138+00	8.75	6.02	-2.73	N/A	N/A	N/A
US-23 NB	152+00	7.65	8.97	1.32	N/A	N/A	N/A

In asphalt pavement sections, GPR measurements generally aligned well with field cores, consistently capturing AC layer thickness with reasonable accuracy (*15-20*). In contrast, for composite pavements, the GPR results appeared less reliable, as a proper distinction between AC and PCC layers was not always possible. This limitation was largely due to noise in the GPR signal, moisture-induced attenuation, and a minimal dielectric contrast between adjacent layers, which made it difficult to interpret layer boundaries. Similar issues have been noted in previous studies, where GPR was

reported to perform reliably in asphalt pavements but less effectively in composite and rigid systems due to signal scattering and weak layer interfaces (*15, 21, 22*). Figure 3-13 shows the GPR record of I-96 (Grand), which is a composite pavement. The difference between clear-layer demarcation based on GPR and noisy signals is evident in the figures.



a. Clean Signal b. Signal with noise

Figure 3-13 GPR testing of I-96 (Grand) EB (composite pavement)

3.2.4 Traffic Speed Deflectometer Testing

The section summarizes the work conducted on the TSD and 3D GPR data analysis. It is important to note that the TSD analysis presented here was conducted only to demonstrate the potential applications of the technology using TSD data collected by MDOT and was not used in the rehabilitation design modeling or calibration in this study due to limited number of projects that do not represent the entire network of MDOT.

3.2.4.1. Objectives

This task aims to demonstrate the benefits of the TSD using data collected for MDOT. The scope of the analysis includes determining:

- The existing pavement layer thickness is based on the available 3DGPR collected during the TSD testing.
- Subgrade modulus variations with project length.
- Layer modulus (backcalculated using Evercalc for asphalt pavements and the area method for concrete and composite pavements).
- Effective and required structural number, remaining service life, and recommended overlay thickness (based on AASHTO 93).
- JPCP load transfer evaluation.
- Asphalt pavement stripping potential (requires 3DGPR data and analysis).

The following sections provide a summary of the projects, deflection data, and GPR results. A complete discussion on methodology, objectives, and their findings are presented in Appendix E.

3.2.4.2. Project Selection

Five projects, totaling approximately 30 miles, were identified for TSD and 3DGPR data analysis. The selected projects represent five pavement types: HMA over HMA, HMA over C&S, JPCP, HMA over rubblized concrete, and HMA full-depth. TSD and 3DGPR data, averaged over 0.01 miles, were obtained from MDOT (note: JPCP includes 5 cm spacing data). Table 3-23 presents the summary of the projects selected for TSD data analysis. The following sections present the results of the TSD data analysis.

Table 3-23 Project selection summary for TSD analysis

Project	From – To	Length, (mi)	Year of Construction	Pavement Type	Plan Thickness, (in.)	20-year ESALs*, (million)	3DGPR Data
I-69 EB	Church Rd to Genessee County Line	8.07	1992	HMA overlay	• HMA – 6.5 to 7.5 • PCC – 9 • Aggregate Base – 3 • Subbase - 14	15.80	No
US-131 NB	Mecosta County Line to 6 Mile Road	6.04	2014	HMA over C&S	• HMA – 4.0 to 6.0 • C&S – 5.5 • Aggregate base – 4 • Subbase - 18	10.30	No
US-131 NB	Cannonsville Road to M-46/ Edgar Rd	5.51	2012	JPCP	• JPCP – 10 • Open-graded base – 6 • Subbase - 10	16.90	Yes
US-131 SB	M-46/17 Mile Rd to Kent County Line	4.84	1999	HMA over rubblized concrete	• HMA – 6.0 • Rubblized – 7 • Aggregate Base – 4 • Subbase – 18	10.60	No
US-127 NB	Price Road to Wildcat Road	4.25	1995	HMA full depth	• HMA – 6.5 • Asphalt permeable base – 4 • Aggregate Base – 4 • Subbase – 24	8.20	Yes

* = Estimated future ESALs per initial date of TSD collection (2020 to 2024)

Since surface curvature index [difference between peak deflection and deflection at 12-inch sensor (SCI_{12})] is a function of the maximum deflection, similar spikes are noted at the same locations of increased maximum deflection. SCI_{12} has been used to quantify pavement structural condition and is described in (*23*).

- Good: $SCI_{12} \leq 1.6$
- Fair: $1.6 > SCI_{12} \leq 3.3$
- Poor: $SCI_{12} > 3.3$

Using these criteria, most projects are in good structural condition (Figure 3-14b). The existing pavement typically has less than 15% alligator cracking (Figure 3-14c). The

maximum deflection spikes do not necessarily correlate with locations of the higher percentage of alligator cracking.

3.2.4.3. I-69 EB HMA Overlay

TSD data collection was conducted on August 23, 2019. At the time of testing, the TSD was not equipped with a 3DGPR unit; therefore, the existing pavement layer thickness was not determined. Figure 3-14 illustrates the maximum deflection, SCI_{12} (defined as the maximum deflection [D_0] minus deflection at 12 inches [D_{12}]), and the total alligator cracking over the project length. The circles represent the measurements for all the figures, while the solid line represents the moving average. For most of the project, the maximum deflection ranges from 4 to 8 mils with increased deflections near chainage 1.85, 5.34, 7.28, and 8.58 (note: final analysis will include milepost locations) (Figure 3-14).

3.2.4.4. US-131 NB HMA Over C&S

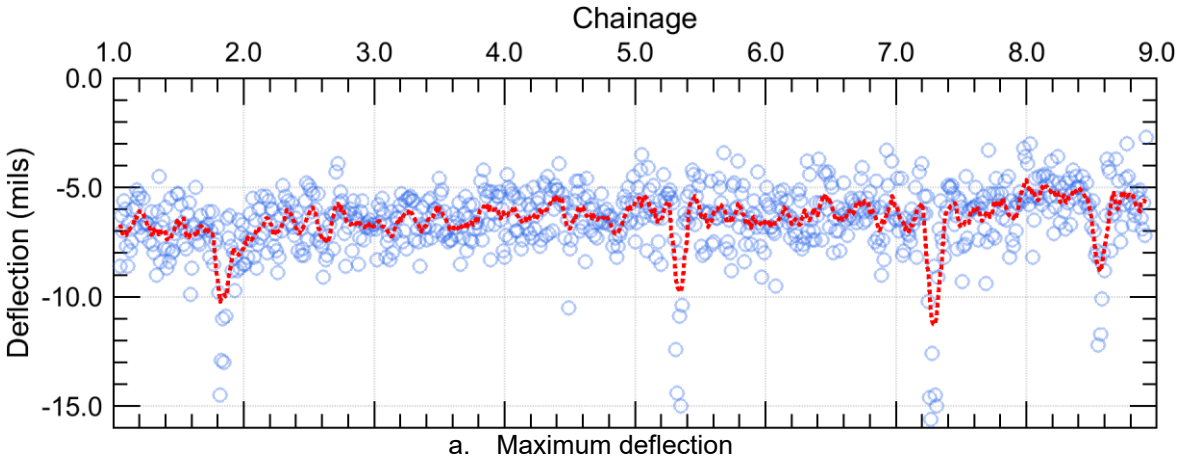
TSD data collection for this section of US-131 was conducted on November 9, 2022. 3D-GPR data were unavailable; therefore, the existing pavement layer thickness could not be determined. Most of the project's maximum deflection ranges from 4 to 8 mils (Figure 3-15a). Based on SCI12, most of the project length is in fair structural condition (Figure 3-15b). On average, the existing pavement has less than 3% alligator cracking (Figure 3-15c).

3.2.4.5. US-131 NB JPCP

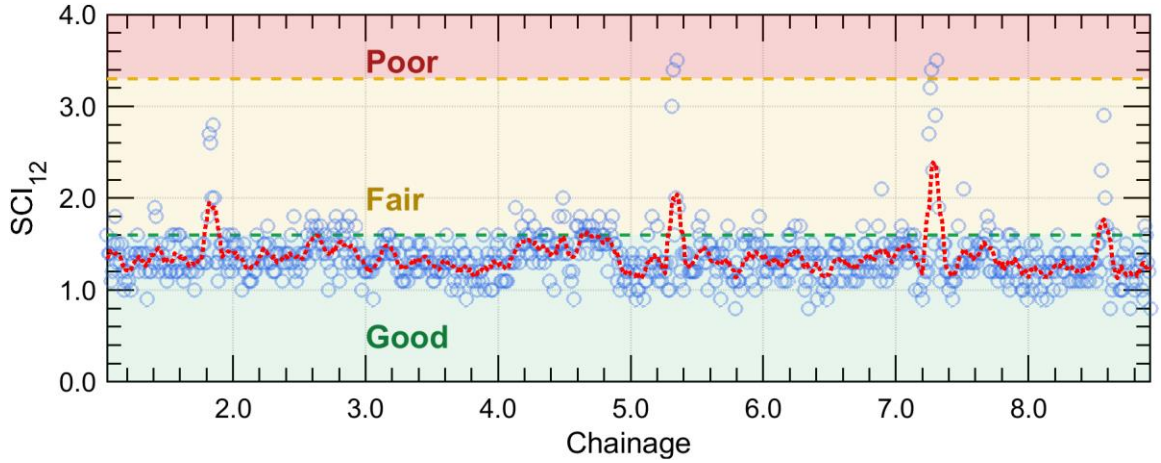
TSD and 3D-GPR data collection for this section of US-131 was conducted on November 9, 2022. Figure 3-16 summarizes the results of the 3D-GPR analysis. The first ½ mile of the project shows an asphalt layer ranging from 3.5 in. to 6.8 in. The remaining portion of the project shows a JPCP layer thickness ranging from 9 in. to 12.5 in. Most of the 3D-GPR results indicate a 10 in. to 11 in. JPCP layer.

3.2.4.6. US-131 SB HMA over Rubblized Concrete

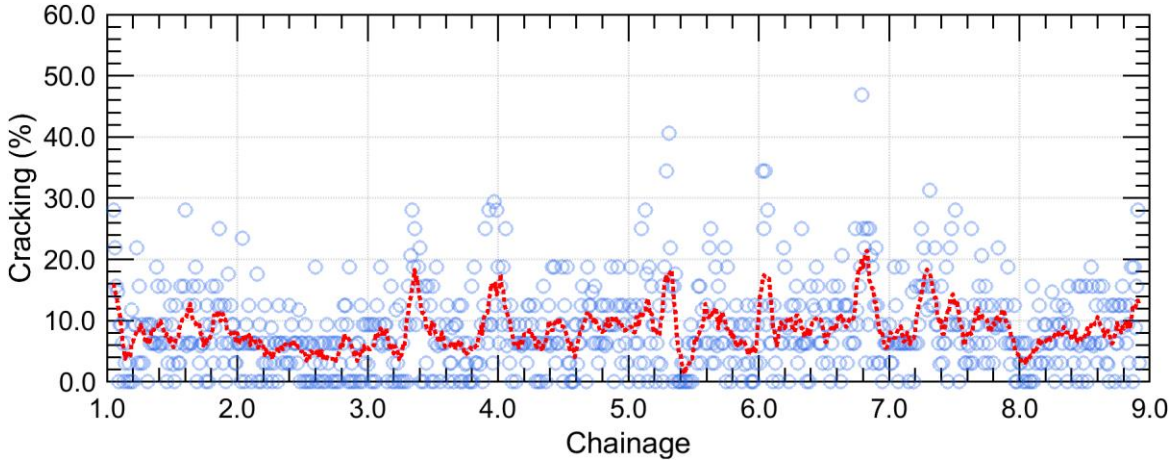
TSD data collection was conducted on November 8, 2022. 3D-GPR data were unavailable; therefore, the existing pavement layer thickness could not be determined. The first ¾ miles of the project appear to be a stiffer section, with deflections typically less than four mils. The remainder of the project has deflections typically ranging from 4 to 8 mils (Figure 3-17a). Comparatively, the project's beginning (and last mile) shows the pavement is in good structural condition, with much of the remaining project length being in fair structural condition (Figure 3-17b). On average, the existing pavement has less than 3% alligator cracking (Figure 3-17c).



a. Maximum deflection

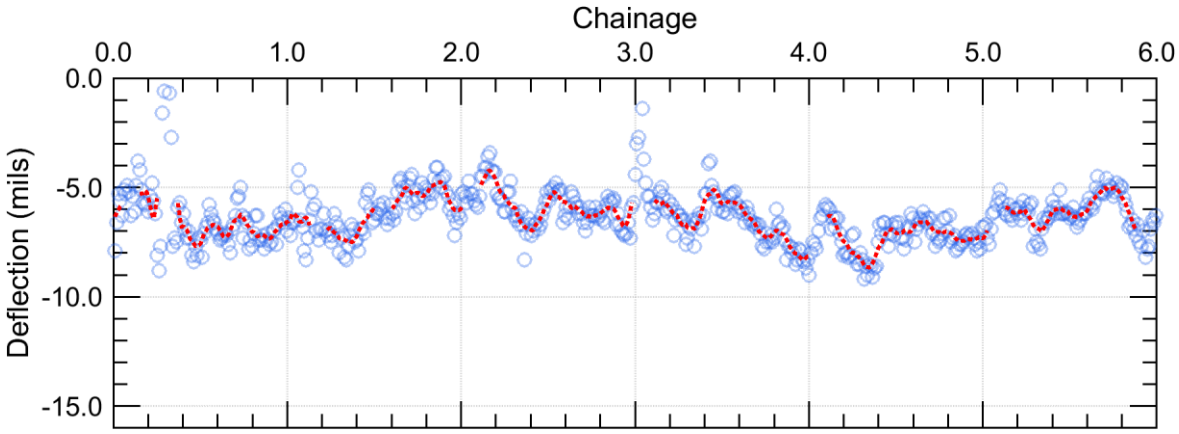


b. SC_{12}

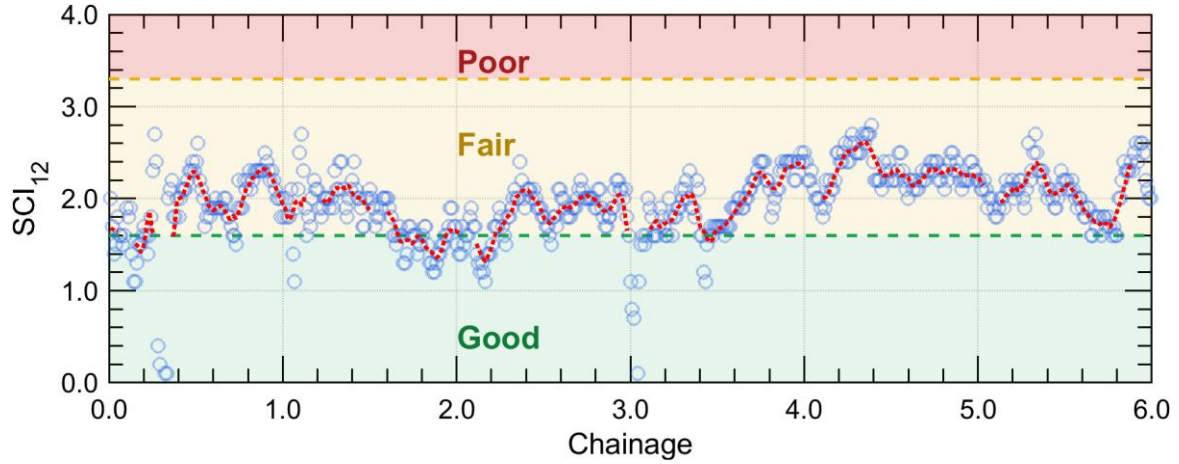


c. Percent alligator cracking (wheel paths)

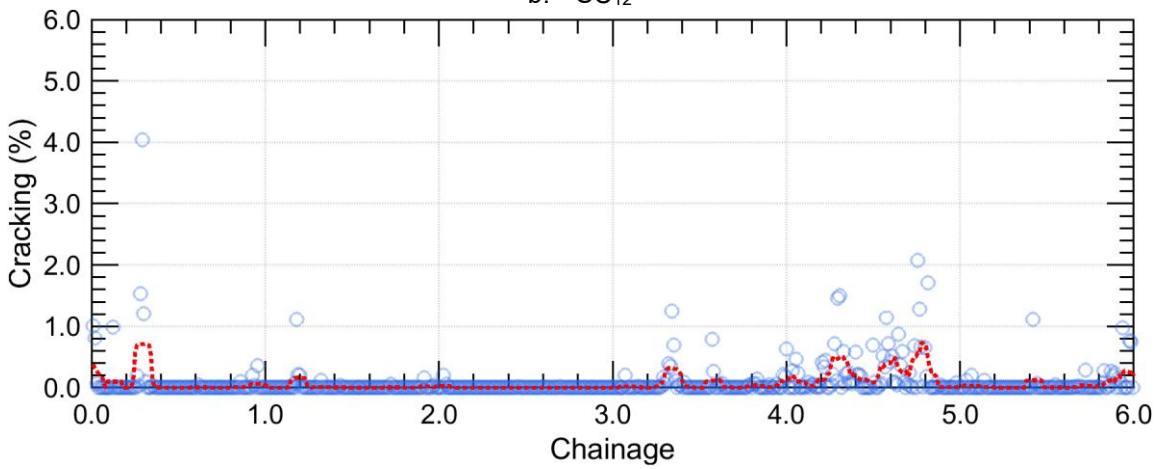
Figure 3-14 TSD analysis summary for I69EB HMA over HMA



a. Maximum deflection



b. SC_{12}



c. Percent alligator cracking (wheel paths)

Figure 3-15 TSD analysis summary for US131 NB HMA over C&S

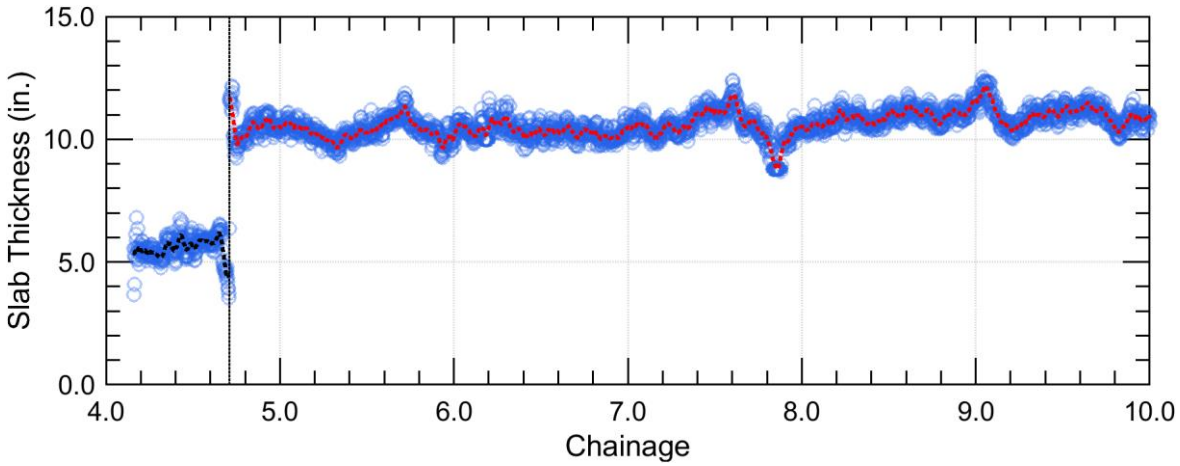
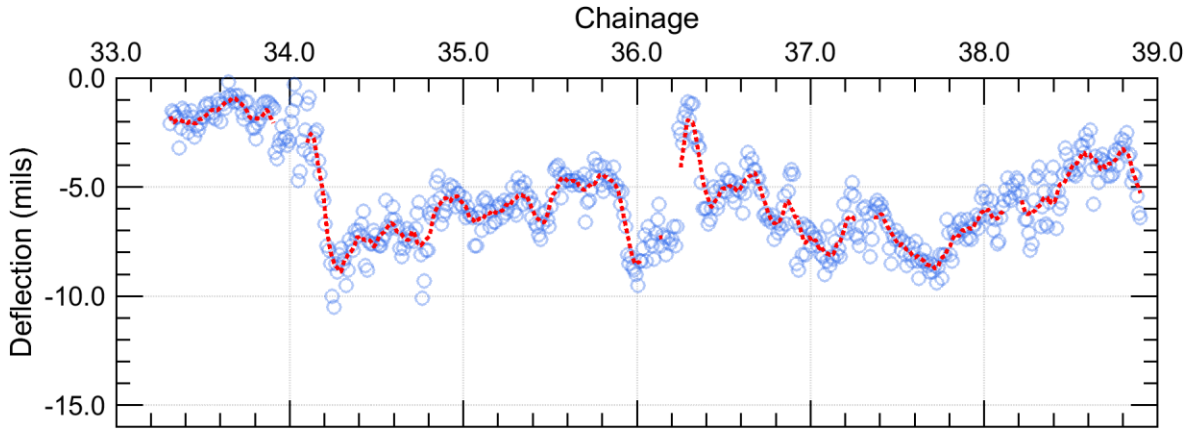


Figure 3-16 JPCP layer thickness US131 NB

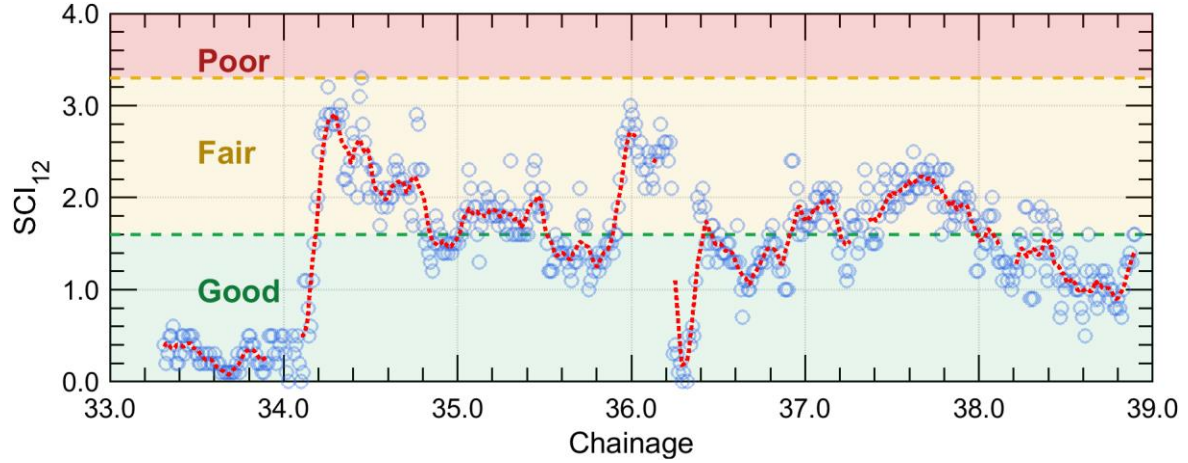
3.2.4.7. US127 NB Full-Depth HMA

TSD and 3D-GPR data collection for US-127 was conducted on November 13, 2022. Figure 3-17a summarizes the results of the 3D-GPR analysis. The determined thickness for the asphalt layer is relatively consistent over the project length, ranging from 7 to 9.1 in. The thickness of the asphalt permeable base varies between 1.7 in. and 5.2 in.

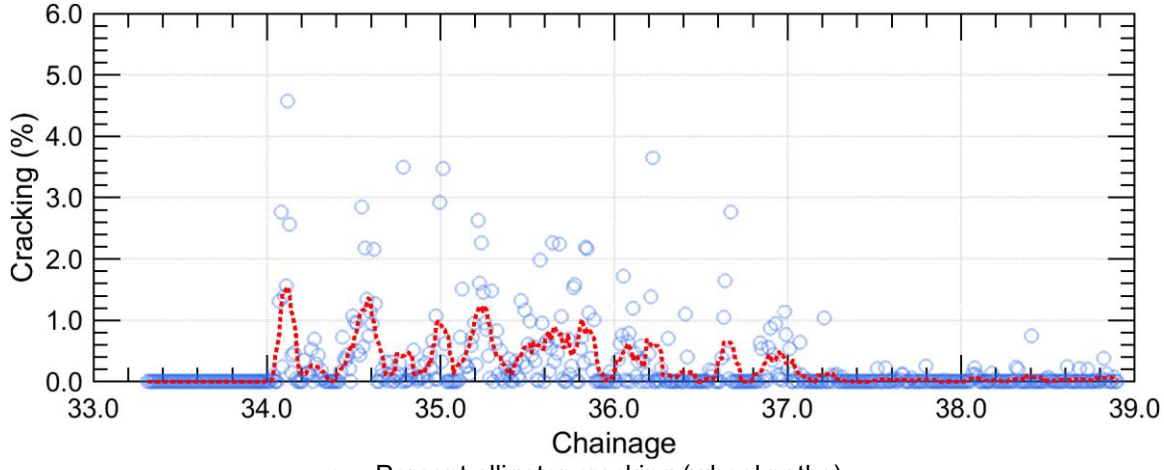
For most of the project, the maximum deflection is four mils or less, with a short section at the end of the project with slightly higher deflections (Figure 3-18b). Given the thickness of the existing pavement, the deflections are within the expected range. Most of the project length is in good structural condition (Figure 3-18c). On average, the existing pavement has less than 2% alligator cracking (Figure 3-18d).



a. Maximum deflection

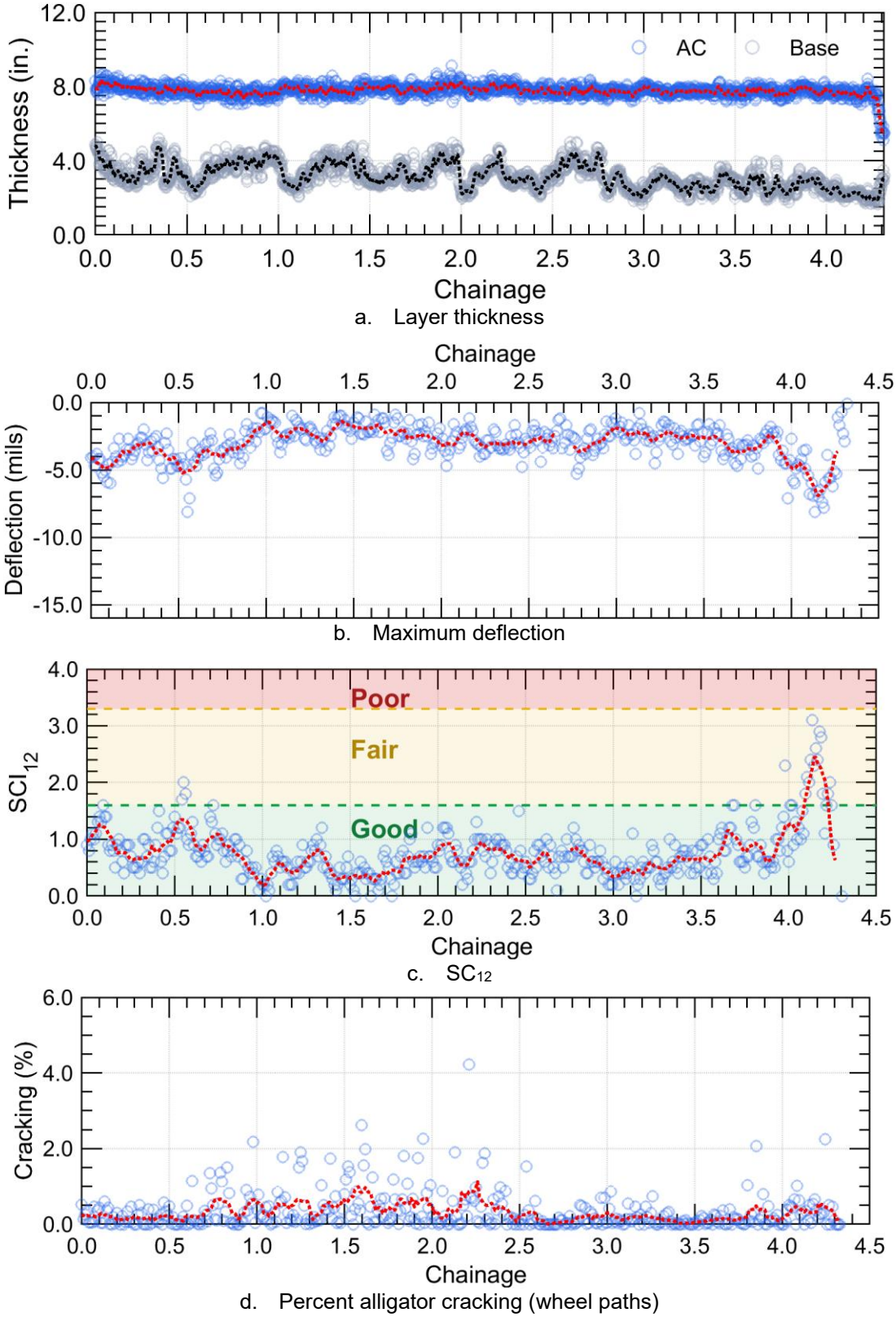


b. SC_{12}



c. Percent alligator cracking (wheel paths)

Figure 3-17 TSD analysis summary for US131 NB HMA over rubblized concrete



a. Layer thickness

b. Maximum deflection

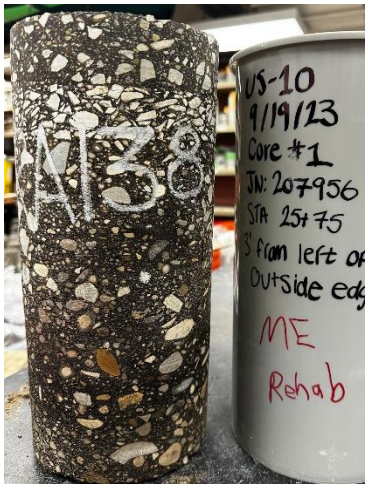
c. SC_{12}

d. Percent alligator cracking (wheel paths)

Figure 3-18 TSD analysis summary for US127 NB full-depth HMA

3.3 LABORATORY CHARACTERIZATION OF MATERIALS

MDOT provided pavement field cores from all construction-related projects. The material samples, including loose ASCRL mixtures, C&S materials for six projects, and rubblized PCC from one project, were also collected. Figure 3-19 shows field cores collected from full-depth HMAs and composite pavements. The existing pavement was constructed in the early 1960s to 1970s and overlaid with multiple asphalt layers over time. For characterization in the lab, these cores were treated as a single layer. Figure 3-20 shows the C&S and rubblized material collected for the selected projects.



(a) US-10 EB – field core



(b) US-131 NB – field core



(c) M-117 SB – field core



(d) I-96 (Grand) EB – field core

Figure 3-19 Field cores collected from full depth and a composite pavement



(a) US-10 EB – field material



(b) US-131 NB – field material



(c) M-117 SB – field material



(d) I-96 (Univ.) EB – field material

Figure 3-20 Collected C&S and rubblized material

3.3.1 HMA Material Testing

MDOT provided field cores from eleven projects. In addition, MDOT provided ASCRL loose-mix from two projects. This section summarizes the results of the HMA material testing. The cores were taken at 3- and 6-foot offsets from the lane/outer shoulder edge for the wheel path (WP) and non-wheel path (NWP) areas of the outer lane (truck lane), respectively. For laboratory testing requirements, cores thicker than 6 inches were cut to 4 inches in diameter and 6 inches in height. For cores that were either not intact or had a thickness of less than 6 inches, smaller samples were extracted from the original cores, resulting in test samples with a diameter of 1.5 inches and a height of 4.3 inches. Table 3-24 summarizes the number of tested samples (4- vs. 1.5-inch diameters) and their locations (WP vs. NWP). Figure 3-21 shows the samples extracted from field cores.

Table 3-24 Tested field core samples for damaged |E*| that have FWD data

Project	Direction	Pavement type	Standard Sample – WP	Standard Sample– NWP	Small Sample- WP	Small Sample– NWP
M-117	NB	Full-depth HMA	3	-	-	2
M-117	SB	Full-depth HMA	3	-	2	-
US-10	EB	Full-depth HMA	3	1	-	-
US-23	NB	Full-depth HMA	3	1	-	-
M-91	NB	Full-depth HMA	3	1	-	-
I-75 BL	NB	Full-depth HMA	2	2	-	-
M-53 (Bay)	NB	Full-depth HMA	2	1	-	-
M-53 (Bay)	NB	HMA over JPCP	-	-	2	-
M-3	NB	Full-depth HMA	3	-	2	-
M-3	SB	HMA over JPCP	-	-	4	2
M-84*	SB	HMA over JPCP	3	1	-	-
I-96 (Grand)	EB	HMA over JPCP	1	1	4	-
I-96 (Grand)	WB	HMA over JPCP	1	1	4	-
M-53 (Metro)	SB	HMA over JPCP	-	-	4	-
US-131	NB	HMA over JPCP	-	-	2	2
US-131	SB	HMA over JPCP	-	-	2	2
Total	**-**	**-**	**27**	**9**	**26**	**8**

* FWD was available on NB only.



(a) US10 EB – sample for |E*| testing



(b) US131 NB – sample for |E*| testing

Figure 3-21 Samples extracted from field cores for |E*| testing

Laboratory characterization of HMA material considered the following tests on the cores and laboratory compacted ASCRL samples from the loose mix received from the MDOT:

- Percent air voids (AASHTO T166)
- Dynamic Modulus (AASHTO PP60, AASHTO T312, AASHTO T342, AASHTO TP132-23, AASHTO R84)
- Binder content by Ignition (AASHTO T308)
- Sieve analysis (ASTM D5444)

3.3.1.1. Percent Air Voids

Air voids strongly affect HMA performance by directly influencing the dynamic modulus. Previous studies confirm that a higher percentage of air voids (AV) reduces dynamic modulus and stiffness under design loading. Studies have found that increasing the percentage of air voids significantly lowers the dynamic modulus and affects the performance of HMA mixtures (*24-29*).

The theoretical maximum specific gravity (Gmm) values for the mix were obtained from job mix formulas (JMFs) for the existing layers (where available). Since the existing pavements were constructed in the late 1960s, JMFs were not available for most projects. In such cases, MDOT specification books and averages were used. The bulk specific gravity (Gmb) of the asphalt mixture in field cores was determined in accordance with AASHTO T166. The percent air voids was calculated using the conventional relationship (Equation 3-16). Figure 3-22 shows the comparison of mean %AV for WP and NWP samples.

$$\% \text{ AV} = \left(1 - \frac{G_{mb}}{G_{mm}}\right) \times 100 \qquad (3\text{-}16)$$

For the ASCRL layers, which are binder-rich, intentionally porous mixes placed over existing concrete to mitigate reflective cracking, the laboratory specimens were prepared with a target air-void content of 15–20%. These levels were selected to replicate field conditions and were used for subsequent dynamic modulus testing.

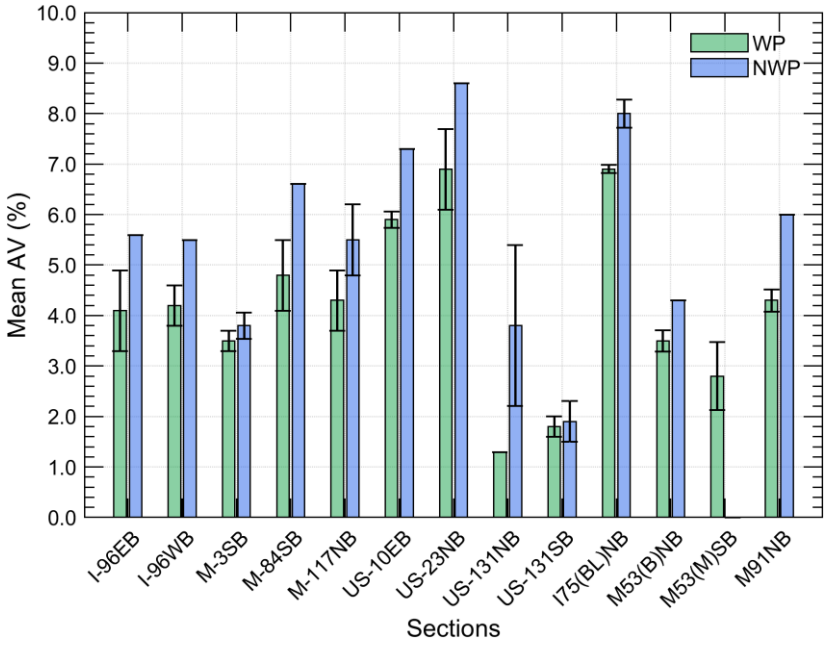


Figure 3-22 Comparison of mean percent air voids for WP and NWP samples

3.3.1.2. Dynamic Modulus

Dynamic modulus testing was conducted to characterize the stiffness of the field cores at different temperatures and loading frequencies, in accordance with AASHTO T342. The average of three replicates was used to generate the dynamic modulus master curves, per AASHTO R84. Each replicate was tested in uniaxial compression mode at temperatures of 4, 20, and 40°C (the highest temperature for ASCRL was 35°C) and loading frequencies of 10, 1.0, 0.5, and 0.1 Hz. Table 3-25 provides descriptive statistics (mean, standard deviation, and coefficient of variation) for a representative project (I-96 EB, Grand) to demonstrate the repeatability and quality of the laboratory-measured damaged dynamic modulus results. All tested sections showed acceptable data variability, with coefficient of variation (CoV) values below 30%, consistent with standard expectations for HMA materials.

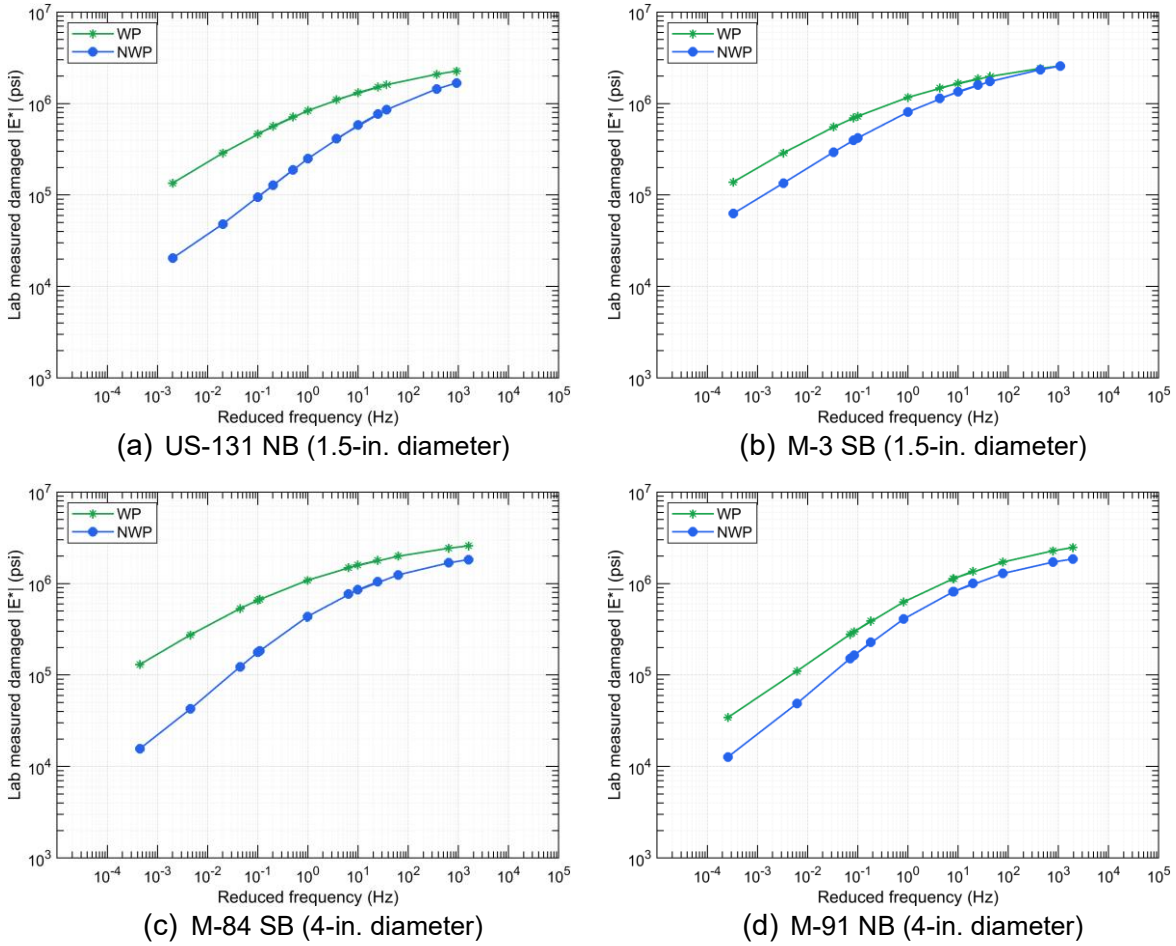
Table 3-25 Summary of damaged dynamic modulus

Temperature (C)	Frequency (Hz)	Sample 1 (psi)	Sample 2 (psi)	Sample 3 (psi)	Mean (psi)	Standard Deviation (psi)	Coefficient of Variation
4.0	10	1,843,723	2,094,349	1,857,067	1,931,713	141,004	7.3%
4.0	1	1,371,479	1,476,922	1,394,105	1,414,168	55,510	3.9%
4.0	0.1	841,365	945,648	921,716	902,909	54,626	6.0%
20.0	10	902,862	971,900	837,304	904,022	67,305	7.4%
20.0	1	482,832	481,671	483,267	482,589	825	0.2%
20.0	0.1	204,359	194,496	220,748	206,534	13,261	6.4%
40.0	10	208,565	167,229	228,000	201,265	31,037	15.4%
40.0	1	68,734	49,922	81,076	66,577	15,689	23.6%
40.0	0.1	21,930	15,084	26,585	21,200	5,786	27.3%
40.0	0.01	9,645	8,064	10,356	9,355	1,173	12.5%

Laboratory-measured damaged dynamic modulus values were compared for the WP and NWP cores. The WP cores exhibited higher modulus values at higher temperatures. Figure 3-23 presents the laboratory-measured damaged dynamic modulus curves for WP and NWP cores for four example sections, using 4-inch and 1.5-inch diameter samples. The results from other cores follow the same trend. WP cores exhibited 1.0 to 1.5 times higher damaged dynamic modulus values than NWP cores, with variations depending on temperature and frequency, except for US-131 NB and M-84 SB. Figures 3-24a and 3-24b illustrate the laboratory-measured damaged dynamic modulus ratios for WP to NWP cores on US-131 NB and M-91 NB, along with a histogram of all project ratios.

The higher damaged dynamic modulus values observed in WP cores could be attributed to long-term compaction resulting from traffic loading. While the PMED assumes that damage occurs in WP due to traffic loading, it is also found that traffic loading can induce densification. This densification is evident in WP cores, as indicated by their lower air-void percentages (Figure 3-22). The absence of visible damage in the cores and the lower percent air voids likely account for the observed higher dynamic modulus values. However, it is essential to note that the PMED framework does not explicitly account for this field densification effect when estimating damaged dynamic

modulus master curves. This comparison between WP and NWP cores highlights a potential limitation in PMED rehabilitation input modeling.



(a) US-131 NB (1.5-in. diameter)

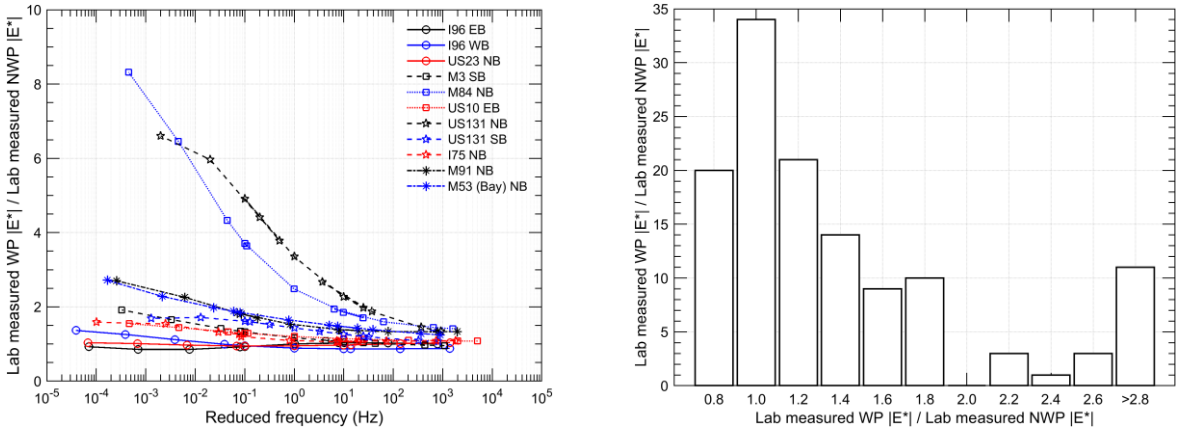
(b) M-3 SB (1.5-in. diameter)

(c) M-84 SB (4-in. diameter)

(d) M-91 NB (4-in. diameter)

Figure 3-23 Laboratory-measured damaged |*E**| comparison for WP and NWP cores

Three replicates from the ASCRL loose mix were compacted to characterize the dynamic modulus. Figure 3-25 shows the gyratory compacted sample, cylindrical specimen for testing, and the dynamic modulus master curve based on three replicate samples.



(a) |*E**| ratio for WP vs. NWP cores (b) WP vs. NWP ratio for all projects

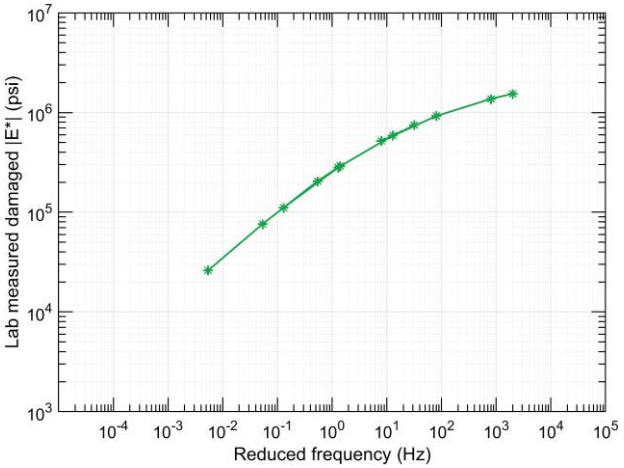
Figure 3-24 Laboratory-measured damaged |*E**| ratios for WP and NWP cores



(a) ASCRL – gyratory compacted sample



(b) 4in. x 6-in. cylinder for |E*| testing

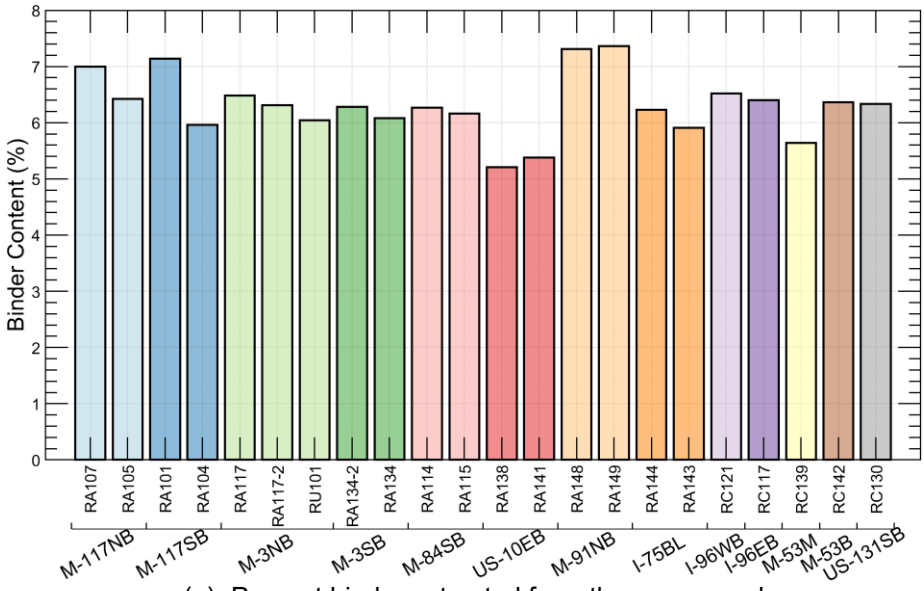


(c) ASCRL |E*| master curve

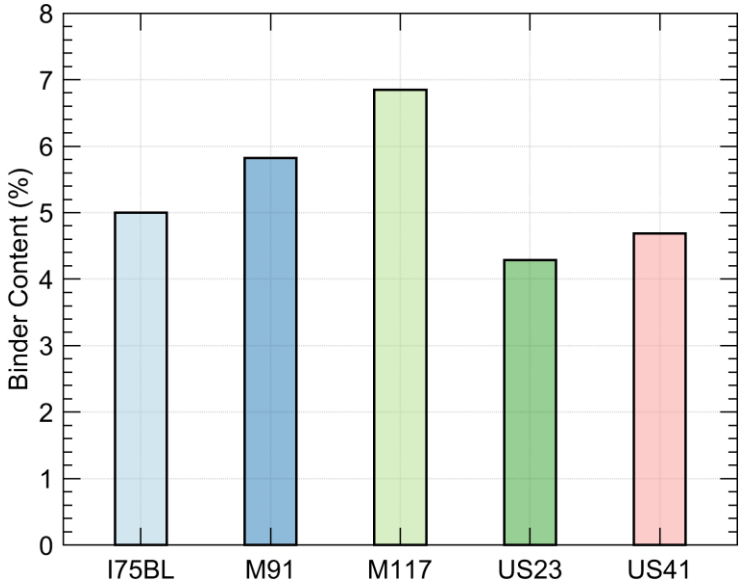
Figure 3-25 ASCRL laboratory testing results for |E*|

3.3.1.3. Binder Content by Ignition

Binder ignition testing was conducted on all field cores and C&S samples in accordance with AASHTO T308 to determine asphalt binder content. This test provided essential material characterization, as the binder content of the existing HMA layer serves as a direct input in PMED rehabilitation design. The team quantified the bitumen fraction by igniting the specimens and measuring the resulting mass loss. These measurements supported volumetric analysis and ensured the laboratory characterization of existing mixtures aligned with PMED requirements. Figures 3-26a and 3-26b show the percentage of binder extracted from the field cores and the C&S samples, respectively.



(a) Percent binder extracted from the core samples



(b) Percent binder extracted from the C&S material

Figure 3-26 Summary percent binder extraction

3.3.1.4. Sieve Analysis of Extracted Aggregates

Mechanical sieve analysis was conducted on the extracted aggregates from cores and the C&S material per ASTM D5444. Table 3-26 shows the percentage of passing extracted aggregate from all cores. Table 3-27 summarizes the gradation of extracted aggregate from the C&S material.

Table 3-26 Percent passing of extracted aggregate from cores after ignition

Sieve Number	I-96 Grand	I-75 BL	M-3	M-84	M-117	US-10	M-91	US-131	M-53 Metro	M-53 Bay
1 1/2"	100.0	100.0	100.0	100.0	100.0	100.0	100.0	100.0	100.0	100.0
1"	100.0	100.0	100.0	100.0	100.0	100.0	100.0	100.0	100.0	100.0
3/4"	100.0	99.0	97.4	98.1	100.0	97.5	100.0	100.0	100.0	100.0
1/2"	97.6	89.0	89.7	87.1	93.1	95.7	94.6	92.0	98.8	98.8
3/8"	90.9	80.4	82.1	79.4	84.3	88.4	87.3	76.9	92.6	91.0
#4	69.7	59.7	63.9	62.4	63.6	69.3	63.2	53.7	70.5	74.0
#10	47.9	46.1	48.1	48.1	45.0	51.9	41.0	36.3	41.8	41.0
#20	33.7	37.0	35.7	37.2	32.3	40.8	29.2	26.4	26.4	25.0
#40	23.5	19.6	24.2	26.6	19.8	27.2	19.1	18.1	16.7	18.0
#100	9.9	2.9	9.0	6.9	3.6	6.1	3.3	6.7	5.7	5.0
#200	6.2	1.5	5.6	2.5	1.4	4.2	1.5	5.3	3.2	4.0

Table 3-27 Percent passing of extracted aggregate from C&S material after ignition

Sieve Number	I-75 BL	M-91	M-117	US-23	US-41
1 1/2"	100.0	100.0	100.0	100.0	100.0
1"	100.0	100.0	100.0	98.8	100.0
3/4"	99.0	99.2	100.0	94.0	99.1
1/2"	92.0	91.5	96.6	86.0	94.5
3/8"	85.9	86.0	90.6	80.0	88.1
#4	73.9	69.3	73.3	63.0	70.9
#10	63.6	51.7	53.9	46.7	53.2
#20	54.9	34.2	40.8	36.7	38.9
#40	34.9	23.7	29.3	26.5	28.1
#100	8.2	8.2	11.3	9.2	11.7
#200	6.4	6.6	7.9	5.8	8.5

Sieve analysis was also attempted for the rubblized PCC material; however, as shown in Figure 3-20(d), the majority of the rubblized concrete pieces were retained on the 2-inch sieve, making standard mechanical sieve analysis in accordance with ASTM D5444 impractical.

3.3.2 PCC Material

To characterize the existing PCC layer, PMED requires compressive strength, elastic modulus, or MOR. The 4-in-diameter by 6-in-height samples were prepared from the cores to test for elastic modulus; however, due to equipment limitations, the tests were unsuccessful. Therefore, all the prepared samples from cores were tested against compressive strength using the "Forney" compression testing machine. The elastic modulus was estimated using the ACI equation (Equation 3-17). Table 3-28 presents the average compressive strength and elastic modulus results for each section.

$$\mathrm{E} = 57{,}000\sqrt{f_c'} \quad (3\text{-}17)$$

where;
E = elastic modulus of concrete.
f_c' = concrete compressive strength

Table 3-28 PCC core compressive strength results from composite pavements

Project	Direction	Total Cores	Core 1 (psi)	Core 2 (psi)	Core 3 (psi)	Average (psi)	Elastic Modulus (x10^6, psi)
I-96 (Grand)	EB	3	7,580	10,276	10,118	9,325	5.5
I-96 (Grand)	WB	3	9,072	8,070	7,675	8,272	5.2
M-3	NB	1	9,024	N/A	N/A	9,024	5.4
M-3	SB	2	10,122	11,202	N/A	10,662	5.9
US-131	NB	3	9,921	8,438	7,570	8,643	5.3
US-131	SB	3	8,726	10,463	8,692	9,294	5.5
M-53 (Bay)	NB	2	12,613	7,577	N/A	10,095	5.7
M-53 (Metro)	SB	3	6,610	9,440	9,160	8,403	5.2

Overall, for all sections, the average compressive strength is 9,215 psi, and the average elastic modulus is 5,500 ksi. The high compressive strength can be attributed to long-term strength gain (from continued cement hydration) and the reinforcement steel in the cores, as most of these cores are derived from JRCP. Figure 3-27 shows the testing machine and a few cores after destruction.

3.3.3 C&S Material

Laboratory testing of unbound material samples included five C&S materials collected from I-75BL, M-91, M-117, US-23, and US-41. Material testing included sieve analysis, binder extraction, and resilient modulus using field compaction data.

3.3.3.1. Resilient Modulus

The C&S material was treated as an aggregate base and tested for MR in the laboratory, in accordance with the standard specifications for the triaxial repeated-load test.

Material Testing System (MTS) 810

The team characterized C&S by MR to comprehend the materials' response to cyclic loading. The specimen preparation used field compaction and sieve analysis test results to prepare the samples. The materials were tested for MR using the MTS 810 testing equipment (Figure 3-28a).



a. Forney machine



b. Breaking point



c. Brittle failure



d. Presence of reinforcement

Figure 3-27 Concrete compressive strength testing

This setup features an external Linear Variable Differential Transformer (LVDT) to measure specimen deformation, a pressure control panel for confining pressure, and a computer-aided system to manage the applied cyclic loads. Specimens were prepared in six layers according to the gradation (Figure 3-28b). Each layer was thoroughly mixed and compacted at the field moisture content in a 6 in. diameter by 12 in. high mold, using a vibratory hammer (Figure 3-28c). The specimen after testing is shown in Figure 3-28d.

The MR tests apply 2,000 load cycles, including 500 during conditioning and 100 per sequence at five different confining pressures. Table 3-29 shows the five confining pressures, corresponding load cycles, and the number of sequences per cycle.



a. MTS 810



b. Ready to test the sample



c. Sample preparation mold



d. Sample after testing

Figure 3-28 Laboratory testing of C&S materials

Table 3-29 Testing sequences for base and subbase materials

Seq. No.	Confining Pressure (kPa)	Cyclic Stress (kPa)	No. of Load Applications
0	103.4	93.1	500–1000
1	20.7	18.6	100
2	20.7	37.3	100
3	20.7	55.9	100
4	34.5	31.0	100
5	34.5	62.0	100
6	34.5	93.1	100
7	68.9	62.0	100
8	68.9	124.1	100
9	68.9	186.1	100
10	103.4	62.0	100
11	103.4	93.1	100
12	103.4	186.1	100
13	137.9	93.1	100
14	137.9	124.1	100
15	137.9	248.2	100

The MR was calculated using a confining pressure of 35.0 kPa and a deviatoric stress of 103.0 kPa (*30*). The MR for each sequence was calculated by averaging the last five cycles of each testing sequence. The Witczak model was then used to calculate the predicted MR and to estimate the regression constant (*30*):

$$M_R = k_1 P_a \left(\frac{\theta}{P_a}\right)^{k_2} \left(\frac{\tau_{oct}}{P_a} + 1\right)^{k_3} \quad (3\text{-}18)$$

where:
P_a = atmospheric pressure.
k1, k2, and k3 are regression constants.
θ = bulk stress ($\theta = \sigma_1 + \sigma_2 + \sigma_3 = \sigma_1 + 2\sigma_3$)
$\sigma_1, \sigma_2, \sigma_3$ = principal stresses.
τ_{oct} = octahedral shear stress [$\tau_{oct} = \sqrt[1/3]{(\sigma_1 - \sigma_2)^2 + (\sigma_1 - \sigma_3)^2 + (\sigma_2 - \sigma_3)^2}$]

Results

Three replicate samples from each project were tested at 20 ºC. M-117 has the highest binder content, so two replicates were tested at 4 °C to see the effect of temperature on the C&S material. Table 3-30 summarizes the resilient modulus results for both projects. Figure 3-29 shows the measured and predicted resilient modulus values for all projects along a reference line.

Table 3-30 Summary of resilient modulus testing

Road	Sample	Confining pressure (kPa)	MR (ksi)	K_1	K_2	K_3	Temperature, C
M-117	1	35	18.00	6.62	0.69	-0.01	20
M-117	2	35	19.96	6.79	0.61	-0.02	20
M-117	3	35	18.75	6.7	0.69	-0.1	20
M-117	4	35	36.59	7.36	0.66	-0.02	4
M-117	5	35	39.07	7.49	0.63	-0.15	4
I-75	1	35	28.08	7.25	0.5	-0.15	20
I-75	2	35	26.89	7.16	0.53	-0.06	20
I-75	3	35	26.33	7.18	0.51	-0.08	20
M-91	1	35	28.9	7.28	0.49	-0.12	20
M-91	2	35	28.43	7.26	0.51	-0.14	20
M-91	3	35	26.41	7.16	0.52	-0.1	20
US-23	1	35	74.95	8.47	0.12	-0.04	20
US-23	2	35	72.65	8.38	0.18	-0.01	20
US-23	3	35	60.53	8.16	0.25	-0.03	20
US-23	4	35	71.74	8.37	0.2	-0.04	20

The average MR for US-23 is 75 ksi, and 26 ksi for the remaining projects. The following possible reasons can explain the difference between the projects:

- The US-23 material contains a large amount of virgin aggregate (Figures 3-20c). The large particle size directly affects stress distribution. Moreover, the US-23 material has a lower binder content than that of all other projects. US-23 material properties could be more inclined towards an unbound aggregate base.
- The M-117 project is in the Superior region, and the binder used in this project is less stiff than that used in US-23. The M-117 has a higher percentage of coarser particles, but overall, its particles are smaller than those of the US-23. Moreover,

after ignition, US-23 has the lowest percentage of finer materials of all the projects.

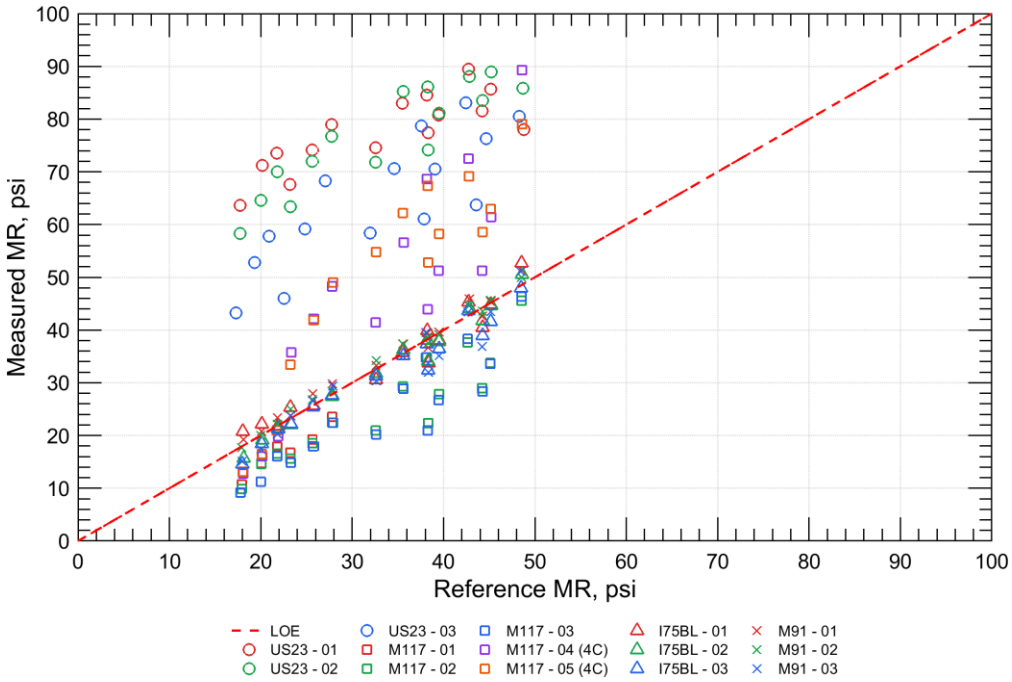


Figure 3-29 Resilient modulus summary

It is pertinent to note that in MTS, vertical displacement is measured by an actuator, which can lead to inaccurate results due to various factors (e.g., inaccurate load cell calibration or improper equipment setup). To verify the results, a dynamic testing system was used to measure the sample's actual displacement.

Dynamic Testing System (DTS-30)

Figure 3-30 illustrates the full testing setup of the DTS-30. Figure 3-30a shows the testing apparatus in the controlled testing chamber along with the computer control system. The specimens were placed in a triaxial chamber, which was enclosed to maintain confining pressure using compressed air (Figure 3-30b). After positioning the specimen in the triaxial chamber, two LVDTs were installed on a custom-built laboratory fixture to measure axial deformation (Figure 3-30c). LVDTs provide high-resolution, continuous strain measurements, enabling precise assessment of material stiffness and deformation behavior under load.

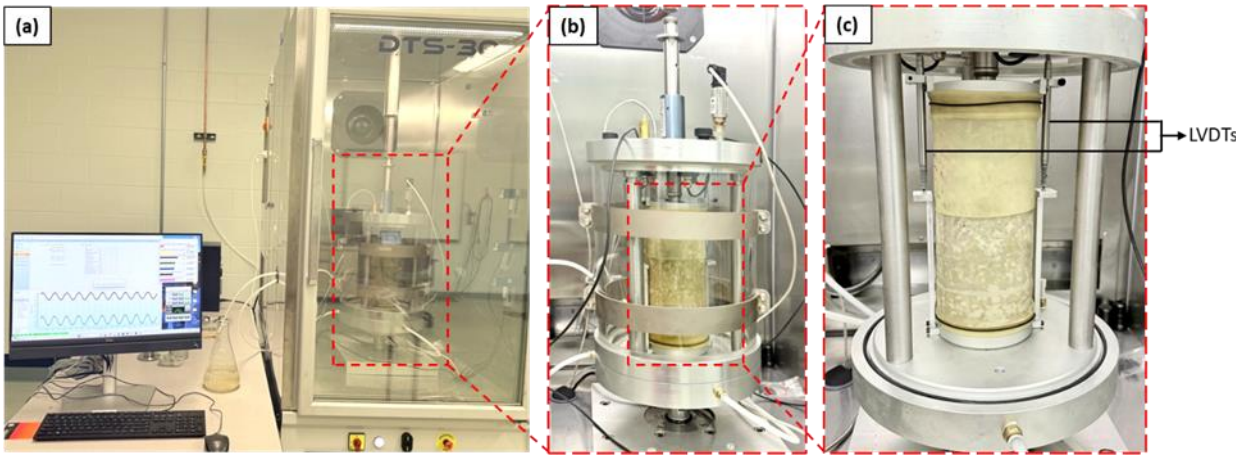


Figure 3-30 Testing Setup using DTS-30

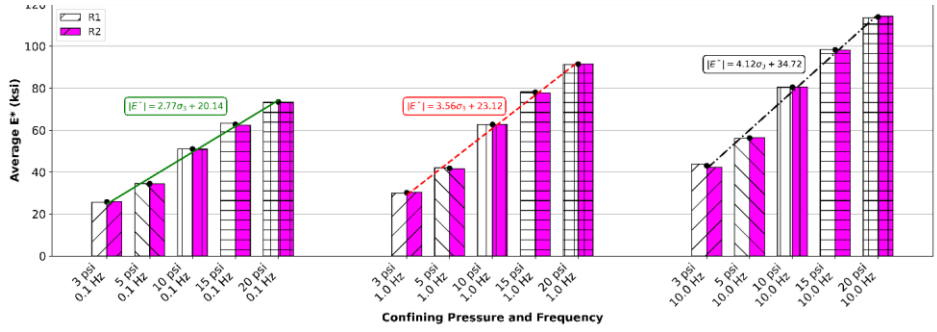
Since C&S material is like reclaimed asphalt pavement (RAP), it may behave as a viscoelastic material. To confirm this hypothesis, dynamic modulus and resilient modulus tests were conducted in accordance with standard protocols. Testing was performed at 4°C, 20°C, and 35°C. The samples were compacted in a mold with a 4-inch diameter and 8-inch height at their respective maximum dry density and optimum moisture content (OMC). Compaction was performed in six equal layers using a proctor hammer to reach the target height. The C&S specimens were compacted to meet 90–95% of the maximum dry density as specified in the guidelines (*31*). Samples were conditioned before testing: first overnight at 4°C, then for 2 hours at 20°C and 35°C to ensure uniform temperature distribution within the specimen, as per the test standards.

Dynamic Modulus– Effect of Confinement

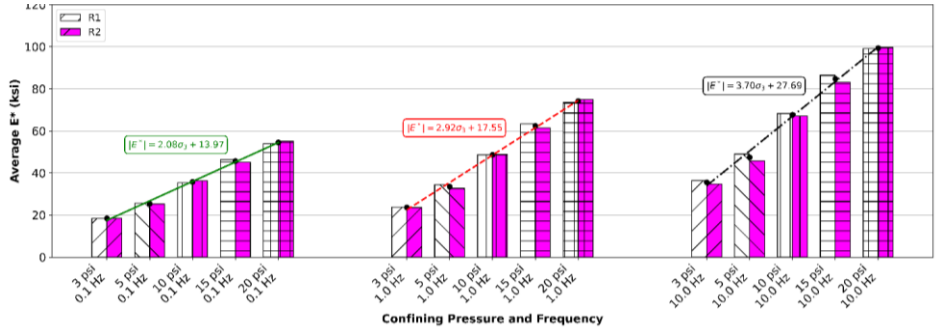
The dynamic modulus of the M-117 C&S material consistently increases with confining pressure across all temperatures and loading frequencies, emphasizing the importance of confinement in enhancing the stiffness of these materials (Figure 3-31). This relationship is expressed by Equation 3-19.

$$|\mathrm{E}^*| = m\sigma_3 + C \quad (3\text{-}19)$$

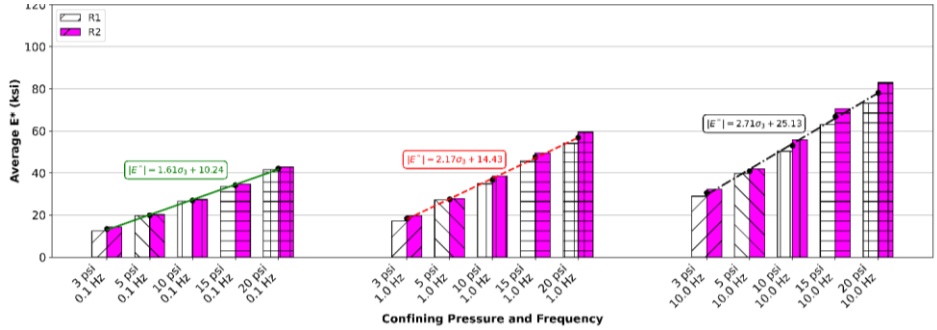
where;
$|\mathrm{E}^*|$= dynamic modulus, psi.
m = slope representing sensitivity to confinement.
σ_3 = confining pressure.
C = estimated modulus at zero confinement.



(a) M-117 (4°C)



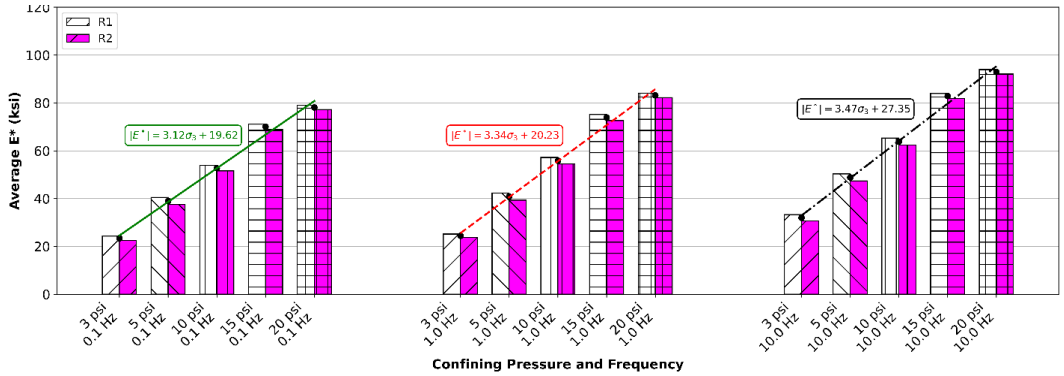
(b) M-117 (20°C)



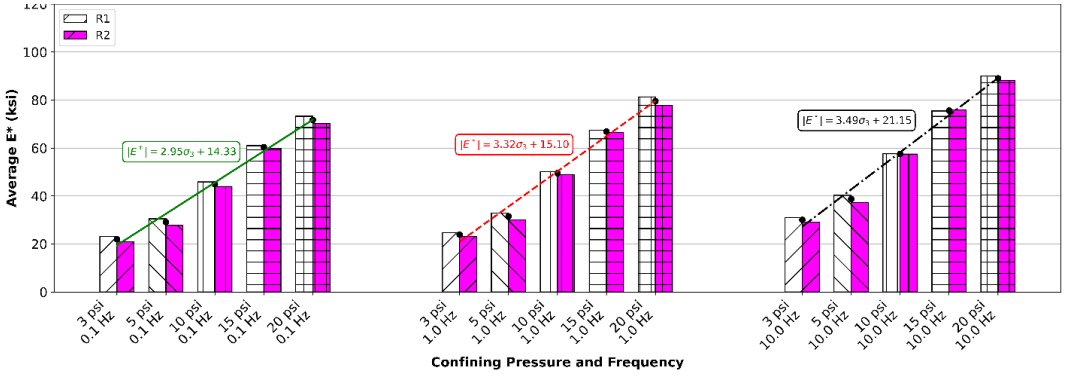
(c) M-117 (35°C)

Figure 3-31 Variation of the average dynamic modulus of M-117

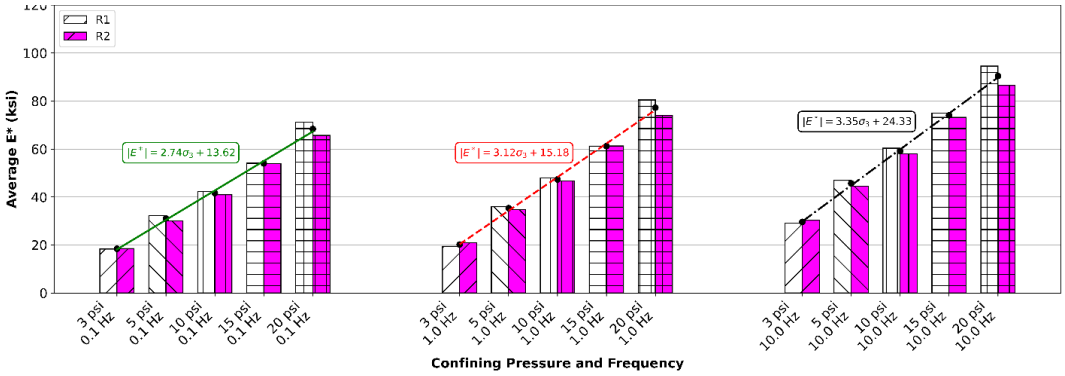
I-75BL exhibits steep slopes at 4°C across all test temperatures and frequencies, indicating high sensitivity to confinement at low temperatures (Figure 3-32a). However, both the dynamic modulus and slope magnitude values are lower than those observed for M-117 under similar conditions. This difference might be attributed to the lower binder content in I-75BL, which reduces its capacity to stiffen under pressure. Additionally, possible binder aging may contribute to the diminished confinement response, especially at higher loading rates, where elastic behavior typically dominates.



(a) I-75BL (4°C)



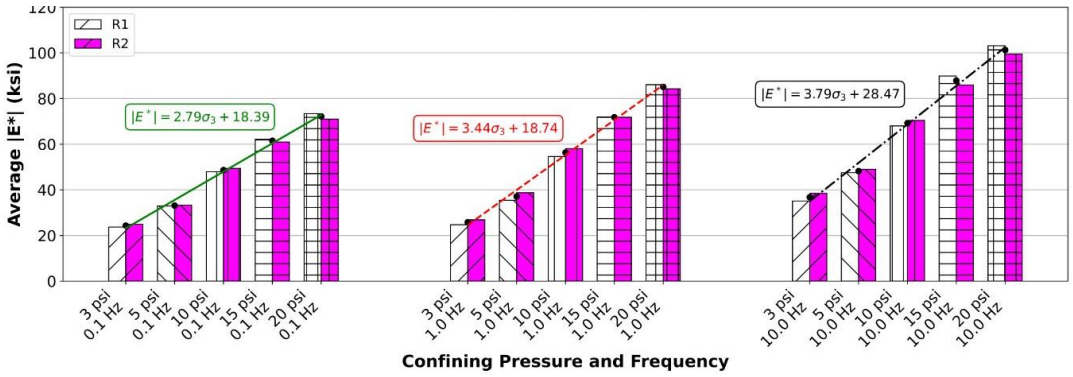
(b) I-75BL (20°C)



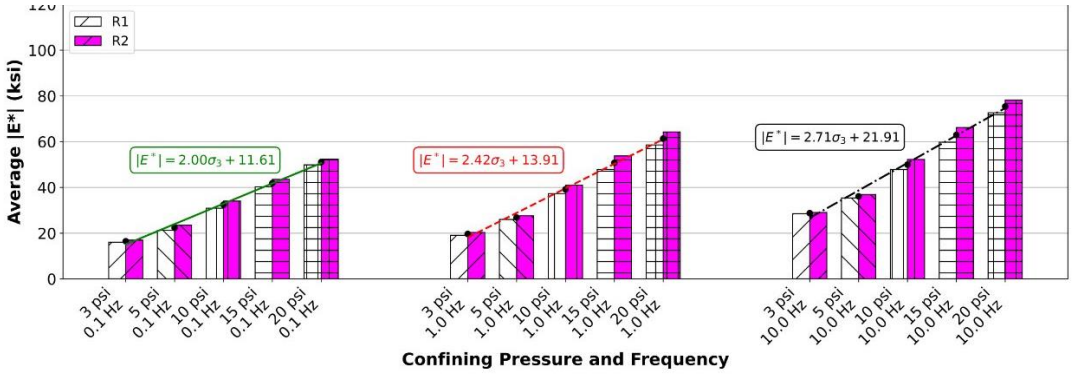
(c) I-75BL (35°C)

Figure 3-32 Variation of the average dynamic modulus of I-75BL

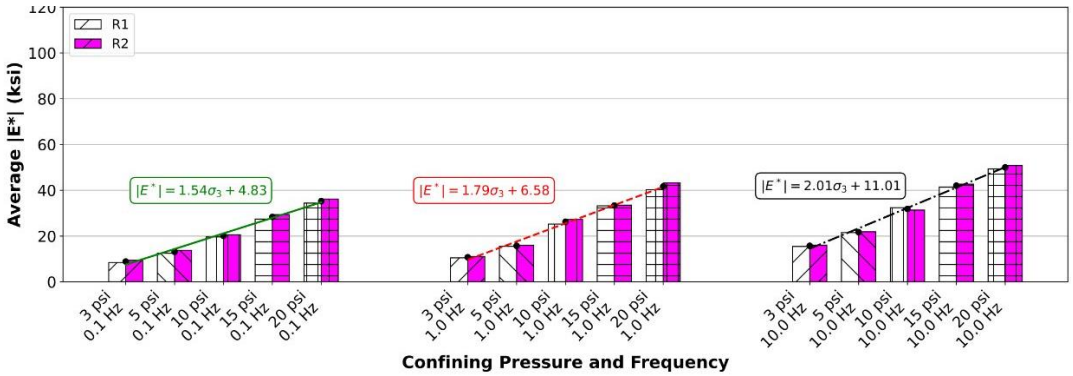
The lowest binder content was estimated in the C&S material from US-41. Figure 3-33 shows the effect of confinement on US-41 samples. The |E*| values were lower than I-75BL and M-117. At higher temperatures, the reduction in modulus was more noticeable than with I-75BL.



(a) US-41 (4°C)



(b) US-41 (20°C)



(c) US-41 (35°C)

Figure 3-33 Variation of the average dynamic modulus of US-41

Table 3-31 compares slope and intercept values at increments of confinement for all tested materials.

Table 3-31 Regression parameters (slope and intercept) of |*E**| per frequency (confinement effect)

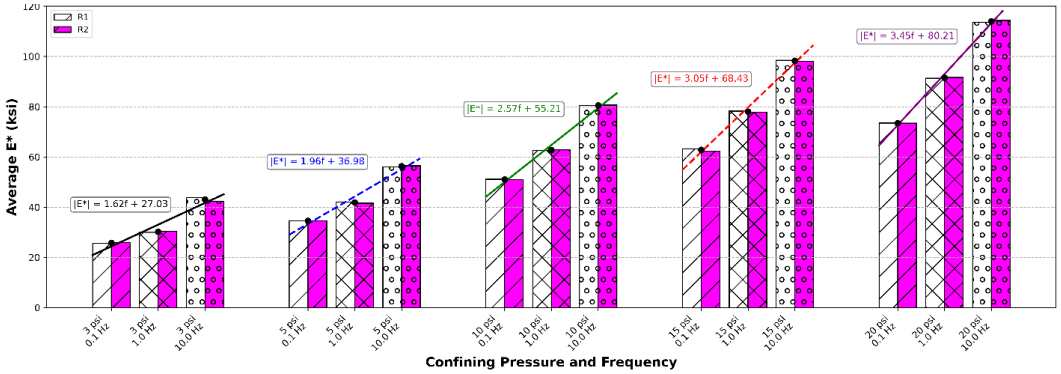
Material	Temperature (°C)	0.1 Hz *m*	0.1 Hz *C*	1 Hz *m*	1 Hz *C*	10 Hz *m*	10 Hz *C*
M-117	4	2.77	20.14	3.56	23.12	4.12	34.72
M-117	20	2.08	13.97	2.92	17.55	3.70	27.69
M-117	35	1.61	10.24	2.17	14.43	2.71	25.13
I-75BL	4	3.12	19.62	3.34	20.23	3.47	27.35
I-75BL	20	2.95	14.33	3.32	15.10	3.49	21.15
I-75BL	35	2.74	13.62	3.12	15.18	3.35	24.33
US-41	4	2.79	18.39	3.44	18.74	3.79	28.47
US-41	20	2.00	11.61	2.42	13.91	2.71	21.91
US-41	35	1.54	4.83	1.79	6.58	2.01	11.01

Dynamic Modulus– Effect of Frequency

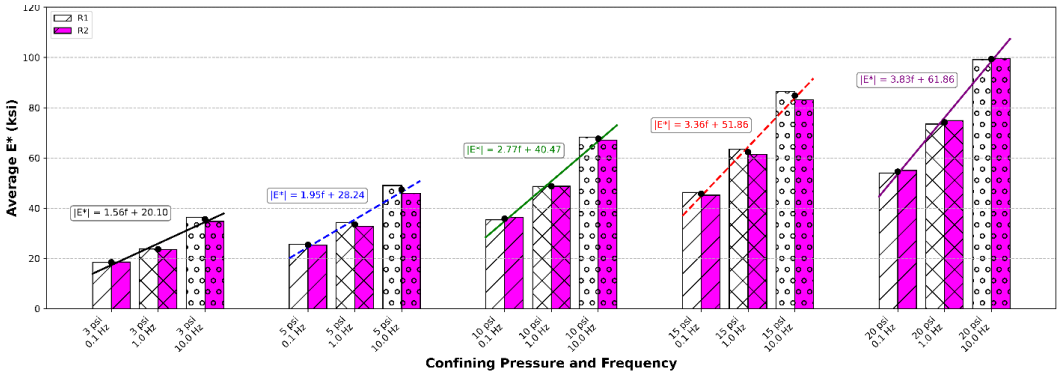
The dynamic modulus results presented in Figures 3-34 to 3-36 illustrate the frequency-dependent behavior of the M-117, I-75BL, and US-41 material at three temperatures (4°C, 20°C, and 35°C) under increasing confining pressure. In each case, Equation 3-20 describes the linear regression relationship between dynamic modulus and frequency. All corresponding slope and intercept values are summarized in Table 3-32 for comparison.

$$|\mathrm{E}^*| = f\sigma_3 + C \tag{3-20}$$

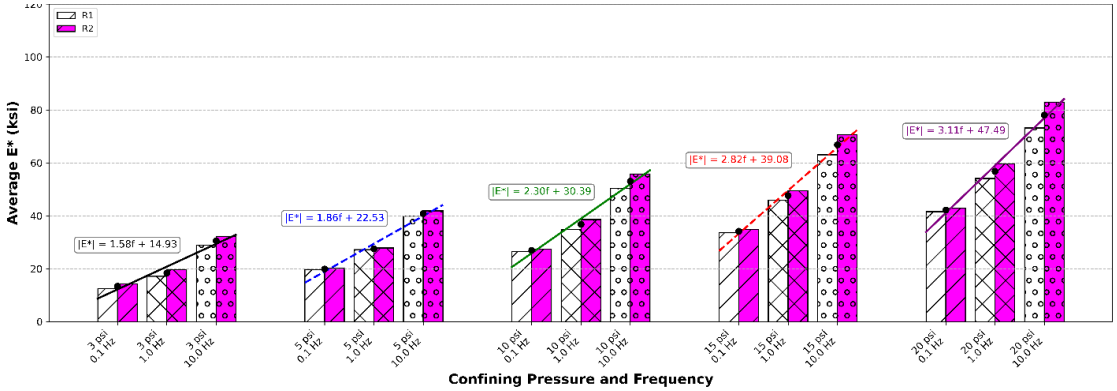
where;
$|\mathrm{E}^*|$= dynamic modulus, psi.
m = slope representing sensitivity to confinement.
f = testing frequency.
C = estimated modulus at zero confinement.



(a) M-117 (4°C)

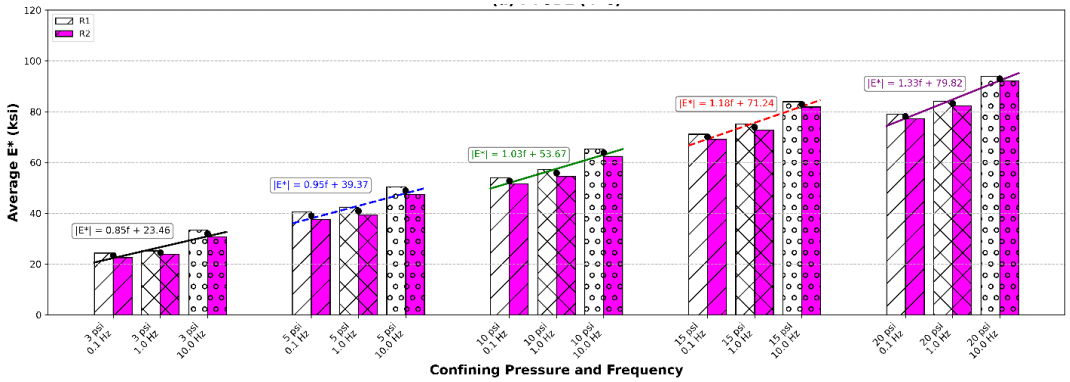


(b) M-117 (20°C)

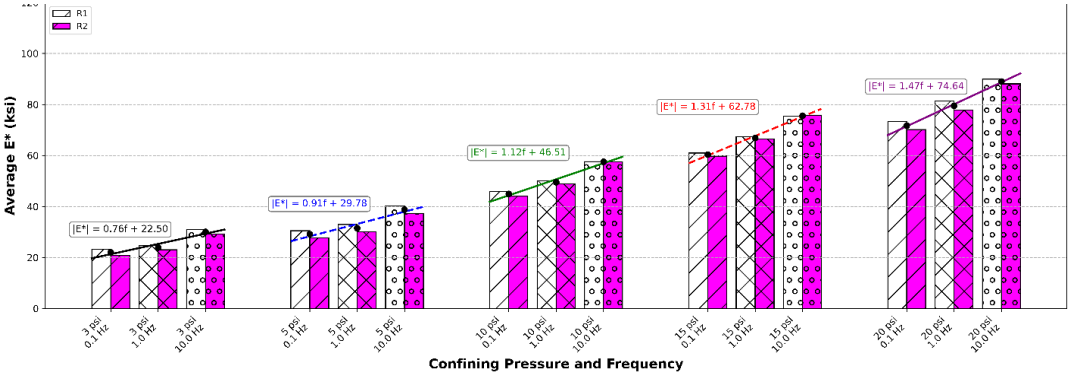


(c) M-117 (35°C)

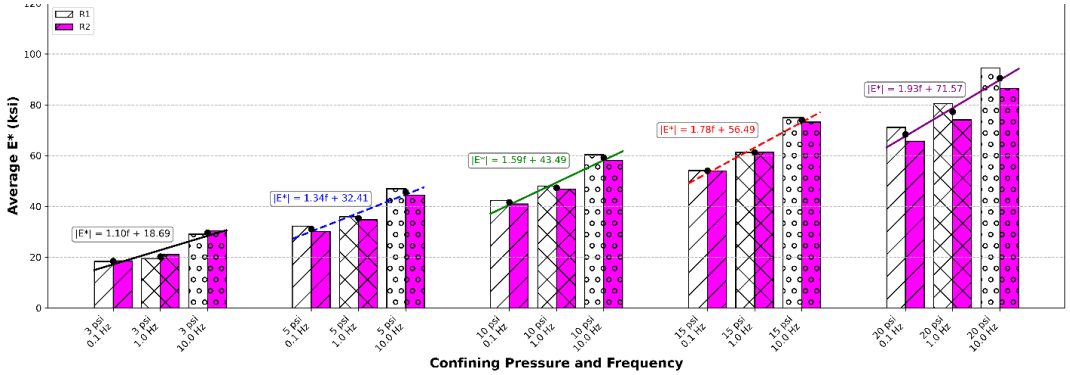
Figure 3-34 Variation of the average dynamic modulus of M-117 with frequency



(a) I-75BL (4°C)

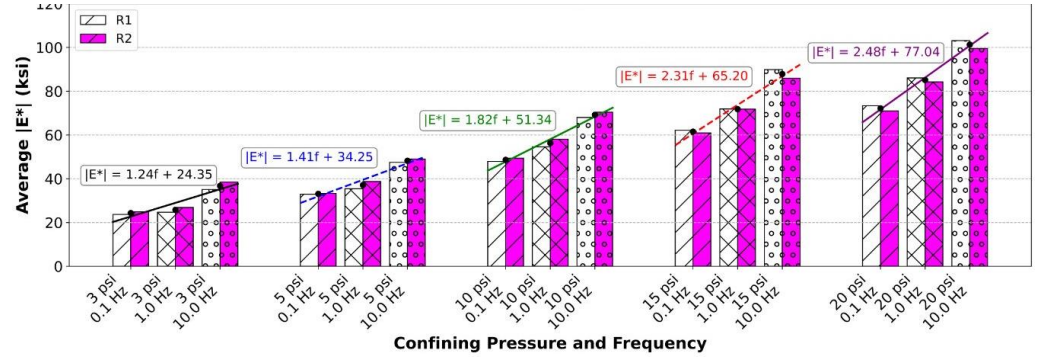


(b) I-75BL (20°C)

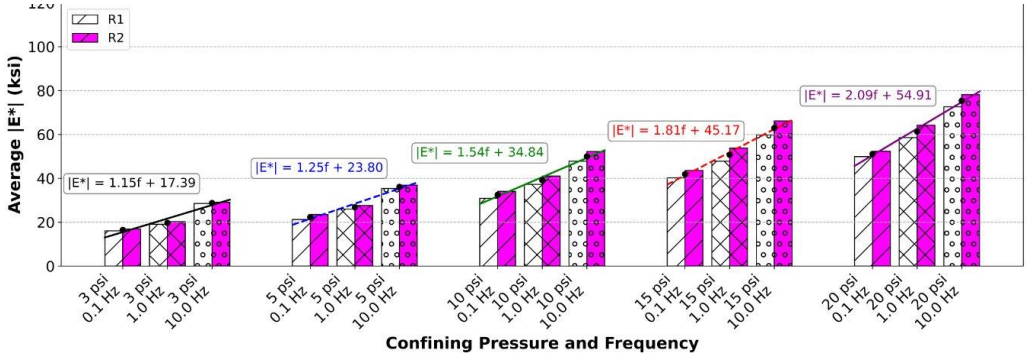


(c) I-75BL (35°C)

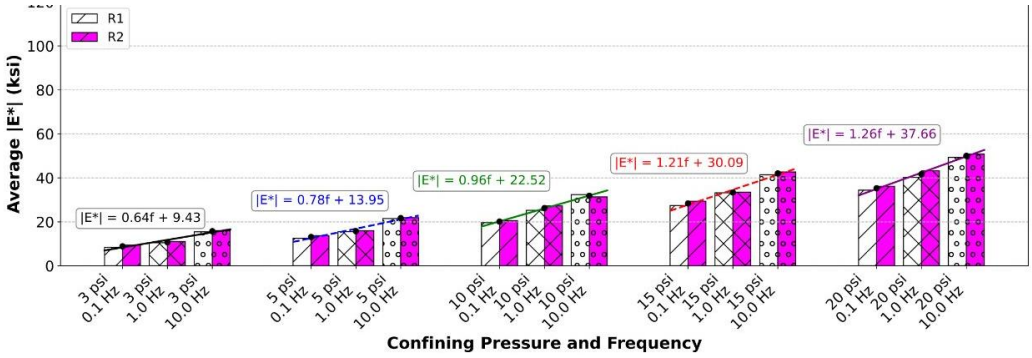
Figure 3-35 Variation of average dynamic modulus of I-75BL with frequency



(a) US-41 (4°C)



(b) US-41 (20°C)



(c) US-41 (35°C)

Figure 3-36 Variation of average dynamic modulus of US-41 with frequency

Table 3-32 Dynamic modulus slope and intercept per confinement (frequency effect)

Material	Temperature (°C)	3 psi *m*	3 psi *C*	5 psi *m*	5 psi *C*	10 psi *m*	10 psi *C*	15 psi *m*	15 psi *C*	20 psi *m*	20 psi *C*
M-117	4	1.62	27.03	1.96	36.98	2.57	55.21	3.05	68.43	3.45	80.21
M-117	20	1.56	20.10	1.95	28.24	2.77	40.47	3.36	51.86	3.83	61.86
M-117	35	1.58	14.93	1.86	22.53	2.30	30.39	2.82	39.08	3.11	47.49
I-75 BL	4	0.85	23.46	0.95	39.37	1.03	53.67	1.18	71.24	1.33	79.82
I-75 BL	20	0.76	22.50	0.91	29.78	1.12	46.51	1.31	62.78	1.47	74.64
I-75 BL	35	1.10	18.69	1.34	32.41	1.59	43.49	1.78	56.49	1.93	71.57

**m = slope; C = intercept at 0.1 Hz, 1 Hz, 10 Hz frequency*

Resilient Modulus Results

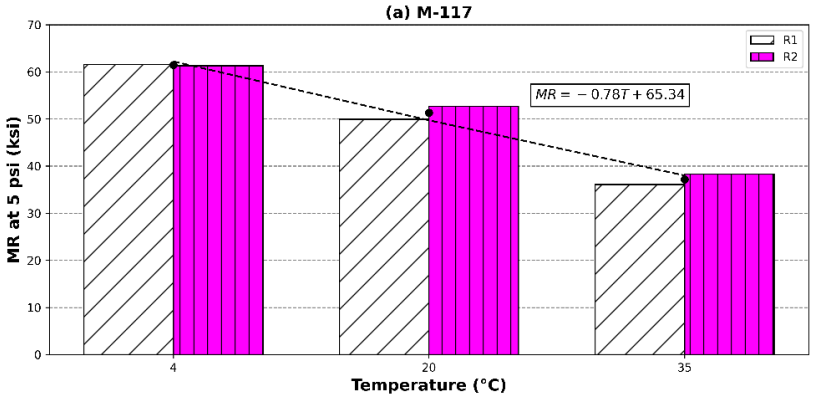
The variation in resilient modulus with temperature at a constant confinement pressure of 5 psi for M-117, I-75BL, and US-41 materials is presented in Figure 3-37. The resilient modulus values were predicted using the NCHRP 1-37A model. A best-fit linear trendline was then applied to represent the temperature dependence using Equation 3-21, where T is the test temperature in °C. Test results are shown for two replicates (R1 and R2) to assess repeatability.

$$MR = mT + C \quad (3\text{-}21)$$

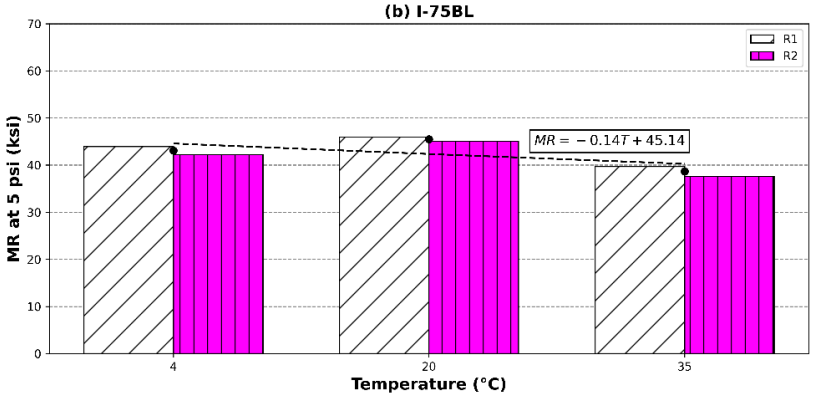
where;
MR = resilient modulus, psi.
m = slope representing sensitivity to confinement.
T = testing temperature, °C.
C = estimated modulus at zero confinement.

In Figures 3-37a and 3-37b, M-117 and US-41 show a clear decreasing trend in MR with increasing temperature. The fitted equation reveals a relatively steep negative slope, indicating strong temperature sensitivity. This behavior is expected due to the binder's viscoelastic nature, which softens at higher temperatures, reducing the material's resistance to repeated loading. The close match between R1 and R2 confirms the test's reliability and consistency.

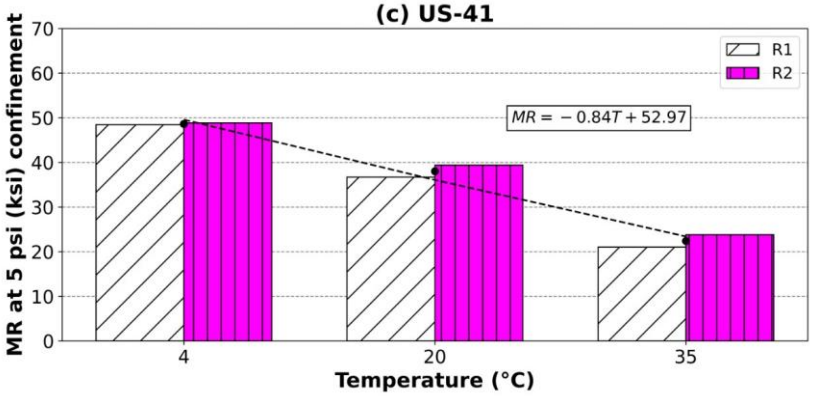
Figure 3-37c shows a similar trend for I-75BL but with a much milder slope, suggesting that this material is less affected by temperature. The minor change in MR is likely due to a lower binder content, resulting in mechanical behavior more governed by aggregate structure than by binder stiffness. This yields more stable modulus values across the temperature range, with less softening observed. It is pertinent to note that US-41 has the lowest binder content, yet it shows the viscoelastic effect more prominently than I-75BL.



(a) M-117



(b) I-75BL



(c) US-41

Figure 3-37 Resilient modulus (MR) at 5 psi confining pressure plotted against temperature

The M-117 section exhibited the highest MR, reaching nearly 60 ksi at 20 °C. The higher stiffness reflects its binder-rich mix, which provides greater viscoelastic resistance to deformation. In comparison, I-75BL showed an MR of about 45 ksi at the same temperature. The lower modulus suggests reduced stiffness, likely due to binder aging and a greater dependence on aggregate structure rather than binder elasticity. The US-41 section recorded the lowest MR, approximately 40 ksi at 20 °C, indicating

that its stiffness is primarily governed by particle interlock and contact stresses. The regression slopes plotted in the figures confirm the expected reduction in MR with increasing temperature across all projects. However, the sensitivity of MR to temperature varied: I-75BL showed a much smaller slope than M-117 or US-41, suggesting that factors beyond binder content influence the thermal response. For instance, M-117 exhibited the steepest decline, consistent with the behavior of binder-rich mixes, while US-41 showed similar sensitivity despite its lower binder content. These observations suggest that binder content and type have a significant impact on stiffness; however, field performance is influenced by the combined effects of material composition, binder grade, pavement age, climate exposure, and traffic loading history. Table 3-33 summarizes resilient modulus at 20 °C.

Table 3-33 Summary MR (ksi) for C&S at 20 ˚C using DTS30

Project	Replicate 1	Replicate 2	Average
M-117	49.94	52.70	51.32
I-75	45.92	45.04	45.48
US-41	36.70	39.39	38.05

3.4 SUMMARY

A comprehensive field and laboratory characterization of materials was conducted to generate reliable inputs for PMED. The FWD analysis confirmed that a four-layered backcalculation framework most effectively characterizes existing pavements, as it allows separate estimation of base and subbase moduli that can be directly incorporated into PMED. Among the backcalculation methods, Modulus 7.0 and BcT consistently produced stable, realistic HMA and PCC moduli, while the Boussinesq solution provided a reasonable check of subgrade resilient modulus. The reduced AREA method, applied only to composite sections, tended to overestimate PCC stiffness and underestimate subgrade response. To address spatial variability, the team adopted the 15th percentile of distributed modulus values as representative design inputs.

The LWD testing program provided additional insight into the behavior of C&S and rubblized layers. Resilient modulus values generally ranged from 4,700 to 17,000 psi, though results showed greater variability when fewer drops were available. In all cases, LWD values trended lower than FWD-derived moduli, consistent with the device's intended role as a QA tool for relative stiffness and uniformity rather than as a source of design-level inputs.

Similarly, GPR thickness measurements showed strong alignment with field cores for asphalt pavement layers. Still, they were inconsistent in composite sections, where signal noise and weak dielectric contrasts limited the ability to resolve HMA and PCC interfaces. TSD and 3D-GPR data provided network-level evidence of structural condition, service life, and load-transfer behavior, which were used to support field characterization.

Laboratory testing complemented field data by quantifying the material properties of HMA, PCC, and C&S layers. For HMA, air voids, binder content, and dynamic modulus master curves were determined from field cores and ASCRL specimens. WP cores exhibited higher stiffness than NWP cores, confirming the influence of long-term traffic densification. Binder ignition tests ensured accurate characterization of binder content, a direct input to PMED. For PCC, compressive strength and estimated modulus of elasticity were determined using ACI correlations due to equipment limitations, and for C&S materials, resilient modulus testing conducted with both MTS-810 and DTS-30 systems revealed strong dependency on temperature, frequency, and confining pressure, highlighting their viscoelastic and bound-like behavior rather than that of conventional unbound aggregates. The DTS-30 results, which directly measured vertical displacements with LVDTs, were deemed the most reliable, and resilient modulus values at 20 °C from this system were recommended for PMED calibration.

Overall, the findings reinforce the importance of capturing existing layer properties with sufficient resolution to support mechanistic–empirical rehabilitation design. The results highlight the value of four-layered FWD analysis, the reliability of BcT and Modulus 7.0 for HMA and PCC moduli, the use of Boussinesq for subgrade checks, and the reliance on DTS-30 for accurate resilient modulus of C&S materials. Together, these outcomes establish a defensible set of inputs that account for material variability and mechanistic response, thereby strengthening the foundation for the subsequent performance modeling and calibration presented in later chapters.

CHAPTER 4 - DATA SYNTHESIS FOR LOCAL CALIBRATION

4.1 INTRODUCTION

A critical step in local calibration involves selecting enough pavement sections that accurately represent the range of construction practices, traffic levels, and environmental conditions within the study area. For this study, a pavement section refers to a specific roadway segment corresponding to a construction project (identified by an MDOT job number), with separate segments defined for undivided directions or other unique identifiers. Although segments within a project often share similar data inputs, they may exhibit differences in measured pavement performance or subtle variations in traffic or cross-section. Accordingly, the number of sections is always greater than or equal to the number of projects.

Once candidate sections are identified, the necessary data must be compiled for each section, including pavement performance records, maintenance history, and the PMED inputs for materials, traffic, and climate. Predicted performance is subsequently compared to the actual performance of the as-constructed pavement sections. Since PMED performance predictions rely on the quality of the input data, assembling accurate and complete information for each section is essential.

The previous local calibration effort focused on selecting pavement projects and performance data from 1991 to 2019 *(1)*. Accordingly, this study began with a comprehensive review of all projects in MDOT's databases to determine the availability of additional sections and distress data. Notably, the recently available MDOT PAVETrack database was also used to identify additional sections or supplemental performance data points that could extend existing distress time-series trends and improve data completeness. All available MDOT rehabilitation fixes from 2011 onward were evaluated. PMED inputs for existing calibration sections were also reassessed to incorporate more recent or higher-level data inputs.

This chapter summarizes the project identification and selection process, the compilation of their PMED inputs, and performance data for all sections included in the local calibration analysis.

4.2 MDOT CONDITION DATA

The MDOT PMS and other available construction data sources were reviewed to identify the available condition data, performance measurement units, and the best possible estimates. The SPR-1723 report compiled all of the PMS data up to 2019 for the most common fix types (*2*). For this study, additional performance data points collected after 2019 were obtained for the selected roadway sections.

MDOT collects and reports performance data at 0.1-mile intervals. Each 0.1-mile interval was reviewed to assess the extent of distress and evaluate the reasonableness

and consistency of the reported performance measures. Subsequently, for each section, the performance values represent the average of all 0.1-mile intervals within that section.

4.2.1 Pavement Condition Measures and PMED Data Conversions

SPR-1723 comprehensively addressed the extraction, conversion, and verification of MDOT PMS performance data (*2*). The project documented the mapping of principal distress (PD) codes to PMED predicted distresses, unit conversions for compatibility, and adjustments to account for sampling practices. This study builds upon established procedures and enhances the database by incorporating condition data beyond 2019 using PAVETrack and the PMS database.

4.2.1.1. Selected distresses

The relevant asphalt and concrete pavement distresses are reproduced as explained in the following sections, which form the foundation for the synthesized datasets used in this research study.

4.2.1.2. Pavement distress unit conversion for asphalt pavement designs

For calibration of different rehabilitation fixes, only the distress types predicted by the PMED were used. The corresponding MDOT PDs were identified and aligned with the PMED distress categories to determine whether any unit adjustments or data conversions were required. MDOT measured pavement distress related to HMA pavements is listed in Table 4-1. PD code 501 corresponds to no distress condition and has been used in all distresses except rutting and IRI. SPR-1723 documented comprehensive procedures for converting distress types to PMED-compatible formats (*2*).

Table 4-1 Asphalt pavement distress measurement by MDOT

Performance measure	PDs	MDOT units	PMED units	Conversion needed?
IRI	Directly measured	in/mile	in/mile	No
Top-down cracking	204, 205, **724, 725**, 501	miles	% area	Yes
Bottom-up cracking	234, 235, **220, 221, 730, 731**, 501	miles	% area	Yes
Thermal cracking	**101,** 103, 104, 114, **701, 703, 704,** 110, 501	No. of occurrences	ft/mile	Yes
Rutting	Directly measured	in	in	No
Reflective cracking	No specific PD	None	% area	N/A

Note: Bold numbers represent older PDs that are not currently in use; PD code 501 = No distress

A concise summary of those procedures is presented below:

IRI

MDOT collects IRI data directly in PMED-compatible units; therefore, no additional conversion or adjustment was required for IRI.

Top-Down Cracking

Top-down cracking was represented in the MDOT PMS database by PDs 204, 205, 724, and 725, which capture early-stage longitudinal wheel-path cracking. These PDs were converted into percent area cracking using Equation 4-1. The lane width was assumed to be 12 ft. The typical wheel path width of 3 feet was assumed, as recommended by the LTPP distress identification manual *(3)*.

$$\%\, AC_{top-down} = \frac{\text{Length of cracking (miles)} \times \text{width of wheelpaths (feet)}}{\text{Length of section (miles)} \times \text{Lane width (feet)}} \times 100 \quad (4\text{-}1)$$

Research indicates that HMA layer thickness controls whether cracking initiates at the surface (top-down) or from the bottom. Cracking was classified using Equation (4-1) as top-down or bottom-up based on the thickness of the HMA layer. MDOT studies established these thresholds through mechanistic analyses using Mechanistic-Empirical Asphalt Pavement Analysis (MEAPA), which simulated MDOT design inputs under a standard axle load (*2*). Top-down cracking was identified when surface tensile strains exceeded those at the bottom of the layer. The resulting threshold thicknesses for each fix type are summarized in Table 4-2.

Table 4-2 HMA minimum thicknesses for top-down cracking

Fix type	Threshold thickness (in)
HMA over rubblized concrete	6
HMA over composite or JPCP	6
HMA over C&S	4
HMA over HMA	6
New or reconstructed	5

Bottom-Up Cracking

The PDs 234, 235, 220, 221, 730, and 731 match alligator cracking requirements in the MDOT PMS database (*2*). The PDs have units of miles; however, to make these compatible with the PMED alligator cracking units, conversion to a percentage of the total area was achieved by using the following Equation (4-2):

$$\%HMA_{bottom-up} = \frac{\text{Length of cracking (miles)} \times \text{width of wheelpaths (feet)}}{\text{Length of section (miles)} \times \text{Lane width (feet)}} \times 100 \quad (4\text{-}2)$$

The width of each wheel path and lane was assumed to be 3 feet and 12 feet, respectively. The typical wheel path width of 3 feet is recommended by the LTPP distress identification manual *(3)*.

Thermal Cracking

In the previous study, thermal cracks were converted to feet per mile for PMED compatibility by multiplying the number of occurrences by 3 ft for PDs 114 and 701; these PDs are defined as “tears” (short cracks) less than half the lane width, and by 12 ft for all other PDs. The project length normalized the total transverse crack length. Equation 4-3 was used to convert the number of occurrences into PMED compatible units.

$$TC = \frac{\sum \text{No. of Occurrences} \times \text{Lane Width (ft)}}{\text{Section Length (miles)}} \quad (4\text{-}3)$$

PMED limits thermal cracking predictions to a maximum of 2,112 ft/mile, corresponding to a minimum crack spacing of 30 ft. Due to this constraint and the SPR-1723 recommendations, the measured thermal cracking values were limited to a maximum value of 2,112 ft/mile for calibration purposes (*2*).

Rut Depth

The rut depth is the total surface rutting contributed by all asphalt and unbound layers. The average rut depth (left & right wheel paths) was determined for the entire project length. No conversion was necessary. It is assumed that the measured rutting corresponds to the total surface rutting predicted by the PMED.

Reflective Cracking

MDOT does not have PDs for reflective cracking. However, separating thermal and reflective cracks at the surface is challenging. Therefore, the total measured transverse cracking was considered a combination of thermal and reflective cracking, and both models were calibrated. For total transverse cracking (thermal + reflective), PMED does not restrict the prediction to 2,112 ft/mile. Total transverse cracking predictions were calibrated against measured transverse cracking.

4.2.1.3. Pavement distress unit conversion for JPCP designs

For JPCP unbonded overlays, transverse cracking requires a unit conversion. For all other distresses, MDOT records PMED compatible units. Table 4-3 summarizes the distress related to JPCP overlays, and the conversion process is discussed below:

Table 4-3 Concrete pavement distress measurement by MDOT

Performance prediction	PD	MDOT units	PMED units	Conversion needed?
IRI	Directly measured	in/mile	in/mile	No
Faulting	Directly measured	in	in	Yes
Transverse cracking	112, 113, 501	No. of occurrences	% slabs cracked	Yes

Note: PD code 501 = No distress

IRI

The IRI in the MDOT sensor database does not need any conversion; the values were used directly.

Faulting

The PMED predicts faulting as an average per joint. MDOT's sensor data records the number of faults (FaultNum), average faulting (avgFault), and the maximum faulting (FaultMax) for every 0.1-mile segment. From 2000 to 2011, faulting values were limited to maximum faulting (i.e., not average values). After 2012, both the average and maximum faulting values are available. A correlation was developed between the maximum and average faulting values using data from 2013 to 2017. Since the pseudo-faulting values may, for example, originate from cracking, spalling, or bridge segments, the maximum number of fault counts was limited to 36, and the average faulting was limited to 0.4 inches. Accordingly, any 0.1-mile section above these restricted faulting values was omitted from the calibration data (*2*).

The average joint faulting is calculated based on the number of faults in a 0.1-mile section. It is assumed that if the number of faults is less than or equal to the number of joints, faulting occurs at the joints only. In that case, the faulting unit conversion equation is given by Equation (4-4). If, for any 0.1-mile section, the number of faults is greater than the number of joints, that section is removed (cut) from the calibration data, as previously mentioned.

$$Fault = \frac{\mathrm{FAULnum} \times \mathrm{FAULi}}{\mathrm{N_{joints}}} \tag{4-4}$$

where,
Fault = average joint faulting, in.
FAULnum = number of faults in a 0.1 mile
FAULi = $(\mathrm{FAULT_(Avg_Right)} + \mathrm{FAULT_(Avg_Left)})/2$ = Average faulting in a 0.1 mile (inches)
N_{joints} = number of joints in 0.1-mile (528 ft) segments, i.e., $\mathrm{N_{joints}}$=528/Joint Spacing.

Transverse Cracking

PMED predicts transverse cracking as the percentage of slabs cracked. However, MDOT measures the number of transverse cracks (PDs 112 and 113). The estimated transverse cracking is converted to percent cracked slabs using Equations (4-5).

$$\%\ \text{Slabs Cracked} = \frac{\sum PD_{112,113}}{\left(\frac{\text{Section Length (miles)} \times 5280\,ft}{\text{Joint Spacing (ft)}}\right)} \times 100 \quad (4\text{-}5)$$

4.2.2 Condition Database for Local Calibration

To efficiently analyze the condition of selected PDs, customized databases were created during SPR-1723 that included distress and sensor data spanning multiple years. These databases were compiled in Microsoft Access, enabling easy extraction of relevant data for projects of any length. For divided highways, which can have an increasing or decreasing direction to indicate north/south or east/west, both directions were included in the time-series data and treated as separate sections. In contrast, distress data was collected in one direction for undivided highways (*2*).

4.3 PROJECT SELECTION CRITERIA FOR LOCAL CALIBRATION

Selecting in-service pavement sections that represent Michigan's pavement design, current materials, construction practices, and performance is essential for local calibration. The selected sections also needed to capture the full range of MDOT rehabilitation strategies. To achieve this, selection criteria were developed to ensure the chosen projects would serve as reliable representatives of the MDOT's pavement network. The process followed a structured sequence as highlighted in previous studies (*2*):

1. Determine the minimum number of pavement sections required for calibration based on the statistical requirements.
2. Identify all available in-service pavement projects.
3. Extract all pavement distresses (pavement condition data) from the customized database for all identified projects in Step 2.
4. Assess the measured performance for all the identified projects.
5. Identify projects with adequate data, age, trend, and PMED inputs, and use this to develop a refined list.

4.3.1 Minimum Number of Recommended Sections for Calibration

The *MEPDG Local Calibration Guide* provides a method for determining the minimum number of pavement sections required for each distress type (*4*). These minimums serve as guidance to help users identify the number of sections that would be statistically sufficient for a representative calibration. However, these values are recommendations, not requirements. Accordingly, a dataset with fewer sections may still be adequate if those sections are themselves broadly representative of the

pavement type. Conversely, meeting the minimum number does not guarantee representativeness if the selected sections do not adequately reflect the full range of conditions. Therefore, the recommended minimums are used as a relative benchmark to provide a general understanding of the sections that may be needed.

The recommended minimum number of pavement sections for calibration was determined using Equation 4-6:

$$n = \left(\frac{Z_{\alpha/2} \times \sigma}{e_t}\right)^2 \quad (4\text{-}6)$$

where;
$Z_{\alpha/2}$ = z-value from a standard normal distribution.
n = minimum number of pavement sections.
σ = performance threshold.
e_t = tolerable bias $Z_{\frac{\alpha}{2}} \times SEE$.
SEE = standard error of the estimate.

Table 4-4 presents the minimum number of recommended sections for each rehabilitation fix type.

Table 4-4 Minimum number of sections required for rehabilitation calibration

Performance Model	Nationally calibrated SEE	Z_{90}	Threshold	*N* (required number of sections)
Fatigue, bottom-up (%)[1]	5.01	1.64	20%	16
Fatigue, top-down (ft/mile or %)[1]	583	1.64	2000	12
Fatigue, top-down (ft/mile or %)[1]	583	1.64	or 20%	12
Thermal cracking (ft/mile)[1]	-	1.64	1000	-
Rutting (in) [1]	0.107	1.64	0.5	22
IRI (in/mile) [1]	18.9	1.64	172	83
Transverse cracking (%)[2]	4.52	1.64	15	11
Joint faulting (in) [2]	0.033	1.64	0.125	14
IRI (in/mile) [2]	22	1.64	172	61

1 = Flexible pavements; 2 = Rigid pavements

4.3.2 Available In-Service Pavement Projects

The common rehabilitation types applied to Michigan roadways include the following:

1. HMA over C&S
2. HMA over existing HMA
3. HMA over rubblized concrete
4. HMA over existing PCC (including composite HMA over PCC)
5. JPCP (unbonded) over existing JPCP or JRCP

The pavement sections were selected for local calibration based on performance trends and to accommodate a wide range of different inputs, including layer thicknesses, traffic, and region.

4.3.3 Project Selection Criteria

To ensure a robust and appropriate set of data, the criteria used for pavement section selection included the following:

- The section must have at least three measured pavement condition data points over time. There are some exceptions to this criterion. Bottom-up cracking has relatively few data points; some sections, with as few as two points, have been included. The exact process was followed by transverse cracking in JPCP unbonded overlay sections.
- At least one of the section's distresses should have an increasing trend. Any section with decreasing or no trends over time was excluded from the list.
- The section must have a last recorded Distress Index (DI) of at least 5. DI is the weighted average of different distress types (*2*). DI was observed and limited to ensure sufficient distress for calibration and to capture adequate trends in pavement performance.

Figures 4-1 through 4-3 illustrate the progression of distress in various types of asphalt overlays. Top-down cracking was initially reported in feet per mile and later converted to a percentage. Construction (dashed red line) and maintenance (dotted blue line) activities are included in the figures, with rehabilitation events, such as cold milling and resurfacing (CM&R), and clearly reflected reductions in measured distress (Figure 4-3). The effect of the rehabilitation event is noticeable, as indicated by a drop in measured distress in individual distress plots. Therefore, in this case, pavement section performance can be considered for the period from 2001 to 2011. Generally, minor maintenance activities, such as crack treatment (CT) or joint sealing (JS), do not significantly affect the time series trend, as they primarily involve non-structural fixes. It is also noted that a consistent drop in rutting during 2012–2013 across sections appears to be related to changes in data collection rather than to actual pavement performance.

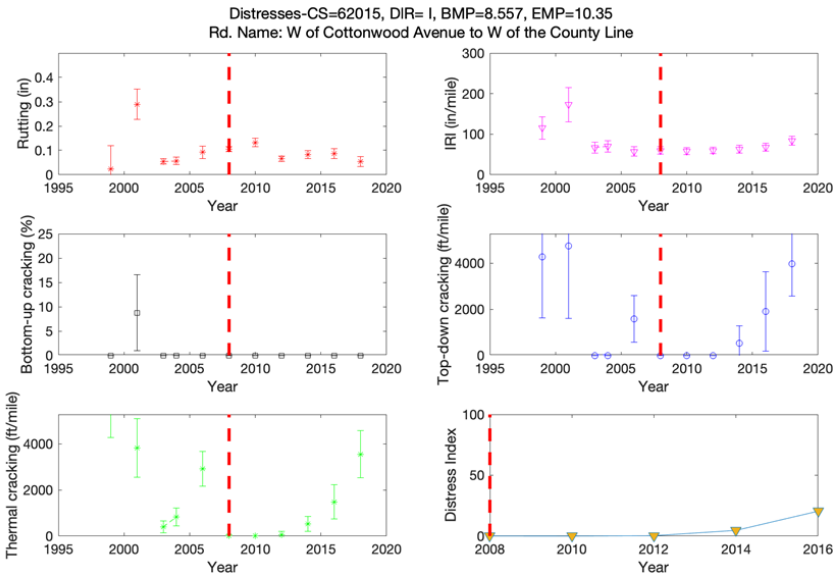


Figure 4-1 Example of distress progression of HMA over C&S

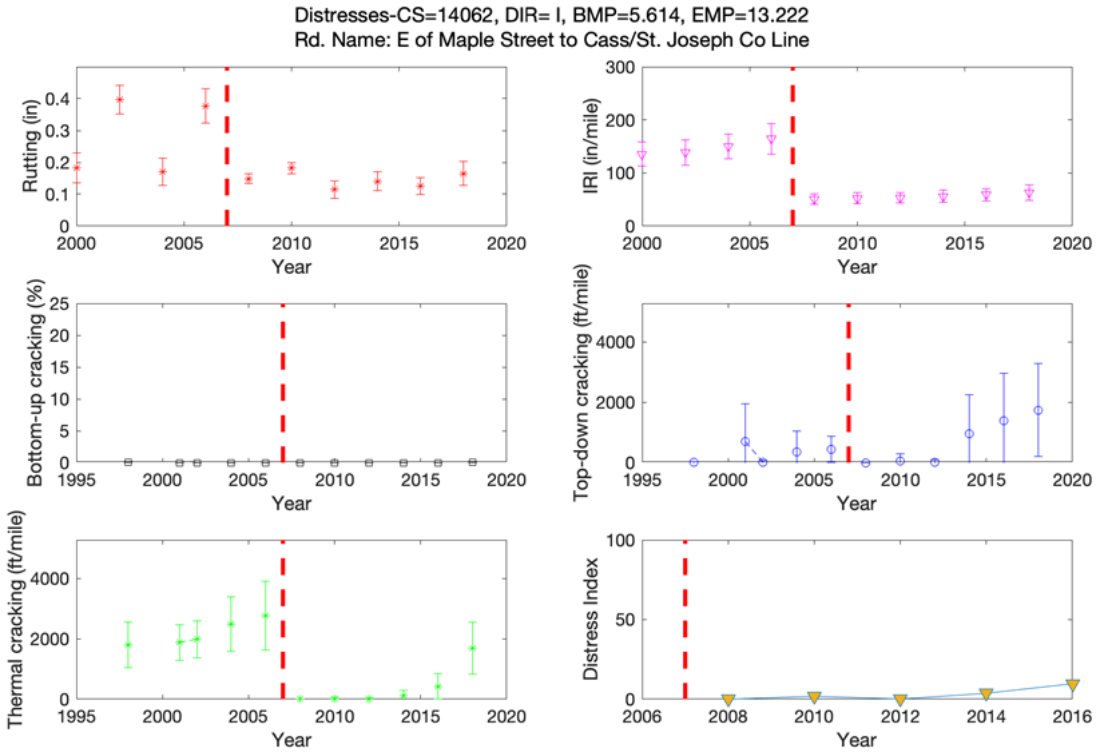


Figure 4-2 Example of distress progression of HMA over rubblized concrete

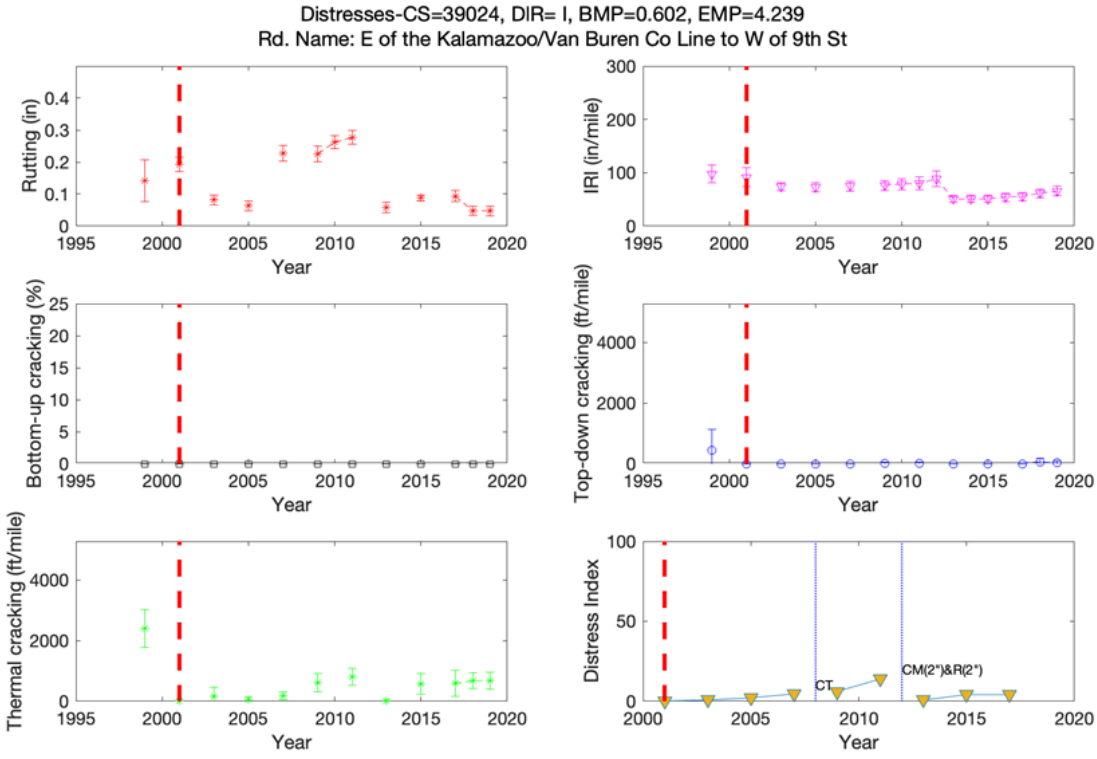


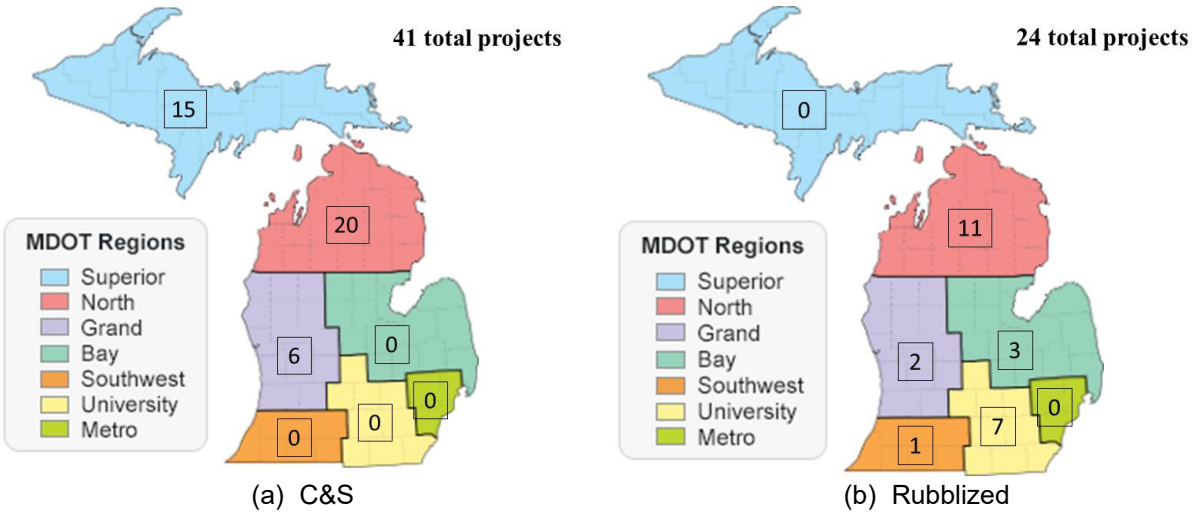
Figure 4-3 Example of distress progression of multicourse HMA over HMA

To represent the overall pavement condition and section selection criteria, pavement sections were selected based on good, fair, and poor performance. Moreover, sections with Superpave mixes are used solely to calibrate the thermal cracking model, ensuring consistent Level 1 input in the PMED (*2*). The detailed discussion on the section selection criteria is outlined in SPR-1723 (*2*).

4.3.4 Summary of the Selected Projects for Local Calibration

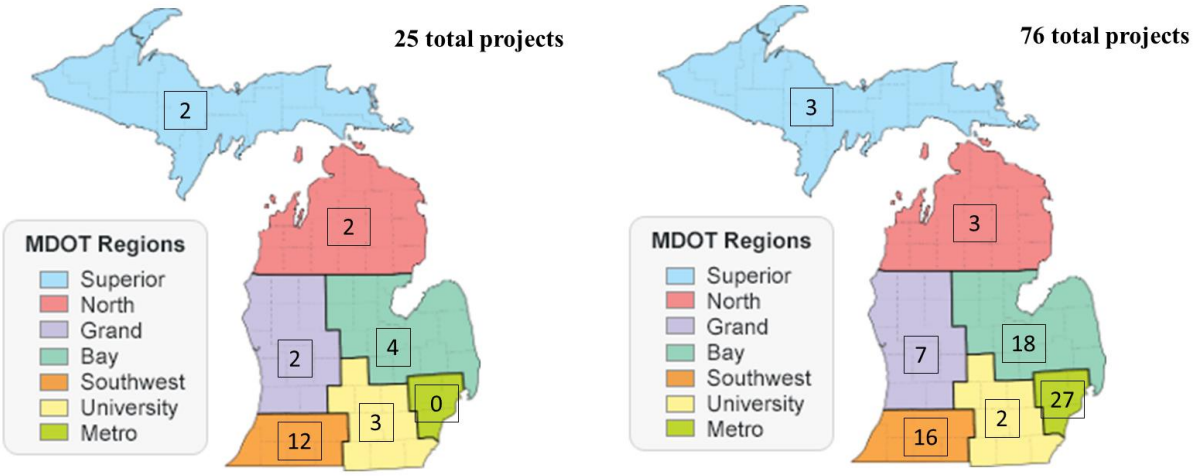
Based on the evaluation of available in-service pavement sections, including adequacy of data, ages, performance trends, and available PMED inputs, a total of 336 rehabilitation sections were selected for calibration. This includes 308 HMA overlay sections and 28 concrete overlay sections, representing a broad range of pavement sections across Michigan. These sections comprise 198 rehabilitation projects: 186 asphalt overlay projects and 12 JPCP unbonded overlay projects.

Figures 4-4 to 4-6 show the geographical distribution of selected sections by region, with numbers indicating the number of selected sections per region. Table 4-5 summarizes the selected rehabilitation sections based on the design matrix, accounting for traffic, thickness, and age for each section.



(a) C&S (b) Rubblized

Figure 4-4 Geographical location of selected HMA over C&S and rubblized sections(*2*)



(a) HMA over HMA (b) Composite

Figure 4-5 Geographical location of selected HMA over HMA sections (*2*)

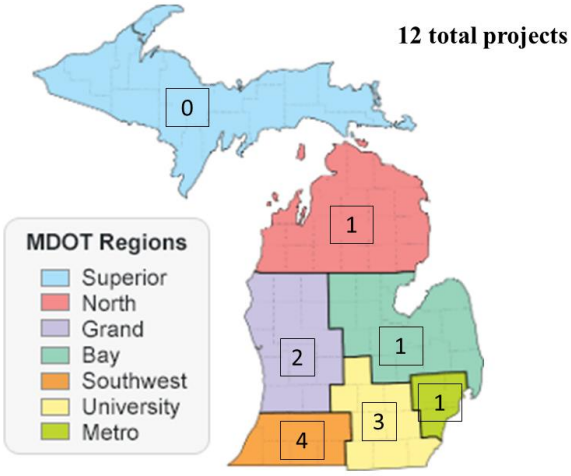


Figure 4-6 Geographical location of selected JPCP (unbonded) overlay sections (*2*)

Table 4-5 Selection matrix displaying selected rehabilitation sections

Rehabilitation type	Traffic level*	Overlay thickness level**	Age <10 years	Age 10 to 20 years	Age >20 years	Total
HMA over Crush and shape	1	1	-	-	4	4
HMA over Crush and shape	1	2	11	17	12	40
HMA over Crush and shape	2	2	-	7	10	17
HMA over Crush and shape	3	2	-	-	1	1
HMA over rubblized PCC	1	2	-	14	6	20
HMA over rubblized PCC	1	3	-	3	4	7
HMA over rubblized PCC	2	2	-	11	1	12
HMA over rubblized PCC	3	2	-	-	8	8
HMA over rubblized PCC	3	3	-	-	4	4
HMA over PCC (composite)	1	1	-	1	-	1
HMA over PCC (composite)	1	2	5	67	2	74
HMA over PCC (composite)	2	2	2	21	10	33
HMA over PCC (composite)	3	2	10	32	6	48
HMA over HMA	1	1	-	-	9	9
HMA over HMA	1	2	3	16	4	23
HMA over HMA	2	2	-	1	4	5
HMA over HMA	3	2	-	-	2	2
JPCP unbonded overlay	2	3	-	-	5	5
JPCP unbonded overlay	3	3	-	21	2	23
Total	-	-	31	211	94	336

* Traffic levels: 1 <1,000; 2 =1,000-3,000; 3 >3,000.

** Overlay thickness levels: 1 <3in.; 2 =3-7in.; 3 >7in.

4.4 CALIBRATION SECTION PERFORMANCE DATA SUMMARY

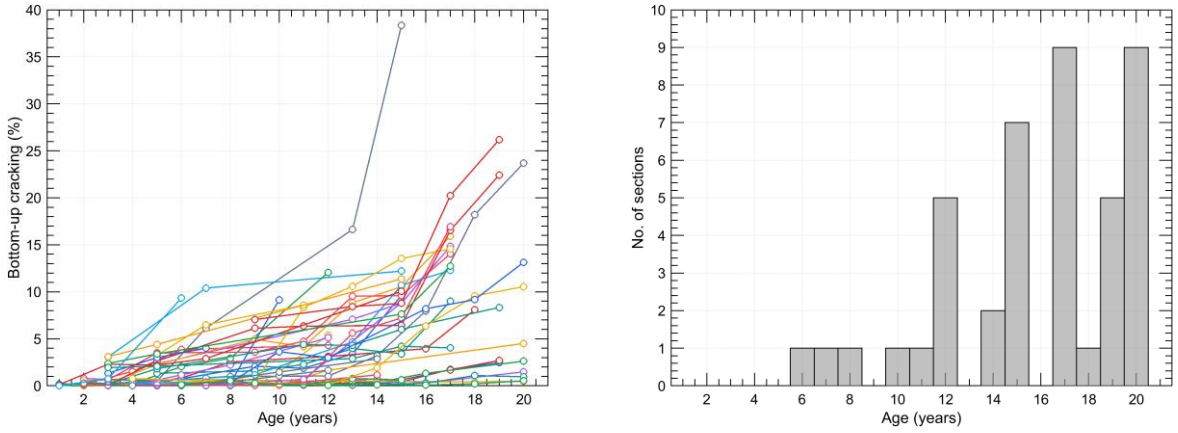
A comprehensive review of all pavement sections considered for local calibration was conducted to assess measured performance. Calibration requires comparing measured performance with predicted values for each project, and this is only meaningful if the observed distress levels span a reasonable range above and below the threshold limits for each distress type. To support this, distress data for all selected sections were compiled and analyzed to establish their ranges. This section summarizes the performance of the rehabilitation sections chosen for calibration.

It is important to note that the measured values presented in this section correspond to PMED predictions at 50% reliability. In practice, pavement designs incorporate higher reliability levels to account for variability in traffic, climate, materials, and construction, which produces higher predicted distress values. Therefore, while the calibration sections provide a representative foundation for design, subsequent pavement designs (that use a higher reliability level) should not be expected to mirror the exact performance of the calibration sections.

4.4.1 Asphalt Overlay Performance Data

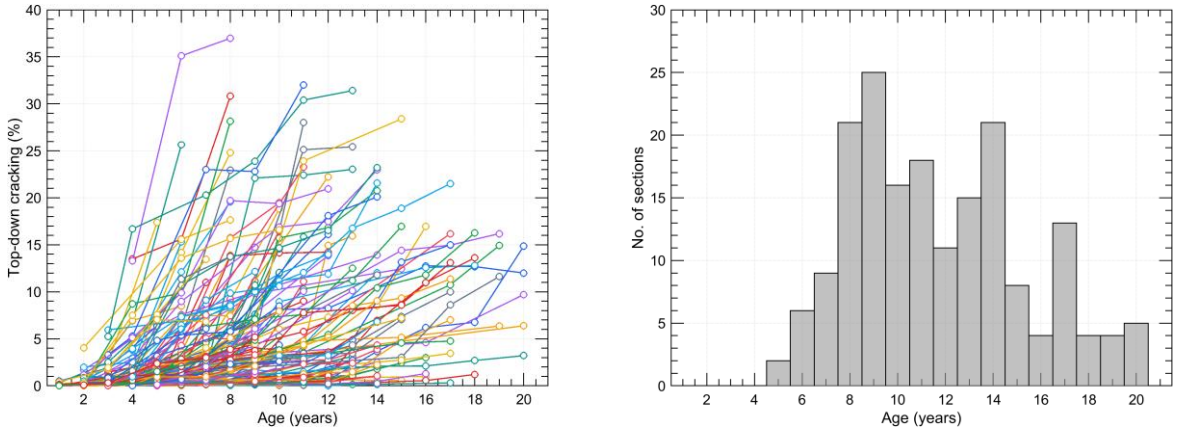
The time series and age distribution for the asphalt overlay (HMA over HMA, HMA over PCC, HMA over C&S, and HMA over rubblized) projects are shown in Figures 4-7 to 4-11. The following observations can be made from the results:

- Bottom-up fatigue cracking: Most sections exhibit low bottom-up cracking, with only a few reaching the 20% threshold (Figure 4-7). The age at maximum distress ranged from 5 to 20 years.
- Longitudinal/top-down fatigue cracking: Top-down cracking is observed more frequently than bottom-up cracking. The age at maximum distress ranged from 5 to 20 years (Figure 4-8).
- Rutting: Most sections did not exhibit significant rutting, with none exceeding 0.5 inches. The age distribution ranged from 3 to 19 years (Figure 4-9).
- Thermal cracking: The thermal cracking observed in the rehabilitation projects was significant, with two sections having nearly 5,000 feet/mile. The age at which the maximum thermal cracking occurred ranged from 6 to 20 years (Figure 4-10). Sections with Superpave (PG) binder have been used for calibration of thermal cracking. It should be noted that some of the thermal cracks could be reflective cracks.
- IRI: Only two sections exceeded the 172 in/mile threshold. The age at maximum IRI ranged from 7 to 20 years (Figure 4-11). It is worth noting that only sections with an initial IRI of 82 inches per mile or less were selected for calibration of the IRI model.



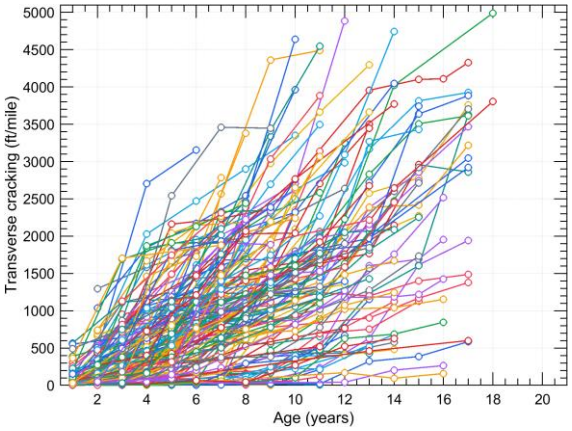
(a) Time series (b) Age distribution

Figure 4-7 Selected asphalt rehabilitation sections — Bottom-up cracking

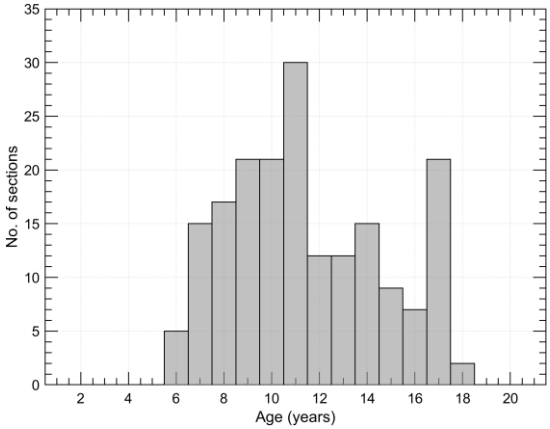


(a) Time series (b) Age distribution

Figure 4-8 Selected asphalt rehabilitation sections — Top-down cracking

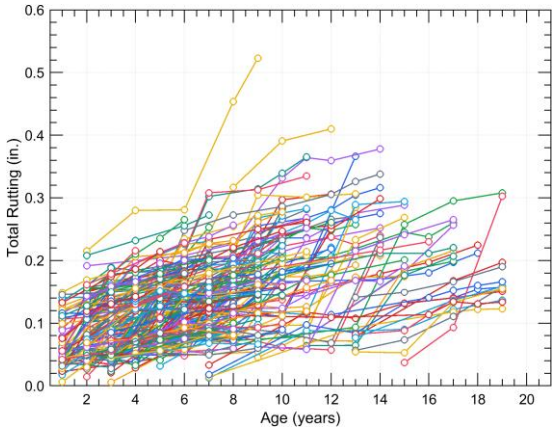


(a) Time series

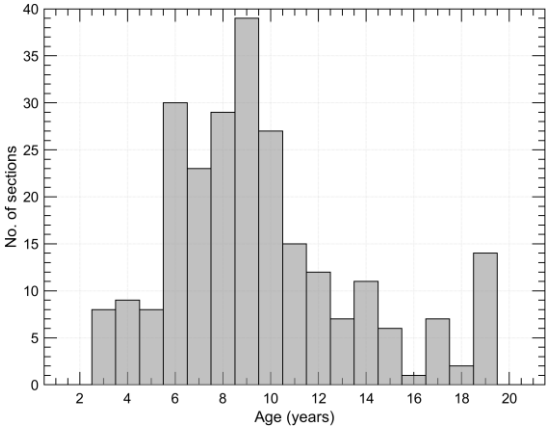


(b) Age distribution

Figure 4-9 Selected asphalt rehabilitation sections — Transverse (thermal) cracking

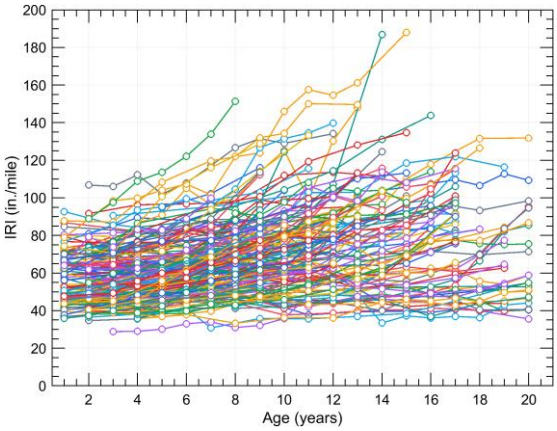


(a) Time series

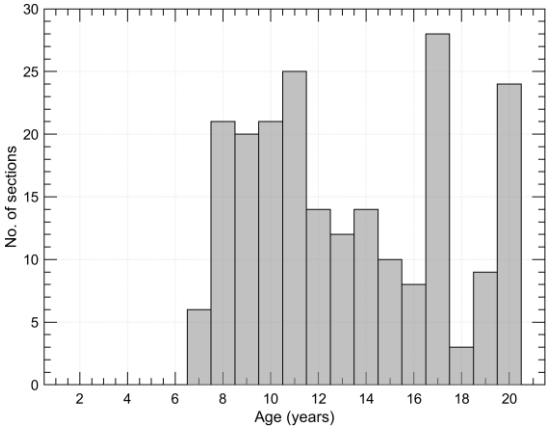


(b) Age distribution

Figure 4-10 Selected asphalt rehabilitation sections — Total rutting



(a) Time series



(b) Age distribution

Figure 4-11 Selected asphalt rehabilitation sections — IRI

Figure 4-12 presents the distribution of good, fair, and poor sections for the selected asphalt overlay sections and the full set of MDOT sections (noted as “All MDOT sections” in the figure). Details on the good, fair, and poor category definitions are provided in SPR-1723 (*2*), except for faulting. For faulting, the FHWA Highway Performance Monitoring System (HPMS) reporting classifications are used, where good is less than 0.10 inches, fair is from 0.10 to 0.15 inches, and poor is greater than 0.15 inches. The “All MDOT sections” dataset includes reconstruction sections. These are provided for comparison purposes. As shown, most sections fall into the good category, as expected, since MDOT maintains its pavement to ensure adequate performance. Accordingly, once maintenance is performed, the resulting post-maintenance data are excluded from calibration analyses.

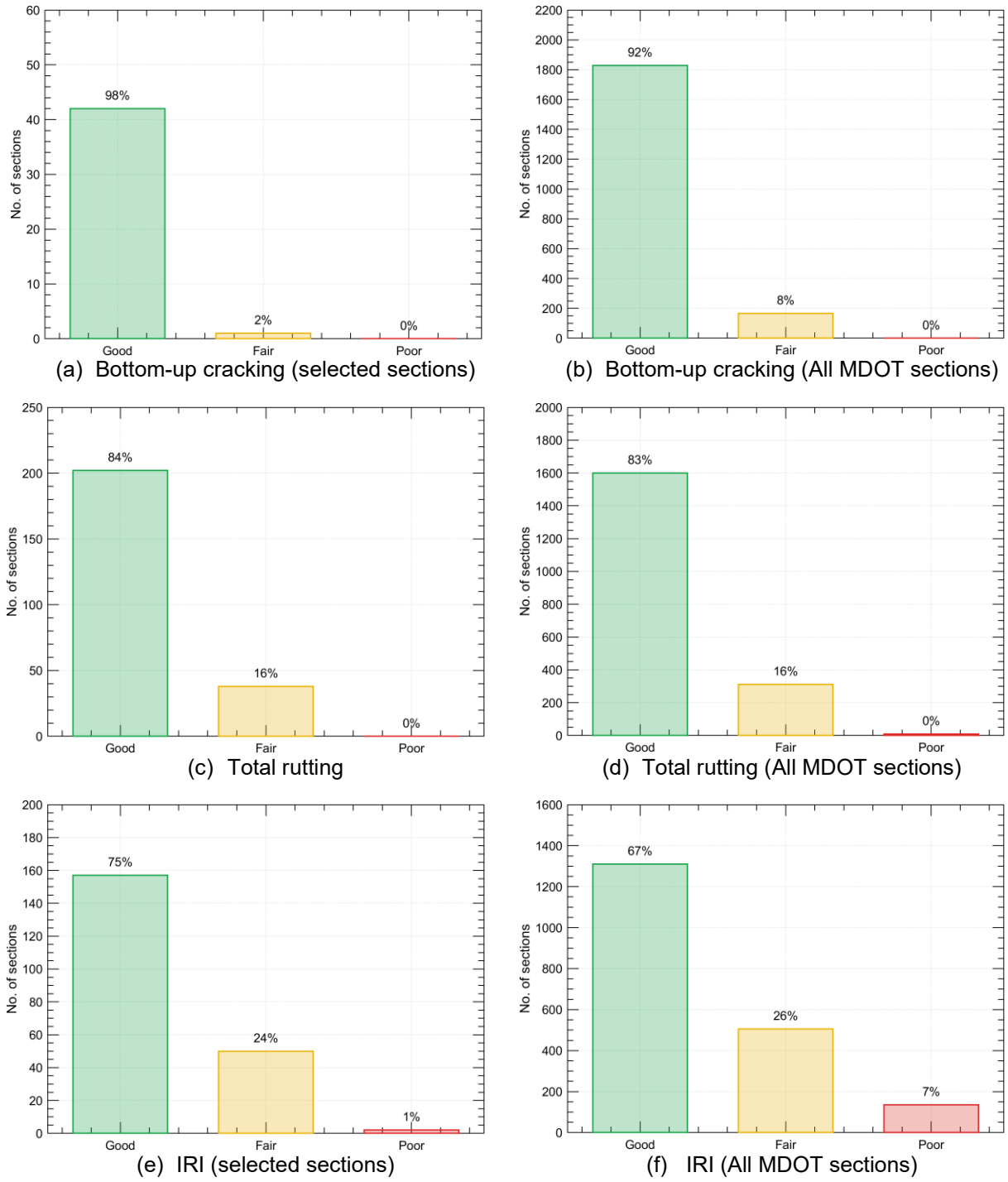
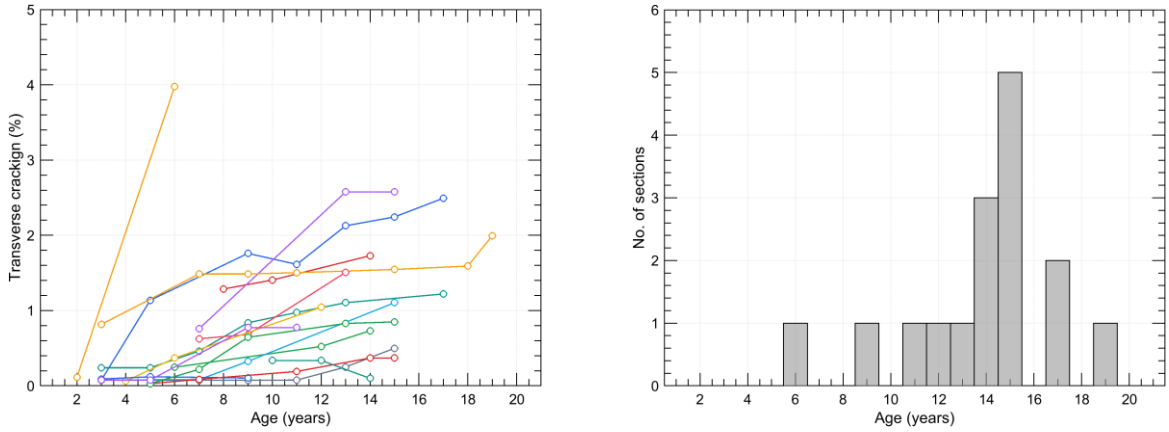


Figure 4-12 Condition distribution of asphalt overlay sections with all MDOT sections

4.4.2 JPCP Unbonded Overlay Performance Data:

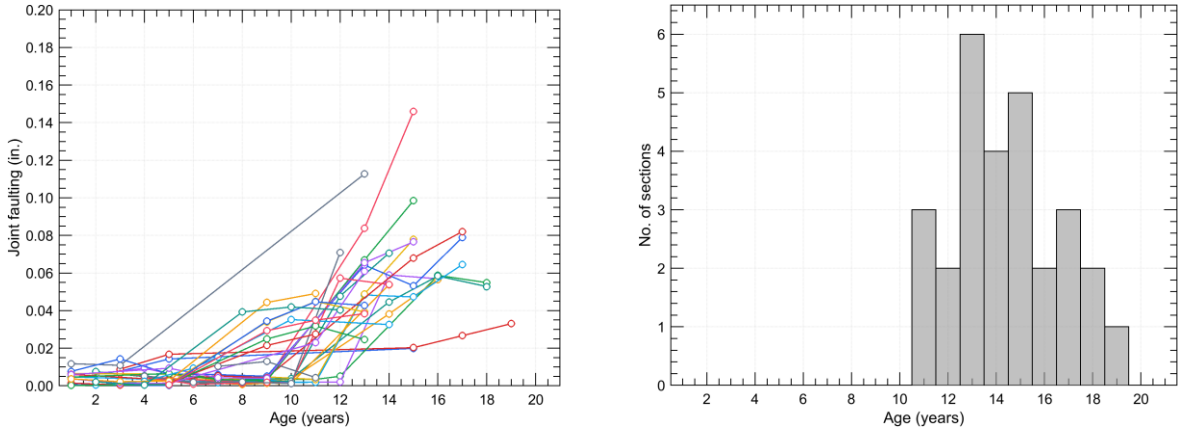
Figures 4-13 to 4-15 show the magnitude and age distribution for the JPCP rehabilitation projects. The following observations can be made:

- Transverse cracking: Low values are observed, with none of the projects exceeding the distress threshold of 15% of slabs cracked. The maximum transverse cracking observed is 4%. The age distribution ranges from 6 to 19 years (Figure 4-13).
- Transverse joint faulting: One section exceeds the joint faulting threshold of 0.125 inches with a maximum value of 0.14 inches. The age distribution ranges from 11 to 19 years (Figure 4-14). As previously described, to provide a robust and practical calibration, measured tenth-mile joint-faulting values above 0.4 inches were excluded when compiling data for each section.
- IRI: A maximum IRI of 144 in/mile was observed for the unbonded overlay sections. None of the sections exceeded the IRI threshold of 172 in/mile. The age at maximum IRI ranges from 13 to 19 years (Figure 4-15). As described in SPR-1723, this study also limited the initial IRI to 82 inches per mile (2). Accordingly, only sections with less than or equal to 82 in/mile were used to calibrate the IRI model.



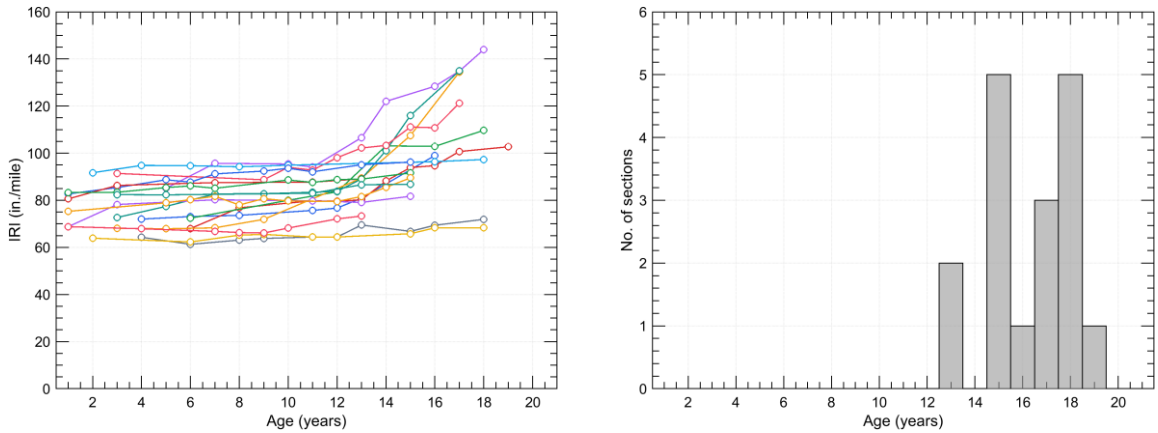
(a) Time series (b) Age distribution

Figure 4-13 Selected JPCP unbonded overlay sections — Transverse cracking



(a) Time series (b) Age distribution

Figure 4-14 Selected JPCP unbonded overlay sections — Joint faulting



(a) Time series (b) Age distribution

Figure 4-15 Selected JPCP unbonded overlay sections — IRI

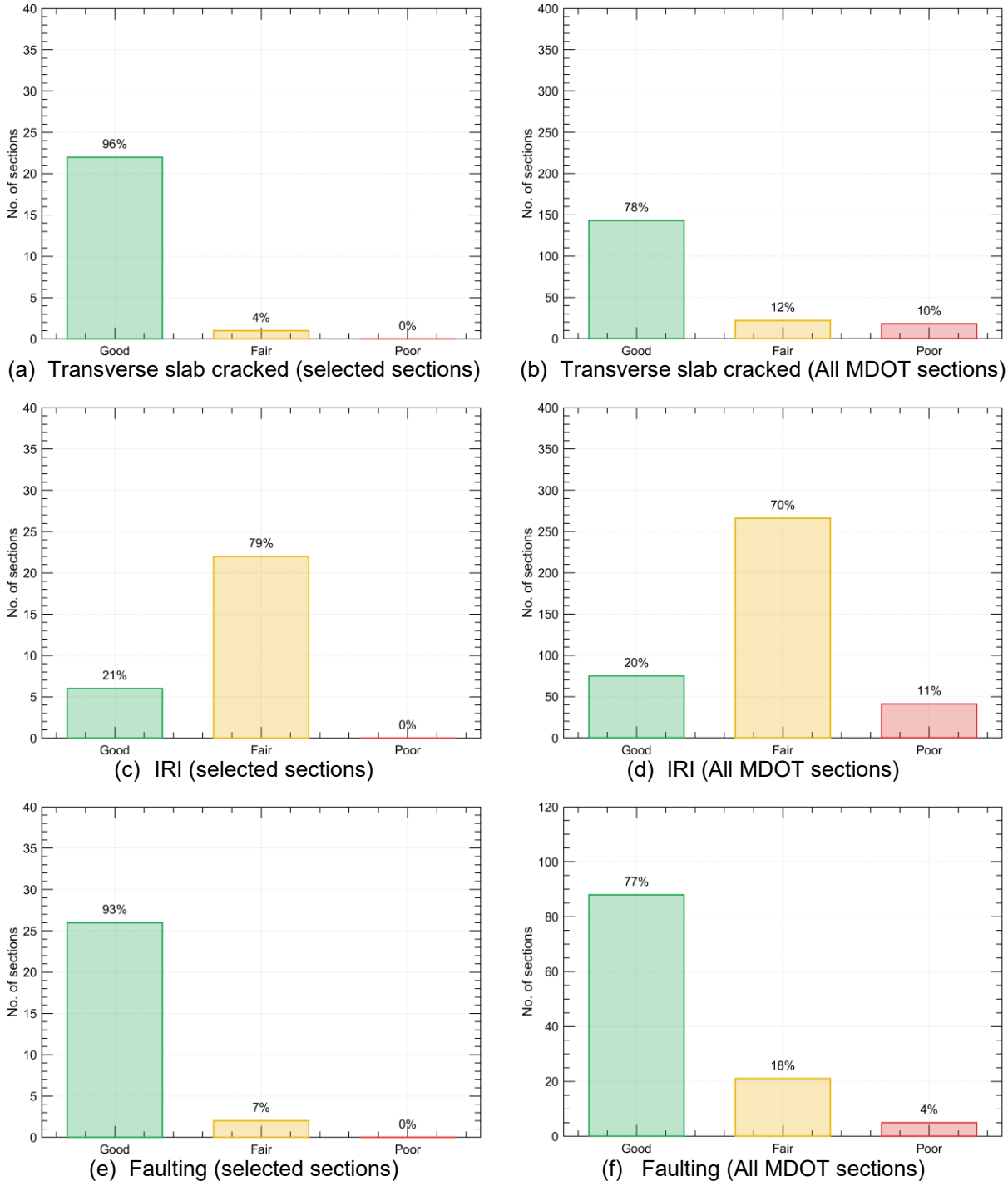
Figure 4-16 presents the distribution of good, fair, and poor sections for the selected concrete overlay sections and the full set of MDOT sections (noted as “All MDOT sections” in the figure). Details on the good, fair, and poor category definitions are provided in SPR-1723 (*2*). The “All MDOT sections” dataset includes reconstruction sections. These are provided for comparison purposes. As shown, most sections fall into the good category, as expected except IRI. Accordingly, once maintenance is performed, the resulting post-maintenance data are excluded from calibration analyses.

4.5 CALIBRATION INPUTS FOR MATERIALS, TRAFFIC, AND CLIMATE

PMED requires a large set of detailed input parameters, making data assembly a resource-intensive process. Many of these inputs are further organized into three hierarchical input levels, which define the degree of precision available for analysis. This section outlines procedures for assembling the as-constructed pavement structure, material properties, traffic inputs, and climatic data for each calibration section. It also summarizes the data sources, approaches for addressing missing information, and the selection of appropriate values. For each calibration pavement section, the team consistently relied on the highest input level supported by the available information. A complete listing of all material, traffic, and climate inputs is provided in Appendix B.

4.5.1 Pavement Cross-Section and Layer Configuration

Construction records, plans, JMFs, and MDOT databases (i.e., Pavement Historical Database and PAVETrack) were used to identify pavement cross-sections and material properties during construction. MDOT provided test results to estimate the best possible values for missing data. When data were missing or incomplete, practical assumptions were discussed with MDOT, and values were selected to represent anticipated field conditions best. This comprehensive approach allowed the assembling of the most reliable input dataset. Table 4-6 presents the mean cross-sectional details for the selected projects.



(a) Transverse slab cracked (selected sections)

(b) Transverse slab cracked (All MDOT sections)

(c) IRI (selected sections)

(d) IRI (All MDOT sections)

(e) Faulting (selected sections)

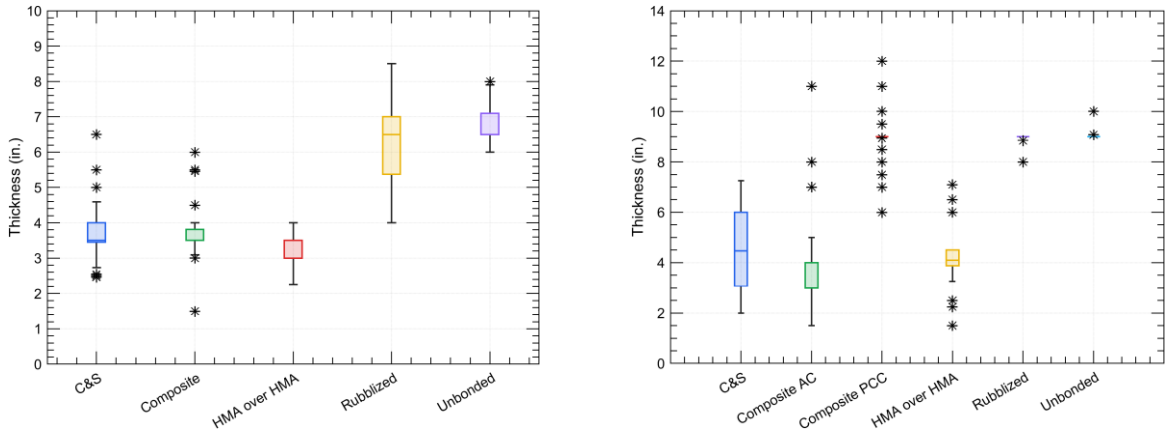
(f) Faulting (All MDOT sections)

Figure 4-16 Condition distribution of concrete overlay sections with all MDOT sections

Table 4-6 Average rehabilitation treatment thicknesses

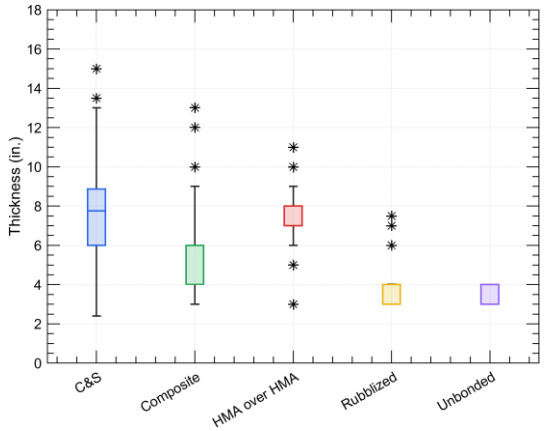
Rehabilitation type	Overlay thickness (in.)	Existing pavement thickness (in.)	Base thickness (in.)	Subbase thickness (in.)
HMA over C&S	3.64	4.46	7.55	20.97
HMA over rubblized PCC	6.28	8.83	3.92	11.79
HMA over PCC (composite)	3.65	8.93	5.21	12.77
HMA over HMA	3.29	4.19	7.87	16.68
JPCP unbonded overlay	6.93	9.07	3.68	11.64

Figure 4-17 shows the distribution of thicknesses of different pavement layers for all rehabilitation sections.

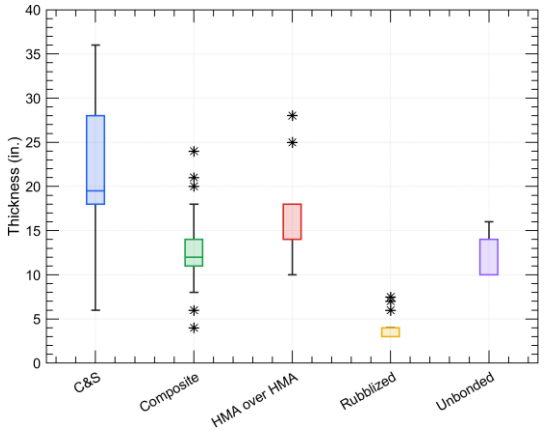


(a) Overlay layers (HMA or PCC)

(b) Existing layers (HMA or PCC)



(c) Existing aggregate base layer



(d) Existing sand subbase layer

Figure 4-17 Layer thickness distribution amongst different rehabilitation types

4.5.2 Material Inputs

The as-constructed material inputs were obtained from the construction records, JMFs, and other test records. Ideally, these inputs are recorded at the time of construction. These inputs range between project-specific and statewide average values. This section discusses the material properties of each pavement structural layer. The following is a summary of data resources for material inputs:

a. For the new HMA mix and binder properties, MDOT provided mix-specific values based on construction practices. These values have been obtained from laboratory testing of the mix and refined over time based on field performance (*2, 5*).
b. For the existing HMA and PCC, as described in Chapter 3, field cores were tested for dynamic modulus and concrete compressive strength. MDOT also provided FWD, LWD, and GPR data for 12 projects to estimate the in-situ properties of the existing materials.
c. The team used backcalculation results from this study, as described in Chapter 3, and compared them with past MDOT studies to estimate the stiffness of unbound materials.

4.5.2.1. HMA layer inputs

All inputs were collected at the highest available hierarchy level; however, the needed data were not available for all pavement sections. In that case, the data was collected using other correlations/sources. Data collection for new and existing HMA layers input includes:

New HMA (Overlay) Layers

- Dynamic modulus (*E**): MDOT provided *dynamic modulus* values for specific mix and binder combinations, determined through laboratory testing conducted in a previous study *(5)*. *Dynamic modulus* for the Superpave mixes was directly obtained from the database. For older mixes (marshal mixes), the volumetric, binder, and gradation information were used to predict the *dynamic modulus* using DYNAMOD's Artificial Neural Networks. D*ynamic modulus* was obtained at Level 1.
- Binder (*G**): MDOT also provided *complex shear modulus* based on the region and binder information. *Complex shear modulus* was obtained at Level 1.
- Creep compliance (D(t)): MDOT also provided creep compliance. Creep compliance was obtained at Level 1 for Performance Grade (PG) sections and Level 3 for other sections.
- Indirect Tensile Strength (IDT): MDOT also provided IDT at Level 2 for PG sections. Level 3 was used for other sections containing the older mixes.
- HMA layer thickness: These were obtained from construction records as previously mentioned.
- Air voids and binder content: As-constructed, air voids and binder content were obtained from the construction records. Table 4-7 summarizes the average as-constructed air voids for different pavement types. Historical test records were used to obtain an average value for unavailable data by mix type, as shown in Table 4-8.
- Aggregate gradation: Gradation was obtained from JMFs. Table 4-8 summarizes the average gradation of the top, leveling, and base layers for different pavement types. For unavailable data, historical test records were used to obtain average values by mix type, as shown in Table 4-9.

It is essential to note that Level 1 G* and Level 2 IDT data were used to calibrate the thermal cracking model.

Table 4-7 As-constructed percent air voids for HMA layers

HMA layer	Rehabilitation Type	Average as-constructed air voids
Top course	HMA over C&S	6.1
Top course	HMA over rubblized PCC	6.8
Top course	HMA over HMA	6.2
Top course	HMA over PCC (composite)*	6.1
Leveling course	HMA over C&S	6.2
Leveling course	HMA over rubblized PCC	6.4
Leveling course	HMA over HMA	6.2
Base course	HMA over C&S	5.8
Base course	HMA over rubblized PCC	5.8

* = an average %AV for all new HMA layers over PCC

Table 4-8 HMA layer average aggregate gradation

HMA layer	Rehabilitation type	Effective HMA binder content	% Passing 3/4" Sieve	% Passing 3/8" Sieve	% Passing #4 Sieve	% Passing #200 Sieve
Top course	HMA over C&S	11.5	100.0	89.7	68.4	5.2
Top course	HMA over rubblized PCC	11.9	99.4	89.8	67.3	5.9
Top course	HMA over HMA	12.3	100.0	93.4	72.2	5.6
Top course	HMA over PCC (composite)*	12.5	100.0	94.4	72.1	5.6
Leveling course	HMA over C&S	10.6	100.0	81.8	61.1	5.0
Leveling course	HMA over rubblized PCC	11.2	100.0	87.0	67.8	5.2
Leveling course	HMA over HMA	11.3	100.0	84.9	64.0	5.2
Base course	HMA over C&S	10.8	99.6	77.9	60.3	4.6
Base course	HMA over rubblized PCC	10.6	99.3	78.9	59.9	4.8

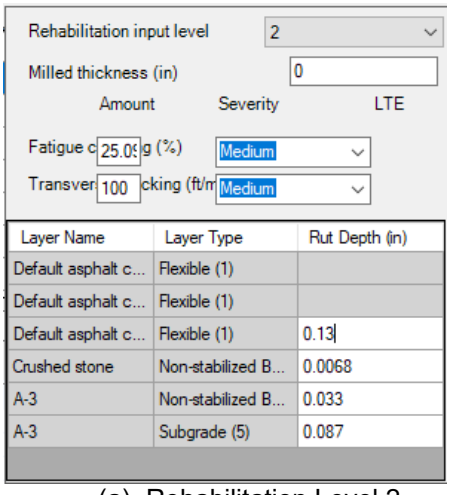
* = average values of %binder and gradations for all new HMA layers over PCC

Table 4-9 MDOT recommended values, volumetrics, and gradation

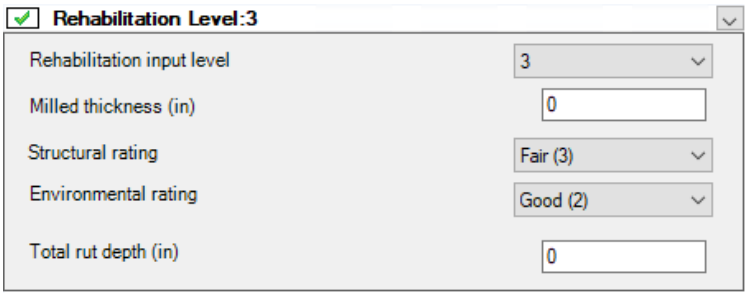
Mix type	Air voids (%)	Effective binder content (%)	% Passing 3/4" Sieve	% Passing 3/8" Sieve	% Passing #4 Sieve	% Passing #200 Sieve
3E1	5.8	10.8	99.85	80.44	62.94	4.40
4E1	6.1	11.5	100.00	87.24	70.43	5.11
5E1	6	12.6	100.00	97.14	78.23	5.63
2E3	4.8	9.7	92.65	68.70	53.95	4.40
3E3	5.8	10.8	99.63	77.88	60.33	4.56
4E3	6.1	11.5	100.00	86.91	68.66	4.92
5E3	6	12.6	100.00	97.86	79.81	5.49
2E10	4.8	9.7	94.55	73.50	59.70	4.50
3E10	5.8	10.8	99.78	80.27	62.78	4.84
4E10	6.1	11.5	100.00	87.65	70.06	5.26
5E10	6	12.6	100.00	98.30	81.27	5.67
2E30	4.8	9.7	99.00	71.80	60.60	4.20
3E30	5.8	10.8	99.95	79.20	59.82	4.40
4E30	6.1	11.5	100.00	88.63	66.90	4.33
5E30	6	12.6	100.00	99.00	81.24	5.68

Existing HMA Layers

The PMED characterizes existing HMA layers at three rehabilitation levels, as discussed in Chapter 2. Level 1 uses FWD backcalculated moduli; Level 2 employs percent fatigue cracking on existing surfaces; and an overall structural rating is used at Level 3. In this study, Levels 2 and 3 were used to characterize the existing HMA, as FWD data for HMA overlay sections were not available. Figure 4-18 shows the inputs required to characterize existing HMAs at rehabilitation Levels 2 and 3.



(a) Rehabilitation Level 2



(b) Rehabilitation Level 3

Figure 4-18 The PMED characterization of existing HMA at rehabilitation Levels 2 and 3

Data were extracted from the PMS database on percent fatigue cracking, transverse cracking, and total rutting for the most recent years available before the placement of the overlay. The total rutting was distributed into HMA, aggregate base, and subgrade rutting as per the findings of SPR 1723 (2). Fair-condition values, in consultation with

MDOT, were assumed when data were missing. Tables 4-10 and 4-11 present the structural and environmental rating criteria for bottom-up fatigue and thermal cracking, respectively.

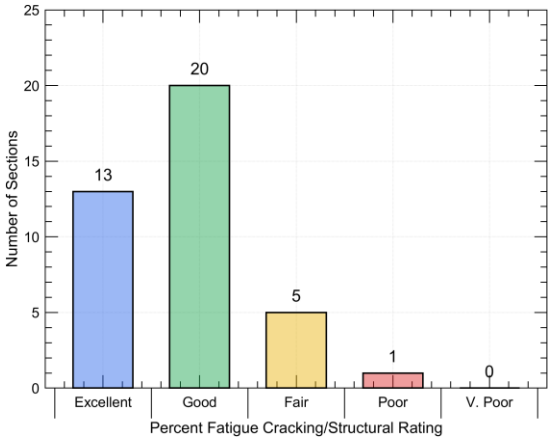
Table 4-10 Structural rating criteria per the corresponding bottom-up fatigue cracking

Structural Rating (Level 3)	**Damage index (d_{HMA}) interval**	**Damage value used in PMED**	**Corresponding fatigue cracking (%)**
Excellent	0.00 – 0.20	0.1	< 7.0
Good	0.20 – 0.40	0.3	7.0-20.9
Fair	0.40 – 0.80	0.6	21.0-35.9
Poor	0.80 – 1.20	1.0	36.0-50.0
Very poor	> 1.20	1.2	> 50.0

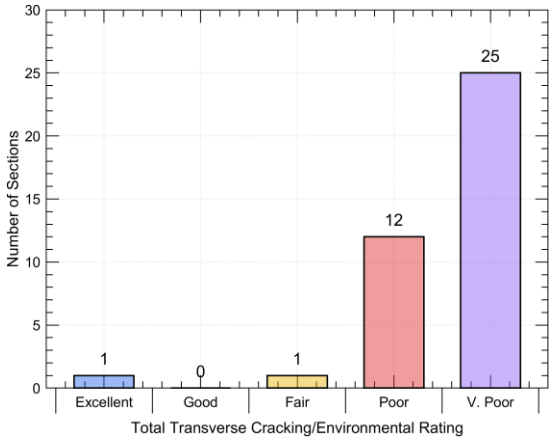
Table 4-11 Environmental rating criteria per the corresponding thermal cracking

Environmental Rating (Level 3)	**Corresponding Thermal cracking (ft/mile)**
Excellent	Less than 100
Good	100 - 200
Fair	200 - 500
Poor	500 – 1,000
Very poor	Above 1,000

Figure 4-19 shows the distribution of sections for percent fatigue cracking, total transverse cracking, structural rating, and environmental rating for HMA over HMA overlays.



(a) Percent fatigue cracking



(b) Total transverse cracking

Figure 4-19 Distribution of fatigue and transverse cracking for HMA over HMA overlays

The percent binder content and mix gradation of field cores were estimated and summarized in Chapter 3, Figure 3-26(a) and Table 3-25. The average binder content was 6.2%. The average gradation of field cores closely matched that of the 4E mix. Therefore, the 4E mix properties were used for existing HMA layers. A sensitivity analysis was conducted to determine the impact of the existing layer's G* on predicted performance. It was observed that G* of the existing HMA layer has minimal effect on PMED predicted performance; therefore, a PG64-22 binder was recommended for existing HMA layers.

4.5.2.2. PCC material inputs

The PMED transverse cracking prediction model is very sensitive to concrete strength. The PCC material-related inputs were obtained from material testing results. If these results were unavailable, typical MDOT values were used.

New PCC Layers

As part of SPR-1723, MDOT collected compressive-strength data from cores obtained near construction time. The MOR values were estimated based on the ACI correlation (Equations 4-7). The remaining values were used in accordance with MDOT specifications (*6*).

$$MOR = 9.5 \times \sqrt{f_c'} \quad (4\text{-}7)$$

where;
MOR = modulus of rupture of concrete (psi).
$\sqrt{f_c'}$ = concrete compressive strength (psi).

Strength of Existing PCC Layers

The PMED characterizes existing PCC layers using the concrete elastic modulus. The transverse cracking prediction is sensitive to the existing concrete's elastic modulus. The default PMED value for existing concrete is 2,000,000 psi. To establish representative properties, twenty field cores obtained from existing composite and PCC pavement sections were tested for compressive strength. Compressive strength values were converted to elastic modulus using the established correlation presented in Chapter 3. The corresponding results are summarized in Table 3-27, with calculated elastic modulus values ranging from 5,200,000 psi to 5,900,000 psi. Accordingly, an elastic modulus of 5,000,000 psi was selected as a representative design value, accounting for potential variability in material properties, particularly for non-reinforced sections, which may have a lower modulus. However, to account for field conditions of the existing PCC layer and recognizing that core samples were obtained from visually intact slabs, the laboratory-based design elastic modulus was adjusted using a C_{BD} factor of 0.6[1], resulting in a representative design value of approximately 3,000,000 psi.

Condition of Existing PCC Layers under HMA Overlays

PMED requires that existing PCC layers be present to simulate the performance of rehabilitated pavements. The PMED uses the condition of the existing slab to account for the pre-existing level of slab distress when estimating future damage progression. The model uses user-defined inputs to represent the extent of cracking or replacement before restoration, before overlay placement. The PMED user guide defines these inputs as follows (*7*):

[1] As per PMED manual of practice, the condition of existing concrete cores were considered as “Good”.

- **Slabs distressed/replaced before restoration (%)** – Represents the percentage of slabs exhibiting cracking before rehabilitation. This value characterizes the initial condition of the existing PCC and includes all visible slab cracking before overlay placement.
- **Slabs repaired/replaced after restoration (%)** – Defines the percentage of slabs repaired or replaced during rehabilitation. The difference between distressed and replaced slabs indicates the portion of slabs that remain cracked after restoration.

MDOT does not record these inputs as part of their data collection. In consultation with MDOT and the DI, the DI and the percent of slabs cracked before overlay placement on all concrete pavements were used to estimate these inputs. The slabs distressed/replaced before restoration were assumed to be twice the pre-overlay DI value, or up to 90%. The "slabs repaired/replaced after restoration" were taken, and half of the "slabs distressed/replaced before restoration".

4.5.2.3. Aggregate base/subbase and subgrade input values

MDOT recommends resilient modulus values of 33,000 psi and 20,000 psi for new base and subbase layers, respectively (*2*). The subgrade material type and resilient modulus are based on recommendations from the subgrade resilient modulus study *(8, 9)*. MDOT's previous calibration studies used resilient modulus values of 30,000 psi for base, 13,500 psi for sand subbase materials, 125,000 psi for C&S, and 70,000 psi for rubblized concrete.

Resilient modulus testing was attempted for the rubblized material; however, laboratory MR testing was not feasible due to the large fragment sizes produced by rubblization. As shown in Figure 3-20(d), most fragments were retained above the 2-inch sieve. They could not be compacted in a 6-inch-diameter MR mold while satisfying the standard requirement that the nominal maximum aggregate size be less than one-fourth of the specimen diameter. Attempts to isolate smaller particles resulted in non-representative specimens. As discussed in Chapter 2, reported resilient modulus values for rubblized concrete from various DOT studies range approximately from 35,000 psi to 170,000 psi. Accordingly, a representative value of 70,000 psi was adopted, consistent with prior MDOT calibration efforts (*2, 10-12*).

FWD deflection data was used to backcalculate the resilient modulus of the existing aggregate base, sand subbase, and C&S layers. The results of this analysis were provided in Chapter 3. Representative resilient modulus values for unbound layers were based on backcalculated values from this research and previous studies (*9, 13*). SPR-1723 also reports laboratory testing of existing resilient modulus values for the base and subbase (*2*).

For this research study, C&S material was tested in the laboratory to determine the resilient modulus.

Table 4-12 summarizes resilient modulus for the existing base and subbase based on results from both current and previous studies.

Table 4-12 Summary of existing base and subbase resilient modulus values

	SPR-1548[1] Base (psi)	SPR-1548[1] Subbase (psi)	SPR-1723[2] Base (psi)	SPR-1723[2] Subbase (psi)	This Study[3] Base (psi)	This Study[3] Subbase (psi)
Weighted Mean	**35,323**	**24,825**	**33,862**	**19,585**	**27,956**	**19,155**
Minimum	8,087	2,894	22,610	11,900	8,100	3,367
Maximum	70,007	39,980	47,520	30,060	69,467	39,967
Std. Dev.	17,498	8,219	11,422	10,977	15,982	10,265
Standard Error (SE)	851	694	2,949	2,662	1,465	1,020
95% CI (Upper)	*37,025*	26,215	*39,760*	*24,910*	30,887	21,195
95% CI (Lower)	*33,621*	23,436	*27,964*	*14,261*	25,025	17,117
Mean+Std Dev.	52,822	33,044	45,284	30,562	43,938	29,420
Mean-Std Dev.	17,825	16,607	22,440	8,608	11,974	8,891
15th Percentile	**14,318**	**15,401**	**26,399**	**13,087**	**11,325**	**6,967**
85th Percentile	**57,076**	**34,493**	**41,689**	**24,958**	**47,245**	**31,587**
Total number of tests	2,017	1,998	15	17	448	448
Number of included tests	1,723	1,700	15	17	364	364

[1] Based on FWD deflections and backcalculation (field in-situ moduli)
[2] Lab measured resilient modulus values from material samples
[3] Based on FWD deflections and backcalculation (field in-situ moduli)

Table 4-13 summarizes the structural layer coefficients used in MDOT's rehabilitation designs, based on the AASHTO 93 Guide, and the estimated resilient modulus values based on the following correlation used by PMED (*7*).

$$MR = 30{,}000 \times \left({}^{a_i}/_{14}\right) \quad (4\text{-}8)$$

where;
MR = resilient modulus
a_i = layer coefficient

Table 4-13 Structural layer coefficients for existing unbound layers

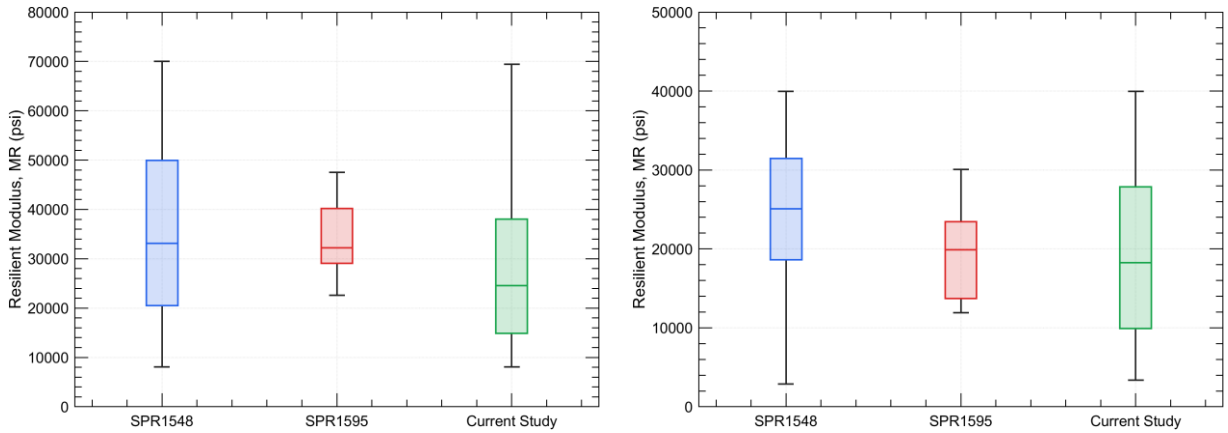
Layer Type	Notes	Structural Coefficient (a_i)	Estimated Resilient modulus (psi)
Existing Aggregate Base	No evidence of pumping, degradation, or contamination by fines	0.130	27,857
Existing Aggregate Base	Evidence of pumping, degradation, or contamination by fines	0.060	12,857
Existing Sand Subbase	No evidence of pumping, degradation, or contamination by fines	0.090	19,286
Existing Sand Subbase	Evidence of pumping, degradation, or contamination by fines	0.040	8,571
New DGAB	None	0.140	30,000
New DGAB	ME resilient modulus conversion to structural coefficient	0.154*	33,000
New OGDC	None	0.130	27,857
New Sand Subbase	None	0.100	21,429
New Sand Subbase	ME resilient modulus conversion to structural coefficient	0.093*	20,000

* Structural coefficient estimated from the MDOT PMED value.

The backcalculated and laboratory-tested resilient modulus values of C&S layers were also evaluated from triaxial testing (Table 4-14). Figure 4-20 illustrates the distribution of existing base and subbase resilient moduli from previous and current studies.

Table 4-14 Summary of C&S layer resilient modulus values

	Backcalculation 3-Layered (psi)	Backcalculation 4-Layered (psi)	Laboratory Determined (psi)
Weighted Mean	**61,460**	**61,553**	**40,595**
Minimum	20,567	18,700	18,000
Maximum	111,200	109,500	74,950
Std. Dev.	26,294	22,928	22,305
Standard Error (SE)	5,475	4,851	11,259
95% CI (Upper)	72,411	71,255	63,113
95% CI (Lower)	50,510	51,851	18,077
Mean+Std Dev.	87,755	84,481	62,900
Mean-Std Dev.	35,166	38,624	18,290
15th Percentile	**16,240**	**31,678**	**24,419**
85th Percentile	**76,940**	**76,778**	**63,893**
Total number of tests	232	232	13
Number of included tests	154	154	13



(a) Existing aggregate base (b) Existing sand subbase

Figure 4-20 Distribution of resilient modulus values of existing base and subbase

Evaluating data from recent and previous projects suggests the following resilient modulus ranges:

- Existing aggregate base – 25,000 to 39,000 psi.
- Existing sand subbase – 14,000 to 28,000 psi.
- C&S – 35,000 to 88,000 psi.

These ranges reflect in situ testing results, making it difficult to recommend a single resilient modulus value due to regional differences, material types, timing of FWD testing, and variations in moisture conditions. Establishing a representative design value requires extensive non-destructive testing (NDT) and laboratory testing. As highlighted above, environmental factors significantly influence the resilient modulus of unbound layers. Conducting monthly FWD tests at specific sites in each MDOT region helps capture seasonal impacts on resilient modulus and account for this variability. Considering the data shown in Tables 4-11 to 4-13, earlier calibration efforts, and consultation with MDOT, the team recommended the following single representative design values:

- Existing aggregate base – 28,000 psi.
- Existing sand subbase – 18,000 psi
- C&S existing HMA – 60,000 psi
- Rubblized PCC base – 70,000 psi

Annual representative values for subgrade resilient modulus were used in PMED based on SPR-1531 (*8*). The recommended resilient modulus value for the soil type is shown in Table 4-15.

Table 4-15 Average roadbed soil resilient modulus values (*2*)

USCS	AASHTO	Laboratory-determined (psi)	Back-calculated (psi)	Recommended design resilient modulus value (psi)
SM	A-2-4, A-4	17,028	24,764	5,200
SP1	A-1-a, A-3	28,942	27,739	7,000
SP2	A-1-b, A-3	25,685	25,113	6,500
SP-SM	A-1-b,A-2-4, A-3	21,147	20,400	7,000
SC-SM	A-2-4, A-4	23,258	20,314	5,000
SC	A-2-6, A-6, A-7-6	18,756	21,647	4,400
CL	A-4, A-6, A-7-6	37,225	15,176	4,400
ML	A-4	24,578	15,976	4,400
SC/CL/ML	A-2-6, A-4, A-6, A-7-6	26,853	17,600	4,400

4.5.3 Traffic Inputs

Traffic data were collected from the construction records and the MDOT Transportation Data Management System (TDMS). Level 2 (cluster grouping) data were used to determine the traffic inputs for all sections. MDOT provided a spreadsheet with the PMED traffic input tables for the following:

- Vehicle class distribution
- Hourly distribution (only for concrete sections)
- Monthly adjustment factor
- Number of axles per truck
- Single axle load spectra
- Tandem axle load spectra
- Tridem axle load spectra
- Quad axle load spectra

To determine the applicable inputs, the section attributes, including road type, number of lanes, and percentage of class 9 vehicles, were used to identify the appropriate cluster group. Table 4-16 summarizes the Level 2 attributes and categories used for traffic input selection.

Table 4-16 MDOT Level 2 Attributes and Subcategories for Traffic inputs

Attribute	Categories
Percentage of vehicle class 9	• Less than 45 • 45 to 70 • Above 70
Region type	• Rural • Urban
Corridors of Highest Significance (COHS) type	• National • Regional • Statewide
Number of lanes	• 2 • 3 • 4+

The team extracted two-way average annual daily truck traffic (AADTT) and the number of lanes from the project plans. The range and average two-way AADTT values for rehabilitation projects are summarized in Table 4-17. Figure 4-21 shows the overall distribution of the AADTT across different rehabilitation types for the selected sections.

Table 4-17 Ranges of AADTT for all rehabilitation projects

Rehabilitation Type	Minimum AADTT	Maximum AADTT	Average AADTT
HMA over C&S	35	1,784	599
HMA over rubblized PCC	173	3,707	1,514
HMA over PCC (composite)	113	20,876	2,809
HMA over HMA	61	3,780	695
JPCP unbonded overlay	1,458	6,100	4,472

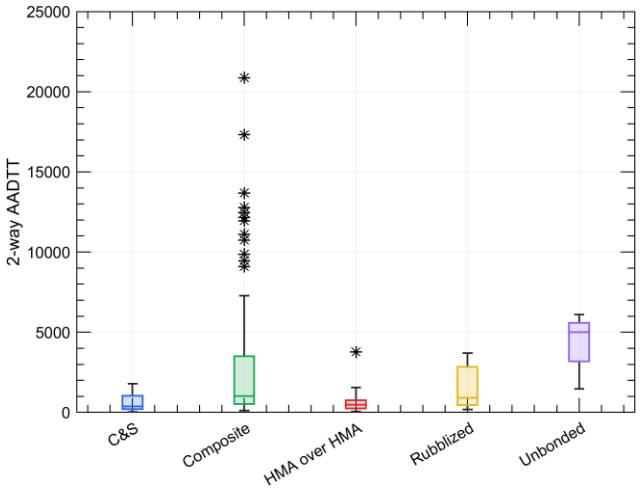


Figure 4-21 Distribution of 2-way AADTT

A lane distribution value of 50% and a directional distribution value of 90% were assumed for all calibration sections. When the number of lanes was unavailable, it was estimated from Google Maps aerial imagery. The Physical Reference (PR) number and beginning and ending milepost were used to determine the COHS type. The percentage of Class 9 vehicles was estimated for each section using the MDOT TDMS database (*14*). For sections where traffic data was unavailable, values from nearby locations within the same corridor were used.

4.5.4 Climatic Inputs

For climatic data, this study used the updated North American Regional Reanalysis (NARR) files for Michigan as revised in SPR-1626 *(15)*. The PMED default NARR climatic files were corrected and supplemented with additional data from the ASOS and the Michigan RWIS to improve spatial and temporal coverage*(2, 16)*.

The previous calibration study, SPR-1723, provided a comprehensive evaluation of PMED inputs by comparing data from the Modern-Era Retrospective Analysis for Research and Applications (MERRA) and NARR datasets to determine the most suitable source for Michigan conditions (*2*). Using overlapping hourly records from 2000

to 2013, the study found that NARR provided more reliable data for temperature, humidity, and wind speed, whereas MERRA exhibited inconsistencies, particularly in humidity and precipitation.

Following the recommendations of SPR-1723, this study adopted the improved MDOT NARR climatic files for all calibration analyses (*2*). These files, formatted as *.hcd and directly compatible with PMED, were assigned to each selected project using the nearest climate station. Table 4-18 summarizes the MDOT climatic files used for calibration (*2*).

Table 4-18 Michigan climate station information

HCD filename	City/Location	Climate identifier	Latitude	Longitude
4847	Adrian	Adrian Lenawee County Arpt	41.868	-84.079
94849	Alpena	Alpena Co Rgnl Airport	45.072	-83.581
94889	Ann Arbor	Ann Arbor Municipal Arpt	42.224	-83.74
14815	Battle Creek	W K Kellogg Airport	42.308	-85.251
94871	Benton Harbor	Sw Michigan Regional Arpt	42.129	-86.422
14822	Detroit	Detroit City Airport	42.409	-83.01
94847	Detroit	Detroit Metro Wayne Co Apt	42.215	-83.349
14853	Detroit	Willow Run Airport	42.237	-83.526
14826	Flint	Bishop International Arpt	42.967	-83.749
4854	Gaylord	Otsego County Airport	45.013	-84.701
94860	Grand Rapids	Gerald R Ford International Airport	42.882	-85.523
14858	Hancock	Houghton County Memo Arpt	47.169	-88.506
4839	Holland	Tulip City Airport	42.746	-86.097
94814	Houghton Lake	Roscommon County Airport	44.368	-84.691
94893	Iron Mountain/Kingsford	Ford Airport	45.818	-88.114
14833	Jackson	Jakson Co-Rynolds Fld Arpt	42.26	-84.459
94815	Kalamazoo	Klmazo/Btl Creek Intl Arpt	42.235	-85.552
14836	Lansing	Capital City Airport	42.78	-84.579
14840	Muskegon	Muskegon County Airport	43.171	-86.237
14841	Pellston	Pton Rgl Ap Of Emmet Co Ap	45.571	-84.796
94817	Pontiac	Oakland Co. Intnl Airport	42.665	-83.418
14845	Saginaw	Mbs International Airport	43.533	-84.08
14847	Sault Ste Marie	Su Ste Mre Muni/Sasn Fl Ap	46.467	-84.367
14850	Traverse City	Cherry Capital Airport	44.741	-85.583
AMN	Alma	Gratiot Community Airport	43.322	-84.688
BAX	Bad Axe	Huron County Memorial Airport	43.78	-82.985
CFS	Caro	Tuscola Area Airport	43.459	-83.445
ERY	Newberry	Luce County Airport	46.311	-85.4572
ESC	Escanaba	Delta County Airport	45.723	-87.094
FKS	Frankfort	Frankfort Dow Memorial Field Airport	44.625	-86.201
IRS	Sturgis	Kirsch Municipal Airport	41.813	-85.439
ISQ	Manistique	Schoolcraft County Airport	45.975	-86.172
IWD	Ironwood	Gogebic Iron County Airport	46.527	-90.131
LDM	Ludington	Mason County Airport	43.962	-86.408
MOP	Mount Pleasant	Mount Pleasant Municipal Airport	43.622	-84.737
OSC	Oscoda	Oscoda Wurtsmith Airport	44.452	-83.394
PHN	Port Huron	Saint Clair County Intnl Airport	42.911	-82.529
RQB	Big Rapids	Roben Hood Airport	43.723	-85.504
SAW	Gwinn	Sawyer International Airport	46.354	-87.39

4.6 SUMMARY

This chapter outlines the steps for collecting data, selecting projects and calibration sections, and obtaining the PMED inputs for the calibration sections. Details about each input, its source, and potential estimates in the event of unavailable data have also been discussed. In addition, the number of sections for each rehabilitation type and performance criteria has been summarized. PMED inputs used for calibration during his project are included in Appendix B. The following primary inputs were used during the calibration process:

- Rehabilitation levels: Level 2 or 3 for calibration – both options evaluated.
- Structural and environmental ratings: As per Tables 4-10 and 4-11.
- Existing HMA layer:
    - MDOT recommended 4E mix properties.
    - PG64-22 for G* of existing HMA.
- New HMA (overlay) layer:
    - All inputs were used in accordance with the latest MDOT specifications (*6*).
- Existing PCC layer:
    - Elastic modulus of 3,000,000 psi.
    - Slabs distressed/replaced before restoration (%) – two times of pre-overlay DI.
    - Slabs repaired/replaced after restoration (%) – half of the slabs were distressed/replaced before restoration.
- New PCC (overlay) layer:
    - All inputs were used in accordance with the latest MDOT specifications (*6*).
- Unbound materials:
    - Existing aggregate base resilient modulus – 28,000 psi.
    - Existing sand subbase resilient modulus – 18,000 psi.
    - Existing C&S HMA resilient modulus – 60,000 psi.
    - Existing rubblized PCC resilient modulus – 70,000 psi

CHAPTER 5 - REHABILITATION MODEL SELECTION

5.1 INTRODUCTION

Before calibrating performance prediction models, it is necessary to establish appropriate rehabilitation modeling approaches that accurately represent the range of pavement fixes implemented by MDOT. The PMED software provides a mechanistic–empirical platform for analyzing pavement responses and estimating long-term performance under varying traffic and environmental conditions. PMED categorizes pavement structures as flexible, rigid, or overlaid systems, each governed by specific modeling assumptions, stress–strain formulations, and material property inputs. Selecting an appropriate modeling type is therefore critical to ensure that predicted distresses, such as fatigue cracking, rutting, and joint faulting, reflect realistic field performance.

MDOT employs a range of rehabilitation strategies to address existing pavement conditions, structural adequacy, and material compatibility. These strategies include asphalt overlays on asphalt or concrete pavements, unbonded PCC overlays, rubblization of existing concrete before asphalt resurfacing, and C&S operations for distressed asphalt pavements. Each rehabilitation fix type exhibits unique structural behavior and requires specific characterization of the existing layers in PMED. For example, the condition of the existing HMA layer will impact the performance of HMA overlays. On the other hand, the modulus of rubblized or C&S layers will impact the performance of new asphalt layers.

Because PMED applies standardized layer configurations and bonding conditions, not all MDOT rehabilitation fixes can be designed directly. Specific complex strategies, such as short-jointed concrete overlays with fiber reinforcement or unique layers, such as overlays incorporating ASCRL, exceed the current modeling capabilities of PMED versions 2.6 and 3.0. Identifying these limitations is essential for determining which rehabilitation designs can be realistically analyzed within PMED and which require future methodological development.

This chapter presents the classification of MDOT rehabilitation fix types and their corresponding mechanistic–empirical design representations. It delineates the fixes that can be modeled directly, those that are not currently supported, and those that may be indirectly modeled. The outcome of this classification establishes a consistent analytical framework for subsequent calibration and validation of rehabilitation performance models. The following rehabilitation strategies were evaluated for MDOT modeling as part of this study:

1. HMA over JPCP
2. HMA over JRCP
3. HMA over CRCP

4. HMA with ASCRL over JPCP
5. HMA with ASCRL over JRCP
6. HMA with ASCRL over CRCP
7. HMA over HMA/JPCP (composite pavement)
8. HMA over HMA/JRCP (composite pavement)
9. HMA over HMA/CRCP (composite pavement)
10. HMA over HMA (full depth)
11. HMA over rubblized concrete
12. HMA over C&S
13. HMA over aggregate-lift sections of existing PCC
14. HMA over aggregate-lift sections of existing HMA
15. Concrete over JPCP
16. Concrete over JRCP
17. Concrete over CRCP
18. Concrete over HMA/JPCP (composite)
19. Concrete over HMA/JRCP (composite)
20. Concrete over HMA/CRCP (composite)
21. Concrete over HMA (full depth)
22. JPCP over aggregate-lift sections of existing PCC
23. JPCP over aggregate-lift sections of existing HMA
24. SJPCP (including fibers) over JPCP
25. SJPCP (including fibers) over JRCP
26. SJPCP (including fibers) over CRCP
27. SJPCP (including fibers) over HMA/JPCP (composite)
28. SJPCP (including fibers) over HMA/JRCP (composite)
29. SJPCP (including fibers) over HMA/CRCP (composite)
30. SJPCP (including fibers) over HMA (full depth)

These fix types include the primary rehabilitation options MDOT considers for restoring structural capacity and extending pavement service life across the state's network. Their representation within the PMED framework forms the foundation for assessing modeling feasibility and guiding the calibration of performance prediction models in subsequent sections. Figure 5-1 shows the available rehabilitation modeling options in PMED V2.6.

5.2 FIX TYPES MODELED DIRECTLY IN THE PMED

Several MDOT rehabilitation fix types can be modeled directly in PMED using its existing structural configurations and input parameter framework. These fixes align with PMED's predefined mechanistic–empirical pavement categories and can be analyzed without modifying the software's design logic. They represent standard rehabilitation practices, such as asphalt overlays on asphalt or concrete pavements and unbonded concrete overlays, that are fully compatible with PMED's modeling assumptions and performance prediction capabilities. The following subsections present a detailed discussion of each fix type, outlining its structural configuration, material characterization, and the corresponding PMED modeling approach. All calibration inputs are summarized in Appendix B.

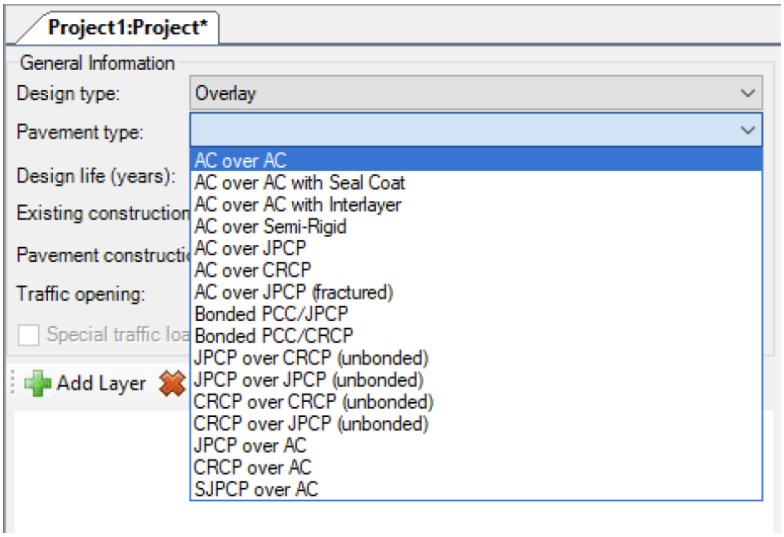


Figure 5-1 Overlay modeling options available in the PMED V2.6 (*1*)

5.2.1 HMA over HMA

HMA overlays are applied to flexible and composite pavements to restore surface profile, structural capacity, and ride quality. The overlay configuration and pre-overlay treatments are selected based on the existing pavement condition, subgrade support, and traffic demand. This fix type is directly modeled by the PMED design/pavement type of “Overlay, AC over AC”. The following subsections summarize the key considerations and findings associated with this design type.

5.2.1.1. Rehabilitation Levels

As mentioned in Chapter 2, the PMED characterizes the existing HMA layer at three rehabilitation levels. Due to the unavailability of FWD data for rehabilitation Level 1 for most projects, the team evaluated the feasibility of calibrating this fix type using rehabilitation Levels 2 and 3.

Rehabilitation Level 3 characterizes the existing pavement based on the total rut depth (per inch) and structural and environmental ratings. The rutting input for existing layers is taken as total rutting in existing pavement only. The structural and environmental ratings are associated with a predefined HMA damage index value to estimate damage. Using the methodology explained in Chapter 2 section 2.5.1, the predefined damage index is used to calculate the bottom-up fatigue cracking. At rehabilitation Level 3, the distress severity levels and corresponding load transfer efficiency (LTE) are predefined based on the overall condition rating. See Tables 4-10 and 4-11 for the corresponding bottom-up and thermal cracking associated with structural and environmental ratings.

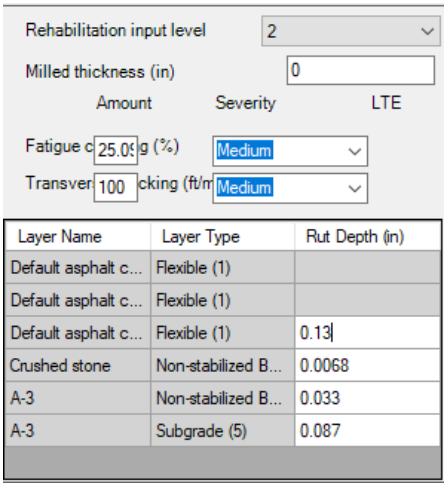
For reference and comparison, FHWA assigns three condition rating categories for existing pavements based on the percentage of alligator (bottom-up) cracking. In contrast, PMED assigns five condition rating categories based on the damage index of the existing HMA layer. Table 5-1 shows the condition ratings of FHWA and PMED and their corresponding ranges of alligator cracking (*1-3*).

Overall, since the ratings are subjective and imprecise estimates, Level 3 rehabilitation is not recommended.

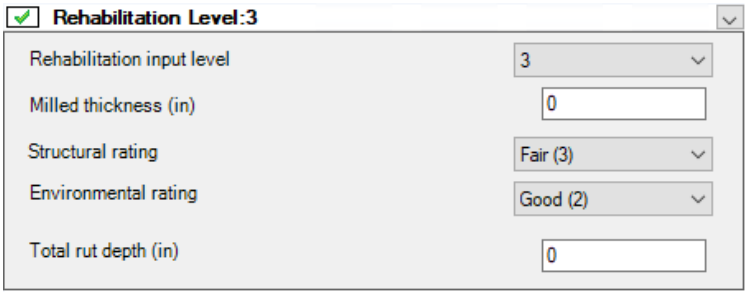
Table 5-1 FHWA pavement condition rating

Pavement Condition Rating Category	FHWA alligator cracking (%)	PMED estimated alligator cracking (%)
Excellent	N/A	Less than 7.0
Good	Less than 5.0	7.0 - 20.9
Fair	5.0 – 20.0	21.0 - 35.9
Poor	Greater than 20.0	36.0 - 50.0
Very Poor	N/A	Greater than 50.0

Rehabilitation Level 2 characterizes the existing pavement based on actual measured fatigue and transverse cracking, along with their severity levels. Additionally, Level 2 requires entry of rutting in existing HMA and unbound layers. Figure 5-2 shows the differences between the rehabilitation Levels 2 and 3 inputs in the PMED.



(a) Rehabilitation Level 2



(b) Rehabilitation Level 3

Figure 5-2 The PMED rehabilitation Levels 2 and 3

5.2.1.2. Performance Prediction Models

The PMED analyzes asphalt overlays placed over existing flexible and composite pavements using the same distress models applied to new flexible pavement designs. The distress prediction framework considers both the initiation of new damage in the overlay and the ongoing deterioration of the underlying pavement layers. Fatigue cracking is evaluated at the bottom of the overlay (new HMA layers) using the alligator cracking model. In contrast, reflective and thermal cracking are predicted using mechanistic–empirical fracture-mechanics relationships. It is essential to note that PMED estimates rutting in all asphalt and unbound layers, accounting for ongoing deformation in the existing materials.

The rutting model uses existing rutting to assess the stage of plastic deformation in the mix and to determine the point at which strain accumulation occurs in the strain-versus-

load cycles relationship (*1*). Figure 5-3 shows typical load cycles and a plastic deformation curve. For example, if the existing layers have a total rutting of 0.2 inches, the program will likely set the rate of deformation to the slower-gain steady-state zone (depending on other project parameters). Whereas, if no existing rutting is entered, then the program assumes the pavement has not yet undergone the initial faster gain in the primary zone. Accordingly, if rutting values are not provided (because the existing pavement has not experienced measurable rutting during its service life or are unavailable), PMED will predict higher total rutting, since the strain point initiates in the primary deformation zone. As a result, for equivalent structural overlay designs, the design with initial rutting will have a lower final total AC rutting prediction than one without initial rutting. Therefore, it is vital to provide an initial rutting value for existing layers to avoid incorrect rutting estimates in designs.

Based on this investigation and consultation with MDOT, the research team recommends using an average total rut depth of 0.22 inches for existing pavement layers when measured rutting data is unavailable, and a minimum value of 0.20 inches when measured rut depth is less than this amount. The total rut depth should then be allocated across the pavement layers following the rutting distribution observed for MDOT HMA overlay sections – 75% in the HMA layer, 17% in the unbound layers (base plus subbase), and 8% in the subgrade – before entering the values into PMED at rehabilitation Level 2. For additional details on rut distributions, see SPR 1723 (*4*). For example, if the minimum total rutting is 0.20 inches, then the PMED Level 2 existing rut depth inputs should be 0.15 inches (75.0%) for HMA, 0.017 inches (8.5%) for base, 0.017 inches (8.5%) for subbase, and 0.016 inches (8.0%) for subgrade.

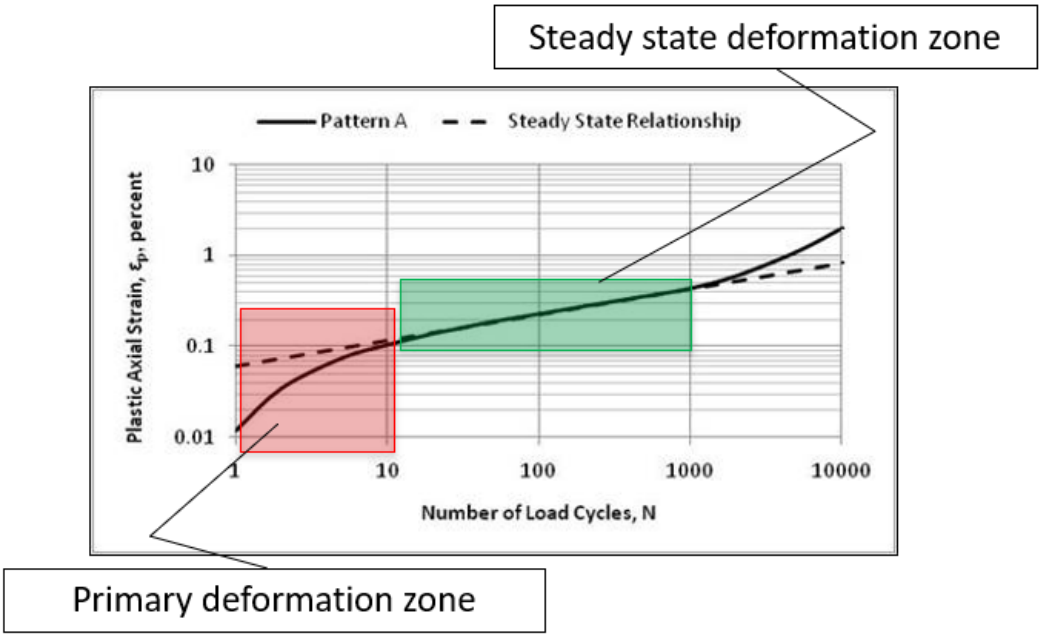
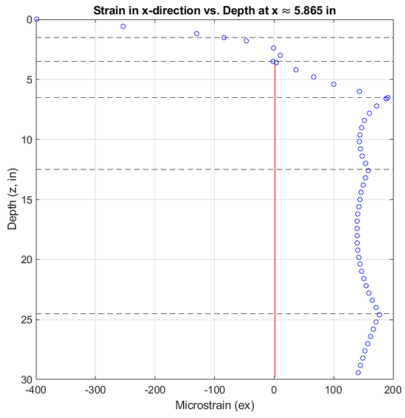


Figure 5-3 Load cycles vs. plastic axial strain (*1*)

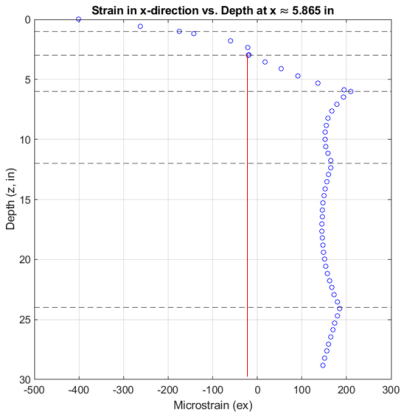
5.2.1.3. Critical Strain at Bottom of Overlay Layer

Identifying the critical HMA layer thickness is important because it defines the point at which the bottom of the asphalt layer transitions from a tensile to a compressive strain zone. Once this transition occurs, PMED no longer predicts bottom-up fatigue cracking, since the critical tensile strain that primarily causes fatigue damage is no longer present. Understanding this threshold helps distinguish between thicknesses where fatigue cracking governs performance and those where it becomes negligible.

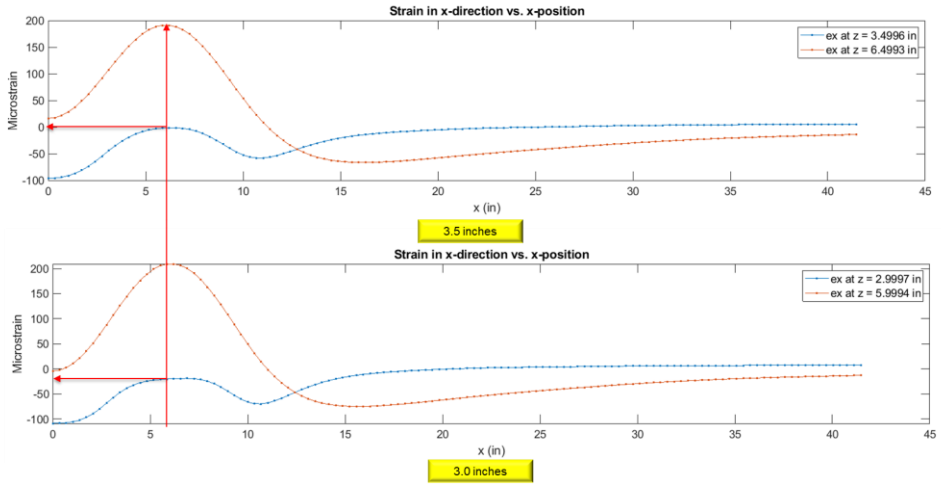
To determine the transition thickness for HMA overlays, the research team utilized the Material Layered Elastic Analysis (MATLEA) program, developed by Michigan State University researchers, to evaluate the strain response at the bottom of the asphalt layer across varying thicknesses (*5*). The team selected a section with a 3.0- and 3.5-inch overlay thickness over the existing 5.0-inch asphalt to estimate strains within the overlay and the existing layers. Figure 5-4 shows the strain accumulated at the bottom of the overlay and existing layers using MATLEA. As shown, the strain at the bottom of the 3.0-inch overlay is in compression, whereas the 3.5-inch overlay exhibits tensile strain.



(a) Overlay of 3.5 in.



(b) Overlay of 3.0 in.



(c) Strains at the bottom of overlay layers

Figure 5-4 Horizontal strain profiles in overlay and existing layers from MATLEA

5.2.2 HMA over JPCP or JRCP

HMA overlays on existing JPCP pavements are a widely used rehabilitation strategy to restore smoothness, reduce joint faulting, and extend structural capacity. In PMED, these sections are modeled as asphalt overlays placed over intact PCC slabs, with performance primarily governed by reflective cracking originating from underlying joints. The design approach accounts for the overlay thickness, existing slab condition, and subgrade support characteristics to evaluate the long-term effectiveness of the rehabilitation treatment. PMED provides direct modeling options for JPCP but does not include a distinct JRCP option. For design and analysis purposes, JRCP sections are treated as JPCP, as their joint behavior and reflective cracking characteristics are considered sufficiently similar for overlay performance prediction. Accordingly, these are directly modeled by specifying the PMED design/pavement type “Overlay, AC over JPCP”. The following subsections detail the inputs and describe the performance modeling for HMA over existing jointed PCC pavements.

5.2.2.1. Fatigue Damage in Existing PCC Layers

The addition of an asphalt overlay significantly influences the fatigue behavior of the underlying PCC slab by moderating temperature-induced stresses and reducing tensile strain responses. Even thin HMA overlays can substantially decrease the magnitude of top-down and bottom-up fatigue damage in the existing concrete. In PMED, the accumulated fatigue damage before rehabilitation is quantified using the percentage of slabs exhibiting transverse cracking and those previously repaired or replaced, which together represent the total past damage that is used in the fatigue transfer function to predict future cracking in the overlay (*1*). As discussed in Chapter 4, subsection 4.5.2.2, the past damage was estimated based on the DI of existing concrete pavements.

The research team conducted a sensitivity analysis to assess the influence of pre-overlay slab conditions on predicted performance, using a triangular matrix of input combinations representing the percentages of slabs distressed before restoration and those repaired or replaced after restoration. A matrix ranging from 10% to 90% for both parameters was used to evaluate their combined impact on fatigue-related distress and overall pavement performance. This analysis was performed using global coefficients, a 95% design reliability level, and a CADT of 8,500. The modeled pavement structure consisted of a three-layer HMA overlay (1.5 in. 5EMH 70-28P, 2.5 in. 4EMH 70-28P, and 3.0 in. 3EMH 64-22), over 12 in. of existing PCC, 4 in. of OGDC, 10 in. of sand subbase, and a CL subgrade. The Southwest region climate (Benton Harbor) was used across all simulations. Tables 5-2 through 5-4 summarize the outcomes of the sensitivity analysis performed using a diagonal matrix framework to evaluate the influence of pre-overlay condition inputs and their impact on predicted IRI, JPCP transverse cracking, and total transverse cracking.

Table 5-2 Sensitivity of predicted IRI

SRAR	SDBR 10	SDBR 20	SDBR 30	SDBR 40	SDBR 50	SDBR 60	SDBR 70	SDBR 80	SDBR 90
5	164.5	164.9	165.2	165.5	165.8	166.2	166.5	166.8	167.1
10	164.4	164.7	165	165.4	165.7	166	166.3	166.6	167
15	-	164.5	164.9	165.2	165.5	165.8	166.2	166.5	166.8
20	-	164.4	164.7	165	165.4	165.7	166	166.3	166.6
25	-	-	164.5	164.9	165.2	165.5	165.8	166.2	166.5
30	-	-	164.4	164.7	165	165.4	165.7	166	166.3
35	-	-	-	164.5	164.9	165.2	165.5	165.8	166.2
40	-	-	-	164.4	164.7	165	165.4	165.7	166
45	-	-	-	-	164.5	164.9	165.2	165.5	165.8
50	-	-	-	-	164.4	164.7	165	165.4	165.7
55	-	-	-	-	-	164.5	164.9	165.2	165.5
60	-	-	-	-	-	164.4	164.7	165	165.4
65	-	-	-	-	-	-	164.5	164.9	165.2
70	-	-	-	-	-	-	164.4	164.7	165
75	-	-	-	-	-	-	-	164.5	164.9
80	-	-	-	-	-	-	-	164.4	164.7
85	-	-	-	-	-	-	-	-	164.5
90	-	-	-	-	-	-	-	-	164.4

SDBR = Slab distressed/replaced before restoration, (%)
SRAR = Slab repaired/restored after restoration, (%)

Table 5-3 Sensitivity of predicted JPCP transverse cracking

SRAR	SDBR 10	SDBR 20	SDBR 30	SDBR 40	SDBR 50	SDBR 60	SDBR 70	SDBR 80	SDBR 90
5	16.36	30.97	43.77	55.91	67.67	79.19	90.54	100.00	100.00
10	1.23	24.06	37.49	49.90	61.83	73.46	84.89	96.18	100.00
15	-	16.36	30.97	43.77	55.91	67.67	79.19	90.55	100.00
20	-	1.23	24.06	37.49	49.90	61.83	73.46	84.90	96.18
25	-	-	16.36	30.97	43.77	55.91	67.67	79.20	90.55
30	-	-	1.23	24.06	37.49	49.90	61.83	73.47	84.90
35	-	-	-	16.36	30.97	43.77	55.91	67.68	79.20
40	-	-	-	1.23	24.06	37.49	49.90	61.84	73.47
45	-	-	-	-	16.36	30.97	43.77	55.92	67.68
50	-	-	-	-	1.23	24.06	37.49	49.91	61.84
55	-	-	-	-	-	16.36	30.97	43.79	55.92
60	-	-	-	-	-	1.23	24.06	37.50	49.91
65	-	-	-	-	-	-	16.36	30.98	43.79
70	-	-	-	-	-	-	1.23	24.08	37.50
75	-	-	-	-	-	-	-	16.37	30.98
80	-	-	-	-	-	-	-	2.46	24.08
85	-	-	-	-	-	-	-	-	16.37
90	-	-	-	-	-	-	-	-	2.46

SDBR = Slab distressed/replaced before restoration, (%)
SRAR = Slab repaired/restored after restoration, (%)

Table 5-4 Sensitivity of predicted total transverse cracking

SRAR	SDBR 10	SDBR 20	SDBR 30	SDBR 40	SDBR 50	SDBR 60	SDBR 70	SDBR 80	SDBR 90
5	3778	3939	4099	4259	4420	4580	4740	4900	5060
10	3698	3858	4019	4179	4340	4500	4660	4820	4980
15	-	3778	3939	4099	4259	4420	4580	4740	4900
20	-	369	3858	4019	4179	4340	4500	4660	4820
25	-	-	3778	3939	4099	4259	4420	4580	4740
30	-	-	3698	3858	4019	4179	4340	4500	4660
35	-	-	-	3778	3939	4099	4259	4420	4580
40	-	-	-	3698	3858	4019	4179	4340	4500
45	-	-	-	-	3778	3939	4099	4259	4420
50	-	-	-	-	3698	3858	4019	4179	4340
55	-	-	-	-	-	3778	3939	4099	4259
60	-	-	-	-	-	3698	3858	4019	4179
65	-	-	-	-	-	-	3778	3939	4099
70	-	-	-	-	-	-	3698	3858	4019
75	-	-	-	-	-	-	-	3778	3939
80	-	-	-	-	-	-	-	3698	3858
85	-	-	-	-	-	-	-	-	3778
90	-	-	-	-	-	-	-	-	3698

SDBR = Slab distressed/replaced before restoration, (%)
SRAR = Slab repaired/restored after restoration, (%)

The sensitivity analysis of the pre-overlay condition inputs —percent of slabs distressed before restoration and percent of slabs repaired after restoration —showed minimal influence on most predicted pavement distresses, with the most notable on JPCP transverse cracking and total transverse cracking. The predicted IRI values remained relatively stable across all combinations, ranging from approximately 164 to 167 in/mi, indicating that surface roughness predictions are largely insensitive to variations in pre-overlay condition inputs. In contrast, predicted JPCP transverse cracking exhibited a significant increase with higher pre-overlay distress, as this parameter directly designates PMED's estimation of past fatigue damage in the existing slab. It is important to note that this cracking indicates deterioration in the underlying PCC layer and does not represent surface cracking in the HMA overlay. Consequently, using JPCP transverse cracking alone as a performance threshold is not recommended, since the condition of the HMA surface principally defines the rehabilitation performance or serviceability. The total transverse cracking, which includes the influence of underlying slab cracking transmitted through the overlay, showed a more gradual increase across the input matrix and serves as a more realistic indicator of visible surface performance. All remaining distress types, including rutting and bottom-up fatigue, were unaffected by these input variations. Therefore, MDOT should rely on total transverse cracking as the primary performance indicator for HMA over JPCP sections, since the underlying JPCP cracking is already incorporated within the reflective cracking model and should not be evaluated separately.

5.2.2.2. JPCP Design Properties

The research team, in consultation with MDOT, standardized the concrete slab design properties across all calibration sections to maintain consistency in the analysis and

address the limitations of the PMED software. As previously noted, the MDOT network includes existing JPCP and JRCP sections; however, PMED does not provide a separate design category for JRCP. Therefore, all HMA overlays of jointed PCC sections were modeled as “AC over JPCP”. Accordingly, for all calibration sections, the existing JPCP properties used a 15-ft joint spacing, with dowels spaced at 12 inches and a 1.25-inch diameter. The widened slab input was not used, and all slabs were modeled as standard slabs. A curl/warp temperature differential of −10°F was assigned to all calibration sections based on the value obtained from previous calibration efforts (*4*). Information on tied and untied shoulders came directly from the construction records to ensure accurate representation of edge-support conditions.

5.2.2.3. Transverse Cracking Prediction

During the sensitivity evaluation of HMA overlay thickness, the research team observed inconsistencies in the prediction of total transverse cracking within PMED. As the overlay thickness increased from 3.5 to 5.5 inches, the predicted total transverse cracking initially increased, then decreased with further increases in overlay thickness. This non-monotonic trend was unexpected, as thicker overlays are generally associated with reduced tensile strain and improved thermal resistance.

To further investigate this behavior, the team conducted sensitivity analyses using both global default coefficients and locally calibrated coefficients (from the prior research project) for the same fix type (*4*). The response pattern remained consistent across the two calibration sets, with maximum cracking at approximately 4.5 inches and then decreasing with increasing thickness. Subsequent discussion with PMED support staff suggested that the anomaly likely arises from how PMED discretizes pavement sublayers and from the depth assignment of temperature nodes in the Enhanced Integrated Climate Model (EICM). The interaction between thermal gradient computation and layer subdivision may distort the temperature-stress relationship in thinner overlays, leading to inaccurate cracking predictions below a critical thickness threshold.

Based on these findings, it is recommended that PMED transverse cracking predictions for HMA overlays thinner than 4.5 inches be interpreted with caution, and that the model be applied primarily for overlays exceeding this thickness. Figure 5-5 illustrates the variation in predicted total transverse cracking with overlay thickness (at 95% reliability), highlighting the observed peak near an overlay thickness of 4.5 inches.

5.2.3 HMA over CRCP

MDOT's network contains very limited in-service CRCP pavements and even fewer that are overlaid with HMA; therefore, there were insufficient sections available to support model calibration for HMA overlays on CRCP. As a result, the research team did not calibrate this fix type and utilized national default parameters for review. Understanding the modeling framework for HMA over CRCP remains essential for interpreting potential performance trends and for supporting future calibration efforts once additional CRCP sections become available.

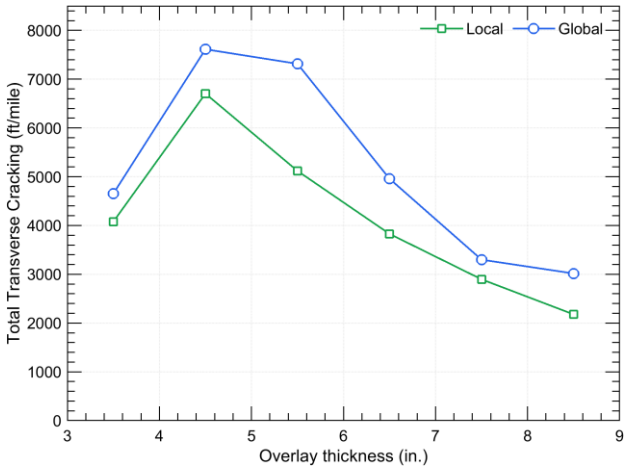


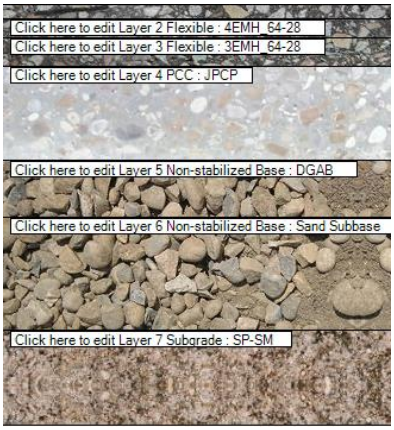
Figure 5-5 Comparison of thermal and total transverse cracking

5.2.3.1. Fatigue Damage in Existing PCC Layers

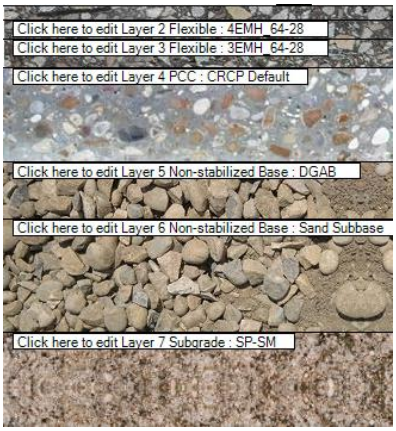
For CRCP pavements receiving HMA overlays, the estimate of past fatigue damage is based on the extent of existing punchouts. The PMED procedure uses the total number of medium- and high-severity punchouts per mile, combined with the number of repaired punchouts per mile, to represent accumulated fatigue damage. This total serves as a key input for determining the pavement's initial damage state before overlay placement. It is essential to note that PMED assumed all these punchouts as full-depth repairs (*1*). PMED applies the nationally calibrated fatigue damage–punchout relationship to calculate cumulative fatigue damage and to predict the future development of punchouts over the design period. Next, PMED simulates month-by-month damage accumulation under the expected traffic and climatic conditions (*1*). The estimated damage is used to calculate the fatigue cracking in the asphalt overlay.

5.2.3.2. Performance Comparison of HMA Overlay over JPCP vs. CRCP

The research team initially selected a section designed for an HMA overlay of JPCP and replicated it, using existing CRCP instead of the original JPCP (all other design inputs remain the same). The remaining coefficients were the same. Figure 5-6 shows the comparison between the two designs. Designs were evaluated for HMA overlay thicknesses of 3.5, 4.0, and 6.5 inches. The existing layer thicknesses are: 10-inch PCC, 6-inch DGAB, 12-inch sand subbase, and SP-SM subgrade with an MR of 7,000 psi. For this example, all analyses were performed using a Lansing climate station, a CADT of 1,020, 95% design reliability, and global calibration coefficients. For the JPCP scenario, pre- and post-repair percentages of 50% and 25%, respectively, were assumed, while for the CRCP scenario, 20 total punchouts (repaired and unrepaired) were used for analysis.



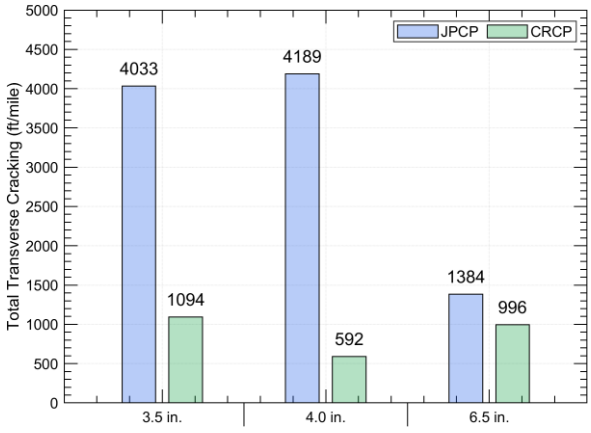
(a) HMA over JPCP



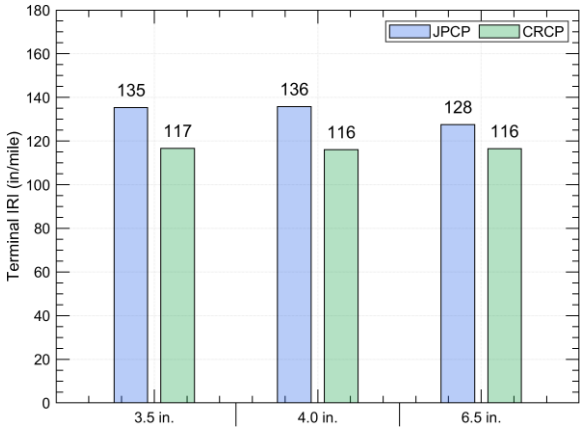
(b) HMA over CRCP

Figure 5-6 HMA overlay of JPCP vs. CRCP cross-sections

Figure 5-7 shows the comparison between the HMA overlay of JPCP and CRCP, along with the overlay thickness. Since no sections were available for CRCP calibration, the team used the global default CRCP calibration coefficients. The results indicate that HMA overlays over CRCP consistently yield better performance predictions than those over JPCP across all thicknesses. The difference is most pronounced in total transverse cracking and IRI. JPCP overlays predicted higher total transverse (thermal plus reflective) cracking, exceeding 4,000 ft/mile at thinner overlays, while CRCP overlays maintained cracking below 1,100 ft/mile. This outcome highlights the influence of the underlying slab type on overlay performance. The continuous steel reinforcement in CRCP minimizes joint-related stress concentrations, reducing reflective cracking and improving overall durability. Given the reduced potential for reflective cracking in existing CRCP (due to the absence of transverse joints), the team recommends using the new flexible pavement thresholds of 2,000 ft/mile for transverse (thermal) cracking and 2,500 ft/mile for total transverse cracking when designing HMA over CRCP. However, based on these results and the use of global calibration, there is lower confidence in design-level applications, so the research team recommends that the HMA over CRCP model within PMED be used only as a reference or closely monitored.



(a) Total transverse cracking



(b) IRI

Figure 5-7 Predicted performance comparison of HMA over JPCP vs. CRCP

5.2.4 JPCP (Unbonded) overlay of Existing JPCP, JRCP, or CRCP

Concrete overlays are classified as bonded and unbonded. A bonded concrete overlay consists of a 2- to 8-inch concrete layer placed directly over an existing concrete pavement, with full bond ensured between the new and existing slabs (*6, 7*). An unbonded concrete overlay consists of a 5- to 11-inch concrete layer applied over existing concrete, separated by a 1- to 2-inch HMA or fabric interlayer. This interlayer prevents bonding and allows independent movement between the old and new layers, reducing the potential for reflective cracking (*6, 7*).

MDOT utilizes an interlayer (typically HMA, but a fabric interlayer in some instances) or places the concrete overlay on existing HMA surfaces, so unbonded overlays will be evaluated for design applications. MDOT concrete overlays generally utilize standard slab widths (12 ft) and spacings (12 to 16 ft) with tie bars and dowels. However, thinner concrete overlays less than 6 inches are SJPCP, with short, square joint spacings (half the lane width), fibers in the concrete mix, and non-doweled joints.

For standard (non-SJPCP) concrete overlays, a sensitivity analysis using the PMED global default coefficients showed an unexpected trend: predicted cracking increased with overlay thickness up to about 6.5 inches, then decreased as thickness continued to increase (Figure 5-8). This anomaly likely occurs because PMED is not optimized for overlays thinner than approximately 6.5 inches, in part because the LTPP database, on which PMED's models and calibration are based, lacks such thin overlay sections. Another contributing factor may be the assumption of constant joint spacing (12 ft) and dowel bar diameter (1 inch) for overlays thinner than 8 inches – an assumption necessitated by MDOT's minimal dowel bar diameter and PMED's joint spacing limit of 10 ft. These constraints increase the dowel bar diameter-to-slab thickness ratio, which, in theory, improves the estimated load-transfer performance and may contribute to this observed behavior. Based on these findings, the research team recommends avoiding PMED for evaluating unbonded JPCP overlays thinner than 6.5 inches under these assumptions, or if used, closely monitoring the design outcomes.

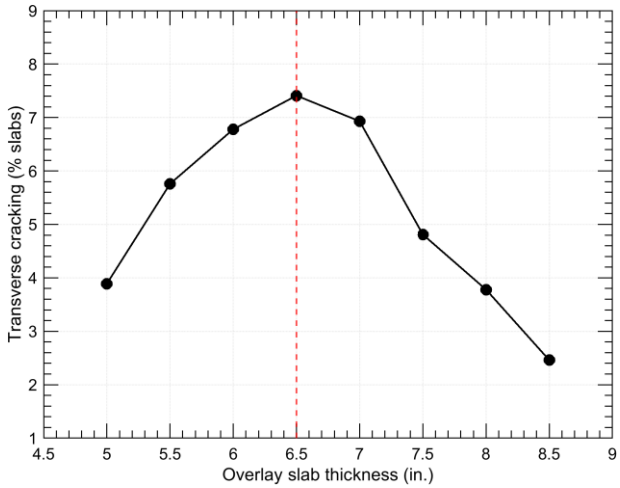


Figure 5-8 Predicted transverse cracking versus overlay thickness

As previously noted, PMED does not include separate options for JRCP; therefore, such sections are modeled as JPCP. For CRCP, MDOT's network contains very limited or no in-service sections, preventing local calibration. Consequently, the global default parameters were reviewed.

5.2.4.1. Existing Condition of PCC

PMED models the existing PCC layer as a stiff foundation-type layer, using only the elastic modulus for characterization, regardless of whether it is JPCP or CRCP. As explained in Chapter 4, the team recommended an elastic modulus of 3.0 million psi for the existing concrete, based on laboratory testing of field cores and conversion to equivalent modulus using PMED methodology (*1*).

5.2.5 Concrete over Full-Depth HMA Pavements

Concrete overlays placed over full-depth HMA pavements can be effectively modeled in PMED as JPCP over AC, with the existing HMA layer serving as the primary structural foundation for the new concrete layer. In PMED, the interface between the JPCP and HMA layers is typically assumed to remain bonded until the defined friction loss period, after which partial slip is introduced to simulate long-term interface degradation. Since there are only a few MDOT sections with this fix type, local calibration is not feasible at this time. However, the models used for this rehabilitation type are the same as those applied to new/reconstruction JPCP, and the underlying HMA layer is simulated like a stabilized base. Therefore, the research team recommends using the PMED calibration coefficients established under SPR-1723 for new/reconstructed JPCP pavements (*4*).

Preliminary sensitivity analyses showed that the CTE of the new JPCP and the presence of tied shoulders exerted a moderate influence on predicted performance, particularly in governing transverse cracking initiation and IRI progression. In contrast, the existing HMA thickness, its input for rehabilitation level (i.e., Level 3 structural condition rating of fair versus poor), the assumed time to friction loss, and the erodibility index exhibited only marginal effects on design outcomes.

These findings indicate that this PMED fix type can be applied to MDOT pavements and in rehabilitation evaluations, with routine performance checks and periodic reassessment as PMED designs are implemented and new sections are constructed.

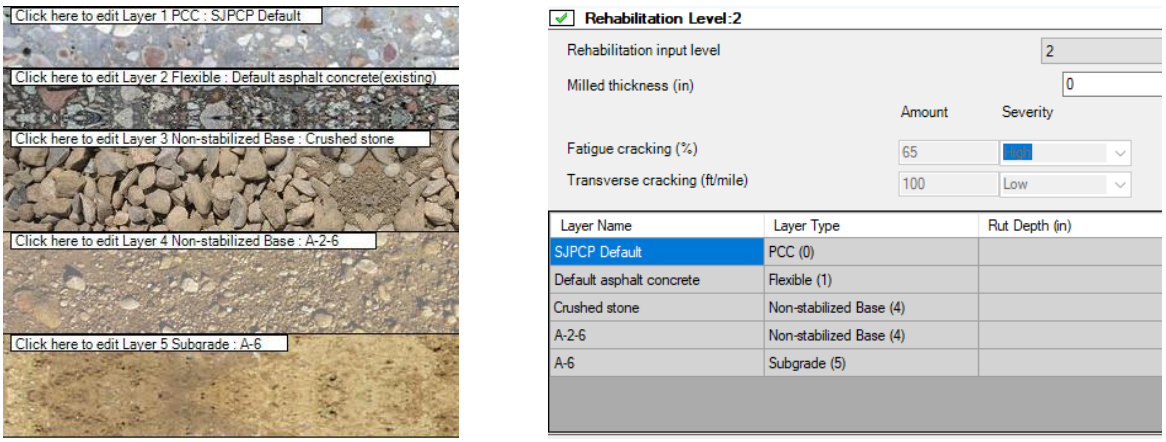
5.2.6 SJPCP over HMA

MDOT has used SJPCP overlays to control cracking through tighter joint spacing for thin concrete overlays. PMED includes only one modeling option for SJPCP overlays: SJPCP over existing HMA. As a result, no other pavement types are supported, so it does not accommodate configurations in which short-jointed or fiber-reinforced slabs are placed over existing rigid or composite pavements. See subsection 5.4.1 for additional discussion.

Within the available SJPCP over AC option, PMED automatically defines the existing HMA layer as being in very poor structural condition. This limits the user's ability to

assign stiffness or condition values that accurately reflect field-measured performance. Consequently, support conditions may be underestimated when the existing HMA base remains in fair or good condition. Figure 5-9 illustrates the available PMED modeling configuration for SJPCP over AC. It highlights the auto-selected fatigue cracking of 65% by PMED at rehabilitation Level 2, which corresponds to a very poor structural rating at Level 3.

Given these constraints, the research team recommends that MDOT continue to design SJPCP with fiber-reinforced concrete overlays using its established engineering procedures rather than relying on the PMED module for this configuration.



(a) SJPCP over AC (b) Rehabilitation Level 2 characterization

Figure 5-9 PMED modeling of SJPCP over AC

5.2.7 HMA over C&S Pavement

C&S is an in-place recycling technique that reuses existing HMA pavement by pulverizing and recompacting it to form a new aggregate base layer. Unlike RAP, which is milled, stockpiled, and later reused in new HMA mixtures, the C&S process is performed entirely in place. It involves scarifying, trenching, and pulverizing the existing pavement, typically incorporating 1 to 2 inches of the underlying aggregate base, followed by mixing, grading, and compaction to the desired cross-section. The resulting layer generally exhibits uniform gradation, with 95% passing 1.5 in. and no particles larger than 4.0 in. Water is added during processing to control moisture and achieve the target compaction.

In SPR-1723, C&S pavements were modeled in PMED as new flexible pavement structures, since V2.6 did not include a dedicated design type for in-place recycled layers. The crushed material was represented as an unbound aggregate base with a resilient modulus of 125,000 psi, based on literature values (*4, 8*). PMED V3.0 introduced new design options, such as full-depth reclamation (FDR), that provide additional methods for characterizing and analyzing C&S materials. These options should be considered in future studies. However, it should be noted that PMED V3.0 still recommends modeling the C&S layer as an unbound granular type if viscoelastic-bound properties are minimally exhibited.

For this study, the research team designed the C&S sections as new flexible pavements, modeling the PMED layer as "cold recycled asphalt – RAP pulverized in place" (unbound granular layer type). Laboratory testing was conducted on C&S material to determine its MR, complemented by analysis of FWD deflection data for field validation. Based on both laboratory and backcalculated results, the team recommended an MR value of 60,000 psi for use in calibration and design. Additionally, consistent with PMED practice, the gradation for this layer should be specified to match dense-graded aggregate base. Pulverized RAP typically produces a well-graded blend with a gradation like that of a granular base, making it most suitable for PMED modeling. All calibration and validation analyses in this study were performed using this approach for modulus and gradation properties.

5.2.8 HMA over Rubblized Concrete

Rubblization is a pavement rehabilitation technique that fractures an existing concrete slab into small interlocked pieces, typically 3 to 8 inches in size, to eliminate slab action and minimize reflective cracking in subsequent HMA overlays (*9*). A relatively small number of states have analyzed HMA overlays over fractured JPCP using PMED. These efforts modeled the rubblized concrete layer as an unbound aggregate base with high stiffness, treating the pavement as a new flexible system. Reported modulus values vary significantly: Iowa DOT estimated 78,000 psi (*10*), NAPA recommended 100,000–150,000 psi (*11*), Wisconsin reported a range of 35,000–120,000 psi (*12*), Indiana DOT found an average of 170,000 psi (*13*), and Ohio characterized six rubblization projects and found that the modulus of fractured slabs, backcalculated using EVERCALC, ranged from 100 ksi to 309 ksi, with an average of 272 ksi. This range reflects the influence of slab fragmentation, subgrade stiffness, and interlock quality on structural response (*14*). The PMED Level 3 default modulus is 150,000 psi (*15*).

In older MDOT studies, HMA overlays over rubblized PCC were modeled in PMED as new flexible pavements, with the rubblized layer treated as an unbound aggregate base with an MR of 70,000 psi. This approach was adopted because PMED V2.6 does not include a dedicated design type for rubblized or fractured concrete layers (*4, 16, 17*). Lali et al. further validated this approach, demonstrating that modeling rubblized layers as unbound bases within new flexible pavement structures yielded consistent, realistic performance predictions for Michigan data (*18*). Specifically, the gradation for this layer should be specified to match dense-graded aggregate base, as is current PMED standard practice. Although rubblized concrete typically contains coarser fragments than a conventional granular base, PMED requires the use of this gradation category to provide the closest available representation for modeling purposes.

Following these studies, the current research applied the same methodology, representing rubblized concrete layers as unbound dense-graded aggregate bases with an MR value of 70,000 psi for calibration and design purposes.

5.3 FIX TYPES REPRESENTED THROUGH EQUIVALENT MODELING APPROACHES

This section describes the pavement rehabilitation fix types analyzed using equivalent modeling approaches in PMED. Due to limitations in available field data or software modeling options, certain fix types were represented through comparable pavement structures. The following subsections outline these equivalent modeling strategies, associated assumptions, and recommendations for MDOT's design and calibration practices.

5.3.1 HMA over HMA/JPCP, JRCP, or CRCP (composite pavement)

The performance modeling and calibration approach for composite pavement systems comprising HMA overlays on existing HMA, JPCP, JRCP, and CRCP structures requires adaptations due to limitations in PMED V2.6. This version of the software cannot model multiple overlays, such as HMA placed over existing composite pavements (HMA over PCC). Therefore, an equivalent modeling approach was adopted to represent these fix types within PMED's framework. The research team modeled all such sections as HMA over existing JPCP, treating the existing HMA layer as a new HMA layer with reduced E* to simulate the degraded condition of the in-place material. Although this is not a standard modeling practice, this approach provided the most practical representation of composite behavior under available constraints.

The primary limitation of this method is that PMED computes fatigue damage based on tensile strain at the bottom of the HMA overlay. When the existing HMA layer is modeled as a new flexible layer with reduced E*, the program may underestimate or mischaracterize reflective cracking propagation, as it cannot fully capture the composite interaction between the existing and new HMA layers. Nevertheless, this modified approach still enables evaluation of the pavement’s overall crack potential, as the damaged HMA layer will approximate the effects of reflective cracking. The following subsections describe in detail the modeling considerations and assumptions applied to represent existing bound layers within these composite pavement systems.

5.3.1.1. Existing HMA Layer for HMA Over Composite Pavement

As previously noted, the existing HMA layer in composite pavement systems was modeled in PMED as a new flexible layer, with its |E*| reduced to represent the level of field deterioration. For PMED HMA overlays of existing HMA, the software allows the user to characterize existing pavement condition at rehabilitation Level 3 using a structural rating. Accordingly, for each category, the |E*| reduction was determined by comparing the undamaged |E*| with the PMED predicted damaged |E*| values at rehabilitation Level 3. The results were averaged within each category to establish representative stiffness-reduction factors for application to HMA in composite pavements.

Sections with a good structural rating exhibited an average |E*| ratio of 0.95, representing a 5% reduction in modulus. Fair sections averaged 0.80, indicating a 20%

reduction, and poor sections averaged 0.58, corresponding to approximately a 42% reduction. These rating categories and their associated multipliers can then be applied to the |E*| of the HMA layer directly above the existing PCC, based on the pavement's condition rating.

In the MDOT database, bottom-up fatigue cracking is not typically observed in composite pavement sections (based on assumed longitudinal crack locations that may or may not represent actual bottom-up cracking). Therefore, it was not feasible to characterize these calibration sections solely on the basis of fatigue cracking. After consultation with MDOT and review of relevant agency literature, including the MDOT Scoping Manual (2022), the team selected the DI to classify the existing composite pavements into condition categories of good, fair, and poor. Table 5-5 presents the pavement condition criteria based on DI values, while the pre-overlay DI from each calibration section was used to assign the corresponding category. Figure 5-10 illustrates the percentage distribution of sections classified as Good, Fair, and Poor within the calibration dataset (*19*). A total of 150 in-service composite pavement sections were evaluated based on measured fatigue cracking and categorized following these thresholds.

Table 5-5 MDOT pavement condition criteria based on DI (*19*)

Pavement rating	DI
Good	0-20
Fair	26-49
Poor	≥50

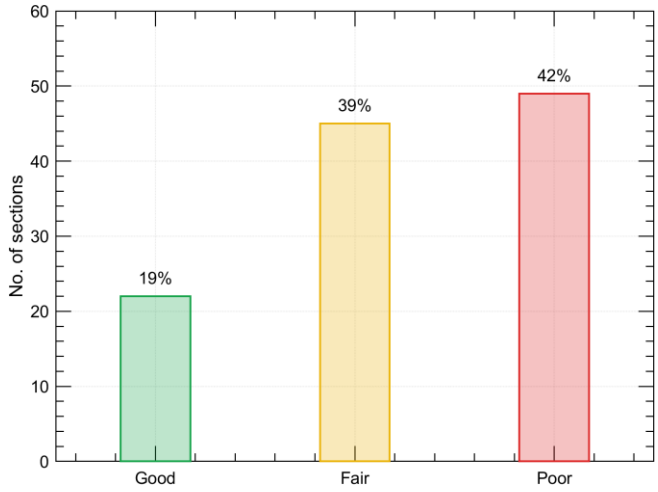


Figure 5-10 Distribution of composite pavement sections' condition based on DI

5.3.1.2. Existing PCC Layer for HMA Over Composite Pavement

The modeling of existing PCC layers in composite pavements followed the same approach described earlier for HMA overlays of JPCP (and JRCP) sections. Pre-overlay fatigue damage was represented through the percentage of slabs exhibiting transverse cracking or previous repairs, consistent with the PMED rehabilitation framework. See subsection 5.2.2 for further details regarding design inputs and other estimations. As

noted in subsection 5.2.3, due to insufficient CRCP sections and corresponding material data in the MDOT database, this fix type could not be feasibly calibrated. As a result, national default parameters were reviewed for pavement design application.

5.3.2 HMA or JPCP over Aggregate-Lift (Agg-Lift) Sections

Agg-lift resurfacing is a rehabilitation technique commonly used by MDOT, particularly in the Superior Region, where challenging terrain and budget constraints often limit the feasibility of full-depth reconstruction, rubblization, or in-place recycling. This fix type involves placing a new aggregate over the existing pavement surface — typically damaged HMA or PCC — followed by resurfacing with either new HMA or JPCP. The agg-lift restores proper grade and cross-slope, improves drainage, enhances structural capacity, and provides a separation layer to reduce reflective cracking. The treatment is considered a cost-effective alternative when extensive milling, lifting, or in-place rehabilitation techniques such as C&S or rubblization are not practical or economically justified.

Currently, MDOT designs agg-lift sections using the AASHTO 93 method, as PMED does not include a direct modeling option for this fix type (*8*). Depending on the existing pavement type and proposed surface, six potential design configurations can be used for agg-lift resurfacing. Each configuration can be modeled differently in PMED to represent the structural interactions among the new surface, agg-lift, and underlying layers. The possible combinations include:

- HMA over agg-lift over existing HMA
- HMA over agg-lift over existing PCC
- HMA over agg-lift over existing HMA/PCC (composite)
- PCC over agg-lift over existing HMA
- PCC over agg-lift over existing PCC
- PCC over agg-lift over existing HMA/PCC (composite)

The following subsections discuss each of these configurations in general, outlining the theoretical design approach and corresponding PMED modeling options to represent them equivalently for general guidance. As will be explained in the following subsections, each equivalent configuration provides a practical framework for representing agg-lift sections. The research team validated a few designs using these approaches. Chapter 7 discusses the results of the validation sections. Due to the limited number of agg-lift sections in the MDOT database and modeling limitations, they were excluded from the calibration dataset. Therefore, the research team recommends using PMED for such fix types with caution.

5.3.2.1. HMA over Agg-Lift over Existing HMA

Figure 5-11 illustrates the theoretical design and corresponding PMED equivalent approach for HMA over the agg-lift of existing HMA. This configuration can be modeled as a new flexible pavement, with the agg-lift represented as a sandwich granular layer between two HMA layers. The lower HMA layer can be treated as the existing pavement, with its modulus reduced according to the condition-based factors described

in Section 5.3.1.1 (good = 0.95, fair = 0.80, poor = 0.58). The agg-lift layer can be modeled as an unbound granular base with an MR of 33,000 psi, consistent with MDOT's recommended value for a new dense-graded aggregate base. The upper HMA layer can be modeled as a new surface course using project-specific mix properties. This equivalent modeling approach provides a practical representation of agg-lift rehabilitation in PMED. In addition, because the design type is treated as a new flexible pavement, the same local calibration coefficients can be applied. As a result, this can serve as a guideline or starting point for design, recognizing that further field performance data are needed for calibration.

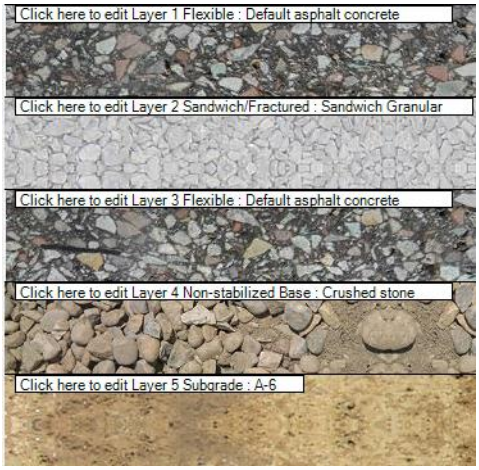


Figure 5-11 PMED design approach for HMA over agg-lift over existing HMA

5.3.2.2. HMA over Agg-Lift over Existing PCC

Figure 5-12 illustrates the theoretical design and PMED equivalent modeling approach for HMA over the agg-lift of existing PCC. Since PMED does not allow a sandwich granular layer directly between HMA and an existing PCC layer, the existing PCC can be modeled as a stiff unbound aggregate base (DGAB) with a modulus of 2,000,000 psi to simulate its reduced load transfer and fractured behavior. The agg-lift layer can be represented as a granular base using the standard MR value. The HMA overlay can be modeled as a new surface layer using project-specific mix properties. Again, because this configuration is modeled as a new flexible pavement, the same local calibration coefficients can be used.

5.3.2.3. HMA over Agg-Lift over Existing HMA/PCC

Figure 5-13 presents the PMED equivalent modeling for HMA over the agg-lift of existing HMA/PCC. In this configuration, the existing HMA layer can be modeled with a reduced modulus as discussed in Section 5.3.1.1. At the same time, the underlying PCC is represented as a stiff, unbound base (DGAB) with a modulus of 2,000,000 psi to capture its remaining structural contribution (since PMED does not allow a concrete sublayer to be directly included in this design type). The agg-lift is modeled as a standard granular base layer. As in previous cases, modeling the system as a new flexible pavement allows the use of the same local calibration coefficients.

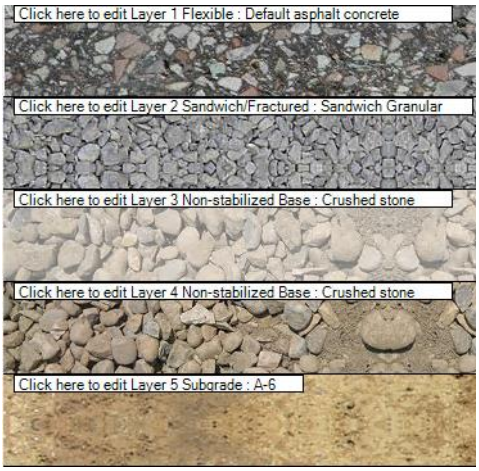


Figure 5-12 PMED design approach for HMA over agg-lift over existing PCC

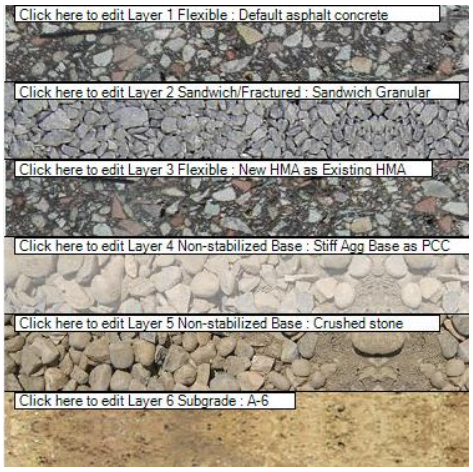


Figure 5-13 PMED design approach for HMA over agg-lift over existing HMA/PCC

5.3.2.4. PCC over Agg-Lift over Existing HMA

Figure 5-14 illustrates the PMED equivalent modeling approach for PCC over the agg-lift of existing HMA. In this setup, the pavement can be modeled as a new JPCP pavement, with the agg-lift treated as a granular base layer (using the same properties described in Section 5.3.2.1), and the existing HMA layer modeled with a reduced modulus (as discussed in Section 5.3.1.1). All remaining unbounded layers can be modeled using standard design practices. Because the PMED design type is treated as a new JPCP pavement, the applicable local calibration coefficients can be used.

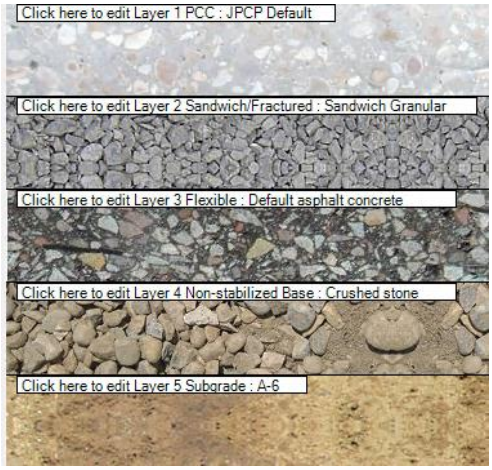


Figure 5-14 PMED design approach for PCC over agg-lift over existing HMA

5.3.2.5. PCC over Agg-Lift over Existing PCC

Figure 5-15 shows the PMED equivalent modeling approach for PCC over the agg-lift of the existing PCC. This configuration is modeled as a new JPCP pavement, enabling the use of the same local calibration coefficients. In this case, the existing PCC should be modeled as a chemically stabilized layer with a higher modulus (2,000,000 psi), better reflecting the PCC's stiffness. This approach is required because PMED does not allow a concrete sublayer to be directly included within this design type. Other inputs remain the same as previously discussed.

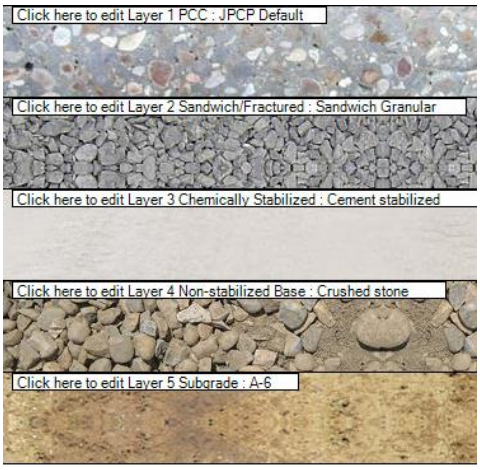


Figure 5-15 PMED design approach for PCC over agg-lift over existing PCC

5.3.2.6. PCC over Agg-Lift over Existing HMA/PCC

Figure 5-16 shows the PMED equivalent for PCC over the agg-lift of existing composite HMA/PCC pavement. This configuration can be modeled as a new JPCP pavement design, with the existing HMA treated as a new HMA layer with reduced modulus (per Section 5.3.1.1), and the existing PCC is modeled as a chemically stabilized layer to represent its residual stiffness. The agg-lift is modeled as a granular base consistent

with Section 5.3.4.1. As with the other rigid pavement cases, treating the section as a new JPCP allows the use of the same local calibration coefficients.

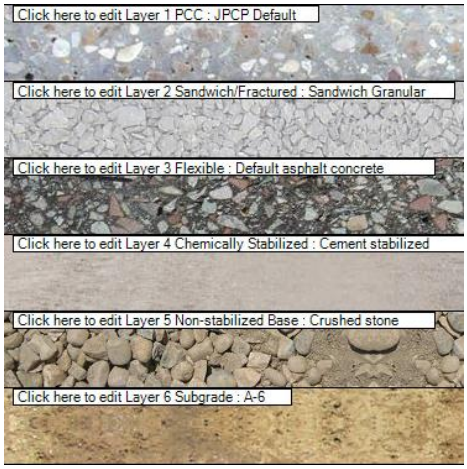


Figure 5-16 PMED design approach for PCC over agg-lift over existing HMA/PCC

5.3.3 Concrete over Composite Pavements (HMA/JPCP, HMA/JRCP, or HMA/CRCP)

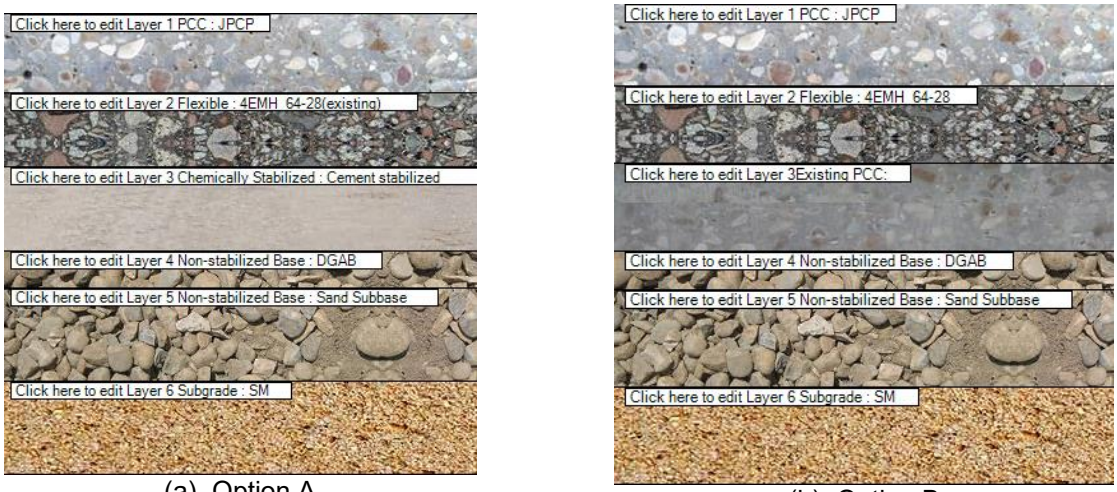
Concrete overlays placed over composite pavements consisting of HMA over existing JPCP, JRCP, or CRCP structures were modeled in PMED V2.6 using two distinct theoretical configurations, as illustrated in Figure 5-17.

Option A modeled the overlay as a JPCP over HMA, with the underlying concrete layer represented as a cement-stabilized base having an elastic modulus equivalent to the intact PCC (3,000,000 psi). This approach preserves the stiffness contribution of the existing slab while allowing the existing asphalt layer to degrade mechanistically in accordance with PMED's temperature- and age-dependent modulus predictions. This method accounts for base friction at the HMA interface, indicating partial bonding. The inputs and rehabilitation level for the existing HMA layer were characterized using the same procedure applied to HMA over HMA rehabilitation fix types (as described in subsection 5.2.1).

Option B modeled the system as an unbonded JPCP over JPCP, with the existing HMA specified as the separator layer, debonding the new PCC from the existing concrete base. In this case, the HMA modulus was reduced proportional to its observed condition (as described in Section 5.3.1.1). At the same time, the underlying PCC could be retained as a structural layer to represent the effective composite foundation. This method aligns with the PMED guidelines for unbonded overlays and is particularly applicable when field observations indicate separation at the asphalt–concrete interface. Performance predictions in this configuration remained governed by the JPCP models.

The research team modeled both theoretical configurations illustrated in Figure 5-17 for representative concrete-over-composite rehabilitation sections located in the Lansing

region. In both cases, the new PCC overlay thickness, joint spacing, and load transfer parameters were kept identical to isolate the effect of foundation representation. For Option A (bonded configuration), the existing HMA layer was modeled at rehabilitation Level 2, with 20% fatigue cracking. In Option B (unbonded configuration), the team modeled the separator HMA layer with its modulus reduced to reflect a "fair" structural condition, corresponding to approximately 20% fatigue cracking as per section 5.3.1.1. The existing PCC layer was represented with an elastic modulus of 3,000,000 psi in both cases. All other design coefficients, material properties, traffic inputs, and climatic parameters remained unchanged across both simulations. The locally calibrated coefficients established during SPR-1723 for new JPCP pavements were applied to both models with a design reliability of 95%, ensuring consistency in the performance prediction framework and enabling a direct mechanistic comparison of the two modeling approaches.



(a) Option A (b) Option B

Figure 5-17 Theoretical cross-sections modeled for concrete-over-composite pavements

The PMED-predicted performance outcomes for the two modeling configurations are presented in Table 5-6. The comparatively lower prediction levels in Option B can be attributed to the reduced stiffness of the modeled interlayer, which effectively dissipates load-induced and thermally induced stresses, thereby reducing crack propagation and differential slab deflection. Conversely, the higher cracking and roughness values predicted in Option A reflects the influence of the bonded-interface assumption, which transfers a greater proportion of strain energy from the deteriorated substructure to the new overlay, amplifying reflective cracking tendencies.

Table 5-6 Predicted performance comparison

Performance/design options	Option A	Option B
Terminal IRI (in/mile)	172.28	162.71
Mean joint faulting (in)	0.09	0.08
JPCP transverse cracking (percent slabs)	17.76	7.42

The research team did not perform local calibration for Option A. Similarly, Option B has not been formally validated against field-measured performance for this fix type. Therefore, these predictions should be interpreted as preliminary mechanistic trends rather than validated design outcomes.

MDOT standard practice considers the existing HMA as an unbonded separator, which supports the use of Option B (unbonded JPCP over PCC with a reduced-modulus HMA interlayer) for mechanistic design and evaluation. Accordingly, Option B may be considered under the same design framework and calibration used for other unbonded JPCP overlays. However, because validation specifically for concrete over composite sections is limited, users should pair design decisions with targeted monitoring of constructed sections so that any necessary adjustments to calibration or modelling assumptions can be made as field data accrue.

5.3.4 HMA with ASCRL over JPCP or JRCP

Reflective cracking remains one of the most challenging distresses to isolate and identify in asphalt overlays placed over existing concrete pavements. Previous studies, as outlined in Chapter 2, consistently demonstrate that compliant, viscoelastic layers with high air-void contents (typically 15 to 25%) can delay or significantly reduce reflective cracking by dissipating stress concentrations at underlying concrete joints. However, long-term performance depends heavily on interlayer bonding, gradation, and asphalt binder characteristics.

In alignment with these findings, the research team characterized MDOT's ASCRL as a viscoelastic, open-graded mixture placed between the concrete substrate and HMA overlay. Three field cores were tested using the CoreLok method, and the results indicated an average air void content of 20%, which was used to prepare gyratory-compacted cylindrical samples for E* evaluation. The team modeled the ASCRL layer in PMED as an HMA overlay over the existing concrete, with the ASCRL serving as the HMA base course. Sensitivity analysis on three air void and effective binder content levels revealed negligible effects on predicted distresses for both thin (4.0 inch) and thick (6.5 inch) overlays. The research team recommended using the following inputs in the PMED:

- 20% air voids (per average of field cores).
- An effective binder content equal to twice the ASCRL mixture binder content by volume (as per the MDOT JMF) (*20, 21*).
- The laboratory-measured E* values reported in Chapter 3 are for subsequent local calibration.

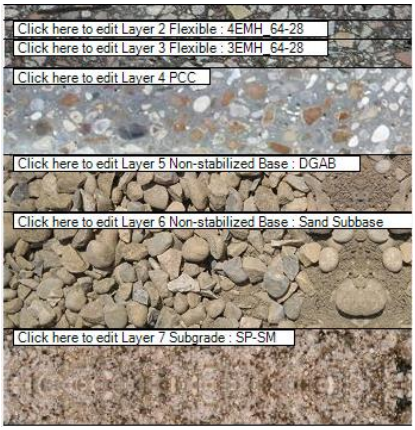
5.3.4.1. Impact of ASCRL on Predicted Performance

Using the recommended ASCRL material properties, the research team conducted a comparative performance analysis by designing pavement sections in three representative climate zones of Michigan: Lansing, Kalamazoo, and Marquette (Upper Peninsula). In each zone, two sections were modeled in PMED: one incorporating a 3EMH mix as the base course and the other incorporating an ASCRL layer as the base

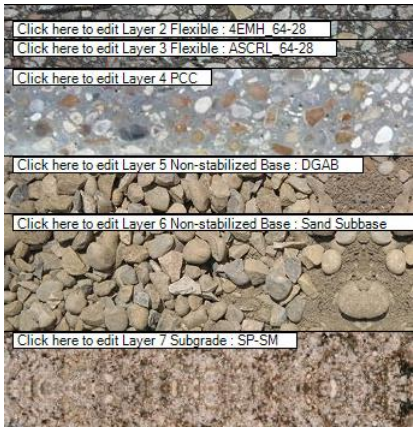
course. All other material, structural, and traffic inputs were kept identical across the comparison, including:

- 6.5 in HMA (1.5 in. top, 2.0 in. leveling, and 3.0 in. base) for the thick section
- 4.0 in HMA (1.5 in. top and 2.5 in. base) for the thin section
- 9.0 in. existing PCC
- 6.0 in. DGAB
- 12.0 in. sand subbase
- SP-SM subgrade
- CADT = 1,000
- 95% design reliability
- Locally calibrated coefficients for HMA overlay of JPCP

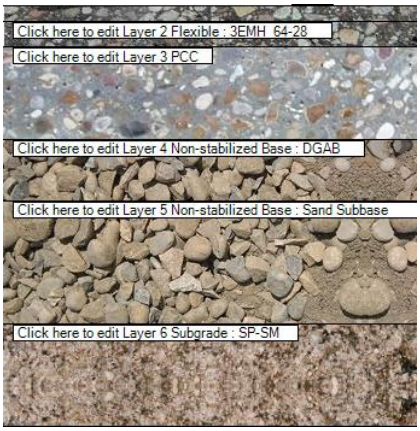
The team analyzed each configuration for both thin and thick overlay designs to capture sensitivity across structural conditions. The purpose of this analysis was to evaluate the impact of the ASCRL layer on predicted performance, particularly on total fatigue cracking and total transverse cracking, since both distresses are influenced by PMED's reflective cracking model. Figure 5-18 illustrates the PMED structural configurations used for this evaluation.



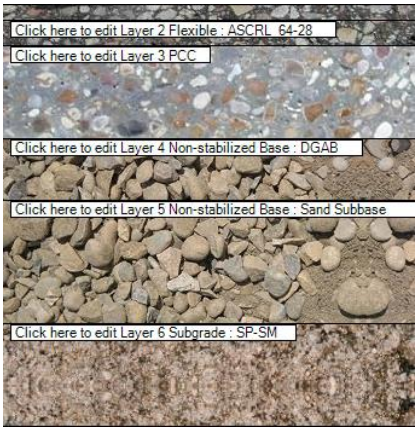
(a) Thick section with 3EMH base course



(b) Thick section with ASCRL base course



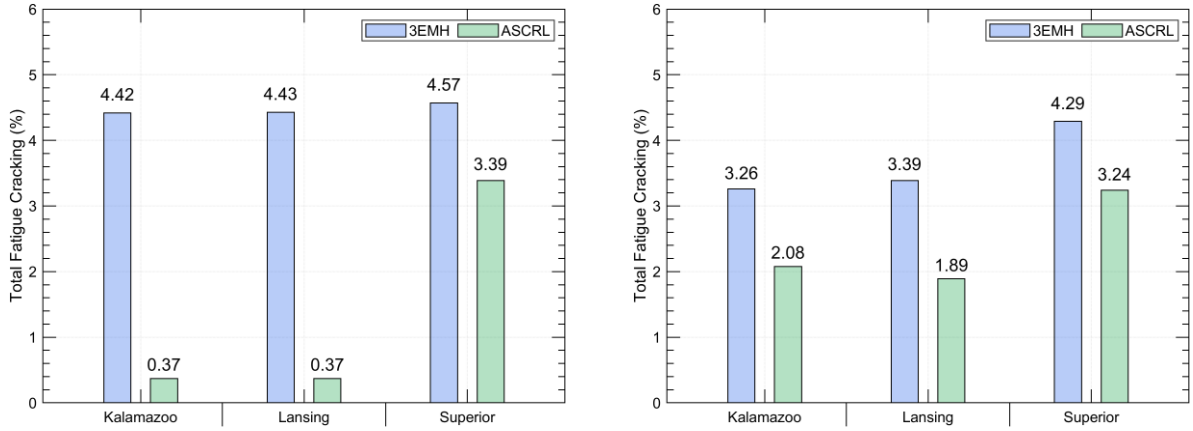
(c) Thin section with 3EMH base course



(d) Thin section with ASCRL base course

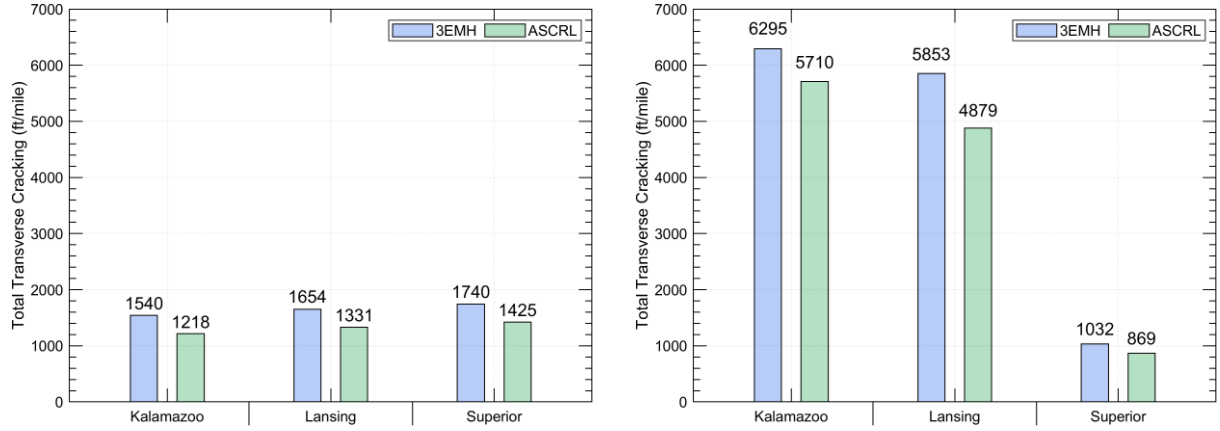
Figure 5-18 PMED structural configurations for ASCRL and 3EMH sections

Figures 5-19 and 5-20 present comparisons of total fatigue and transverse cracking for pavement sections incorporating ASCRL and conventional 3EMH base courses across Michigan's three climatic regions, for both thin and thick overlays. The results demonstrate that integrating the ASCRL layer between the HMA overlay and existing concrete pavement substantially reduced both total fatigue cracking and total transverse cracking. This improvement is primarily attributed to the ASCRL's ability to attenuate reflective cracking, which is the governing distress mechanism in rehabilitated composite pavements.



(a) Thick section (b) Thin section

Figure 5-19 Total fatigue cracking comparison



(a) Thick section (b) Thin section

Figure 5-20 Total transverse cracking comparison

5.3.5 HMA with ASCRL over CRCP

The modeling approach for HMA overlays incorporating ASCRL over CRCP follows the same general procedure as that used for HMA overlays of CRCP. The only distinction lies in the use of the ASCRL as the base HMA layer over the existing concrete pavement. As previously noted, the ASCRL layer is intended to absorb stress concentrations and further delay the onset of reflective cracking from the underlying concrete. However, because CRCP provides a continuous reinforcement system

without joints, reflection cracking is already significantly reduced, as illustrated in Figure 5-7(a). The inclusion of an ASCRL would further enhance this benefit by dissipating thermal and shrinkage-induced stresses. Given MDOT's limited CRCP network, this fix type should follow the same recommendations as HMA over CRCP, as noted in subsection 5.2.3.

5.4 FIX TYPES NOT ADDRESSED BY PMED

Several rehabilitation fix types identified in the MDOT network could not be modeled directly or indirectly within the current PMED framework because the corresponding structural configurations or predictive models were unavailable. The following subsection briefly outlines the fix types, describes the limitations encountered in PMED implementation, and provides recommendations for their future analytical treatment.

5.4.1 SJPCP over Existing PCC or AC/JPCP, JRCP, or CRCP (composite)

SJPCPs over JPCPs, JRCP, CRCP, or composite pavements represent a recognized rehabilitation category for MDOT. However, these configurations are not explicitly supported within the PMED structural framework. As previously noted, (in 5.2.6), although PMED includes a modeling option for SJPCP over AC, it does not accommodate configurations where short-jointed or fiber-reinforced slabs are placed over existing rigid or composite pavements.

Within the available SJPCP over AC option, PMED imposes fixed assumptions (as described in 5.2.6) that make it extremely difficult to modify or equate to other representative existing pavement types. Because of these hard-coded constraints, it cannot be adequately adapted to represent SJPCP placed over rigid/composite foundations.

For these limitations, the research team recommends that MDOT continue to design SJPCP with fiber-reinforced concrete overlays using its established engineering procedures rather than attempting to apply the PMED SJPCP model outside its narrow-intended use.

5.5 DISTRESS THRESHOLDS

Performance thresholds define the allowable limits of pavement distress or roughness used to evaluate design adequacy and determine rehabilitation needs within the PMED framework. These criteria represent serviceability limits beyond which pavement performance is considered unacceptable for a given functional class and/or traffic level. When predicted distress exceeds these limits, adjustments to the design, such as increased thickness or other material properties, are required. The following section explains the threshold criteria for PMED rehabilitation fix types and initial recommended values.

5.5.1 Asphalt Overlays (of intact pavements)

For asphalt overlays, PMED applies predefined distress thresholds that define the acceptable limits of performance over the design life. These thresholds serve as benchmarks for evaluating predicted pavement responses, such as roughness, rutting, and cracking, ensuring that rehabilitation designs meet required serviceability and durability standards. Table 5-7 shows the PMED default thresholds for HMA overlays (of intact pavements).

Table 5-7 PMED default thresholds for asphalt overlays

Performance Criteria	Limit
Terminal IRI (in/mile)	172.00
AC total fatigue cracking: bottom up + reflective (% lane area)*	25.00
AC total transverse cracking: thermal + reflective (ft/mile)	2500.00
Permanent deformation - total pavement (in)*	0.75
Permanent deformation - AC only (in)	0.25
AC bottom-up fatigue cracking (% lane area)	25.00
AC thermal cracking (ft/mile)	1000.00
AC top-down fatigue cracking (% lane area)	25.00
JPCP transverse cracking (percent slabs)**	15.00
CRCP punchouts (1/mile)***	10.00

* Applies only to AC over AC
** Applies only to AC over JPCP/composite types
*** Applies only to AC over CRCP/composite types

The research team evaluated the measured field performances to assess the suitability of the existing thresholds for HMA overlays and identify potential revisions. The following sections describe the basis for selecting the recommended threshold for each performance criterion. It should be noted that the recommended thresholds are presented as initial recommendations and may be refined based on MDOT review and/or additional design validation.

AC total fatigue cracking: bottom up + reflective

This criterion is only applicable to asphalt overlays of existing HMA. Figure 5-21(a) shows the measured bottom-up cracking in these overlays. Most sections exhibit low bottom-up cracking, with only a few reaching the default 25% threshold at maximum ages ranging from 5 to 20 years. However, as documented in SPR-1723, all longitudinal cracking types, including potential top-down cracking, were combined for calibration and to evaluate potential bottom-up fatigue cracking. This approach was adopted due to the inherent difficulty in distinguishing surface cracking mechanisms and to capture total longitudinal distress, as shown in Figure 5-21(b). When top-down cracking is examined separately, the number of sections exceeding 25% increases. However, it is important to note that this criterion accounts for cracking in both the new overlay and potential reflective cracking initiated by the existing sublayers. MDOT's HMA reconstruction threshold for bottom-up cracking alone is 20%. The PMED default value of 25%, therefore, provides appropriate allowance for the additional reflective cracking expected in overlay systems. As a result, the PMED default threshold is recommended for this criterion.

AC bottom-up fatigue cracking

This value defines the not-to-exceed limit for bottom-up cracking alone. For AC over AC PMED designs, this threshold is hardcoded at the 50% reliability level because it is used only as an informational output, with the primary design criterion being total fatigue cracking (which incorporates this measure). However, for HMA overlays of rigid or composite pavements, this measure remains applicable since total fatigue cracking is not a performance measure for these pavement types. In these cases, reconstruction-based considerations can be applied to the new HMA overlay, as reflective cracking is not included in this measure. Therefore, the MDOT 20% bottom-up cracking threshold for HMA reconstruction can be equally applied to these overlays.

AC top-down fatigue cracking

Figure 5-21 (b) shows the measured top-down cracking for the selected overlay sections. The age at maximum distress ranged from 5 to 20 years. However, the top-down model does not give reasonable predictions for Michigan conditions, and SPR 1595 identified some mathematical anomalies in the top-down cracking model (*4*). Consequently, as previously noted, all observed top-down cracking should be combined with bottom-up cracking, and this criterion alone should be omitted from design evaluation. This PMED default threshold may be retained, as this measure is not used for design assessment.

Permanent deformation - total pavement (Total Rutting)

Figure 5-21 (c) shows the measured rutting for the selected overlay sections. Most sections did not exhibit significant rutting, and none reached the 0.75 threshold. The maximum age of the sections ranged from 3 to 19 years. Figure 4-15 (c) in Chapter 4 shows the distribution of categories (good, fair, and poor) for these sections. As shown, all these sections fall into the good and fair categories for rutting, indicating their field performance. Therefore, the team recommends using the lower MDOT reconstruction threshold of 0.5 inches for rutting.

AC total transverse cracking: thermal + reflective (ft/mile)

Figure 5-21 (d) shows the observed total transverse cracking for the selected overlay sections. The thermal cracking observed in the rehabilitation projects was significant, with two sections nearing 5,000 feet/mile. The age at which the maximum thermal cracking occurred ranged from 6 to 20 years. Sections with Superpave (PG) binder have been used for calibration of thermal cracking. It should be noted that some of the thermal cracks may be reflective cracks, as MDOT PMS cannot distinguish between the two.

MDOT increased the reconstruction thermal cracking threshold to 2,000 ft/mile (from 1,000 ft/mile) during the last calibration efforts based on its measured thermal cracking trends (*4*). For asphalt overlays, the default thresholds of thermal cracking and total transverse cracking (thermal plus reflective) are 1,000 ft/mile and 2,500 ft/mile, respectively. Considering MDOT's revised thermal cracking threshold and an Iowa DOT study recommending 4,000 ft/mile (*22*), a higher total transverse cracking threshold is warranted. Therefore, the research team recommends setting the total transverse

cracking threshold at 3,500 ft/mile, based on field performance trends and relative to the reconstruction criteria, given consideration of additional reflective cracking. For HMA overlays of CRCP, the total predicted transverse cracking has minimal influence of reflective cracking due to continuous reinforcement with no transverse joints. Therefore, it is rational to use a threshold of 2,500 ft/mile for total transverse cracking in HMA overlays of CRCP pavements.

IRI

Figure 5-21 (e) shows the observed IRI for the asphalt overlay sections. The IRI time series is generally flat, with two sections exceeding the 172 in/mile threshold. The age of maximum IRI ranged from 7 to 20 years. It is worth noting that only sections with an initial IRI of 82 inches per mile or less were selected for calibration of the IRI model to ensure that only practical measures were considered (*4*). Almost all sections fall under good or fair categories (as shown in Figure 4-15 (e) in Chapter 4). Although the total transverse and fatigue cracking models contribute to the IRI model, the measured IRI remains consistent with reconstruction sections. Therefore, the team recommends retaining the reconstruction IRI threshold (as is also the PMED default).

Table 5-8 summarizes the recommended thresholds for HMA overlays, with values that differ from the PMED defaults shown in bold. For HMA overlays over JPCP or CRCP, it is recommended that their concrete-related criteria retain the default PMED thresholds, as these are primarily used for informational purposes. Design evaluation should instead rely on the remaining surface HMA criteria, which more directly indicate the rehabilitation's serviceability.

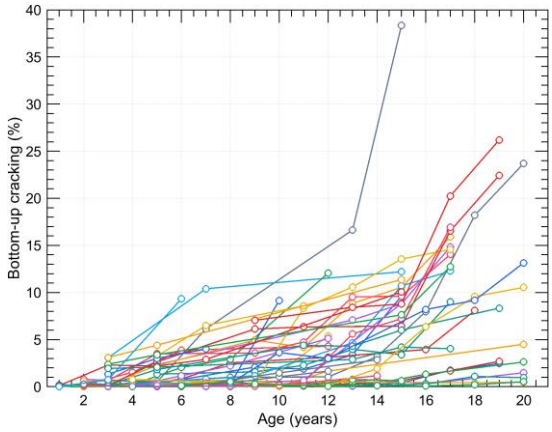
Table 5-8 Recommended thresholds for HMA overlays

Performance Criteria	Limit
Terminal IRI (in/mile)	172.00
AC total fatigue cracking: bottom up + reflective (% lane area)*	25.00
AC total transverse cracking: thermal + reflective (ft/mile)	**3500.00/2500.00*** **
Permanent deformation - total pavement (in)*	**0.50**
Permanent deformation - AC only (in)	0.25
AC bottom-up fatigue cracking (% lane area)	**20.00**
AC thermal cracking (ft/mile)	**2000.00**
AC top-down fatigue cracking (% lane area)	25.00
JPCP transverse cracking (percent slabs)**	15.00
CRCP punchouts (1/mile)***	10.00

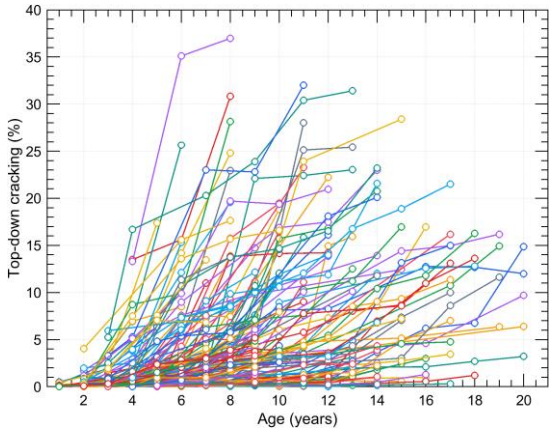
* Applies only to AC over AC
** Applies only to AC over JPCP/composite types
*** Applies only to AC over CRCP/composite types

5.5.2 Concrete Overlays

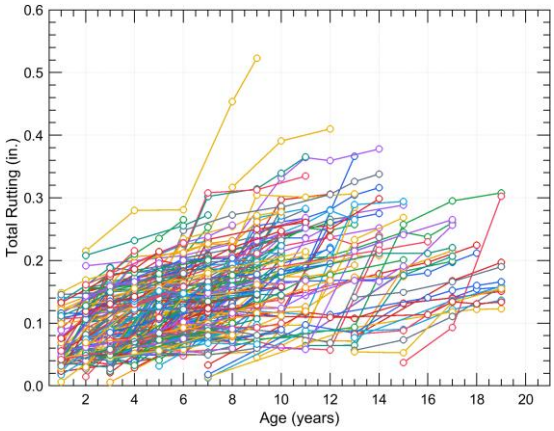
For concrete overlays, the PMED framework defines performance thresholds based on key distress indicators that govern structural integrity and ride quality. These include slab cracking, joint faulting, and smoothness. Current MDOT reconstruction thresholds are generally consistent with the PMED defaults for concrete overlays, with the only notable difference being a slightly higher allowable mean joint faulting value of 0.125 inches (versus 0.12 inches for the default).



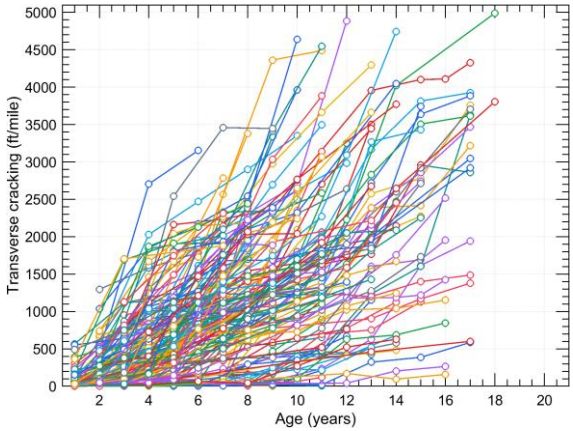
(a) Bottom-up cracking



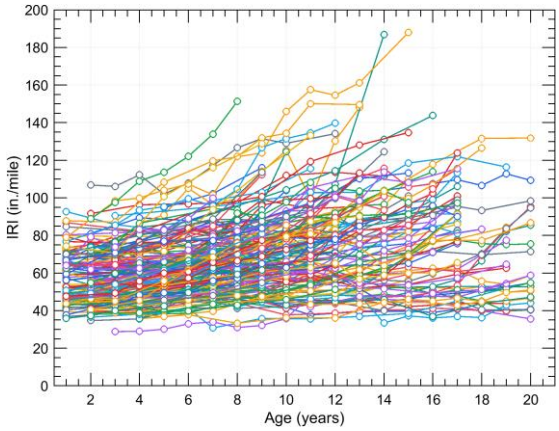
(b) Top-down cracking



(c) Rutting



(d) Transverse cracking



(e) Time series

Figure 5-21 Field-measured performance for asphalt overlay sections

Table 5-9 presents the PMED default thresholds for concrete overlays, along with the corresponding MDOT joint-faulting threshold.

Table 5-9 PMED default thresholds for concrete overlays (*1*)

Distress Type	Target
Terminal IRI (in/mile)	172.0
Mean joint faulting (in)	0.12 ***(MDOT = 0.125)***
JPCP transverse cracking (percent slabs)	15.0

The following section explains the selection of the design threshold for MDOT designs.

JPCP Transverse Cracking

Figure 5-22 (a) shows the observed transverse cracking on concrete overlay sections. Low values are observed for transverse cracking, with none of the projects exceeding the distress threshold of 15% of slabs cracked. The maximum transverse cracking observed is 4%. The age distribution ranges from 6 to 19 years. Transverse cracking is not a significant performance issue requiring modification to the threshold, so retaining the PMED default is appropriate.

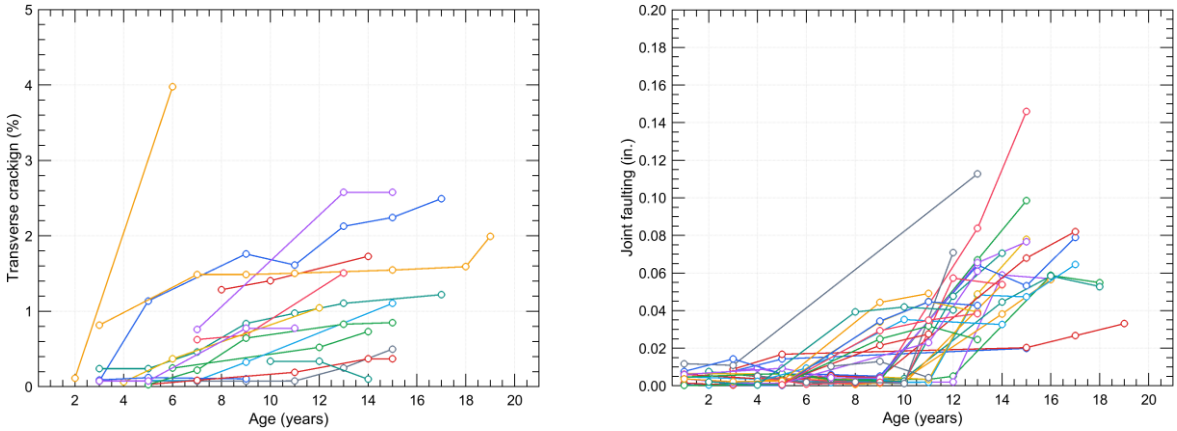
Mean Joint Faulting

Figure 5-22 (b) reflects the measured joint faulting for concrete overlay sections. One section exceeds the joint-faulting threshold of 0.125 inches, with a maximum value of 0.14 inches. The age distribution ranges from 11 to 19 years. Based on these observations, the default PMED or MDOT reconstruction threshold remains suitable.

IRI

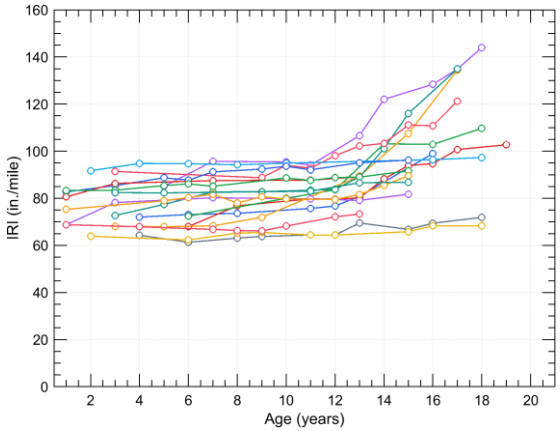
Figure 5-22 (c) shows the observed IRI for concrete overlay sections. A maximum IRI of 144 in/mile was observed for the unbonded overlay sections. None of the sections exceeded the IRI threshold of 172 in/mile. The age at maximum IRI ranges from 13 to 19 years. These mostly remain consistent with the reconstruction counterparts. Therefore, the research team recommends matching the reconstruction threshold to the PMED default.

The research team recommends using the current MDOT thresholds for JPCP reconstruction (Table 5-9), as they remain applicable to PCC overlays.



(a) Transverse cracking

(b) Transverse joint faulting



(c) IRI

Figure 5-22 Measured performance of concrete overlay sections

5.6 PMED LIMITATIONS

PMED V2.6 remains capable of modeling most rehabilitation fix types used by MDOT; however, several agency-specific fix types present inherent implementation limitations. These constraints arise from structural configuration options, material characterization defaults, and input parameter restrictions that do not fully align with MDOT's current rehabilitation practices or field conditions. The key software and data limitations identified during this study are summarized below:

- PMED V2.6 does not model multiple overlays. Although V3.0 allows users to model multiple overlays over existing pavements, i.e., AC over AC over JPCP, its usability for the MDOT application has not yet been verified.
- For HMA over HMA overlays, rehabilitation Level 3 uses the pavement's structural rating to assign a predefined damage value. Its subjective and imprecise assignment of pavement ratings means it cannot accurately capture damage in existing pavements.
- PMED V2.6 initializes the AC rutting model based on the existing rut depth to define the stage of plastic strain accumulation. If no existing rutting is specified,

the program assumes the pavement begins in the primary (rapid) deformation zone, leading to artificially high total rutting predictions. Accurate input of in-place rutting is therefore critical to avoid overestimation of final rut depths in overlay designs.

- For HMA overlays of existing HMA thinner than approximately 3.5 inches, the critical strain at the bottom of the overlay is in the compressive zone. At the same time, the PMED fatigue model continues to assume a tensile strain condition for initiating bottom-up cracking. This mismatch leads to inaccurate fatigue predictions for thin overlays, as the model applies a bottom-up cracking mechanism under conditions where tensile strain does not exist.
- Although the MDOT database includes several existing JRCP sections, PMED lacks a dedicated JRCP modeling option; therefore, all JRCP pavements were analyzed as JPCP, potentially introducing bias in predicted cracking and faulting behavior due to differences in joint spacing and load transfer characteristics.
- PMED exhibits unusual transverse cracking predictions for HMA overlays of existing rigid pavement, where total cracking increased with thickness up to 4.5 inches and then decreased for thicker overlays. This behavior contradicts expected mechanistic trends and is attributed to PMED's sublayer discretization and EICM temperature node depth assignments, which can distort thermal stress gradients in thin overlays. As a result, transverse cracking predictions for overlays thinner than 4.5 inches may be unreliable and should be interpreted with caution.
- PMED characterizes the existing concrete layer beneath unbonded concrete overlays solely based on elastic modulus, without incorporating additional surface condition indicators such as transverse cracking, faulting, or surface distress severity.
- Modeling rehabilitation strategies that deviate from standard configurations or equivalent approaches in the PMED can yield inaccurate or overly simplified results. For such fix types, PMED should be used with caution, and its outcomes should be validated against established design practices, such as those based on the AASHTO 93 design methodology, to ensure reliability and engineering consistency.

5.7 SUMMARY

This chapter presented the framework for selecting and modeling rehabilitation fix types within PMED V2.6. It explained the configurations for fix types directly supported in the software and those represented through equivalent approaches, including HMA and PCC overlays over various existing pavement structures. The discussion also addressed fix types not explicitly handled by the PMED, summarized the distress threshold criteria adopted for asphalt and concrete overlays, and outlined key limitations of the program and available input data. Overall, this chapter guides the applicability, practicality, modeling approach, and modeling considerations of MDOT HMA and PCC overlay rehabilitation strategies within the PMED framework.

CHAPTER 6 - LOCAL CALIBRATION PROCEDURES

6.1 INTRODUCTION

The PMED guide was initially developed under the NCHRP Project 1-37A (*1*) to overcome the limitations of the AASHTO 93 method (*2*). The PMED provides a mechanistic–empirical framework for analyzing both new and rehabilitated pavement structures. The methodology integrates traffic loading, material properties, and climate data to estimate pavement mechanical responses and the resulting damage accumulation over time. These calculated damage indices are subsequently converted to field distresses through empirically derived transfer functions. The transfer functions in PMED were calibrated at the national level using the LTPP database (*3*). While these national calibrations offer a reasonable prediction of pavement performance across the United States, they may not fully capture the variability in materials, construction practices, traffic characteristics, and environmental conditions unique to a given state or region. As a result, the nationally calibrated models may either overpredict or underpredict field performance when applied locally. The AASHTO Local Calibration Guide (*4*) recommends recalibrating state-specific distress transfer functions to improve model reliability and prediction accuracy.

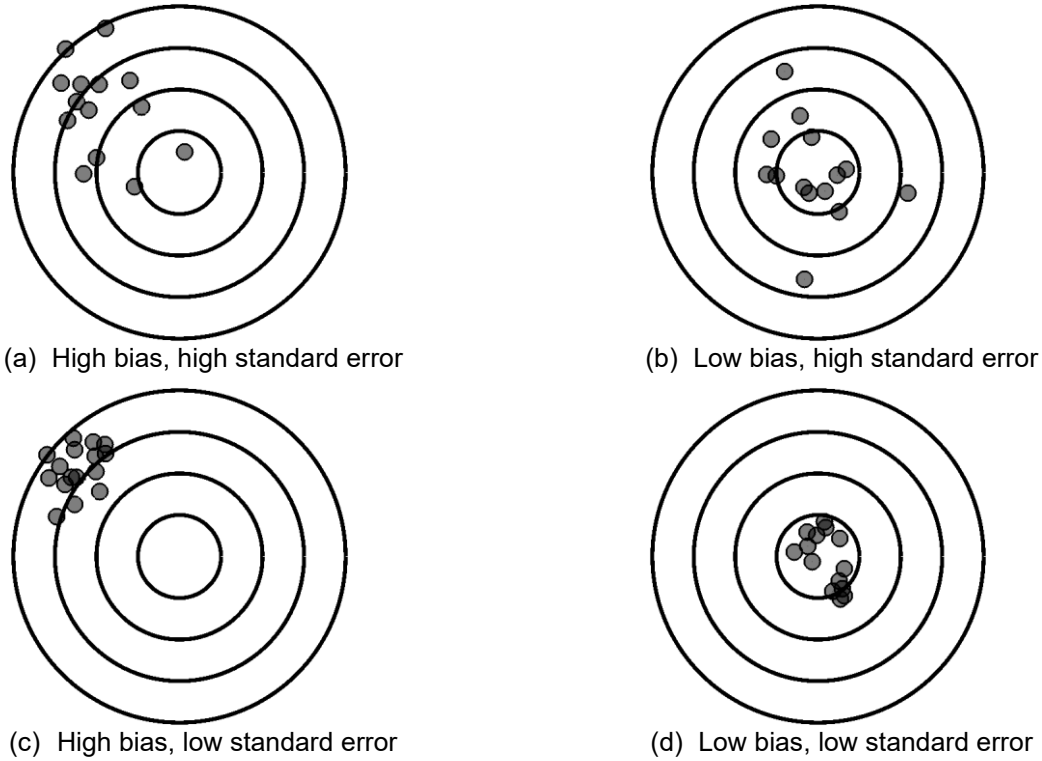
Previous local calibration studies have primarily focused on new and reconstructed pavement sections, particularly for flexible and rigid pavement designs. However, rehabilitation strategies, such as HMA overlays, unbonded PCC overlays, C&S, and rubblized concrete, represent a significant portion of the pavement network and exhibit unique structural and material behaviors that warrant independent calibration. The rehabilitation models within PMED differ from those for new construction because they incorporate pre-existing distress, aged materials, and interface conditions between old and new layers, all of which affect predicted performance. PCC overlay PMED performance distresses include transverse cracking (percentage of slabs cracked), transverse joint faulting (inches), and IRI (in./mile). For flexible pavements, the distresses include bottom-up cracking (percentage), top-down cracking (percentage), rutting (in.), thermal (transverse) cracking (feet/mile), reflective cracking (feet/mile), and IRI (in./mile).

This chapter outlines the overall local calibration process for rehabilitation performance models and types considered in this study. It describes the calibration approaches, resampling and optimization techniques, and the systematic procedure adopted to refine transfer function coefficients for various rehabilitation fix types. The chapter also explains how to evaluate model reliability, ensuring that the calibrated models accurately reflect Michigan-specific material and environmental conditions.

6.2 CALIBRATION APPROACHES

The objective of local calibration in the PMED framework is to refine the model coefficients so that the predicted pavement distress aligns closely with measured field

performance. This process aims to minimize both bias and standard error in model predictions. Bias indicates whether a model systematically over- or under-predicts distress relative to observed data. At the same time, the standard error reflects the degree of variability or scatter around the line of equality, as shown in Figure 6-1.



(a) High bias, high standard error

(b) Low bias, high standard error

(c) High bias, low standard error

(d) Low bias, low standard error

Figure 6-1 Schematic representation of bias and standard error (5)

Minimizing these two metrics ensures that the locally calibrated models provide accurate, consistent performance predictions for Michigan-specific materials, climate, and traffic conditions. The team used a Genetic Algorithm (GA) implemented in MATLAB to optimize the model coefficients. GA is an evolutionary, population-based optimization technique that can converge to a global minimum even in the presence of multiple local minima. The algorithm evolves candidate solutions through several key operations:

- Initialization: A population of potential solutions is randomly generated within the predefined search space.
- Selection: Individual solutions are evaluated using an objective function, and the most suitable candidates are selected for reproduction.
- Generation of offspring: New candidate solutions (offspring) are generated from selected parents via crossover and mutation, promoting diversity and exploration of the search space.
- Termination: The iterative process continues until a convergence criterion is satisfied, such as achieving a minimum objective-function value or reaching the maximum number of generations.

The PMED categorized the empirical transfer functions into two forms:

1. Models that compute the magnitude of distress directly from predicted damage or strain responses.
2. Models that estimate damage index over time and subsequently relate it to surface distress.

Depending on the model formulation, the team adopted two distinct calibration approaches in this study:

1. Approach I – External Optimization: For distresses such as fatigue cracking (bottom-up and top-down), rutting, PCC transverse cracking, and IRI, the required damage indices are readily available in the PMED output files. These models were calibrated outside the PMED environment using MATLAB-based GA optimization.
2. Approach II – CAT: For models where cumulative damage or internal mechanisms are not directly reported by PMED, such as thermal cracking, reflective cracking, and joint faulting, the CAT provided within PMED is used for calibration. The CAT iteratively modifies model coefficients to minimize the difference between measured and predicted distress based on cumulative-damage computations over the analysis period.

Tables 6-1 and 6-2 summarize the transfer functions and the calibration approaches used for asphalt and concrete overlays, respectively.

Table 6-1 Model transfer functions and calibration approaches for asphalt overlays

Performance prediction model	Approach I	Approach II	Model transfer functions
Fatigue cracking – bottom up	✓		$FC_{Bottom} = \left(\frac{1}{60}\right)\left(\frac{6000}{1 + e^{\boldsymbol{C_1}C_1^* + \boldsymbol{C_2}C_2^* Log(DI_{Bottom}100)}}\right)$
Fatigue cracking – top down	✓		$t_0 = \frac{K_{L1}}{1 + e^{\boldsymbol{K_{L2}} \times 100 \times (a_0/2A_0) + \boldsymbol{K_{L3}} \times HT + \boldsymbol{K_{L4}} \times LT + \boldsymbol{K_{L5}} \times log_{10}\ AADTT}}$ $L(t) = L_{MAX} e^{-\left(\frac{\boldsymbol{C_1}\rho}{t - C_3 t_0}\right)^{\boldsymbol{c_2}\beta}}$
Rutting – HMA	✓		$\Delta_{p(HMA)} = \varepsilon_{p(HMA)} h_{HMA} = \boldsymbol{\beta_{1r}} k_z \varepsilon_{r(HMA)} 10^{k_{1r}} n^{k_{2r}\beta_{2r}} T^{k_{3r}\beta_{3r}}$
Rutting – Base/subgrade	✓		$\Delta_{p(soil)} = \boldsymbol{\beta_{s1}} k_{s1} \varepsilon_v h_{soil} \left(\frac{\varepsilon_o}{\varepsilon_r}\right) e^{-\left(\frac{\rho}{n}\right)^{\beta}}$
Thermal cracking		✓	$A = 10^{\boldsymbol{k_t}\beta_t\left(4.389 - 2.52 Log(E_{HMA}\sigma_m\eta)\right)}$
Reflective cracking		✓	$\Delta D = \frac{\boldsymbol{C_1} k_1 \Delta_{bending} + \boldsymbol{C_2} k_2 \Delta_{shearing} + \boldsymbol{C_3} k_3 \Delta_{thermal}}{h_{OL}}$ $RCR = \left(\frac{100}{\boldsymbol{C4} + e^{c5 log\, D}}\right) * EXCRK$
IRI	✓		$IRI = IRI_o + \boldsymbol{C_1}(RD) + \boldsymbol{C_2}(FC_{Total}) + \boldsymbol{C_3}(TC) + \boldsymbol{C_4}(SF)$

*Bold font indicates calibrated coefficients

Table 6-2 Model transfer functions and calibration approaches for concrete overlays

Performance prediction model	Approach I	Approach II	Model transfer functions
Transverse cracking	✓		$CRK_{BU/TD} = \frac{100}{1 + \boldsymbol{C_4}(DI_F)^{\boldsymbol{C_5}}}$ $TCRACK = \left(CRK_{Bottom-up} + CRK_{Top-down} - CRK_{Bottom-up} \cdot CRK_{Top-down}\right) \cdot 100\%$
Transverse joint faulting		✓	$Fault_m = \sum_{i=1}^{m} \Delta Fault_i$ $\Delta Fault_i = C_{34} \times (FAULTMAX_{i-1} - Fault_{i-1})^2 \times DE_i$ $FAULTMAX_i = FAULTMAX_0 + C_7 \times \sum_{j=1}^{m} DE_j \times Log(1 + C_5 \times 5.0^{EROD})^{\boldsymbol{C_6}}$ $FAULTMAX_0 = \boldsymbol{C_{12}} \times \delta_{\text{curling}} \times \left[Log(1 + C_5 \times 5.0^{EROD}) \times Log(\frac{P_{200} \times WetDays}{p_s})\right]^{\boldsymbol{C_6}}$ $C_{12} = \boldsymbol{C_1} + \boldsymbol{C_2} \times FR^{0.25}$ $C_{34} = C_3 + C_4 \times FR^{0.25}$
IRI	✓		$IRI = IRI_I + \boldsymbol{C_1} \times CRK + \boldsymbol{C_2} \times SPALL + \boldsymbol{C_3} \times TFAULT + \boldsymbol{C_4} \times SF$

*Bold font indicates calibrated coefficients

6.3 CALIBRATION TECHNIQUES

Over the years, several calibration and resampling techniques have been employed by transportation agencies to calibrate the PMED performance models. During the previous Michigan calibration study (*6*), four primary approaches — no sampling, split sampling, bootstrapping, and jackknifing — were evaluated in combination with optimization methods, including least-squares and maximum-likelihood estimation (MLE). Among these methods, bootstrapping consistently produced the most stable and statistically reliable results, as it effectively quantified uncertainty and reduced sensitivity to outliers or sample variability.

The current calibration focused on two complementary techniques: the traditional (no-sampling) approach and bootstrapping. These were implemented within the frameworks of Approach I (external MATLAB optimization) and Approach II (PMED CAT-based calibration), both using the least-squares criterion to minimize the difference between measured and predicted distress values. The following subsections describe the procedures and characteristics of each resampling technique applied in this study.

6.3.1 No-Sampling Technique

The no-sampling approach uses the entire dataset of available sections without dividing it into calibration and validation subsets. All data points are used simultaneously to estimate the model coefficients that minimize the standard error of the estimate of the difference between measured and PMED-predicted distress. This method is straightforward, computationally efficient, and appropriate when the dataset is sufficiently large and representative. However, because it does not assess prediction accuracy on independent data, the resulting coefficients represent point estimates only and do not quantify parameter uncertainty. Consequently, this technique primarily serves as a baseline or comparative method alongside more advanced resampling approaches, such as bootstrapping.

6.3.2 Bootstrapping

Bootstrap resampling is a non-parametric statistical technique widely used to estimate the sampling distribution of a parameter and to construct confidence intervals without assuming a specific underlying population distribution. In pavement model calibration, bootstrapping provides a robust framework for quantifying the uncertainty associated with model coefficients derived from limited field data. In this method, numerous bootstrap samples are generated from the original dataset by random sampling with replacement. Each sample has the same size as the original dataset and may contain duplicate observations. For each bootstrap sample, the calibration coefficients are re-estimated, and the resulting distribution of coefficients is used to compute their mean, standard error, and confidence intervals. In this study, 1,000 bootstrap resamples (B = 1,000) were generated for each distress model, and the coefficients were optimized for each resample using the least-squares criterion.

Equation 6-1 shows the standard error of a bootstrap-estimated statistic:

$$\mathrm{SE} = \sqrt{\frac{1}{B-1}\sum(\theta_b - \theta^*)^2} \quad (6\text{-}1)$$

where;
SE = estimated standard error of the statistic
B = number of bootstrap samples
θ_b = value of the statistic for the b_{th} bootstrap sample
θ^* = mean of the B bootstrap sample values.

The confidence interval (CI) for the parameter can be obtained using the percentile method based on the ranked bootstrap sample values, as in Equation 6-2.

$$\mathrm{CI} = (\theta^* - \theta_{\frac{\alpha}{2}}, \theta^* + \theta_{\frac{\alpha}{2}}) \quad (6\text{-}2)$$

where;
CI = bootstrap confidence interval
θ^* = mean of the B bootstrap sample values
$\theta_{\frac{\alpha}{2}}$ = $\frac{\alpha}{2}$th percentile of the bootstrap sample values

The bootstrapping technique offers several advantages: it does not require assumptions of normality, performs well with small or irregular datasets, and provides a direct estimation of coefficient variability. However, it can be computationally intensive for large datasets and may be influenced by biased or unrepresentative samples. Despite these limitations, bootstrapping was adopted as the primary resampling technique in this study due to its demonstrated robustness and reliability in the previous Michigan calibration effort (*6*).

6.3.3 Summary of Resampling Techniques

Among the various resampling methods explored in previous calibration studies, this research employed only the no-sampling and bootstrapping approaches. The no-sampling technique provided a computationally efficient baseline by using the entire dataset to obtain point estimates of calibration coefficients, whereas bootstrapping offered a statistically robust means of quantifying uncertainty and constructing confidence intervals. Both techniques complemented each other within the calibration framework—no-sampling for initial estimation and bootstrapping for assessing the stability of the results. Table 6-3 summarizes the advantages and limitations of no-sampling and bootstrapping.

Table 6-3 Summary of calibration techniques

Technique	Advantages	Limitations
No sampling	• Computationally fast and straightforward • Utilizes the full dataset	• Produces point estimates only • Does not quantify parameter uncertainty
Bootstrapping	• Provides confidence intervals for coefficients • Identify outliers • No distributional assumptions required	• Computationally intensive for large datasets • Sensitive to biased or unrepresentative samples • It may not be suitable for non-normally distributed data

6.4 PROCEDURE FOR CALIBRATION OF PERFORMANCE MODELS

The procedures described in this section outline the overall workflow adopted for the local calibration of PMED distress prediction models for rehabilitation pavement types. The details regarding project selection, data assembly, and performance measurement have already been discussed in earlier Chapters. After compilation of input data, the research team prepared and ran the PMED input files (.dgpx) to generate the corresponding outputs, which included the critical structural responses and predicted distress values for each rehabilitation section:

1. Run PMED using the nationally calibrated (global) coefficients to obtain predicted distress values and critical response parameters for each section.
2. Compare the model-predicted performances with the measured field values to assess the predictive accuracy of the global models.
3. Examine the degree of bias and standard error in the global predictions to determine whether local calibration is warranted.
4. Refine/recalibrate the transfer function coefficients through local calibration to better reflect Michigan-specific conditions.
5. Verify the performance of the calibrated models using independent sections or through statistical evaluation to ensure stability and generalizability.
6. Develop reliability equations based on the relationship between measured and calibrated distress predictions to quantify prediction uncertainty across performance levels.

6.4.1 Testing the Accuracy of the Global Calibration Coefficients

Before initiating local calibration, the predictive accuracy of the global PMED models was evaluated at a 50% reliability level, reflecting the expected mean performance. The research team ran PMED using global coefficients and compared predicted distress values with field-measured data to assess bias and standard error. Predicted versus measured plots were developed for each distress type, using the line of equality (LOE) as a reference. The relationship between measured and predicted distress is expressed as:

$$y_{\text{measured}} = b_o + m \times x_{\text{predicted}} \quad (6\text{-}3)$$

where;
y_{measured} = measured distress.
$x_{\text{predicted}}$ = predicted distress.
b_0 = intercept.
m = slope.

The team tested three statistical hypotheses (H_0) to determine the adequacy of the global models:

- There is no systematic bias between the measured and predicted distress (Equation 6-4). This can be tested using a paired t-test.

$$H_0: \sum(y_{\text{Measured}} - x_{\text{Predicted}}) = 0 \quad (6\text{-}4)$$

- The slope parameter *m* is 1 (Equation 6-5).

$$H_0: m = 1.0 \quad (6\text{-}5)$$

- The intercept parameter b_o is zero (Equation 6-6).

$$H_o: b_o = 0 \quad (6\text{-}6)$$

If any of these conditions were not met, the research team recalibrated the transfer function coefficients to minimize standard error and bias between measured and predicted performance.

6.5 TRANSFER FUNCTION COEFFICIENTS OF ASPHALT OVERLAY

The design distresses in PMED include bottom-up cracking, top-down cracking, rutting, thermal (transverse) cracking, reflective cracking, and IRI for flexible pavements. The following section discusses the calibration of each model and the specific coefficients calculated for each model.

6.5.1 Fatigue Cracking Model (bottom-up)

The fatigue cracking (bottom-up) model was calibrated by optimizing the C_1 and C_2 coefficients (see Table 6-1). In PMED v2.6, coefficient C_1 is a single value, whereas coefficient C_2 has three different values depending on the total HMA thickness. Table 6-4 shows the global values for C_1 and C_2.

Table 6-4 Global values for the bottom-up cracking model coefficients

Calibration coefficient	Global values
C_1	1.31
C_2	H_{ac} < 5 in. : 2.1585
C_2	5 in. <= H_{ac} <=12 in.: (0.867 + 0.2583 × H_{ac}) ×1
C_2	H_{ac} > 12 in.: 3.9666

H_{ac} : Total HMA thickness in inches

Notably, there are no MDOT sections with a total HMA thickness exceeding 12 inches, so C_2 cannot be locally calibrated for this thickness. However, C_2 can be calibrated for the thickness iterations of less than 5 inches and 5 to 12 inches. For a thickness range of 5 to 12 inches, only the multiplying factor 1 (marked in bold here: (0.867 + 0.2583 × H_{ac}) ×**1**) is to be calibrated, while other values (0.867 and 0.2583) are to be kept at global values. The crack initiation time is affected by C_1, whereas the slope of the bottom-up cracking curve is affected by C_2. Nevertheless, since HMA over HMA and HMA over JPCP have minimal field-measured bottom-up fatigue cracking, it cannot be practically calibrated. As a result, bottom-up fatigue cracking was not calibrated for these fix types.

6.5.2 Fatigue Cracking Model (top-down)

The top-down cracking model has been modified in PMED V2.6 (from prior versions). The model consists of a crack initiation function that calculates the time to crack initiation and a crack propagation function that calculates the percentage of the lane area that has cracked. So, the model consists of a total of eight coefficients combined from both functions. Since the actual crack initiation time is not known, it was not possible to calibrate the crack initiation model separately. So, a single function was used by substituting the crack initiation function with the crack propagation function. Initially, an attempt was made to change all eight coefficients simultaneously. This approach had some challenges:

- The model has some mathematical limitations. High C_3 values result in a mathematical error when used in PMED.
- There is limited literature available on the calibration of the top-down cracking model. Therefore, estimating the range for each coefficient to be used in optimization was difficult.
- The model has many coefficient values ranging from 0.011 to 64271618. This diverse range of coefficient values makes convergence in optimization challenging.

Four coefficients from the crack initiation function (*kL2, kL3, kL4, kL5)* and two coefficients from the crack propagation function (C_1, C_2) have been calibrated based on the model's understanding and limitations, as mentioned above.

6.5.3 Rutting Model

Due to axle loads, rutting is the total accumulated plastic strain in different pavement layers (HMA, base/sub-base, and subgrade). It is calculated by summing the plastic strains at the mid-depth of each layer, accumulated over each time increment. In the

PMED, rutting is predicted separately for each layer (HMA, base, and subgrade). The total rutting is the sum of rutting from all layers. The AC rutting model has three coefficients (β_{1r}, β_{2r}, β_{3r}). β_{1r} is a direct multiplier and can be calibrated using optimization outside PMED. In this model, β_{2r} and β_{3r} are powers of the pavement temperature and the number of axle load repetitions. Calibration of β_{2r} and β_{3r} cannot be done outside of the PMED and requires running the PMED multiple times or optimizing these in the CAT tool. Therefore, the team calibrated β_{1r} solely based on discussions from previous calibration efforts *(5)*.

The unbound layers (base and subgrade) rutting model has one calibration coefficient each (β_{s1}). Since β_{s1} is a direct multiplier, it can be calibrated using optimization outside PMED without running the software or CAT. Since both base and subgrade have the same model and calibration coefficient, the base calibration coefficient is referred to as $\beta_{s1,}$ and the subgrade coefficient is referred to as β_{sg1} to avoid confusion. The rutting model in the PMED was calibrated using the following two methods:

1. *Method 1: Individual layer rutting calibrations* — For this approach, the measured rutting from individual layers was matched against the predictions from the PMED (β_{1r}, $\beta_{s1,}$ and β_{sg1} were calibrated separately). The total measured rutting was multiplied by each layer's percent contribution to obtain the measured rutting for that layer. The percentage contribution was used as described in SPR 1723, as shown in Figure 6-2 (*6*). The width and depth of the measured rut channel were used to determine the seat of rutting and the extent of rutting in individual layers. AC layer rutting accounts for more than 70% of all pavement types [based on transverse profile analysis (*7*)]. The standard error equations for rutting in the PMED are separate for individual layers. This method evaluated the standard error equations for rutting in each layer.
2. *Method 2: Total surface rutting calibration* — The total measured rutting was calibrated against the sum of individual predicted rutting (i.e., β_{1r}, $\beta_{s1,}$ and β_{sg1} were calibrated simultaneously).

6.5.4 Thermal Cracking Model

The thermal cracking model in the PMED has three calibration coefficient levels. These levels are based on the level of HMA input. Level 1 *G* and Level 2 IDT have been used to calibrate the thermal cracking model, corresponding to the* Level 1 thermal cracking calibration coefficients. MDOT provided the *G** and IDT values for calibration. In the MDOT database, *G** and IDT values are available only for sections with a PG binder type. Therefore, sections with PG binder type (Superpave mixes) have been used to calibrate the thermal cracking model. In PMED V2.6, the calibration coefficient k_t is originally a function of mean annual air temperature (MAAT), whereas in V2.3 it was a single representative value. For the reconstruction sections, two different approaches were used during the previous calibration effort (*6*):

- Using CAT, an initial attempt was made to calibrate k_t (using the original Equation as a function of MATT).

- A second attempt to calibrate k_t was made by running the PMED multiple times with different k_t values. As was done for the recalibration of reconstructed pavements in SPR-1723, a single k_t value was applied, independent of MAAT (*6*).

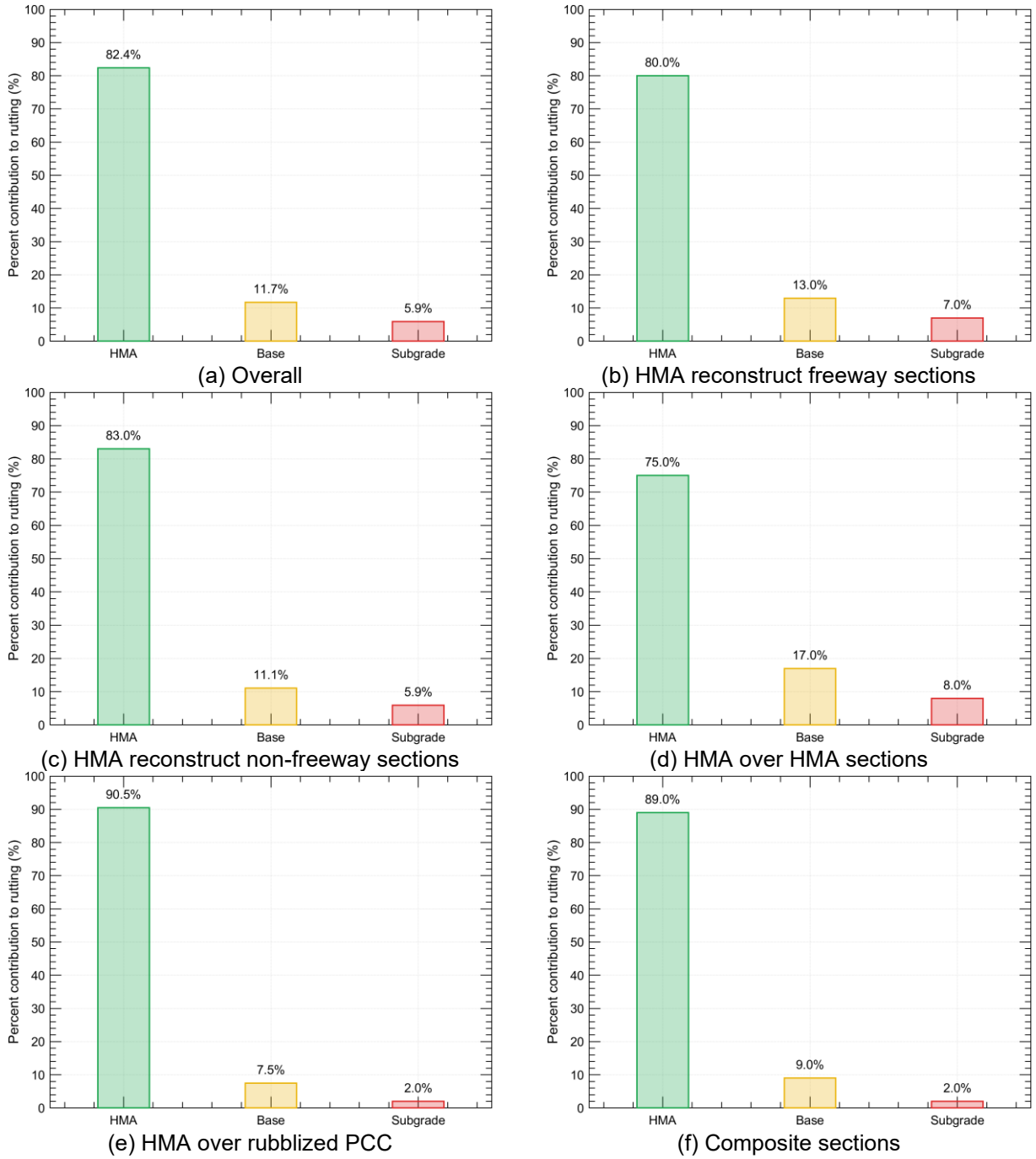


Figure 6-2 Rutting profile analysis results

As consistent with SPR-1723 and for improved practicality of the calibration, this calibration limited the average thermal cracking to 2,112 ft/mile, so values exceeding

this limit were not included. For overlays, MDOT does not differentiate between thermal cracking and reflective cracking. Hence, thermal and reflective cracking coefficients were calibrated for overlays using CAT. However, CAT has limitations on runtime and the total number of coefficient combinations, as well as the restriction to a single coefficient value, k_t. Therefore, for overlays, the team calibrated the thermal cracking coefficient k_t as a function of MAAT using CAT. The following subsection discusses the reflective cracking model. The team calibrated HMA over HMA and composite overlays based on this approach.

6.5.5 Reflective Cracking Model

In the HMA overlay design, damage to existing layers is a critical consideration. PMED uses the existing damage as a starting point for future damage predictions through reflection cracking (*8*). The reflection cracking model implemented in PMED is a mechanistic–empirical formulation developed under NCHRP Project 1-41 and incorporated into the 2015 enhancement of the PMED software (*9*). The model estimates the initiation and propagation of cracks in asphalt overlays using a fracture-mechanics approach governed by Paris' law. Crack growth is expressed as a function of stress intensity factors generated from traffic-induced shear and bending responses, as well as thermally induced tensile responses. These responses are obtained through ANN models trained using finite element simulations for a range of pavement structures.

The model consists of five calibration coefficients (C_1-C_5). Coefficients C_1, C_2, and C_3 represent crack initiation parameters derived from the ANN-based damage functions. Coefficients C_4 and C_5 correspond to damage-propagation parameters that control the relationship between accumulated damage and the percentage of surface cracking reflected from underlying layers. In this study, the research team maintained the C_1 to C_3 coefficients within proximity to their global values to preserve the internal consistency of the ANN-based formulation. Coefficient C_4 was adjusted during calibration to minimize the bias between measured and predicted reflective cracking. The C_5 coefficient could not be varied within CAT due to software limitations and was therefore retained at its global value.

The reflection cracking model is inherently complex because it depends on internally computed ANN outputs, which limit direct access to intermediate damage parameters. This structural constraint reduces calibration flexibility and may influence convergence during optimization. Nevertheless, the calibration improved model performance and reduced prediction bias for HMA overlays over JPCP and HMA pavement sections.

6.5.6 IRI Model for Asphalt Overlay Pavements

IRI is a linear function of initial IRI, rut depth, total fatigue cracking, total transverse cracking, and site factor, as shown in Equation 6-7. The initial IRI was obtained by linear back-casting based on the time-series trend for each section, as recommended by the previous calibration effort (*6*). The total fatigue cracking, rutting, and total transverse cracking models were calibrated before calibrating the IRI model. Since all inputs to the IRI model could be obtained, it was calibrated outside of PMED without using CAT. IRI

has a closed-form solution and does not require a standard error equation in the PMED. The standard error of IRI is calculated from the standard errors of its components.

$$\mathrm{IRI} = \mathrm{IRI_o} + \mathrm{C1(RD)} + \mathrm{C2(FC_{Total})} + \mathrm{C3(TC)} + \mathrm{C4(SF)} \quad (6\text{-}7)$$

where;
IRI_o = Initial IRI after construction, in/mi.
SF = Site factor.
FC_{Total} = Area of fatigue cracking (combined bottom-up and reflection cracking in the wheel path), percent of total lane area.
TC = Length of total transverse cracking (including the reflection of transverse cracks in existing HMA pavements), ft/mi.
RD = Average rut depth, in.

6.6 TRANSFER FUNCTION COEFFICIENTS OF CONCRETE OVERLAY

Design distresses in PMED include transverse cracking, joint faulting, and IRI in rigid pavements. This section covers the impact of calibration coefficients on the predicted performance specific to each model.

6.6.1 Transverse Cracking Model

The coefficients C_4 and C_5 (shown in Table 6-2) were optimized to calibrate the transverse cracking model. These coefficients were calibrated outside PMED without using CAT. C_4 affects the crack initiation time, and C_5 affects the slope of the transverse cracking curve.

6.6.2 Transverse Joint Faulting Model

The joint-faulting model in PMED comprises eight coefficients. Joint faulting could not be predicted using the available inputs outside the PMED; therefore, it was calibrated using CAT. However, CAT has limitations on runtime and on the total number of coefficient combinations that can be calibrated simultaneously. Consequently, it was essential to identify the most sensitive coefficients. Several studies *(10, 11)* show that, among the seven calibration coefficients for the faulting model, C_6 is the most sensitive. C_1 is the next sensitive coefficient, followed by C_2. Using this sequence of sensitivity of the coefficients, C_1 and C_6 were calibrated together. The calibrated coefficients from C_1 and C_6 were then kept fixed, and C_2 was calibrated. In this sequence, the three most sensitive coefficients were calibrated. As previously noted, and explained in Chapter 4, the joint faulting (for every 0.1-mile segment) was limited to a maximum value of 0.4 inches for calibration.

6.6.3 IRI Model for JPCP (Unbonded) Overlay Pavements

IRI in concrete pavements is a linear function of initial IRI, transverse cracking, joint spalling, joint faulting, and site factor, as shown in Equation 6-8. The initial IRI was obtained by linear backcalculation from the time-series trend for each section (*6*). The transverse cracking and joint faulting models were calibrated before calibrating the IRI model. Since all inputs to the IRI model were available, it was calibrated outside PMED without using CAT. IRI has a closed-form solution and does not require a standard error

equation in PMED. The standard error of IRI is calculated from the standard errors of its components.

$$\mathrm{IRI} = \mathrm{IRI_I} + \mathrm{C1} \times \mathrm{CRK} + \mathrm{C2} \times \mathrm{SPALL} + \mathrm{C3} \times \mathrm{TFAULT} + \mathrm{C4} \times \mathrm{SF} \quad (6\text{-}8)$$

where,
IRI = Predicted IRI
IRI_I = Initial IRI at the time of construction
CRK = Percent slabs with transverse cracking (all severities).
SPALL = Percentage of joints with spalling (medium and high severities).
TFAULT = Total joint faulting cumulated per mi
C_1, C_2, C_3, C_4 = Calibration coefficients
SF = Site factor

6.7 DESIGN RELIABILITY

The PMED framework incorporates a reliability-based approach to account for the inherent variability in pavement performance prediction. Although the mechanistic–empirical models in PMED provide rational estimates for design purposes, actual field performance often varies due to uncertainties associated with future traffic loading, material properties, construction variability, measurement errors, and the use of Level 2 and Level 3 input data. To address these sources of uncertainty, PMED defines reliability as the probability that the predicted distress will remain below the critical threshold over the design life. Mathematically, reliability (*R*) can be expressed, as shown in Equation 6-9.

$$\mathrm{Reliability} = \mathrm{P}[\text{distress at the end of design life} < \text{Critical distress}] \quad (6\text{-}9)$$

where;
R = reliability level of the design (probability of satisfactory performance).
P = probability operator.
Distress at the end of the design life = the predicted distress value at the end of the design period.
Critical distress = allowable distress threshold for design performance.

For example, suppose 100 pavement sections are designed at a reliability level of 90%. In that case, approximately 10 of them are expected to exceed the allowable distress before the end of the design period. Design reliability may differ by distress type; however, maintaining consistent reliability across all performance indicators is generally recommended to ensure uniform safety margins *(12)*. Except for IRI, PMED estimates reliability using the relationship between the standard deviation of measured distress (the dependent variable) and the mean predicted distress (the independent variable). The underlying assumption is that prediction errors follow a normal distribution, with a bias toward the upper tail of the distress prediction range (i.e., failures are more likely when the predicted distress exceeds the mean).

Figure 6-3 illustrates the reliability concept for smoothness (IRI). The solid curve represents the mean prediction at 50% reliability, while the dashed curve corresponds to a higher reliability level (e.g., 90%). At 90% reliability, the predicted distress curve must remain below the critical threshold throughout the analysis period. If it exceeds the

threshold, the design does not meet the target reliability, and modifications such as increased structural thickness or improved material properties should be implemented.

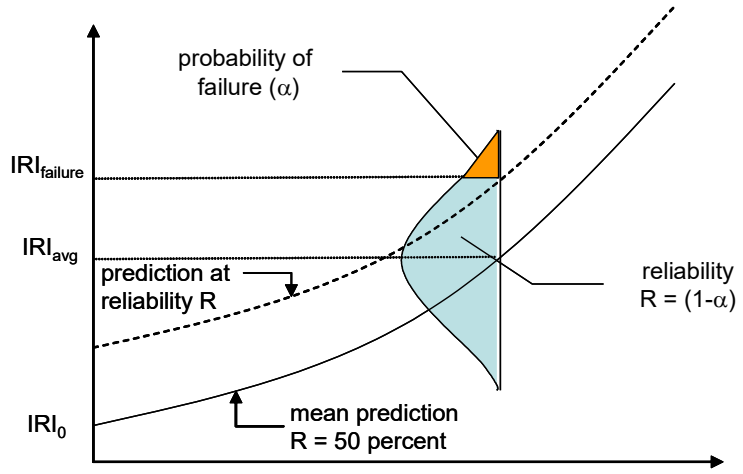


Figure 6-3 Design reliability concept for IRI (*8*)

6.7.1 Reliability Estimation

PMED quantifies reliability as a function of predicted performance, derived from the relationship between measured and simulated distress values. It accounts for variability arising from input data, material behavior, and model prediction error. The following procedure illustrates the reliability estimation process using bottom-up fatigue cracking in HMA overlays as an example. A similar methodology was applied to other distress models, except for IRI, which PMED handles internally.

Step 1 - Data grouping: Predicted and measured cracking data were divided into bins based on the range of predicted bottom-up cracking to ensure a uniform number of data points per group. This grouping minimizes bias in the regression relationship developed in subsequent steps.

Step 2 - Descriptive statistics: For each group, the research team computed the mean and standard deviation of both measured and predicted cracking after the calibration coefficients were finalized. Table 6-5 provides an example of summary statistics for the bottom-up cracking data.

Table 6-5 Example statistics for reliability analysis of HMA overlay bottom-up cracking

Cracking range (%)	No. of data points	Average Measured Cracking	Average Predicted Cracking	Standard dev. of Measured Cracking	Standard dev. of Predicted Cracking
0-1.5	4309	2.309	2.060	2.707	0.283
1.5-2.5	7859	3.136	3.051	3.244	0.286
2.5-3.5	12096	3.421	4.017	3.386	0.286
3.5-4.5	6116	3.364	4.736	3.396	0.144
4.5-5.0	12292	4.343	6.345	3.477	1.282
5.0-100	1884	8.027	10.267	3.264	1.734

Step 3 - Relationship between variability and predicted distress: A regression relationship was developed between the standard deviation of measured cracking and the average predicted cracking, as shown in Equation 6-10. This relationship quantifies the expected dispersion of measured data for a given level of predicted cracking. Figure 6-4 shows the fitted regression curve developed from the grouped data.

$$s_{e(FC)} = 1.0256 + \frac{2.4828}{1 + e^{0.0046 - 5.2091 \times log(D)}} \quad (6\text{-}10)$$

where;
$s_{e(FC)}$= standard deviation of measured fatigue cracking, %.
D = average predicted bottom-up cracking, %.

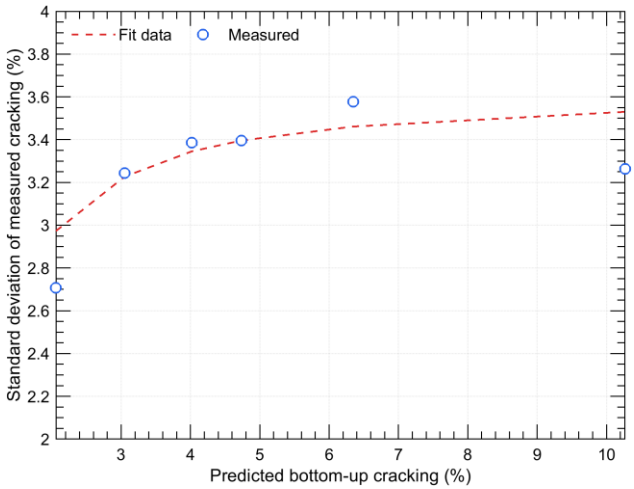


Figure 6-4 Fitting curve for the reliability of bottom-up cracking

Step 4 - Adjustment for reliability: Assuming normally distributed prediction errors, the predicted cracking was adjusted to any target reliability level using Equation 6-11.

$$C_r = C_{50} + S_e \times Z_{a/2} \quad (6\text{-}11)$$

where,
C_r = Predicted cracking at reliability *r* (%).
C_{50} = Predicted cracking at 50% reliability.
S_e = Standard deviation of cracking, which can be estimated using Equation 6-10.
$Z_{a/2}$ = Standardized normal deviate (mean = 0; standard deviation = 1) at reliability *r.*

Step 5 - Verification: Finally, the research team verified the reasonableness of the reliability relationship by comparing adjusted predictions against field-measured data.

The reliability model for IRI differs from those of other models. Since a closed-form solution and the variances of IRI's components are known, the reliability model for IRI is based on variance analysis of its components. The basic assumption implies that the error in predicting IRI is roughly normally distributed. The total error includes input,

repeatability, and model errors. The PMED internally estimates the reliability of the IRI model. Table 6-6 summarizes the global standard error equations for each model.

Table 6-6 Global SE equations for each distress and smoothness model

Pavement Type	Pavement performance prediction model	Standard error equation
Asphalt overlays	Fatigue cracking (bottom-up)	$S_{e(bottom-up)} = 1.13 + \frac{13}{1 + e^{7.57-15.5\times Log(FC_{Bottom}+0.0001)}}$
Asphalt overlays	Fatigue cracking (top-down)	$S_{e(top-down)} = 0.3657 \times FC_{top} + 3.6563$
Asphalt overlays	Total fatigue (includes reflective) cracking	$S_{e(Fatigue+reflective)} = 1.1097(Fatigue)^{0.6804} + 1.23$
Asphalt overlays	Rutting	$S_{e(HMA)} = 0.24(\Delta_{HMA})^{0.8026} + 0.001$ $S_{e(Base)} = 0.1477(\Delta_{Base})^{0.6711} + 0.001$ $S_{e(SG)} = 0.1235(\Delta_{SG})^{0.5012} + 0.001$
Asphalt overlays	Total transverse cracking	$S_{e(Transverse)} = 70.98(Transverse)^{0.2994} + 30.12$
Asphalt overlays	IRI	Estimated internally by the software
JPCP unbonded overlays	Transverse cracking	$S_{e(CRK)} = 3.5522(CRK)^{0.3415} + 0.75$
JPCP unbonded overlays	Faulting	$S_{e(Fault)} = 0.07162(Fault)^{0.368} + 0.00806$
JPCP unbonded overlays	IRI	Estimated internally by the software

6.8 SUMMARY

This chapter describes the local calibration process for PMED rehabilitation models for HMA and JPCP unbonded overlays. The team used the no-sampling and bootstrapping techniques with the least-squares optimization method for calibration. Approach I (MATLAB-based) and Approach II (CAT-based) were applied depending on model type and data availability. The chapter also outlined the procedures for assessing global model accuracy, refining transfer function coefficients, and establishing reliability relationships to account for performance variability.

CHAPTER 7 - LOCAL CALIBRATION

7.1 INTRODUCTION

Local calibration improves the accuracy of PMED performance predictions, better aligning them with the observed behavior of Michigan's rehabilitated pavements. Although PMED's national transfer functions were developed using extensive datasets from various climatic regions, materials, and traffic conditions across the United States, they may not fully capture Michigan's unique characteristics. Differences in material properties, mixture design practices, subgrade stiffness, and environmental conditions can introduce variability in predictions when national coefficients are used alone. Adjusting these coefficients through local calibration reduces this variability, aligning the predicted performance more closely with field-measured data and thereby improving the accuracy and reliability of design outcomes.

This study focused exclusively on rehabilitated pavement sections from MDOT's network. The calibration dataset included five primary rehabilitation fix types:

1. HMA overlay of C&S pavement
2. HMA overlay of rubblized PCC pavement
3. HMA overlay of existing HMA pavement
4. HMA overlay of existing PCC or composite (existing HMA/PCC) pavement
5. JPCP (unbonded) overlays of existing JPCP (or JRCP)

Each fix type exhibits unique structural behavior and distress progression, requiring independent evaluation to determine whether reliable calibration is feasible and, if so, whether it provides improved accuracy and model representation. While the research team endeavored to calibrate all rehabilitation fix types, some currently lack sufficient representative sections to support statistically valid calibration. In these cases, calibration was not performed to avoid generating coefficients that would lack statistical reliability and practical application. Notably, this limitation applies to aggregate lifts, short-jointed concrete overlays, ASCRL overlays, HMA JPCP overlays, and CRCP overlays. See Chapter 5 for further discussion regarding these fix types.

For those fix types that were calibrated, the research team applied two statistical techniques to develop local calibration coefficients and assess prediction variability:

1. No sampling (include all data) – used all available data to compute bias and the SEE.
2. Bootstrapping – resampled the dataset repeatedly to estimate parameter uncertainty and establish confidence intervals for the calibration factors.

The CAT was used to calibrate thermal, total transverse, and total fatigue cracking models for flexible pavements. For all other models, PMED was used to calculate distress and damage outputs, which were then externally calibrated. For each distress

type, the team generated scatterplots of predicted versus measured performance with a 45-degree line of equality to visualize bias and variability. Ideally, points cluster along the equality line, indicating strong model agreement. The calibration process followed the hypothesis-testing procedures outlined in the AASHTO Local Calibration Guide to ensure statistical validity and consistency across models.

The following sections present the locally calibrated coefficients for each rehabilitation fix type and compare the outcomes from the two statistical approaches. These results demonstrate how local calibration can improve the predictive capability of PMED for Michigan's rehabilitated pavements.

7.2 LOCAL CALIBRATION OF ASPHALT OVERLAYS

This section presents the detailed results of the local calibration performed for the various HMA overlay rehabilitation fix types, including overlays placed over existing HMA, composite (HMA/JPCP), C&S, and rubblized PCC pavements. The team analyzed each fix type separately to evaluate its performance trends, calibration coefficients, and prediction accuracy under Michigan conditions.

7.2.1 HMA Overlay of C&S Pavement

MDOT frequently uses HMA overlays over C&S pavements as a rehabilitation strategy. In this study, the research team designed the C&S sections as new flexible pavements, modeling the crushed and shaped layer in PMED as "cold recycled asphalt – RAP pulverized in place" (unbonded granular layer) with an MR of 60,000 psi. The team adopted this MR value based on laboratory characterization and FWD backcalculation analyses as discussed in Chapters 3 and 4. Previous studies have typically used a modulus of 125,000 psi for this layer (*1, 2*). This section presents the local calibration results for the C&S fix type, including fatigue cracking, rutting, transverse (thermal) cracking, and IRI. The calibration aimed to minimize bias and SEE between predicted and measured performance using a total of 62 sections of HMA overlay over existing C&S HMA pavements in service.

7.2.1.1. Fatigue Cracking Model – Bottom-up

The research team calibrated the bottom-up fatigue cracking model using data from 29 C&S pavement sections, applying both the no-sampling and bootstrapping techniques to optimize model coefficients and improve prediction accuracy.

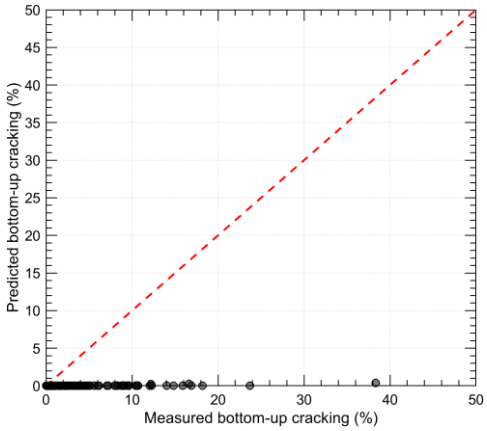
No Sampling

In the no-sampling approach, the team used the entire dataset for calibration to minimize the error between predicted and measured fatigue cracking. Table 7-1 presents the results of the local calibration, including the calibration coefficients, bias, and SEE. Figure 7-1 shows the predicted versus measured bottom-up cracking for both globally and locally calibrated models, along with their comparison over time. The global model underestimates bottom-up cracking, whereas local calibration significantly improves model accuracy.

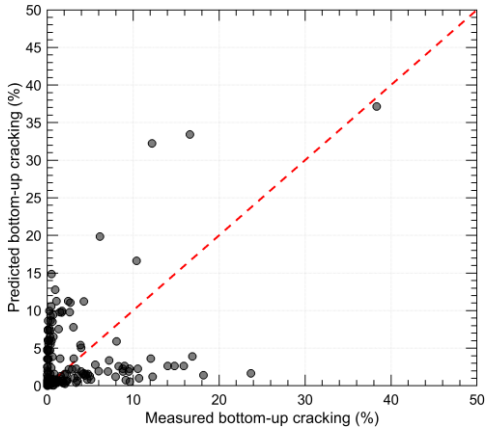
Table 7-2 summarizes the results of the hypothesis tests assessing the statistical significance of the local calibration. Although one or more hypothesis tests were rejected, the local model demonstrates a notable reduction in bias and SEE, indicating improved agreement with field performance.

Table 7-1 Calibration of bottom-up cracking model for C&S (No sampling)

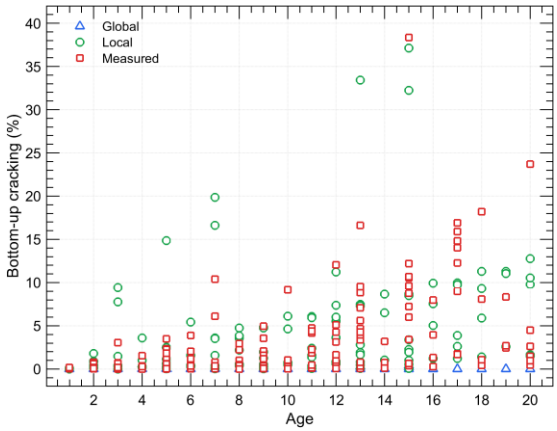
Parameter	Global model	Local model
SEE (% total lane area)	6.17	6.05
Bias (% total lane area)	-3.24	0.60
C_1	1.31	0.23
C_2 (h_{ac} < 5 in.)	2.1585	0.832
C_2 (5 in. <= h_{ac} <=12 in.)	(0.867+0.2583* h_{ac})*1	(0.867+0.2583* h_{ac})*0.28



(a) Global model



(b) Local model



(c) Measured and predicted time series

Figure 7-1 Calibration results of bottom-up cracking for C&S (No sampling)

Table 7-2 Hypothesis testing results for bottom-up cracking (No sampling)

Hypothesis test	Global model	Local model
Mean difference = 0	0.00	0.21
Intercept = 0	0.02	0.00
Slope = 1	0.00	0.00

Bootstrapping

The team used bootstrapping as a resampling technique to calibrate the bottom-up cracking model. One thousand bootstrap samples were generated, with replacement. This approach allowed the team to estimate the variability of the calibration coefficients and to construct CIs for each parameter. Tables 7-3 and 7-4 summarize the model parameters for global and local models, respectively. Local calibration resulted in a slight increase in SEE, whereas it significantly improved bias. Figure 7-2 shows the distribution of parameters for the 1,000 bootstrap samples.

Table 7-3 Bootstrapping global model summary

Parameter	Global model mean	Global model median	Global model lower CI	Global model upper CI
SEE (% total lane area)	6.095	6.085	4.174	8.155
Bias (% total lane area)	-3.238	-3.217	-4.476	-2.175
C_1	1.31	1.31	-	-
C_2 (h_{ac} < 5 in.)	2.1585	2.1585	-	-
C_2 (5 in. <= h_{ac} <=12 in.)	(0.867+0.2583*h_{ac})*1	(0.867+0.2583* h_{ac})*1	-	-

Table 7-4 Bootstrapping local calibration results summary

Parameter	Local model mean	Local model median	Local model lower CI	Local model upper CI
SEE (% total lane area)	6.012	6.053	4.874	7.173
Bias (% total lane area)	0.640	0.557	-0.758	2.396
C_1	0.230	0.230	0.230	0.230
C_2 (h_{ac} < 5 in.)	0.818	0.832	0.677	0.832
C_2 (5 in. <= h_{ac} <=12 in.)	(0.867+0.2583* h_{ac})* 0.532	(0.867+0.2583* h_{ac})* 0.524	(0.867+0.2583* h_{ac})* 0.28	(0.867+0.2583* h_{ac})* 0.8

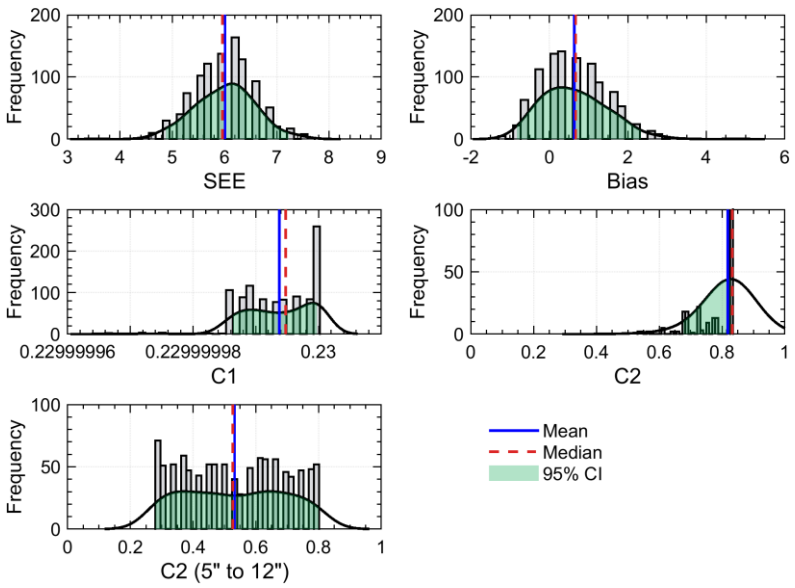


Figure 7-2 Distribution of local calibration parameters (bootstrapping)

Reliability for the bottom-up cracking model

The calibration process and the PMED predictions are obtained at a reliability of 50%. The concept of reliability and method is discussed in detail in Chapter 6. The measured and predicted cracking were sorted into bins based on the expected cracking. The next step was to develop a relationship between the standard deviation of the measured cracking and the mean predicted cracking. Table 7-5 shows the standard error equations for global and local models. Figure 7-3 shows the reliability plots for the global and local models.

Table 7-5 SE equation of the bottom-up cracking model for C&S pavements

Global model equation	Local model equation
$S_{e(Alligator)} = 1.13 + \frac{13}{1 + e^{7.57 - 15.5 \times log(D + 0.0001)}}$	$S_{e(Alligator)} = 0.0825 + \frac{6.44}{1 + e^{0.08 - 2.227 \times log(D)}}$

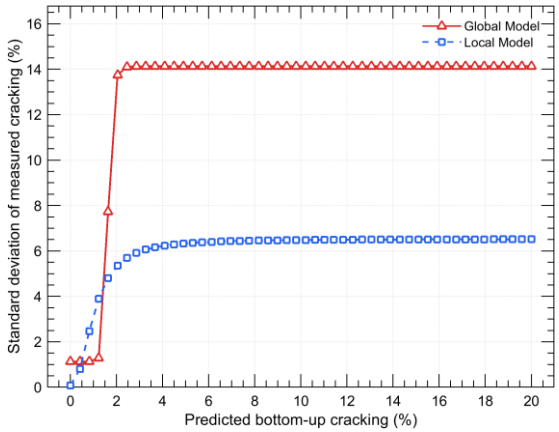


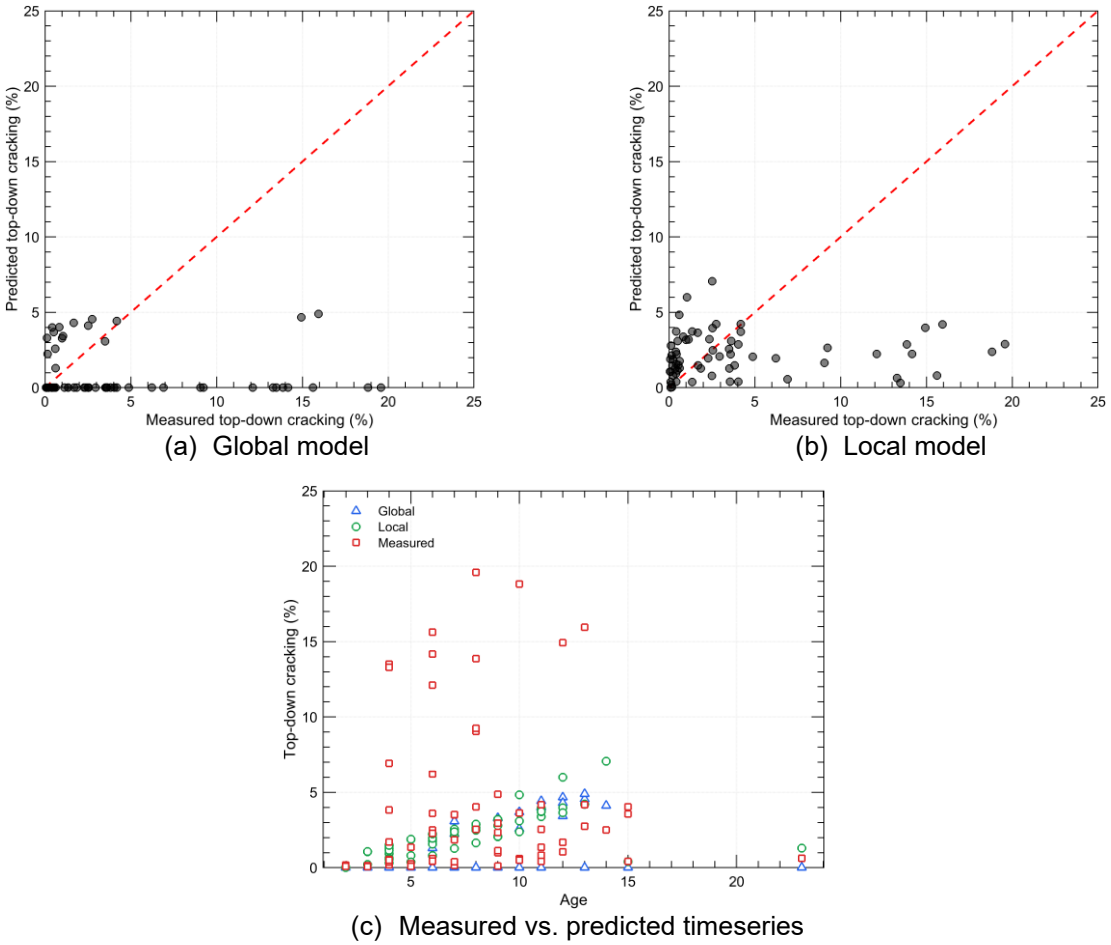
Figure 7-3 SE of global and local models for C&S pavements

7.2.1.2. Fatigue Cracking Model – Top-down

The following section presents the calibration of the top-down cracking model. This model includes both crack initiation and crack propagation components. Since the actual time of crack initiation is unknown for the available pavement sections, the team was unable to independently calibrate the initiation model. Therefore, a single combined function was used by substituting the initiation model with the propagation function. The limitations associated with this modeling approach have already been discussed in Chapter 2.

The team performed the calibration in Microsoft Excel using a combination of engineering judgment and the Solver optimization tool. The team calibrated four coefficients from the initiation function (*kL2, kL3, kL4, kL5)* and two from the crack propagation function (C_1, C_2) using a no-sampling technique across 23 in-service pavement sections.

Figure 7-4 shows the measured vs. predicted values for the global and local models, along with their comparison over time. Table 7-6 shows the calibration results for the top-down cracking model.



(a) Global model (b) Local model

(c) Measured vs. predicted timeseries

Figure 7-4 Measured and predicted top-down-cracking for C&S (time series)

Table 7-6 Calibration results for top-down cracking for C&S

Parameters	Global model	Local model
SEE	6.37	5.59
Bias	-2.36	1.60
K_{L2}	0.2855	0.90
K_{L3}	0.011	0.09
K_{L4}	0.01488	0.1005
K_{L5}	3.266	0.1083
C_1	2.5219	0.453
C_2	0.8069	1.342

Reliability for the top-down cracking model

Table 7-7 shows the standard error equations for global and local top-down cracking models. Figure 7-5 shows the reliability comparison of global and local models.

Table 7-7 SE equation of the top-down cracking model for C&S pavements

Global model equation	Local model equation
$S_{e(Top-down)} = 0.3657 \times TOP + 3.6563$	$S_{e(Top-down)} = 0.1358 \times TOP + 3.233$

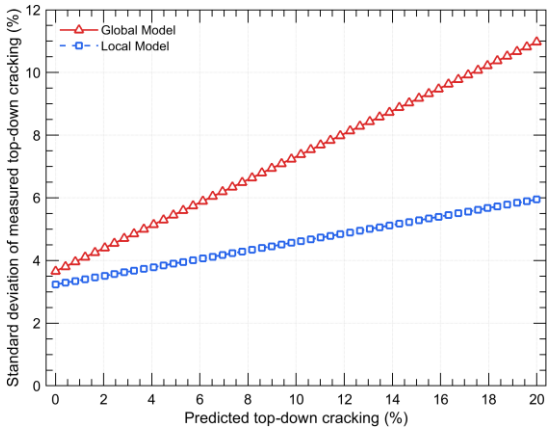


Figure 7-5 SE of global and local top-down cracking models

7.2.1.3. Rutting Model

Rutting in the PMED is a sum of permanent deformations from individual layers. The research team adopted the following methods for calibration of rutting models, using 39 in-service C&S sections:

1. *Method 1: Individual layer rutting calibrations* — This approach matched the measured rutting from individual layers against the predictions from PMED (β_{1r}, $\beta_{s1,}$ and β_{sg1} were calibrated separately). The total measured rutting was multiplied by each layer's percent contribution to obtain the measured rutting for that layer. The percentage contribution was estimated using transverse pavement profile analysis, as discussed in Chapter 6. The standard error equations for rutting in the PMED are separate for individual layers. This method was used to evaluate the standard error equations for rutting in each layer.
2. *Method 2: Total surface rutting calibration* — The total measured rutting was calibrated against the sum of individual predicted rutting (β_{1r}, $\beta_{s1,}$ and β_{sg1} were calibrated simultaneously).

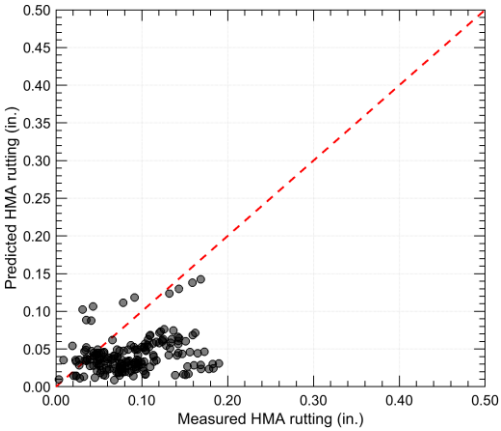
Method 1 - Individual Layer Rutting Calibration

This section outlines the calibration of individual-layer rutting.

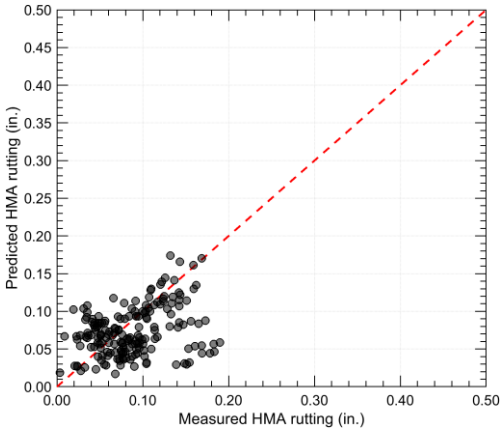
No Sampling

This section presents the calibration of individual-layer rutting using the no-sampling method. The predicted individual-layer rutting was matched to the measured rutting determined from the transverse profile. Figures 7-6 and 7-7 show the predicted vs. measured AC, base, and subgrade rutting for global and local models, and their comparison over time, respectively. The PMED under-predicts AC rutting and over-

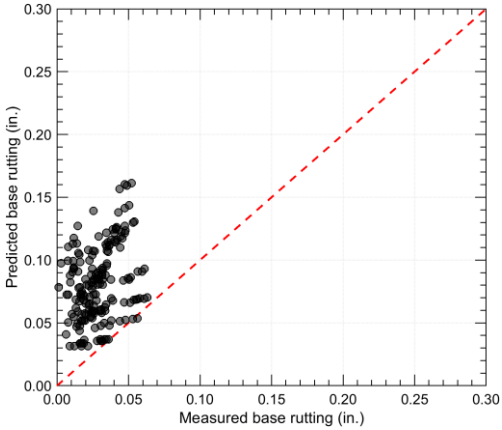
predicts base and subgrade rutting. Table 7-8 shows the hypothesis results for each layer. Both global and local models failed to support any of the hypotheses. Table 7-9 shows the SEE, bias, and calibrated coefficients. Both SEE and bias improved significantly across all layers.



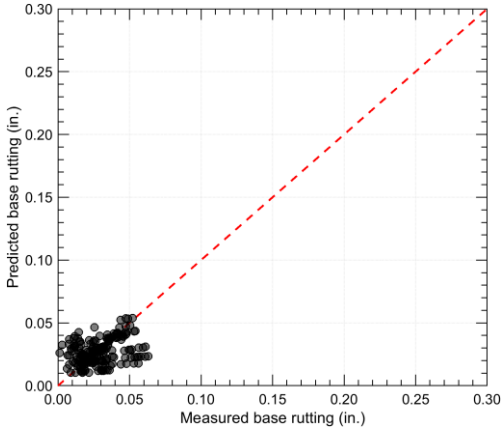
(a) Global model – HMA rut



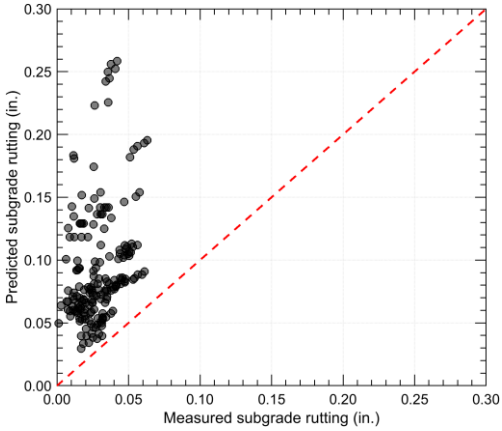
(b) Local model – HMA rut



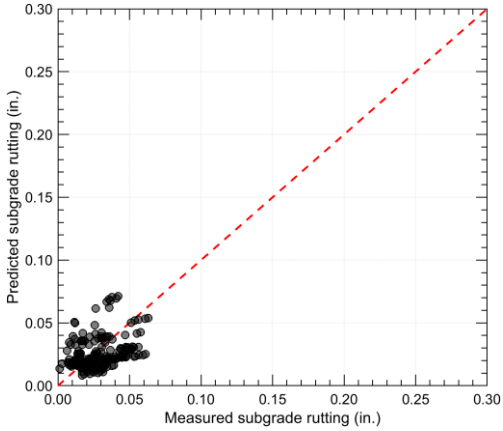
(a) Global model – base rut



(b) Local model – base rut

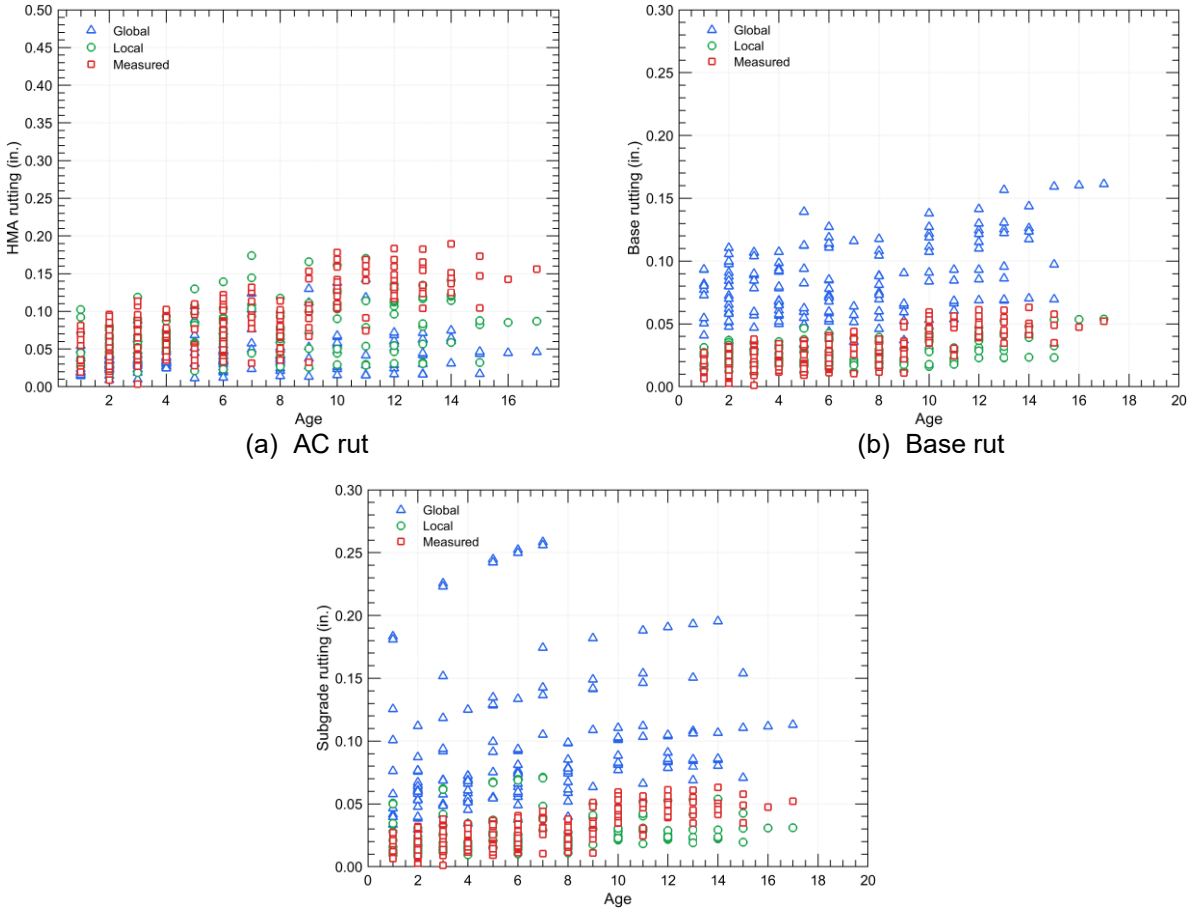


(a) Global model – subgrade rut



(b) Local model – subgrade rut

Figure 7-6 Predicted vs. measured rutting (No sampling)



(a) AC rut (b) Base rut

(c) Subgrade rut

Figure 7-7 Time series of individual layers' rutting for C&S pavements

Table 7-8 Hypothesis testing results of rutting models for C&S pavements

Layer	t-test *p*-value (G)	Intercept *p*-value (G)	Slope = 1 *p*-value (G)	t-test *p*-value (L)	Intercept *p*-value (L)	Slope = 1 *p*-value (L)
HMA rut	0.000	0.000	0.000	0.024	0.000	0.000
Base rut	0.000	0.000	0.000	0.056	0.000	0.000
Subgrade	0.000	0.000	0.000	0.013	0.000	0.000

G = Global; L = Local

Table 7-9 Calibration summary results for C&S pavements – Method 1 (No sampling)

Layer	Global model SEE (in.)	Global model Bias (in.)	Local model SEE (in.)	Local model Bias (in.)
HMA rut	0.062	-0.046	0.053	-0.009
Base rut	0.060	0.052	0.014	-0.002
Subgrade	0.080	0.066	0.016	-0.002
Parameters	Global Model	Global Model	Local Model	Local Model
HMA rutting (br1)	0.4	0.4	0.757	0.757
Base rutting (bs1)	1.0	1.0	0.334	0.334
Subgrade rutting (bsg1)	1.0	1.0	0.276	0.276

Bootstrapping

The team applied bootstrapping as described earlier, generating 1,000 resampled datasets with replacement to calibrate the rutting model for C&S pavements. Tables 7-10 and 7-11 summarize the calibration results for the global and locally calibrated models, while Figure 7-8 shows the parameter distributions and corresponding confidence intervals for the calibrated coefficients.

Table 7-10 Global rutting model for C&S pavements (bootstrapping)

Layer type	Average SEE	SEE Lower CI	SEE Upper CI	Average bias (in.)	Bias Lower CI	Bias Upper CI
HMA	0.0619	0.0514	0.0719	-0.045	-0.055	-0.035
Base	0.059	0.0513	0.0672	0.0517	0.0432	0.0604
Subgrade	0.0795	0.0610	0.0995	0.0657	0.0523	0.0810

Table 7-11 Local rutting model for C&S pavements (bootstrapping)

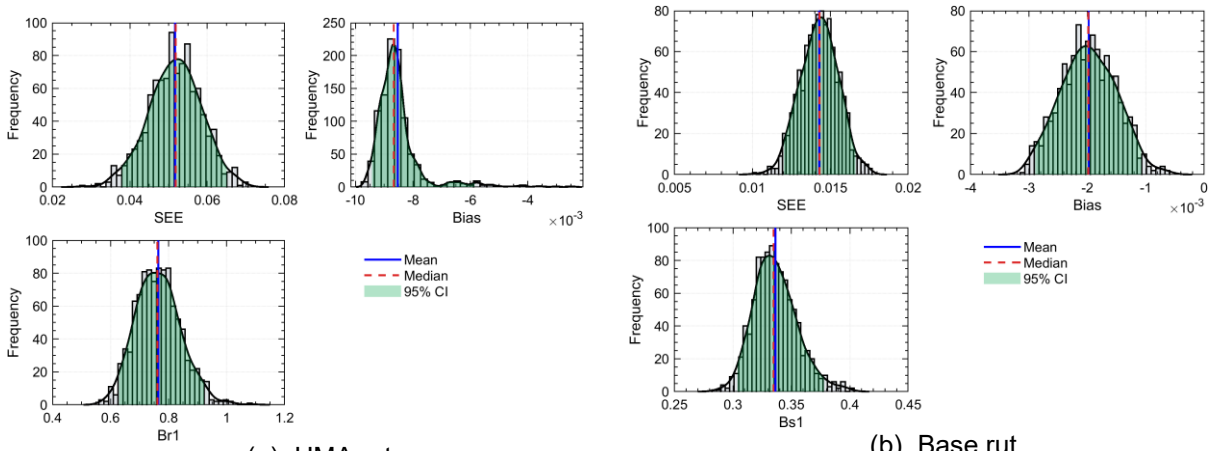
Statistics	HMA rutting	Base rutting	Subgrade rutting
Average SEE (in.)	0.0517	0.0142	0.0157
SEE Lower CI	0.0376	0.0119	0.0131
SEE Upper CI	0.0651	0.0167	0.0178
Average bias (in.)	-0.008	-0.002	-0.002
Bias Lower CI	-0.009	-0.003	-0.003
Bias Upper CI	-0.006	-0.001	-0.001
Average calibration coefficient	0.764	0.336	0.279
Calibration coefficient Lower CI	0.628	0.303	0.237
Calibration coefficient Upper CI	0.927	0.378	0.329

Method 2 – Total Rutting Calibration

This method used the total measured total rutting against the predicted total rutting for calibration. Total predicted rutting is simply the sum of rutting predictions for individual layers. Calibration coefficients of all layers were simultaneously changed to match the total predicted rutting with measured rutting.

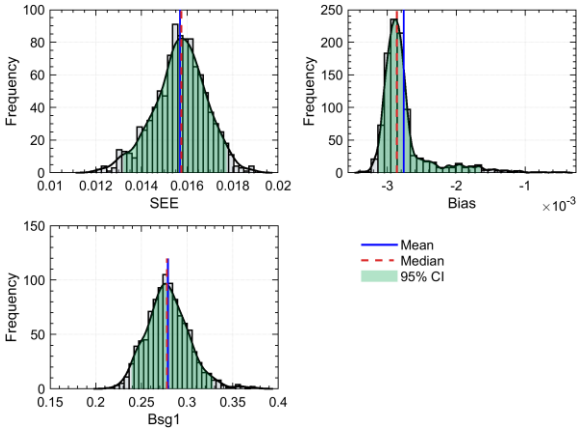
No Sampling

Tables 7-12 and 7-13 present the hypothesis testing and calibration results for the global and local models, obtained without sampling. Figure 7-9 shows the predicted vs. measured total rutting for the global and local models with no sampling, along with their comparison over time.



(a) HMA rut

(b) Base rut



(c) Subgrade rut

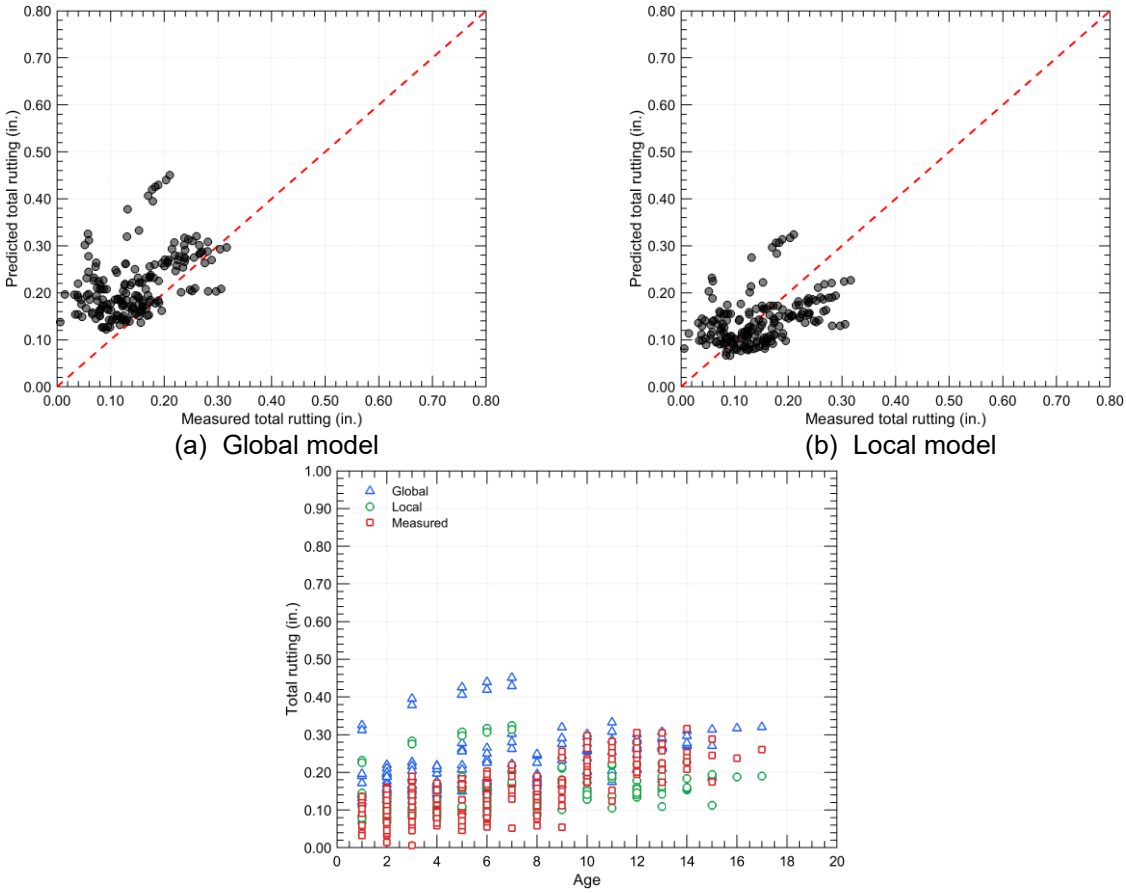
Figure 7-8 Distribution of calibration parameters - AC rutting (Bootstrapping)

Table 7-12 Hypothesis testing results for total rutting

Layer	Global model	Local model
t-test p-value	0.000	0.261
Intercept p-value	0.000	0.000
Slope = 1 p-value	0.000	0.000

Table 7-13 Total rutting model calibration results

Parameters	Global model	Local model
SEE	0.1014	0.0675
Bias	0.0719	-0.0056
HMA rutting (br1)	0.4	0.175
Base rutting (bs1)	1.0	0.385
Subgrade rutting (bsg1)	1.0	0.953



(a) Global model (b) Local model

(c) Time series

Figure 7-9 Predicted vs measured total rutting (No sampling)

Bootstrapping

Tables 7-14 and 7-15 summarize the global and local models, respectively, using bootstrapping. Figure 7-10 shows the distribution of calibration parameters.

Table 7-14 Global model summary for total rutting of C&S pavements (bootstrapping)

Parameter	Global model mean	Global model median	Global model lower CI	Global model upper CI
SEE (in)	0.0948	0.0949	0.0325	0.0433
Bias (in.)	0.0584	0.0586	0.0379	0.0792
br1	0.4	0.4	-	-
bs1	1	1	-	-
bsg1	1	1	-	-

Table 7-15 Local calibration summary for total rutting of C&S pavements (bootstrapping)

Parameter	Local model mean	Local model median	Local model lower CI	Local model upper CI
SEE (in.)	0.0691	0.0691	0.0230	0.0323
Bias (in.)	-0.0088	-0.0088	-0.0132	-0.0041
br1	0.0941	0.0954	0.0212	0.4301
bs1	0.5644	0.5784	0.2170	0.8180
bsg1	1.0034	1.0100	0.6707	1.2779

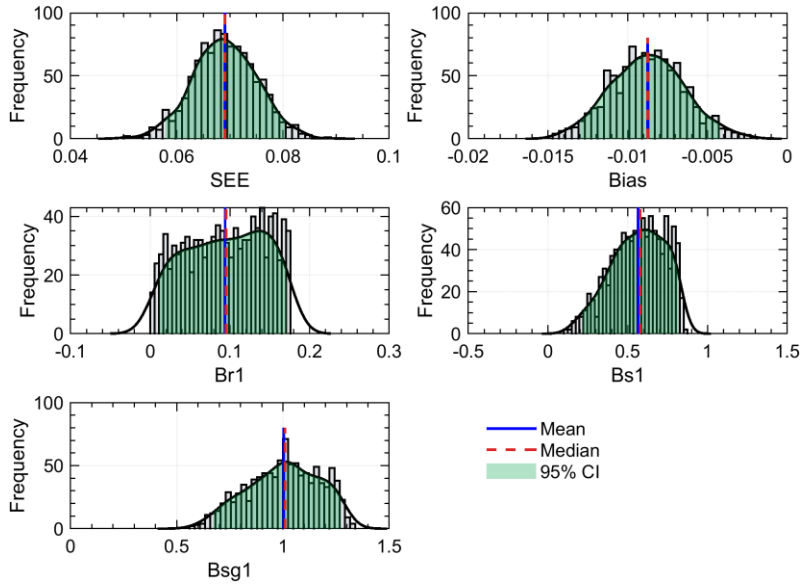


Figure 7-10 Distribution of calibration parameters - total rutting

Reliability for the rutting model

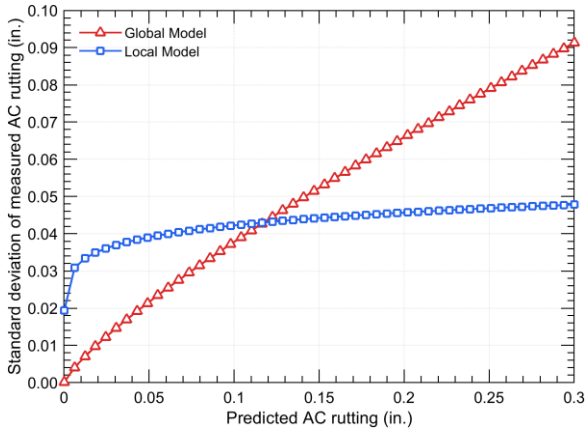
The standard error equations were formulated using the standard deviation of the measured cracking and the mean predicted cracking to incorporate reliability in the model. Table 7-16 shows the standard error equation for individual-layer rutting models. Figure 7-11 shows the reliability comparison of global and local models.

Table 7-16 SE equations of rutting models for C&S pavements

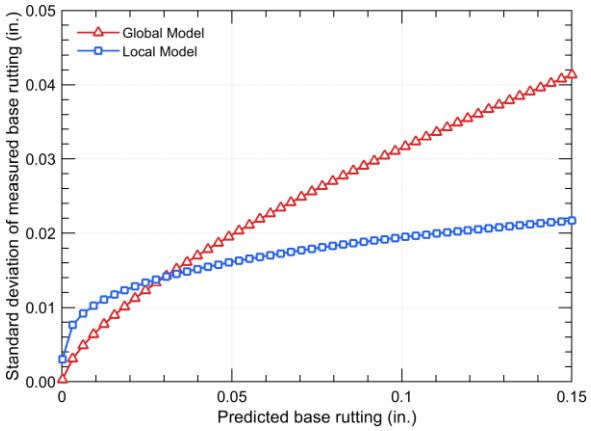
Layer	Global model	Local model
HMA	$s_{e(HMA)} = 0.24(Rut_{HMA})^{0.8026} + 0.001$	$s_{e(HMA)} = 0.0584(Rut_{HMA})^{0.1029}$
Base	$s_{e(base)} = 0.1477(Rut_{base})^{0.6711} + 0.001$	$s_{e(base)} = 0.0362(Rut_{base})^{0.1098}$
Subgrade	$s_{e(subgrade)} = 0.1235\left(Rut_{subgrade}\right)^{0.5012} + 0.001$	$s_{e(subgrade)} = 0.0562\left(Rut_{subgrade}\right)^{0.3114}$

7.2.1.4. Transverse (thermal) Cracking Model

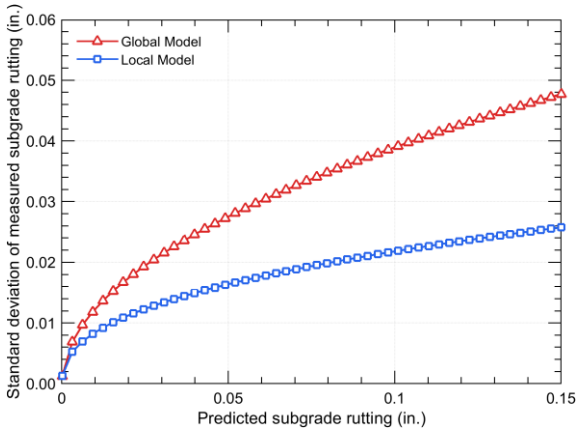
The thermal cracking model was calibrated for Level 1 inputs in the PMED. The model calibration only considered 23 sections with the PG binder type. The team utilized CAT to calibrate the thermal cracking model. As discussed in Chapter 6, the Kt for the thermal cracking model depends on the MAAT. In previous calibration studies, it was calibrated as a single value (*1, 2*). However, in CAT, Kt cannot be calibrated as a single value. The team calibrated the transverse cracking models using CAT as a function of MAAT for this study. Table 7-17 provides the calibration summary. Figure 7-12 presents the measured and predicted thermal cracking, along with their time-series comparison, for C&S sections.



(a) AC rut



(b) Base rut

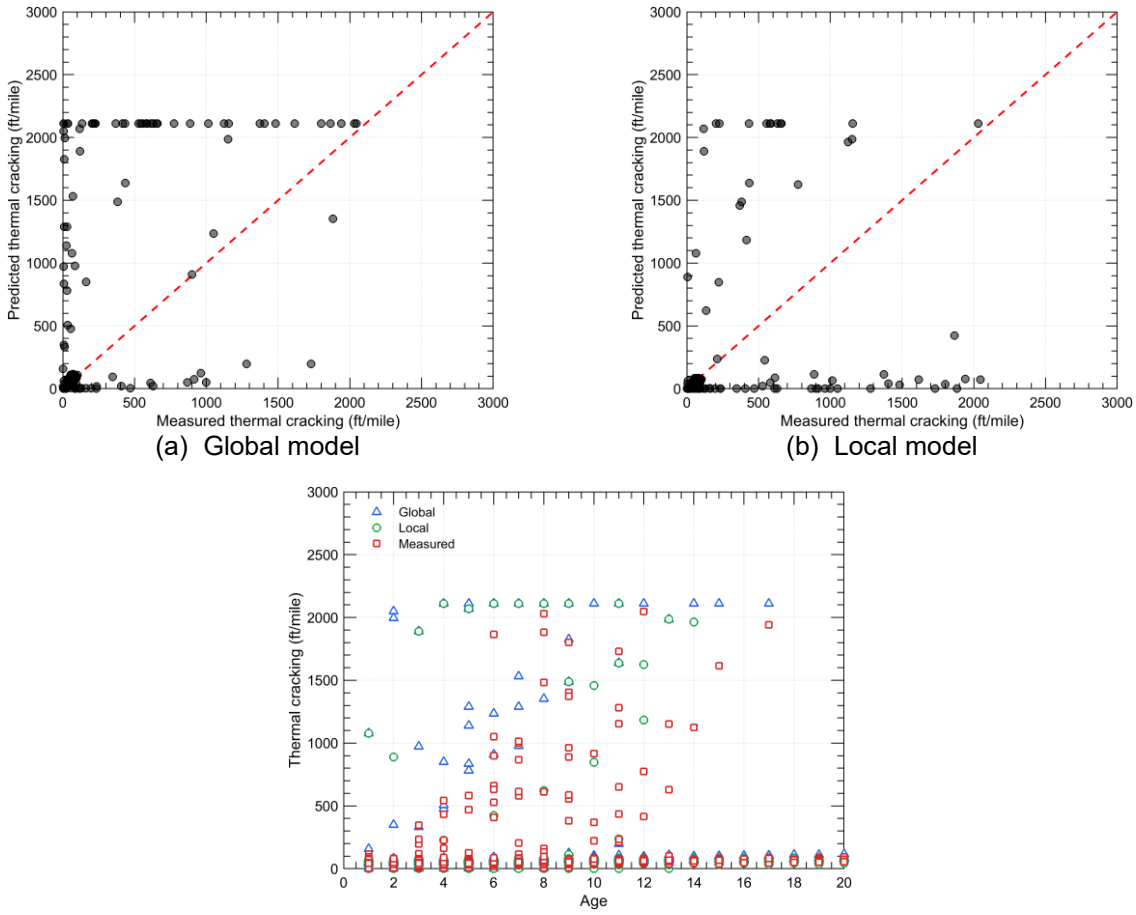


(c) Subgrade rut

Figure 7-11 SE comparison for C&S rutting models

Table 7-17 Transverse (thermal) cracking results – C&S pavements

Parameter	Global model	Local model
SEE	1106	753
Bias	630	-212
K	$K = (3 * POW(10, -7)) * Pow(MAAT, 4.0319)) * 1 + 0$	$K = (3 * POW(10, -7)) * Pow(MAAT, 4.0319)) * 0.629 + 0$



(a) Global model (b) Local model

(c) Time series

Figure 7-12 Predicted vs. measured thermal cracking for C&S pavements

Reliability for the thermal cracking model

The standard error equations for the thermal cracking model were developed using the standard deviation of the measured cracking and the mean predicted cracking to incorporate reliability. Table 7-18 presents the standard-error equation for the thermal cracking model, and Figure 7-13 compares the reliability of the global and locally calibrated models.

Table 7-18 SE equations for the thermal cracking model of C&S pavements

Global model	Local model
$S_{e(Thermal)} = 0.14 \times TC + 168$	$S_{e(Thermal)} = 0.1311 \times TC + 145$

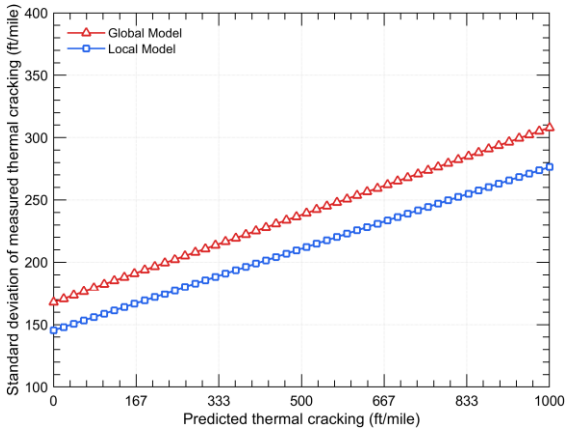


Figure 7-13 SE comparison of thermal cracking model for C&S pavements

7.2.1.5. IRI Model for C&S Pavements

IRI is a linear function of initial IRI, rut depth, total fatigue cracking, transverse cracking, and site factor. The IRI model was calibrated after the local calibration of the fatigue, transverse cracking, and rutting models. The research team used data from 47 C&S pavement sections that showed increasing IRI over time for calibration.

No Sampling

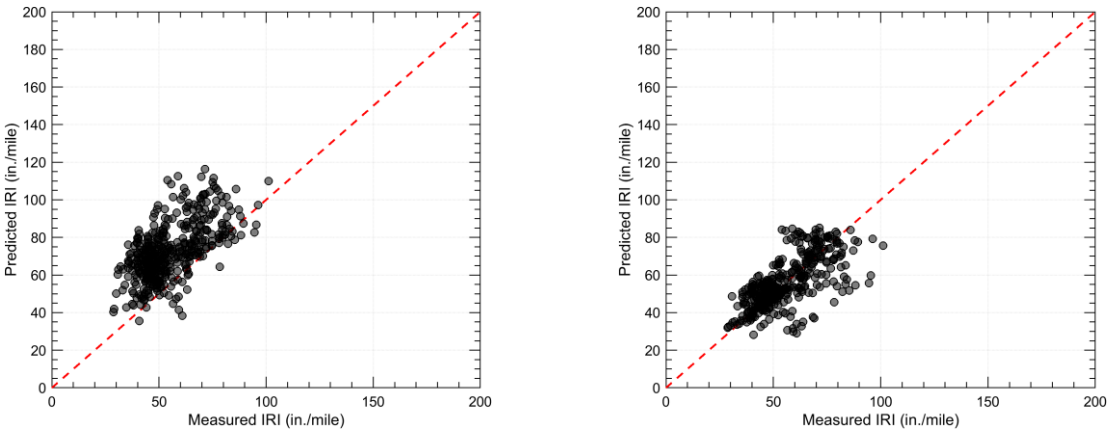
Table 7-19 shows the hypothesis results for global and local models. Table 7-20 summarizes the model parameters and shows significant improvements in SEE and bias following local calibration. Figure 7-14 compares predicted and measured IRI for both global and local models, along with their temporal comparisons with no sampling.

Table 7-19 IRI model hypothesis testing results

Layer	Global model	Local model
t-test p-value	0.000	1.000
Intercept p-value	0.000	0.000
Slope = 1 p-value	0.000	0.000

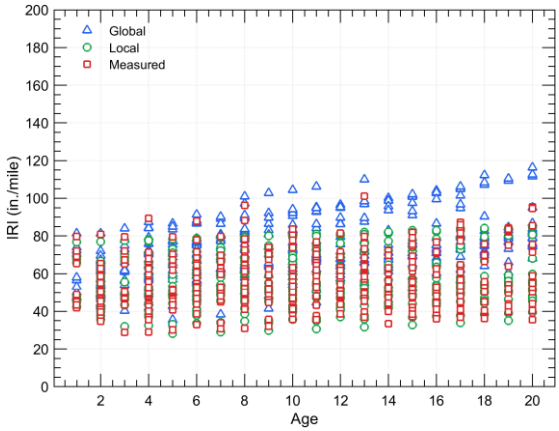
Table 7-20 IRI model calibration results (No sampling)

Model coefficient	Global model	Local model
SEE	21.754	10.629
Bias	17.433	0.000
C1	40.000	19.552
C2	0.4000	0.1049
C3	0.0080	0.0083
C4	0.0150	0.0041



(a) Global model

(b) Local model



(c) Time series

Figure 7-14 Measured vs predicted IRI for C&S pavements

Bootstrapping

The team also calibrated the IRI model using bootstrapping, like other models, as explained above. Tables 7-21 and 7-22 summarize the global and local models, respectively, using bootstrapping. Figure 7-15 shows the distribution of calibration parameters.

Table 7-21 Global model summary for IRI of C&S pavements (bootstrapping)

Parameter	Global model mean	Global model median	Global model lower CI	Global model upper CI
SEE (in)	21.771	21.699	18.893	24.522
Bias (in.)	17.499	17.454	14.419	20.363
C1	40.000	40.000	-	-
C2	0.400	0.400	-	-
C3	0.008	0.008	-	-
C4	0.015	0.015	-	-

Table 7-22 Local calibration summary for IRI of C&S pavements (bootstrapping)

Parameter	Local model mean	Local model median	Local model lower CI	Local model upper CI
SEE (in.)	10.399	10.395	8.489	12.418
Bias (in.)	0.002	0.000	0.000	0.000
C1	19.611	19.279	8.049	33.839
C2	0.143	0.109	0.000	0.474
C3	0.006	0.004	0.002	0.023
C4	0.0032	0.0030	0.000	0.008

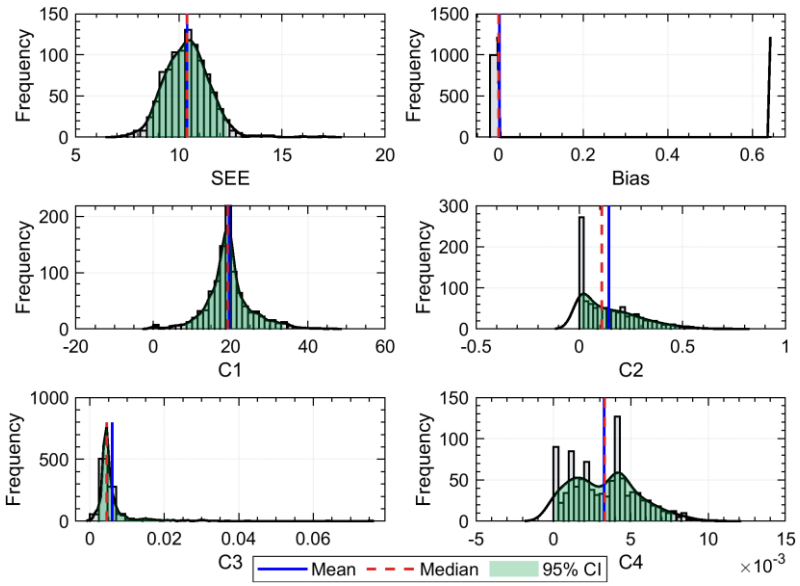


Figure 7-15 Distribution of calibration parameters of the IRI model for C&S pavements

7.2.1.6. Summary for HMA Overlay over C&S Pavements

Based on previous calibration efforts and supporting literature, the team adopted the calibration coefficients obtained through the bootstrapping approach. Bootstrapping provides a more robust estimation technique by capturing the variability and confidence intervals of the model parameters through resampling. Tables 7-23 and 7-24 summarize the final bootstrapped calibration coefficients for all performance models, along with the corresponding standard-error equations developed for reliability analysis.

Table 7-23 Summary coefficients for HMA overlay over C&S pavements

Performance prediction model	Performance models and transfer functions	Local coefficient
Fatigue cracking (bottom-up)	$FC_{Bottom} = \left(\frac{1}{60}\right)\left(\frac{6000}{1 + e^{C_1 C_1^* + C_2 C_2^* Log(DI_{Bottom}*100)}}\right)$	$C_1 = 0.230$ $C_2 = 0.818$ (hac <5 in) $C_2 = (0.867 + 0.2583 * hac) * 0.532$ (5 in <= hac <=12 in)
Fatigue cracking (top-down)	$t_0 = \frac{\mathrm{K}_{L1}}{1 + e^{\mathrm{K}_{L2}\times 100\times(\mathrm{a}_0/2\mathrm{A}_0)+\mathrm{K}_{L3}\times \mathrm{HT}+\mathrm{K}_{L4}\times LT+K_{L5}\times \log_{10}\ \mathrm{AADTT}}}$ $FC_{Top} = \mathrm{Lmax} \times \mathrm{e}^{-(\frac{C_1\rho}{t-C_3 to})^{C_2\beta}}$	$\mathrm{K}_{L2} = 0.90$ $\mathrm{K}_{L3} = 0.090$ $\mathrm{K}_{L4} = 0.1005$ $\mathrm{K}_{L5} = 0.1083$ $C_1 = 0.453$ $C_2 = 1.342$
HMA Rutting	$\Delta_{p(HMA)} = \varepsilon_{p(HMA)} h_{HMA} = \beta_{1r} k_z \varepsilon_{r(HMA)} 10^{k_{1r}} n^{k_{2r}\beta_{2r}} T^{k_{3r}\beta_{3r}}$	$\beta_{1r} = 0.094$ $\beta_{2r} = 0.7$ $\beta_{3r} = 1.3$
Base/subgrade Rutting	$\Delta_{p(soil)} = \beta_{s1} k_{s1} \varepsilon_v h_{soil} \left(\frac{\varepsilon_o}{\varepsilon_r}\right) e^{-\left(\frac{\rho}{n}\right)^{\beta}}$	$\beta_{s1} = 0.564$ $\beta_{sg1} = 1.003$
Thermal cracking	$A = 10^{k_t \beta_t (4.389 - 2.52 Log(E_{HMA}\sigma_m \eta))}$	$K = (3 * POW(10, -7)) * Pow(MAAT, 4.0319)) * 0.629 + 0$
IRI	$IRI = IRI_o + C_1(RD) + C_2(FC_{Total}) + C_3(TC) + C_4(SF)$	$C_1 = 19.611, C_2 = 0.143$ $C_3 = 0.006, C_4 = 0.0032$

Table 7-24 SE equations for HMA overlay over C&S pavements

Performance prediction model	Global model	Local model
Fatigue cracking (bottom-up)	$S_{e(Alligator)} = 1.13 + \frac{13}{1 + \exp(7.57 - 15.5\log(Crack + 0.0001))}$	$S_{e(Alligator)} = 0.0825 + \frac{6.44}{1 + \exp(0.08 - 2.227\log(Crack))}$
Fatigue cracking (top-down)	$S_{e(Top-down)} = 0.3657 \times TOP + 3.6563$	$S_{e(Top-down)} = 0.1358 \times TOP + 3.233$
HMA Rutting	$S_{e(HMA)} = 0.24(Rut_{HMA})^{0.8026} + 0.001$	$S_{e(HMA)} = 0.0584(Rut_{HMA})^{0.1029}$
Base/subgrade Rutting	$S_{e(base)} = 0.1477(Rut_{base})^{0.6711} + 0.001$ $S_{e(subgrade)} = 0.1235(Rut_{subgrade})^{0.5012} + 0.001$	$S_{e(base)} = 0.0362(Rut_{base})^{0.1098}$ $S_{e(subgrade)} = 0.0562(Rut_{subgrade})^{0.3114}$
Thermal	$S_{e(Thermal)} = 0.14 \times TC + 168$	$S_{e(Thermal)} = 0.1311 \times TC + 145$
IRI	Internally calculated by PMED	

7.2.2 HMA Overlays of Rubblized PCC Pavements

MDOT uses HMA overlays over rubblized JPCP as one of its primary rehabilitation strategies. Previous studies recommend designing rubblized pavements as new flexible systems, with the rubblized layer modeled as an unbound aggregate base in Michigan (*2, 3*). MDOT's previous calibration efforts also adopted this approach, using an MR of 70,000 psi for the rubblized layer (*1, 2*). In this study, the team followed the same design methodology, modeling rubblized JPCP pavements as new flexible systems with an MR of 70,000 psi using a 51 in-service HMA overlay of rubblized PCC pavement sections.

7.2.2.1. Fatigue Cracking Model – Bottom-up

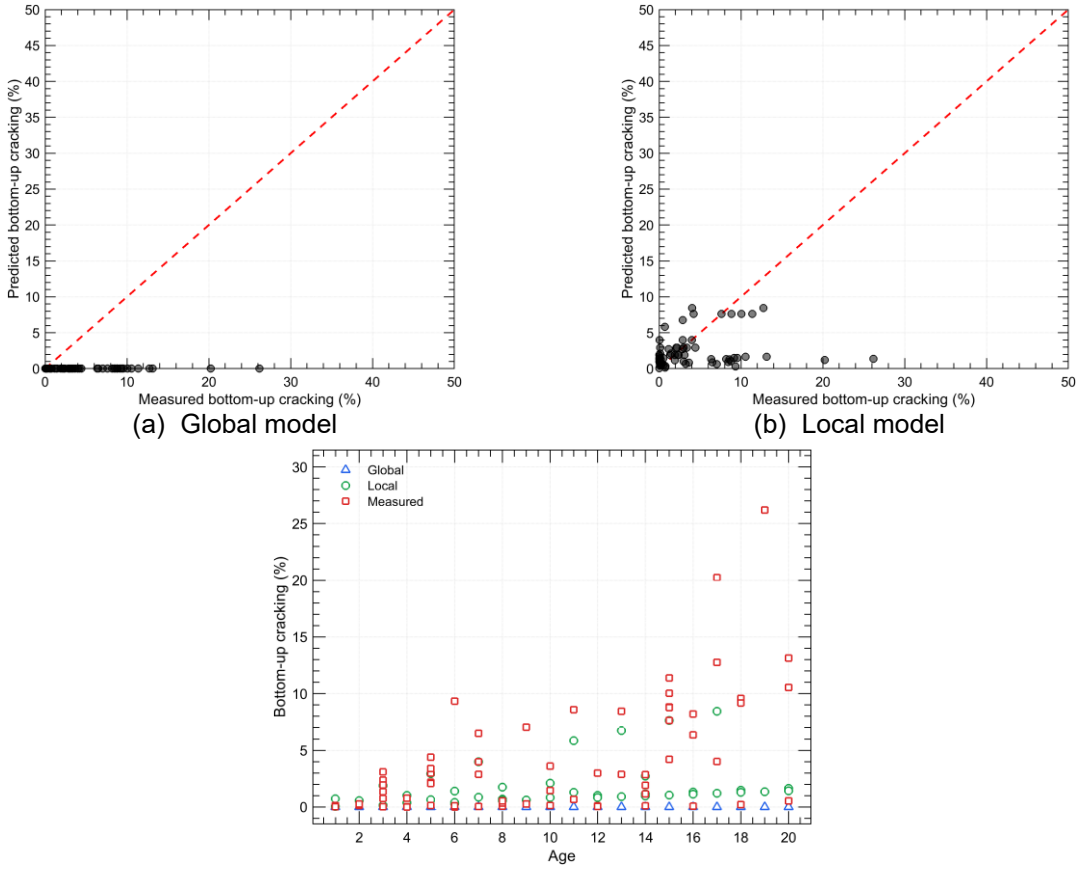
The bottom-up cracking model was calibrated using 14 rubblized pavement sections using no sampling and bootstrapping.

No Sampling

Table 7-25 summarizes the local calibration results for rubblized JPCP pavements, including the coefficients, bias, and SEE. Figure 7-16 compares the predicted and measured bottom-up cracking for the global and locally calibrated models. The local calibration reduces bias and improves SEE. Table 7-26 presents the hypothesis test results, which confirm improved model accuracy despite a few tests failing to meet the acceptance criteria.

Table 7-25 Calibration of bottom-up cracking model for rubblized PCC (No sampling)

Parameter	Global model	Local model
SEE (% total lane area)	6.545	5.405
Bias (% total lane area)	-4.025	-1.689
C_1	1.31	0.24
C_2 (h_{ac} < 5 in.)	2.1585	0.761
C_2 (5 in. <= h_{ac} <=12 in.)	(0.867+0.2583* h_{ac})*1	(0.867+0.2583* h_{ac})*0.35



(a) Global model (b) Local model

(c) Measured and predicted time series

Figure 7-16 Calibration results of bottom-up cracking for rubblized (No sampling)

Table 7-26 Hypothesis testing results for bottom-up cracking (No sampling)

Hypothesis test	Global model	Local model
Mean difference = 0	0.00	0.01
Intercept = 0	0.15	0.00
Slope = 1	0.00	0.00

Bootstrapping

The team applied bootstrapping with 1,000 resampled datasets to calibrate the bottom-up cracking model for rubblized JPCP pavements—this method quantified parameter variability and established confidence intervals for the calibration coefficients. Tables 7-27 and 7-28 present the global and locally calibrated results, and Figure 7-17 shows the parameter distributions from the 1,000 bootstrap samples.

Table 7-27 Bootstrapping global model summary

Parameter	Global model mean	Global model median	Global model lower CI	Global model upper CI
SEE (% total lane area)	6.375	6.341	3.836	9.299
Bias (% total lane area)	-4.025	-3.964	-6.216	-2.192
C_1	1.31	1.31	-	-
C_2 (h_{ac} < 5 in.)	2.1585	2.1585	-	-
C_2 (5 in. <= h_{ac} <=12 in.)	(0.867+0.2583*h_{ac})*1	(0.867+0.2583* h_{ac})*1	-	-

Table 7-28 Bootstrapping local calibration results summary

Parameter	Local model mean	Local model median	Local model lower CI	Local model upper CI
SEE (% total lane area)	4.992	5.250	2.528	7.583
Bias (% total lane area)	-1.692	-1.672	-3.129	-0.318
C_1	0.332	0.300	0.149	0.540
C_2 (h_{ac} < 5 in.)	0.526	0.529	0.034	0.984
C_2 (5 in. <= h_{ac} <=12 in.)	(0.867+0.2583* h_{ac})* 0.283	(0.867+0.2583* h_{ac})* 0.314	(0.867+0.2583* h_{ac})* 0.100	(0.867+0.2583* h_{ac})* 0.4

Reliability for the bottom-up cracking model

The calibration and PMED predictions were performed at a 50% reliability level, as described in Chapter 5. The team grouped the measured and predicted cracking into bins and developed equations for the standard error of the mean of measured cracking as a function of the mean predicted cracking. Table 7-29 lists the equations for the global and local models, and Figure 7-18 compares their reliability plots.

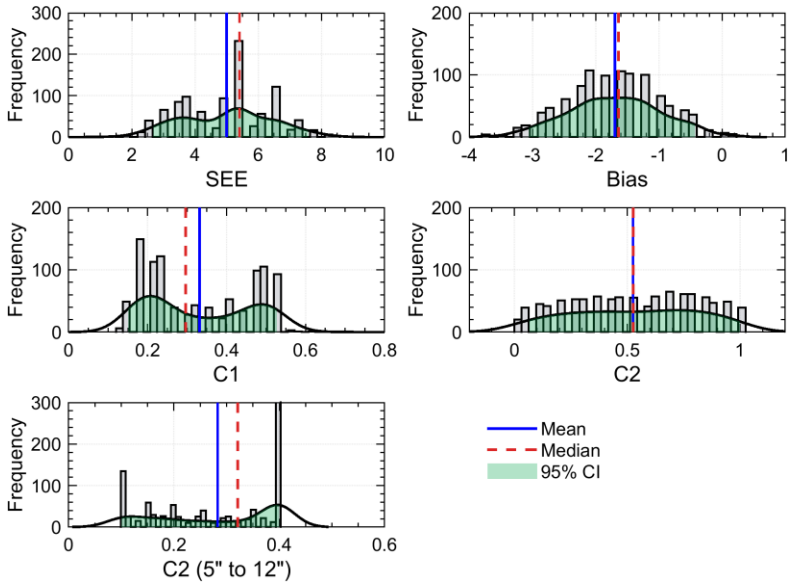


Figure 7-17 Distribution of local calibration parameters (bootstrapping)

Table 7-29 SE equations of the bottom-up cracking model for rubblized PCC

Global model equation	Local model equation
$S_{e(Alligator)} = 0.2262 + \frac{14.2349}{1 + \exp(0.2958 - 0.1441 \log(D))}$	$S_{e(Alligator)} = 3.166 + \frac{1.588}{1 + \exp(0.0967 - 5.626 \log(D))}$

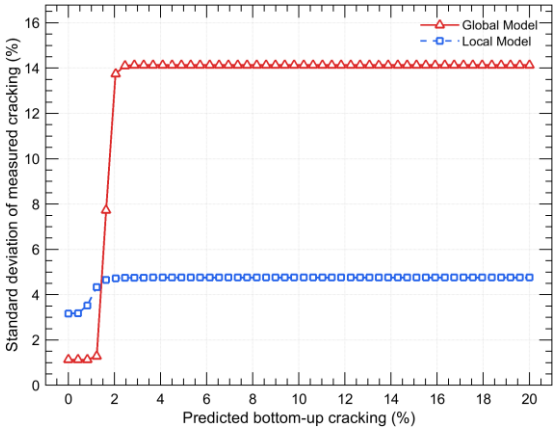
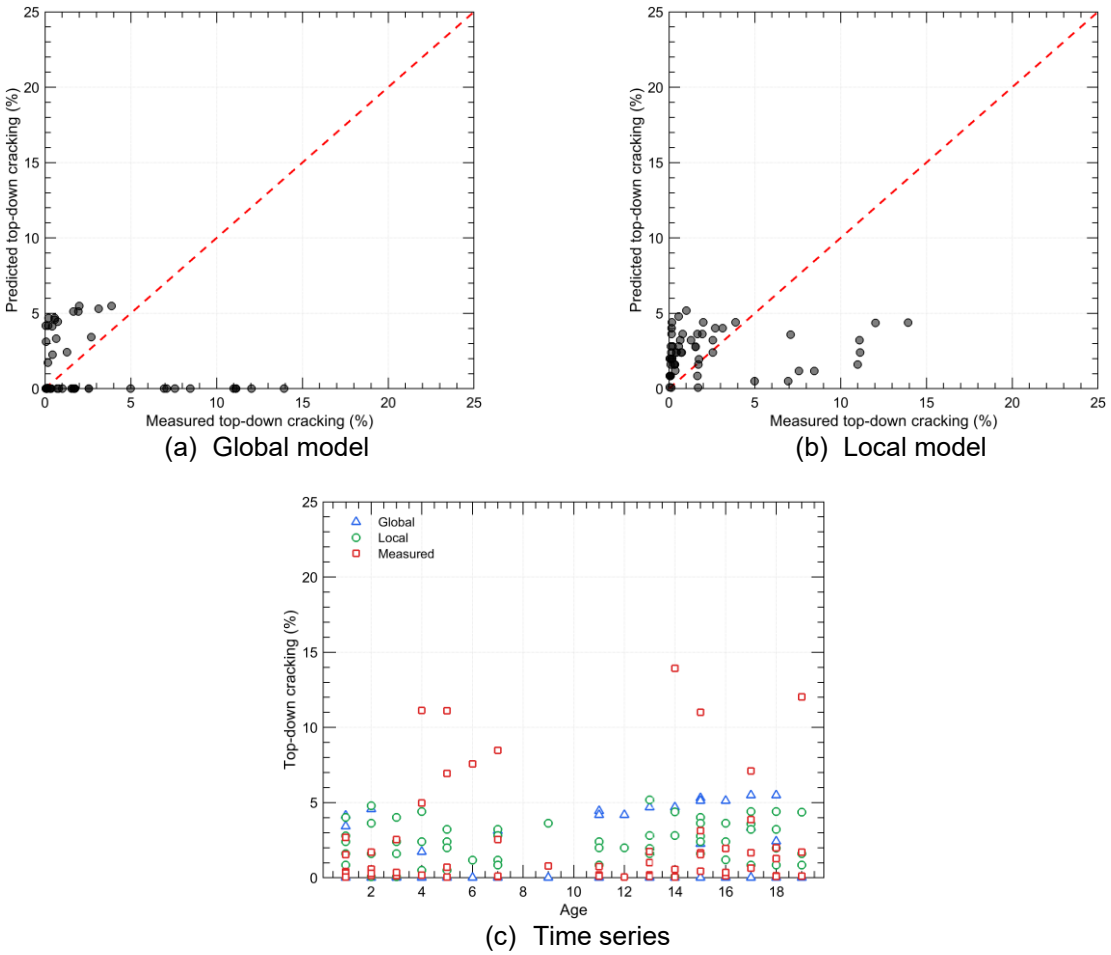


Figure 7-18 SE of global and local models for rubblized PCC

7.2.2.2. Fatigue Cracking Model – Top-down

The calibration procedure for the top-down cracking model followed the same approach used for the C&S pavements. The team calibrated the combined crack initiation and propagation function in Microsoft Excel using the Solver tool and engineering judgment, as the actual crack initiation times were not available. The team applied the no-sampling

calibration method using 17 in-service sections. Figure 7-19 shows the predicted versus measured top-down cracking for the global and locally calibrated models, along with their comparison over time. Table 7-30 presents the calibration results.



(a) Global model (b) Local model

(c) Time series

Figure 7-19 Measured and predicted top-down-cracking for rubblized PCC

Table 7-30 Calibration results of the top-down cracking model for rubblized PCC

Parameters	Global model	Local model
SEE	4.657	3.672
Bias	-1.097	0.000
K_{L2}	0.286	0.657
K_{L3}	0.011	0.100
K_{L4}	0.015	0.092
K_{L5}	3.266	2.044
C_1	2.522	0.097
C_2	0.807	2.416

Reliability for the top-down cracking model

Table 7-31 shows the standard error equations for global and local top-down cracking models. Figure 7-20 shows the reliability comparison of global and local models.

Table 7-31 SE equations of the top-down cracking model for rubblized PCC

Global model equation	Local model equation
$S_{e(Top-down)} = 0.3657 \times TOP + 3.6563$	$S_{e(Top-down)} = 0.2846 \times TOP + 2.8188$

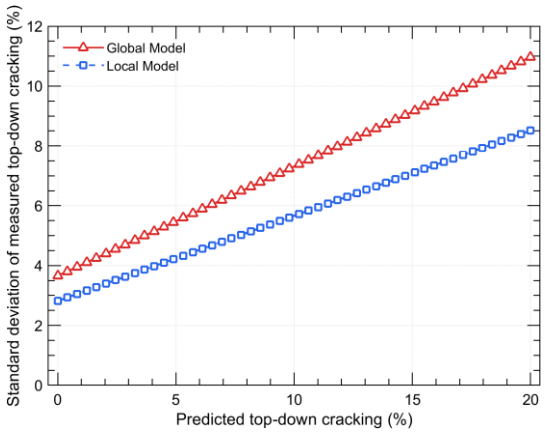


Figure 7-20 SEof the global and local top-down cracking model for rubblized

7.2.2.3. Rutting Model

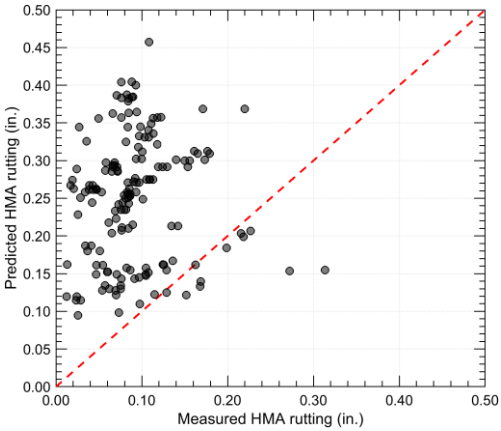
The team followed the same rutting calibration procedure described earlier. Both no-sampling and bootstrapping approaches were applied to calibrate the layer-specific and total surface rutting models for rubblized JPCP pavements using 39 in-service rubblized sections.

Method 1 - Individual Layer Rutting Calibration

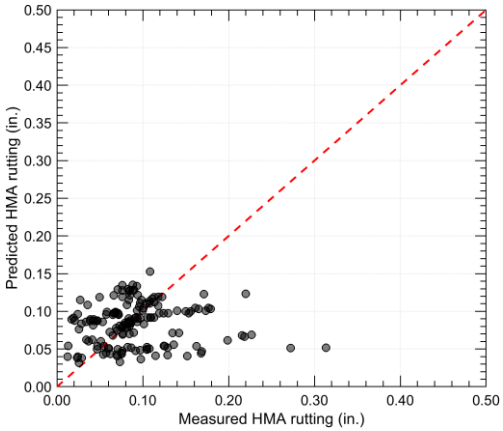
This section outlines the calibration of individual-layer rutting using an HMA overlay over rubblized PCC sections.

No Sampling

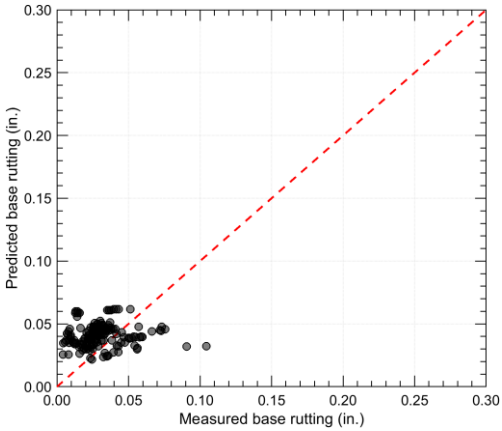
Figures 7-21 and 7-22 show the predicted versus measured rutting for global and locally calibrated models. Tables 7-32 and 7-33 summarize the calibration results and hypothesis test outcomes. The locally calibrated model shows reduced bias and improved alignment with measured performance.



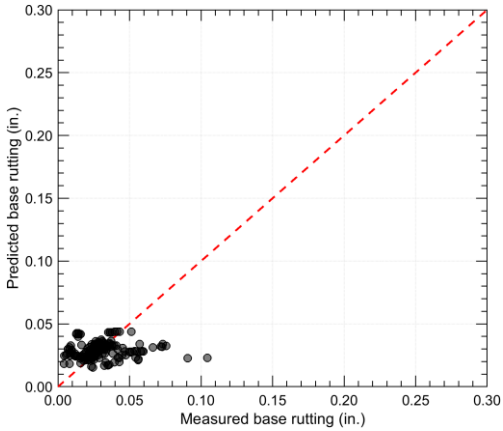
(a) Global model – HMA rut



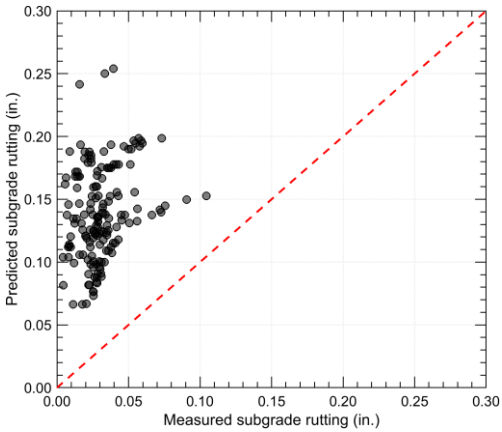
(b) Local model – HMA rut



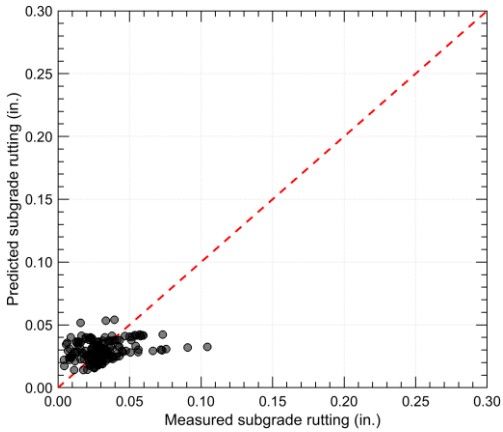
(c) Global model – base rut



(d) Local model – base rut

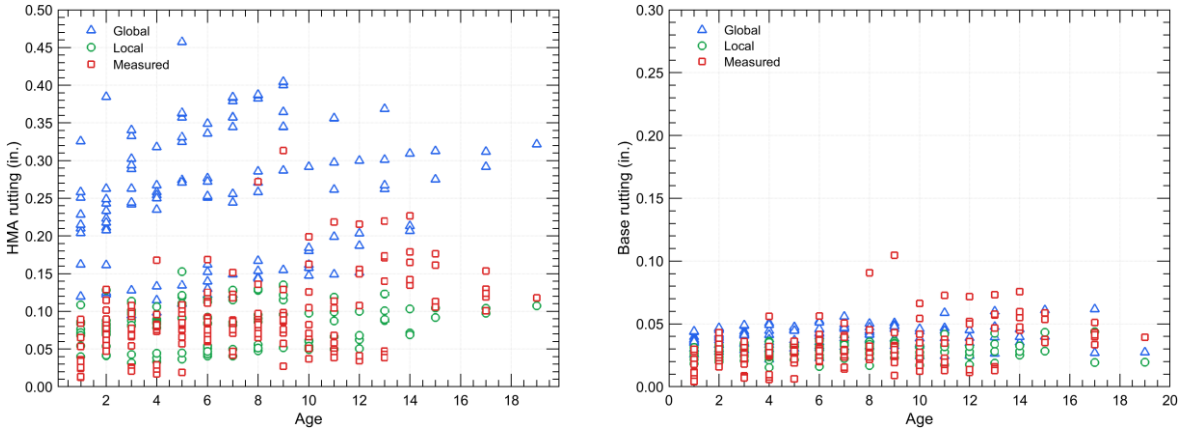


(e) Global model – subgrade rut



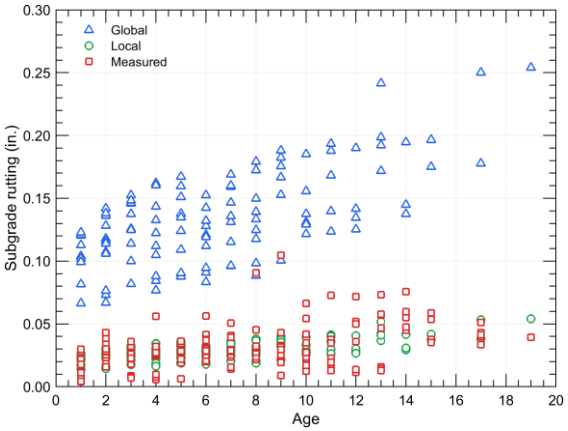
(f) Local model – subgrade rut

Figure 7-21 Predicted vs. measured rutting for rubblized PCC (No sampling)



(a) HMA rut

(b) Base rut



(c) Subgrade rut

Figure 7-22 Individual layers rutting time series for the rubblized PCC

Table 7-32 Hypothesis testing results of rutting models for rubblized PCC

Layer	t-test *p*-value (G)	Intercept *p*-value (G)	Slope = 1 *p*-value (G)	t-test *p*-value (L)	Intercept *p*-value (L)	Slope = 1 *p*-value (L)
HMA rut	0.000	0.000	0.000	0.056	0.000	0.000
Base rut	0.000	0.000	0.000	0.370	0.000	0.000
Subgrade	0.000	0.000	0.000	0.458	0.000	0.000

G = Global; L = Local

Table 7-33 Calibration summary results for rubblized PCC – Method 1 (No sampling)

Layer	Global model SEE (in.)	Global model Bias (in.)	Local model SEE (in.)	Local model Bias (in.)
HMA rut	0.185	0.158	0.055	-0.008
Base rut	0.0212	0.0107	0.017	-0.001
Subgrade	0.1148	0.1082	0.0162	0.000
Parameters	Global Model	Global Model	Local Model	Local Model
HMA rutting (br1)	0.4	0.4	0.134	0.134
Base rutting (bs1)	1.0	1.0	0.712	0.712
Subgrade rutting (bsg1)	1.0	1.0	0.213	0.213

Bootstrapping

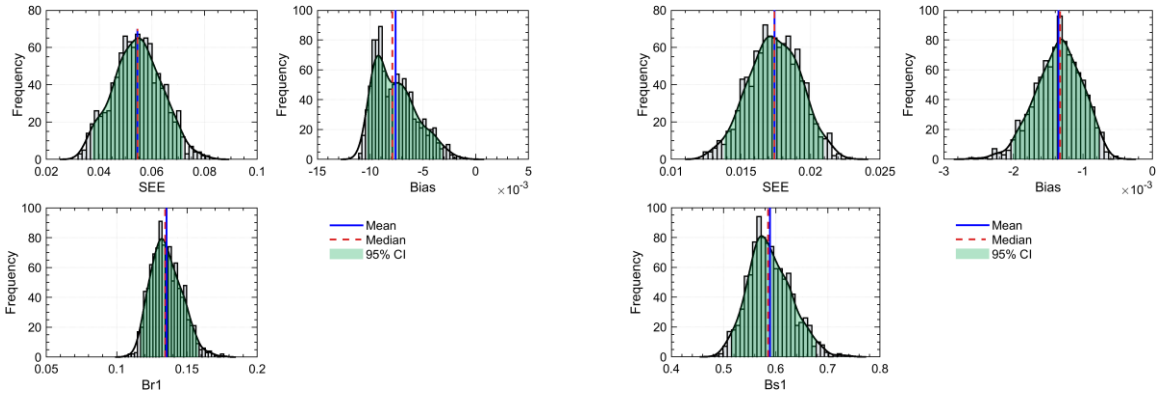
Tables 7-34 and 7-35 summarize the calibration results for the global and locally calibrated models, while Figure 7-23 shows the parameter distributions and corresponding confidence intervals for the calibrated coefficients.

Table 7-34 Global rutting model for rubblized PCC (bootstrapping)

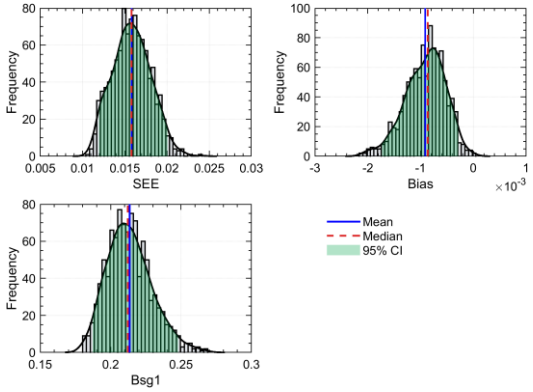
Layer type	Average SEE	SEE Lower CI	SEE Upper CI	Average bias (in.)	Bias Lower CI	Bias Upper CI
HMA	0.1838	0.1603	0.2077	0.1573	0.1283	0.1870
Base	0.0254	0.0234	0.0273	0.0164	0.0119	0.0207
Subgrade	0.1146	0.1025	0.1261	0.1081	0.0961	0.1194

Table 7-35 Local rutting model for rubblized PCC (bootstrapping)

Statistics	HMA rutting	Base rutting	Subgrade rutting
Average SEE (in.)	0.055	0.017	0.016
SEE Lower CI	0.037	0.014	0.012
SEE Upper CI	0.072	0.021	0.020
Average bias (in.)	-0.008	-0.001	-0.001
Bias Lower CI	-0.010	-0.002	-0.002
Bias Upper CI	-0.003	-0.001	0.000
Average calibration coefficient	0.149	0.546	0.538
Calibration coefficient Lower CI	0.117	0.514	0.521
Calibration coefficient Upper CI	0.181	0.578	0.555



(a) HMA rut (b) Base rut



(c) Subgrade rut

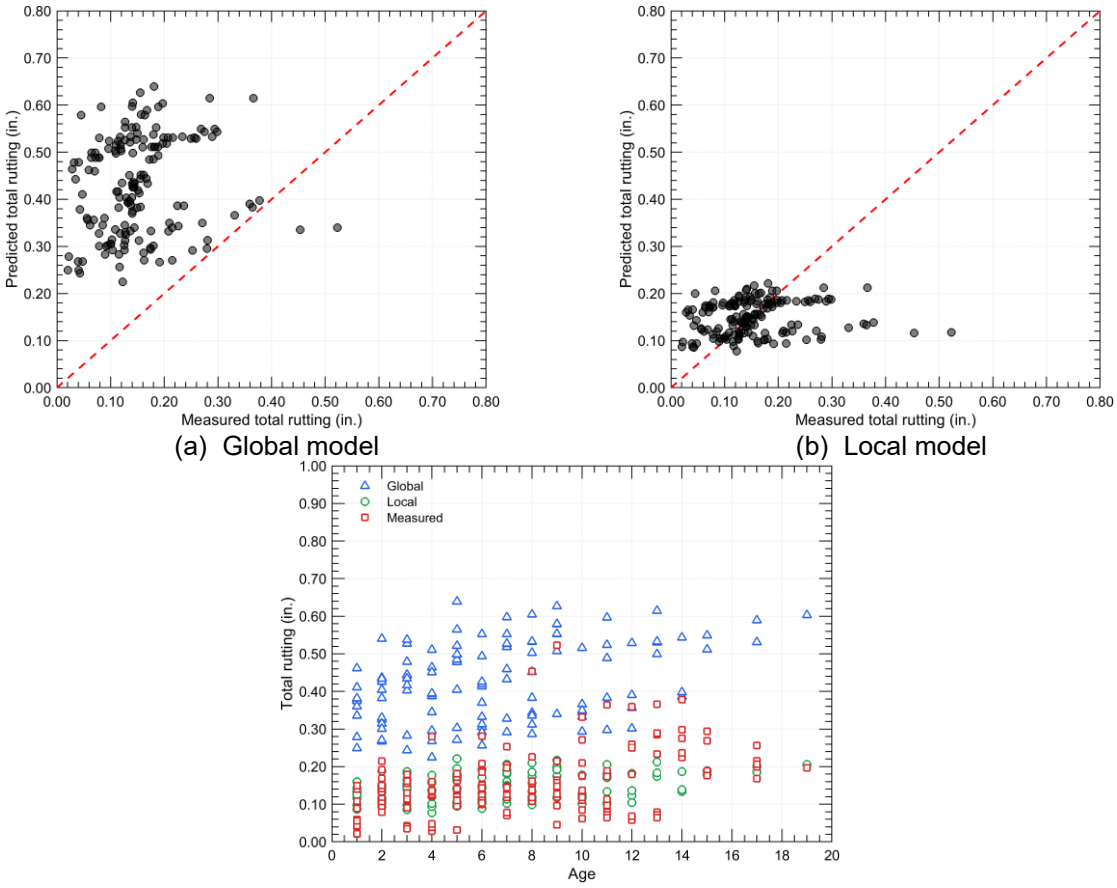
Figure 7-23 Distribution of calibration parameters - AC rutting (Bootstrapping)

Method 2 – Total Rutting Calibration

In this method, the team calibrated the measured total rutting against the sum of the predicted rutting from all layers. The calibration coefficients for each layer were adjusted simultaneously to align the total predicted rutting with the measured values.

No Sampling

Figure 7-24 shows the predicted vs. measured total rutting for the global and local models with no sampling, along with their comparison over time. Tables 7-36 and 7-37 present the hypothesis-testing and calibration results for the global and local models with no sampling.



(a) Global model (b) Local model

(c) Time series

Figure 7-24 Predicted vs measured Total rutting (No sampling)

Table 7-36 Hypothesis testing results for total rutting

Layer	Global model	Local model
t-test p-value	0.000	0.573
Intercept p-value	0.000	0.000
Slope = 1 p-value	0.000	0.000

Table 7-37 Total rutting model calibration results

Parameters	Global model	Local model
SEE	0.305	0.085
Bias	0.277	-0.004
HMA rutting (br1)	0.400	0.137
Base rutting (bs1)	1.000	0.434
Subgrade rutting (bsg1)	1.000	0.330

Bootstrapping

Tables 7-38 and 7-39 summarize the global and local models, respectively, using bootstrapping. Figure 7-25 shows the distribution of calibration parameters.

Table 7-38 Global model summary for total rutting of rubblized PCC (bootstrapping)

Parameter	Global model mean	Global model median	Global model lower CI	Global model upper CI
SEE (in)	0.217	0.217	0.075	0.098
Bias (in.)	0.179	0.180	0.137	0.218
br1	0.400	0.400	-	-
bs1	1.000	1.000	-	-
bsg1	1.000	1.000	-	-

Table 7-39 Local calibration summary for total rutting of rubblized PCC (bootstrapping)

Parameter	Local model mean	Local model median	Local model lower CI	Local model upper CI
SEE (in.)	0.087	0.087	0.023	0.046
Bias (in.)	-0.007	-0.007	-0.013	-0.002
br1	0.149	0.161	0.272	0.551
bs1	0.546	0.561	0.027	1.040
bsg1	0.538	0.540	0.027	1.020

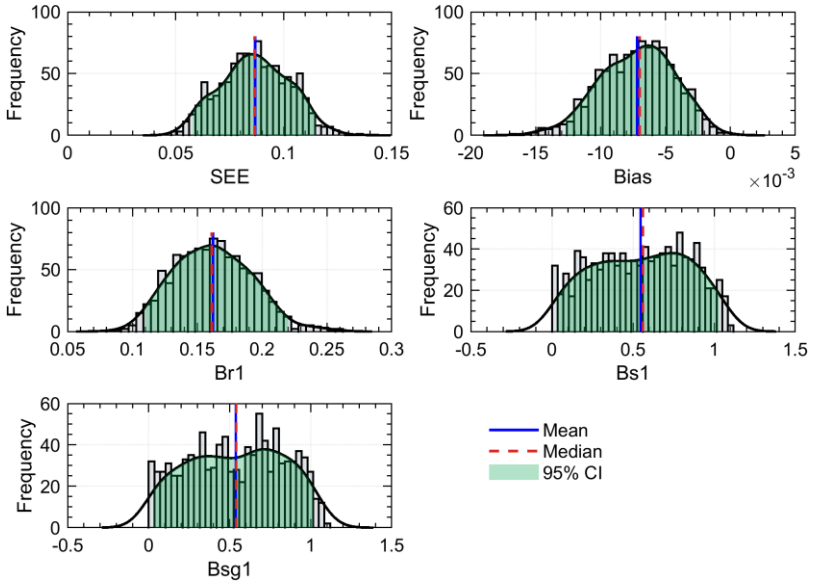


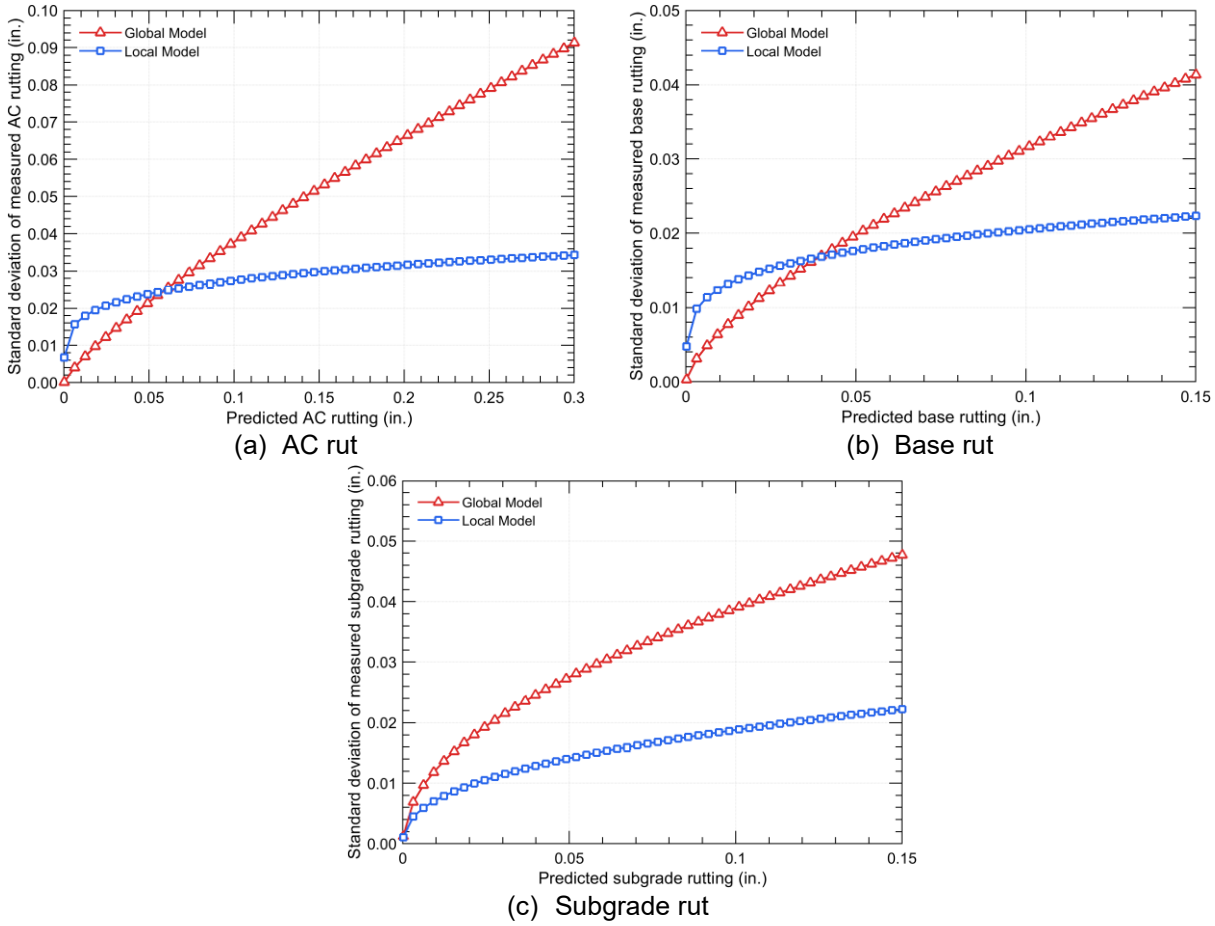
Figure 7-25 Distribution of calibration parameters - total rutting

Reliability for the rutting model

The team developed equations for standard error that relate the standard deviation of measured rutting to the mean predicted rutting, incorporating reliability. Table 7-40 lists the equations for individual layers, and Figure 7-26 compares the reliability of global and local models.

Table 7-40 SE equations of rutting models for rubblized PCC

Layer	Global model	Local model
HMA	$s_{e(HMA)} = 0.24(Rut_{HMA})^{0.8026} + 0.001$	$s_{e(HMA)} = 0.0446(Rut_{HMA})^{0.2185}$
Base	$s_{e(base)} = 0.1477(Rut_{base})^{0.6711} + 0.001$	$s_{e(base)} = 0.0334(Rut_{base})^{0.2122}$
Subgrade	$s_{e(subgrade)} = 0.1235\left(Rut_{subgrade}\right)^{0.5012} + 0.001$	$s_{e(subgrade)} = 0.0952\left(Rut_{subgrade}\right)^{0.5567}$



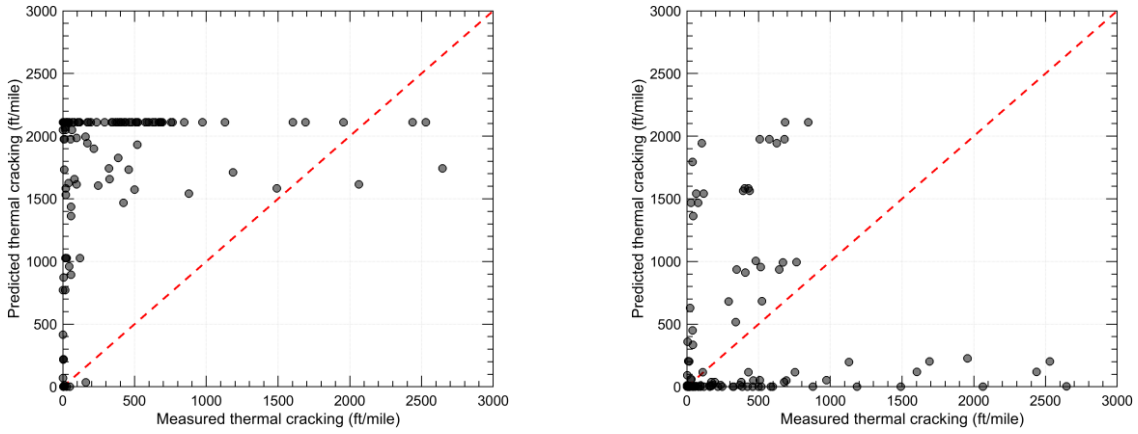
(a) AC rut (b) Base rut

(c) Subgrade rut

Figure 7-26 SE comparison for rubblized PCC

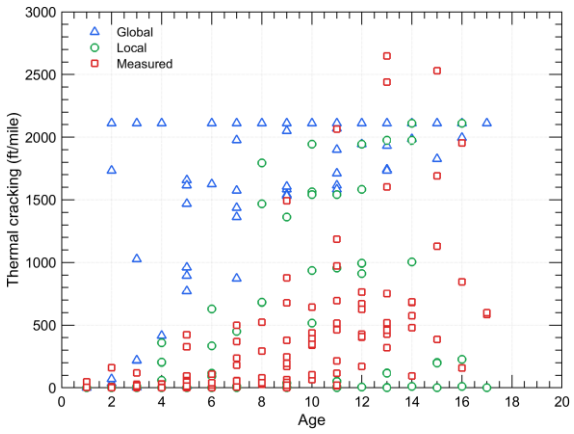
7.2.2.4. Transverse (thermal) Cracking Model

The team calibrated the thermal cracking model for Level 1 inputs in PMED using the same procedure described earlier, with 22 sections and only PG binder types. The calibration was performed in CAT, where Kt was defined as a function of MAAT. Figure 7-27 shows the measured versus predicted thermal cracking and their comparison over time, and Table 7-41 summarizes the calibration results.



(a) Global model

(b) Local model



(c) Time series

Figure 7-27 Predicted vs. measured thermal cracking for rubblized PCC

Table 7-41 Transverse (thermal) cracking results for rubblized PCC

Parameter	Global model	Local model
SEE	1500	-1301
Bias	797	6.32
K	$K = \left(3 * POW(10, -7)\right) * Pow(MAAT, 4.0319)) * 1 + 0$	$K = \left(3 * POW(10, -7)\right) * Pow(MAAT, 4.0319)) * 0.55$

Reliability for the thermal cracking model

The team developed standard-error equations using the standard deviation of the measured data and the mean predicted cracking to incorporate reliability. Table 7-42 lists the equations, and Figure 7-28 compares the reliability of global and local models.

Table 7-42 SE equations for the thermal cracking model of rubblized PCC

Global model	Local model
$S_{e(Thermal)} = 0.14 \times TC + 168$	$S_{e(Thermal)} = 0.0425 \times TC + 142$

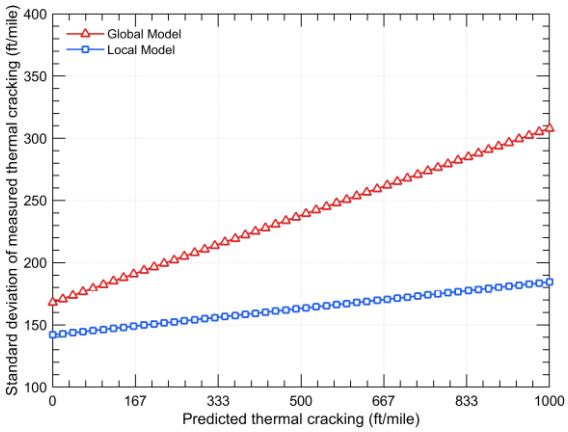


Figure 7-28 SE comparison of thermal cracking model for rubblized PCC

7.2.2.5. IRI Model for Rubblized PCC Pavements

The IRI model represents a linear function of initial IRI, rut depth, total fatigue cracking, transverse cracking, and site factor. The team calibrated the IRI model with 32 in-service rubblized PCC sections.

No Sampling

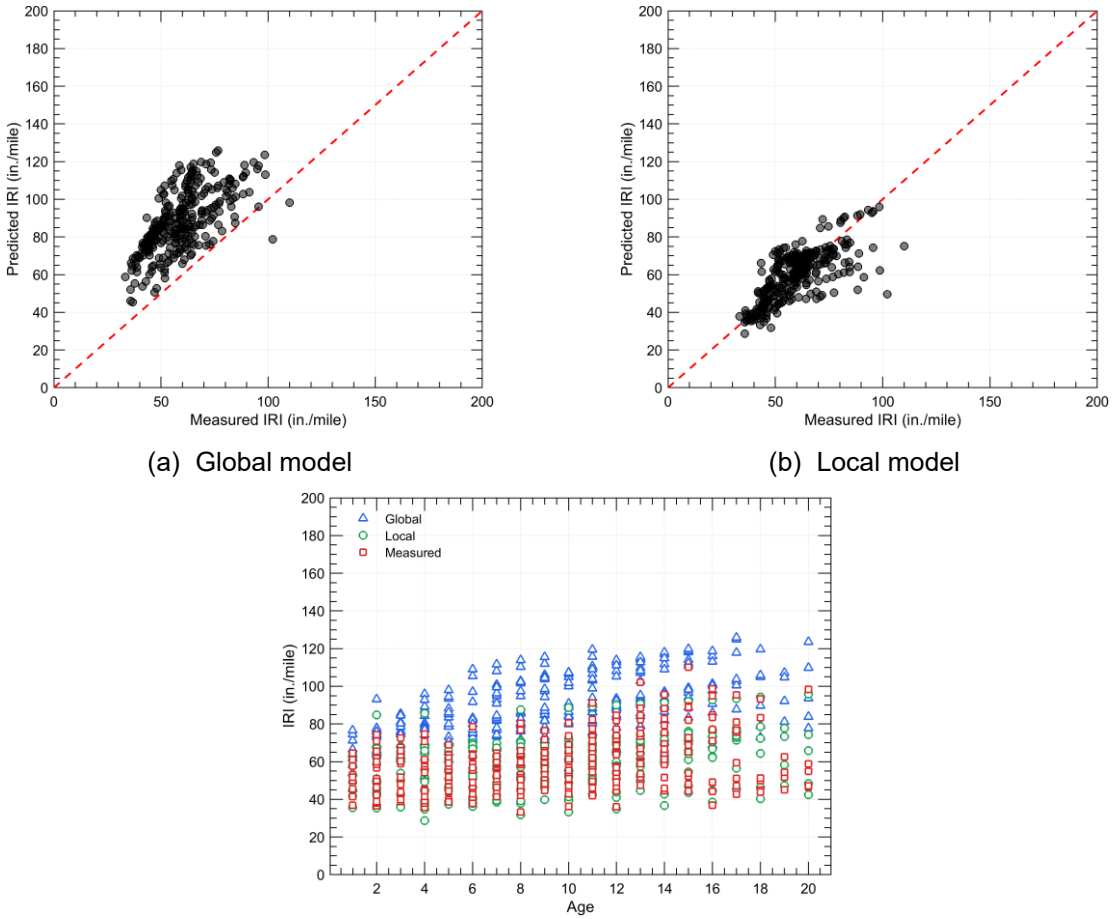
Tables 7-43 and 7-44 present the hypothesis test results and summarize the calibrated parameters for the IRI model, respectively. The local calibration achieved notable reductions in SEE and bias. Figure 7-29 shows the predicted versus measured IRI and their variation over time.

Table 7-43 IRI model hypothesis testing results

Layer	Global model	Local model
t-test p-value	0.000	1.000
Intercept p-value	0.000	0.000
Slope = 1 p-value	0.000	0.000

Table 7-44 IRI model calibration results (No sampling)

Model coefficient	Global model	Local model
SEE	31.358	10.387
Bias	28.510	0.000
C1	40.000	17.520
C2	0.4000	0.5189
C3	0.0080	0.0079
C4	0.0150	0.0066



(a) Global model

(b) Local model

(c) Time series

Figure 7-29 Measured vs predicted IRI for rubblized PCC

Bootstrapping

Tables 7-45 and 7-46 summarize the global and local models, respectively, using bootstrapping. Figure 7-30 shows the distribution of calibration parameters.

Table 7-45 Global model summary for IRI of rubblized PCC (bootstrapping)

Parameter	Global model mean	Global model median	Global model lower CI	Global model upper CI
SEE (in)	31.341	31.266	27.814	34.896
Bias (in.)	28.508	28.474	25.005	31.988
C1	40.000	40.000	-	-
C2	0.400	0.400	-	-
C3	0.008	0.008	-	-
C4	0.015	0.015	-	-

Table 7-46 Local calibration summary for IRI of rubblized PCC (bootstrapping)

Parameter	Local model mean	Local model median	Local model lower CI	Local model upper CI
SEE (in.)	10.515	10.348	8.473	13.583
Bias (in.)	-0.013	0.000	-0.571	0.001
C1	25.719	23.493	8.902	46.407
C2	0.212	0.028	0.000	1.656
C3	0.009	0.007	0.001	0.028
C4	0.005	0.004	0.000	0.012

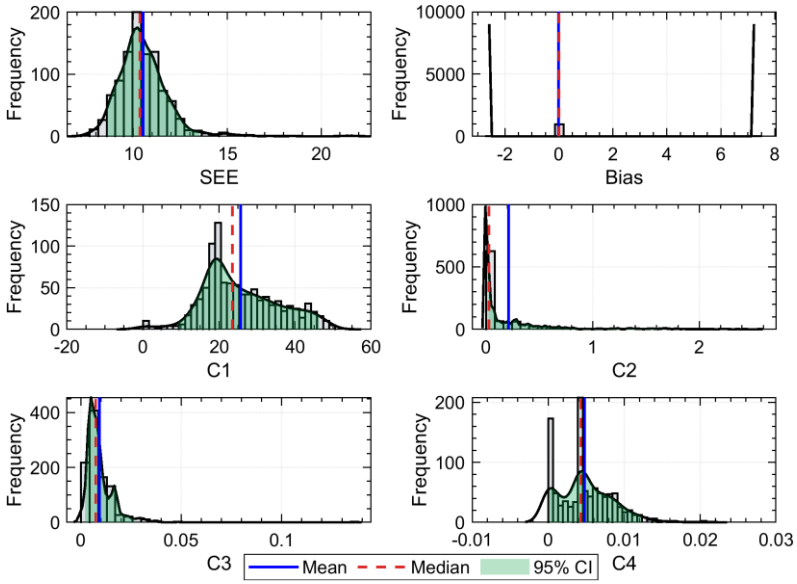


Figure 7-30 Distribution of calibration parameters of the IRI model for rubblized PCC

7.2.2.6. Summary for HMA Overlay over Rubblized PCC Pavements

The team adopted the bootstrapped calibration coefficients as the final set for implementation. Tables 7-47 and 7-48 summarize the selected coefficients for all performance models and the corresponding standard error equations used in reliability evaluation.

Table 7-47 Summary coefficients for HMA overlay over rubblized PCC

Performance prediction model	Performance models and transfer functions	Local coefficient
Fatigue cracking (bottom-up)	$FC_{Bottom} = \left(\frac{1}{60}\right)\left(\frac{6000}{1 + e^{C_1 C_1^* + C_2 C_2^* Log(DI_{Bottom}*100)}}\right)$	$C_1 = 0.332$ $C_2 = 0.526$ (hac <5 in) $C_2 = (0.867 + 0.2583 * hac) * 0.283$ (5 in <= hac <=12 in)
Fatigue cracking (top-down)	$t_0 = \frac{\mathrm{K}_{L1}}{1 + e^{\mathrm{K}_{L2}\times 100\times(\mathrm{a}_0/2\mathrm{A}_0)+\mathrm{K}_{L3}\times \mathrm{HT}+\mathrm{K}_{L4}\times LT+K_{L5}\times \log_{10}\ \mathrm{AADTT}}}$ $FC_{Top} = \mathrm{Lmax} \times \mathrm{e}^{-\left(\frac{C_1\rho}{t - C_3 t_0}\right)^{C_2\beta}}$	$\mathrm{K}_{L2} = 0.657$ $\mathrm{K}_{L3} = 0.100$ $\mathrm{K}_{L4} = 0.092$ $\mathrm{K}_{L5} = 2.044$ $C_1 = 0.097$ $C_2 = 2.416$
HMA Rutting	$\Delta_{p(HMA)} = \varepsilon_{p(HMA)} h_{HMA} = \beta_{1r} k_z \varepsilon_{r(HMA)} 10^{k_{1r}} n^{k_{2r}\beta_{2r}} T^{k_{3r}\beta_{3r}}$	$\beta_{1r} = 0.149$
Base/subgrade Rutting	$\Delta_{p(soil)} = \beta_{s1} k_{s1} \varepsilon_v h_{soil} \left(\frac{\varepsilon_o}{\varepsilon_r}\right) e^{-\left(\frac{\rho}{n}\right)^{\beta}}$	$\beta_{s1} = 0.546$ $\beta_{sg1} = 0.538$
Thermal cracking	$A = 10^{k_t \beta_t \left(4.389 - 2.52 Log(E_{HMA}\sigma_m \eta)\right)}$	$K = \left(3 * POW(10, -7)\right) * Pow(MAAT, 4.0319)) * 0.55 + 0$
IRI	$IRI = IRI_o + C_1(RD) + C_2(FC_{Total}) + C_3(TC) + C_4(SF)$	$C_1 = 25.715, C_2 = 0.212$ $C_3 = 0.0093, C_4 = 0.0048$

Table 7-48 SE equations for HMA overlay over rubblized PCC

Performance prediction model	Global model	Local model
Fatigue cracking (bottom-up)	$S_{e(Alligator)} = 1.13 + \frac{13}{1 + \exp\left(7.57 - 15.5 \log(Crack + 0.0001)\right)}$	$S_{e(Alligator)} = 3.166 + \frac{1.588}{1 + \exp\left(0.0967 - 5.626 \log(Crack)\right)}$
Fatigue cracking (top-down)	$S_{e(Top-down)} = 0.3657 \times TOP + 3.6563$	$S_{e(Top-down)} = 0.2846 \times TOP + 2.8188$
HMA Rutting	$S_{e(HMA)} = 0.0446(Rut_{HMA})^{0.2185}$	$S_{e(HMA)} = 0.0584(Rut_{HMA})^{0.1029}$
Base/subgrade Rutting	$S_{e(base)} = 0.0334(Rut_{base})^{0.2122}$ $S_{e(subgrade)} = 0.0952\left(Rut_{subgrade}\right)^{0.5567}$	$S_{e(base)} = 0.0362(Rut_{base})^{0.1098}$ $S_{e(subgrade)} = 0.0562\left(Rut_{subgrade}\right)^{0.3114}$
Thermal	$S_{e(Thermal)} = 0.14 \times TC + 168$	$S_{e(Thermal)} = 0.0425 \times TC + 142$
IRI	Internally calculated by PMED	

7.2.3 HMA Overlays of Existing HMA Pavements

This section presents the local calibration results for HMA overlays placed over existing HMA pavements (39 in-service sections) using the calibrated PMED performance prediction models. As described in Chapter 5, the calibration was performed at rehabilitation input Level 2, since Level 3 involves broader assumptions that reduce model reliability. Level 3 uses predefined damage values for the existing HMA layer based on pavement structural ratings; however, these ratings differ between PMED and MDOT, as MDOT follows FHWA's structural rating criteria. In addition, Level 3 requires the total rutting across all existing layers to be reported as a single value, potentially leading to inaccurate rutting predictions in the underlying layers. The research team calibrated the HMA over HMA sections at rehabilitation Levels 2 and 3; however, due to the limitations stated above, the team recommended using rehabilitation Level 2 calibration.

7.2.3.1. Fatigue Cracking Model – Bottom-up

The available HMA-over-HMA sections did not provide sufficient performance data to support local calibration of the bottom-up cracking model. Therefore, the team, in consultation with MDOT officials, adopted the coefficients calibrated in the SPR-1723 study for new flexible pavements (*2*).

7.2.3.2. Total Fatigue (Bottom-up + Reflective) Cracking Model

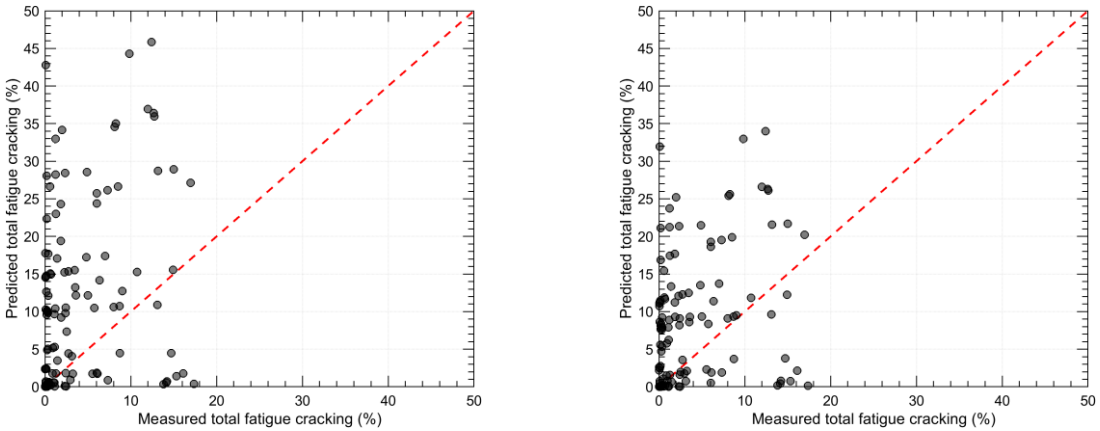
In HMA over HMA overlays, reflective cracking caused by damage in the existing HMA layers is a critical concern for performance. However, the MDOT PMS database does not record reflective cracking separately and instead reports total fatigue cracking without distinguishing between reflective and conventional fatigue cracking. Initially, this model was not locally calibrated, and the global coefficients were recommended. Following further discussions with MDOT, the team decided to calibrate the model against the total measured fatigue cracking (top-down only). This approach introduces inherent limitations because the top-down cracking model was also calibrated using the same dataset. The team used 26 in-service pavement sections for model calibration.

As discussed in Chapter 5, PMED uses an ANN framework to estimate bending, shearing, and thermal fracture damage. These ANN-based coefficients can vary only within a narrow range near the global values. Therefore, only the C4 coefficient was calibrated over a broader range using CAT, resulting in slight improvements in SEE and bias.

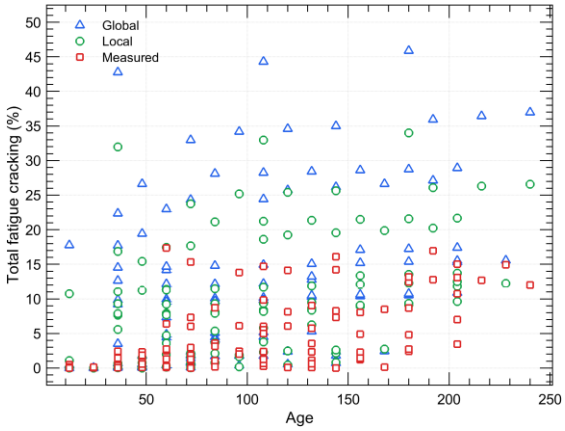
It is important to note that, for the bottom-up cracking component, the team used the previously calibrated coefficients for new flexible pavements from earlier calibration efforts. Table 7-49 summarizes the local calibration results for the total fatigue cracking model, including the calibrated coefficients, bias, and SEE. Figure 7-31 compares measured and predicted total fatigue cracking for the global and locally calibrated models.

Table 7-49 Calibration of the total fatigue cracking model for HMA over HMA

Parameter	Global model	Local model
SEE (% total lane area)	14.41	10.25
Bias (% total lane area)	8.13	5.06
C_1	0.38	0.24
C_2	1.66	1.1
C_3	2.72	2.1
C_4	105.4	140.0
C_5	-7.02	-7.02



(a) Global model (b) Local model



(c) Measured and predicted time series

Figure 7-31 Calibration of the total fatigue cracking model for HMA over HMA

Reliability for the total fatigue cracking model

For total fatigue cracking, the team developed a standard-error equation to account for design reliability. Table 7-50 lists the equations for the global and local models, and Figure 7-32 compares their reliability plots.

Table 7-50 SE equations of the total fatigue cracking model for HMA over HMA

Global model equation	Local model equation
$S_{e(Fatigue+reflective)} = 1.1097(Fatigue)^{0.6804} + 1.23$	$S_{e(Fatigue+reflective)} = 1.065(Fatigue)^{0.482} + 1.11$

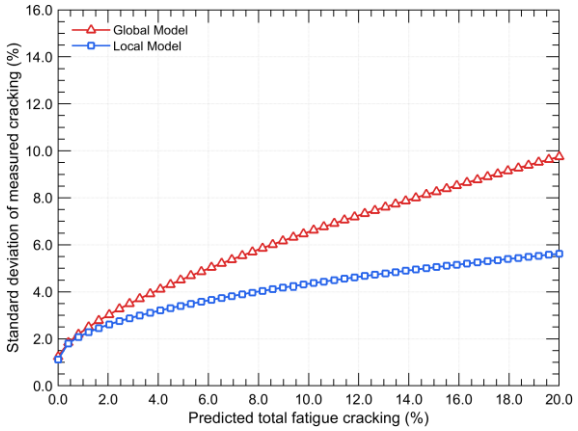


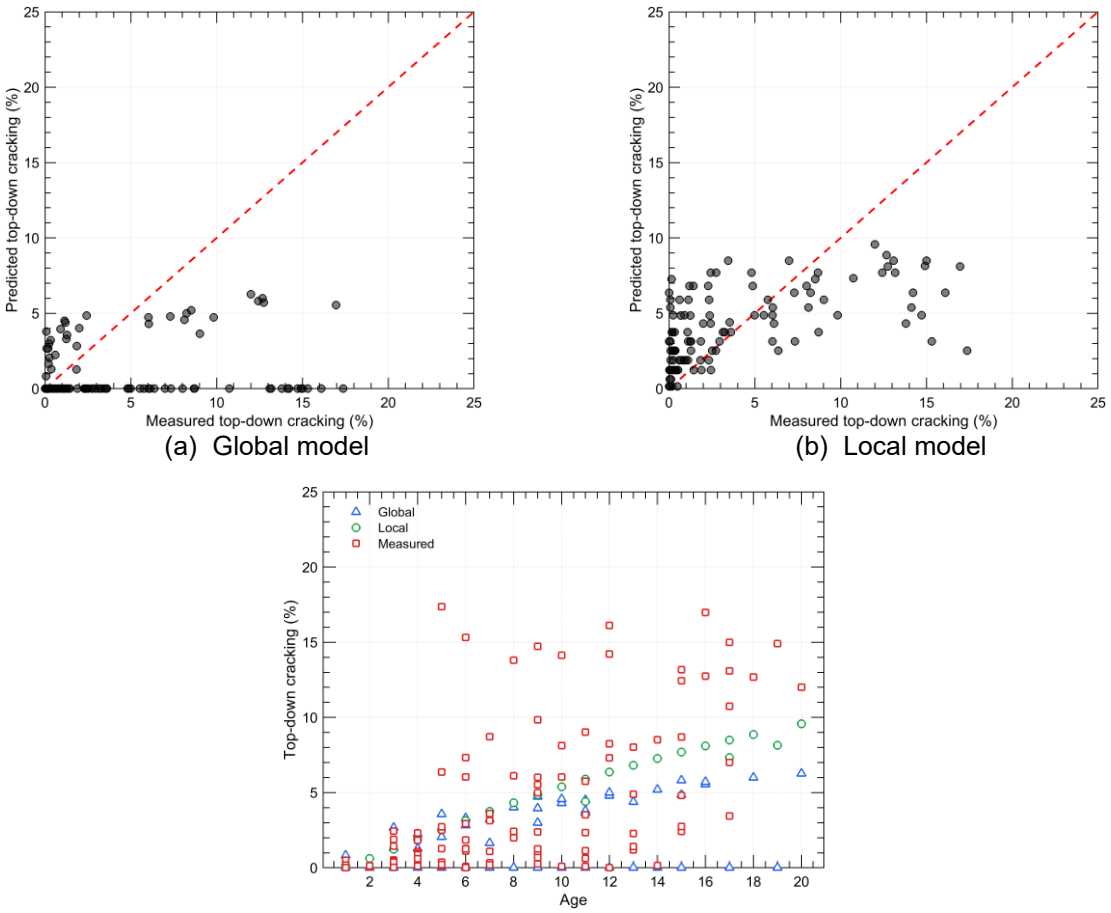
Figure 7-32 SE of global and local models of total fatigue cracking

7.2.3.3. Fatigue Cracking Model – Top-down

The calibration of the top-down cracking model adopted the same approach as explained earlier for other fix types. The combined initiation and propagation function was optimized in Excel using Solver and engineering judgment, given the unavailability of initiation times. The research team calibrated the model using 26 pavement sections, applying the no-sampling technique to estimate the coefficients and minimize prediction error. Table 7-51 and Figure 7-33 present the model comparison and calibration results.

Table 7-51 Calibration results of the top-down cracking model for HMA over HMA

Parameters	Global model	Local model
SEE	5.870	4.100
Bias	-3.11	0.000
K_{L2}	0.286	1.236
K_{L3}	0.011	0.103
K_{L4}	0.015	0.175
K_{L5}	3.266	0.172
C_1	2.522	0.087
C_2	0.807	2.019



(a) Global model (b) Local model

(c) Time series

Figure 7-33 Measured and predicted top-down-cracking for HMA over HMA

Reliability for the top-down cracking model

Table 7-52 shows the standard error equations for global and local top-down cracking models. Figure 7-34 shows the reliability comparison of global and local models.

Table 7-52 SE equations of the top-down cracking model for HMA over HMA

Global model equation	Local model equation
$S_{e(Top-down)} = 0.3657 \times TOP + 3.6563$	$S_{e(Top-down)} = 0.2846 \times TOP + 2.8188$

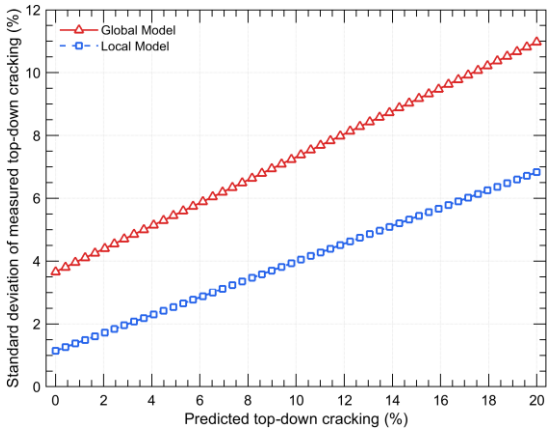


Figure 7-34 SE of the top-down cracking model for HMA over HMA

7.2.3.4. Rutting Model

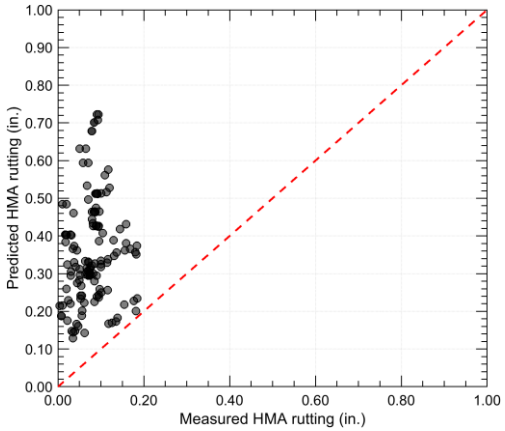
The same calibration procedure was used for rutting, applying both no-sampling and bootstrapping methods to calibrate layer-specific and total surface rutting models across 28 HMA-over-HMA pavement sections. It is vital that PMED predicted zero subgrade rutting in most sections, so the subgrade rutting coefficient was set to the global default value specified by PMED.

Method 1 - Individual Layer Rutting Calibration

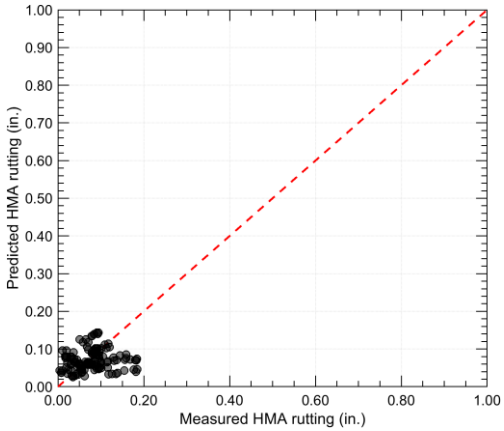
This section presents the calibration of layer-specific rutting for HMA overlays on rubblized PCC sections.

No Sampling

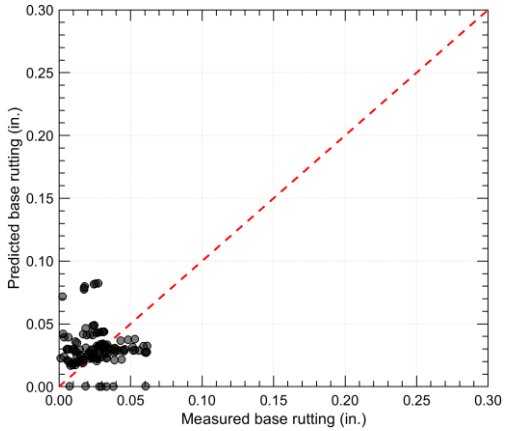
Figures 7-35 and 7-36 show the predicted versus measured rutting for global and locally calibrated models. Tables 7-53 and 7-54 summarize the calibration results and hypothesis test outcomes. The locally calibrated model shows reduced bias and improved alignment with measured performance.



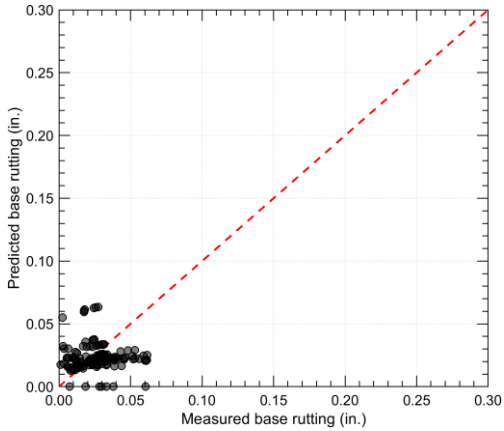
(a) Global model – HMA rut



(b) Local model – HMA rut

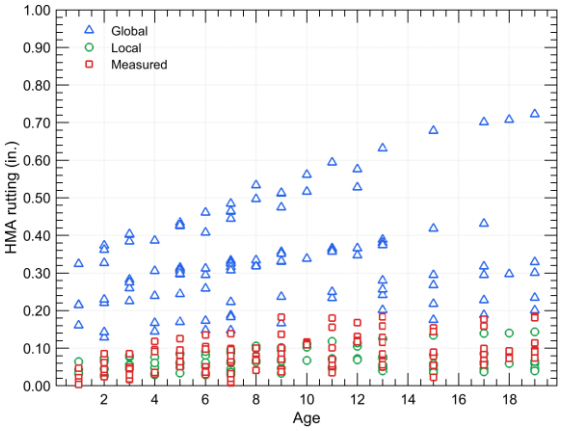


(c) Global model – base rut

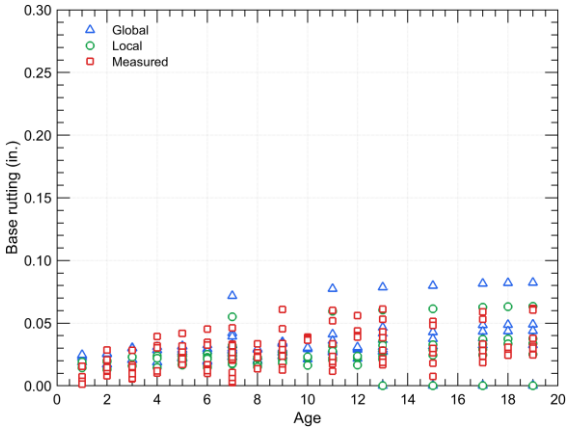


(d) Local model – base rut

Figure 7-35 Predicted vs. measured rutting for HMA over HMA (No sampling)



(a) AC rut



(b) Base rut

Figure 7-36 Individual layers rutting time series for HMA over HMA

Table 7-53 Hypothesis testing results of rutting models for HMA over HMA

Layer	t-test *p*-value (G)	Intercept *p*-value (G)	Slope = 1 *p*-value (G)	t-test *p*-value (L)	Intercept *p*-value (L)	Slope = 1 *p*-value (L)
HMA rut	0.000	0.000	0.000	0.064	0.000	0.000
Base rut	0.000	0.000	0.000	0.112	0.000	0.000
Subgrade	-	-	-	-	-	-

G = Global; L = Local

Table 7-54 Calibration summary results for HAM over HMA (No sampling)

Layer	Global model SEE (in.)	Global model Bias (in.)	Local model SEE (in.)	Local model Bias (in.)
HMA rut	0.316	0.279	0.050	-0.008
Base rut	0.022	0.005	0.020	-0.002
Subgrade	-	-	-	-
Parameters	Global Model	Global Model	Local Model	Local Model
HMA rutting (br1)	0.4	0.4	0.081	0.081
Base rutting (bs1)	1.0	1.0	0.780	0.780
Subgrade rutting (bsg1)	1.0	1.0	1.000	1.000

Bootstrapping

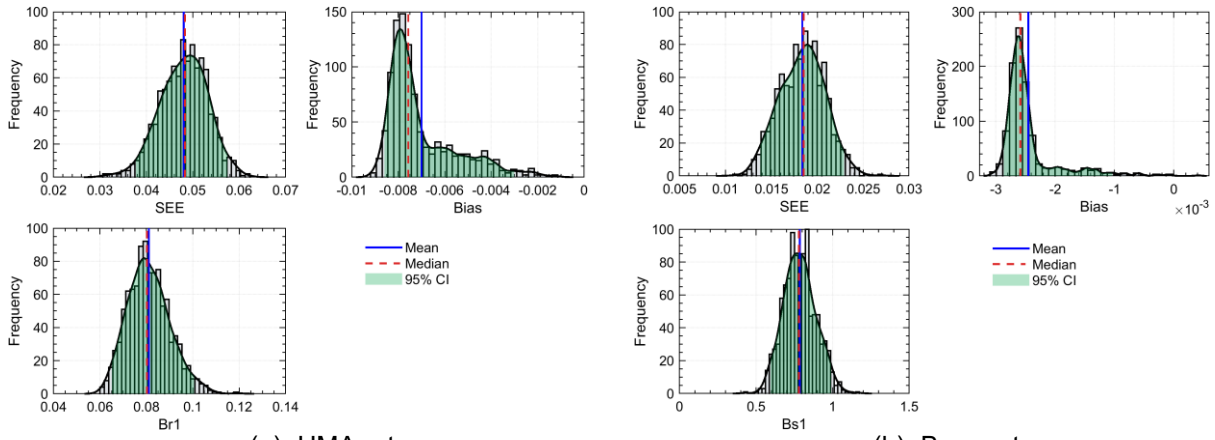
The team applied bootstrapping as described earlier. Tables 7-55 and 7-56 summarize the calibration results for the global and locally calibrated models, while Figure 7-37 shows the parameter distributions and corresponding confidence intervals for the calibrated coefficients.

Table 7-55 Global rutting model for HMA over HMA (bootstrapping)

Layer type	Average SEE	SEE Lower CI	SEE Upper CI	Average bias (in.)	Bias Lower CI	Bias Upper CI
HMA	0.314	0.314	0.252	0.280	0.277	0.225
Base	0.021	0.021	0.015	0.004	0.004	-0.002
Subgrade	-	-	-	-	-	-

Table 7-56 Local rutting model for HAM over HMA (bootstrapping)

Statistics	HMA rutting	Base rutting	Subgrade rutting
Average SEE (in.)	0.048	0.018	-
SEE Lower CI	0.038	0.014	-
SEE Upper CI	0.058	0.023	-
Average bias (in.)	-0.007	-0.002	-
Bias Lower CI	-0.009	-0.003	-
Bias Upper CI	-0.003	-0.001	-
Average calibration coefficient	0.081	0.785	-
Calibration coefficient Lower CI	0.065	0.588	-
Calibration coefficient Upper CI	0.101	0.994	-



(a) HMA rut (b) Base rut

Figure 7-37 Distribution of calibration parameters of the rutting model (Bootstrapping)

Method 2 – Total Rutting Calibration

In this method, the team calibrated the measured total rutting against the sum of the predicted rutting from all layers. The calibration coefficients for each layer were adjusted simultaneously to align the total predicted rutting with the measured values.

No Sampling

Tables 7-57 and 7-58 present the hypothesis-testing and calibration results for the global and local models with no sampling. Figure 7-38 shows the predicted vs. measured total rutting for the global and local models with no sampling, along with their comparison over time.

Table 7-57 Hypothesis testing results for the total rutting of HMA over HMA

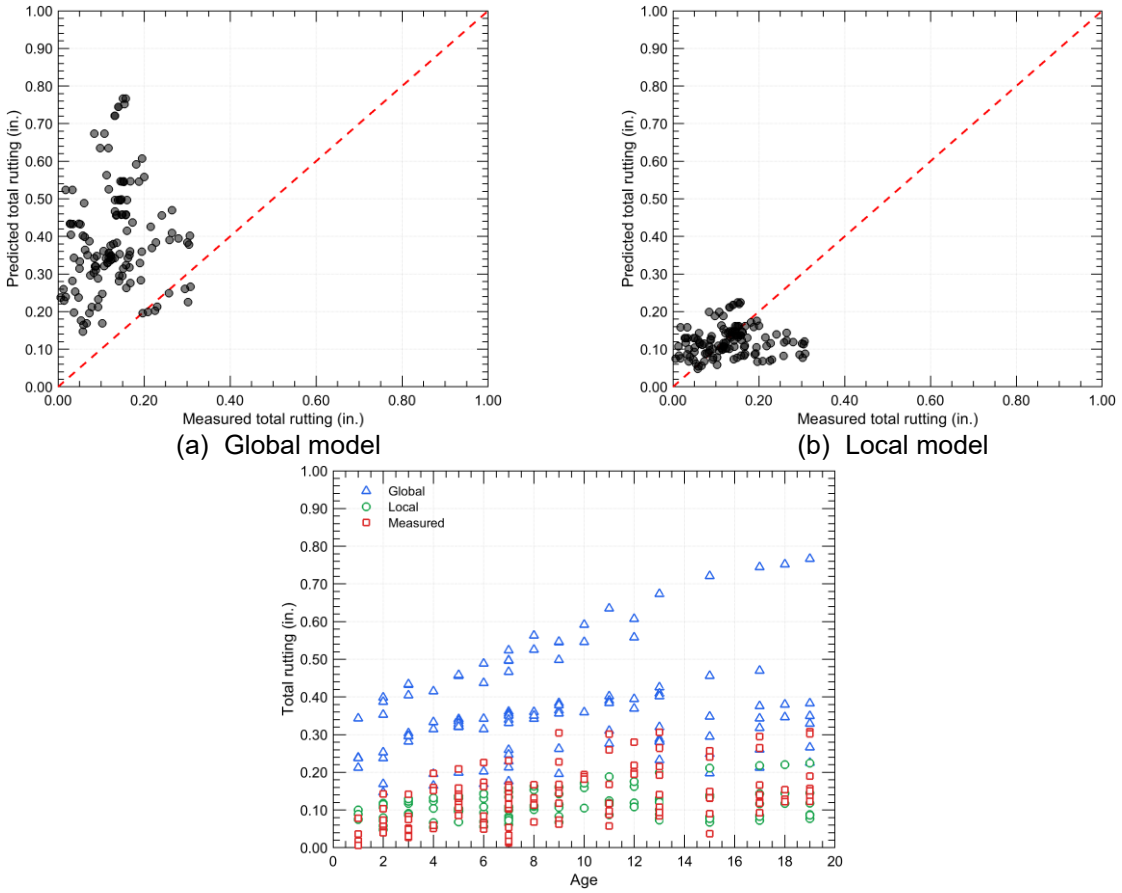
Layer	Global model	Local model
t-test p-value	0.000	0.125
Intercept p-value	0.000	0.000
Slope = 1 p-value	0.000	0.000

Table 7-58 Total rutting model calibration results for HMA over HMA

Parameters	Global model	Local model
SEE	0.304	0.079
Bias	0.261	-0.011
HMA rutting (br1)	0.400	0.104
Base rutting (bs1)	1.000	0.811
Subgrade rutting (bsg1)	1.000	1.000

Bootstrapping

Tables 7-59 and 7-60 summarize the global and local models, respectively, using bootstrapping. Figure 7-39 shows the distribution of calibration parameters.



(a) Global model (b) Local model

(c) Time series

Figure 7-38 Predicted vs measured total rutting of HMA over HMA (No sampling)

Table 7-59 Global model summary for total rutting of HMA over HMA (bootstrapping)

Parameter	Global model mean	Global model median	Global model lower CI	Global model upper CI
SEE (in)	0.328	0.328	0.105	0.157
Bias (in.)	0.286	0.285	0.229	0.348
br1	0.400	0.400	-	-
bs1	1.000	1.000	-	-
bsg1	1.000	1.000	-	-

Table 7-60 Local calibration for total rutting of HAM over HMA (bootstrapping)

Parameter	Local model mean	Local model median	Local model lower CI	Local model upper CI
SEE (in.)	0.080	0.080	0.026	0.037
Bias (in.)	-0.007	-0.008	-0.011	0.000
br1	0.082	0.082	0.141	0.284
bs1	0.691	0.693	0.461	0.932
bsg1	1.002	0.990	0.990	1.100

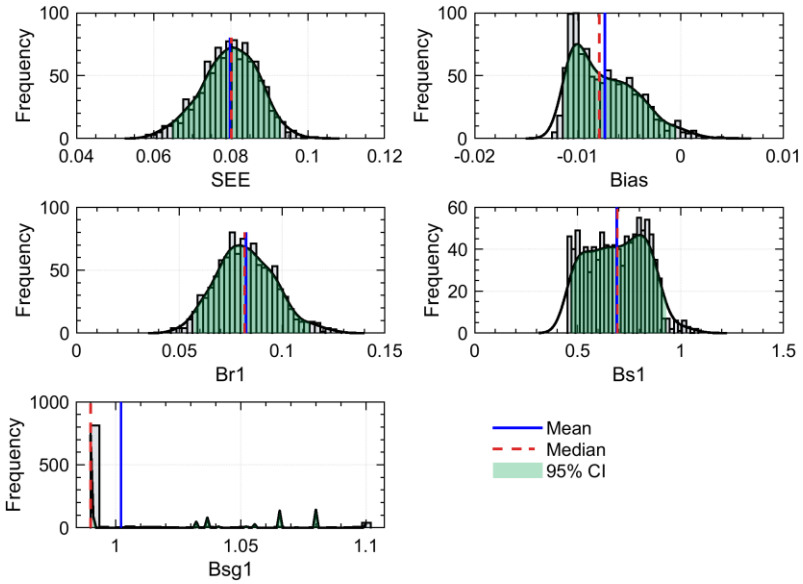


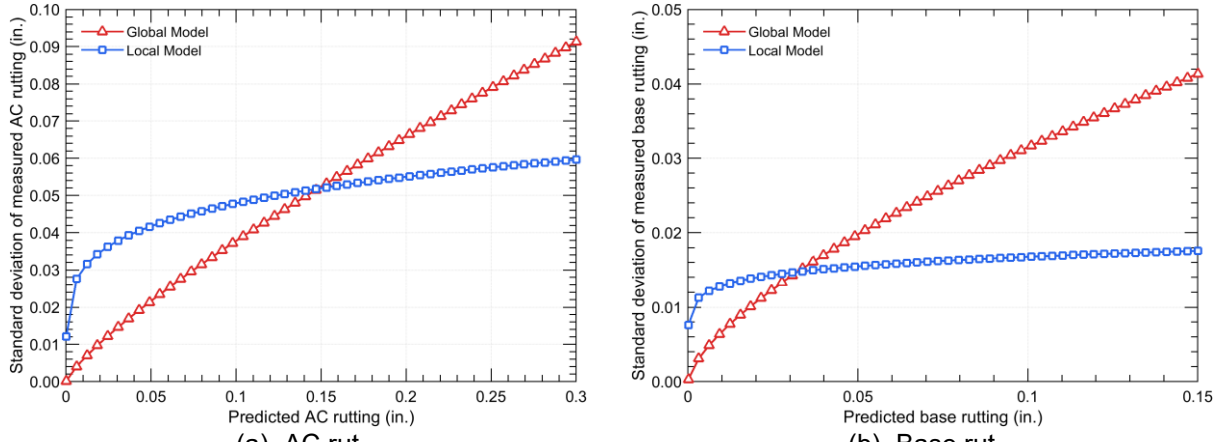
Figure 7-39 Distribution of calibration parameters - total rutting (bootstrapping)

Reliability for the rutting model

The team developed standard-error equations for AC and base-rutting models only. Since the subgrade model was not calibrated, the global standard error equation was adopted. Table 7-61 lists the equations for individual layers, and Figure 7-40 compares the reliability of global and local models.

Table 7-61 SE equations of rutting models for HMA over HMA

Layer	Global model	Local model
HMA	$s_{e(HMA)} = 0.24(Rut_{HMA})^{0.8026} + 0.001$	$s_{e(HMA)} = 0.099(Rut_{HMA})^{0.2314}$
Base	$s_{e(base)} = 0.1477(Rut_{base})^{0.6711} + 0.001$	$s_{e(base)} = 0.0293(Rut_{base})^{0.1802}$
Subgrade	$s_{e(subgrade)} = 0.1235\left(Rut_{subgrade}\right)^{0.5012} + 0.001$	$s_{e(subgrade)} = 0.1235\left(Rut_{subgrade}\right)^{0.5012} + 0.001$

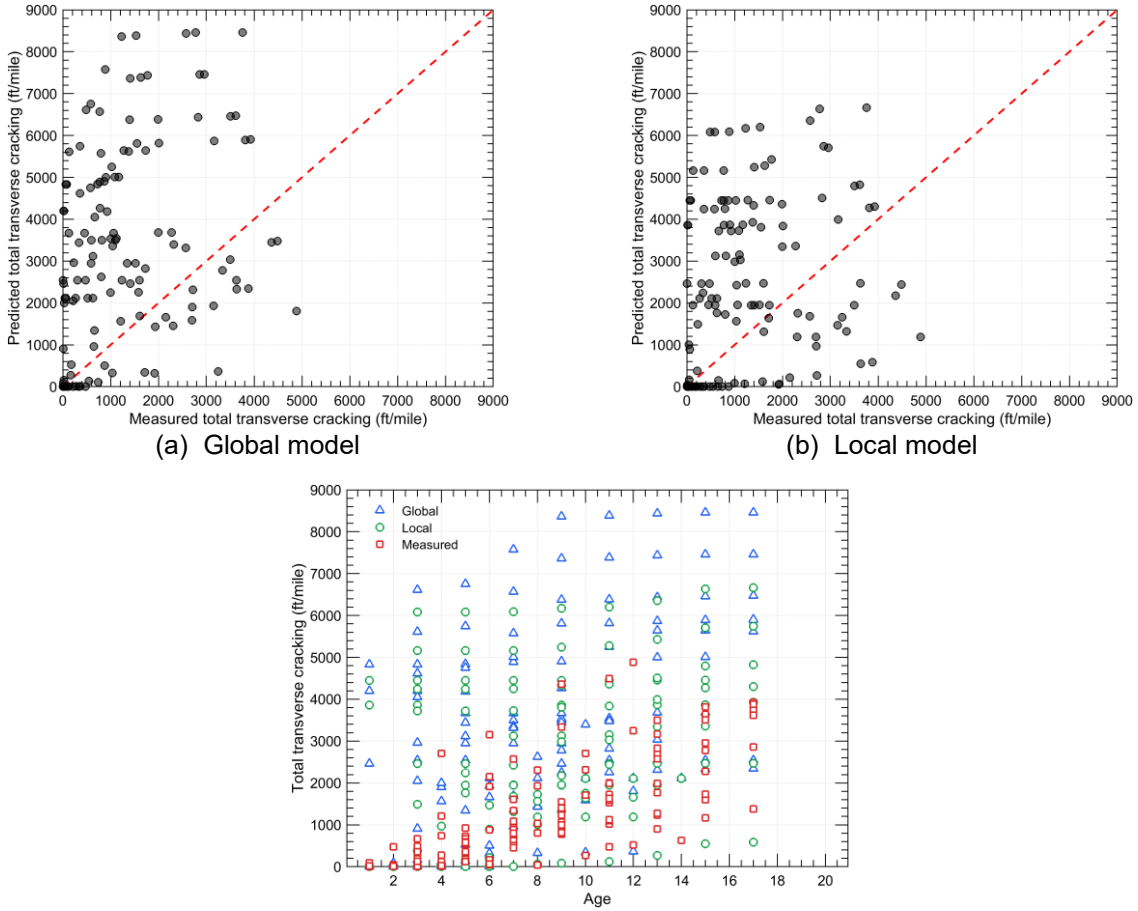


(a) AC rut (b) Base rut

Figure 7-40 SE comparison for HMA over HMA

7.2.3.5. Total Transverse (Thermal + Reflective) Cracking Model

Due to the difficulty of isolating thermal and reflective cracking in MDOT PMS data, the analysis treated all transverse cracking as a combined distress. The research team used the CAT tool to sequentially calibrate the thermal and reflective cracking coefficients for 22 in-service pavement sections. The thermal coefficient Kt was calibrated first, followed by paired calibration of the four reflective cracking coefficients. The coefficients C1 to C3 representing bending, shear, and thermal fracture mechanisms were constrained within narrow bounds of their global values because these parameters are derived from the ANN-based mechanistic framework. Figure 7-41 illustrates the measured versus predicted transverse cracking and their temporal comparison, while Table 7-62 summarizes the resulting global and local calibration parameters.



(a) Global model (b) Local model

(c) Time series

Figure 7-41 Predicted vs. measured total transverse cracking for HMA over HMA

Reliability for the total transverse cracking model

The team developed standard-error equations using the standard deviation of the measured data and the mean predicted cracking to incorporate reliability. Table 7-63 lists the equations, and Figure 7-42 compares the reliability of global and local models.

Table 7-62 Total transverse cracking results for HMA over HMA

Parameters	Global model	Local model
SEE	3058.6	2363.3
Bias	2061.6	1127.9
k	((3 * Pow(10,-7)) * Pow(MAAT,4.0319)) * 1 + 0	((3 * Pow(10,-7)) * Pow(MAAT,4.0319)) * 0.73
C1	3.22	2.65
C2	25.7	24.2
C3	0.1	0.05
C4	133.4	145
C5	-72.4	-72.4

Table 7-63 SE equations of the total transverse cracking for HMA over HMA

Global model	Local model
$S_{e(Transverse)} = 70.98(Transverse)^{0.2994} + 30.12$	$S_{e(Transverse)} = 69.54(Transverse)^{0.271} + 32.54$

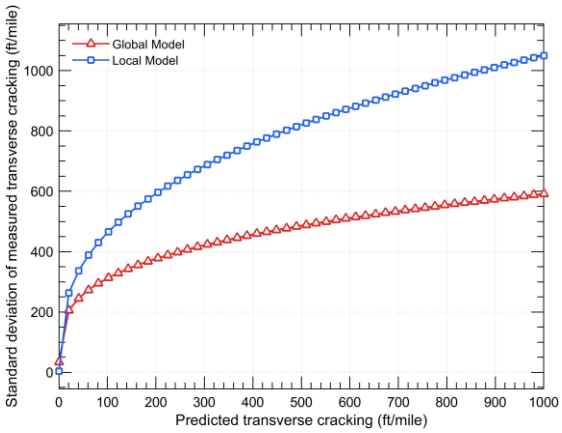


Figure 7-42 SE of the total transverse cracking for HMA over HMA

7.2.3.6. IRI Model for HMA over HMA Pavements

The IRI model represents a linear function of initial IRI, rut depth, total fatigue cracking, total transverse cracking, and site factor. The team calibrated the IRI model by local calibration of the total fatigue, total transverse cracking, and rutting models using 26 HMA overlay sections over HMA pavements.

No Sampling

Tables 7-64 and 7-65 present the hypothesis test results and summarize the calibrated parameters for the IRI model, respectively. The local calibration achieved notable

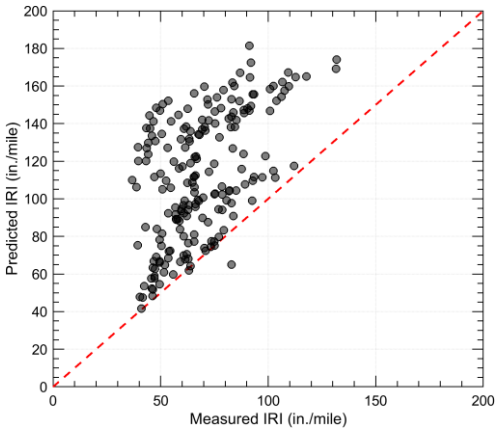
reductions in SEE and bias. Figure 7-43 shows the predicted and measured IRI, along with their temporal variations.

Table 7-64 IRI model hypothesis testing results

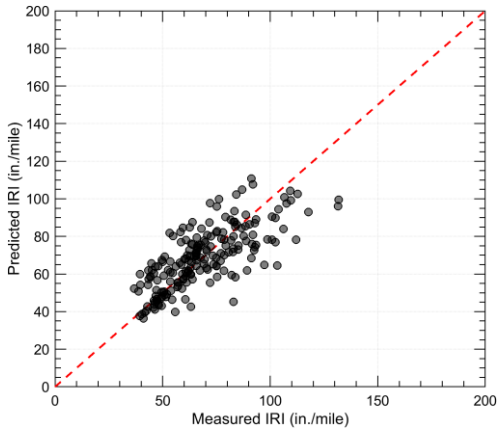
Layer	Global model	Local model
t-test p-value	0.000	1.0000
Intercept p-value	0.000	0.0000
Slope = 1 p-value	0.000	0.0000

Table 7-65 IRI model calibration results (No sampling)

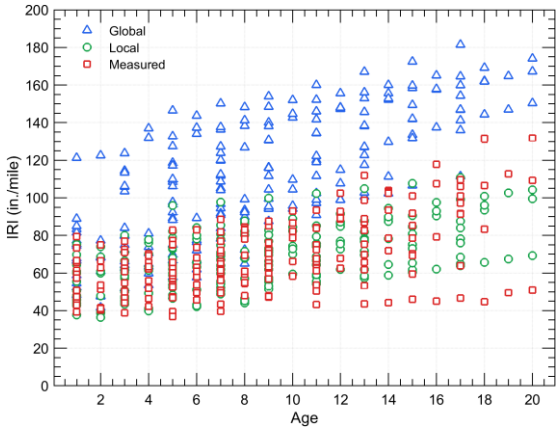
Model coefficient	Global model	Local model
SEE	52.023	13.080
Bias	43.378	0.000
C1	40.000	27.321
C2	0.4000	0.055
C3	0.0080	0.002
C4	0.0150	0.013



(a) Global model



(b) Local model



(c) Time series

Figure 7-43 Measured vs predicted IRI for HMA over HMA

Bootstrapping

Tables 7-66 and 7-67 summarize the global and local models, respectively, using bootstrapping. Figure 7-44 shows the distribution of calibration parameters.

Table 7-66 Global model summary for IRI of HMA over HMA (bootstrapping)

Parameter	Global model mean	Global model median	Global model lower CI	Global model upper CI
SEE (in)	51.811	51.832	41.338	60.519
Bias (in.)	43.389	43.162	33.093	53.535
C1	40.000	40.000	-	-
C2	0.400	0.400	-	-
C3	0.008	0.008	-	-
C4	0.015	0.015	-	-

Table 7-67 Local calibration summary for IRI of HMA over HMA (bootstrapping)

Parameter	Local model mean	Local model median	Local model lower CI	Local model upper CI
SEE (in.)	12.767	12.460	9.537	16.087
Bias (in.)	0.431	0.000	-0.443	2.591
C1	28.200	27.148	25.000	35.000
C2	0.050	0.012	0.009	0.393
C3	0.002	0.001	0.001	0.005
C4	0.016	0.017	0.003	0.027

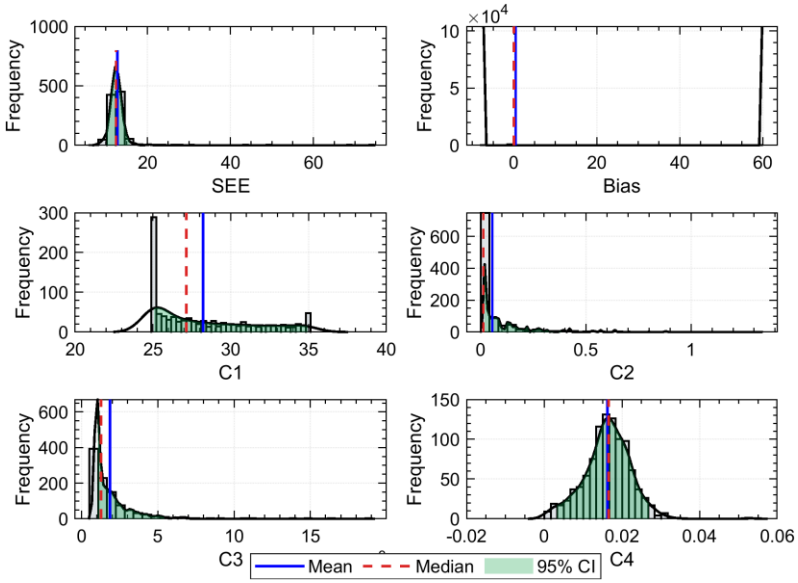


Figure 7-44 Distribution of parameters of the IRI model for HMA over HMA

7.2.3.7. Summary for HMA Overlay over Existing HMA Pavements

The team adopted the bootstrapped calibration coefficients as the final set for implementation. Tables 7-68 and 7-69 summarize the selected coefficients for all

performance models and the corresponding standard error equations used in reliability evaluation.

Table 7-68 Summary coefficients for HMA over HMA

Performance prediction model	Performance models and transfer functions	Local model
Fatigue cracking (Bottom-up)	$FC_{Bottom} = \left(\frac{1}{60}\right)\left(\frac{6000}{1 + e^{C_1 C_1^* + C_2 C_2^* Log(DI_{Bottom}*100)}}\right)$	$C_1 = 0.232$ $C_2 = 0.6998$ (hac <5 in) $C_2 = (0.867 + 0.2583 * hac) * 0.2204$ (5 in <= hac <=12 in) $C_2 = 0.8742$ (hac >12 in)
Fatigue cracking (top-down)	$t_0 = \frac{\mathrm{K}_{L1}}{1 + e^{\mathrm{K}_{L2}\times 100\times(\mathrm{a}_0/2\mathrm{A}_0)+\mathrm{K}_{L3}\times \mathrm{HT}+\mathrm{K}_{L4}\times LT+K_{L5}\times \log_{10}\ \mathrm{AADTT}}}$ $FC_{Top} = \mathrm{Lmax} \times \mathrm{e}^{-(\frac{C_1\rho}{t-C_3 to})^{C_2\beta}}$	$C_1 = 0.087$ $C_2 = 2.019$ $\mathrm{K}_{L2} = 1.236$ $\mathrm{K}_{L3} = 0.103$ $\mathrm{K}_{L4} = 0.175$ $\mathrm{K}_{L5} = 0.172$
Total Fatigue (Bottom-up+ Reflective Cracking)	$\Delta D = \frac{C_1 k_1 \Delta_{bending} + C_2 k_2 \Delta_{shearing} + C_3 k_3 \Delta_{thermal}}{h_{OL}}$ $RCR = \left(\frac{100}{C4 + e^{c5 log\, D}}\right) * EXCRK$	$C_1 = 0.24, C_2 = 1.1$ $C_3 = 2.1, C_4 = 140$
HMA Rutting	$\Delta_{\mathrm{p(HMA)}} = \varepsilon_{p(HMA)} h_{HMA} = \beta_{1r} k_z \varepsilon_{r(HMA)} 10^{k_{1r}} n^{k_{2r}\beta_{2r}} T^{k_{3r}\beta_{3r}}$	$\beta_{1r} = 0.082$ $\beta_{2r} = 0.70$ $\beta_{3r} = 1.30$
Base/subgrade Rutting	$\Delta_{p(soil)} = \beta_{s1} k_{s1} \varepsilon_v h_{soil} \left(\frac{\varepsilon_o}{\varepsilon_r}\right) e^{-\left(\frac{\rho}{n}\right)^{\beta}}$	$\beta_{s1} = 0.69$ $\beta_{sg1} = 1.0$
Thermal Fracture - L1	Level 1 K (MAAT <= 57 deg F) $A = 10^{k_t \beta_t (4.389 - 2.52 Log(E_{HMA} \sigma_m \eta))}$	((3 * Pow(10,-7)) * Pow(MAAT,4.0319)) * 0.73
Thermal Fracture - L1	Level 1 K (MAAT > 57 deg F)	(0.13 * Pow(MAAT,2) - 11.68 * MAAT + 244.14) * 1 + 0
Thermal Fracture - L2	Level 2 K (MAAT <= 57 deg F)	((3 * Pow(10,-7)) * Pow(MAAT,4.0319)) * 1 + 0
Thermal Fracture - L2	Level 2 K (MAAT > 57 deg F)	(0.13 * Pow(MAAT,2) - 11.68 * MAAT + 244.14) * 1 + 0
Thermal Fracture - L3	Level 3 K (MAAT <= 57 deg F)	((3 * Pow(10,-7)) * Pow(MAAT,4.0319)) * 1 + 0
Thermal Fracture - L3	Level 3 K (MAAT > 57 deg F)	(0.13 * Pow(MAAT,2) - 11.68 * MAAT + 244.14) * 1 + 0
Transverse Reflective cracking	$\Delta D = \frac{C_1 k_1 \Delta_{bending} + C_2 k_2 \Delta_{shearing} + C_3 k_3 \Delta_{thermal}}{h_{OL}}$ $RCR = \left(\frac{100}{C4 + e^{c5 log\, D}}\right) * EXCRK$	$C_1 = 2.65, C_2 = 24.2$ $C_3 = 0.05, C_4 = 145$
IRI	$IRI = IRI_o + C_1(RD) + C_2(FC_{Total}) + C_3(TC) + C_4(SF)$	$C_1 = 28.2,$ $C_2 = 0.05$ $C_3 = 0.002,$ $C_4 = 0.016$

Table 7-69 SE equations for HMA over HMA

Performance prediction model	Global model	Local model
Fatigue cracking (bottom-up only)	$S_{e(Alligator)} = 1.13 + \frac{13}{1+\exp(7.57-15.5\log(Crack+0.0001))}$	$S_{e(Alligator)} = 0.2262 + \frac{14.2349}{1+\exp(0.2958-0.1441\log(Crack))}$
Fatigue cracking (top-down)	$S_{e(Top-down)} = 0.3657 \times TOP + 3.6563$	$S_{e(Top-down)} = 0.2845 \times TOP + 1.1414$
Total Fatigue + Reflective Cracking	$S_{e(Fatigue+reflective)} = 1.1097(Fatigue)^{0.6804} + 1.23$	$S_{e(Fatigue+reflective)} = 1.065(Fatigue)^{0.482} + 1.11$
HMA Rutting	$S_{e(HMA)} = 0.24(Rut_{HMA})^{0.8026} + 0.001$	$S_{e(HMA)} = 0.099(Rut_{HMA})^{0.2314}$
Base Rutting	$S_{e(base)} = 0.1477(Rut_{base})^{0.6711} + 0.001$	$S_{e(base)} = 0.0293(Rut_{base})^{0.1802}$
Subgrade Rutting	$S_{e(subgrade)} = 0.1235(Rut_{subgrade})^{0.5012} + 0.001$	$S_{e(subgrade)} = 0.1235(Rut_{subgrade})^{0.5012} + 0.001$
Thermal + Reflective cracking	$S_{e(Transverse)} = 70.98(Transverse)^{0.2994} + 30.12$	$S_{e(Transverse)} = 69.54(Transverse)^{0.271} + 32.54$
IRI	Internally calculated by PMED	

7.2.4 HMA Overlays of PCC/Composite Pavements

This section presents the calibration results for HMA overlays placed over existing JPCP and composite pavements (AC over JPCP) using locally calibrated PMED performance prediction models. Since PMED v2.6 does not allow multiple existing layers, the team modeled all composite pavement sections as HMA overlays over JPCP. For these sections, the existing AC layer was modeled as a new HMA layer with a degraded modulus, following the methodology described in Chapter 5.

The calibration included all relevant distress models for this fix type except the JPCP transverse cracking model. Since transverse cracking in the underlying JPCP primarily drives reflective cracking in the overlay, the model was deemed non-critical once the pavement was overlaid and the concrete surface was no longer exposed. Its effects were inherently captured in the total transverse cracking model, as verified by the sensitivity analyses presented in Chapter 5. In coordination with MDOT, the team adopted the JPCP transverse cracking coefficients from the 2023 calibration of new and reconstructed JPCP sections to maintain consistency across models.

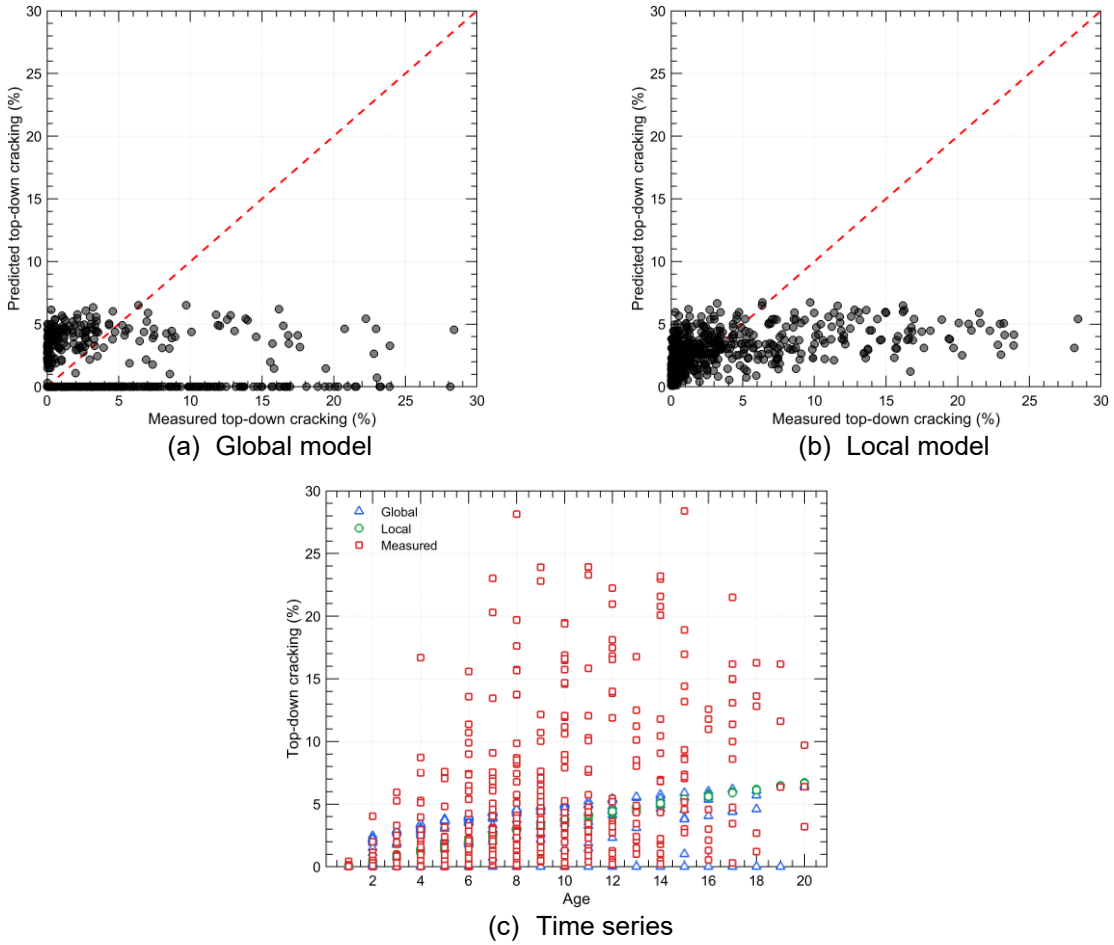
7.2.4.1. Fatigue Cracking Model – Bottom-up

PMED does not predict bottom-up fatigue cracking for composite pavements, as the software primarily considers the structural behavior of the concrete layer beneath the

HMA overlay. The bottom-up fatigue cracking model was not calibrated for composite pavements.

7.2.4.2. Fatigue Cracking Model – Top-down

The calibration procedure for the top-down cracking model followed the same approach discussed earlier, using 116 sections. The team calibrated the combined crack initiation and propagation function in Microsoft Excel, adopting a no-sampling technique. Figure 7-45 shows the predicted versus measured top-down cracking for the global and locally calibrated models, along with their comparison over time. Table 7-70 presents the calibration results.



(a) Global model (b) Local model

(c) Time series

Figure 7-45 Measured and predicted top-down-cracking for HMA over PCC

Table 7-70 Calibration results of the top-down cracking model for HMA over PCC

Parameters	Global model	Local model
SEE	7.210	5.520
Bias	-3.090	-0.710
K_{L2}	0.286	0.475
K_{L3}	0.011	0.097
K_{L4}	0.015	0.104
K_{L5}	3.266	0.206
C_1	2.522	0.132
C_2	0.807	1.635

Reliability for the top-down cracking model

Table 7-71 presents the standard-error equations for global and local top-down cracking models. Figure 7-46 shows the reliability comparison of global and local models.

Table 7-71 SE equation of the top-down cracking model for HMA over PCC

Global model equation	Local model equation
$S_{e(Top-down)} = 0.3657 \times TOP + 3.6563$	$S_{e(Top-down)} = 0.5249 \times TOP + 1.7406$

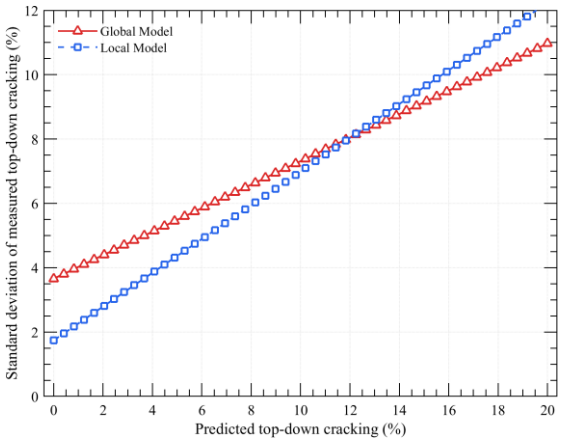


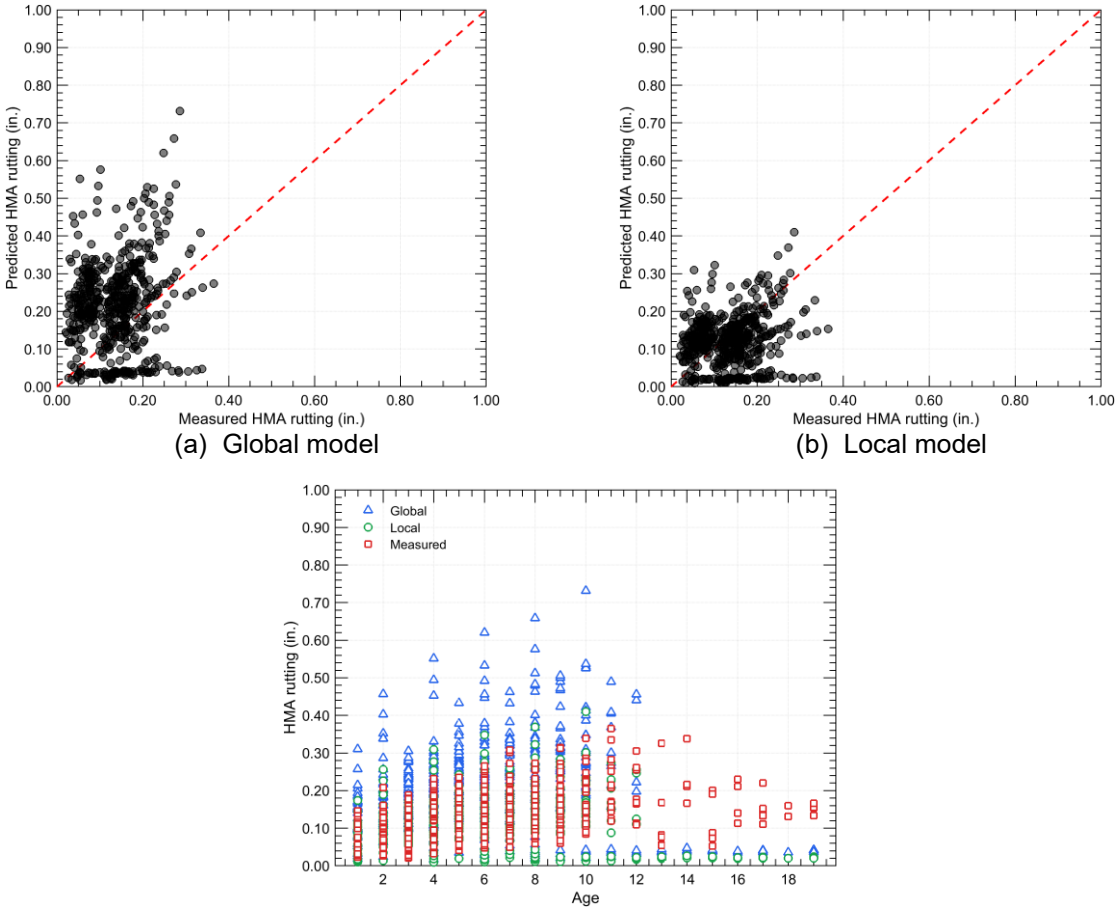
Figure 7-46 SE of the top-down cracking model for HMA over PCC

7.2.4.3. Rutting Model

It is important to note that due to the high stiffness of the underlying concrete layer, PMED does not predict rutting in the base or subgrade for composite sections. Therefore, the calibration for these sections was limited to HMA layer rutting, which was directly compared against the measured surface rutting. A total of 132 HMA over JPCP sections were used for this calibration.

No Sampling

Figure 7-47 shows the predicted vs. measured HMA rutting for the global and local models with no sampling, along with their comparison over time. Tables 7-72 and 7-73 present the hypothesis-testing and calibration results for the global and local models with no sampling.



(a) Global model (b) Local model

(c) Time series

Figure 7-47 Predicted vs measured HMA rutting for HMA over PCC (No sampling)

Table 7-72 Hypothesis testing results of HMA rutting for HMA over PCC

Layer	Global model	Local model
t-test p-value	0.000	0.012
Intercept p-value	0.000	0.000
Slope = 1 p-value	0.000	0.000

Table 7-73 HMA rutting model calibration results for HMA over PCC

Parameters	Global model	Local model
SEE	0.151	0.085
Bias	0.082	-0.01
HMA rutting (br1)	0.400	0.224

Bootstrapping

Tables 7-74 and 7-75 summarize the global and local models, respectively, using bootstrapping. Figure 7-48 shows the distribution of calibration parameters.

Table 7-74 Global model summary for total rutting of rubblized PCC (bootstrapping)

Parameter	Global model mean	Global model median	Global model lower CI	Global model upper CI
SEE (in)	0.151	0.150	0.135	0.167
Bias (in.)	0.082	0.082	0.061	0.103
br1	0.400	0.400	-	-

Table 7-75 Calibration summary for total rutting of rubblized PCC (bootstrapping)

Parameter	Local model mean	Local model median	Local model lower CI	Local model upper CI
SEE (in.)	0.087	0.087	0.076	0.100
Bias (in.)	-0.014	-0.014	-0.014	-0.013
br1	0.225	0.224	0.203	0.251

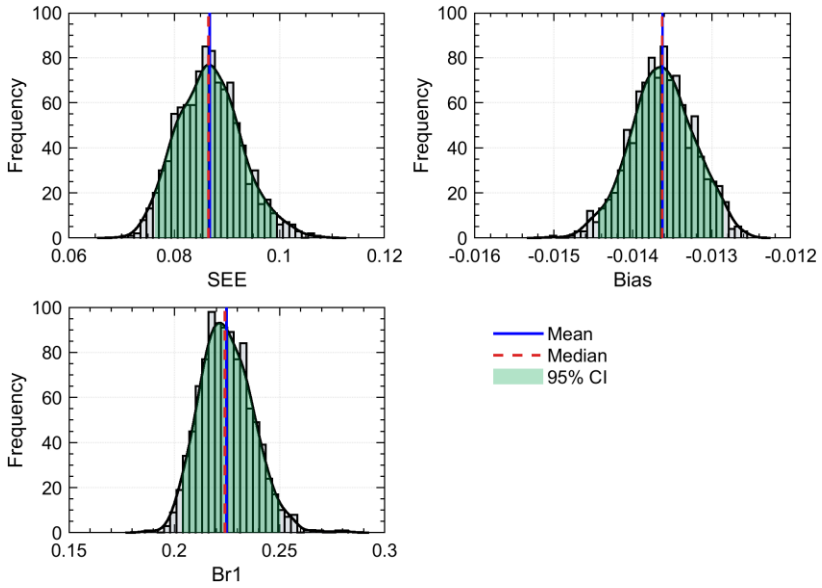


Figure 7-48 Distribution of calibration parameters of HMA rutting

Reliability for the rutting model

The team developed equations for the standard error of the relationship between the standard deviation of measured rutting and the mean predicted rutting, accounting for reliability. Since PMED predicts rutting only within the HMA layer for composite pavements, the standard error equations for the base and subgrade layers were retained at their global default values. Table 7-76 lists the equations for individual layers, and Figure 7-49 compares the reliability of global and local models.

Table 7-76 SE equations of rutting models for rubblized PCC

Layer	Global model	Local model
HMA	$s_{e(HMA)} = 0.24(Rut_{HMA})^{0.8026} + 0.001$	$s_{e(HMA)} = 0.088(Rut_{HMA})^{0.1728}$
Base	$s_{e(base)} = 0.1477(Rut_{base})^{0.6711} + 0.001$	$s_{e(base)} = 0.1477(Rut_{base})^{0.6711} + 0.001$
Subgrade	$s_{e(subgrade)} = 0.1235(Rut_{subgrade})^{0.5012} + 0.001$	$s_{e(subgrade)} = 0.1235(Rut_{subgrade})^{0.5012} + 0.001$

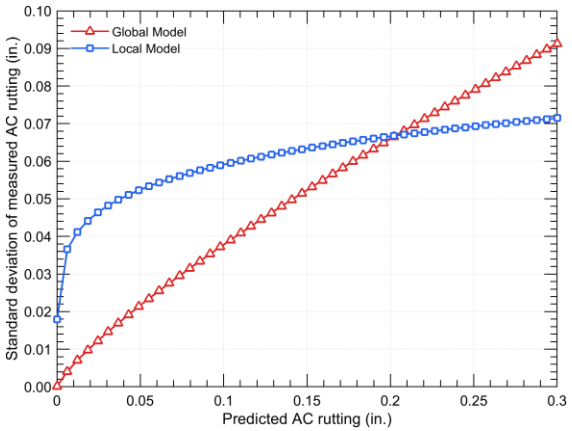


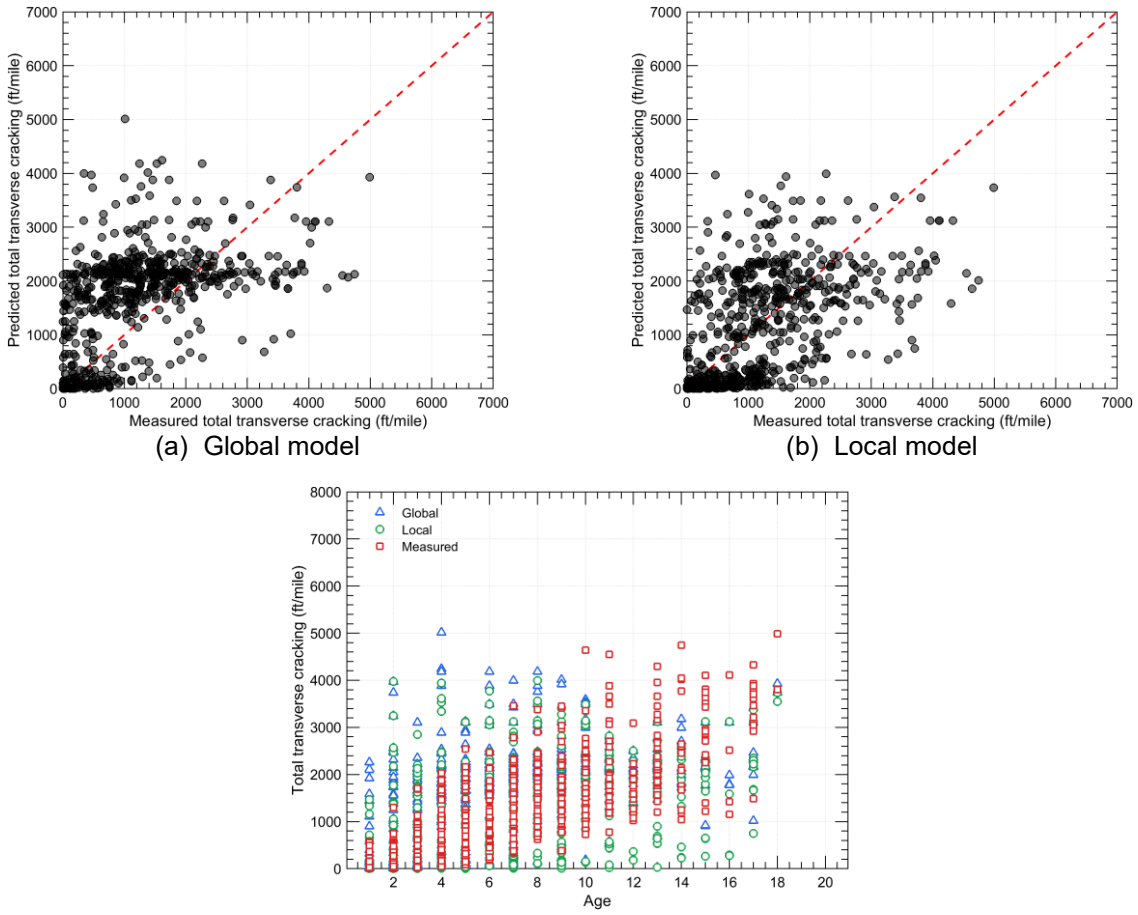
Figure 7-49 SE comparison of HMA rutting for HMA over PCC

7.2.4.4. Total Transverse (Thermal + Reflective) Cracking Model

In HMA overlays over PCC pavements, reflective cracking is a dominant distress mechanism due to underlying PCC slab joints. Accordingly, the calibration focused on accurately modeling the combined thermal and reflective cracking behavior. The team used the CAT tool to sequentially calibrate the thermal cracking coefficient Kt, followed by paired calibration of the four reflective cracking coefficients. A total of 120 sections were used to calibrate this model. The coefficients C1 to C3, corresponding to bending, shear, and thermal fracture mechanisms, were constrained to narrow bounds near their global values because these parameters are derived from the ANN-based mechanistic model. Table 7-77 presents the global and local calibration coefficients, and Figure 7-50 compares the measured and predicted transverse cracking progression over time.

Table 7-77 Total transverse cracking results for HMA over PCC

Parameters	Global model	Local model
SEE	1344.00	1120.00
Bias	596.50	-0.66
k	((3 * Pow(10,-7)) * Pow(MAAT,4.0319)) * 1 + 0	((3 * Pow(10,-7)) * Pow(MAAT,4.0319)) * 0.722
C1	0.10	0.05
C2	0.52	0.40
C3	3.10	2.00
C4	79.5	96.11
C5	-2.71	-2.71



(a) Global model (b) Local model

(c) Time series

Figure 7-50 Predicted vs. measured total transverse cracking for HMA over HMA

Reliability for the total transverse cracking model

The team developed standard-error equations using the standard deviation of the measured data and the mean predicted cracking to incorporate reliability. Table 7-78 lists the equations, and Figure 7-51 compares the reliability of global and local models.

Table 7-78 SE equations of the total transverse cracking for HMA over PCC

Global model	Local model
$s_{e(Transverse)} = 5.1025(Transverse)^{0.6513} + 30.12$	$s_{e(Transverse)} = 5.087(Transverse)^{0.571} + 92.5$

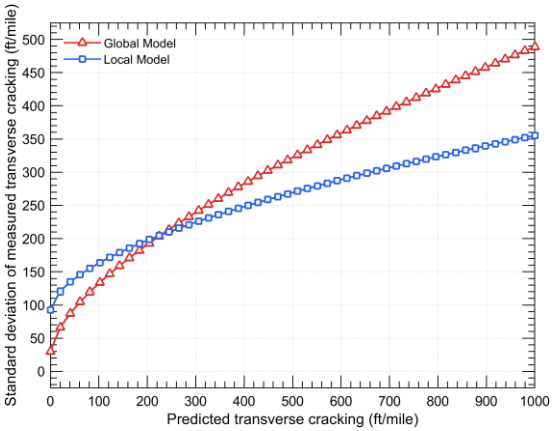


Figure 7-51 SE of the total transverse cracking for HMA over PCC

7.2.4.5. IRI Model for HMA over PCC/Composite Pavements

The IRI model represents a linear function of initial IRI, rut depth, total fatigue cracking, transverse cracking, and site factor. The team calibrated the IRI model using the local calibration of the fatigue, transverse cracking, and rutting models, based on 105 sections.

No Sampling

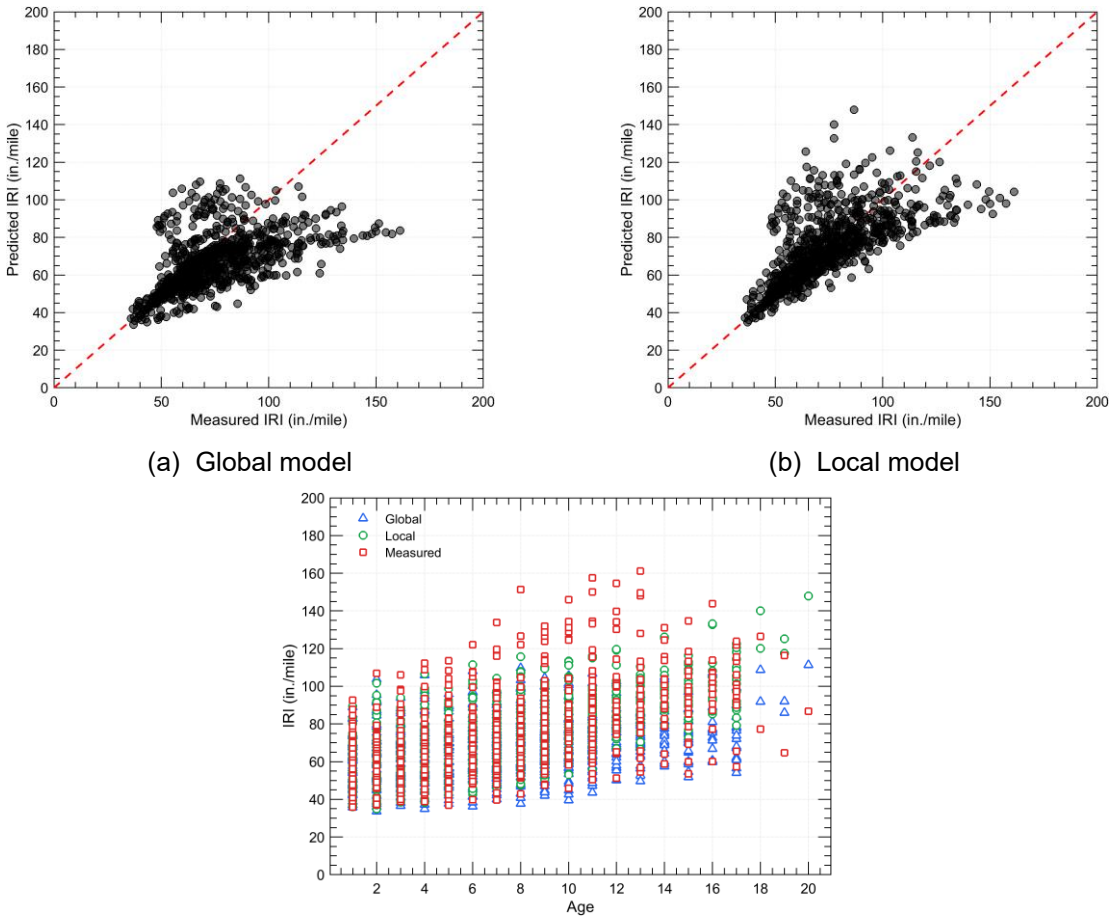
Tables 7-79 and 7-80 present the hypothesis test results and summarize the calibrated parameters for the IRI model, respectively. The local calibration achieved notable reductions in SEE and bias. Figure 7-52 shows the predicted versus measured IRI and their variation over time.

Table 7-79 IRI model hypothesis testing results for HMA over PCC

Layer	Global model	Local model
t-test p-value	0.000	1.000
Intercept p-value	0.000	0.000
Slope = 1 p-value	0.000	0.000

Table 7-80 IRI model calibration results for HMA over PCC (No sampling)

Model coefficient	Global model	Local model
SEE	19.613	16.709
Bias	1.166	0.000
C1	40.000	10.421
C2	0.575	0.0036
C3	0.0014	0.0022
C4	0.00825	0.0298



(a) Global model

(b) Local model

(c) Time series

Figure 7-52 Measured vs predicted IRI for HMA over PCC

Bootstrapping

Tables 7-81 and 7-82 summarize the global and local models, respectively, using bootstrapping. Figure 7-53 shows the distribution of calibration parameters.

Table 7-81 Global model summary for IRI of HMA over PCC (bootstrapping)

Parameter	Global model mean	Global model median	Global model lower CI	Global model upper CI
SEE (in)	19.774	19.744	16.844	22.854
Bias (in.)	1.074	1.068	-2.004	4.440
C1	40.800	40.800	-	-
C2	0.575	0.575	-	-
C3	0.001	0.001	-	-
C4	0.008	0.008	-	-

Table 7-82 Local calibration summary for IRI of HMA over PCC (bootstrapping)

Parameter	Local model mean	Local model median	Local model lower CI	Local model upper CI
SEE (in.)	16.814	16.796	13.981	19.708
Bias (in.)	-0.034	0.000	-0.362	0.000
C1	13.090	10.275	9.076	44.235
C2	0.140	0.190	0.000	0.220
C3	0.0024	0.002	0.002	0.005
C4	0.020	0.028	0.018	0.035

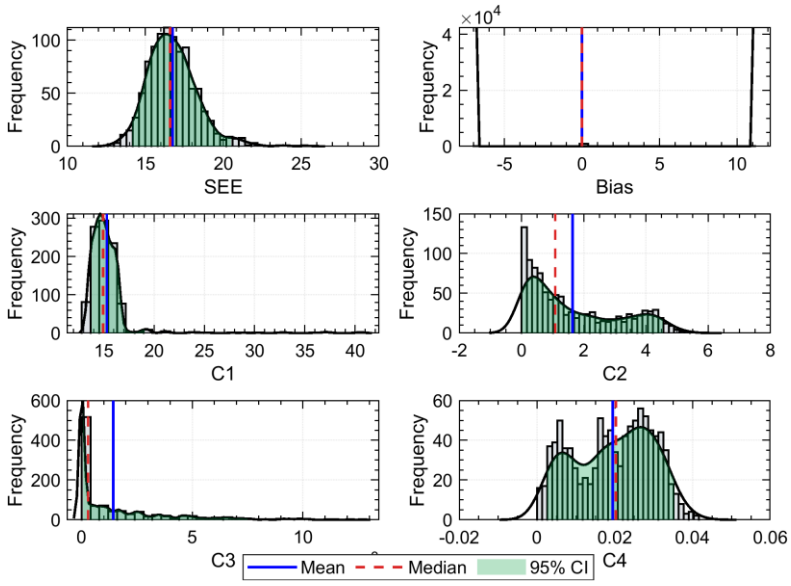


Figure 7-53 Parameters distribution of the IRI model for HMA over PCC

7.2.4.6. Summary for HMA Overlay over PCC/Composite Pavements

The team adopted the bootstrapped calibration coefficients as the final set for implementation. Tables 7-83 and 7-84 summarize the selected coefficients for all performance models and the corresponding standard error equations used in reliability evaluation.

Table 7-83 Summary coefficients for HMA overlay over PCC

Performance prediction model	Performance models and transfer functions	Local model
Fatigue cracking (bottom-up)	$FC_{Bottom} = \left(\frac{1}{60}\right)\left(\frac{6000}{1 + e^{C_1C_1^* + C_2C_2^* Log(DI_{Bottom}*100)}}\right)$	$C_1 = 0.232$ $C_2 = 0.6998$ (hac <5 in) $C_2 = (0.867 + 0.2583 * hac) * 0.2204$ (5 in <= hac <=12 in) $C_2 = 0.8742$ (hac >12 in)
Fatigue cracking (top-down)	$t_0 = \frac{\mathrm{K}_{L1}}{1 + e^{\mathrm{K}_{L2}\times 100\times(\mathrm{a}_0/2\mathrm{A}_0)+\mathrm{K}_{L3}\times \mathrm{HT}+\mathrm{K}_{L4}\times LT+K_{L5}\times \log_{10}\ \mathrm{AADTT}}}$ $FC_{Top} = \mathrm{Lmax} \times \mathrm{e}^{-(\frac{C_1\rho}{t-C_3to})^{C_2\beta}}$	$\mathrm{K}_{L2} = 0.475$ $\mathrm{K}_{L3} = 0.097$ $\mathrm{K}_{L4} = 0.104$ $\mathrm{K}_{L5} = 0.206$ $C_1 = 0.132$ $C_2 = 1.635$
HMA Rutting	$\Delta_{\mathrm{p(HMA)}} = \varepsilon_{p(HMA)} h_{HMA} = \beta_{1r} k_z \varepsilon_{r(HMA)} 10^{k_{1r}} \eta^{k_{2r}\beta_{2r}} T^{k_{3r}\beta_{3r}}$	$\beta_{1r} = 0.224$
Thermal + Reflective cracking	$A = 10^{k_t\beta_t(4.389 - 2.52Log(E_{HMA}\sigma_m\eta))}$ $\Delta D = \frac{C_1k_1\Delta_{bending} + C_2k_2\Delta_{shearing} + C_3k_3\Delta_{thermal}}{h_{OL}}$ $RCR = \left(\frac{100}{C4 + e^{c5 log\, D}}\right) * EXCRK$	$K = \left(3 * POW(10, -7)\right) * Pow(MAAT, 4.0319)) * 0.722$ $C_1 = 0.05,$ $C_2 = 0.40$ $C_3 = 2.0, C_4 = 96.11$
IRI	$IRI = IRI_o + C_1(RD) + C_2(FC_{Total}) + C_3(TC) + C_4(SF)$	$C_1 = 13.09,$ $C_2 = 0.14$ $C_3 = 0.0024,$ $C_4 = 0.020$
JPCP Transverse Cracking (*2*)	$CRK_{BU/TD} = \frac{100}{1 + C_4(DI_F)^{C_5}}$	$C_4 = 0.415,$ $C_5 = -0.965$

Table 7-84 SE equations for HMA overlay over PCC

Performance prediction model	Global model	Local model
Fatigue cracking (Bottom-up)	$S_{e(Alligator)} = 1.13 + \frac{13}{1 + \exp(7.57 - 15.5\log(D + 0.0001))}$	$S_{e(Alligator)} = 0.2262 + \frac{14.2349}{1 + \exp(0.2958 - 0.1441\log(D))}$
Fatigue cracking (top-down)	$S_{e(Top-down)} = 0.3657 \times TOP + 3.6563$	$S_{e(Top-down)} = 0.5249 \times TOP + 1.7406$
HMA Rutting	$S_{e(HMA)} = 0.24(Rut_{HMA})^{0.8026} + 0.001$	$S_{e(HMA)} = 0.088(Rut_{HMA})^{0.1728}$
Thermal + Reflective cracking	$S_{e(Transverse)} = 5.1025(Transverse)^{0.6513} + 30.12$	$S_{e(Transverse)} = 5.087(Transverse)^{0.571} + 92.5$
JPCP Transverse Cracking (*2*)	$S_{e(CRK)} = 2.9004(CRK)^{0.5074}$	$S_{e(CRK)} = 2.9004(CRK)^{0.5074}$
IRI	Internally calculated by PMED	

7.3 LOCAL CALIBRATION OF CONCRETE OVERLAYS

Concrete overlays are categorized as bonded or unbonded. A bonded overlay consists of a 2 to 8 in. concrete layer placed directly over an existing concrete pavement, ensuring full bond between the new and existing slabs. In contrast, an unbonded overlay consists of a 5 to 11 in. concrete layer, separated from the existing pavement by a 1 to 2 in. gap. HMA interlayer or other separator to prevent bonding and allow independent slab movement, thereby reducing reflective cracking (7, 8).

MDOT currently designs unbonded JPCP overlays 6 in. or thicker using the AASHTO 93 procedure. For thinner overlays, an HMA interlayer is often introduced and treated as unbonded, which deviates from the conventional practice and intended performance of true unbonded systems. This modeling assumption may cause inconsistencies in transverse cracking predictions within the PMED. As discussed in Chapter 5, the research team recommends avoiding the use of PMED for unbonded JPCP overlays thinner than 6.5 in. under these conditions.

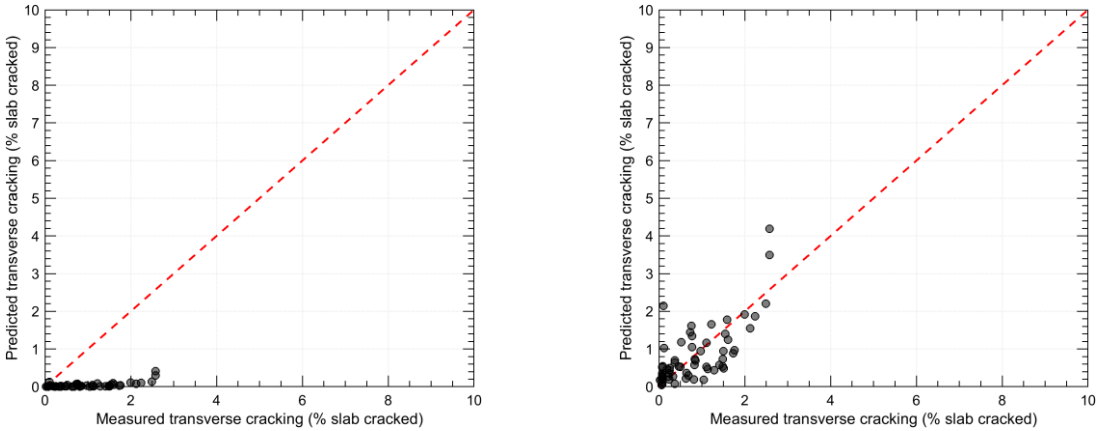
This section presents the local calibration of transverse cracking, joint faulting, and IRI models for unbonded overlays, based on data from 28 pavement sections. However, the limited number of available sections introduces inherent uncertainty in the calibration process and may affect the reliability of the resulting coefficients for design applications.

7.3.1 Transverse Cracking Model

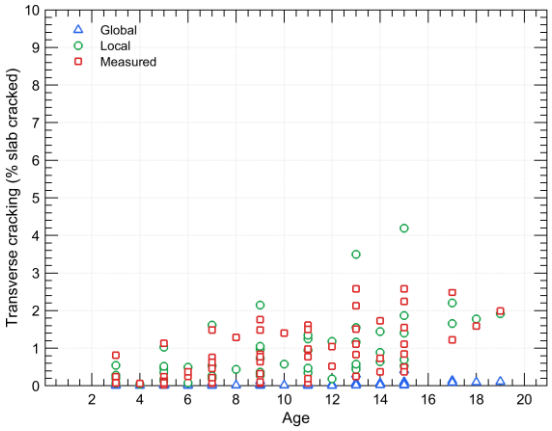
The transverse cracking model was calibrated by minimizing the error between measured and predicted cracking. The number of available unbonded overlay sections is fewer than the number of reconstructed JPCP sections used in the previous calibration study (*2*).

7.3.1.1. No Sampling

The no-sampling approach considered all available sections for calibration. Figure 7-54 shows the predicted versus measured transverse cracking for the global and locally calibrated models, along with their comparison over time. The global model underpredicts transverse cracking. Table 7-85 shows the hypothesis test results. The global model fails all tests, whereas the local model passes one. Table 7-86 shows the local calibration results. The SEE is reduced from 1.154 to 0.732, whereas the bias is reduced from -0.812 to -0.074. Although two out of three hypothesis tests were rejected, the SEE and bias values significantly improved.



(a) Global model (b) Local model



(c) Time series

Figure 7-54 Local calibration results of transverse cracking

Table 7-85 Global model hypothesis testing results

Hypothesis test	Global model	Local model
t-test p-value	0.000	0.399
Intercept p-value	0.346	0.000
Slope = 1 p-value	0.000	0.000

Table 7-86 Local calibration results using the entire dataset (No sampling)

Parameter	Global model	Local model
SEE (% slabs cracked)	1.154	0.732
Bias (% slabs cracked)	-0.812	-0.074
C_4	0.52	0.908
C_5	-2.17	-1.088

7.3.1.2. Bootstrapping

Bootstrapping was used to calibrate the transverse cracking model, with 1000 bootstrap samples with replacement. Tables 7-87 and 7-88 summarize the model parameters for global and local models, respectively. Figure 7-55 shows the distribution of SEE, bias,

and model coefficients. Bootstrap provides mean, median, and CI for the model parameters.

Table 7-87 Transverse cracking global model using bootstrapping for unbonded overlays

Parameter	Global Model Mean	Global Model Median	Global model lower CI	Global model upper CI
SEE	1.1404	1.1416	0.7950	1.4669
Bias	-0.8090	-0.8043	-1.1268	-0.5134
C4	0.5200	0.5200	-	-
C5	-2.1700	-2.1700	-	-

Table 7-88 Transverse cracking local model using bootstrapping for unbonded overlays

Parameter	Local Model Mean	Local Model Median	Local model lower CI	Local model upper CI
SEE (percent slabs cracked)	0.7208	0.7119	0.4591	1.0256
Bias (percent slabs cracked)	-0.1116	-0.1045	-0.2505	-0.0134
C4	0.5592	0.5724	0.1919	0.8701
C5	-1.2319	-1.2071	-1.4855	-1.0633

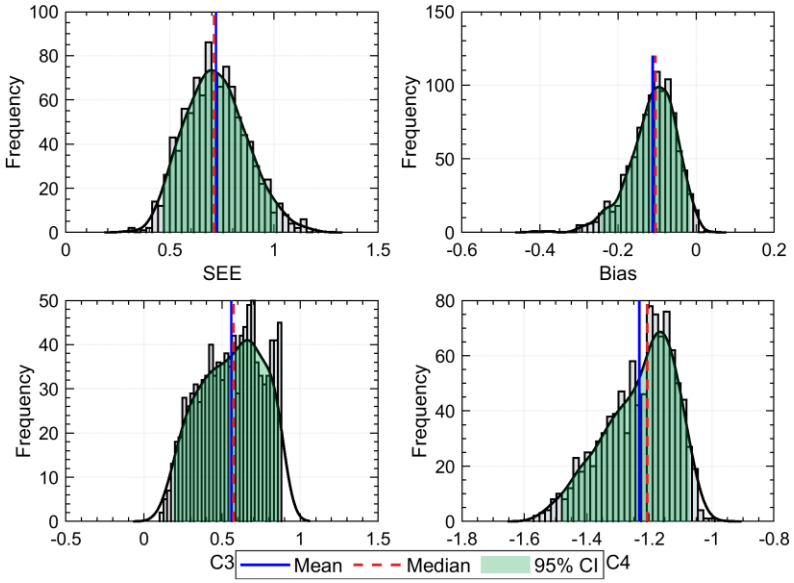


Figure 7-55: Bootstrap sampling calibration results for the transverse cracking model

7.3.1.3. Reliability for the transverse cracking model

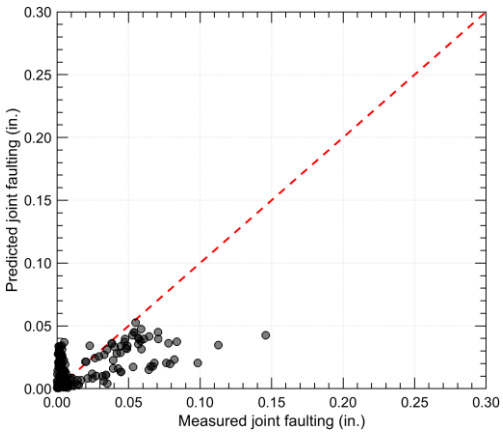
The team developed the SE equation for the calibrated cracking models to establish the relationship between the standard deviation of measured cracking and the mean predicted cracking, as explained in Chapter 6. These relationships are used to calculate the cracking for specific reliability. Table 7-89 summarizes the standard error equations for the global and local models.

Table 7-89 SE equations for transverse cracking

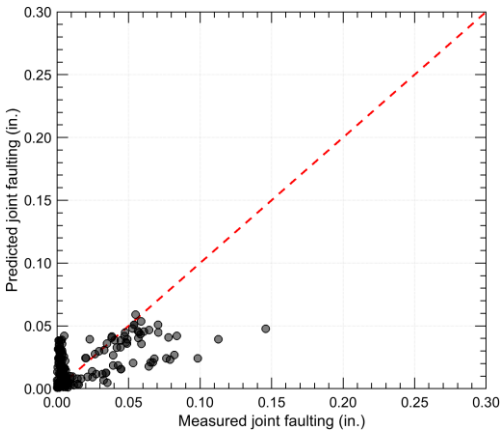
Global model equation	Local model equation
$S_{e(CRK)} = 3.5522(CRK)^{0.3415} + 0.75$	$S_{e(CRK)} = 0.6855(CRK)^{0.2987}$

7.3.2 Faulting Model

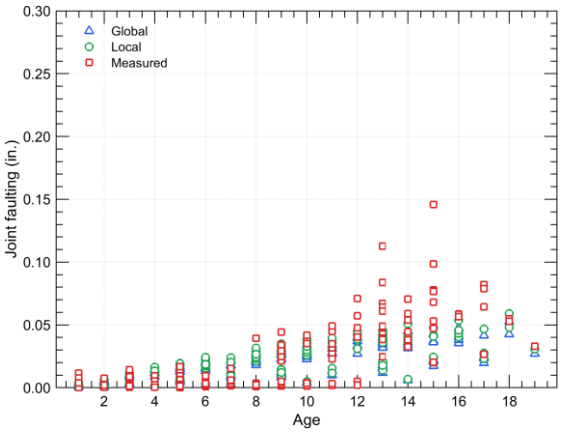
The research team used CAT, employing the no-sampling technique to calibrate the faulting model. The most sensitive coefficients, C1 and C6, were simultaneously calibrated in the initial step. Subsequently, while maintaining the calibrated values of C1 and C6, C2 was calibrated. The remaining coefficients (C3, C4, C5, C7, and C8) were not calibrated and retained at global values. Due to limited runtime and the number of coefficient combinations that could be calibrated simultaneously, it was not feasible to calibrate all coefficients at once. The measured faulting was cut to 0.4 inches, as mentioned in Chapter 4. This threshold means that any 0.1-mile section with mean faulting above 0.4 inches was removed from calibration. Figure 7-56 shows the predicted and measured joint faulting, along with their time-series comparison. Table 7-90 summarizes local calibration and the corresponding model parameters. SEE and bias are significantly improved.



(a) Global model



(b) Local model



(c) Time series

Figure 7-56 Calibration results of joint faulting for unbonded overlays

Table 7-90 Summary of faulting model calibration

Parameter	Global	Local
SEE	0.02	-0.003
Bias	0.02	0.000
C1	0.595	0.667
C2	1.636	1.5789
C3	0.00217	0.00217
C4	0.00444	0.00444
C5	250	250
C6	0.47	0.32
C7	7.3	7.3
C8	400	400

7.3.2.1. Reliability for the faulting model

The standard errors of the calibrated faulting models were developed by analyzing the relationship between the standard deviation of the measured faulting and the mean predicted faulting, as explained in Chapter 6. Table 7-91 summarizes standard error equations for the faulting model.

Table 7-91 SE equations for the faulting model

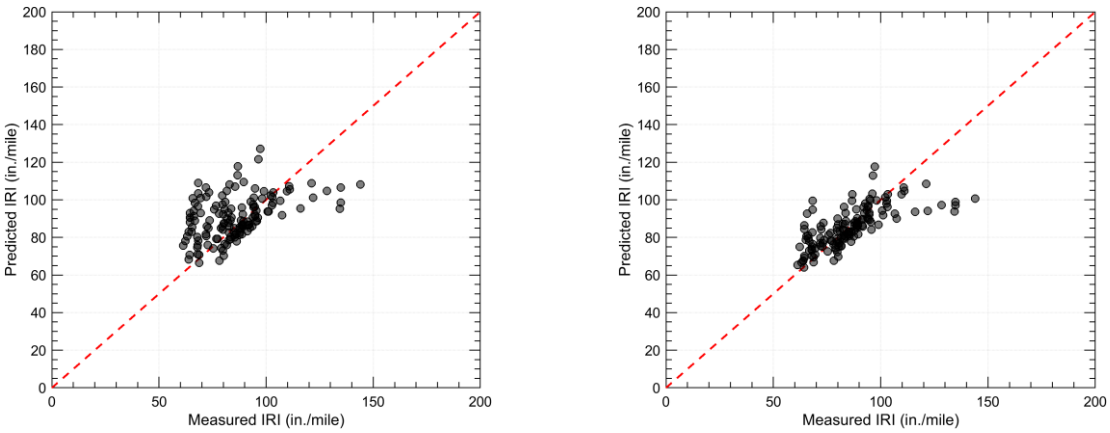
Global model equation	Local model equation
$s_{e(Fault)} = 0.07162(Fault)^{0.368} + 0.00806$	$s_{e(Fault)} = 0.2457(Fault)^{0.6267}$

7.3.3 Rigid Pavement Roughness (IRI) Model

IRI in rigid pavements is a linear function of initial IRI, transverse cracking, joint spalling, joint faulting, and site factor. Transverse cracking and faulting models were calibrated before calibrating the IRI model.

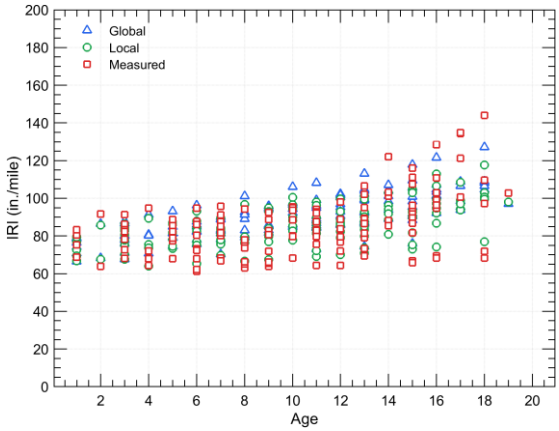
7.3.3.1. No Sampling

Figure 7-57 shows the predicted and measured IRI, along with their comparison over time, using the no-sampling approach. The local model predictions are well within the range of measured values. Table 7-92 shows the calibration results for unbonded overlay using no sampling. The SEE reduced from 15.91 to 11.26, and the bias reduced from 5.23 to 0.00.



(a) Global model

(b) Local model



(c) Time series

Figure 7-57 IRI calibration results for unbonded overlays using no sampling

Table 7-92 Calibration results for IRI (No sampling)

Parameters	Global model	Local model
SEE	15.917	11.526
Bias	5.234	0.000
C1	0.820	0.022
C2	0.441	1.269
C3	1.492	2.605
C4	25.240	0.101

7.3.3.2. Bootstrapping

The team also used bootstrapping to calibrate the IRI model. Tables 7-93 and 7-94 show the bootstrap parameters for global and local models, respectively. Figure 7-58 shows the distribution of these parameters.

Table 7-93 IRI global model using bootstrapping for unbonded overlays

Parameter	Global model mean	Global model median	Global model lower CI	Global model upper CI
SEE	15.756	15.765	11.876	19.345
Bias	5.145	5.059	-0.319	10.883
C1	0.820	0.820	-	-
C2	0.441	0.441	-	-
C3	1.492	1.492	-	-
C4	25.240	25.240	-	-

Table 7-94 IRI local model using bootstrapping for unbonded overlays

Parameter	Local model mean	Local model median	Local model lower CI	Local model upper CI
SEE	11.001	11.106	6.944	14.567
Bias	-0.012	0.000	-0.219	0.000
C1	0.056	0.052	0.045	0.095
C2	1.003	0.871	0.016	2.747
C3	2.645	2.717	1.860	3.228
C4	1.891	0.020	0.000	13.130

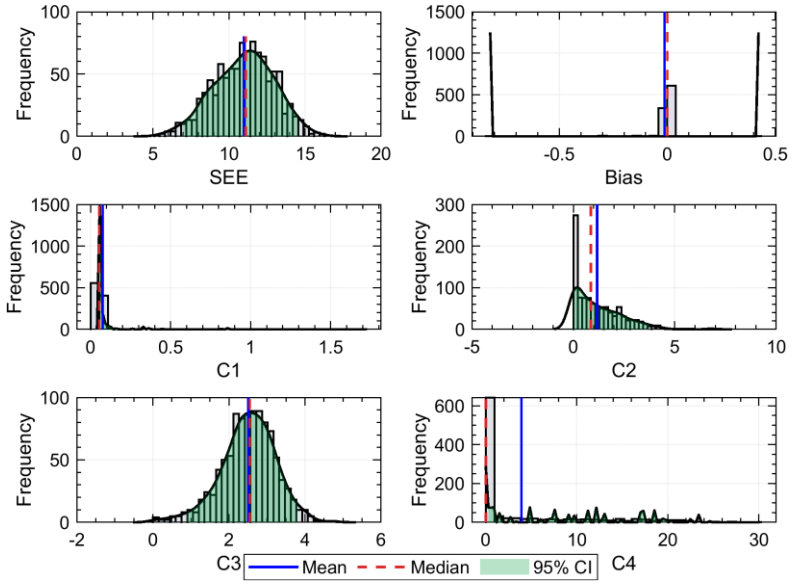


Figure 7-58 Bootstrap sampling calibration results for the IRI model

7.3.4 Summary of JPCP (Unbonded) Overlays

Due to the limited number of available unbonded overlay sections, the calibration accuracy for this fix type is subject to inherent statistical and representational limitations. The small dataset limits the model's ability to capture the full variability across different traffic levels, climate zones, and layer configurations. To ensure more stable and reliable design outcomes, the research team recommends adopting the new/reconstructed JPCP calibration coefficients developed under SPR-1723, which were derived from a larger and more diverse dataset encompassing a broader range of Michigan pavement conditions. Tables 7-95 and 7-96 show the calibration coefficients

and standard error equations for new/reconstruction JPCP pavements calibrated during the previous calibration study (*2*).

Table 7-95 Summary of unbonded overlay pavement performance models

Performance prediction model	Performance models and transfer functions	Local coefficient
Transverse cracking	$CRK_{BU/TD} = \frac{100}{1 + C_4(DI_F)^{C_5}}$	$C_4 = 0.415$ $C_5 = -0.965$
Transverse joint faulting	$Fault_m = \sum_{i=1}^{m} \Delta Fault_i$ $\Delta Fault_i = C_{34} \times (FAULTMAX_{i-1} - Fault_{i-1})^2 \times DE_i$ $FAULTMAX_i = FAULTMAX_0 + C_7 \times \sum_{j=1}^{m} DE_j \times Log(1 + C_5 \times 5.0^{EROD})^{C_6}$ $FAULTMAX_0 = C_{12} \times \delta_{\text{curling}} \times \left[Log(1 + C_5 \times 5.0^{EROD}) \times Log(\frac{P_{200} \times WetDays}{p_s})\right]^{C_6}$ $C_{12} = C_1 + C_2 \times FR^{0.25}$ $C_{34} = C_3 + C_4 \times FR^{0.25}$	$C_1 = 0.6$ $C_2 = 1.611$ $C_3 = 0.00217$ $C_4 = 0.00444$ $C_5 = 250$ $C_6 = 0.2$ $C_7 = 7.3$ $C_8 = 400$
IRI	$IRI = IRI_I + C_1 \times CRK + C_2 \times SPALL + C_3 \times TFAULT + C_4 \times SF$	$C_1 = 0.0942$ $C_2 = 1.5471$ $C_3 = 1.797$ $C_4 = 23.7529$

Table 7-96 SE equations of unbonded overlays

Performance prediction model	Global	Local
Transverse cracking	$S_{e(CRK)} = 3.5522(CRK)^{0.3415} + 0.75$	$S_{e(CRK)} = 2.9004(CRK)^{0.5074}$
Transverse joint faulting	$S_{e(Fault)} = 0.07162(Fault)^{0.368} + 0.00806$	$S_{e(Fault)} = 0.0919(Fault)^{0.2249}$
IRI	Internally calculated by PMED	

7.4 COMPARISON AND VALIDATION OF REHABILITATION DESIGNS USING CALIBRATED MODELS

The research team validated the locally calibrated PMED models by designing representative pavement sections for each rehabilitation fix type and comparing the results with those generated using MDOT's standard AASHTO 93-based pavement design procedures. Although PMED is not intended to replicate AASHTO 93 outcomes, AASHTO 93 designs provide a practical reference for comparison. Most of the selected pavement sections originate from projects previously analyzed via MDOT's LCCA, providing a practical and consistent basis for comparison. The LCCA packages contain detailed material, traffic, and location inputs that can be readily translated into PMED,

enabling improved comparison between the two approaches. As needed, additional theoretical or non-LCCA sections were developed using closely estimated inputs for each design method to ensure full representation of the major rehabilitation fix types.

This validation effort aimed to (a) evaluate the differences between rehabilitation designs produced using locally calibrated PMED models and those based on MDOT's AASHTO 93 procedures, and (b) assess the practical implications of these differences for rehabilitation design in Michigan.

Detailed input parameters used for the validation sections are provided in Appendix C. See Chapter 5 for the PMED design approach and criteria threshold values used for the following designs. Each section was designed in PMED using a 95% reliability level to align with the MDOT AASHTO 93 standard practice. Although reliability is applied differently in the two methods, using 95% provides a reasonable basis for comparison. The following subsections present the validation results for each primary rehabilitation fix type.

7.4.1 HMA Overlay of C&S Pavement

The research team used four representative C&S pavement sections for validation. Table 7-97 summarizes the key details of these sections, including route, MDOT climate region, CADT, existing layer thicknesses, and moduli.

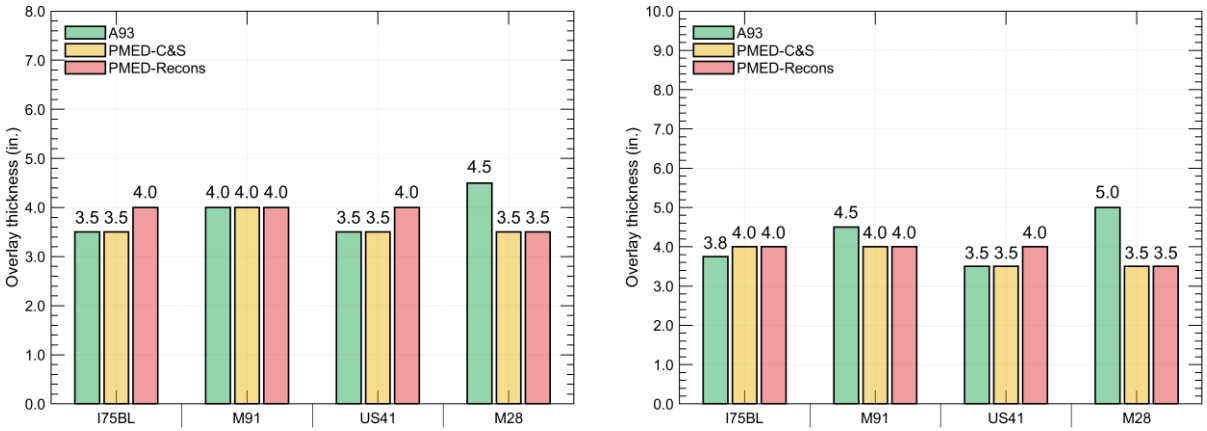
Table 7-97 Summary of validation sections for HMA overlays of C&S pavements

Route	I-75BL	M-91	US-41	M-28
Region	North	Grand	Superior	Superior
CADT	405	155	173	148
C&S layer thickness (inch)	5.0	7.0	5.5	5.75
Aggregate Base Thickness (inch)	5.0	6.0	6.0	3.75
Aggregate Base MR (psi)	28,000	28,000	28,000	28,000
Subbase Thickness (inch)	18.0	N/A	18.0	11.0
Subbase MR (psi)	18,000	N/A	18,000	18,000
Subgrade type	SM	SC	SP	CL
Subgrade MR, Annual Average (psi)	5,200	4,400	6,500	4,400

Since the C&S fix type was calibrated under the new flexible pavement category, MDOT requested an additional comparison using the new/reconstructed flexible pavement calibration coefficients developed in SPR-1723 (*2*). Accordingly, the research team designed the same sections using both the C&S-specific calibrated coefficients and the new flexible pavement coefficients to evaluate differences in resulting design thicknesses. Figures 7-59 show the design thickness comparison for 15- and 20-year design lives. A minimum overlay thickness of 3.5 inches was applied to all C&S comparisons.

Across both design lives, PMED overlay thicknesses were generally within ±0.5 inches of the corresponding AASHTO 93 thicknesses, indicating consistency with current MDOT design outcomes. The only notable deviation occurred for the M-28 section, where PMED produced a 1.0 to 1.5 inch reduction in thickness. This difference is most

likely attributable to the low estimated subgrade modulus, which has a more significant effect on AASHTO 93 calculations, but a comparatively smaller influence in PMED. Overall, the close correspondence between the C&S-specific and reconstruction flexible pavement coefficients confirms the robustness of the local calibration and its suitability for future MDOT rehabilitation design applications.



(a) 15-year design thickness (b) 20-year design thickness

Figure 7-59 Design thickness comparison for C&S pavements

7.4.2 HMA Overlay of Rubblized PCC Pavement

Four representative rubblized PCC pavement sections were used to validate the locally calibrated PMED models for this type of rehabilitation. The selected sections represent different MDOT climate regions and traffic categories, ensuring coverage of typical field conditions across the state. Table 7-98 summarizes key details, including route, CADT, and existing layer configurations with corresponding material moduli. For comparison purposes, the existing base and subbase moduli are representative of new construction conditions to maintain consistency with the AASHTO 93 design assumptions.

Table 7-98 Summary of validation sections for HMA overlays of rubblized pavements

Route	I-75	M-52	US-127	US-10
Region	North	University	University	Bay
CADT	1,790	284	2,755	1,364
Rubblized PCC thickness (inch)	9.2	9.0	9.0	9.0
Aggregate Base thickness (inch)	N/A	3.0	4.0	N/A
Aggregate Base MR (psi)	N/A	33,000	33,000	N/A
Subbase thickness (inch)	14.0	12.0	14.0	14.0
Subbase MR (psi)	20,000	20,000	20,000	20,000
Subgrade type	CL	CL	SM	SC
Subgrade MR, Annual Average (psi)	4,400	4,400	5,000	4,400

All rubblized sections were designed for a 20-year service life. Because HMA over rubblized pavements behaves structurally as full-depth reconstruction flexible systems (with unbound base), the team also compared these designs with the new/reconstruction flexible pavement calibrations to evaluate differences in predicted

performance and design thickness. A minimum overlay thickness of 6.5 inches was applied to all rubblize comparisons.

Accordingly, Figure 7-60 shows the AASHTO 93–based overlay thicknesses with those obtained from PMED using the rubblized-specific and flexible reconstruction calibrations. PMED design thicknesses were generally close to the AASHTO 93 results, typically within 1.0 inch. The rubblized-specific calibration produced slightly thinner designs for I-75 and US-127, whereas it produced marginally thicker designs for US-10 and M-52. Although these differences appear to be grouped by traffic level, they are primarily driven by climatic sensitivity in PMED. This is because the standard mix-binder combination for the specific climatic region requires slightly thicker surface courses to control thermal cracking, which explains the thicker PMED overlays for these routes. It should be noted that alternate mix-binder types may be employed to reduce the reliance on thickness to mitigate cracking; however, such alternatives were outside the scope of this analysis.

Although PMED is not intended to replicate AASHTO 93 outcomes, the observed alignment provides additional confidence in design results and practical expectations. Additionally, the results indicate that both the rubblized-specific calibration and the flexible reconstruction calibration coefficients yield reasonable, comparable designs, supporting their applicability to MDOT rehabilitation design practice.

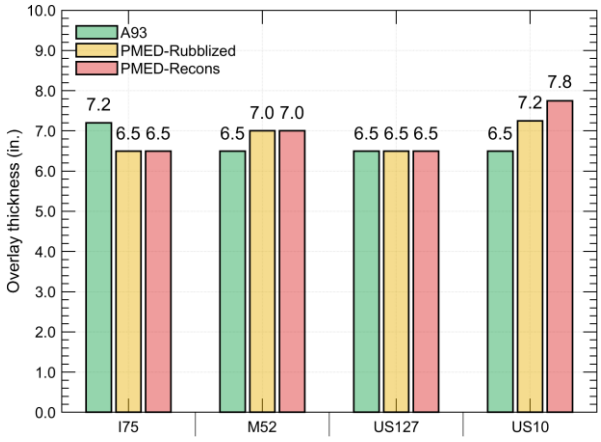


Figure 7-60 Design thickness comparison for rubblized PCC pavements

7.4.3 HMA Overlay of Existing HMA Pavement

Three representative sections were used to validate the locally calibrated PMED model for HMA overlays of existing HMA pavements. Table 7-99 summarizes key design and material parameters for these sections.

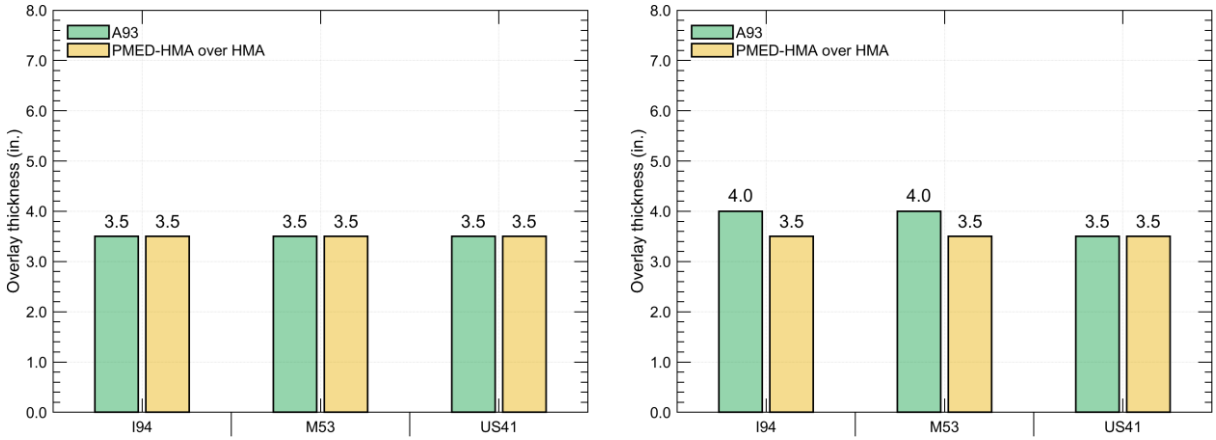
Table 7-99 Summary of validation sections for HMA over HMA

Route	M-53	US-41	I-94
Region	Bay	Superior	Southwest
CADT	1,118	315	161
Existing HMA layer thickness (inch)	8.0	5.0	7.0
Fatigue cracking (%) before overlay	5.0	10.0	10.0
Transverse cracking (ft/mile) before overlay	100	350	350
Aggregate Base Thickness (inch)	8.0	6.0	N/A
Aggregate Base MR (psi)	28,000	28,000	N/A
Subbase Thickness (inch)	16.0	12.0	24.0
Subbase MR (psi)	18,000	18,000	18,000
Subgrade type	CL	SP	CL
Subgrade MR, Annual Average (psi)	4,400	5,000	4,400

The team analyzed each section using both 15- and 20-year design lives. The analysis considered the influence of pre-overlay distresses, including fatigue and transverse cracking, on overlay performance and thickness requirements. Figures 7-61 and 7-62 compare overlay thicknesses from AASHTO 93 and PMED for 15- and 20-year design periods, respectively. A minimum overlay thickness of 3.5 inches was applied to all HMA over HMA comparisons.

For both design periods, the locally calibrated PMED model produced overlay thicknesses that closely matched those of the AASHTO 93 designs, with minimal deviation across all sections. Still, as discussed in Chapter 5, bottom-up cracking predictions apply only to the new HMA layers, which may not fully represent the full-depth structural condition. In addition, HMA over HMA bottom-up and thermal cracking predictions are particularly sensitive to climate inputs, especially in cold-weather locations (such as the Superior Region) when the new HMA overlay is less than roughly 6.5 inches. For example, even though the resulting thicknesses did not show this effect, the Superior Region project (US-41) exhibited thermal cracking predictions close to the failure threshold.

Overall, the locally calibrated PMED model produced rational overlay designs that were consistent with AASHTO 93. However, results for high-volume (very thick pavement) or cold-climate projects should be closely monitored for potential anomalies associated with these model sensitivities.



(a) 15-year design thickness (b) 20-year design thickness

Figure 7-61 Design thickness comparison for HMA over HMA

7.4.4 HMA Overlay of PCC/Composite Pavement

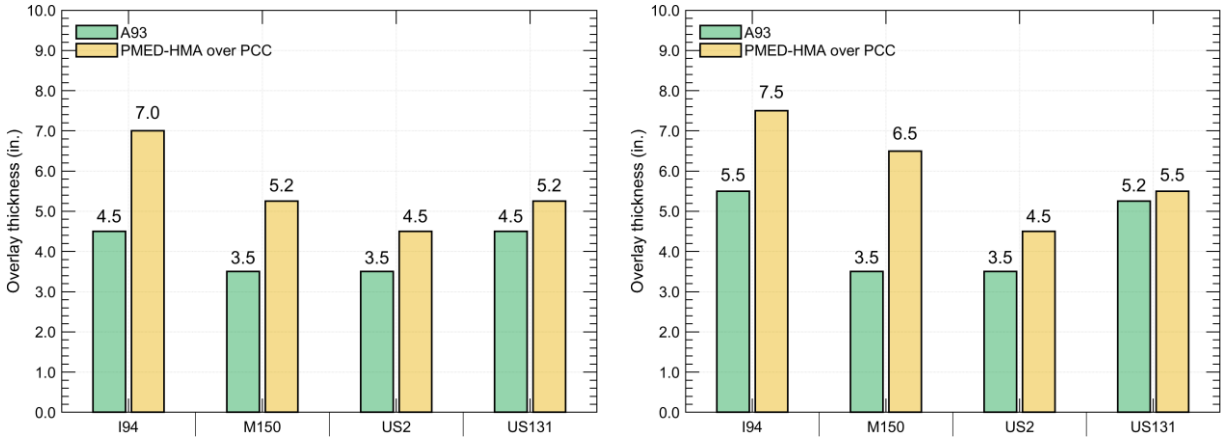
The research team used four representative pavement sections to validate the locally calibrated PMED models for HMA overlays of PCC and composite pavements. The selected sections represent a range of climatic and traffic conditions across Michigan, including both freeway and non-freeway facilities. The design and material properties for these sections are summarized in Table 7-100.

Table 7-100 Summary of validation sections for HMA over PCC/composite pavements

Route	I-94	M-150	US-2	US-131
Region	Southwest	Metro	Superior	Southwest
CADT	8,575	1,325	140	5,918
Existing HMA layer thickness (inch)	N/A	N/A	4.5	3.5
Existing PCC layer thickness (inch)	12.0	9.0	6.0	9.0
Aggregate Base Thickness (inch)	4.0	N/A	N/A	4.0
Aggregate Base MR (psi)	28,000	N/A	N/A	28,000
Subbase Thickness (inch)	12.0	16.0	8.0	12.0
Subbase MR (psi)	18,000	18,000	18,000	18,000
Subgrade type	CL	CL	CL	SM
Subgrade MR, Annual Average (psi)	4,400	3,700	4,400	5,200

PMED V2.6 does not explicitly model multiple existing layers for composite pavements. Therefore, the existing HMA layer was modeled as a new HMA layer with a reduced modulus, following the methodology described in Chapter 5. Each section was designed for both 15- and 20-year design periods, and the results were compared with the AASHTO 93–based overlay thicknesses. A minimum overlay thickness of 3.5 inches was applied to all HMA overlays of existing PCC/composite comparisons.

Figure 7-62 provides the overlay thicknesses obtained from AASHTO 93 and PMED for the 15- and 20-year design periods. The locally calibrated PMED model predicted thicker HMA overlays than AASHTO 93, with the relative increase depending on traffic level, existing structure, and design life.



(a) 15-year design thickness (b) 20-year design thickness

Figure 7-62 Design thickness comparison for HMA over PCC/composite pavements

For the 15-year designs, PMED resulted in HMA overlay thicknesses ranging from 4.5 to 7.0 inches, compared to 3.5 to 4.5 inches from AASHTO 93. The thicker PMED overlays resulted primarily from the model's consideration of reflective and thermal cracking. In contrast, AASHTO 93 accounts only for the influence of reflective cracks, thereby omitting the effect of thermal cracking.

For the 20-year designs, PMED yielded HMA overlay thicknesses of 4.5 to 7.5 inches, while AASHTO 93 yielded 3.5 to 5.5 inches. However, MDOT standard practice is to use a minimum thickness of 6.5 inches for 20-year designs. When applying this minimum, all 20-year designs would be 6.5 inches, except for I-94, which would have AASHTO 93 and PMED thicknesses of 6.5 and 7.5 inches, respectively.

Overall, the PMED results are governed by total transverse cracking rather than fatigue cracking. This valuation of fatigue cracking aligns with AASHTO 93, where the underlying structure significantly controls HMA overlays, so when the existing layers provide sufficient structural capacity, the required overlay thickness (to achieve structural requirements) will be lower. However, since AASHTO 93 largely overlooks thermal cracking and reflective cracking, this method may overlook an important climate-related cracking mechanism.

As a result, PMED may offer a more effective approach to evaluating total transverse cracking in composite sections, resulting in rational thicknesses and/or mix types that align with observed performance and MDOT's design expectations. Still, the sensitivity of PMED to total transverse cracking, particularly for shorter design periods, should be monitored to ensure that these influences do not produce overly conservative HMA overlay recommendations.

7.4.5 JPCP (Unbonded) Overlay of existing JPCP (or JRCP)

Four representative unbonded JPCP overlay sections were used to validate the locally calibrated PMED models. These sections represent a range of traffic volumes and climatic conditions across Michigan, including both freeway and non-freeway corridors.

Table 7-101 summarizes the input parameters used for validation, including layer configurations, moduli, and subgrade properties.

Table 7-101 Summary of validation sections for JPCP (unbonded) overlays

Route	I-75 (a)	I-75 (b)	I-94	US-23
Region	Bay	Bay	Southwest	Metro
CADT	1,644	1,400	8,575	4,600
HMA Separator layer thickness (inch)	1.0	1.0	1.0	1.0
Existing PCC thickness (inch)	9.0	9.0	12.0	9.0
Aggregate Base Thickness (inch)	4.0	3.0	6.0	4.0
Aggregate Base MR (psi)	28,000	28,000	28,000	28,000
Subbase Thickness (inch)	10.0	10.0	10.0	10.0
Subbase MR (psi)	18,000	18,000	18,000	18,000
Subgrade type	SM	SC-SM	CL	CL
Subgrade MR, Annual Average (psi)	4,400	5,000	4,400	4,400

The research team analyzed each section using the newly calibrated coefficients derived specifically from the 28 unbonded JPCP overlay sections evaluated in this study, as well as the new/reconstructed JPCP design coefficients developed under the SPR-1723 study (*2*). All analyses were conducted using a 20-year design period. A minimum overlay thickness of 6.0 inches was applied to all JPCP overlay designs.

Figure 7-65 compares the design slab thicknesses obtained from AASHTO 93 and PMED using both sets of calibration coefficients. For low to medium traffic levels, both PMED calibrations produced thicknesses like those of the AASHTO 93 design. However, in higher-traffic sections (e.g., I-94 and US-23), PMED produced thicker overlays than AASHTO 93. This outcome reflects PMED's greater sensitivity to cumulative traffic loading and slab bending stress under high-volume conditions. In addition, all sections except for I-94 had untied shoulder conditions, which become more significant in PMED designs for high-volume corridors.

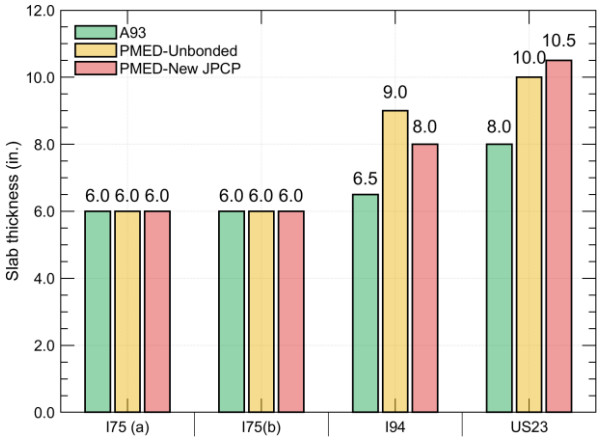


Figure 7-63 Design thickness comparison for JPCP (unbonded) overlays

The research team recommends the new/reconstructed JPCP coefficients for unbonded overlay design (*2*) because they provide results consistent with those from the

unbonded JPCP-specific calibration while being derived from a broader dataset encompassing a wider range of traffic, climatic, and structural conditions. Accordingly, this calibration offers improved reliability and applicability for statewide implementation. Given the thickness difference observed at high traffic volumes, it may be beneficial to adopt a PMED design restriction, as MDOT currently does for PMED reconstruction designs, requiring the PMED result to be no more than 1 inch different from the AASHTO 93 result.

7.4.6 JPCP Overlay of existing HMA Pavement

The same four representative sections as used in the JPCP overlay of existing JPCP were also used to evaluate the PMED modeling of the JPCP overlay of existing HMA pavement. Table 7-102 summarizes the input parameters used for validation, including layer configurations, moduli, and subgrade properties. These designs are theoretical because the sections are not existing HMA structures; therefore, the existing cross-sections were estimated based on traffic levels and MDOT HMA pavement and sublayer thicknesses.

Table 7-102 Summary of validation sections for JPCP overlay of existing HMA

Route	US-23	I-75 (a)	I-94	I-75 (b)
Region	Metro	Bay	Southwest	Bay
CADT	4,600	1,644	8,575	1,400
Existing HMA thickness, post-milling (inch)	8.0*	7.5*	12.5*	7.25*
Aggregate Base Thickness (inch)	4.0	4.0	6.0	3.0
Aggregate Base MR (psi)	28,000	28,000	28,000	28,000
Subbase Thickness (inch)	18.0*	18.0*	18.0*	18.0*
Subbase MR (psi)	18,000	18,000	18,000	18,000
Subgrade type	CL	SM	CL	SC-SM
Subgrade MR, Annual Average (psi)	4,400	4400	4,400	5,000

** Theoretical estimated thickness*

As described in Chapter 5, there are only a few MDOT sections with this fix type, so local calibration is not feasible at this time. However, the models used for this rehabilitation type are the same as those applied to new/reconstruction JPCP, and the underlying HMA layer is simulated like a stabilized base. Therefore, the PMED calibration coefficients for new/reconstructed JPCP pavements established in SPR-1723 (*2*) can be applied to these designs. All analyses were performed using a 20-year design period and use a minimum overlay thickness of 6.0 inches for all JPCP overlays.

Figure 7-64 compares the design slab thicknesses obtained from AASHTO 93 and PMED. Relative to JPCP over PCC, the JPCP over HMA designs tend to produce higher predicted percent slabs cracked, which, along with terminal IRI, serves as a key design criterion in PMED. This outcome is reasonable given that the HMA pavement typically provides less structural stiffness than a PCC base. In addition, the PMED design thicknesses are very consistent with the estimated AASHTO 93 results, with all thicknesses within 0.5 inches of each other. Based on these findings, the PMED design approach for JPCP overlay of existing HMA pavement provides a reliable and practical basis for implementation.

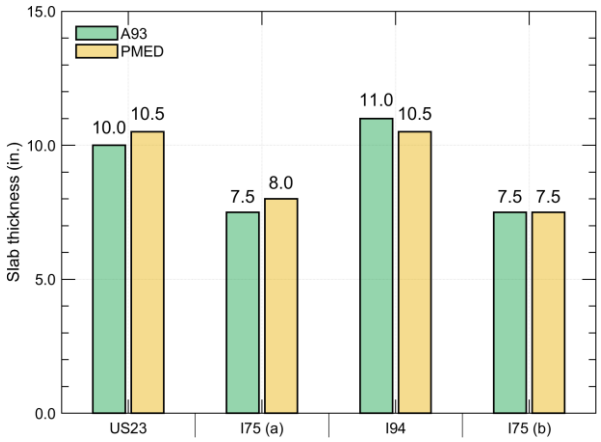
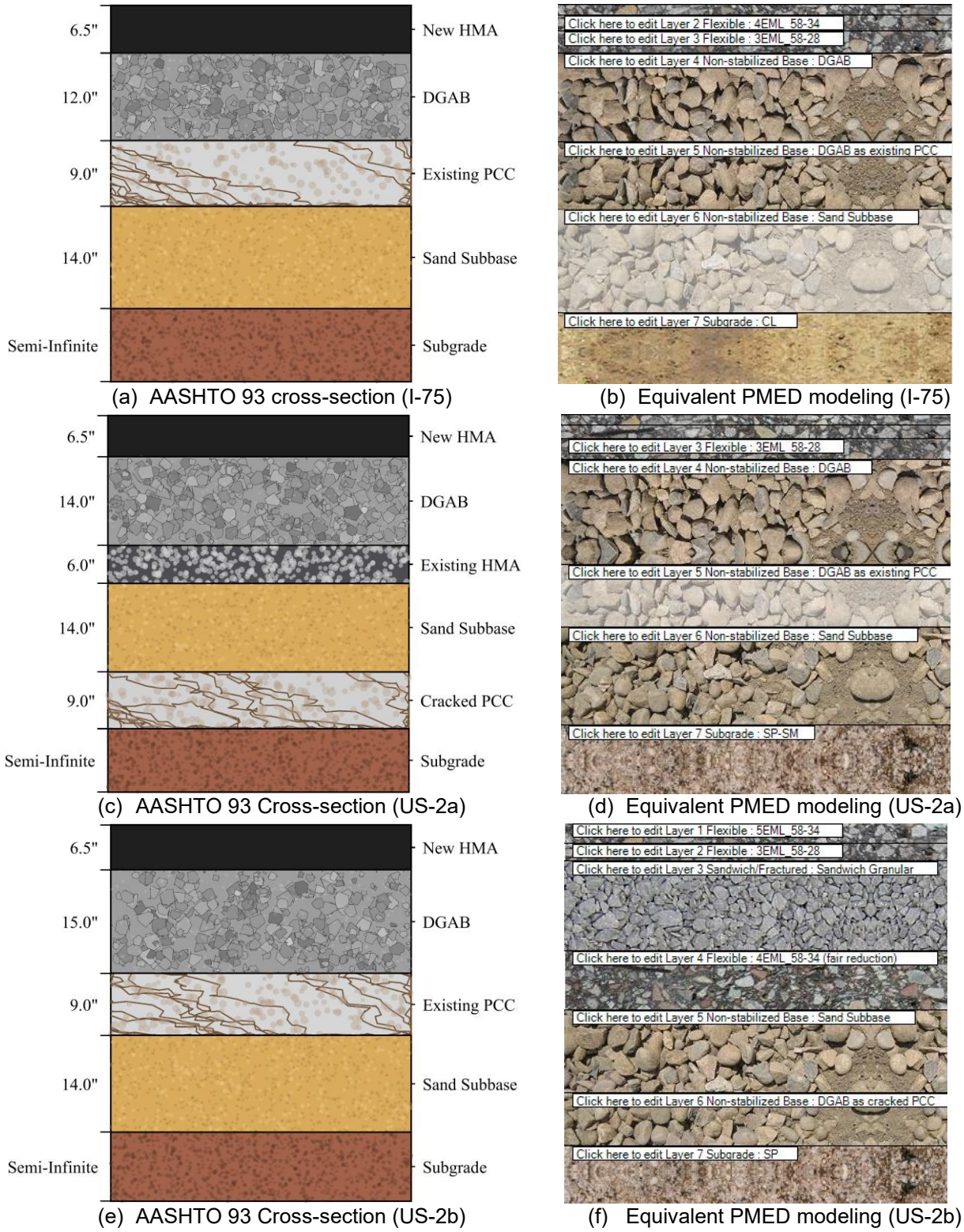


Figure 7-64 Design thickness (20-years) comparison for JPCP over HMA pavement

7.4.7 HMA/PCC over Aggregate Lift over Existing Pavement

This category includes resurfacing designs in which either existing HMA or PCC layers are covered by a thick aggregate base, known as an aggregate lift, and surfaced with new HMA or PCC pavement. The aggregate lift serves to restore grade, improve drainage, enhance structural capacity, and provide a separation layer to minimize reflective cracking from the underlying pavement. The team selected representative designs for both surface types from the MDOT LCCA database. Figures 7-65 and 7-66 compare the AASHTO 93 design configurations with the equivalent PMED models developed for both surface types.



(a) AASHTO 93 cross-section (I-75)

(b) Equivalent PMED modeling (I-75)

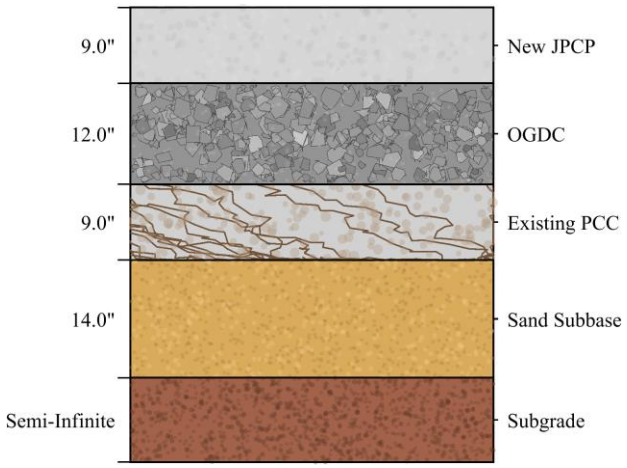
(c) AASHTO 93 Cross-section (US-2a)

(d) Equivalent PMED modeling (US-2a)

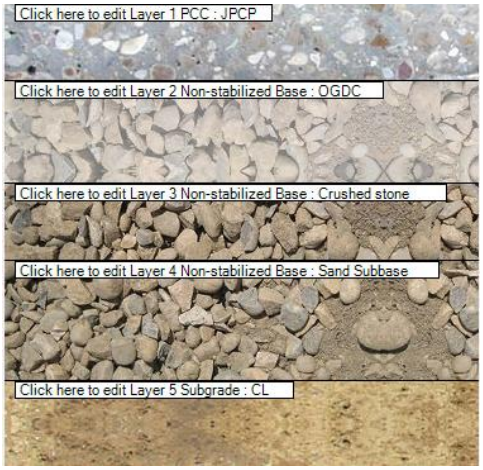
(e) AASHTO 93 Cross-section (US-2b)

(f) Equivalent PMED modeling (US-2b)

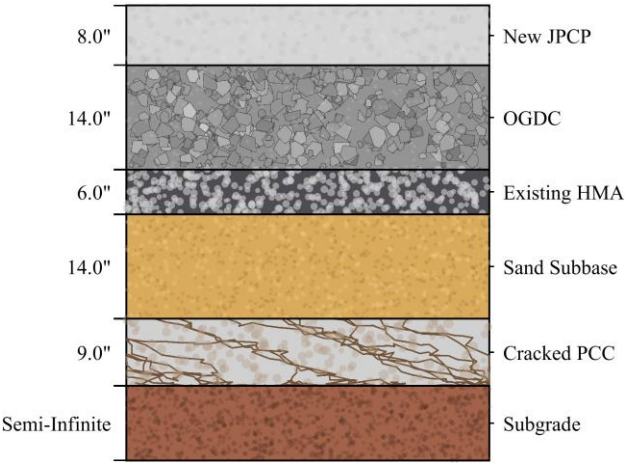
Figure 7-65 HMA over aggregate-lift over existing pavement



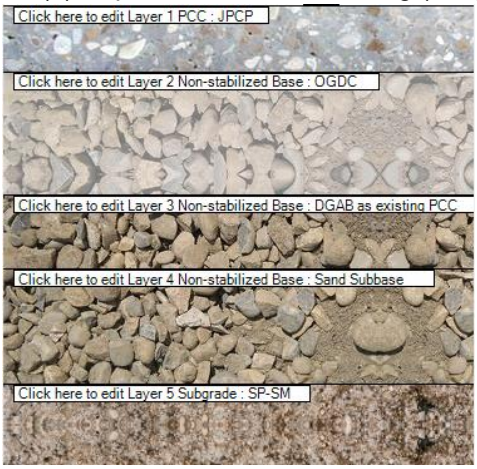
(a) AASHTO 93 Cross-section (I-75)



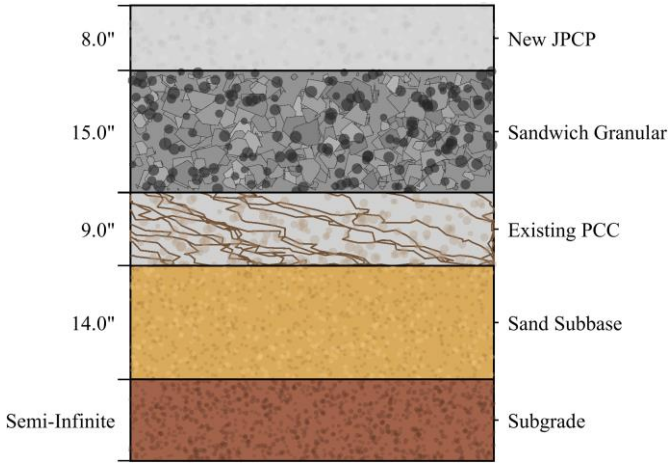
(b) Equivalent PMED modeling (I-75)



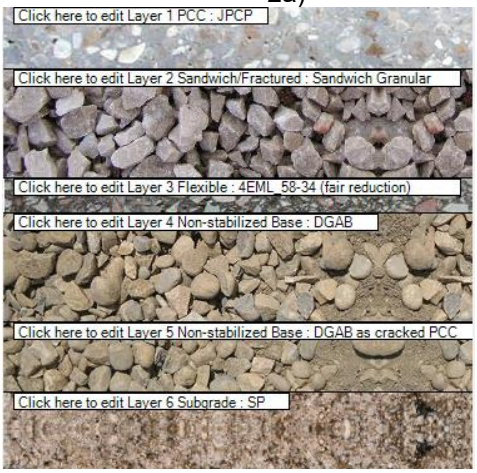
(c) AASHTO 93 Cross-section (US-2a)



(d) Equivalent PMED modeling (US-2a)



(e) AASHTO 93 Cross-section (US-2b)



(f) Equivalent PMED modeling (US-2b)

Figure 7-66 PCC over aggregate-lift over existing pavement

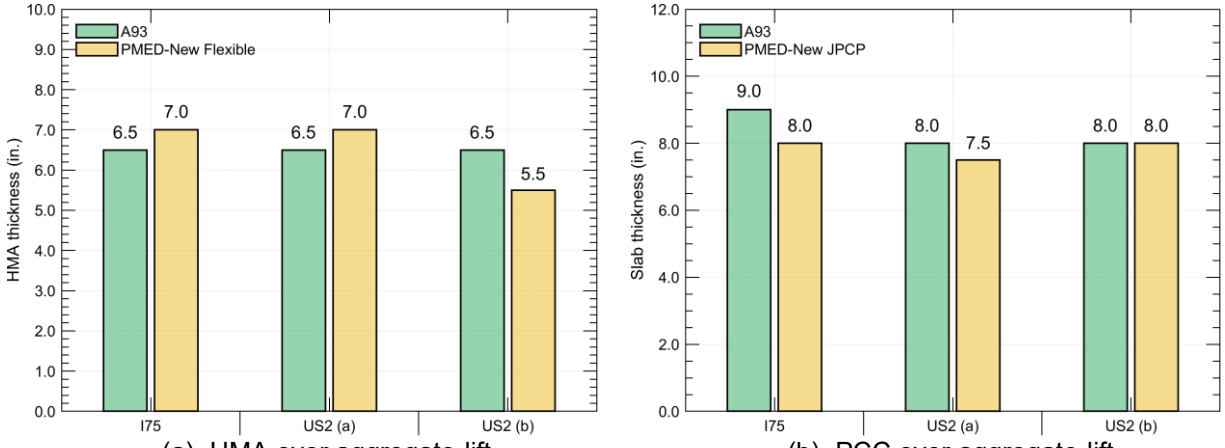
For HMA-over-aggregate-lift sections, the pavement structures were modeled in PMED using the new flexible pavement approach, as described in Chapter 5. The modeling approach represents the aggregate lift and existing layers according to their equivalent

structural roles and condition-based stiffness adjustments. The new/reconstructed flexible pavement calibration coefficients developed under SPR-1723 were applied for performance prediction (*2*). A minimum overlay thickness of 6.5 inches was applied to all HMA designs. For PCC-over-aggregate-lift sections, the pavements were modeled as new JPCP structures following the equivalent modeling framework outlined in Chapter 5. The new JPCP calibration coefficients from SPR-1723 were used (*2*). A minimum overlay thickness of 8.0 inches was applied to all JPCP designs. Accordingly, Figure 7-67 compares the AASHTO 93 and PMED-based overlay thicknesses for HMA and PCC surfaces placed over aggregate-lift systems.

For HMA overlays, PMED predicted thicknesses within approximately ±1.0 inches of the AASHTO 93 design values, indicating a reasonable agreement between the two methodologies. The slightly higher thicknesses in some sections are attributed to PMED's sensitivity to thermal cracking criteria, which are not explicitly considered in AASHTO 93.

For JPCP overlays, PMED produced designs generally 0.5 to 1.0 inches thinner than AASHTO 93. This difference is consistent with PMED's mechanistic approach, which captures the enhanced structural efficiency of the PCC layer and its interaction with the aggregate-lift base.

These results should still be interpreted cautiously, as PMED's current framework cannot fully represent the complex stress transfer and partial confinement effects within the aggregate-lift and underlying layers. Therefore, the research team recommends using PMED analyses primarily for comparative assessment and sensitivity evaluation until improved modeling capabilities are developed for aggregate-lift rehabilitation systems.



(a) HMA over aggregate-lift (b) PCC over aggregate-lift

Figure 7-67 Design thickness (20-years) comparison for HMA/PCC over aggregate-lift

7.5 CATALOG DESIGN

The development of a rehabilitation design catalog is intended to support the broader implementation of PMED within MDOT, particularly for regional offices and design engineers. While PMED offers a robust framework for modeling pavement performance under site-specific conditions, its complexity, data-intensive input requirements, and software accessibility challenges can limit its practicality for routine rehabilitation design.

The catalog design approach was developed to bridge this gap by providing pre-evaluated, performance-based solutions using the calibrated PMED framework. These catalog designs are a streamlined resource for selecting appropriate pavement structures based on defined traffic levels, material conditions, and expected performance outcomes. The catalog uses validated performance thresholds to guide thickness recommendations and enables engineers to design consistent, reliable, and efficient rehabilitation solutions without running full PMED simulations for every project.

The research team established a standardized set of input parameters that reflect the key factors influencing pavement performance, ensuring that the catalog designs are robust, practical, and broadly applicable across Michigan's diverse roadway network. These parameters were selected to represent typical field conditions while enabling consistency in PMED-based rehabilitation designs. The core factors considered include traffic loading, climate region, existing HMA pavement condition, subgrade modulus, and estimated thicknesses of the base and subbase layers. These inputs play a vital role in shaping pavement response and long-term durability. The following sections describe each parameter's rationale and selected values to guide catalog development rooted in realistic, implementable design practices. As an initial assessment of catalog feasibility, the rehabilitation types evaluated were limited to HMA over HMA, HMA over C&S, and HMA over rubblized concrete.

7.5.1 Traffic Levels

To define the traffic inputs, which are a significant factor in pavement design, an approximate AASHTO 93 ESAL value was estimated. Three standardized traffic levels were selected to represent general statewide ESAL ranges. The selected traffic levels are:

- Low traffic: Approximately 3 million ESALs (or less)
- Medium traffic: Approximately 7 million ESALs
- High traffic: Approximately 16 million ESALs (or more)

These traffic levels were selected in consultation with MDOT and used consistently in developing the rehabilitation design catalog.

Accordingly, the ESAL values were estimated using the following PMED traffic inputs. Note that a different combination of CADT and vehicle class distribution was used for the HMA over HMA fix type to obtain each ESAL level. This approach allows for estimating ESALs based on different traffic input combinations to produce possible variations in the PMED catalog outputs.

- CADT
    - C&S and rubblized: low=950, medium=2700, and high=6000
    - HMA over HMA: low=500, medium=2200, and high=4800
- Directional Distribution = 51%
- Lane Distribution = 90%
- Vehicle class distribution
    - C&S and rubblized: Class 9 distribution = 37.75%
    - HMA over HMA: Class 9 distribution = 59.73%
- GR =1.5% compound
- Axle load spectra
    - C&S and rubblized: Urban Regional
    - HMA over HMA: Rural Regional
- MAF = as per MDOT level 2 traffic input tables

7.5.2 Condition of Existing HMA Pavement

The condition of the existing HMA pavement is a key input in rehabilitation design, as it governs the remaining structural capacity of in-place materials. At the time the catalog design effort was initiated, local calibration of the PMED rehabilitation models had been completed only for rehabilitation Level 3 for HMA over HMA overlays. Therefore, Level 3 rehabilitation was adopted to characterize the existing HMA pavements in this catalog.

Under rehabilitation Level 3, the structural condition of the existing HMA is represented using a fatigue cracking-based structural rating. FHWA pavement condition guidelines were used to define the existing HMA condition per the following three representative categories and these were assigned to PMED input for existing layer structural rating:

- Good: Fatigue cracking < 5%
- Fair: Fatigue cracking between 5% and 20%
- Poor: Fatigue cracking > 20%

These categories were used as discrete condition inputs in the catalog to represent typical field conditions and corresponding structural effectiveness. Rehabilitation Level 3 also requires an environmental rating, typically based on transverse cracking. For catalog development, the environmental rating was assumed to match the structural rating to simplify application and maintain consistency across design scenarios.

7.5.3 Subgrade Modulus

Subgrade support is fundamental to pavement performance, particularly in rehabilitation design, where foundation conditions vary widely. For catalog development, two

representative subgrade modulus levels were selected to reflect the range of soil types commonly encountered across Michigan. Based on MDOT's roadbed soil resilient modulus database (Table 4-15), the recommended design resilient modulus values range from approximately 4,400 psi for weaker fine-grained soils such as CL, ML, and SC to approximately 7,000 psi for stronger granular soils such as SP and SP-SM. Accordingly, the following two subgrade modulus levels were adopted in the catalog:

- Low subgrade support: 4,400 psi (representing SC or similar fine-grained soils)
- High subgrade support: 7,000 psi (representing SP-SM or similar granular soils)

These values were used as fixed input conditions in PMED for all catalog design cases to provide a practical and consistent basis for evaluating rehabilitation performance across different pavement structures.

7.5.4 Cross-section of Existing Pavement Layers

Representative pavement cross-sections were defined for catalog development to reflect typical existing layer configurations observed on MDOT rehabilitation projects. Historic construction records and project documentation were reviewed as part of the calibration effort, and average layer thicknesses for different rehabilitation fix types were summarized in Chapter 4 (Table 4-6 and Figure 4-17). These averages were used to establish consistent and practical assumptions for the existing pavement structure in the catalog analyses. Accordingly, for catalog development, the following existing aggregate base and sand subbase layer thicknesses were adopted:

- HMA over HMA: existing HMA = 4.2 in., aggregate base = 7.5 in., sand subbase = 16 in.
- HMA over C&S: existing C&S HMA = 4.5 in., aggregate base = 7.5 in., sand subbase = 21 in.
- HMA over rubblized PCC: existing rubblized PCC = 8.8 in., aggregate base = 4 in., sand subbase = 11 in.

These assumed cross-sections were consistently used in all PMED catalog simulations to represent typical existing pavement conditions, while limiting the number of design combinations and maintaining a practical, implementation-oriented catalog structure.

7.5.5 Climate Region Grouping

To account for environmental variability in pavement performance, Michigan was divided into representative climate regions based on the existing MDOT regional structure, which includes seven regions: Superior (1), North (2), Grand (3), Bay (4), Southwest (5), University (6), and Metro (7). To develop the catalog and streamline the number of climate-based design scenarios, these regions were consolidated into four climate groups with similar temperature and precipitation characteristics. The groups and corresponding climate stations used for design (shown in parentheses) are listed as follows:

- Superior – Region 1 (Gwinn)
- North – Region 2 (Gaylord)
- Grand and Southwest – Regions 3 and 5 (Kalamazoo)
- Bay, University, and Metro – Regions 4, 6, and 7 (Pontiac)

7.5.6 Selection of Material Properties

The selection of HMA mix and binder combinations for catalog design followed MDOT's standard material selection criteria based on regional climate conditions and traffic levels. The appropriate HMA mixture type and PG binder were assigned according to MDOT specifications for each climate region and traffic category used in the catalog. These combinations ensure that the selected materials are compatible with MDOT's regional performance expectations and align with field practices. Table 7-103 shows the HMA mix and binder combinations used to develop this catalog.

For the underlying layers, standardized MDOT material properties were used:

- Existing Base Layer: Modeled using MDOT DGAB properties and modulus value of 28,000 psi.
- Existing Subbase Layer: Modeled using MDOT Sand Subbase properties and modulus value of 18,000 psi.

Table 7-103 Mix and binder selection by climate region, traffic level, and layer

Traffic Level (million ESALs)	Climate Region (number)	Top – Mix	Top – Binder	Leveling – Mix	Leveling – Binder	Base – Mix	Base – Binder	Existing* – Binder
3	2	5EML	64-28	4EML	64-28	3EML	58-28	64-22
7	2	5EMH	64-28	4EMH	64-28	3EMH	58-28	64-22
16	2	5EMH	70-28P	4EMH	70-28P	3EMH	64-28	64-22
3	3/5	5EML	64-28	4EML	64-28	3EML	58-22	64-22
7	3/5	5EMH	70-28P	4EMH	64-28	3EMH	58-22	64-22
16	3/5	5EMH	70-28P	4EMH	70-28P	3EMH	64-22	64-22
3	1	5EML	58-34	4EML	58-34	3EML	58-28	64-22
7	1	5EMH	58-34	4EMH	58-34	3EMH	58-28	64-22
3	4/6/7	5EML	64-28	4EML	64-28	3EML	58-22	64-22
7	4/6/7	5EMH	64-28	4EMH	64-28	3EMH	58-22	64-22
16	4/6/7	5EMH	70-28P	4EMH	70-28P	3EMH	64-22	64-22

* = Not applicable to C&S and rubblized design types.

7.5.7 Design Selection Criteria and Performance Evaluation

For each catalog scenario, PMED analyses were conducted for the combinations of traffic level, climate region, subgrade modulus, existing structure, and material properties defined in Sections 7.5.1 through 7.5.6. All catalog designs were evaluated using the locally calibrated PMED performance models as produced in this study, under a 20-year design life and 95% reliability. Predicted performance was assessed against the predefined structural distress criteria used for catalog development, including IRI, bottom-up fatigue cracking, top-down fatigue cracking, and total rutting. Thermal

(transverse) cracking was not used as a governing threshold in this evaluation, as it represents a non-structural distress that can typically be addressed through adjustments in binder grade or mix type without altering the structural design. The minimum HMA thickness satisfying the governing criteria was selected for each scenario.

In addition to meeting PMED-predicted performance criteria, all selected designs were subsequently checked against MDOT minimum layer thickness requirements, consistent with the MDOT ME User Manual (*4*) and the minimum thickness considerations discussed in Chapter 5 (Section 5.2.1.3). As a result, two sets of output tables were prepared for each fix type:

- Performance-based thickness table – shows values selected solely based on PMED performance outcomes, including cases where the required thickness was below MDOT's minimum threshold.
- Final catalog thickness table – applies MDOT's minimum thickness requirements by adjusting any design that met performance criteria but fell below the minimum limit. In such cases, the minimum allowable thickness was selected to ensure compliance with MDOT standards.

This dual-table approach allows users to distinguish between model-driven recommendations and adaptable designs that meet performance and policy-based requirements. The following tables summarize both the PMED performance-based thickness selections and the final catalog thicknesses that account for minimum layer requirements for each rehabilitation fix type:

- Table 7-104: Performance-based design thicknesses for HMA over HMA
- Table 7-105: Final catalog thicknesses for HMA over HMA
- Table 7-106: Performance-based design thicknesses for HMA over C&S
- Table 7-107: Final catalog thicknesses for HMA over C&S
- Table 7-108: Performance-based design thicknesses for HMA over Rubblized
- Table 7-109: Final catalog thicknesses for HMA over Rubblized

Table 7-104 Performance-based design thicknesses for HMA over HMA

Traffic Level (million ESALs)	Climate Region (number)	Good / SG 4,400	Good / SG 7,000	Fair / SG 4,400	Fair / SG 7,000	Poor / SG 4,400	Poor / SG 7,000
3	2	2.00	1.50	2.75	1.50	3.50	2.00
7	2	4.00	2.25	4.75	2.75	5.50	3.50
16	2	5.25	3.75	5.75	4.25	7.50	4.75
3	3/5	2.00	1.50	2.75	2.25	4.50	4.00
7	3/5	4.00	2.25	4.75	2.75	5.50	4.50
16	3/5	5.25	3.75	5.75	4.25	6.50	4.75
3	1	2.00	1.50	2.75	1.50	3.50	2.00
7	1	4.00	2.25	4.75	2.75	5.50	3.50
3	4/6/7	2.00	1.50	2.75	2.25	3.50	3.00
7	4/6/7	4.00	2.25	4.75	2.75	5.50	3.50
16	4/6/7	5.25	3.75	5.75	5.25	6.50	5.75

Note: Good, fair, and poor are the existing HMA condition level and SG is the subgrade.

Table 7-105 Final catalog thicknesses for HMA over HMA

Traffic Level (million ESALs)	Climate Region (number)	Good / SG 4,400	Good / SG 7,000	Fair / SG 4,400	Fair / SG 7,000	Poor / SG 4,400	Poor / SG 7,000
3	2	3.50	3.50	3.50	3.50	3.50	3.50
7	2	4.00	3.50	4.75	3.50	5.50	3.50
16	2	5.25	3.75	5.75	4.25	7.50	4.75
3	3/5	3.50	3.50	3.50	3.50	4.50	4.00
7	3/5	4.00	3.50	4.75	3.50	5.50	4.50
16	3/5	5.25	3.75	5.75	4.25	6.50	4.75
3	1	3.50	3.50	3.50	3.50	3.50	3.50
7	1	4.00	3.50	4.75	3.50	5.50	3.50
3	4/6/7	3.50	3.50	3.50	3.50	3.50	3.50
7	4/6/7	4.00	3.50	4.75	3.50	5.50	3.50
16	4/6/7	5.25	3.75	5.75	5.25	6.50	5.75

Note: Good, fair, and poor are the existing HMA condition level and SG is the subgrade.

Table 7-106 Performance-based design thicknesses for HMA over C&S

Traffic Level (million ESALs)	Climate Region (number)	Subgrade - 4,400 psi	Subgrade - 7,000 psi
3	2	3.00	1.50
7	2	4.50	2.75
16	2	6.00	5.00
3	3/5	3.00	1.50
7	3/5	4.50	2.75
16	3/5	6.00	5.00
3	1	3.00	1.50
7	1	4.50	2.75
3	4/6/7	3.00	1.50
7	4/6/7	4.50	2.75
16	4/6/7	6.00	5.00

Table 7-107 Final catalog thicknesses for HMA over C&S

Traffic Level (million ESALs)	Climate Region (number)	Subgrade - 4,400 psi	Subgrade - 7,000 psi
3	2	3.50	3.50
7	2	4.50	3.50
16	2	6.00	5.00
3	3/5	3.50	3.50
7	3/5	4.50	3.50
16	3/5	6.00	5.00
3	1	3.50	3.50
7	1	4.50	3.50
3	4/6/7	3.50	3.50
7	4/6/7	4.50	3.50
16	4/6/7	6.00	5.00

Table 7-108 Performance-based design thicknesses for HMA over rubblized PCC

Traffic Level (million ESALs)	Climate Region (number)	Subgrade - 4,400 psi	Subgrade - 7,000 psi
3	2	4.50	2.50
7	2	6.00	4.00
16	2	7.50	5.50
3	3/5	4.50	2.50
7	3/5	6.00	4.00
16	3/5	7.50	5.50
3	1	5.00	3.50
7	1	7.00	5.00
3	4/6/7	5.00	2.50
7	4/6/7	6.00	4.00
16	4/6/7	7.50	5.00

Table 7-109 Final catalog thicknesses for HMA over rubblized PCC

Traffic Level (million ESALs)	Climate Region (number)	Subgrade - 4,400 psi	Subgrade - 7,000 psi
3	2	4.50	3.50
7	2	6.00	4.00
16	2	7.50	5.50
3	3/5	4.50	3.50
7	3/5	6.00	4.00
16	3/5	7.50	5.50
3	1	5.00	3.50
7	1	7.00	5.00
3	4/6/7	5.00	3.50
7	4/6/7	6.00	4.00
16	4/6/7	7.50	5.00

7.5.8 Summary of Catalog Results and Limitations

The catalog tables presented in this section provide HMA thickness recommendations developed using locally calibrated PMED models for the three rehabilitation fix types

evaluated: HMA over HMA, HMA over C&S, and HMA over rubblized PCC. The results reflect expected trends, with required thickness generally increasing with higher traffic levels and lower subgrade support. For HMA over HMA rehabilitation, existing pavement condition also has a pronounced influence on thickness requirements, with poorer conditions requiring thicker overlays.

The catalog was developed using a limited set of representative input levels for traffic, climate, subgrade modulus, existing pavement condition, and pavement structure to support practical implementation. However, ME rehabilitation design is inherently project-specific, as site-specific factors, including existing pavement condition, material properties, traffic loading characteristics, and local climate, influence pavement response and vary across projects. As a result, these parameters may not be fully captured by the discrete scenarios included in the catalog.

Furthermore, in many catalog scenarios, the final recommended HMA thickness was governed by minimum thickness requirements, necessitated by the simplified assumptions used in catalog development. Additionally, an important feature of PMED – thermal cracking – was not included in the catalog analyses, which further limits the usefulness of catalog-based PMED results.

For these reasons, the catalog thicknesses should be viewed as representative guidance rather than optimized project-level designs. The catalog can serve as a general screening and potential starting point for ME rehabilitation design, so practitioners are encouraged to perform project-specific PMED analyses using site-specific inputs when developing final rehabilitation designs, rather than relying on catalog values.

Catalogs for additional rehabilitation types were not pursued within this study due to the inherent limitations as described and because they provide minimal practical benefit over the existing AASHTO 93 approach. In addition, variability in existing pavement structure, distress conditions, and rehabilitation inputs makes it impractical to prescribe catalog thicknesses without risking misapplication.

7.6 SUMMARY OF FINDINGS

This chapter presented the local calibration and validation of PMED performance models for a comprehensive set of rehabilitation fix types used in Michigan. The local calibration effort employed both the no-sampling and bootstrapping techniques to evaluate model robustness and optimize coefficient suitability. Bootstrapping was found to improve statistical consistency and reduce prediction error across several models. Still, the no-sampling method was retained for cases where the available data were limited or computationally constrained. The team calibrated the following five rehabilitation fix types:

1. HMA overlay of C&S pavements
2. HMA overlay of rubblized PCC pavement
3. HMA overlay of existing HMA pavement

4. HMA overlay of existing PCC or composite (existing HMA/PCC) pavement
5. JPCP (unbonded) overlays of existing JPCP (or JRCP) pavement

Table 7-110 summarizes the locally calibrated rehabilitation fix types and lists the corresponding tables containing the recommended calibration coefficients and standard error equations.

Table 7-110 Summary of calibrated rehabilitation fix types

Fix Type	Calibration Coefficients	Standard Error Equations
HMA overlay of C&S HMA	Table 7-23	Table 7-24
HMA overlay of rubblized PCC	Table 7-47	Table 7-48
HMA overlay of existing HMA	Table 7-68	Table 7-69
HMA overlay of existing PCC/composite pavement	Table 7-83	Table 7-84
JPCP (unbonded) JPCP overlay	Table 7-95	Table 7-96

In addition, validation analyses were conducted for seven fix types, including aggregate-lift resurfacing systems, to evaluate the performance of calibrated models under representative design scenarios using historical MDOT project data. Validation indicated that the locally calibrated PMED models generally produce practical design thicknesses across traffic levels and climatic regions, and these outcomes align with those obtained using the AASHTO 93 method. Although PMED implementation may require varying levels of engineering assessment or limitations depending on fix type and site conditions, the PMED calibrated approaches presented in this chapter may be considered for potential statewide implementation.

Building on the local calibration results, an initial rehabilitation design catalog was developed to demonstrate the application of locally calibrated PMED models for representative rehabilitation types. The catalog reflects the design assumptions, input ranges, and modeling limitations present at the time of development. While the catalog results generally aligned with expected design trends, such as increasing HMA thickness with higher traffic and lower subgrade support, many catalog thicknesses were controlled by minimum thickness requirements and do not account for thermal cracking. These limitations restrict the usefulness of PMED within a catalog format.

Therefore, catalogs are not intended to replace project-specific ME rehabilitation design. Instead, they provide a generalized framework to support early-stage evaluation and consistency in rehabilitation design. In contrast, final design decisions should continue to rely on project-level PMED analyses using site-specific inputs. Based on the findings of this study, using PMED catalogs is not recommended as the full benefits of PMED cannot be realized through a catalog alone, and they do not offer significant advantages over the existing AASHTO 93 approach.

CHAPTER 8 - CONCLUSIONS AND RECOMMENDATIONS

8.1 SUMMARY

This study evaluated the use of PMED V2.6 in designing Michigan rehabilitation treatments. These include HMA over HMA, HMA over PCC (JPCP and CRCP), HMA with ASCRL layers over PCC, rubblized PCC, C&S pavements, aggregate-lift sections, thin and unbonded concrete overlays, and composite rehabilitation designs. Additionally, fourteen projects were evaluated using FWD, LWD, and GPR testing, supported by laboratory characterization of asphalt, concrete, and C&S materials. This data was used to establish representative material characterization for new and existing pavement layers and to support the development of calibration input parameters.

For calibration, the team selected 308 sections with asphalt overlays and 28 sections with concrete overlays from the MDOT PMS and PAVETrack databases. These projects were selected to represent the range of Michigan's traffic levels, climatic regions, construction practices, and pavement ages. The main objectives of this project are as follows:

1. Review and evaluate current MDOT pavement design practices, protocols, data, and past research for reconstruction and rehabilitation. The scope of the work includes the following rehabilitation fix types:

    - HMA over rubblized concrete
    - Unbonded concrete overlay (6 inches or more)*
    - Thin concrete overlay (less than 6 inches)*
    - HMA over C&S HMA
    - Multicourse HMA overlay*
    - Multicourse HMA with ASCRL overlay of existing concrete pavement

    * Over existing concrete, asphalt, or composite (asphalt over concrete) pavements

2. Recommend the appropriate PMED modeling selection (i.e., PMED design type and pavement type categories) for each rehabilitation fix type.
3. Compare different hierarchical input levels for rehabilitation pavement designs, including (a) evaluation of reliability and performance criteria thresholds, (b) recommendations on how to characterize existing pavement cross-section materials (including their thicknesses) based on the readily available data in MDOT's databases, and (c) MDOT practicality.
4. Evaluate and update the PMED performance model calibration coefficients for each rehabilitation treatment type, if warranted.
5. Provide a comparison of performance predictions and/or design thicknesses for selected pavements designed using the AASHTO 1993 Guide and PMED to quantify and qualify the differences for each rehabilitation fix type.
6. Deliver updated guidance for MDOT pavement rehabilitation designs.

The calibration employed two approaches: external optimization using MATLAB for direct-response models (fatigue cracking, rutting, transverse cracking, and IRI) and the PMED CAT for cumulative-damage models (thermal, reflective, and faulting). The team used no sampling techniques and bootstrap resampling to minimize bias and reduce the SEE of the calibrated coefficients.

Verification of the global models demonstrated that nationally calibrated coefficients did not adequately represent Michigan rehabilitation performance. Local calibration produced significant improvements in prediction accuracy for all distress types, with bootstrapping yielding the most statistically consistent results. Six rehabilitation fix types were subsequently validated using independent data to confirm the accuracy and applicability of the locally calibrated models.

This report documents the calibrated model coefficients, associated reliability equations, and recommended PMED design type, and data guidelines to support statewide implementation of the locally calibrated PMED framework for rehabilitation pavements.

8.2 MATERIAL CHARACTERIZATION

A comprehensive laboratory and field-testing program were conducted to characterize the materials used in rehabilitation pavement structures and to establish representative data inputs for PMED calibration. Fourteen rehabilitation projects, representing Michigan's primary fix types and climatic regions, were tested from 2023 to 2025. Field investigations included FWD, LWD, GPR, and TSD measurements. Laboratory testing was performed on asphalt, concrete, and C&S materials collected from the same projects. The following subsections summarize the key findings.

8.2.1 Field Testing

This section summarizes the field tests, including FWD, LWD, GPR, and TSD.

- A total of 1,119 pre-overlay and 1,344 post-overlay FWD deflection basins were evaluated across ten flexible and six composite sections. Convergence rates of approximately 72% (flexible) and 70% (composite) confirmed the stability and reliability of modulus backcalculation using Modulus 7.0 and BcT. The corresponding FWD data are provided in Appendix A.
- FWD analyses using both Modulus 7.0 and BcT achieved stable convergence, with four-layer backcalculation yielding the modulus of existing HMA, base, subbase, and subgrade layers.
- The 15th percentile backcalculated HMA moduli were adopted to account for spatial variability, with a reliability of 85%.
- The outer-AREA method overestimated the PCC stiffness and underestimated the subgrade modulus in FWD backcalculation of composite pavements. This finding suggests that direct use of outer-AREA results could lead to an underestimation of pavement support in PMED inputs.

- Review of current FWD backcalculation and prior MDOT studies produced the following representative resilient-modulus values for use in the PMED calibration and design, modeled as unbound granular layers:

    - Existing aggregate base: 28,000 psi.
    - Existing sand subbase: 18,000 psi.
    - C&S HMA: 60,000 psi.
    - Rubblized PCC: 70,000 psi.

- Based on LWD testing of rubblized layers, the resilient moduli ranged from 4.7 to 17 ksi. There are significant differences in loading magnitude and influence depth between LWD and FWD testing. Therefore, the LWD-based moduli are not comparable with FWD and laboratory-estimated values. These values are only useful for assessing relative uniformity and identifying weak spots within a project, but they should not be used directly in design.
- GPR accurately measured HMA thicknesses and detected layer discontinuities. In composite pavements, signal attenuation limited identification of HMA over PCC interfaces, but overall thickness trends agreed with construction records.
- TSD deflection and curvature indices correlated well with FWD trends and provided an efficient method for network-level structural screening. Most tested sections exhibited SCI_{12} values consistent with PMS-based "good" or "fair" classifications.

8.2.2 Laboratory Testing

This section summarizes the laboratory testing conducted on the material during this project.

- Sixty field cores from eleven projects were tested, including HMA and composite pavements, ASCRL loose mix from two sections, and C&S loose material from five projects.
- HMA cores were tested for %AV, dynamic modulus (|E*|), binder content (estimated by the ignition method), and aggregate gradation of the mix. The average aggregate gradation of the HMA field cores fell between MDOT's typical 5E and 4E mixes. The average % binder extracted was 6.2%, aligning more closely with a 4E mix.
- Wheel-path cores showed higher |E*| and lower air-void contents than non-wheel-path cores, indicating densification from repeated traffic loading.
- PCC cores from composite sections exhibited compressive strengths ranging from 7.5 to 10.5 ksi, corresponding to calculated elastic moduli between 5,000 and 5,800 ksi. A reduction factor was applied to adjust the estimated modulus for damage in existing PCC per the PMED guidelines, selecting a representative value of 3,000 ksi.

- Laboratory triaxial testing (MTS-810 and DTS-30) confirmed partially bound behavior of C&S materials, with MR values ranging from 25 to 75 ksi. Testing of C&S material for |E*| at different temperatures and frequencies revealed a strong dependence on both temperature and frequency, reflecting the viscous behavior of C&S materials with an average binder content of 5%.
- Laboratory-compacted ASCRL samples were prepared with a target air void content of 20% (representative of the field core average) and tested for |E*|. The resulting values are recommended for future use in design and analysis.

8.3 MDOT REHABILITATION FIX TYPES AND PMED MODELING

Thirty MDOT asphalt and concrete rehabilitation fix types were evaluated across different pavement types (listed in Chapter 5, section 5.1) and appropriate PMED V2.6 modeling approaches, input requirements, and confidence levels for design were identified.

Field performance data confirmed that PMED's default distress thresholds generally represent HMA overlay performance in Michigan and are therefore suitable, except for transverse cracking, where Michigan sections exhibited higher thermal cracking levels than those predicted by the national calibration. Accordingly, for evaluation purposes, the total transverse cracking threshold was increased from 2,500 to 3,500 ft/mile, while the thermal cracking threshold of 2,000 ft/mile established in previous MDOT calibrations was retained to reflect Michigan's climatic conditions (*1*).

Key findings and PMED modeling considerations are summarized below:

- **Directly modeled strategies:** Most rehabilitation strategies, including HMA overlays, rubblized concrete, C&S, and unbonded JPCP, can be modeled directly in PMED using existing categories. For rubblized concrete and C&S layers, these materials are classified as non-stabilized base layers, using standard inputs for dense-graded aggregate base with the MR adjusted to their recommended values.
- **Equivalent modeling requirements:** Configurations involving aggregate lift, ASCRL, composite pavements, and SJPCP systems require alternative modeling or modified layer approaches, as PMED V2.6 cannot design these structures directly.
- **HMA overlay framework:** HMA overlays (of any pavement type) are analyzed using flexible pavement distress models that account for new damage in the overlay and continued deterioration in the underlying layers.
- **Existing HMA rehabilitation hierarchical input level:** PMED rehabilitation Level 2 provides more reliable characterization than Level 3 because it incorporates measured cracking data, whereas Level 3 relies on simplified condition ratings that may not adequately reflect the range of existing conditions and are subjective.
- **Existing rutting inclusion:** Using measured rutting in existing layers as inputs is essential, as it defines the stage of deformation along the rutting progression

curve. When such data are unavailable, an average value of 0.22 inches for total rutting is representative of typical field conditions for Michigan pavements considered for rehabilitation. Using a value less than 0.20 inches is not recommended, as PMED will overestimate the existing rutting. In these instances, a minimum value of 0.20 inches for total rutting should be used.

- **HMA overlay thickness sensitivity of existing HMA:** The strain analysis of HMA over HMA design sections using MATLEA identified approximately 3.5 inches as the critical overlay thickness separating tensile and compressive strain behavior at the bottom of the overlay. Overlays thinner than 3.5 inches are considered to experience compressive strain alone, so PMED does not predict bottom-up fatigue cracking in these thinner overlays.
- **Representation of Rubblized and C&S layers:** Rubblized and C&S layers can be modeled as unbound bases with resilient moduli of 70 ksi and 60 ksi, respectively, consistent with field-derived and laboratory-measured values.
- **Degradation of existing HMA in Composite Pavements:** The existing HMA layer in composite pavements was modeled with reduced |E*| values to account for material degradation. The reduction factors were based on condition ratings: 0.95 (Good), 0.80 (Fair), and 0.58 (Poor). This approach approximates the stiffness loss in aged materials while preserving the structural behavior of composite sections within the PMED framework.
- **HMA overlay thickness sensitivity of composite pavements:** In composite pavement designs, thicknesses below 4.5 inches result in variable predictions of transverse cracking in PMED. Designers should exercise caution with such thin sections, as model-prediction variability tends to increase.
- **Existing JPCP/JRCP pavement damage representation:** Damage in existing JPCP/JRCP was estimated using the MDOT distress index. Considering that the typical scale of pavement performance is 0 to 50 (from very good to very poor), the percentage of slabs distressed or replaced before restoration was taken as twice the pre-overlay DI value (up to 90%). The percentage of slabs repaired or replaced after rehabilitation was assumed to be half that value. This method provides a practical means for estimating PMED inputs when detailed pre- and post-rehabilitation conditions are unavailable.
- **HMA over CRCP performance:** HMA overlays over CRCP showed substantially lower predicted transverse cracking and IRI than those over JPCP. This is attributed to the continuous steel reinforcement in CRCP that reduces joint-related stress concentrations and reflective cracking. However, due to the limited number of CRCP sections in Michigan, local calibration could not be performed; therefore, these designs were analyzed using default model coefficients with lower confidence in prediction accuracy.
- **Aggregate-lift modeling:** Because PMED V2.6 currently lacks direct modeling capabilities for Aggregate lift configurations, equivalent structural representations were developed. These approximations modify the interaction between layers and the assumed bonding mechanisms, which may not fully reproduce actual field performance. Therefore, these design options were classified as lower-confidence modeling applications due to limited field performance data and the

simplified structural representation required in PMED V2.6. See section 8.7 and Tables 8-11 and 8-12 for further information.

- **ASCRL evaluation:** ASCRL sections were excluded from calibration due to limited field data; however, estimated design comparisons (HMA overlay over JPCP) using ASCRL and 3E mix as base layers indicated that ASCRL provides improved resistance to reflective cracking under both thin and thick overlays. Future field studies are recommended to verify this finding and enable full calibration of ASCRL. In the meantime, ASCRL can be modeled using standard HMA overlay calibration factors with HMA layer input adjustments to represent ASCRL layer properties.
- **JPCP (unbonded) overlay of existing JPCP (or JRCP):** Due to the additional number of sections and improved calibration results, unbonded concrete overlays were modeled using new/reconstructed rigid pavement performance models, with the existing slab assigned a modulus of 3,000 ksi. Reliable performance was achieved when the overlay thickness exceeded 6.5 inches.
- **Concrete overlays over composite pavements:** Since PMED V2.6 cannot model concrete overlays directly, two allowable PMED configurations were used to represent the design and the existing pavement layers. Option A applies the JPCP design type to HMA, with the underlying PCC treated as a stiff, cement-stabilized base. This approach assumes partial bonding at the HMA interface. Option B uses the JPCP over JPCP design type with the existing HMA represented as a reduced-modulus separator layer. This approach assumes fully unbonded conditions. Comparison of these configurations showed that the unbonded configuration (Option B) produced lower predicted transverse cracking and roughness. The possible reason is that it dissipates load-induced and thermal stresses from the underlying layers more effectively, which aligns better with the expectations of this design type.
- **Short-jointed plain concrete pavement overlays:** PMED V2.6 only offers SJCP over existing HMA, so overlays of existing concrete or composite pavements cannot be modeled. The available "SJPCP over AC" option automatically assigns 65% fatigue cracking at rehabilitation Level 2 and a "Very Poor" condition rating at Level 3, which the user cannot modify. Consequently, this limitation prevents a realistic and accurate representation of actual support conditions in MDOT applications.

8.4 LOCAL CALIBRATION FINDINGS

Local calibration was performed for five major rehabilitation fix types (for which an adequate number of sections and performance data are available) to improve the accuracy of PMED distress models under Michigan conditions. The calibration process focused on the following fix types:

- HMA overlay of C&S pavement
- HMA overlay of rubblized PCC pavement
- HMA overlay of HMA pavement
- HMA overlay of concrete or composite pavement (existing HMA/JPCP)

- JPCP (unbonded) overlay of existing JPCP (or JRCP)

The calibration sought to optimize PMED model coefficients to reflect better Michigan's traffic, climate, and material conditions. Both no-sampling and bootstrap resampling techniques were employed to minimize bias and assess the variability of calibration parameters. Measured distress data for the MDOT calibration sections were determined from the MDOT PMS database, with data provided in Appendix C. Local climate data from MDOT ground-based weather stations were utilized. PMED material inputs for the calibration sections were developed using historical project plans, available test records, and laboratory and field testing of existing layers, along with distress data to characterize existing pavement conditions, supplemented by general estimates where necessary. See Appendix B for a complete list of the PMED inputs used in the calibration.

The following subsections summarize the calibration findings, along with the final calibrated coefficients and SE equations established for each fix type.

8.4.1 HMA Overlay of C&S Pavements

The performance models for HMA overlays of C&S HMA pavements were calibrated using the PMED model for "New, Flexible Pavement" design type. The C&S was represented as an unbonded granular layer with the same gradation properties as dense-graded aggregate base, but with an increased modulus of 60 ksi. The calibration included all performance criteria for this PMED design type: bottom-up and top-down fatigue cracking, rutting, transverse (thermal) cracking, and IRI models. Analysis of field data showed that the global PMED models consistently underpredicted fatigue cracking and rutting for this fix type. By adjusting the transfer function coefficients through local calibration, prediction bias was reduced, correlation with measured performance was improved, and reliability equations were developed to better reflect the variability observed in Michigan conditions. Tables 8-1 and 8-2 summarize the coefficients and SE equations.

Table 8-1 Final local calibrated coefficients for HMA overlay of C&S pavements

Performance prediction model	Performance models and transfer functions	Local coefficient
Fatigue cracking (bottom-up)	$FC_{Bottom} = \left(\frac{1}{60}\right)\left(\frac{6000}{1 + e^{C_1 C_1^* + C_2 C_2^* Log(DI_{Bottom}*100)}}\right)$	$C_1 = 0.230$ $C_2 = 0.818$ (hac <5 in) $C_2 = (0.867 + 0.2583 * hac) * 0.532$ (5 in <= hac <=12 in)
Fatigue cracking (top-down)	$t_0 = \frac{\mathrm{K}_{L1}}{1 + e^{\mathrm{K}_{L2}\times 100\times(\mathrm{a_0}/2\mathrm{A_0})+\mathrm{K}_{L3}\times\mathrm{HT}+\mathrm{K}_{L4}\times LT+K_{L5}\times\log_{10}\ \mathrm{AADTT}}}$ $FC_{Top} = \mathrm{Lmax} \times \mathrm{e}^{-(\frac{C_1\rho}{t-C_3 to})^{C_2\beta}}$	$\mathrm{K}_{L2} = 0.90$ $\mathrm{K}_{L3} = 0.090$ $\mathrm{K}_{L4} = 0.1005$ $\mathrm{K}_{L5} = 0.1083$ $C_1 = 0.453$ $C_2 = 1.342$
HMA rutting	$\Delta_{p(HMA)} = \varepsilon_{p(HMA)} h_{HMA} = \beta_{1r} k_z \varepsilon_{r(HMA)} 10^{k_{1r}} \eta^{k_{2r}\beta_{2r}} T^{k_{3r}\beta_{3r}}$	$\beta_{1r} = 0.094$ $\beta_{2r} = 0.7$ $\beta_{3r} = 1.3$
Base/subgrade rutting	$\Delta_{p(soil)} = \beta_{s1} k_{s1} \varepsilon_v h_{soil} \left(\frac{\varepsilon_o}{\varepsilon_r}\right) e^{-\left(\frac{\rho}{n}\right)^{\beta}}$	$\beta_{s1} = 0.564$ $\beta_{sg1} = 1.003$
Thermal cracking	$A = 10^{k_t \beta_t (4.389 - 2.52 Log(E_{HMA}\sigma_m \eta))}$	$K = \left(3 * POW(10, -7)\right) * Pow(MAAT, 4.0319)) * 0.629 + 0$
IRI	$IRI = IRI_o + C_1(RD) + C_2(FC_{Total}) + C_3(TC) + C_4(SF)$	$C_1 = 19.611, C_2 = 0.143$ $C_3 = 0.006, C_4 = 0.0032$

Table 8-2 SE equations for HMA overlay of C&S pavements

Performance prediction model	Global model	Local model
Fatigue cracking (bottom-up)	$s_{e(Alligator)} = 1.13 + \frac{13}{1 + \exp(7.57 - 15.5\log(Crack + 0.0001))}$	$s_{e(Alligator)} = 0.0825 + \frac{6.44}{1 + \exp(0.08 - 2.227\log(Crack))}$
Fatigue cracking (top-down)	$s_{e(Top-down)} = 0.3657 \times TOP + 3.6563$	$s_{e(Top-down)} = 0.1358 \times TOP + 3.233$
HMA rutting	$s_{e(HMA)} = 0.24(Rut_{HMA})^{0.8026} + 0.001$	$s_{e(HMA)} = 0.0584(Rut_{HMA})^{0.1029}$
Base/subgrade rutting	$s_{e(base)} = 0.1477(Rut_{base})^{0.6711} + 0.001$ $s_{e(subgrade)} = 0.1235\left(Rut_{subgrade}\right)^{0.5012} + 0.001$	$s_{e(base)} = 0.0362(Rut_{base})^{0.1098}$ $s_{e(subgrade)} = 0.0562\left(Rut_{subgrade}\right)^{0.3114}$
Thermal	$s_{e(Thermal)} = 0.14 \times TC + 168$	$s_{e(Thermal)} = 0.1311 \times TC + 145$
IRI	Internally calculated by the PMED	

8.4.2 HMA Overlay of Rubblized PCC Pavements

The local calibration of the performance models for rubblized pavement was modeled as "New, Flexible Pavement" design type in PMED. The rubblized material was represented as an unbound base layer with the same gradation properties as dense-graded aggregate base, but with an MR of 70 ksi. The calibration included all performance criteria for this PMED design type. Analysis of field performance indicated that the nationally calibrated models generally underestimated fatigue cracking and over-predicted rutting, transverse cracking, and IRI. Adjusting the model coefficients improved the SEE and reduced bias. The parameters obtained from the bootstrapped calibration were adopted as the final coefficients and SE equations for this fix type, as summarized in Tables 8-3 and 8-4.

Table 8-3 Final local calibrated coefficients for HMA overlay of rubblized pavements

Performance prediction model	Performance models and transfer functions	Local coefficient
Fatigue cracking (bottom-up)	$FC_{Bottom} = \left(\frac{1}{60}\right)\left(\frac{6000}{1 + e^{C_1 C_1^* + C_2 C_2^* Log(DI_{Bottom}*100)}}\right)$	$C_1 = 0.332$ $C_2 = 0.526$ (hac <5 in) $C_2 = (0.867 + 0.2583 * hac) * 0.283$ (5 in <= hac <=12 in)
Fatigue cracking (top-down)	$t_0 = \frac{\mathrm{K}_{L1}}{1 + e^{\mathrm{K}_{L2}\times 100\times(\mathrm{a_0}/2\mathrm{A_0})+\mathrm{K}_{L3}\times\mathrm{HT}+\mathrm{K}_{L4}\times LT+K_{L5}\times\log_{10}\ \mathrm{AADTT}}}$ $FC_{Top} = \mathrm{Lmax} \times \mathrm{e}^{-(\frac{C_1\rho}{t-C_3 to})^{C_2\beta}}$	$\mathrm{K}_{L2} = 0.657$ $\mathrm{K}_{L3} = 0.100$ $\mathrm{K}_{L4} = 0.092$ $\mathrm{K}_{L5} = 2.044$ $C_1 = 0.097$ $C_2 = 2.416$
HMA rutting	$\Delta_{p(HMA)} = \varepsilon_{p(HMA)} h_{HMA} = \beta_{1r} k_z \varepsilon_{r(HMA)} 10^{k_{1r}} n^{k_{2r}\beta_{2r}} T^{k_{3r}\beta_{3r}}$	$\beta_{1r} = 0.149$
Base/subgrade rutting	$\Delta_{p(soil)} = \beta_{s1} k_{s1} \varepsilon_v h_{soil} \left(\frac{\varepsilon_o}{\varepsilon_r}\right) e^{-\left(\frac{\rho}{n}\right)^{\beta}}$	$\beta_{s1} = 0.546$ $\beta_{sg1} = 0.538$
Thermal cracking	$A = 10^{k_t \beta_t (4.389 - 2.52 Log(E_{HMA}\sigma_m \eta))}$	$K = (3 * POW(10, -7)) * Pow(MAAT, 4.0319)) * 0.55 + 0$
IRI	$IRI = IRI_o + C_1(RD) + C_2(FC_{Total}) + C_3(TC) + C_4(SF)$	$C_1 = 25.715, C_2 = 0.212$ $C_3 = 0.0093, C_4 = 0.0048$

Table 8-4 SE equations for HMA overlay of rubblized pavements

Performance prediction model	Global model	Local model
Fatigue cracking (bottom-up)	$S_{e(Alligator)} = 1.13 + \frac{13}{1 + \exp(7.57 - 15.5\log(Crack + 0.0001))}$	$S_{e(Alligator)} = 3.166 + \frac{1.588}{1 + \exp(0.0967 - 5.626\log(Crack))}$
Fatigue cracking (top-down)	$S_{e(Top-down)} = 0.3657 \times TOP + 3.6563$	$S_{e(Top-down)} = 0.2846 \times TOP + 2.8188$
HMA rutting	$S_{e(HMA)} = 0.0446(Rut_{HMA})^{0.2185}$	$S_{e(HMA)} = 0.0584(Rut_{HMA})^{0.1029}$
Base/subgrade rutting	$S_{e(base)} = 0.0334(Rut_{base})^{0.2122}$ $S_{e(subgrade)} = 0.0952(Rut_{subgrade})^{0.5567}$	$S_{e(base)} = 0.0362(Rut_{base})^{0.1098}$ $S_{e(subgrade)} = 0.0562(Rut_{subgrade})^{0.3114}$
Thermal	$S_{e(Thermal)} = 0.14 \times TC + 168$	$S_{e(Thermal)} = 0.0425 \times TC + 142$
IRI	Internally calculated by PMED	

8.4.3 HMA Overlay of Existing HMA Pavements

Local calibration of the PMED performance models for HMA overlays of existing HMA pavements was conducted using the PMED "AC over AC" pavement design type. The calibration included the performance criteria for total fatigue (bottom-up plus reflective) cracking, top-down cracking, rutting, total transverse (thermal plus reflective) cracking, and IRI.

Because material bottom-up fatigue cracking cannot be separated from existing reflective cracks, the MDOT calibration for "New, Flexible Pavement" bottom-up fatigue cracking from SPR-1723 was adopted (*1*) and not separately calibrated. Additionally, since surface measures from the MDOT PMS database were used, approximations are needed to separate top-down from bottom-up cracking. Accordingly, the HMA over existing HMA sections did not indicate bottom-up cracking per these estimations.

Therefore, the total fatigue cracking model was calibrated by assuming that any surface longitudinal cracking (including reflective cracks and the assumed top-down cracking) contributed to the total fatigue cracking. This is consistent with the SPR-1723 approach for bottom-up cracking calibration, which included all longitudinal cracking types (*1*).

Two separate local calibrations were conducted utilizing rehabilitation input Levels 2 and 3. The global PMED models generally underpredicted fatigue and transverse cracking, while overpredicted rutting and IRI. For each calibration set, local calibration reduced bias and SEE. Tables 8-5 and 8-6 summarize the final coefficients and SE equations for HMA overlay of existing HMA pavements for rehabilitation Level 2 only.

8.4.4 HMA overlay of PCC/Composite Pavements

The local calibration of PMED models was performed for HMA overlays of existing JPCP or composite pavements using the PMED "AC over JPCP" pavement design type. The calibration was based on 150 MDOT pavement sections. Due to the high stiffness of the existing concrete layer, the tensile strains at the bottom of the HMA overlay are negligible. As a result, the mechanistic model predicts negligible bottom-up fatigue cracking. Although this is largely consistent with the MDOT performance database, calibrating this distress model would yield distress predictions that are impractically low. Therefore, bottom-up fatigue cracking was not calibrated. Instead, the coefficients developed for new flexible bottom-up fatigue cracking from SPR-1723 were adopted (*1*). These coefficients use the same PMED models and a larger dataset, thereby improving robustness and practicality. Accordingly, the calibration effort focused on top-down cracking, rutting, total transverse (thermal plus reflective) cracking, and IRI models. For composite pavements, the existing asphalt layers were modeled as a single, damaged HMA layer, with a reduction factor applied to its estimated modulus.

Global coefficients resulted in over-predictions of cracking, rutting, and IRI. The sensitivity analysis showed that the pre-overlay condition inputs—percent slabs distressed before restoration and percent slabs repaired after restoration—primarily affected total transverse cracking and JPCP transverse cracking. Because JPCP cracking is already incorporated into PMED's reflective cracking model, its impact is indirectly accounted for through the total transverse cracking observed on the HMA surface. Therefore, the JPCP transverse cracking model was not calibrated, and the SPR-1723-developed coefficients were used instead. Local calibration refined the model coefficients, reduced bias, and established reliability equations. Tables 8-7 and 8-8 represent the final selected coefficients and SE equations.

Table 8-5 Final local calibrated coefficients for HMA overlay of HMA pavements

Performance prediction model	Performance models and transfer functions	Local model
Fatigue cracking (Bottom-up) (SPR-1723) (*1*)	$FC_{Bottom} = \left(\frac{1}{60}\right)\left(\frac{6000}{1 + e^{C_1 C_1^* + C_2 C_2^* Log(DI_{Bottom} * 100)}}\right)$	$C_1 = 0.232$ $C_2 = 0.6998$ (hac <5 in) $C_2 = (0.867 + 0.2583 * hac) * 0.2204$ (5 in <= hac <=12 in) $C_2 = 0.8742$ (hac >12 in)
Fatigue cracking (top-down)	$t_0 = \frac{\mathrm{K}_{L1}}{1 + e^{\mathrm{K}_{L2} \times 100 \times (\mathrm{a}_0/2\mathrm{A}_0) + \mathrm{K}_{L3} \times \mathrm{HT} + \mathrm{K}_{L4} \times LT + K_{L5} \times \log_{10} \mathrm{AADTT}}}$ $FC_{Top} = \mathrm{Lmax} \times \mathrm{e}^{-(\frac{C_1 \rho}{t - C_3 to})^{C_2 \beta}}$	$C_1 = 0.087$ $C_2 = 2.019$ $\mathrm{K}_{L2} = 1.236$ $\mathrm{K}_{L3} = 0.103$ $\mathrm{K}_{L4} = 0.175$ $\mathrm{K}_{L5} = 0.172$
Total Fatigue (Bottom-up+ Reflective Cracking)	$\Delta D = \frac{C_1 k_1 \Delta_{bending} + C_2 k_2 \Delta_{shearing} + C_3 k_3 \Delta_{thermal}}{h_{OL}}$ $RCR = \left(\frac{100}{C4 + e^{c5 log\, D}}\right) * EXCRK$	$C_1 = 0.24, C_2 = 1.1$ $C_3 = 2.1, C_4 = 140$
HMA rutting	$\Delta_{\mathrm{p(HMA)}} = \varepsilon_{p(HMA)} h_{HMA} = \beta_{1r} k_z \varepsilon_{r(HMA)} 10^{k_{1r}} n^{k_{2r} \beta_{2r}} T^{k_{3r} \beta_{3r}}$	$\beta_{1r} = 0.082$ $\beta_{2r} = 0.70$ $\beta_{3r} = 1.30$
Base/subgrade rutting	$\Delta_{p(soil)} = \beta_{s1} k_{s1} \varepsilon_v h_{soil} \left(\frac{\varepsilon_o}{\varepsilon_r}\right) e^{-\left(\frac{\rho}{n}\right)^{\beta}}$	$\beta_{s1} = 0.69$ $\beta_{sg1} = 1.0$
Thermal Fracture - L1	Level 1 K (MAAT <= 57 deg F) $A = 10^{k_t \beta_t (4.389 - 2.52 Log(E_{HMA} \sigma_m \eta))}$	((3 * Pow(10,-7)) * Pow(MAAT,4.0319)) * 0.73
	Level 1 K (MAAT > 57 deg F)	(0.13 * Pow(MAAT,2) - 11.68 * MAAT + 244.14) * 1 + 0
Thermal Fracture - L2	Level 2 K (MAAT <= 57 deg F)	((3 * Pow(10,-7)) * Pow(MAAT,4.0319)) * 1 + 0
	Level 2 K (MAAT > 57 deg F)	(0.13 * Pow(MAAT,2) - 11.68 * MAAT + 244.14) * 1 + 0
Thermal Fracture - L3	Level 3 K (MAAT <= 57 deg F)	((3 * Pow(10,-7)) * Pow(MAAT,4.0319)) * 1 + 0
	Level 3 K (MAAT > 57 deg F)	(0.13 * Pow(MAAT,2) - 11.68 * MAAT + 244.14) * 1 + 0
Transverse Reflective cracking	$\Delta D = \frac{C_1 k_1 \Delta_{bending} + C_2 k_2 \Delta_{shearing} + C_3 k_3 \Delta_{thermal}}{h_{OL}}$ $RCR = \left(\frac{100}{C4 + e^{c5 log\, D}}\right) * EXCRK$	$C_1 = 2.65, C_2 = 24.2$ $C_3 = 0.05, C_4 = 145$
IRI	$IRI = IRI_o + C_1(RD) + C_2(FC_{Total}) + C_3(TC) + C_4(SF)$	$C_1 = 28.2,$ $C_2 = 0.05$ $C_3 = 0.002,$ $C_4 = 0.016$

Table 8-6 SE equations for HMA overlay of HMA pavements

Performance prediction model	Global model	Local model
Fatigue cracking (bottom-up only) (SPR-1723) (*1*)	$S_{e(Alligator)} = 1.13 + \frac{13}{1+\exp(7.57-15.5\log(Crack+0.0001))}$	$S_{e(Alligator)} = 0.2262 + \frac{14.2349}{1+\exp(0.2958-0.1441\log(Crack))}$
Fatigue cracking (top-down)	$S_{e(Top-down)} = 0.3657 \times TOP + 3.6563$	$S_{e(Top-down)} = 0.2845 \times TOP + 1.1414$
Total Fatigue + Reflective Cracking	$S_{e(Fatigue+reflective)} = 1.1097(Fatigue)^{0.6804} + 1.23$	$S_{e(Fatigue+reflective)} = 1.065(Fatigue)^{0.482} + 1.11$
HMA rutting	$S_{e(HMA)} = 0.24(Rut_{HMA})^{0.8026} + 0.001$	$S_{e(HMA)} = 0.099(Rut_{HMA})^{0.2314}$
Base rutting	$S_{e(base)} = 0.1477(Rut_{base})^{0.6711} + 0.001$	$S_{e(base)} = 0.0293(Rut_{base})^{0.1802}$
Subgrade rutting	$S_{e(subgrade)} = 0.1235\left(Rut_{subgrade}\right)^{0.5012} + 0.001$	$S_{e(subgrade)} = 0.1235\left(Rut_{subgrade}\right)^{0.5012} + 0.001$
Thermal + Reflective cracking	$S_{e(Transverse)} = 70.98(Transverse)^{0.2994} + 30.12$	$S_{e(Transverse)} = 69.54(Transverse)^{0.271} + 32.54$
IRI	Internally calculated by PMED	

Table 8-7 Final local calibrated coefficients for HMA overlay of PCC/composite pavements

Performance prediction model		Performance models and transfer functions	Local model
Fatigue cracking (bottom-up) (SPR-1723) (*1*)		$FC_{Bottom} = \left(\frac{1}{60}\right)\left(\frac{6000}{1+e^{C_1C_1^*+C_2C_2^*Log(DI_{Bottom}*100)}}\right)$	$C_1 = 0.232$ $C_2 = 0.6998$ (hac <5 in) $C_2 = (0.867 + 0.2583 * hac) * 0.2204$ (5 in <= hac <=12 in) $C_2 = 0.8742$ (hac >12 in)
Fatigue cracking (top-down)		$t_0 = \frac{\mathrm{K}_{L1}}{1+e^{\mathrm{K}_{L2}\times 100\times(\mathrm{a}_0/2\mathrm{A}_0)+\mathrm{K}_{L3}\times \mathrm{HT}+\mathrm{K}_{L4}\times LT+K_{L5}\times\log_{10}\mathrm{AADTT}}}$ $FC_{Top} = \mathrm{Lmax}\times \mathrm{e}^{-(\frac{C_1\rho}{t-C_3to})^{C_2\beta}}$	$\mathrm{K}_{L2} = 0.475$ $\mathrm{K}_{L3} = 0.097$ $\mathrm{K}_{L4} = 0.104$ $\mathrm{K}_{L5} = 0.206$ $C_1 = 0.132$ $C_2 = 1.635$
Rutting	HMA	$\Delta_{\mathrm{p(HMA)}} = \varepsilon_{p(HMA)}h_{HMA} = \beta_{1r}k_z\varepsilon_{r(HMA)}10^{k_{1r}}\eta^{k_{2r}\beta_{2r}}T^{k_{3r}\beta_{3r}}$	$\beta_{1r} = 0.224$
Thermal + Reflective cracking		$A = 10^{k_t\beta_t(4.389-2.52Log(E_{HMA}\sigma_m\eta))}$ $\Delta D = \frac{C_1k_1\Delta_{bending} + C_2k_2\Delta_{shearing} + C_3k_3\Delta_{thermal}}{h_{OL}}$ $RCR = \left(\frac{100}{C4+e^{c5log\,D}}\right) * EXCRK$	$K = \left(3 * POW(10,-7)\right) * Pow(MAAT, 4.0319)) * 0.722$ $C_1 = 0.05,$ $C_2 = 0.40$ $C_3 = 2.0, C_4 = 96.11$
IRI		$IRI = IRI_o + C_1(RD) + C_2(FC_{Total}) + C_3(TC) + C_4(SF)$	$C_1 = 13.09,$ $C_2 = 0.14$ $C_3 = 0.0024,$ $C_4 = 0.020$
JPCP Transverse Cracking (SPR-1723) (*1*)		$CRK_{BU/TD} = \frac{100}{1+C_4(DI_F)^{C_5}}$	$C_4 = 0.415,$ $C_5 = -0.965$

Table 8-8 SE equations for HMA overlay of PCC/composite pavements

Performance prediction model	Global model	Local model
Fatigue cracking (Bottom-up) (SPR-1723) (*1*)	$S_{e(Alligator)} = 1.13 + \frac{13}{1 + \exp(7.57 - 15.5\log(D + 0.0001))}$	$S_{e(Alligator)} = 0.2262 + \frac{14.2349}{1 + \exp(0.2958 - 0.1441\log(D))}$
Fatigue cracking (top-down)	$S_{e(Top-down)} = 0.3657 \times TOP + 3.6563$	$S_{e(Top-down)} = 0.5249 \times TOP + 1.7406$
HMA rutting	$S_{e(HMA)} = 0.24(Rut_{HMA})^{0.8026} + 0.001$	$S_{e(HMA)} = 0.088(Rut_{HMA})^{0.1728}$
Thermal + Reflective cracking	$S_{e(Transverse)} = 5.1025(Transverse)^{0.6513} + 30.12$	$S_{e(Transverse)} = 5.087(Transverse)^{0.571} + 92.5$
JPCP Transverse Cracking (SPR-1723) (*1*)	$S_{e(CRK)} = 2.9004(CRK)^{0.5074}$	$S_{e(CRK)} = 2.9004(CRK)^{0.5074}$
IRI	Internally calculated by PMED	

8.4.5 JPCP (Unbonded) Overlays of existing JPCP (or JRCP)

The research team conducted local calibration of PMED performance models for unbonded JPCP overlays using the PMED "JPCP over JPCP" pavement design type. The calibration included all performance criteria for this PMED design type, including transverse cracking, joint faulting, and IRI models. The measured performance of 28 MDOT concrete overlay sections was used. Due to the limited number of sections, calibration results may carry higher statistical uncertainty.

The global model's coefficients consistently underpredicted transverse cracking and overpredicted faulting and roughness. Local calibration refined the model coefficients, reducing bias and improving consistency between measured and predicted performance. However, because the small sample size could not capture the full variability of Michigan conditions, the coefficients developed for new and reconstructed JPCP pavements under SPR-1723 were recommended for use in design (*1*). Tables 8-9 and 8-10 summarize the local model coefficients and SE equations.

Table 8-9 Locally calibrated coefficients of unbonded overlay pavements

Performance prediction model	Performance models and transfer functions	Local coefficient
Transverse cracking (SPR-1723) (*1*)	$CRK_{BU/TD} = \frac{100}{1 + C_4(DI_F)^{C_5}}$	$C_4 = 0.415$ $C_5 = -0.965$
Transverse joint faulting (SPR-1723) (*1*)	$Fault_m = \sum_{i=1}^{m} \Delta Fault_i$ $\Delta Fault_i = C_{34} \times (FAULTMAX_{i-1} - Fault_{i-1})^2 \times DE_i$ $FAULTMAX_i = FAULTMAX_0 + C_7 \times \sum_{j=1}^{m} DE_j \times Log(1 + C_5 \times 5.0^{EROD})^{C_6}$ $FAULTMAX_0 = C_{12} \times \delta_{\text{curling}} \times \left[Log(1 + C_5 \times 5.0^{EROD}) \times Log(\frac{P_{200} \times WetDays}{p_s})\right]^{C_6}$ $C_{12} = C_1 + C_2 \times FR^{0.25}$ $C_{34} = C_3 + C_4 \times FR^{0.25}$	$C_1 = 0.6$ $C_2 = 1.611$ $C_3 = 0.00217$ $C_4 = 0.00444$ $C_5 = 250$ $C_6 = 0.2$ $C_7 = 7.3$ $C_8 = 400$
IRI (SPR-1723) (*1*)	$IRI = IRI_I + C_1 \times CRK + C_2 \times SPALL + C_3 \times TFAULT + C_4 \times SF$	$C_1 = 0.0942$ $C_2 = 1.5471$ $C_3 = 1.797$ $C_4 = 23.7529$

Table 8-10 SE equations of unbonded overlay pavements

Performance prediction model	Global	Local
Transverse cracking (SPR-1723) (*1*)	$s_{e(CRK)} = 3.5522(CRK)^{0.3415} + 0.75$	$s_{e(CRK)} = 2.9004(CRK)^{0.5074}$
Transverse joint faulting (SPR-1723) (*1*)	$s_{e(Fault)} = 0.07162(Fault)^{0.368} + 0.00806$	$s_{e(Fault)} = 0.0919(Fault)^{0.2249}$
IRI (SPR-1723) (*1*)	Internally calculated by PMED	

8.5 COMPARISON AND VALIDATION OF CALIBRATED REHABILITATION DESIGNS

To verify the practicality of the calibrations and design approaches, the research team validated the locally calibrated PMED models by comparing the resulting design thicknesses for representative rehabilitation fix types with those from previously designed MDOT pavements as developed using the AASHTO 93 method. Although PMED is not intended to replicate AASHTO 93 outcomes, AASHTO 93 designs provide a practical reference for comparison. For consistency and equivalent comparison, ME designs used corresponding input estimates for existing conditions, materials, traffic, and a 95% reliability level relative to the AASHTO 93 designs. Other inputs not defined in AASHTO 93, such as climate, were estimated using available project information and

MDOT standard PMED procedures. See Appendix D for a complete list of the PMED inputs used for the validation designs.

- **HMA overlay of C&S pavements:** PMED predicted overlay thicknesses within approximately ± 0.5 inch of AASHTO 93 for 15-year designs and up to ±1 inch thinner for 20-year designs. Both the C&S calibration and SPR-1723 flexible pavement coefficients yielded nearly identical results, confirming model consistency.
- **HMA overlays of rubblized PCC pavements:** The locally calibrated PMED model produced 20-year design thicknesses for most sections within ±1 inch of the AASHTO 93 specification. The rubblized-specific and new/reconstruction calibrations yielded comparable results, reflecting PMED climatic sensitivity across both sets of calibration coefficients.
- **HMA overlays of existing HMA pavements:** PMED results were generally within ±0.5 inch of AASHTO 93 for both 15- and 20-year analysis periods, except in colder climates, such as the Superior region, where designs are driven by thermal-cracking considerations not captured in AASHTO 93.
- **HMA overlays of PCC/composite pavements:** PMED generally produced thicker overlays than AASHTO 93 due to explicit modeling of thermal cracking as part of total transverse cracking. Since AASHTO 93 omits this performance condition, PMED may offer a more effective approach to account for total transverse cracking in composite sections. Differences were more pronounced in higher-volume routes and longer design lives, consistent with the mechanistic representation of climate-driven cracking.
- **JPCP (unbonded) overlay of existing JPCP (or JRCP):** The calibration of unbonded overlays used 28 field sections, leading to higher statistical uncertainty. The locally calibrated PMED model produced slab thicknesses that differed from AASHTO 93 by approximately 1.5 to 2.5 inches. Due to the limited dataset and variability in layer configurations, the research team adopted the new JPCP coefficients developed under SPR-1723 (*1*), which were derived from a larger and more representative database. These coefficients yielded design thicknesses within ±1 inch of AASHTO 93 for high-traffic sections and nearly identical results for low-traffic conditions.
- **JPCP overlays of HMA pavements:** Due to the limited number of sections available for local calibration, the new/reconstruction JPCP coefficients from SPR-1723 (*1*) were utilized for this evaluation. PMED slab thicknesses were in close agreement with AASHTO 93, with differences of 0.5 inch or less across all sections. Relative to JPCP overlays of PCC, higher slab cracking was predicted for JPCP overlays of HMA, which is consistent with the lower structural stiffness of the HMA support layer. Overall, the results indicate that the new/reconstructed JPCP calibration coefficients from SPR-1723 (*1*) provide a reasonable and practical basis for designing JPCP overlays on HMA pavements.
- **HMA and PCC placed over aggregate-lift systems:** Since PMED does not have a direct design approach for this fix type, the pavements were modeled as equivalent new flexible or JPCP structures (for details, see Chapter 5, Section 5.3.2) using the corresponding coefficients developed under SPR-1723 (*1*).

Predicted overlay thicknesses were within ± 0.5 inch of AASHTO 93 for HMA surfaces and approximately 0.5 to 1 inch thinner for PCC surfaces. However, because these results are based on an alternative modeling approach, the outcomes should be interpreted with caution.

Overall, the validation demonstrated that the locally calibrated PMED models produce overlay thicknesses that are in close agreement with AASHTO 93 designs, typically within ±1 inch for most rehabilitation types, while providing a more mechanistic basis that captures material, climatic, and distress-interaction effects relevant to Michigan pavement performance.

8.6 CATALOG DESIGN

The research team conducted detailed PMED analyses of HMA over HMA, HMA over C&S, and HMA over rubblized pavement systems to formulate catalog designs tailored to Michigan practices, materials, and environmental conditions. However, the catalog evaluation revealed that required overlay thicknesses vary significantly by fix type, traffic level, climate, and subgrade stiffness, making it challenging to apply standardized catalog thicknesses uniformly across the statewide network. The following summarizes the observed trends across the three rehabilitation categories and the overall conclusion regarding catalog applicability.

- **HMA over HMA:** Generally, minimum MDOT thickness requirements controlled the design at low traffic (3 million ESALs), resulting in a consistent 3.5-inch overlay across most climate and subgrade conditions. At medium traffic (7 million ESALs), required thicknesses increased to approximately 3.5–5.5 inches, while high-traffic scenarios (16 million ESALs) demanded 3.75–7.50 inches depending on climate and subgrade stiffness.
- **HMA over C&S:** Designs similarly defaulted to the 3.5-inch minimum at low traffic, with PMED-controlled thicknesses ranging from roughly 3.5–4.5 inches for medium traffic and 5.0–6.0 inches for high traffic. These results reflect increased sensitivity to traffic loading once MDOT minimums are exceeded.
- **HMA over Rubblized PCC:** Overlay thicknesses were more variable, ranging from 3.5–5.0 inches for low traffic, 4.0–7.0 inches for medium traffic, and 5.0–7.5 inches for high traffic.

While the catalog demonstrated consistent performance trends across fix types, the rehabilitation overlay design remains highly project-specific. Variability in existing pavement structure, distress conditions, and rehabilitation inputs makes it impractical to prescribe statewide catalog thicknesses. Doing so could risk misapplication of the catalog and does not offer a significant benefit over the existing AASHTO 93 approach.

8.7 RECOMMENDATIONS

The following recommendations are based on the findings and analyses presented in this study:

1. **Existing Unbound Granular Layers**: Adopt updated MR values for existing unbound layers based on FWD backcalculated results, laboratory testing, and prior MDOT studies. For PMED rehabilitation designs, these should be entered as non-stabilized base layers using standard inputs, with the MR adjusted to the recommended values as shown below. Note that C&S and rubblized materials should be modeled using standard dense-graded aggregate base inputs with the modified MR value.

    - Existing aggregate base: 28,000 psi
    - Existing sand subbase: 18,000 psi
    - C&S existing HMA: 60,000 psi
    - Rubblized existing PCC: 70,000 psi

2. **Existing HMA Layer Properties:** Use MDOT 4E mix properties for existing HMA layers. The average gradation and binder content (6.2%) of the field cores closely matched those of the 4E mix. Sensitivity analysis indicated that the G* of the existing HMA layer has minimal influence on PMED-predicted performance; therefore, a PG 64-22 binder grade is recommended for existing HMA layers in rehabilitation design. For composite pavements (HMA over PCC), the existing layer should be modeled as a new HMA layer with degraded dynamic modulus |E|* values to reflect material aging. Reduction factors of 0.95 (Good), 0.80 (Fair), and 0.58 (Poor) are recommended based on surface condition ratings. This approach provides a consistent, practical method for representing stiffness loss in aged HMA while maintaining the structural behavior of composite sections within the PMED framework.
3. **Existing PCC Layer Modulus:** Based on testing of field cores from existing PCC and composite pavement sections, the research team determined an average elastic modulus of 5.0 million psi, which was reduced using a condition factor (C_{BD} = 0.6) to reflect in-service damage (*2*); therefore, an effective modulus of 3.0 million psi is recommended for existing PCC layers (including JPCP, JRCP, and CRCP types) in rehabilitation design.
4. **ASCRL Layer Modeling:** Model the ASCRL layer in PMED using the newly tested |E*| values, an air-void content of 20%, and an effective binder content equal to twice the mixture binder content by weight. These inputs are based on field cores showing an average air-void content of 20% and on laboratory-compacted ASCRL specimens prepared at the same target air-voids (for details, see Chapter 3, section 3.3.1).
5. **HMA over JPCP Rehabilitation Estimation:** Estimate the condition of existing JPCP (includes JPCP and JRCP) layers under HMA overlays using the DI as a surrogate measure for pre-overlay slab distress. The percentage of slabs distressed before restoration should be taken as twice the pre-overlay DI value (up to a maximum of 90 percent). If the extent of slab repairs cannot be determined or verified (due to preliminary plans or the presence of existing HMA overlay), the percentage of slabs repaired or replaced after restoration should be assumed to be half of the pre-restoration value.

6. **HMA over JPCP Performance Indicators:** For HMA over JPCP (includes JPCP and JRCP) sections, total transverse cracking should be used as the primary performance indicator for transverse cracking. The JPCP transverse cracking output should be considered informational only, since PMED includes it as reflective cracking when calculating total transverse cracking. Other PMED performance indicators (e.g., IRI and bottom-up fatigue cracking) remain applicable for design.
7. **HMA over HMA Rehabilitation Level:** Use Rehabilitation Level 2 for HMA over HMA designs in PMED, as it incorporates field-measured fatigue and transverse cracking data, providing a more objective and nuanced representation of existing pavement conditions. Rehabilitation Level 3 should be used with caution, and care should be exercised when assigning pavement condition categories, as the method relies on subjective ratings and assumed damage indices. For Level 2, use fatigue and transverse cracking on the existing pavement before overlay placement.
8. **HMA over HMA Rutting Input:** For HMA over HMA designs, when rutting measurements in existing layers are unavailable, use an average value of 0.22 inches for total rutting. If the measured rutting is less than 0.20 inches, use a minimum value of 0.20 inches for total rutting. In both cases, the total rut depth must be allocated across the pavement layers according to the rutting distribution observed for MDOT HMA overlay sections, which is, on average, 75% in the HMA layer, 17% in the unbound base, and 8% in the subgrade, before entering the values for rehabilitation Level 2. These inputs ensure that PMED initiates strain accumulation in the steady-state deformation zone and prevents overestimation of total predicted rutting to provide a practical result.
9. **HMA over HMA Minimum HMA Overlay Thickness:** Use a minimum HMA overlay thickness of 3.5 inches in rehabilitation designs. Analysis using the MATLEA program showed that overlays thinner than 3.5 inches experience compressive strain at the bottom of the asphalt layer, eliminating tensile strain and invalidating bottom-up fatigue predictions in PMED. Maintaining at least 3.5 inches ensures realistic fatigue behavior and reliable overlay performance modeling.
10. **HMA over PCC/Composite Minimum HMA Overlay Thickness:** PMED designs for HMA over PCC/composite pavements are not recommended for overlays thinner than 4.5 inches. Sensitivity analysis showed irregular behavior in transverse-cracking predictions for overlays thinner than 4.5 inches, caused by how PMED assigns temperature nodes within the EICM climatic model. While MDOT currently specifies a minimum HMA overlay thickness of 3.5 inches (for rehabilitation), PMED results for overlays below 4.5 inches should be interpreted with caution, as the model may not provide reliable outcomes.
11. **Performance Criteria Thresholds for HMA Overlays:** The recommended performance criteria threshold values for HMA overlays of existing intact pavements are summarized in Table 5-8. Notably, the total transverse cracking threshold of 3,500 ft/mi and thermal cracking threshold of 2,000 ft/mi align with measured field performance and provide practical serviceability targets for overlay design. Other recommended thresholds are consistent with current

MDOT criteria for reconstruction pavements. The total fatigue cracking (bottom-up plus reflective) threshold of 25% matches the PMED default recommendation, which is supported by MDOT's HMA reconstruction criterion of 20%, with the additional 5% accounting for potential reflective cracking. These thresholds are presented as initial recommendations and may be refined based on MDOT review and/or additional design validation.

12. **Performance Criteria Thresholds for PCC Overlays:** Recommended thresholds for PCC overlays of existing intact pavements are summarized in Table 5-9. These thresholds align with MDOT reconstruction criteria (which are the same or very similar to the default PMED recommended values, with a slight increase to allowable cracking). Unlike HMA overlays, PCC overlays do not include a separate measure to account for reflective cracking, so new threshold values are not required. Measured transverse cracking, joint faulting, and IRI data from field sections remain within these criteria and serve to produce practical outcomes, confirming that the reconstruction limits are also appropriate for overlay designs.
13. **Recommended PMED Modeling Framework:** Tables 8-11 and 8-12 summarize the PMED modeling approaches for MDOT rehabilitation fix types. These tables identify the applicable design thresholds, PMED pavement classifications, confidence levels, and recommended design method. They serve as a practical framework for optimizing the use of PMED and promoting statewide consistency in rehabilitation design applications.

    Confidence levels are presented in 5 categories, ranging from very low to very high, and reflect the overall design confidence of using PMED for each fix type. These levels consider practical performance outcomes (validation results), local calibration accuracy (or lack thereof), the number of required assumptions, and whether direct or indirect PMED models are used. A very high confidence level indicates strong practical outcomes, accurate calibration (low error/bias), minimal assumptions, and direct PMED modeling.

    The recommended design approach is aligned with these confidence levels, which are interpreted as follows:

    - High or very high confidence supports full use of PMED with minimal precautions.
    - Medium confidence suggests that PMED may be used, but results should be monitored and reviewed for potential inconsistencies before relying solely on PMED outcomes.
    - Low or very low confidence indicates that PMED should be used with caution, applied in pilot or side-by-side comparisons with existing MDOT design methods, or deferred until further refinement is available.

14. **Use of PMED for Uncalibrated Fix Types:** Some rehabilitation fix types have not been locally calibrated due to limited available MDOT sections or because available sections are early in their service life. These include overlays of CRCP,

HMA overlays with ASCRL, SJPCP, and Agg-Lifts. HMA overlays with ASCRL may be used in PMED with minimal precautions, as the general HMA overlay calibration can be applied. Similarly, for HMA overlays of CRCP, the HMA overlay calibration may be used in combination with the global CRCP calibration. For PCC overlays of CRCP, the CRCP is treated as a stiff foundation layer, allowing the MDOT calibration for reconstruction pavements to be used. In contrast, SJPCP and Agg-Lift projects should be used with caution, as they have little or no relation to available local calibration data and few representative sections. In these cases, PMED outcomes should be monitored and compared with initial evaluations from AASHTO 93-based designs until sufficient field data become available for calibration and verification.

15. **Use of PMED for Fix Types That Cannot Be Directly Modeled:** There are fix types that cannot be directly modeled in PMED, including HMA overlays with ASCRL, overlays of composite pavement, Agg-Lifts, and SJPCP over PCC/composite pavements. HMA overlays with ASCRL may be used with minimal precautions by treating the ASCRL layer as an equivalent HMA layer with modified material properties. Similarly, overlays of composite pavement may be evaluated using existing PMED approaches by modifying an HMA layer to represent existing pavement. Conversely, Agg-Lift projects require substantial assumptions about the existing subsurface structure and its mechanistic contribution, so these PMED designs should be used with caution. Finally, there is no practical or analogous method to model SJPCP over PCC/composite pavements in PMED. Consequently, this fix type cannot use PMED at this time.
16. **Catalog Design:** Based on the catalog evaluation and the variability observed across traffic levels, climate regions, subgrade stiffness, and existing pavement conditions, the research team does not recommend adopting fixed catalog overlay thicknesses for MDOT rehabilitation design at this time. Although the catalog analyses provided thicknesses for each fix type based on the selected inputs, the results demonstrated that rehabilitation overlay design is inherently project-specific, with required thicknesses strongly influenced by localized conditions. Accordingly, designers should continue to use project-level PMED analyses with appropriate rehabilitation inputs rather than rely on prescriptive catalog tables. The catalog findings may serve as a technical reference for understanding general performance behavior, but they should not replace complete PMED evaluations for MDOT rehabilitation projects.
17. **Expansion of Calibration Dataset:** Continue adding performance data for the pavement sections included in this study and incorporate new sections into future calibration datasets once sufficient performance history becomes available. Expanding the dataset will improve the robustness and reliability of the future PMED local calibrations.
18. **Enhanced Collection of Field Data:** Accurate characterization of existing pavement is critical for reliable PMED rehabilitation design. Collect as much field data as possible from rehabilitation projects through coring, FWD testing, and other in-situ evaluations to define layer properties and existing conditions more accurately.

19. **Additional Testing for Rubblized and C&S Pavements:** Conduct additional FWD testing on rubblized and C&S pavement sections to improve the characterization of these materials. Current MR values of rubblized concrete are primarily based on literature and limited FWD testing, as laboratory testing does not adequately capture its in-situ behavior. For C&S materials, which exhibit partial binding properties, further investigation should focus on evaluating their viscoelastic response to better represent field performance in PMED. Consider conducting FWD testing across multiple and different seasons to capture potential viscoelastic variations.
20. **Regular Calibration Updates:** Perform local calibrations every six years to incorporate newly collected performance data and maintain model accuracy. Over this period, most pavement sections are expected to accumulate at least three additional performance data points, enabling more reliable updates to PMED calibration coefficients and standard error functions.
21. **Transition to PMED Version 3.0:** Future calibration efforts should transition to PMED Version 3.0, the new web-based platform that incorporates updated modeling assumptions and improved analysis capabilities. Version 3.0 also enables simulation of multiple HMA overlay configurations (e.g., HMA over HMA over HMA). In addition, Version 2.6 is scheduled to sunset in 2027, further supporting the need to adopt the latest version.

Table 8-11 Summary of asphalt overlay rehabilitation fix types

No.	Fix types	Design type	Pavement type	Recommended Rehab Threshold	Recommended Rehab Calibration Coefficients	Confidence Level	Recommended Design Approach
1	HMA over JPCP	Overlay	AC over JPCP	Recommended HMA overlay (Table 5-9)	Flexible = Tables 8-7 & 8-8, Rigid = Recon JPCP (SPR-1723)	Very High	PMED
2	HMA over JRCP	Overlay	AC over JPCP	Recommended HMA overlay (Table 5-9)	Flexible = Tables 8-7 & 8-8, Rigid = Recon JPCP (SPR-1723)	Very High	PMED
3	HMA over CRCP	Overlay	AC over CRCP	Recommended HMA overlay (Table 5-9)	Flexible = Tables 8-7 & 8-8, New Rigid = PMED Default	Medium	PMED - Monitor Designs
4	HMA (with ASCRL) over JPCP	Overlay	AC over JPCP	Recommended HMA overlay (Table 5-9)	Flexible = Tables 8-7 & 8-8, Rigid = Recon JPCP (SPR-1723)	High	PMED
5	HMA (with ASCRL) over JRCP	Overlay	AC over JPCP	Recommended HMA overlay (Table 5-9)	Flexible = Tables 8-7 & 8-8, Rigid = Recon JPCP (SPR-1723)	High	PMED
6	HMA (with ASCRL) over CRCP	Overlay	AC over CRCP	Recommended HMA overlay (Table 5-9)	Flexible = Tables 8-7 & 8-8, New Rigid = PMED Default	Medium	PMED - Monitor Designs
7	HMA over HMA/JPCP [COMPOSITE]	Overlay	AC over JPCP	Recommended HMA overlay (Table 5-9)	Flexible = Tables 8-7 & 8-8, Rigid = Recon JPCP (SPR-1723)	High	PMED
8	HMA over HMA/JRCP [COMPOSITE]	Overlay	AC over JPCP	Recommended HMA overlay (Table 5-9)	Flexible = Tables 8-7 & 8-8, Rigid = Recon JPCP (SPR-1723)	High	PMED
9	HMA over HMA/CRCP [COMPOSITE]	Overlay	AC over CRCP	Recommended HMA overlay (Table 5-9)	Flexible = Tables 8-7 & 8-8, New Rigid = PMED Default	Medium	PMED - Monitor Designs
10	HMA over HMA	Overlay	AC over AC	Recommended HMA overlay (Table 5-9)	Flexible = Tables 8-5 & 8-6	Medium	PMED - Monitor Designs
11	HMA over Rubblized Concrete	New Pavement	Flexible pavement	MDOT Recon flexible (MDOT ME User Guide)	Flexible = MDOT Recon Flexible (SPR-1723)	Very High	PMED
12	HMA over Crush & Shape HMA	New Pavement	Flexible pavement	MDOT Recon flexible (MDOT ME User Guide)	Flexible = MDOT Recon Flexible (SPR-1723)	Very High	PMED
13	HMA over Agg-Lift over Concrete Pavement	New Pavement	Flexible pavement	MDOT Recon flexible (MDOT ME User Guide)	Flexible = MDOT Recon Flexible (SPR-1723)	Low	PMED - Pilot Designs
14	HMA over Agg-Lift over Asphalt Pavement	New Pavement	Flexible pavement	MDOT Recon flexible (MDOT ME User Guide)	Flexible = MDOT Recon Flexible (SPR-1723)	Low	PMED - Pilot Designs

Table 8-12 Summary of concrete overlay rehabilitation fix types

No.	Fix types	Design type	Pavement type	Recommended Rehab Threshold	Recommended Rehab Calibration Coefficients	Confidence Level	Recommended Design Approach
1	Concrete over JPCP	Overlay	JPCP over JPCP (Unbonded)	MDOT Recon JPCP (MDOT ME User Guide)	Unbonded Rigid = MDOT Recon Rigid (SPR-1723)	Very High	PMED
2	Concrete over JRCP	Overlay	JPCP over JPCP (Unbonded)	MDOT Recon JPCP (MDOT ME User Guide)	Unbonded Rigid = MDOT Recon Rigid (SPR-1723)	Very High	PMED
3	Concrete over CRCP	Overlay	JPCP over CRCP (Unbonded)	MDOT Recon JPCP (MDOT ME User Guide)	Unbonded Rigid = MDOT Recon Rigid (SPR-1723)	Medium	PMED - Monitor Designs
4	Concrete over HMA/JPCP [COMPOSITE]	Overlay	JPCP over JPCP (Unbonded)	MDOT Recon JPCP (MDOT ME User Guide)	Unbonded Rigid = MDOT Recon Rigid (SPR-1723)	Medium	PMED - Monitor Designs
5	Concrete over HMA/JRCP [COMPOSITE]	Overlay	JPCP over JPCP (Unbonded)	MDOT Recon JPCP (MDOT ME User Guide)	Unbonded Rigid = MDOT Recon Rigid (SPR-1723)	Medium	PMED - Monitor Designs
6	Concrete over HMA/CRCP [COMPOSITE]	Overlay	JPCP over CRCP (Unbonded)	MDOT Recon JPCP (MDOT ME User Guide)	Unbonded Rigid = MDOT Recon Rigid (SPR-1723)	Medium	PMED - Monitor Designs
7	Concrete over HMA	Overlay	JPCP over AC	MDOT Recon JPCP (MDOT ME User Guide)	Unbonded Rigid = MDOT Recon Rigid (SPR-1723)	High	PMED
8	JPCP over Agg-Lift over Concrete Pavement	New Pavement	JPCP	MDOT Recon JPCP (MDOT ME User Guide)	Unbonded Rigid = MDOT Recon Rigid (SPR-1723)	Low	PMED - Pilot Designs
9	JPCP over Agg-Lift over Asphalt Pavement	New Pavement	JPCP	MDOT Recon JPCP (MDOT ME User Guide)	Unbonded Rigid = MDOT Recon Rigid (SPR-1723)	Low	PMED - Pilot Designs
10	Concrete with short-jointed concrete (including fibers) over JPCP	N/A	N/A	N/A	N/A	Very Low	AASHTO 93 (existing MDOT approach)
11	Concrete with short-jointed concrete (including fibers) over JRCP	N/A	N/A	N/A	N/A	Very Low	AASHTO 93 (existing MDOT approach)
12	Concrete with short-jointed concrete (including fibers) over CRCP	N/A	N/A	N/A	N/A	Very Low	AASHTO 93 (existing MDOT approach)
13	Concrete with short-jointed concrete (including fibers) over HMA/JPCP [COMPOSITE]	N/A	N/A	N/A	N/A	Very Low	AASHTO 93 (existing MDOT approach)
14	Concrete with short-jointed concrete (including fibers) over HMA/JRCP [COMPOSITE]	N/A	N/A	N/A	N/A	Very Low	AASHTO 93 (existing MDOT approach)
15	Concrete with short-jointed concrete (including fibers) over HMA/CRCP [COMPOSITE]	N/A	N/A	N/A	N/A	Very Low	AASHTO 93 (existing MDOT approach)
16	Concrete with short-jointed concrete (including fibers) over HMA (full-depth)	Overlay	SJCP over AC	PMED Default	New Rigid = PMED Default	Low	AASHTO 93 (existing MDOT approach)

REFERENCES

CHAPTER 1

1. AASHTO, *Guide for Design of Pavement Structures*, vol. 1: AASHTO, 1993.
2. Huang, Y. H., *Pavement analysis and design*, vol. 2: Pearson/Prentice Hall Upper Saddle River, NJ, 2004.
3. Khanum, T., "Kansas rigid pavement analysis following new mechanistic-empirical design guide," Kansas State University, 2005.
4. NCHRP 1-37A, "Guide for Mechanistic-Empirical Design of New and Rehabilitated Pavement Structures," 2004.
5. Li, Q., D. X. Xiao, K. C. Wang, K. D. Hall, and Y. Qiu, "Mechanistic-empirical pavement design guide (MEPDG): a bird's-eye view," *Journal of Modern Transportation*, 2011.
6. Robbins, M. M., C. Rodezno, N. Tran, and D. Timm, "Pavement ME design–A summary of local calibration efforts for flexible pavements," *NCAT Rep*, pp. 1-98, 2017.
7. Haider, S. W., N. Buch, and K. Chatti, "Evaluation of ME PDG for rigid pavements—Incorporating the state-of-the-practice in Michigan," 2008, pp.
8. Haider, S. W., N. Buch, K. Chatti, and J. Brown, "Development of traffic inputs for mechanistic–empirical pavement design guide in Michigan," *Transportation Research Record*, vol. 2256, pp. 179–190, 2011.
9. Buch, N., K. Chatti, S. W. Haider, G. Baladi, W. Brink, and I. Harsini, "Preparation for implementation of the mechanistic-empirical pavement design guide in Michigan : part 2 - evaluation of rehabilitation fixes.," RC-1594, 2013.
10. Haider, S. W., N. Buch, W. Brink, K. Chatti, and G. Baladi, "Preparation for implementation of the mechanistic-empirical pavement design guide in Michigan, part 3: local calibration and validation of the pavement-ME performance models.," RC-1595, 2014.
11. Haider, S. W., G. Musunuru, N. Buch, O. I. Selezneva, P. Desaraju, and J. Q. Li, "Updated analysis of Michigan traffic inputs for pavement-ME design," Michigan State University. Dept. of Civil and Environmental Engineering 2018.
12. Haider, S. W., G. Musunuru, N. Buch, and W. C. Brink, "Local Recalibration of JPCP Performance Models and Pavement-ME Implementation Challenges in Michigan," *Journal of Transportation Engineering, Part B: Pavements*, vol. 146, pp. 04019037, 2020.
13. Haider, S. W., M. E. Kutay, B. Cetin, R. R. Singh, H. B. Muslim, C. Santos, Z. You, D. Jin, K. Xin, and W. Hansen, "Testing protocol, data storage, and recalibration for pavement-ME design," Michigan. Dept. of Transportation. Research Administration 2023.
14. AASHTO, *Guide for the Local Calibration of the Mechanistic-Empirical Pavement Design Guide*, 2010.
15. Nair, H., B. Saha, and G. Merine, "Developing an Implementation Strategy for Virginia Department of Transportation Pavement Rehabilitation Design Using Mechanistic-Empirical Concepts," Virginia Transportation Research Council (VTRC) 2022.

16. Utah Department of Transportation (UDOT), "Pavement Design Manual of Instruction," 2020.
17. Islam, S., M. Hossain, C. Jones, Y. Gao, X. Wu, and S. Romanoschi, "Implementation of the AASHTO Mechanistic-Empirical Design Guide (AASHTOWare Pavement ME Design) for Pavement Rehabilitation," Kansas Department of Transportation. Bureau of Research 2023.
18. Huang, B., H. Gong, and X. Shu, "Local Calibration of Mechanistic-Empirical Pavement Design Guide in Tennessee," Tennessee. Department of Transportation 2016 2016.
19. Kim, S., H. Ceylan, D. Ma, and K. Gopalakrishnan, "Calibration of pavement ME design and mechanistic-empirical pavement design guide performance prediction models for Iowa pavement systems," *Journal of Transportation Engineering*, vol. 140, pp. 04014052, 2014.
20. AASHTO, *Mechanistic-empirical pavement design guide: A manual of practice (3rd ed.). American Association of State Highway and Transportation Officials*: American Association of State Highway and Transportation Officials, 2020.
21. Lali, F. A., R. R. Singh, S. W. Haider, M. E. Kutay, K. Chatti, and J. P. Schenkel, "Characterizing the damaged dynamic modulus master curves of existing Hot Mix Asphalt (HMA) layers for rehabilitation design," *Construction and Building Materials*, vol. 483, pp. 141808, 2025.
22. Lali, F. and S. W. Haider, "Comparison of Existing Flexible Pavements Damage Index for PMED Rehabilitation Levels," in *Airfield and Highway Pavements 2025*, 2025, pp. 47-59.
23. Velasquez, R., K. Hoegh, I. Yut, N. Funk, G. Cochran, M. Marasteanu, and L. Khazanovich, "Implementation of the MEPDG for new and rehabilitated pavement structures for design of concrete and asphalt pavements in Minnesota," 2009.
24. Von Quintus, H. and A. A. Sufian, "2023 Implementation Plan for the AASHTOWare Pavement ME Design Software," Idaho Transportation Department 2023.
25. Selezneva, O., H. Von Quintus, and W. Brink, "Exploring the Importance of Traffic Data Input Levels for Mechanistic-Empirical Pavement Design," *TechBrief*, 2021.

CHAPTER 2

1. NCHRP 1-37A, "Guide for Mechanistic-Empirical Design of New and Rehabilitated Pavement Structures," 2004.
2. Officials, T., *AASHTO Guide for Design of Pavement Structures, 1993*, vol. 1: Aashto, 1993.
3. Li, Q., D. X. Xiao, K. C. Wang, K. D. Hall, and Y. Qiu, "Mechanistic-empirical pavement design guide (MEPDG): a bird's-eye view," *Journal of Modern Transportation*, 2011.
4. Kang, M., T. Adams, and A. Kang, "Local calibration for fatigue cracking models used in the Mechanistic-empirical pavement design guide," 2007.

5. Von Quintus, H. L. and J. S. Moulthrop, "Mechanistic-Empirical Pavement Design Guide Flexible Pavement Performance Prediction Models for Montana--Volume I Executive Research Summary," 2007.
6. Muthadi, N. R. and Y. R. Kim, "Local Calibration of Mechanistic-Empirical Pavement Design Guide for Flexible Pavement Design," *Transportation Research Record*, vol. 2087, pp. 131-141, 2008.
7. Haider, S. W., G. Musunuru, N. Buch, and W. C. Brink, "Local Recalibration of JPCP Performance Models and Pavement-ME Implementation Challenges in Michigan," *Journal of Transportation Engineering, Part B: Pavements*, vol. 146, pp. 04019037, 2020.
8. Tabesh, M. and M. S. Sakhaeifar, "Local calibration and Implementation of AASHTOWARE Pavement ME performance models for Oklahoma pavement systems," *International Journal of Pavement Engineering*, pp. 1–12, 2021.
9. Buch, N., K. Chatti, S. W. Haider, G. Baladi, W. Brink, and I. Harsini, "Preparation for implementation of the mechanistic-empirical pavement design guide in Michigan : part 2 - evaluation of rehabilitation fixes.," RC-1594, 2013.
10. Haider, S. W., G. Musunuru, N. Buch, O. I. Selezneva, P. Desaraju, and J. Q. Li, "Updated analysis of Michigan traffic inputs for pavement-ME design," Michigan State University. Dept. of Civil and Environmental Engineering 2018.
11. Haider, S. W., N. Buch, W. Brink, K. Chatti, and G. Baladi, "Preparation for implementation of the mechanistic-empirical pavement design guide in Michigan, part 3: local calibration and validation of the pavement-ME performance models.," RC-1595, 2014.
12. Haider, S. W., N. Buch, K. Chatti, and J. Brown, "Development of traffic inputs for mechanistic–empirical pavement design guide in Michigan," *Transportation Research Record*, vol. 2256, pp. 179–190, 2011.
13. Buch, N., S. W. Haider, J. Brown, and K. Chatti, "Characterization of truck traffic in Michigan for the new mechanistic empirical pavement design guide.," Michigan. Dept. of Transportation. Construction and Technology Division 2009.
14. Haider, S. W., N. Buch, and K. Chatti, "Simplified Approach for Quantifying Effect of Significant Input Variables and Designing Rigid Pavements using Mechanistic-Empirical Pavement Design Guide," 2009.
15. Haider, S. W., N. Buch, and K. Chatti, "Evaluation of ME PDG for rigid pavements—Incorporating the state-of-the-practice in Michigan," 2008, pp.
16. Buch, N., K. Chatti, S. W. Haider, and A. Manik, "Evaluation of the 1–37A Design Process for New and Rehabilitated JPCP and HMA Pavements," Michigan. Dept. of Transportation 2008.
17. Haider, S. W., M. E. Kutay, B. Cetin, R. R. Singh, H. B. Muslim, C. Santos, Z. You, D. Jin, K. Xin, and W. Hansen, "Testing protocol, data storage, and recalibration for pavement-ME design," Michigan. Dept. of Transportation. Research Administration 2023.
18. Huang, Y. H., *Pavement analysis and design*, vol. 2: Pearson/Prentice Hall Upper Saddle River, NJ, 2004.
19. MDOT, *Michigan DOT User Guide for Mechanistic-Empirical Pavement Design - January 2025 Edition*: Michigan Department of Transportation, Construction Field Services Division, 2025.

20. AASHTO, *Mechanistic-empirical pavement design guide: A manual of practice (3rd ed.). American Association of State Highway and Transportation Officials*: American Association of State Highway and Transportation Officials, 2020.
21. Sufian, A. A., "Local calibration of the mechanistic empirical pavement design guide for Kansas," Kansas State University, 2016.
22. Islam, S., M. Hossain, C. Jones, Y. Gao, X. Wu, and S. Romanoschi, "Implementation of the AASHTO Mechanistic-Empirical Design Guide (AASHTOWare Pavement ME Design) for Pavement Rehabilitation," Kansas Department of Transportation. Bureau of Research 2023.
23. Harsini, I., W. C. Brink, S. W. Haider, K. Chatti, N. Buch, G. Y. Baladi, and E. L. Kutay, "Sensitivity of Input Variables for Flexible Pavement Rehabilitation Strategies in the MEPDG," 2013.
24. Brink, W. C., I. Harsini, S. W. Haider, N. Buch, K. Chatti, G. Y. Baladi, and E. Kutay, "Sensitivity of input variables for rigid pavement rehabilitation strategies in the MEPDG," *Airfield and Highway Pavement 2013: Sustainable and Efficient Pavements*, pp. 528-538, 2013.
25. AASHTO, "Mechanistic-empirical pavement design guide: A manual of practice, 2nd Edition," 2015.
26. Singh, R. R., F. Lali, H. B. Muslim, S. W. Haider, and K. D. Dolan, "Scaled Sensitivity of Pavement–Mechanistic-Empirical Transfer Function Coefficients for Flexible and Rigid Pavements," *Transportation Research Record*, pp. 03611981241295707, 2025.
27. Lali, F. A., R. R. Singh, S. W. Haider, M. E. Kutay, K. Chatti, and J. P. Schenkel, "Characterizing the damaged dynamic modulus master curves of existing Hot Mix Asphalt (HMA) layers for rehabilitation design," *Construction and Building Materials*, vol. 483, pp. 141808, 2025.
28. Lali, F. and S. W. Haider, "Comparison of Existing Flexible Pavements Damage Index for PMED Rehabilitation Levels," in *Airfield and Highway Pavements 2025*, 2025, pp. 47-59.
29. Salour, F. and S. Erlingsson, "Investigation of a pavement structural behaviour during spring thaw using falling weight deflectometer," *Road Materials and Pavement Design*, vol. 14, pp. 141-158, 2013.
30. Dawson, A. R., M. J. Mundy, and M. Huhtala, "European research into granular material for pavement bases and subbases," *Transportation Research Record*, vol. 1721, pp. 91-99, 2000.
31. Watson, D. K. and R. Rajapakse, "Seasonal variation in material properties of a flexible pavement," *Canadian Journal of Civil Engineering*, vol. 27, pp. 44-54, 2000.
32. Cary, C. E. and C. E. Zapata, "Enhanced model for resilient response of soils resulting from seasonal changes as implemented in mechanistic–empirical pavement design guide," *Transportation research record*, vol. 2170, pp. 36-44, 2010.
33. Muslim, H. B., S. W. Haider, and K. Chatti, "Seasonal and diurnal variations of back-calculated layer moduli in flexible pavement and FWD testing guidelines," *Canadian Journal of Civil Engineering*, vol. 49, pp. 83-94, 2022.

34. Ji, R., N. Siddiki, T. Nantung, and D. Kim, "Evaluation of resilient modulus of subgrade and base materials in Indiana and its implementation in MEPDG," *The Scientific World Journal*, vol. 2014, pp. 372838, 2014.
35. Popik, M., P. Eng, C. Olidis, P. Eng, and S. Tighe, "The effect of seasonal variations on the resilient modulus of unbound materials," presented at 2005 Annual Conference of Transportation Association of Canada. Calgary, Alberta, 2005, pp. 3-5.
36. Mayrberger, T. and R. J. Hodek, "Resilient modulus at the limits of gradation and varying degrees of saturation," 2007.
37. George, K., "Prediction of resilient modulus from soil index properties," University of Mississippi 2004.
38. Richter, C. A., "Seasonal variations in the moduli of unbound pavement layers," United States. Federal Highway Administration 2006.
39. Yang, W.-s., "Mechanistic analysis of nondestructive pavement deflection data," 1988.
40. Newcomb, D. E., S. W. Lee, J. P. Mahoney, and N. C. Jackson, "The use of falling weight deflectometer data in monitoring flexible pavement systems," in *Nondestructive testing of pavements and backcalculation of moduli*: ASTM International, 1989.
41. Uzan, J., "Characterization of granular material," *Transportation research record*, vol. 1022, pp. 52-59, 1985.
42. Brown, S. and A. Hyde, "Significance of cyclic confining stress in repeated-load triaxial testing of granular material," *Transportation research record*, 1975.
43. Tutumluer, E. and M. R. Thompson, "Anisotropic modeling of granular bases in flexible pavements," *Transportation research record*, vol. 1577, pp. 18-26, 1997.
44. Virgil Ping, W., Z. Yang, C. Liu, and B. Dietrich, "Measuring resilient modulus of granular materials in flexible pavements," *Transportation Research Record*, vol. 1778, pp. 81-90, 2001.
45. Yuan, D. and S. Nazarian, "Variation in moduli of base and subgrade with moisture," presented at Transportation Research Board 82nd Annual Meeting, Washington, DC, 2003, pp. 12-16.
46. Baladi, G. Y., A. Thottempudi, and T. Dawson, "Backcalculation of unbound granular layer moduli," 2011.
47. Darter, M. I., H. Von Quintus, B. B. Bhattacharya, and J. Mallela, "Calibration and implementation of the AASHTO mechanistic-empirical pavement design guide in Arizona.," Arizona. Dept. of Transportation. Research Center 2014.
48. Mallela, J., L. Titus-Glover, S. Sadasivam, B. Bhattacharya, M. Darter, and H. Von Quintus, "Implementation of the AASHTO mechanistic-empirical pavement design guide for Colorado," Colorado. Dept. of Transportation. Research Branch 2000.
49. Von Quintus, H. L., M. I. Darter, B. B. Bhattacharya, and L. Titus-Glover, "Calibration of the MEPDG transfer functions in Georgia: task order 2 report.," Georgia. Dept. of Transportation 2015.
50. Wu, Z. and D. X. Xiao, "Development of DARWin-ME Design Guideline for Louisiana Pavement Design," Louisiana Transportation Research Center 2016.

51. Moon, F., *Local Calibration of Pavement ME and Performance Evaluation of Pavement Rehabilitation and Preservation Asphalt Overlays in Louisiana*: Louisiana State University and Agricultural & Mechanical College, 2021.
52. Fick, S. B., *Evaluation of the AASHTO empirical and mechanistic-empirical pavement design procedures using the AASHO road test*: University of Maryland, College Park, 2010.
53. Titus-Glover, L., C. Rao, and S. Sadasivam, "Local Calibration of the Pavement ME for Missouri," Missouri. Department of Transportation. Construction and Materials Division 2020 2020.
54. Williams, R. C. and R. Shaidur, "Mechanistic-empirical pavement design guide calibration for pavement rehabilitation.," Oregon. Dept. of Transportation. Research Section 2013.
55. Huang, B., H. Gong, and X. Shu, "Local Calibration of Mechanistic-Empirical Pavement Design Guide in Tennessee," Tennessee. Department of Transportation 2016 2016.
56. Darter, M., L. Titus-Glover, and H. Von Quintus, "Draft User's Guide for UDOT Mechanistic-Empirical Pavement Design Guide," Report No. UT-09.1 a, 2009.
57. VDOT, "AASHTOWare Pavement ME User Manual," 2018.
58. Loulizi, A., G. W. Flintsch, and K. McGhee, "Determination of in-place hot-mix asphalt layer modulus for rehabilitation projects by a mechanistic–empirical procedure," *Transportation Research Record*, vol. 2037, pp. 53-62, 2007.
59. Nair, H., B. Saha, and G. Merine, "Developing an Implementation Strategy for Virginia Department of Transportation Pavement Rehabilitation Design Using Mechanistic-Empirical Concepts," Virginia Transportation Research Council (VTRC) 2022.
60. Miner, M. A., "Cumulative damage in fatigue," 1945.
61. AASHTO, "Top-Down Cracking Enhancement https://me-design.com/MEDesign/Documents.," in *AASHTOWare*, 2020.
62. Ling, M., X. Luo, Y. Chen, F. Gu, and R. L. Lytton, "Mechanistic-empirical models for top-down cracking initiation of asphalt pavements," *International Journal of Pavement Engineering*, vol. 21, pp. 464–473, 2020.
63. Titus-Glover, L., B. B. Bhattacharya, D. Raghunathan, J. Mallela, and R. L. Lytton, "Adaptation of NCHRP project 1-41 reflection cracking models for semirigid pavement design in AASHTOWare pavement ME design," *Transportation Research Record*, vol. 2590, pp. 122-131, 2016.
64. Lytton, R. L., F. L. Tsai, S. I. Lee, R. Luo, S. Hu, and F. Zhou, "Models for predicting reflection cracking of hot-mix asphalt overlays," *NCHRP report*, vol. 669, pp. 48-56, 2010.
65. Li, Q. J., K. C. Wang, G. Yang, J. Y. Zhan, and Y. Qiu, "Data needs and implementation of the Pavement ME Design," *Transportmetrica A: Transport Science*, vol. 15, pp. 135–164, 2019.
66. Schwartz, C., R. Li, H. Ceylan, S. Kim, and K. Gopalakrishnan, "Sensitivity evaluation of MEPDG performance prediction," NCHRP Report 1-47, 2011 2011.
67. Schwartz, C. W., R. Li, H. Ceylan, S. Kim, and K. Gopalakrishnan, "Global Sensitivity Analysis of Mechanistic–Empirical Performance Predictions for

Flexible Pavements," *Transportation Research Record*, vol. 2368, pp. 12-23, 2013.
68. Ceylan, H., K. Gopalakrishnan, S. Kim, C. W. Schwartz, and R. Li, "Global sensitivity analysis of jointed plain concrete pavement mechanistic–empirical performance predictions," *Transportation research record*, vol. 2367, pp. 113–122, 2013.
69. Ceylan, H., S. Kim, K. Gopalakrishnan, C. W. Schwartz, and R. Li, "Sensitivity quantification of jointed plain concrete pavement mechanistic-empirical performance predictions," *Construction and Building Materials*, vol. 43, pp. 545–556, 2013.
70. Kutay, M. E. and A. Jamrah, "Preparation for Implementation of the Mechanistic-Empirical Pavement Design Guide in Michigan: Part 1 – HMA Mixture Characterization.," RC-1593, 2013.
71. Baladi, G., T. Dawson, and C. Sessions, "Pavement subgrade MR design values for Michigan's seasonal changes: table E5.," 2010 2010.
72. Baladi, G. Y., K. A. Thottempudi, and T. Dawson, "Backcalculation of unbound granular layer moduli, final report," *Michigan Department of Transportation, Construction and Technology Division, PO Box*, vol. 30049, 2010.
73. Buch, N. and S. Jahangirnejad, "Quantifying coefficient of thermal expansion values of typical hydraulic cement concrete paving mixtures," Michigan. Dept. of Transportation. Construction and Technology Division 2008.
74. You, Z., X. Yang, J. Hiller, D. Watkins, and J. Dong, "Improvement of Michigan Climatic Files in Pavement ME Design–Final Report (RC-1626)," 2015.
75. Smith, K. D., J. E. Bruinsma, M. J. Wade, K. Chatti, J. Vandenbossche, and H. T. Yu, "Using falling weight deflectometer data with mechanistic-empirical design and analysis, volume I," United States. Federal Highway Administration 2017.
76. Pierce, L., K. Smith, J. Bruinsma, and N. Sivaneswaran, "Case Studies Using Falling Weight Deflectometer Data with Mechanistic-empirical Designand Analysis," presented at Pavement Performance: Current Trends, Advances, and Challenges, 2012, pp. 205-218.
77. Pierce, L. M., J. E. Bruinsma, K. D. Smith, M. J. Wade, K. Chatti, and J. Vandenbossche, "Using falling weight deflectometer data with mechanistic-empirical design and analysis, volume III: Guidelines for deflection testing, analysis, and interpretation," United States. Federal Highway Administration 2017.
78. Bruinsma, J. E., J. Vandenbossche, K. Chatti, and K. D. Smith, "Using falling weight deflectometer data with mechanistic-empirical design and analysis, volume ii: Case study reports," United States. Federal Highway Administration 2017.
79. Baladi, G., T. Dawson, and C. Sessions, "Pavement subgrade MR design values for Michigan’s seasonal changes: table E5," 2010.
80. Chatti, K., M. E. Kutay, N. Lajnef, I. Zaabar, S. Varma, and H. S. Lee, "Enhanced analysis of falling weight deflectometer data for use with mechanistic-empirical flexible pavement design and analysis and recommendations for improvements to falling weight deflectometer," Turner-Fairbank Highway Research Center 2017.

81. Nazzal, M. D., *Field evaluation of in-situ test technology for Q (C)/Q (A) during construction of pavement layers and embankments*: Louisiana State University and Agricultural & Mechanical College, 2007.
82. Davich, P., F. Camargo, B. Larsen, R. Roberson, and J. Siekmeier, "Validation of DCP and LWD moisture specifications for granular materials," 2006.
83. Senseney, C. T. and M. A. Mooney, "Characterization of two-layer soil system using a lightweight deflectometer with radial sensors," *Transportation Research Record*, vol. 2186, pp. 21-28, 2010.
84. Fan, H., J. Zhang, and S. Zhang, "Dynamic response of an axisymmetric transversely isotropic medium with its modulus varying with depth subjected to LWD load," *International Journal of Pavement Engineering*, vol. 24, pp. 2144306, 2023.
85. Shin, B., N. Tiwari, P. J. Becker, and A. Bobet, "Improved Light Weight Deflectometer Test (LWD) and Analysis," 2024.
86. Witczak, M., K. Kaloush, T. Pellinen, M. El-Basyouny, and H. Von Quintus, "Simple performance test for superpave mix design: Nchrp report no. 465. washington dc: Transportation research board, national research council," 2002.
87. Bari, J., *Development of a new revised version of the Witczak E* predictive models for hot mix asphalt mixtures*: Arizona State University, 2005.
88. Christensen Jr, D., T. Pellinen, and R. Bonaquist, "Hirsch model for estimating the modulus of asphalt concrete," *Journal of the Association of Asphalt Paving Technologists*, vol. 72, 2003.
89. Pellinen, T. K. and M. W. Witczak, "Use of stiffness of hot-mix asphalt as a simple performance test," *Transportation Research Record*, vol. 1789, pp. 80-90, 2002.
90. Program, N. C. H. R., "Independent review of the mechanistic-empirical pavement design guide and software," Transportation Research Board Washington, DC, 2006.
91. Mohammad, L. N., M. Kim, A. Raghavendra, and S. Obulareddy, "Characterization of Louisiana asphalt mixtures using simple performance tests and MEPDG," Louisiana. Dept. of Transportation and Development 2014.
92. Killingsworth, B. and H. L. Von Quintus, "Analyses Relating to Pavement Material Characterizations and Their Effects on Pavement Performance," US Department of Transportation. Federal Highway Administration, Research … 1998.
93. Yau, A. and H. L. Von Quintus, "Study of LTPP laboratory resilient modulus test data and response characteristics," Turner-Fairbank Highway Research Center 2002.
94. Baladi, G., T. Dawson, and C. Sessions, "Pavement subgrade MR design values for michigan's seasonal changes, final report," *Michigan Department of Transportation, Construction and Technology Division, PO Box*, vol. 30049, 2009.
95. Yang, Z., J. Sun, Y. Zhang, J. Liu, E. Oh, and Z. Ma, "A systematic evaluation of the empirical relationships between the resilient modulus and permanent deformation of pavement materials," *Buildings*, vol. 15, pp. 663, 2025.
96. Islam, K. M., S. Gassman, and M. M. Rahman, "Field and laboratory characterization of subgrade resilient modulus for pavement mechanistic-

empirical pavement design guide application," *Transportation research record*, vol. 2674, pp. 921-930, 2020.
97. Thompson, M. R., "Factors affecting the resilient moduli of soil and granular materials," presented at Proceeding, Workshop on Resilient Modulus Testing State-of-the-Practices, 1989, pp.
98. Zaman, M., D.-H. Chen, and J. Laguros, "Resilient moduli of granular materials," *Journal of transportation engineering*, vol. 120, pp. 967-988, 1994.
99. Chowdhury, S. R. M., *Evaluation of resilient modulus of unbound coarse materials in Idaho*: University of Idaho, 2019.
100. Helwany, S., M. B. Elias, and H. Titi, "Determination of typical resilient modulus values for selected soils in Wisconsin," Wisconsin Highway Research Program 2006.
101. AASHTO, *Guide for the Local Calibration of the Mechanistic-Empirical Pavement Design Guide*, 2010.
102. AASHTO, *Mechanistic-empirical pavement design guide: A manual of practice; 2nd Edition*: AASHTO, 2015.
103. Velasquez, R., K. Hoegh, I. Yut, N. Funk, G. Cochran, M. Marasteanu, and L. Khazanovich, "Implementation of the MEPDG for new and rehabilitated pavement structures for design of concrete and asphalt pavements in Minnesota," 2009.
104. Wu, Z., D. X. Xiao, and Z. Zhang, "Research implementation of AASHTOWare pavement ME design in Louisiana," *Transportation Research Record*, vol. 2590, pp. 1-9, 2016.

CHAPTER 3

1. Smith, K. D., J. E. Bruinsma, M. J. Wade, K. Chatti, J. Vandenbossche, and H. T. Yu, "Using falling weight deflectometer data with mechanistic-empirical design and analysis, volume I," United States. Federal Highway Administration 2017.
2. Darter, M. I., L. Khazanovich, and S. D. Tayabji, "Backcalculation of layer parameters for LTPP test sections, volume I: slab on elastic solid and slab on dense-liquid foundation analysis of rigid pavements," Turner-Fairbank Highway Research Center 2001.
3. McPeak, T. J. and L. Khazanovich, "Backcalculation of Asphalt-Overlaid Concrete Pavements," presented at Aircraft/Pavement Technology In the Midst of ChangeASCE, Air Transport Division, Airfield Pavement CommitteeAmerican Society of Civil Engineers, 1997, pp.
4. Hoffman, M. S., *Mechanistic interpretation of nondestructive pavement testing deflections*: University of Illinois at Urbana-Champaign, 1980.
5. Hall, K. T. and M. I. Darter, "Improved methods for asphalt-overlaid concrete pavement backcalculation and evaluation," presented at Nondestructive Testing of Pavements and Backcalculation of Moduli: Second Volume, 1994, pp. 83-102.
6. Hall, K. T., M. I. Darter, T. Hoerner, and L. Khazanovich, "LTPP Data Analysis, Phase I: Validation of Guidelines for K-Value Selection and Concrete Pavement Performance Prediction," United States. Department of Transportation. Federal Highway Administration 1997.

7. Ioannides, A. and L. Khazanovich, "Backcalculation procedures for three-layered concrete pavements," presented at 4th international conference, bearing capacity of roads and airfieldsFHWA, U of Minnesota, Army Corps of Engineers, NRC Canada, FAA, 1994, pp.
8. Ullidtz, P., *Pavement Analysis. Developments in Civil Engineering, 19*, 1987.
9. Lei, L., *Backcalculation of asphalt concrete complex modulus curve by layered viscoelastic solution*: Michigan State University. Civil Engineering, 2011.
10. NCHRP 1-37A, "Guide for Mechanistic-Empirical Design of New and Rehabilitated Pavement Structures," 2004.
11. Vennapusa, P. K. and D. J. White, "Comparison of light weight deflectometer measurements for pavement foundation materials," *Geotechnical Testing Journal*, vol. 32, pp. 1-13, 2009.
12. Schwartz, C. W., Z. Afsharikia, and S. Khosravifar, "Standardizing lightweight deflectometer modulus measurements for compaction quality assurance," Maryland. State Highway Administration 2017.
13. Shin, B., N. Tiwari, P. J. Becker, and A. Bobet, "Improved Light Weight Deflectometer Test (LWD) and Analysis," 2024.
14. Zhang, X., L. Jenny, B. Riad, and C. Liu, "Implementing the LWD for MoDOT Construction Acceptance of Unbound Material Layers," Missouri. Department of Transportation. Construction and Materials Division 2022.
15. Al-Qadi, I. L. and S. Lahouar, "Measuring rebar cover depth in rigid pavements with ground-penetrating radar," *Transportation Research Record*, vol. 1907, pp. 80-85, 2005.
16. Kassem, E., A. Chowdhury, T. Scullion, and E. Masad, "Application of ground-penetrating radar in measuring the density of asphalt pavements and its relationship to mechanical properties," *International Journal of Pavement Engineering*, vol. 17, pp. 503-516, 2016.
17. Shangguan, P., I. L. Al-Qadi, Z. Leng, R. L. Schmitt, and A. Faheem, "Innovative approach for asphalt pavement compaction monitoring with ground-penetrating radar," *Transportation research record*, vol. 2347, pp. 79-87, 2013.
18. Wang, S., S. Zhao, and I. L. Al-Qadi, "Continuous real-time monitoring of flexible pavement layer density and thickness using ground penetrating radar," *Ndt & E International*, vol. 100, pp. 48-54, 2018.
19. Wang, S., S. Zhao, and I. L. Al-Qadi, "Real-time monitoring of asphalt concrete pavement density during construction using ground penetrating radar: Theory to practice," *Transportation Research Record*, vol. 2673, pp. 329-338, 2019.
20. Wang, S., S. Zhao, and I. L. Al-Qadi, "Real-time density and thickness estimation of thin asphalt pavement overlay during compaction using ground penetrating radar data," *Surveys in Geophysics*, vol. 41, pp. 431-445, 2020.
21. Evans, R., M. Frost, M. Stonecliffe-Jones, and N. Dixon, "A review of pavement assessment using ground penetrating radar (GPR) in 12th International Conference on Ground Penetrating Radar, June 16-19, 2008," *Birmingham, UK*, 2008.
22. Loken, M., "Current state of the art and practice of using GPR for Minnesota roadway applications," *Commercially Unpublished Final Report for Investigation*, 2005.

23. Huynh, N., S. Gassman, R. Mullen, C. E. Pierce, Y. Chen, and N. Ahmed, "Utilization of Traffic Speed Deflectometer for Pavement Management," South Carolina. Dept. of Transportation. Office of Materials and Research 2021.
24. Muslim, H. B., *Quality of Flexible Pavement Longitudinal Joints Using Non-Destructive Testing*: Michigan State University, 2024.
25. Shook, J., B. Kallas, N. McLeod, F. Finn, P. Pell, L. Krchma, R. Haas, and K. Anderson, "Factors influencing dynamic modulus of asphalt concrete," presented at Association of Asphalt Paving Technologists Proc, 1969, pp.
26. Seo, Y., O. El-Haggan, M. King, S. Joon Lee, and Y. Richard Kim, "Air void models for the dynamic modulus, fatigue cracking, and rutting of asphalt concrete," *Journal of Materials in Civil Engineering*, vol. 19, pp. 874-883, 2007.
27. Roy, N., A. Veeraragavan, and J. M. Krishnan, "Influence of air voids of hot mix asphalt on rutting within the framework of mechanistic-empirical pavement design," *Procedia-Social and Behavioral Sciences*, vol. 104, pp. 99-108, 2013.
28. Lali, F. A., R. R. Singh, S. W. Haider, M. E. Kutay, K. Chatti, and J. P. Schenkel, "Characterizing the damaged dynamic modulus master curves of existing Hot Mix Asphalt (HMA) layers for rehabilitation design," *Construction and Building Materials*, vol. 483, pp. 141808, 2025.
29. Chen, S., S. Adhikari, and Z. You, "Relationship of coefficient of permeability, porosity, and air voids in fine-graded HMA," *Journal of Materials in Civil Engineering*, vol. 31, pp. 04018359, 2019.
30. Witczak, M. W., *Harmonized Test Methods for Laboratory Determination of Resilient Modulus for Flexible Pavement Design: Asphalt Concrete Material*: Transportation Research Board, 2003.
31. MDOT, "Standard Specifications for Construction, Michigan Department of Transportation," 2020.

CHAPTER 4

1. Haider, S. W., N. Buch, W. Brink, K. Chatti, and G. Baladi, "Preparation for implementation of the mechanistic-empirical pavement design guide in Michigan, part 3: local calibration and validation of the pavement-ME performance models," Michigan. Dept. of Transportation. Office of Research Administration 2014.
2. Haider, S. W., M. E. Kutay, B. Cetin, R. R. Singh, H. B. Muslim, C. Santos, Z. You, D. Jin, K. Xin, and W. Hansen, "Testing protocol, data storage, and recalibration for pavement-ME design," Michigan. Dept. of Transportation. Research Administration 2023.
3. Kutay, M. E. and A. Jamrah, "Preparation for Implementation of the Mechanistic-Empirical Pavement Design Guide in Michigan: Part 1–HMA Mixture Characterization," 2013.
4. You, Z., X. Yang, J. Hiller, D. Watkins, and J. Dong, "Improvement of Michigan climatic files in pavement ME design," Michigan. Dept. of Transportation 2015.
5. Miller, J. S. and W. Y. Bellinger, "Distress identification manual for the long-term pavement performance program," United States. Federal Highway Administration. Office of Infrastructure … 2003.

6. NCHRP 1-37A, "Guide for Mechanistic-Empirical Design of New and Rehabilitated Pavement Structures," 2004.
7. AASHTO, *Mechanistic-empirical pavement design guide: A manual of practice; 2nd Edition*: AASHTO, 2015.
8. MDOT, *Michigan DOT User Guide for Mechanistic-Empirical Pavement Design - January 2025 Edition*: Michigan Department of Transportation, Construction Field Services Division, 2025.
9. AASHTO, *Mechanistic-empirical pavement design guide: A manual of practice (3rd ed.). American Association of State Highway and Transportation Officials*: American Association of State Highway and Transportation Officials, 2020.
10. Baladi, G., T. Dawson, and C. Sessions, "Pavement subgrade MR design values for michigan's seasonal changes, final report," *Michigan Department of Transportation, Construction and Technology Division, PO Box*, vol. 30049, 2009.
11. Baladi, G. Y., A. Thottempudi, and T. Dawson, "Backcalculation of unbound granular layer moduli," 2011.
12. Baladi, G. Y., K. A. Thottempudi, and T. Dawson, "Backcalculation of unbound granular layer moduli, final report," *Michigan Department of Transportation, Construction and Technology Division, PO Box*, vol. 30049, 2010.
13. Singh, R. R., S. W. Haider, M. E. Kutay, B. Cetin, and N. Buch, "Impact of Climatic Data Sources on Pavement Performance Prediction in Michigan," *Journal of Transportation Engineering, Part B: Pavements*, vol. 148, pp. 04022048, 2022.

CHAPTER 5

1. AASHTO, *Mechanistic-empirical pavement design guide: A manual of practice (3rd ed.). American Association of State Highway and Transportation Officials*: American Association of State Highway and Transportation Officials, 2020.
2. Beg, M. A., "Pavement Management Programs Based on Quantitative Performance Targets," *Transportation Research Record*, vol. 2676, pp. 721-730, 2022.
3. Grogg, M., T. Van, R. Rozycki, R. Vaughn, T. Roff, J. Clarke, W. Beatty, J. Buck, A. Christenson, and C. Chang, "FHWA Computation Procedure for the Pavement Condition Measures," United States. Federal Highway Administration 2018.
4. Kutay, M. and M. Lanotte, "Formulations of the pavement performance prediction models in the mechanistic-empirical asphalt pavement analysis (MEAPA) web application," *Michigan State University*, 2020.
5. Haider, S. W., M. E. Kutay, B. Cetin, R. R. Singh, H. B. Muslim, C. Santos, Z. You, D. Jin, K. Xin, and W. Hansen, "Testing protocol, data storage, and recalibration for pavement-ME design," Michigan. Dept. of Transportation. Research Administration 2023.
6. MDOT, *Michigan DOT User Guide for Mechanistic-Empirical Pavement Design - January 2025 Edition*: Michigan Department of Transportation, Construction Field Services Division, 2025.

7. Vespa, J. W., "An evaluation of interlayer stress absorbing composite (ISAC) reflective crack relief system," Illinois. Dept. of Transportation. Bureau of Materials and Physical Research 2005.
8. Elseifi, M. and N. Dhakal, "Mitigation strategies of reflection cracking in pavements," 2015.
9. Torres, H. N., D. S. Harrington, and R. O. Rasmussen, *Design of Concrete Overlays Using Existing Methodologies*: National Concrete Pavement Technology Center, 2011.
10. Texas Department of Transportation, *Pavement Manual*: Texas Department of Transportation, 2021.
11. MDOT, *Project Scoping Manual - revised August 2022*: Michigan Department of Transportation, Construction Field Services Division, 2022.
12. ACPA, "Rubblizing of Concrete Pavements: A Discussion of its Use," *American Concrete Pavement Association*, 1998.
13. Kim, S., K. Gopalakrishnan, and H. Ceylan, "Structural characterization of Iowa's rubblized PCC pavements," *Journal of transportation engineering*, vol. 138, pp. 406-413, 2012.
14. NAPA, "Guidelines for use of HMA overlays to rehabilitate PCC pavement," *NAPA information series*, vol. 117, 1999.
15. Von Quintus, H. L., *Guidance, parameters, and recommendations for rubblized pavements*: Wisconsin Highway Research Program, University of Wisconsin--Madison, 2007.
16. Galal, K. A., B. J. Coree, J. E. Haddock, and T. D. White, "Structural adequacy of rubblized portland cement concrete pavement," *Transportation Research Record*, vol. 1684, pp. 172-177, 1999.
17. Rajagopal, A., "Evaluation of rubblization project in Ohio," Infrastructure Management and Engineering Inc. 2011.
18. NCHRP 1-37A, "Guide for Mechanistic-Empirical Design of New and Rehabilitated Pavement Structures," 2004.
19. Lali, F. A., R. R. Singh, and S. W. Haider, "Mechanistic-Empirical Design for Rubblized Pavements in Michigan," *Journal of Transportation Engineering, Part B: Pavements*, vol. 151, pp. 04025020, 2025.
20. Gopisetti, L. S. P., H. Ceylan, S. Kim, B. Cetin, and O. Kaya, "Investigation on Pavement ME Design Reflective Cracking, Faulting, IRI Prediction Models, Concrete Overlays Design Tool, and Performance Threshold Levels for Iowa Pavement Systems," 2021.

CHAPTER 6

1. NCHRP 1-37 A, "Guide for Mechanistic–Empirical Design of New and Rehabilitated Pavement Structures," *Final Rep., NCHRP Project 1-37A*, 2004.
2. AASHTO, "Guide for design of pavement structures," AASHTO, Washington, DC, 1993.
3. Li, Q., D. X. Xiao, K. C. Wang, K. D. Hall, and Y. Qiu, "Mechanistic-empirical pavement design guide (MEPDG): a bird's-eye view," *Journal of Modern Transportation*, vol. 19, pp. 114-133, 2011.
4. Officials, T., *Guide for the Local Calibration of the Mechanistic-Empirical Pavement Design Guide*: AASHTO, 2010.
5. Haider, S. W., N. Buch, W. Brink, K. Chatti, and G. Baladi, "Preparation for implementation of the mechanistic-empirical pavement design guide in Michigan, part 3: local calibration and validation of the pavement-ME performance models," Michigan. Dept. of Transportation. Office of Research Administration 2014.
6. Haider, S. W., M. E. Kutay, B. Cetin, R. R. Singh, H. B. Muslim, C. Santos, Z. You, D. Jin, K. Xin, and W. Hansen, "Testing protocol, data storage, and recalibration for pavement-ME design," Michigan. Dept. of Transportation. Research Administration 2023.
7. Haider, S. W., N. Buch, W. Brink, K. Chatti, and G. Baladi, "Preparation for implementation of the mechanistic-empirical pavement design guide in Michigan, part 3: local calibration and validation of the pavement-ME performance models.," RC-1595, 2014.
8. AASHTO, *Mechanistic-empirical pavement design guide: A manual of practice (3rd ed.). American Association of State Highway and Transportation Officials*: American Association of State Highway and Transportation Officials, 2020.
9. AASHTO, *Mechanistic-empirical pavement design guide: A manual of practice; 2nd Edition*: AASHTO, 2015.
10. Kim, S., H. Ceylan, D. Ma, and K. Gopalakrishnan, "Calibration of pavement ME design and mechanistic-empirical pavement design guide performance prediction models for Iowa pavement systems," *Journal of Transportation Engineering*, vol. 140, pp. 04014052, 2014.
11. Dong, S., J. Zhong, S. L. Tighe, P. Hao, and D. Pickel, "Approaches for local calibration of mechanistic-empirical pavement design guide joint faulting model: a case study of Ontario," *International Journal of Pavement Engineering*, vol. 21, pp. 1347-1361, 2020.
12. Officials, T., "Mechanistic-empirical pavement design guide: A manual of practice, 2nd Edition," *AASHTO: Washington, DC, USA*, 2015.

CHAPTER 7

1. Buch, N., K. Chatti, S. W. Haider, G. Baladi, W. Brink, and I. Harsini, "Preparation for implementation of the mechanistic-empirical pavement design guide in Michigan: Part 2 - Evaluation of rehabilitation fixes.," RC-1594, 2013.
2. Haider, S. W., M. E. Kutay, B. Cetin, R. R. Singh, H. B. Muslim, C. Santos, Z. You, D. Jin, K. Xin, and W. Hansen, "Testing protocol, data storage, and

recalibration for pavement-ME design," Michigan. Dept. of Transportation. Research Administration 2023.
3. Lali, F. A., R. R. Singh, and S. W. Haider, "Mechanistic-Empirical Design for Rubblized Pavements in Michigan," *Journal of Transportation Engineering, Part B: Pavements*, vol. 151, pp. 04025020, 2025.

CHAPTER 8

1. Haider, S. W., M. E. Kutay, B. Cetin, R. R. Singh, H. B. Muslim, C. Santos, Z. You, D. Jin, K. Xin, and W. Hansen, "Testing protocol, data storage, and recalibration for pavement-ME design," Michigan. Dept. of Transportation. Research Administration 2023.
2. AASHTO, *Mechanistic-empirical pavement design guide: A manual of practice (3rd ed.). American Association of State Highway and Transportation Officials*: American Association of State Highway and Transportation Officials, 2020.